

IAEA-TECDOC-638

# ***Technical aspects of high converter reactors***

*Proceedings of a Technical Committee Meeting  
held in Nuremberg, 26–29 March 1990*



INTERNATIONAL ATOMIC ENERGY AGENCY **IAEA**

February 1992

The IAEA does not normally maintain stocks of reports in this series.  
However, microfiche copies of these reports can be obtained from

INIS Clearinghouse  
International Atomic Energy Agency  
Wagramerstrasse 5  
P.O. Box 100  
A-1400 Vienna, Austria

Orders should be accompanied by prepayment of Austrian Schillings 100,—  
in the form of a cheque or in the form of IAEA microfiche service coupons  
which may be ordered separately from the INIS Clearinghouse.

TECHNICAL ASPECTS  
OF HIGH CONVERTER REACTORS  
IAEA, VIENNA, 1992  
IAEA-TECDOC-638  
ISSN 1011-4289

Printed by the IAEA in Austria  
February 1992

## FOREWORD

For some time, the Agency has given increased attention to improvements in fuel utilization through the organization of meetings and symposia. Improvements can be achieved by changes in either:

- a) the fuel, e.g. by improving the fuel performance of current operating nuclear power plants and/or developing advanced fuel cycle concepts;
- b) the reactor design, e.g. by modifying the characteristics of the current operating plants and/or developing advanced reactor concepts (or, of course, by changing both). During the last decade the attention has been concentrated on water cooled reactors.

Developments in water reactor fuel have been addressed at the IAEA Symposium on Improvements in Water Reactor Fuel Technology and Utilization, held in Stockholm, from 15 to 19 September 1986 and developments in water reactor design at the IAEA Technical Committee Meeting on Advanced Light and Heavy Water Reactors for Improved Fuel Utilization, held in Vienna, from 26 to 29 November 1984.

In addition, the IAEA set up an International Working Group on Advanced Technologies for Water Cooled Reactors (IWGATWR) as a response following to the Chernobyl accident. The IWGATWR provides a forum for Member States to exchange information on technology developments incorporating enhanced safety features and on advanced technologies and new concepts for water cooled reactors. The publication of a status report on advanced water cooled reactors, including a few high converter reactor types, has been the first major task of the group.

From 26 to 29 March 1990, the Agency convened a Technical Committee Meeting on Technical and Economic Aspects of High Converters at the Carlton Hotel in Nuremberg to provide an opportunity to review and discuss national R&D programmes, various technical aspects of and worldwide progress in the implementation of high conversion reactors.

The meeting was attended by 66 participants from 18 countries and 2 international organizations presenting 33 papers. All papers presented at the meeting are included in this TECDOC.

## **EDITORIAL NOTE**

*In preparing this material for the press, staff of the International Atomic Energy Agency have mounted and paginated the original manuscripts as submitted by the authors and given some attention to the presentation.*

*The views expressed in the papers, the statements made and the general style adopted are the responsibility of the named authors. The views do not necessarily reflect those of the governments of the Member States or organizations under whose auspices the manuscripts were produced.*

*The use in this book of particular designations of countries or territories does not imply any judgement by the publisher, the IAEA, as to the legal status of such countries or territories, of their authorities and institutions or of the delimitation of their boundaries.*

*The mention of specific companies or of their products or brand names does not imply any endorsement or recommendation on the part of the IAEA.*

*Authors are themselves responsible for obtaining the necessary permission to reproduce copyright material from other sources.*

*This text was compiled before the unification of Germany in October 1990. Therefore the names German Democratic Republic and Federal Republic of Germany have been retained.*

## CONTENTS

|  |   |
|--|---|
| Summary of the Technical Committee Meeting ..... | 7 |
|--|---|

### HIGH CONVERSION REACTOR (HCR) CONCEPTS (Session 1)

|   |    |
|---|----|
| Rationale for pressurized water high conversion reactor (PWHCR) development strategy .....  | 19 |
| <i>C.A. Goetzmann, H. Märkl, H. Moldaschl</i>   |    |
| The convertible spectral shift reactor .....  | 28 |
| <i>J.P. Millot</i>  |    |
| Analysis of VVER characteristics with tight lattice and MOX fuel .....  | 44 |
| <i>V. Pshenin, I. Levina, A. Suslov, A. Gagarinskij, A. Lazarenko, D. Machov, L. Kobzar, V. Semenov, N. Alekseev</i>  |    |
| The concept of axially heterogeneous high conversion light water reactors .....   | 53 |
| <i>Y. Ishiguro, Y. Murao, S. Yasukawa, T. Iwamura, K. Okumura, O. Sato</i>  |    |
| Improved fuel utilization with a slightly enriched spectral shift reactor .....   | 64 |
| <i>J.C. Lee, W.R. Martin, M.C. Edlund</i>   |    |
| Preliminary physics design of advanced heavy water reactors (AHWRs) .....   | 70 |
| <i>K. Balakrishnan, A. Kakodkar</i>   |    |
| Fuel cycle cost evaluation of a HCPWR .....   | 77 |
| <i>H. Hishida, R. Shimada</i>   |    |
| A conceptual core design of a plutonium generation boiling water reactor .....  | 85 |
| <i>R. Takeda, M. Aoyama, Y. Ishii, O. Yokomizo, K. Ishii, N. Sadaoka, S. Uchikawa</i>   |    |
| Steam-water power reactor concept .....   | 90 |
| <i>P.N. Alekseev, E.I. Grishanin, Yu.A. Zverkov, V.V. Kuznetsov, A.G. Morozov, V.V. Orlov, I.S. Slesarev, V.A. Stukalov, S.A. Subbotin, T.D. Shchepetina, L.N. Falkovskij</i> |    |
| High conversion thorium fuel alternatives for CANDU reactors .....  | 98 |
| <i>D. Serghiuta, V. Raica, D. Gamulescu, E. Nichita</i>   |    |

### HIGH CONVERSION REACTOR (HCR) DESIGNS (Session 2)

|   |     |
|---|-----|
| General advantages of hexagonal fuel assemblies .....   | 109 |
| <i>H. Moldaschl, P.J. Rau, I. Rummel</i>  |     |
| Nuclear core design studies for a tight lattice PWR .....   | 117 |
| <i>G.J. Schlosser, H.-D. Berger, M. Schatz, K. Thieme</i>   |     |
| Neutron physics and thermohydraulics design of a reference high conversion PWR .....                          | 122 |
| <i>C.H.M. Broeders, M. Dalle Donne</i>  |     |
| Present status of design studies on a HCPWR with semi-tight core configuration .....                          | 132 |
| <i>H. Hishida, T. Kondo</i>   |     |
| Critical power characteristics of a high conversion boiling water reactor .....                               | 139 |
| <i>K. Arai, S. Tsunoyama, S. Yokobori, K. Yoshimura</i>   |     |
| Mechanical design aspects of KWU's PWHCR .....  | 148 |
| <i>W. Meier, P.J. Rau, D. Umlauff</i>   |     |
| Radiation field in the reflector and RPV region of the high converter reactor<br>designed by Siemens AG ..... | 154 |
| <i>W. Hofmann, J. Koban</i>   |     |

## CODES AND DATA BASES (Session 3)

|   |     |
|---|-----|
| Development of calculational procedures for the neutron physics design of advanced reactors .....                       | 163 |
| <i>C.H.M. Broeders</i>  |     |
| HEXNOD and HEXMED, nodal reactor codes for the design of high converter reactors ....                                   | 178 |
| <i>M.R. Wagner, W. Francis</i>  |     |
| UO <sub>2</sub> -PuO <sub>2</sub> criticality analysis based on a coupled system NJOY/AMPX-II/<br>Hammer-Technion ..... | 185 |
| <i>A. Dos Santos, C.R. Ferreira, M.A. Rodrigues Fernandes</i>   |     |
| HEXTIME: A hexagonal space-time kinetics code for the analysis of PWHCR transients ....                                 | 192 |
| <i>H. Finnemann, R. Böhm, J. Hüskens, R. Müller, J. Mackiewicz</i>  |     |
| Improvements in the prediction of LWHCR lattice parameters .....  | 204 |
| <i>R. Böhme, J. Axmann, C.H.M. Broeders, S. Pelloni, M. Schatz</i>  |     |
| Evaluation of critical heat flux and flooding experiments for high conversion PWRs .....                                | 213 |
| <i>M. Dalle Donne</i>   |     |

## EXPERIMENTS (Session 4)

|  |     |
|--|-----|
| Experimental support to tight lattice and plutonium core studies .....                     | 229 |
| <i>J.L. Nigon, J. Mondot</i>   |     |
| The PROTEUS Phase II experiments as data base for LWHCR physics validation .....           | 251 |
| <i>R. Chawla, H.-D. Berger, H. Hager, R. Seiler</i>  |     |
| Status of tight lattice thermal hydraulics .....   | 258 |
| <i>S. Bethke, W. Zeggel, X. Cheng, C. Monir</i>  |     |
| Experimental investigation on CHF of tight lattice PWRs .....                              | 272 |
| <i>W. Zeggel, F.J. Erbacher</i>  |     |
| Experimental investigations on emergency core cooling of tight lattice PWRs in a LOCA .... | 282 |
| <i>F.J. Erbacher, K. Wiehr</i>   |     |
| The NEPTUN experiments on LOCA thermal hydraulics for tight lattice PWRs .....             | 287 |
| <i>J. Dreier, R. Chawla, N. Rouge, S. Yanar</i>  |     |

## R&D PROGRAMMES (Session 5)

|  |     |
|--|-----|
| Lessons learned from the PWHCR development .....   | 297 |
| <i>R. Brogli, B. Kuczera, H. Moldaschl, W. Oldekop</i>   |     |
| Overview of Belgian activities in the frame of improved fuel utilization and<br>high conversion reactors .....             | 302 |
| <i>G. Minsart</i>  |     |
| Investigation of intermediate conversion pressurized water reactors for small or medium<br>nuclear systems .....           | 309 |
| <i>V. Knapp, D. Pevec, D. Grgić</i>  |     |
| Progress report on the research activities on high conversion reactors at the<br>Centro Atómico Bariloche, Argentina ..... | 312 |
| <i>M.J. Abbate, M.M. Sbaaffoni, N.E. Patiño</i>  |     |
| Reactor physics research connected with the LR-O reactor .....   | 322 |
| <i>J. Bárdos</i>   |     |
| LIST OF PARTICIPANTS .....   | 330 |

## SUMMARY OF THE TECHNICAL COMMITTEE MEETING

### SUMMARY (Chairman H. Küsters)

Any future development of new nuclear power stations has to compete with 2 aspects:

- New stations have to be at least economically competitive with nowadays PWRs, or preferably cost even less; this should be valid also with respect to other energy sources.
- These new plants must be considered under the very stringent limitations of present day safety considerations and public acceptance.

There is a consensus now reached in the high conversion reactor community:

For physical/thermal hydraulic reasons the originally envisaged very tight lattice has to be widened up relatively close to a PWR - but with a hexagonal lattice.

The physics predictions for the most important parameters seem to be now in an acceptable range of accuracy - although there are some compensations effects which have not yet been cleared up. This seems to be a topic for follow up activities, although not with a very high urgency.

Next, for the semi/wide lattice, thermal-hydraulics investigations by far have not reached the same accuracy as those for neutron physics, but it seems that there are no real obstacles in the way to go.

The safety questions in this wider lattice seem also to be solvable, especially if there are real plans to build such a reactor plant. But at first there is the incentive to increase the fuel burnup, up to about 50 GWd/t, of present PWRs.

All efforts should be put together to prepare the reactor of the future, may it be a modified PWR with hexagonal lattice, high burnup and accepted in a possibly even more stringent licensing procedure - or may it be a fast reactor with improved inherent safety features. In any case, one has to avoid any possibility of a core melt-down. Although a safety argumentation with very small probabilities for the occurrence of a heavy accident is helpful technically to find out weak points in a reactor design, it is very difficult to reach full public acceptance in this way: The public just does not understand sufficiently well this line of argumentation. In addition, fast reactors could be better accepted publicly, if they could help to reduce the long-term hazards arising from the transportation and storage of long-lived radioactive nuclides in the nuclear waste.

## TECHNICAL COMMITTEE

### Session 1: High Conversion Reactor (HCR) Concepts

(Rapporteur: H. Moldaschl)

A rationale for PWR-HCR development strategy is the influence that the TMI and Chernobyl incidents have had on the public acceptance of nuclear energy. This provides an additional incentive, besides the fundamental one of safety for its own sake, for operational and safety improvements designed to avoid unacceptable radiological impact on the environment. The concept is clear and unified (no spectral shift rods, no blankets), with its main features having their basis in the Konvoi technology. The stage of development is advanced, based on proven technology, and some features of the concept of pitch to diameter ratio are similar to the actual spectral shift concepts. Thus, the concept could in principle be used for next generation reactors. Continuation of the development is planned, with the amount to be decided in the middle of the year.

Various programmes for spectral shift reactors have been under investigation. The cost benefit for this of approximately 30% seems to be too high. The additional amount for adapting a conventional core to a spectral shift core is estimated to be only 1-2% of capital cost, despite the fact that spectral shift tools need a highly sophisticated technology and much experimentation. According to detailed investigations, the stage of the development of these concepts is advanced, and is also based on proven technology.

The stage of development is fairly low for improved VVERs using a tight lattice and MOX fuel. First attempts have been made, and a preliminary analysis has been performed showing the basic feasibility of such improvements. However, no concrete design activities have performed, and an extensive experimental and theoretical programme is missing. There remains, also, room for the improvement of codes.

Similarly, only preliminary investigations have been performed for axially heterogeneous HCLWRs. The concept of a flat pancake core with a very tight pitch seems to be physically feasible and advantageous with respect to the void coefficient. Nevertheless, the axially different enrichments may cause several serious problems, e.g. extensive quality assurance, clad stress and problems concerning cooling conditions. Various topics have to be investigated very carefully, such as pump trip, ATWS, and large and small break LOCA. The design has physically interesting aspects, but seems to be complicated with respect to realization and licensing.

The calculational results for a slightly-enriched spectral shift reactor indicated the feasibility of achieving substantial improvement in fuel utilization in open fuel cycles with acceptable nuclear and thermal-hydraulic characteristics. Although detailed mechanical designs for the spectral shift rods were not presented, the first (and interesting) theoretical investigations which have been performed showed that the semi-tight HCR design can be optimized without the need for a hexagonal lattice. Based on standard square-lattice PWR geometry, with proven safety characteristics retained, the design offers the potential for early implementation in operating PWRs. Further study is suggested to resolve potential power peaking problems, and to improve neutronic methodology for tight lattice analysis.

Detailed thermohydraulic and emergency core cooling investigations are necessary for Advanced Heavy Water Reactors with light water coolant, for which only preliminary theoretical work has as yet been performed. The core and driver zones must be balanced very carefully, particularly with regard to the void coefficient. This seems to be very difficult in reality, and any joint reduction of safety margins will further reduce the economy of a plant, the costs of which are already comparatively high. Further problems are likely to be caused by the fact that the licensing of this concept seems to be very complicated.

Very interesting strategy calculations for the evaluation of HCLWR fuel costs have been performed. Extrapolation beyond 20 years does not seem to be hazardous, and it appears as though flexible HCPWR concepts might be necessary to meet the unforeseen fluctuations in economics and strategy trends in the future. Extension of those calculations seems to be very useful, but one should also take into account fusion and "renewable" energy resources as soon as their technological and economical backgrounds become sufficiently reliable for comparison.

As in the above case, investigations with respect to "alternative" energy scenarios should also be improved in the case of strategic calculations for the conceptual core design of plutonium generation Boiling Water Reactors. These calculations were also presented with a rather broad, and perhaps unrealistic time scale (to the year 2000).

The ancient concept of a steam/water cooled and moderated core is based on VVER type reactors, and is in the process of undergoing a renaissance, albeit on a comparatively narrow technological basis. The basic idea of the steam/water cooled breeder is a common one, but the solution of technical problems by extrapolation from the VVER and LMFBR as proposed does not seem to be feasible. Many further experimental/theoretical investigations are required. Additional independent systems for reactivity control are also necessary, which would cause licensing problems to arise.

Different scenarios for high conversion thorium fuel alternatives for the CANDU reactors were investigated, with the fuels thorium oxide and metallic Th. The results are very interesting, although somewhat unrealistic, and fuel problems such as temperature behaviour were not discussed. Realization of realistic concepts in connection with these investigations should be elaborated.

#### Session 2: High Conversion Reactor (HCR) Designs (Rapporteur: B. Kuczera)

The more generic advantages of hexagonal fuel subassembly geometries, which have been developed in the framework of tight lattice HCRs, are derived from symmetry and modeling aspects. They are supposed to facilitate the simulation technique for a more realistic approximation of real core conditions, and thus improve the overall investigations.

A 1300 MW HCPWR design with a very tight lattice core geometry was presented. The initial moderator-to-fuel volume ratio  $V_{mf}$  had been 0.5, but was then modified in several steps to the current value of  $V_{mf} = 1.23$

(fuel pin diameter = 9.5 mm, which is equal to the Convoy-value). In this design, the excess reactivity is compensated for by soluble boron in the coolant. The boron concentration is a function of the burnup, and the void reactivity behaviour of the design is comparable to standard PWR conditions. An assessment of the main pros and cons of thermal plutonium burner concepts was presented next, together with HCR neutron physics, and design problems and methods which have been applied in the solution procedure. Characteristic design data are  $V_{mf} = 1.23$ , conversion ratio CR = 0.75 and burnup B = about 60 Gwd/t.

The conceptual HCR design state was illustrated in further contributions, in which a prototype of an HCR grid spacer, and the design of the complex control element guide structure were presented. Radiation aspects related to the core reflector and the reactor pressure vessel were reported on as well.

The Mitsubishi HCPWR concept sponsored by the Japanese utilities is quite different from the axially heterogeneous JAERI concept described during the first session. For the time being, Mitsubishi favours a triangular lattice design, combined with a mechanical spectral shift concept which allows the modification of the moderator-to-fuel volume fraction from 1.21 to 1.41. Due to the additional spectral shift rod drive mechanisms, some thermal-hydraulic problems (vibrations) have occurred in the upper plenum region, and alternative solutions are being investigated carefully. Characteristic design data are  $V_{mf} = 1.21$  to 1.41, CR = 0.85 and B = 45 Gwd/t.

An inter-comparison of both design concepts mentioned above seems to indicate certain converging trends.

In Japan, BWR plants are also considered to be a proven and established electricity generation system. Insofar as this, HCBWR represents an evolutionary step in the further system development. Critical power correlations for tight triangular lattice configurations were addressed, and particular emphasis was given to critical steam quality correlations. Significant improvements have been achieved with respect to predictive methods based on experimental evidence. First accident analyses indicate an operational transient behaviour, which is comparable to corresponding standard BWR behaviour. Characteristic HCBWR data are  $V_{mf} = 1.0$ , CR = 0.85 and B = 45 Gwd/t.

### Session 3: Codes and Data Bases

(Rapporteur: J.N. Nigon)

Within the last six years tremendous improvements have been achieved in the cell and burnup calculation field. These improvements can be attributed to new evaluations of experimental data such as JEF-1 and ENDF/B-5, and to modeling refinements, mostly in the area of slowing down and of resonance self- and mutual-shielding. Evidence of this is given by the accuracy of reaction rates assessment of 240-Pu, and also by the remaining uncertainty on the capture rate of 242-Pu which still has to be reduced. Most of these developments have been performed on the basis of WIMS-type cell codes. The way to multi-parametric, few group, condensed macroscopic and microscopic cross-sections to be used in reactor calculations still relies on the "supercell" technique for spectrum interaction evaluation.

Many FBR computer codes have been adapted, or at least constitute an important background for the development of the hexagonal multi-group space calculations. These codes have become more and more general, and are also applicable for HTGR calculations. It should be noted that nodal codes are widely used because of their computing time efficiency, and various options and numerous combinations of codes are assembled in consistent systems for design purposes.

A major extension of the critical heat flux (CHF) data base has been achieved for standard lattices with triangular pitch and various geometrical parameters. The correlations seem to be becoming more and more efficient in order to represent satisfactorily varying geometries. They are, however, limited to an accuracy of around  $\pm 20\%$ . As far as reflooding is concerned, the standard lattice and the semi-tight lattice seem to be well represented by the present modeling, at least by the most advanced ones. This is not yet the case for very tight lattices.

Additional work is required to improve the individual isotope reaction rates even if, by some compensation effects, the global parameters such as multiplication factors are well evaluated. This is particularly the case for individual isotope burnup predictions, and for the plutonium and higher actinide build-up rate. Heterogeneity effects are also not always adequately taken into account, and an effort to incorporate these would be profitable to those who do not use cell-interaction procedures. The methods of calculation near the macroscopic interfaces between media with very different spectra, particularly for blanket calculation, should be improved on as well.

For further work, the present methodology which is applied by most of the participating teams should be encouraged. Basic data libraries should always be assessed first, with the improvement and assessment of detailed modeling as a second step. The adjustment of microscopic data to global results, unless it is performed within the experimental uncertainty range, should be avoided as far as possible, as should the adjustment of multigroup cross-sections for reactor calculations on the basis of global results only. If such adjustments are unavoidable, an attempt should be made to try and find out an adjustment procedure which is based on modeling (such as transport-diffusion correction).

#### Session 4: Experiments

(Rapporteur: R. Chawla)

The 4th session dealt mainly with experimental programmes in support of high converter designs - either completed or in progress in France, Switzerland and Germany. In general, the impression given was that a comprehensive experimental data base has now been generated for both reactor physics and thermal-hydraulics aspects of tight-lattice LWRs, but that the testing and development of appropriate design tools has still to make full use of the different types of information available. An obstacle in this regard has been the rather restricted sharing of detailed experimental results and experience - something which is necessary before any further experimental needs can be defined clearly.

The French programme includes zero-power and burnup-related physics, stationary and reflooding thermal-hydraulics, and also the testing of new components. The main conclusion drawn was that semi-tight high converter designs have been shown to be feasible, while the very tight designs do not appear to be so.

An overview of the PROTEUS Phase II zero-power physics experiments in Switzerland showed that the data base provided was broad - both in terms of LWHCR design characteristics covered, as well as in the types of integral measurements made.

The validity of sub-channel analysis for the evaluation of critical heat flux (CHF) experiments at the TU Braunschweig was discussed, and the need for extensive individual-effect experiments was stressed.

Results from some of the KRISTA freon-CHF experiments at Karlsruhe showed satisfactory agreement with predictions. The importance of evaluating the freon/water scaling laws on the basis of the Siemens/KWU Karlstein experiments was stressed.

The emergency core cooling (ECC) experiments at the FLORESTAN facility at Karlsruhe were reviewed. Results for forced- and gravity-feed experiments for a very tight ( $p/d = 1.06$ ) assembly, as well as for deformation tests with a zircaloy ( $p/d = 1.20$ ) assembly, were discussed.

The description of the NEPTUN-LWHCR programme concerned re-flooding experiments which are conducted in Switzerland. Rewetting for the tight ( $p/d = 1.13$ ) assembly was found to occur in all bottom forced-feed tests employing reasonably LWHCR representative values for the thermal-hydraulics parameters.

#### Session 5: R & D Programmes

(Rapporteur: R.H. Brogli)

This session was devoted to R&D aspects for high converter reactors in general, and not to specific aspects of the tight-lattice PWR.

It was noted that new reactors for providing the additional electricity needed in the coming years should be accepted by the public as well as by the utilities. These reactors should be safer, reliable, economic and flexible in their fuel utilization. The R&D activities for LWHCR are a right move in this direction. The results obtained so far are impressive, but more work has yet to be done.

Physics experiments were, and are being performed for MOX fuel at various locations in Belgium, as in the VENUS facility. In the BR3, numerous types of fuels have been irradiated. Material tests, including power recycling, have been done in the reactor BR2. The Belgian facilities could also be used for LWHCR testing in a yet to be defined cooperative effort.

Investigations on the feasibility and gains from an intermediate conversion PWR core in terms of fuel utilization in an open fuel cycle were presented. Conceptual calculations are in progress to determine the range of  $V_m/V_f$  ratios at the beginning and end of the cycle.

The development and validation of calculational tools for designing high conversion reactors in Argentina have yielded improvements in the self-shielding correction and in the heterogeneity treatment. The validation of the code using the NEACRP benchmark and the Proteus-I experiment has also proved to be acceptable.

Experimental investigations at the LR-0 reactor in the Czech and Slovak Federal Republic were orientated to develop a fuel cycle with gadolinium for VVER. The burnup modalization and the  $k_{\infty}$  management were described for this fuel, and experiments for determining the effective radius of the burnable absorbers during burnup were discussed.

## W O R K S H O P

### Workshop Session 1: Reactor Physics

(Chairman: Chawla)

The principal objective of this workshop session was the identification of further R&D needs for the reactor physics design of high converters. The physics-related papers presented at the Technical Committee were found to be in three broad categories, namely the validation of lattice codes, the development of design tools, and special aspects.

Bearing these presentations in mind, questions related to the current status, obvious and potential shortcomings and, finally, requirements for achieving target calculational accuracies, were discussed.

Among the principal findings and recommendations that emerged from the proceeding, was that nuclear data for the higher-energy resonances of the principal fuel nuclides, inelastic scattering cross-sections for  $^{238}\text{U}$  and burnup need closer attention. The last includes fission-product cross-sections (from the viewpoint of reactivity prediction) and higher actinide data (important for assessing Am and Cm build-up in the context of fuel fabrication procedures). Some data will be provided through the JEF-2 or ENDF/B-6 activities.

Considerable efforts has already been invested in the validation of cross-section processing schemes and lattice codes. Features which particularly need to be borne in mind are the choice of group structures in the resolved resonance region (important also in the treatment of the higher  $^{240}\text{Pu}$  and  $^{241}\text{Pu}$  resonances), mutual shielding effects and multizone modeling of the cell. There is a need for reducing the relatively large uncertainty (reported spreads of up to 10%) which currently exists in conversion ratio predictions, and it was recommended that a numerical benchmark exercise be conducted for this purpose.

Whereas physics design tools for high converters have been developed and applied to a large extent, there has been little validation of the space and energy condensation procedures involved. A benchmark exercise for assembly calculations is urgently needed. It would be advantageous to define this in as simple a form as possible, e.g. a set of calculations for an inserted/withdrawn central control rod. This applies also to whole-reactor calculations. Here, a two-stage benchmark exercise is recommended - to be conducted after evaluation of the assembly benchmark. The first stage should be "mathematical" (with pre-specified macroscopic cross-sections) and the second should be "physical" (based, if possible, on an experimental configuration with significant high-converter-type leakage characteristics). It is also recommended that sensitivity and uncertainty analysis methods, such as have been applied in the evaluation of calculational accuracies for high converter lattice parameters, be extended to assess, for example, design uncertainties in such work.

As regards safety-related physics, there is a long-term need for detailed investigations of high converter transients, e.g. ATWS. This would involve the use of suitably benchmarked, space-time kinetics codes with thermal-hydraulics coupling.

Detailed experimental results from the latest French and Swiss/German programmes of high converter physics measurements have not been published in the open literature. It is desirable that these be made widely available. Following this, the various individual groups should meet to define further experimental needs.

## Workshop Session 2: Thermal Hydraulics and Mechanical Design

(Chairman: M. Dalle Donne)

### 1. Steady State Critical Heat Flux

There are correlations available today that are able to predict the critical heat flux (CHF) for an infinitely large array of rods (not disturbed by the rod cluster boundary) with tight triangular lattice, with both grid and spiral wire or integral spacers with an uncertainty band of  $\pm 20\%$ . This may be sufficient for scoping or optimization investigations, but the correlations should be complemented by experiments with the correct geometry for any particular case. For this purpose, it is important that coolant water (correct pressure and mass velocity) be used instead of freon. The number of rods, which should be of the right diameter and pitch, and sufficiently long (full length, if possible), ought to exceed 37. The right spacers and spacer axial distance should also be used.

Besides the infinite array geometries, other local effects should be investigated as well, such as the effects of control rod guide tubes, sub-assembly border and spacer local effects, the effects of sub-assembly inlet and outlet, rod swelling effects, and the CHF in the narrow annulus between control guide tube and control rod. In the investigation of such local effects, as well as for infinite array data, tests with freon 12 are helpful.

For the reduction of the data and the application of the results, information is required concerning friction factors in the flow direction, and mixing factors in the direction perpendicular to the flow (single, sub-cooled boiling and two-phase flow).

### 2. Large Break Loss of Coolant Accidents

In the Blow-Down Phase, this item generally requires very large and expensive tests. It is felt that the experience gained for the PWR and BWR is very useful. However, tests with the proper core geometry (tight fuel rod lattice) are required to check the accuracy of the available codes. Additionally, further experimental information is required in the area of Transient CHF. Although this is generally higher than the Steady State Critical Heat Flux, experimental data are required to account for the higher hydraulic resistance of the fuel rod clusters and possibly stronger flow reductions. Preliminary tests with freon-12 are useful here as well. Experiments are necessary in the area of Post CHF Heat Transfer also, especially to account for the tight lattice geometry of the core. This would allow the checking of the accuracy of the available PWR and BWR codes.

Experiments with the proper geometry should be performed for the Reflooding Phase as well (the full fuel rod length is important here also!). These experiments should be with forced feed for easy interpretation with the available codes. The experiments with gravity feed should be performed while taking care to simulate well the hydraulic resistance, level, volume and length of the rest of the circuit.

### 3. Small Break Loss of Coolant Accident

General experiments are probably not required. The available codes should be checked. Special experiments are probably required for some special conditions (partially uncovered cores).

### 4. Zircaloy Cladding Ballooning

Ballooning tests of zircaloy tubes (constant inside pressure, increasing temperature) should be performed with the proper chosen geometry. Reflooding tests with the swollen rods are recommended.

### 5. Special Recommendations for BWR

Special attention should be given to the two-phase flow phenomena. The correlations should be checked for lower ranges of pressures and high steam quality.

### 6. Design

Particular attention should be paid to the components inside the pressure vessel, which could be quite different from the usual PWR and BWR components. The basic design criteria and the conceptual design of major items are of special interest. The former refers to the boundary of the sub-channels in the fuel assemblies, spacers dimensions, fuel assembly structures, control rod assembly and dimensions, reflector, control rod guides, water flow path in the upper plenum and so on. Of particular importance with respect to the latter are the structures above the core and the control rod guides.

## Workshop Session 3: Economic and Licensing Aspects of the HCR Introduction (Chairman: Hishida)

No member states have as yet a definite plan for HCR introduction before the year 2005. Technical acceptance of a hexagonal lattice is considered to be one of the key steps in this regard.

An HCR with a flexible core (transition capability between a semi-tight lattice core and a loose core through the replacement of fuel assemblies only) would be desirable in order to meet the fluctuations in economic and strategic trends expected during the life of the plant. Such a transition scheme could be one of the R&D objectives associated with design optimization.

It was agreed that the increase in the capital cost of an HCR would have to be minimized. Based on current estimates for design modifications, spectral shift control drive mechanisms, reactor coolant pump power, spent fuel assemblies and radiation shields for new fuel storage facilities should be included. However, the expected capital cost increase should be less than 3%.

Annual natural uranium savings of more than 40% were estimated in the closed cycle with utilization of MOX fuel, while in the open cycle, about 20% savings could be achieved. The amount of savings would depend on Pu availability. The increase in discharge burnup would be the primary determinant of the savings in fuel cycle cost. Through the optimization in HCR design, the net impact of fuel cycle cost may be negligible. The recycling of Pu is also important with respect to future uranium savings, and the sharing of information and experience with Pu recycling and MOX fuel should be encouraged.

Licensing issues for an HCR are dependant on the designs under consideration in member states, and it is difficult to come to any one conclusion. However, it was reported that an HCR with a semi-tight lattice core may satisfy the safety standards for a conventional LWR without difficulties, and for an HCR with a tight lattice, licensing issues may be compromised by design optimization.

## HIGH CONVERSION REACTOR (HCR) CONCEPTS

(Session 1)

Chairman

**H. MOLDASCHL**  
Germany

# RATIONALE FOR PRESSURIZED WATER HIGH CONVERSION REACTOR (PWHCR) DEVELOPMENT STRATEGY

C.A. GOETZMANN, H. MÄRKL, H. MOLDASCHL  
Siemens AG,  
Unternehmensbereich KWU,  
Erlangen, Federal Republic of Germany

## Abstract

The paper describes the rationale and the status of the research and development work for the High Conversion PWR (PWHCR) under investigation at SIEMENS KWU in cooperation with the Nuclear Research Center Karlsruhe, the Paul Scherrer Institute Wuerenlingen, Switzerland, and the Institute for Reactor Technology of the Technical University of Braunschweig.

The distinguishing feature of the PWHCR is that it provides a significant better fuel utilization than in a standard PWR and yet maintains to an extraordinary large degree the latter's plant technology. The capital cost risk, typical for a new concept, would thus be substantially minimized once the development has been completed with satisfactory results.

Increased fuel utilization still is the ultimate target of all fission reactor development. It is the prime motive for breeder reactors which are capable of providing an assured energy supply for many centuries. In light of the ever increasing CO<sub>2</sub> accumulation with its adverse effects on global climate, the benefits of nuclear power are expected to be re-appreciated in the long run and would thus require maintaining and furthering the option of fast breeder reactors.

The PWHCR fits logically into such a strategy since its fuel cycle is basically compatible with that of the breeder. Whilst by far not providing a degree of utilization as that of the breeder, it improves that of the thermal spectrum reactors and nevertheless maintains a sufficient stockpile for starting a large-scale introduction of breeders whenever the pertinent need arises.

Flexibility in fuel cycle adaptability is thus a characteristic feature of PWHCRs as will be described in this paper and the other ones given at this conference. Based on the encouraging R & D results obtained thus far it is concluded that the concept is technically feasible and that it should be accordingly pursued further.

## 1. Introduction and Objectives

The ultimate goal of nearly all civilian nuclear power programs has been, and essentially continues to be, the development and commercial deployment of fast breeder reactors (FBR). This objective was based on the early recognition that only in a fast neutron spectrum it is possible to fully convert the predominant non-fissile part of natural uranium into fissile material to extract energy for power production. With breeders, the availability of nuclear fuel can be assured for many centuries to come under any energy consumption scenario. Primarily due to an appreciably lower growth rate in electricity consumption than originally anticipated and to the difficulty to readily match the capital cost of light water reactors (LWR), commercial introduction of the FBR has been delayed into the next century.

In the past couple of decades thermal converter reactors, particularly LWRs, with a certain quantitative dominance of the pressurized water reactor (PWR) type, have achieved full technical, economic and operational, i.e., commercial maturity. The present paper addresses a LWR concept designed to be operated in the epithermal spectrum range. To better understand the underlying development rationale it would seem appropriate to broadly describe the premises upon which such a concept has to be based. Special aspects of the technical design will be given in the numerous other papers of this conference.

In the Federal Republic of Germany the so-called KONVOI projects, a rigidly standardized series of 1300 MWe PWR nuclear power plants (NPP) commissioned during the past three years represent an extremely high standard regarding safety and operational performance.

Hence the KONVOI technology offers a solid basis to further improvements for the next generation of PWRs in the FRG.

Two different development objectives are being pursued independently:

- a) Further operational and safety performance improvements particularly in the following areas [1]
  - Novel instrumentation and control (I & C) systems using exclusively digital microprocessor-based technology in order to enhance process control and man-machine interface by providing advanced process information and surveillance [2, 3]

- Evolutionary introduction of further inherent and passive design features wherever reasonably practicable
- Consistent implementation of both preventive and mitigative accident management measures in order to maintain core coolability and containment integrity, respectively, even in postulated beyond design events

These development efforts the results of which will be available for project implementation prior to 1995 are expected to contribute markedly to regain and re-establish public acceptance

b) The second objective is oriented towards improving the fuel cycle performance [4] regarding

- fuel cycle costs
- cycle length potential maintaining proven load follow capability, and, in particular
- enhanced fuel utilization including use of plutonium (Pu)

Enhanced fuel resource utilization will turn out to be the more important the sooner the renaissance of nuclear energy utilization will occur and the faster nuclear expansion will take place

In spite of the tendency of certain energy supply saturation phenomena observable in some highly industrialized countries there is undoubtedly a fast increasing energy demand to be anticipated for the coming decades

Particularly due to the rapidly growing awareness that continuation of CO<sub>2</sub> emission at the present or even an enhanced level will lead via the greenhouse effect to a highly alarming global warming, continued operation and construction of fossil fueled power plants will have to be decisively limited and, as a result, due to lack of alternative energy sources, the share of nuclear power will have to be increased correspondingly

In an appeal recently directed to President George Bush by the Union of Concerned Scientists, signed by 49 Nobel Prize Winners and 700 distinguished sci-

entists [5], global warming has been denoted as the most serious environmental threat of the 21st century requiring a policy including a o increased use of nuclear power As a quantitative indication as to which extent energy conservation and conventional power plant efficiency improvement can be supplemented by an increased share of nuclear energy in order to reduce CO<sub>2</sub> emissions Fig. 1 shows for the European Community (EC 12) the additional nuclear capacity required to keep constant or to decrease present CO<sub>2</sub> emission rates by the year 2010 [6] The assessment is based on an electricity demand forecast amounting to a growth rate of 1 75 %/a on the average The goal of keeping CO<sub>2</sub> emissions at present levels would necessitate an additional nuclear capacity of about 47 GWe Implementation of the resolution made at the Toronto Conference 1988 to reduce CO<sub>2</sub> emissions to 80 % of the present value by 2005 would require an additional nuclear capacity of about 67 GW meaning that the share of nuclear energy in the European Community would have to increase from presently 32 % to 50 % This may not appear to be very realistic

However, in the light of growing nuclear energy need to be anticipated in the short to medium range already on the one hand, and of the delay in commercial FBR availability on the other hand, the commercially proven and mature LWRs as the work horses will have to take the predominant share in providing the required nuclear capacity

In order not to rapidly exhaust the finite and limited natural uranium resources, the uranium utilization of the LWR requires appreciable improvement, i e , its conversion ratio will have to be increased markedly above its present value of  $\approx 0.55$

This requirement amounts to, in essence, modifying the core of current PWRs with the moderating ratio (moderator-to fuel volume ratio) being the most important design and optimization parameter for achieving high conversion capability

## 2. Siemens/KWU's High Conversion Reactors as a Link in an Evolutionary Development Chain

As pointed out in the preceding paragraph, further improvement of safety and operational performance of the PWR type NPP is being pursued at Sie-

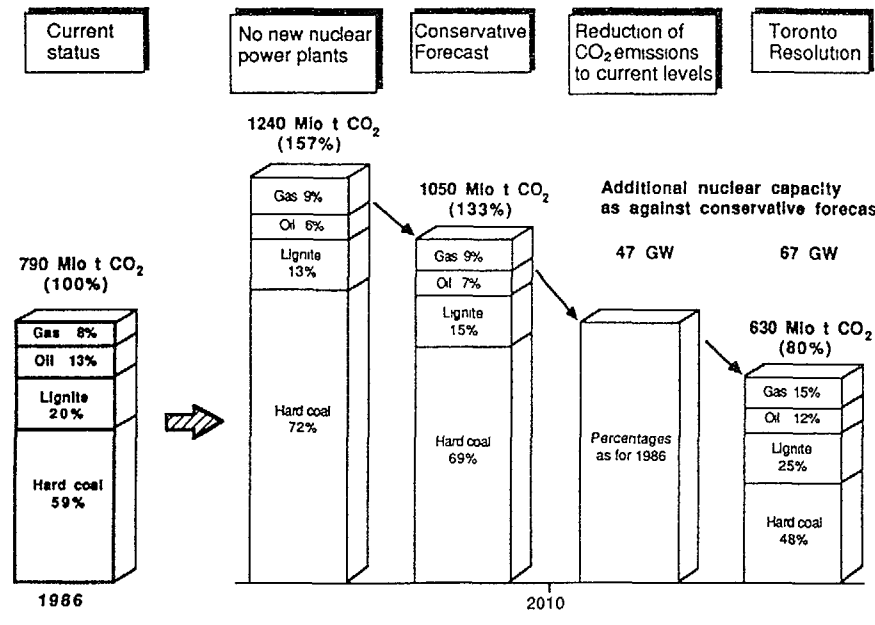


FIG. 1. Development of carbon dioxide emissions by 2010 resulting from fossil fuel electricity generation in the European Community (average electricity generation growth rate 1.75%/a).

mens/KWU with the KONVOI technology being the reference and basis for that evolutionary development

The major objectives are

- to further reduce the probability of occurrence of a beyond design event, i.e., of an accident not coped with by the safety systems, by means of extended use of passive safety features, and, in addition
- to maintain containment integrity by introduction of both design provisions and mitigative accident management measures such that even a core melt accident will not expose the environment to an unacceptable radiological impact, thus rendering external evacuation measures unnecessary

The multilevel defense-in-depth concept traditionally adhered to in the FRG will be extended in order to comply with these targets, as is illustrated in Fig 2

The high conversion reactor (HCR) will likewise have to meet these development objectives

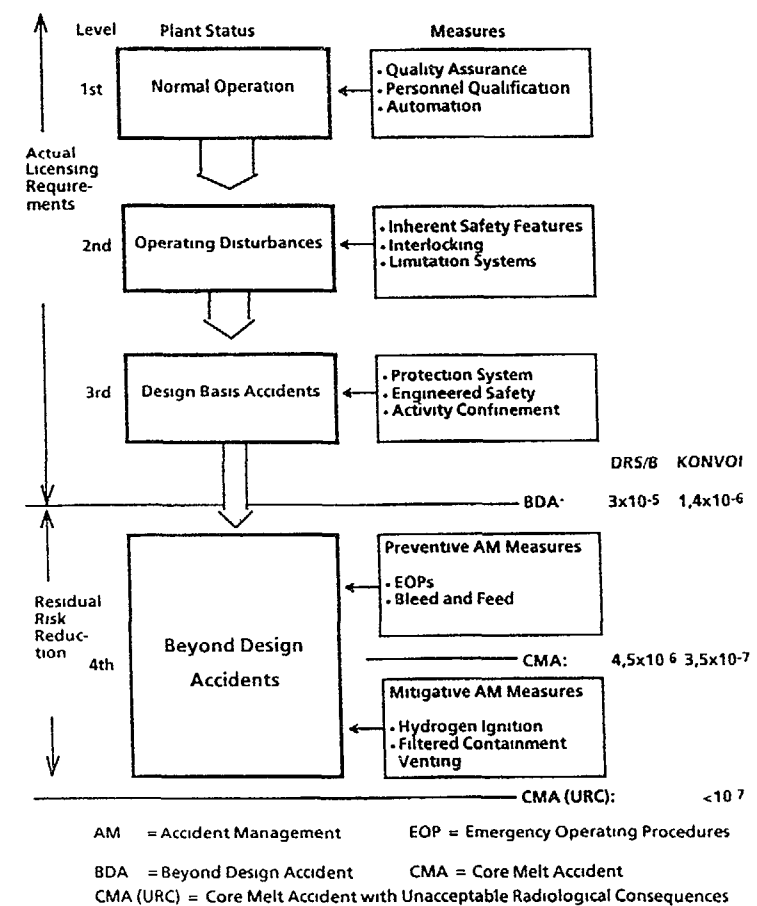


FIG. 2. Multilevel defence-in-depth nuclear power plant safety concept.

Simultaneously, however, the fuel rod lattice will be tightened such that the conversion ratio can be increased markedly beyond its current value of  $\approx 0.55$ . As shown in Fig. 3 the HCR represents a link in an evolutionary development chain of the PWR.

**Development stage number 1** indicates the classical situation of a PWR fueled with uranium fuel exclusively, as is the case in the once-through fuel cycle mode, world-wide most customarily in use in current PWRs.

In the FRG thermal Pu recycling, consistently sponsored by the Federal Ministry for Research and Technology (BMFT) and performed by utilities and manufacturers since 1972, has achieved a high technical and commercial standard [7]. As of March 1990 more than 50 000 mixed oxide (MOX) fuel rods in some 400 MOX fuel assemblies have been inserted and irradiated in Siemens/KWU supplied LWR fuel elements, typically in the so-called self-generated recycle (SGR) mode (**development stage 2**), where one quarter to one third of the core is loaded with MOX-fuel. The maximum number of MOX fuel assemblies in one core loading that has been licensed so far amounts to 50 %. The maximum burnups which have been successfully achieved are beyond 52 MWd/kg.

The **third development stage** differs from the second in that the Pu generated in several LWRs is recycled into one that contains an all-plutonium core (Pu-burner).

According to the experience accumulated with SGR, a Pu burner appears to be a feasible technical extrapolation from development stage 2.

The first three core variants exhibit an identical fuel rod lattice with a square rod arrangement having a moderator-to-fuel volume ratio of  $\approx 2$ . The conversion ratio is slightly increasing with rising Pu contents in the core due to neutron spectrum hardening.

**Development stage 4**, while still maintaining a square fuel rod lattice and keeping the fuel assembly outer dimensions constant, results from the preceding version by decreasing the moderating ratio through fuel rod diameter increase, requiring a slight change in the spacer grid. The rod cluster control assembly can remain unchanged.

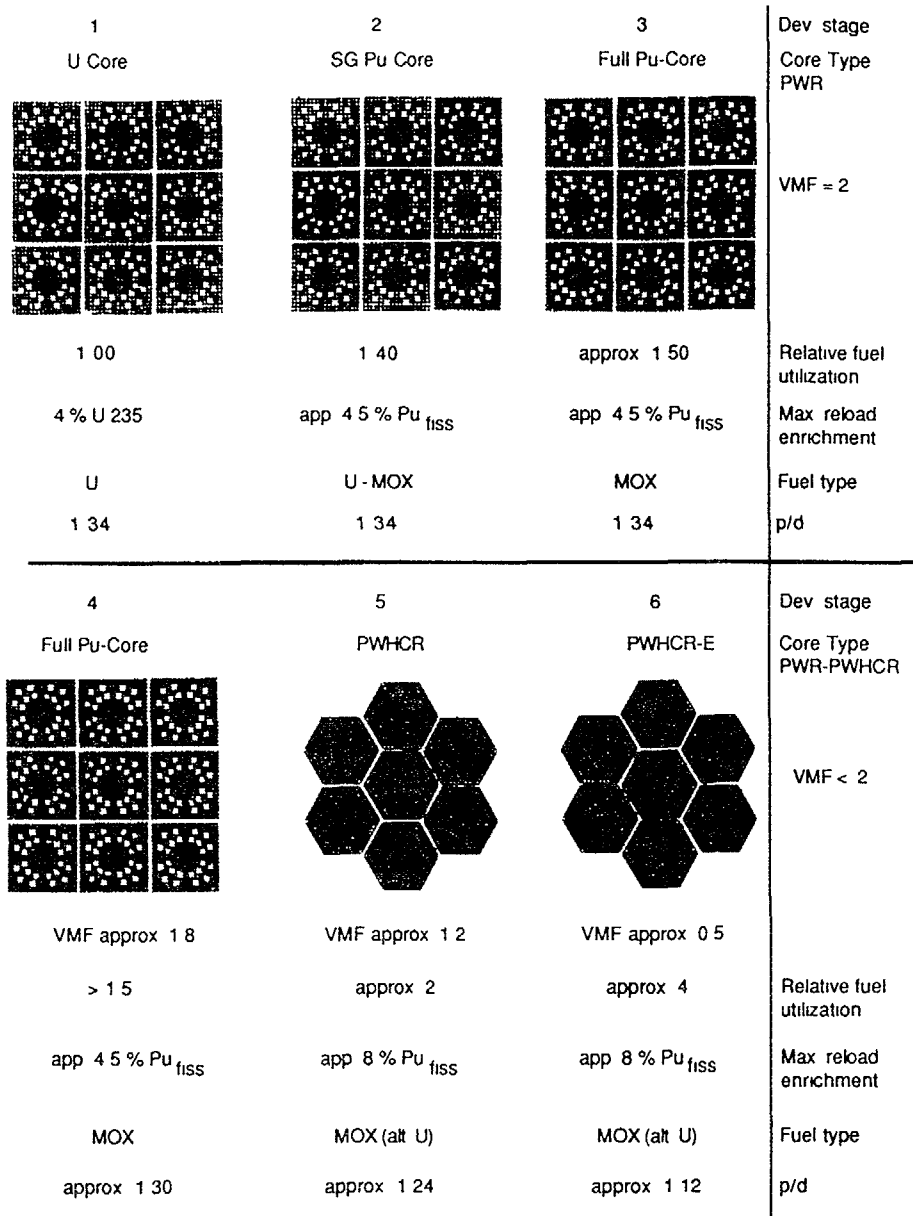


FIG. 3. Evolutionary development chain of PWR cores.

**Development stage 5**, based on a triangular fuel rod array within a hexagonal fuel assembly, represents a major step regarding fuel element shape and moderating ratio. With a moderator-to-fuel volume ratio of  $\sim 1.2$  the relative fuel utilization, defined as actually - to - theoretically achievable energy extraction from a unit mass of heavy metal, normalized to the once-through uranium fuel cycle mode in current PWR standard lattices, can be increased to approximately 2.0, as shown in Fig. 4. A corresponding preliminary design of the so-called PWHCR concept is described in the subsequent chapter.

The sixth and last link in the PWR evolutionary development chain is constituted by the HCR designed for a very tight lattice exhibiting a moderating ratio of  $\approx 0.50$  that can be flexibly brought about by increasing the fuel rod diameter while keeping the lattice pitch and the fuel assembly outer geometry constant. In principle, this version offers the achievement of a conversion ratio beyond 0.90 equivalent to a relative fuel utilization of between 2.5 and 5.0 for average batch burnups between 50 and 70 MWd/kg as illustrated in Fig. 4.

The limit for lattice tightening will be set by a positive integral void reactivity effect. Whether, or under which conditions concerning Pu enrichment and average discharge burnup, such a very tight lattice can be realized remains to be clarified in future development efforts.

Moderator-to-fuel volume ratios (VMF) down from currently 2.0 to 0.7 appear technically feasible and offer already an appreciable increase in fuel utilization in comparison to self generated Pu recycle. As a result, the PWHCR only slightly burns the Pu inventory. Rather, it acts as an "active plutonium stockpile" offering the unique feature to avoid unproductive out-pile Pu stockpiling on the one hand and to nevertheless save the fissile inventory for FBR installations once the breeder reactor is needed and commercially available.

It has to be noted that the evolutionary development strategy shown in Figures 3 and 4 is based to the highest possible extent on the existing and well proven PWR plant system and component technology with only minor design changes required in pressure vessel internals the core and fuel assemblies constituting the only components subject to major but even reversible changes.

Hence, the PWHCR appears to be an excellent, versatile and flexible link between the current PWR and the future FBR. Fig. 5 attempts to visualize such an evolutionary long-term NPP strategy capable of adapting nuclear power use to changing boundary conditions and to actual future needs.

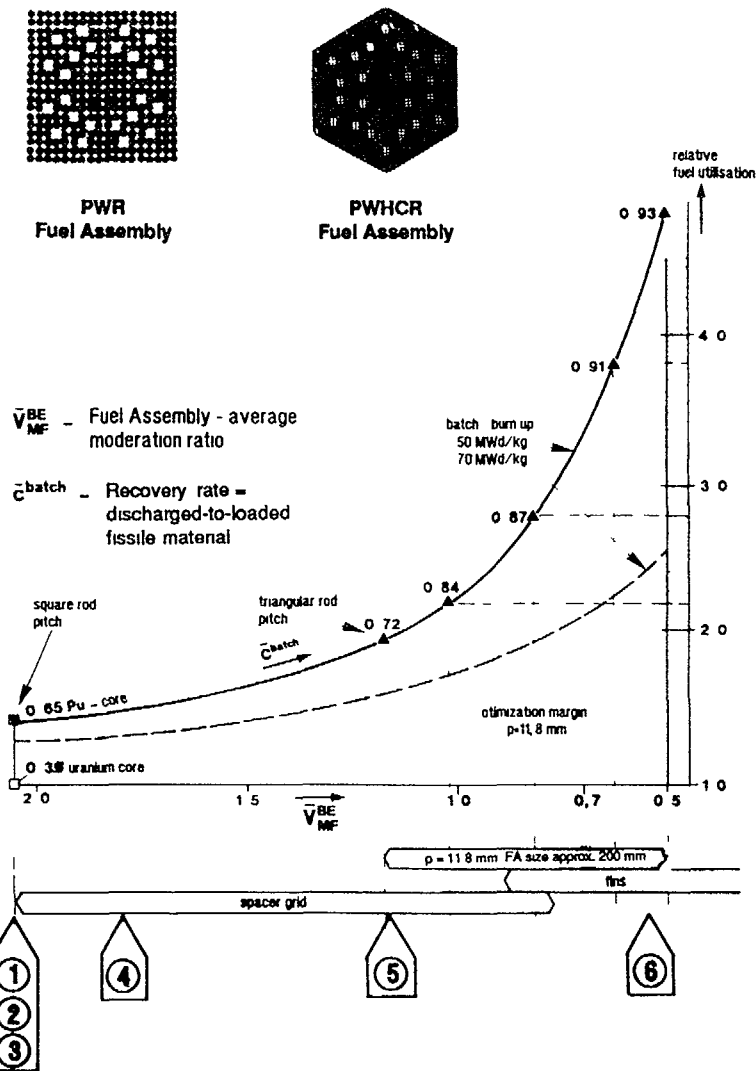


FIG. 4. PWHCR stagewise increase of fuel utilization

|                          |   |   |           |
|--------------------------|---|---|-----------|
| Goal:                    | Reduction of fossil fuel emission ( $\text{CO}_2$ ) by ecological reasons | Preservation of fossil fuel and natural uranium resources |           |
| $U_{\text{nat}}$ -Price: | < 30\$/lb   | < 60\$/lb   | > 60\$/lb |

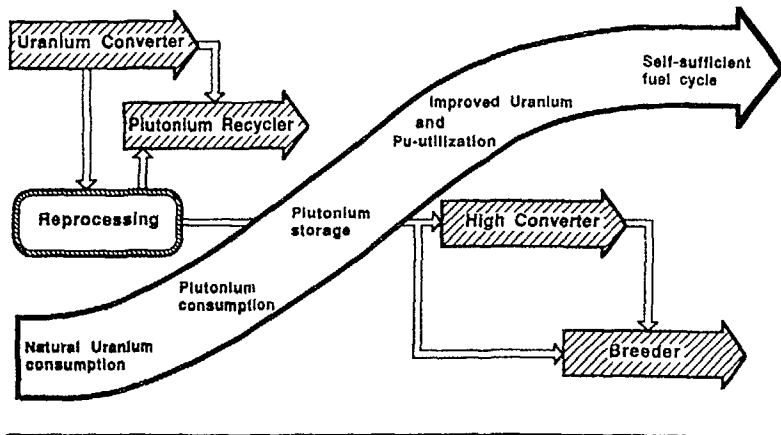


FIG. 5. Buildup of an evolutionary NPP strategy. Objective: versatile and reversible concept, adaptable to actual future needs.

### 3. The Siemens/KWU PWHCR Design

For more than a decade Siemens/KWU has been investigating various conceptual designs of a PWHCR. During the last four years the company internal activities have been enhanced by a cooperation with the Karlsruhe Nuclear Research Center (KfK), the Wuerenlingen Paul Scherrer Institute (PSI) and the Braunschweig Technical University (TUBS).

Initial theoretical and experimental activities were aimed at exploring design limits regarding

- physics phenomena, particularly void reactivity effect, conversion potential and control rod worth
- Thermal-hydraulics, i.e. core coolability under normal and accidental conditions like loss-of-coolant accidents and various transients
- mechanical fuel assembly and core design

The subsequent table lists some interim results achieved through the joint efforts of the cooperation partners in the different problem areas

| Key Problem Area       | Main Activity  | Institution               | Interim Results   | Further Activities  |
|------------------------|--|---------------------------|---|---|
| Physics                | measurements of reaction rates   | PSI                       | <ul style="list-style-type: none"> <li>- void coefficient negative for PWHCR lattice</li> <li>- essential reduction of calculation uncertainty</li> <li>- void coefficient positive for the infinite very tight lattice with <math>\text{VMF} = 0.5</math></li> </ul> | <ul style="list-style-type: none"> <li>- measurement of heterogeneous pattern (water holes)</li> <li>- measurements in wide lattices (<math>\text{VMF} &gt;&gt; 1</math>)</li> <li>- preparation of code interfaces</li> <li>- quality assurance</li> </ul> |
|                        | codes  | TUBS<br>KWU<br>PSI<br>KfK | - 1st set of codes under operation  |   |
|                        | core design  | KWU                       | <ul style="list-style-type: none"> <li>- preliminary design finished</li> <li>- enrichment and power density distribution, burnup, control rod and boron worth, Xe, reactivity coefficients</li> </ul>  |   |
| Thermal-hydraulics     | high pressure experiments  | KWU<br>TUBS<br>KfK        | <ul style="list-style-type: none"> <li>- coolability (DNB margin) guaranteed</li> <li>- essential questions clarified</li> </ul>  | <ul style="list-style-type: none"> <li>- detailed data analysis</li> <li>- core design</li> <li>- code adaptation</li> </ul>  |
| Emergency core cooling | reflooding   | PSI<br>KfK                | <ul style="list-style-type: none"> <li>- coolability for <math>\text{VMF} &gt; 1.5</math> verified</li> <li>- coolability for <math>\text{VMF} &lt;&lt; 1</math> to be carefully checked</li> </ul>   | <ul style="list-style-type: none"> <li>- detailed analysis of data</li> <li>- high pressure experiments for code validation</li> </ul>  |
| Mechanical design      | fuel assembly<br>core internals<br>control assemblies<br>shut down systems | KWU                       | - generic problems solved<br>- fuel, fuel rod, cladding, spacer, CA, CA drive, RPV internals, shut down systems   | - detailed design   |
| Material behaviour     | irradiation experiments  | KWU                       | - stainless steel under irradiation   | - continuation of the experiments only for tighter lattices important   |

Based on the results obtained within the development partnership a preliminary HCR design has been performed designated PWHCR

#### Main Features

- The core is of a "homogeneous type" with a uniform moderation ratio (VMF) within the hexagonally shaped fuel assembly
- VMF of the PWHCR development stage has been chosen to be 1.2  
By an adaptation of the fuel rod diameter while keeping the lattice pitch and the fuel assembly outer dimension constant VMF can be flexibly varied down to 0.5 corresponding to a very tight lattice for an advanced PWHCR  
Although the feasibility of very tight lattices with  $VMF \ll 1$  could not be proved yet, there are good indications suggesting the plausibility of lattices having a VMF appreciably below 1.2
- The average linear heat generation rate has been fixed to be 146 W/cm
- The mechanical design of the PWHCR has been performed in sufficient detail to enable a reliable check of its physics and thermal-hydraulic feasibility during normal and accidental, e.g. emergency core cooling or upset transient conditions

#### Fuel Assembly Design Parameters

|  |   |
|--|---|
| - Fuel rod lattice pitch                   | 11.8 mm                                 |
| - Cladding outside diameter                | 9.5 mm                                  |
| - Pitch-to-diameter ratio                  | 1.24                                    |
| - Cladding material                        | Zry                                     |
| - Cladding wall thickness                  | 0.6 mm                                  |
| - Volumetric moderation (VMF)              | 1.2                                     |
| - Fuel assembly (FA) distance across flats | 200 mm                                  |
| - Spacer type                              | grid                                    |
| - Number of fuel rods per assembly         | 247                                     |
| - Active core height                       | 3000 mm                                 |
| - Fuel                                     | UO <sub>2</sub> /PuO <sub>2</sub> (MOX) |
| - Maximum fissile Pu enrichment            | 7 - 8 w/o                               |
| - Maximum average discharge burnup         | 55- 60 MWd/kg                           |

#### Core Design Parameters

|  |          |
|--|----------|
| - Thermal output                                 | 3765 MW  |
| - Average linear heat generation rate            | 146 W/cm |
| - Average volumetric power density               | 105 kW/l |
| - Total number of fuel assemblies                | 349      |
| - Number of control assembly drives              | 85       |
| - Number of FAs that can hold a control assembly | 127      |

Fig. 6 shows a horizontal, Fig. 7 a vertical cross section through the reactor pressure vessel

#### 4. Summary

The generic results obtained within the German-Swiss cooperation can be summarized as follows

- |                                |  |
|--------------------------------|--|
| <b>Physics:</b>                | <ul style="list-style-type: none"> <li>- the integral void reactivity effect (zero void <math>\rightarrow</math> 100 % void) is sufficiently negative</li> <li>- the Pu recovery rate (<math>Pu_{fiss\ (out)}/Pu_{fiss\ (in)}</math>) is approx 0.75, as compared to a fissile recovery rate of <math>\approx 0.35</math> for a uranium fueled classical PWR</li> <li>- controllability is feasible</li> </ul> |
| <b>Thermal-hydraulics:</b>     | <ul style="list-style-type: none"> <li>- the PWHCR core configuration is coolable at nominal power with a satisfactory DNB margin</li> <li>- hexagonal FAs can guarantee comparatively higher critical heat fluxes (CHF)</li> </ul>  |
| <b>Emergency core cooling:</b> | <ul style="list-style-type: none"> <li>- the core configuration is coolable under emergency conditions</li> <li>- ballooning effect must be investigated carefully</li> </ul>  |
| <b>Mechanical design:</b>      | <ul style="list-style-type: none"> <li>- the essential mechanical design features have been elaborated</li> <li>- neither prohibitive nor serious problems were encountered</li> </ul>   |

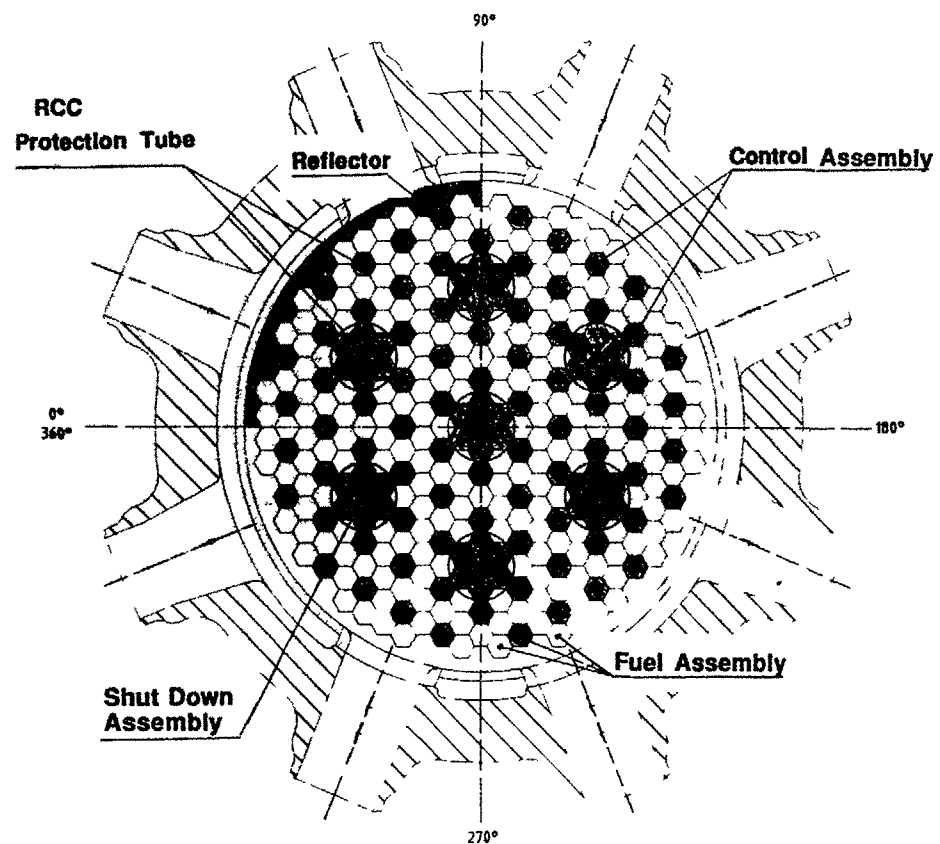


FIG 6 PWHCR core and pressure vessel

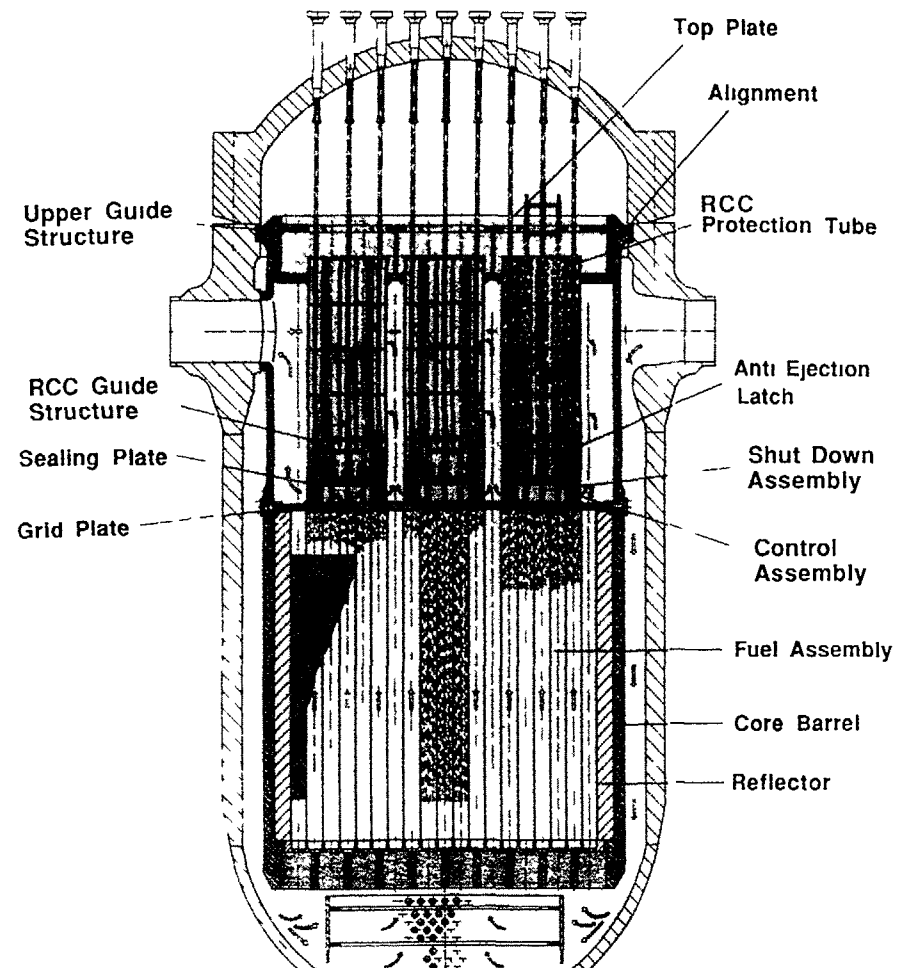


FIG 7 PWHCR upper guide structure

|                  |   |   |
|------------------|---|---|
| <b>Materials</b> | - due to the utilization of standard materials no serious problems are to be expected<br>material investigation for very tight lattices and high burnup values appear expedient | [3] Hofmann, H , Fischer, H D , Lochner, K-H , Mertens, U , Microprocessor based information and control system for non-safety and safety applications in nuclear power plants of the 1990s<br>Paper submitted to the ENC '90 conference to be held 24 - 28 September in Lyon, France |
| <b>Systems.</b>  | - standard systems and components can be employed<br>- no problems could be identified  | [4] Markl, H , Holzer, R , Advanced core and fuel design for light water reactors, Atomkernenergie-Kerntechnik Vol 50 (1987) No 4   |
| <b>Codes:</b>    | - standard codes and adapted codes are available<br>- quality assurance is necessary  | [5] Union of Concerned Scientists Appeal by American Scientists to Prevent Global Warming, Letter to President George W Bush, January 31, 1990  |

In conclusion it can be stated that the PWHCR is conceptionally feasible. No serious problems have been identified that would endanger technical and economic realization of the concept irrespective of the advisability to perform and complete more detailed investigations on various subjects

These encouraging results would suggest that the development of the HCR be continued. The major thrust of a pertinent program should be on the one hand a harmonisation of the different HCR-concepts currently under investigation in Europe and its adaptation to the requirements of the next generation of thermal LWRs on the other hand. This next development phase would also greatly benefit from a direct interaction of the utility industry since their requirements are of top priority

- [3] Hofmann, H , Fischer, H D , Lochner, K-H , Mertens, U , Microprocessor based information and control system for non-safety and safety applications in nuclear power plants of the 1990s  
Paper submitted to the ENC '90 conference to be held 24 - 28 September in Lyon, France
- [4] Markl, H , Holzer, R , Advanced core and fuel design for light water reactors, Atomkernenergie-Kerntechnik Vol 50 (1987) No 4
- [5] Union of Concerned Scientists Appeal by American Scientists to Prevent Global Warming, Letter to President George W Bush, January 31, 1990
- [6] Frewer, H , Future Challenge of Nuclear Power in the European Community, Nuclear Europe, Journal of ENS, No 1/2 1990, pp 63 - 75
- [7] Krebs, W -D , Schlosser, G J , Status of fuel assembly design and core management experience with MOX fuel in the FRG for Siemens/KWU type LWRs, IAEA Technical Committee Meeting on Recycling of Plutonium and Uranium in Water Reactor Fuels, Cadarache, France (1989)

#### REFERENCES

- [1] Markl, H , Safety Aspects of Advanced LWR Designs in the FRG International Workshop on the Safety of Nuclear Installations of the Next Generation and Beyond, August 28 - 31, 1989, Chicago, IL
- [2] Hofmann, H , Jung M , Konig N , BELT-D offers plant-wide integration of digital I & C Nuclear Engineering International, pp 49 - 51, Dec 1989

## THE CONVERTIBLE SPECTRAL SHIFT REACTOR

J P MILLOT

Framatome,  
Paris-La Défense, France

### Abstract

In 1981, after the preliminary design stage for the N4 project had been completed, Framatome initiated a research and development effort aimed at defining new core concepts. A first phase was devoted to analyzing the capabilities offered by undermoderated reactors burning plutonium and by spectral shift reactors using uranium. Subsequently the field was broadened in order to anticipate utilities' medium-term requirements. It was concluded that priority should be given to:

- cost savings,
- flexibility in utilization of fissile material,
- operating versatility.

At the beginning of the twenty-first century, two main trends will govern fissile material supply: increased availability of plutonium produced by light water reactors (though not in sufficient quantities to cover demand) and the fact that natural uranium will be available at reasonable prices for many years to come. This led us to define the convertible spectral shift reactor concept as early as 1984. Such a reactor uses both types of fissile material to optimum effect, but is still based on existing PWR fabrication and fuel facilities. At about the same time, following the first assessments, a basic research program to investigate the neutronics, thermal hydraulics and safety of tight lattice plutonium cores was launched by the CEA and EdF (DER), bringing in Framatome. The CEA was also involved in Framatome's work on the convertible spectral shift reactor, since it performed the various feasibility demonstration tests. The study was completed in 1988, with the conclusion that the convertible spectral shift reactor is a feasible proposition. This work will be presented in greater detail at the technical meeting.

Now, EdF has initiated a program to define the characteristics of a future plant series, the PWR 2000, with the convertible spectral shift reactor as a possible option for the steam supply system.

### INTRODUCTION

France currently generates over 70 % of its electricity by means of nuclear power plants, essentially of the pressurized water reactor (PWR) type. Due to increasing domestic electricity consumption and the electricity-export possibilities that are appearing, the most pessimistic assumptions lead to an estimation for the country's total installed nuclear electric generating capacity of 65 GW in the year 2000.

France's large number of operating PWR units and the spent-fuel reprocessing policy that it has adopted have led to already having a large stock of plutonium on hand. At present, some of this material is being recycled in the existing 900 MWe class PWR units.

- In 1987, one fuel reload containing plutonium was carried out at the Saint Laurent nuclear power plant (NPP)
- In 1988, two such reloads were implemented
- In 1989, new fuel assemblies containing mixed uranium and plutonium oxide (MOX) fuel were loaded into three other PWR units

This type of Pu recycling has been proven to be cost-competitive, using existing industrial facilities. However, such Pu recycling in PWRs, perfectible as it may be, has its limitations, because of the influence that it has on the reactivity balance in the reactor and the isotropic degradation of the plutonium during its irradiation.

In view of the surplus plutonium stocks that will be available in France by the beginning of the 21st century (on the order of 100 tonnes), and taking into account an increasing rate of consumption of the quantity produced annually by the spent-fuel reprocessing plants (approximately 6.5 tonnes), Framatome has developed the concept of an optimized plutonium-using light water reactor. This is the *convertible spectral shift reactor*, known in France as the RCVS (for "Reacteur Convertible à Variation de Spectre").

### DESIGN GOALS

The design goals originally set for the RCVS were as follows:

- 1) To be able to use Pu fuel to a burnup of at least 60 000 MWd/tonne,
- 2) To limit the consumption of fissile material,
- 3) To be able to recycle the Pu indefinitely, without any limitations imposed by its isotopic degradation during irradiation in the reactor core,

4) To be able to use either uranium or MOX fuel, and to be able to shift from one to the other at any reactor refueling, and

5) With either type of fuel, to reduce the fuel cycle cost with respect to a PWR, even taking into account the planned improvements to the latter

#### DESCRIPTION OF THE RCVS

To enable reducing the moderator ratio without reducing the fuel array pitch, the internal configuration of each fuel assembly is a hexagonal array

The moderator ratio adopted for the MOX fuel is the result of a tradeoff between the advantages of a lower ratio, to increase the conversion factor and reduce the isotopic degradation of the Pu, and the disadvantages of such a lower ratio as concerns the reactivity balance. For uranium fuel, the moderator ratio has been optimized by replacing certain fissile rods by water tubes. The different fuel assemblies are thus hydraulically compatible with the moderator ratio adopted, given in the following table.

Table 1 Possibilities of modulating the moderator ratio

| Fertile rod position | Moderator ratio |         |
|----------------------|-----------------|---------|
|                      | U core          | Pu core |
| Withdrawn            | 2.04            | 1.47    |
| Inserted             | 1.60            | 1.16    |

The present pitch of the RCVS fuel array, at this stage of development, is very near that of a PWR.

Certain measures are taken to optimize the consumption of fissile material and the initial enrichment in the RCVS

1) To reduce neutron losses, the reactor is equipped with a heavy stainless-steel reflector and

- Axial blankets, with a uranium core, or
- Radial and axial blankets, with a core containing Pu

2) To improve the production of Pu and optimize the initial enrichment, at the beginning of the fuel cycle, a mechanical spectrum-variation device is employed. Its effectiveness is enhanced by the possibility of inserting fertile gadolinium rods into the core

This concept led Framatome to analyze the feasibility of a fuel assembly with a hexagonal pitch (Figure 1) and the overall RCVS design (Figure 2)

#### MAIN RESULTS OBTAINED

Framatome began its RCVS feasibility study in 1986. Today, taking into account all the analyses performed during this phase, the preliminary results can be summarized as follows:

#### CORE PERFORMANCE

##### Enrichment

For the reference core configurations adopted for the feasibility study, the results obtained are given below:

- Uranium core, 60 000 MWD/tonne burnup, annual refueling, enrichment = 3.9 %
- Pu core, 60 000 MWD/tonne burnup, annual refueling, enrichment = 5.7 %

The radial blankets for the Pu core are cycled, like the core, by sixths and their stay time in the core is identical to that of the fissile elements.

On the basis of this study, it is of course possible to draw conclusions for other core configurations (influence of the burnup, the type of cycling, etc.)

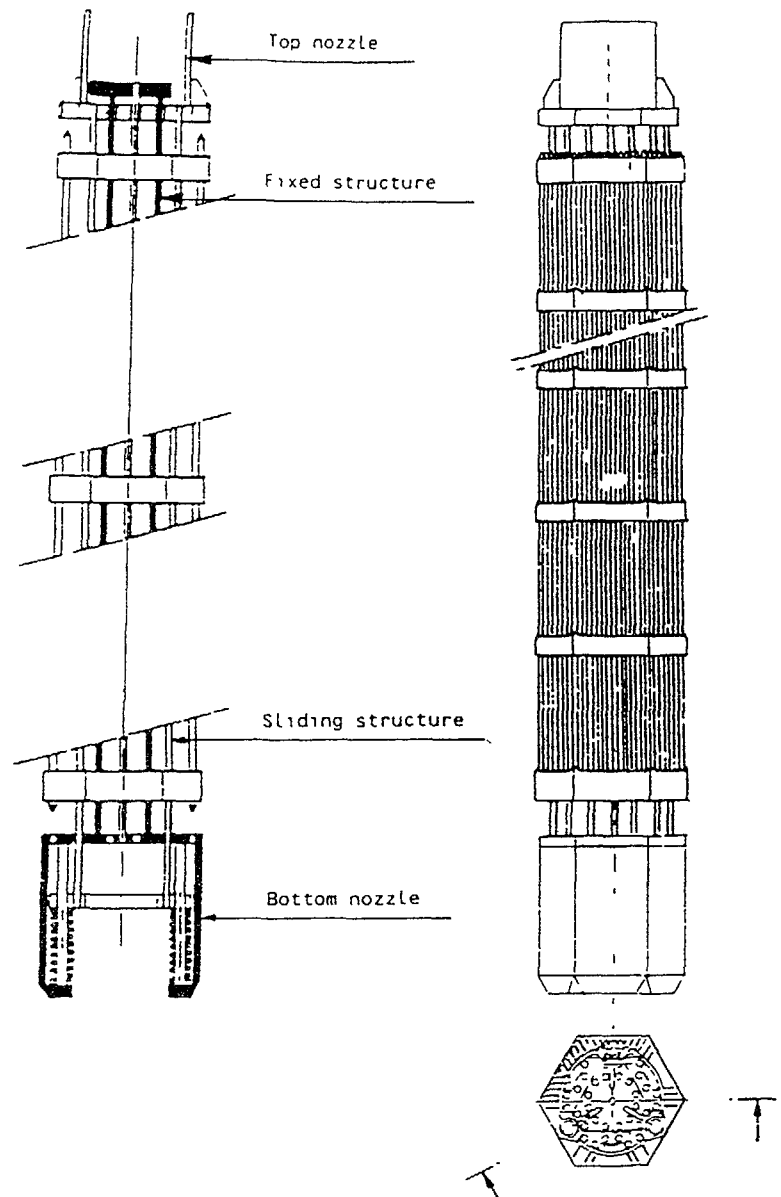


FIG. 1. Conceptual design of a hexagonal RCVS fuel assembly.

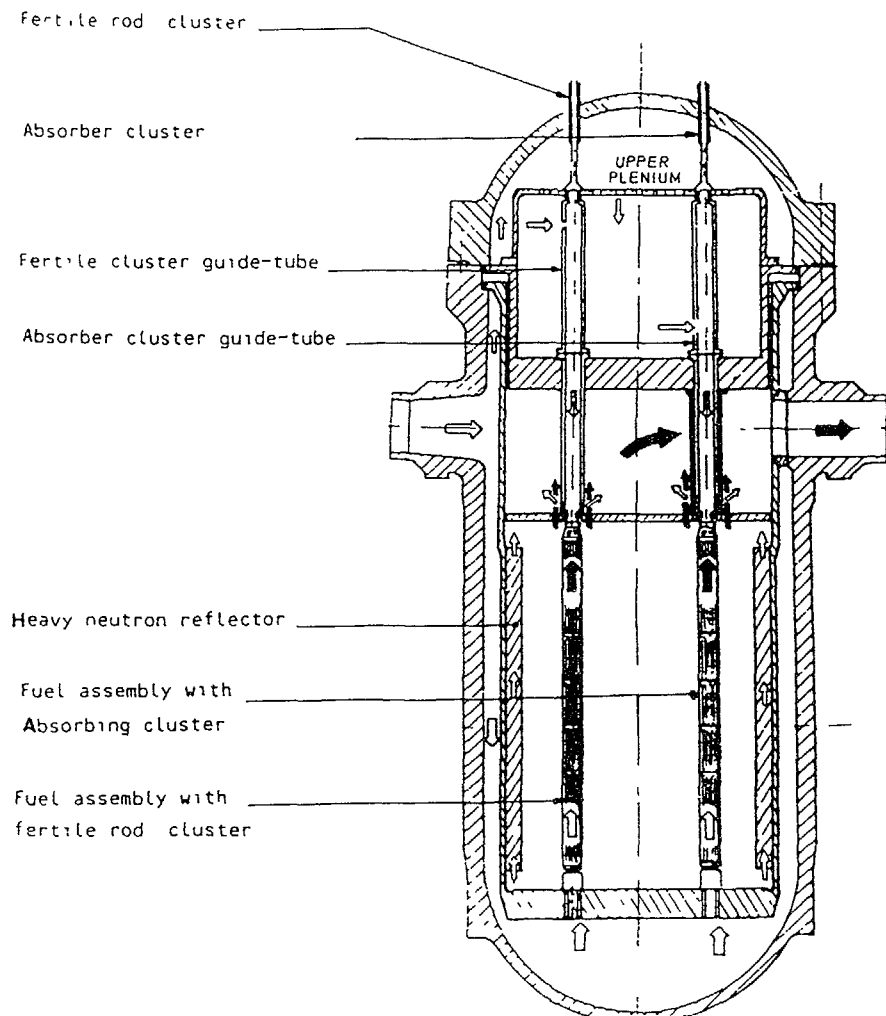


FIG. 2. Partial cross-section of the RCVS showing coolant flow paths.

*Mass Balance*

For the core and the annual cycling under consideration, the fissile material mass balances between the core loading and unloading are as follows:

*Plutonium core*

Table 2. First cycle balance for a fissile Pu reload.

|                 | Initial Pu    | End of 1st cycle |
|-----------------|---------------|------------------|
| Core            | 987 kg        | 719 kg           |
| Axial blankets  | --            | 26 kg            |
| Radial blankets | --            | 65 kg            |
| Fertile rods    | --            | 35 kg            |
| <b>TOTAL</b>    | <b>987 kg</b> | <b>846 kg</b>    |

Table 3. Equilibrium cycle balance for a fissile Pu reload.

|                 | Initial Pu    | End of cycle  |
|-----------------|---------------|---------------|
| Core            | 987 kg        | 747 kg        |
| Axial blankets  | --            | 26 kg         |
| Radial blankets | --            | 65 kg         |
| Fertile rods    | --            | 35.5 kg       |
| <b>TOTAL</b>    | <b>987 kg</b> | <b>874 kg</b> |

*Uranium core*

Table 4. Balance for a reload.

|                  | Initial<br>mass in kg | EIN (U5) | EFIN (U5) | EFIN (FPu) | Final FPu<br>mass in kg |
|------------------|-----------------------|----------|-----------|------------|-------------------------|
| Fissile material | 19 536                | 3.9 %    | 0.4 %     | 0.75 %     | 147                     |
| Axial blankets   | 964                   | 0.2 %    | --        | 0.75 %     | 7.3                     |
| Fertile rods     | 3075                  | 0.2 %    | --        | 0.64 %     | 20                      |

*Possibility of Multiple Recycling*

The possibility of multiple recycling was examined on the basis of the following hypotheses:

1) This would be self-recycling. This is a pessimistic hypothesis, because the mixture of Pu from the RCVS and the Pu from a PWR makes it possible to have Pu fuel of higher isotopic quality.

2) The fertile rods have a stay time in the core of three refueling cycles for a core having a burnup of 60 000 MWd/tonne.

3) The radial blankets remain in the core for six refueling cycles and are managed by sixths, like the fuel.

Using the plutonium from a PWR, for which the burnup is approximately 45 000 MWd/tonne, and taking into account the following isotopic content:

| Pu <sup>238</sup> | Pu <sup>239</sup> | Pu <sup>240</sup> | Pu <sup>241</sup> | Pu <sup>242</sup> |
|-------------------|-------------------|-------------------|-------------------|-------------------|
| 1.9 %             | 58.7 %            | 22.8 %            | 10.9 %            | 5.7 %             |

the isotopic content of the RCVS plutonium at fuel unloading is as follows:

Table 5. Isotopic content of RCVS Pu at discharge after six fuel cycles.

|                   | Core | Blankets | Fertile rods | Average |
|-------------------|------|----------|--------------|---------|
| Pu <sup>238</sup> | 3.2  | 0.2      | 0.2          | 2.8     |
| Pu <sup>239</sup> | 45.3 | 80.2     | 85.5         | 50.9    |
| Pu <sup>240</sup> | 26.2 | 11.9     | 9.0          | 23.7    |
| Pu <sup>241</sup> | 18.1 | 7.1      | 5.0          | 16.3    |
| Pu <sup>242</sup> | 7.2  | 0.6      | 0.3          | 6.2     |

The "average" composition of the plutonium assumes mixing of the plutonium from the core, the fertile rods, and blankets. It is calculated taking into account the mass balances given earlier.

Based on this data, the plutonium was recycled three times in the reactor, i.e. for a time period equivalent to the life of the latter. The final Pu content obtained is very near the equilibrium content for such a reactor. It is given in the following table.

Table 6. Final Pu isotopic content after three fuel cycles.

|                   | Initial PWR Pu | RCVS 1st cycle | RCVS equilibrium |
|-------------------|----------------|----------------|------------------|
| Pu <sup>238</sup> | 1.9 %          | 2.8 %          | 2.8 %            |
| Pu <sup>239</sup> | 58.7 %         | 50.9 %         | 49.0 %           |
| Pu <sup>240</sup> | 22.8 %         | 23.7 %         | 24.0 %           |
| Pu <sup>241</sup> | 10.9 %         | 16.3 %         | 18.0 %           |
| Pu <sup>242</sup> | 5.7 %          | 6.2 %          | 6.2 %            |

Based on these compositions, and taking into account the degradation of the Pu quality during the time it is not in the reactor ( $\text{Pu}^{241} \rightarrow \text{Am}^{241}$ ), the possibility of using this plutonium has been verified.

The composition of the plutonium when removed from the uranium RCVS core is given in the next table.

Table 7. Isotopic content of the Pu at the end of the cycle.

|                   | Core plus blankets | Fertile rods | Average |
|-------------------|--------------------|--------------|---------|
| Pu <sup>238</sup> | 4.6 %              | 0.3 %        | 4.1 %   |
| Pu <sup>239</sup> | 45.5 %             | 72.1 %       | 48.6 %  |
| Pu <sup>240</sup> | 24.7 %             | 16.8 %       | 24.8 %  |
| Pu <sup>241</sup> | 15.0 %             | 9.3 %        | 14.4 %  |
| Pu <sup>242</sup> | 10.2 %             | 1.5 %        | 9.2 %   |

The plutonium from the uranium core has an isotopic composition very close to that of the equilibrium plutonium from the Pu core. Its use therefore does not pose any specific problems.

#### Reactivity Balance

The reactor control strategy employed (control without using soluble boron) is covered in another presentation. The criteria defining the reactivity requirements are as follows:

- At hot shutdown, a reactivity margin of 1000 pcm, assuming that one shutdown RCC is stuck in the withdrawn position.

- 2) At intermediate shutdown ( $180^{\circ}\text{C}$ ), a reactivity margin of 1000 pcm, assuming that one shutdown RCC is stuck or that the mechanism is equipped with double detection of low control rod cluster positions
  
- 3) At refueling shutdown or in case of severe accident, a reactivity margin of 5000 pcm, with all the shutdown RCCs inserted

The margin with respect to the steam line break accident does not need to be taken into account, because of the type of control assumed (no boron during power operation, the shutdown control rod bank having sufficient worth to be able to compensate for the reactivity until shift over to the residual heat removal system)

With respect to these criteria and taking into account the proposed reactor control strategy, the situation with regard to the reactivity is as follows

#### *Plutonium core*

The worth of the natural soluble boron is very low. Depending on the situation, it is only

- under hot conditions 1 51 pcm/ppm with the fertile rods inserted, and 1 83 pcm/ppm with the fertile rods withdrawn,
- under cold conditions 2 57 pcm/ppm with the fertile rods inserted, and 3 12 pcm/ppm with the fertile rods withdrawn

The compensation control rod bank must be capable of accomplishing, starting from hot shutdown, all of the power evolutions. Therefore, when it is fully inserted into the core, the reactor is subcritical regardless of the position of the shutdown control rod bank. Its total worth is determined by the following requirements

- Residual reactivity due to burnup 1000 pcm
  - Xenon effect 1000 pcm
  - Power operation 2000 pcm
  - Control margin 500 pcm
- |       |           |
|-------|-----------|
| Total | 4500 pcm, |
|-------|-----------|

or about 90 pcm per control rod cluster

The worth of the shutdown rod bank is evaluated at 9100 pcm, with a precision of 1000 pcm. It is thus sufficient with respect to the first criterion. At the reactor scram signal, the two banks fall into the core, providing safety redundancy

The reactivity requirement to go to intermediate shutdown (necessary to shift to the residual heat removal system) starting from hot shutdown is 6100 pcm. Taking the above criteria into account, the worth of the shutdown RCCs therefore must be at least 7100 pcm, to which must be added an uncertainty factor of 1400 pcm, by statistically combining the errors. The worth of the shutdown rod bank is thus sufficient to ensure this function

The reactivity requirement to go from hot shutdown to cold shutdown for refueling is 7800 pcm, to which must be added 5000 pcm. This implies a negative reactivity from boron (taking uncertainties into account) of 5100 pcm, which is possible with an injection of borated water, using natural boron in a solution of 2000 ppm

#### *Uranium core*

The worth of the soluble boron is practically the same as for a PWR. The reactivity requirements with respect to the compensation control rod bank are as follows

|                                     |                |
|-------------------------------------|----------------|
| • Residual reactivity due to burnup | 1000 pcm       |
| • Xenon effect                      | 2000 pcm       |
| • Power operation                   | 2000 pcm       |
| • Control margin                    | <u>500 pcm</u> |
| Total                               | 5500 pcm,      |

The average worth of a compensation control rod cluster is thus about 80 pcm

The worth of the shutdown rod banks being 11 600 pcm, it is sufficient to respect the hot-shutdown criterion. The two banks fall into the core simultaneously, and the residual heat removal system is redundant

Taking the necessary margin into account, the necessary reactivity worth to go to the intermediate shutdown state is 7200 pcm, to which must be added 2000 pcm to take account of the uncertainties in evaluating the reactivity and in the worth of the control rod clusters. The worth of the shutdown control rod banks is thus sufficient with respect to this criterion. In case of system failure, the boron injection system ensures redundancy.

The worth of the boron also means that the refueling shutdown criterion is met.

#### SAFETY

With respect to a PWR, certain special features of the RCVS have to be taken into account during safety analyses:

- The compactness of the fuel assembly array, which modifies the conditions of coolant flow through the core, and in particular the capacities of the safety injection systems necessary to ensure correct core cooling in case of a loss of coolant accident (LOCA),
- The presence of fertile fuel rod clusters, which also must be cooled, under the same accident conditions, whether the clusters are inserted into the core or not,
- The plutonium fuel, with greater reactivity and less sensitivity to the action of the soluble boron, which favors reactivity excursions in case of core voiding and control rod ejection, and
- The absence of soluble boron under hot conditions, which makes it necessary to guarantee until intermediate shutdown the negative reactivity necessary to keep the reactor subcritical, using only the control rod clusters. This modifies the sequence of a possible steam-line break accident scenario.

Consequently, among all of the accident transients generally analyzed, only three were considered for the RCVS safety analysis, because they could, *a priori*, cause effects specific to this design. These were:

- 1) LOCAs involving large and medium-sized breaks,
- 2) Steam-line breaks, and
- 3) Control rod ejection

In addition, an analysis of the evolution of the reactivity as a function of the void fraction enabled verifying under which conditions one of the fundamental bases of traditional PWR safety analysis is not compromised in the RCVS, in other words that core voiding always leads to a loss of reactivity.

#### *Large-Break LOCA*

##### *Problems specific to the RCVS design*

Because of the compactness of its core, the RCVS behaves differently than a PWR, both during the decompression phase and during the core reflooding phase. The analysis of its behavior must take into account certain specific effects:

- Cold dome effects, which are highly beneficial during the decompression,
- The increased volume of the dome, and
- Slower decompression of the dead under-dome volume (increase in the pressure drops at the dome-control rod cluster junction)

In addition, certain other specific aspects of the RCVS design require special analyses:

- 1) The fertile rods of the spectrum-variation clusters. When inserted, they remain confined in guide tubes. For this reason, due to possible plugging of these tubes by swelling, the energy released is assumed to be evacuated only by radiation, since cooling by convection can not be guaranteed.
- 2) The heavy stainless-steel neutron reflector, which presents a greater hot structural mass than does a conventional baffle.

## Development and qualification of methods

The computational "codes" (programs) and methods for the decompression phase, qualified for the PWR, remain applicable to the RCVS configuration, provided that certain modifications are made, related to the geometry of the array

Preliminary core reflooding tests carried out at the CEA on the Echo B loop have confirmed the computations made with the PWR design codes (see Figure 3). Computations have also shown that the reflector does not have an appreciable impact on the accident sequence

## Results of the analyses

### a) Fissile core cooling

The evolution of the maximum temperatures of the fissile rod and fertile rod cladding is presented in Figure 4

The penalizing aspects of the core geometry, mainly sensitive during the core-reflooding phase, are entirely countered by the beneficial effects especially related to the decompression. Thus, the maximum temperature of the fissile rod cladding evolves with a delay of about 100 seconds with respect to that of a PWR, but attains a peak of the same order of magnitude, thus respecting the criteria of Appendix K.

The maximum plugging factor is 77 % for the transient envisaged. If PWR core experience is extrapolated to this subject, such a plugging factor has no impact on the core cooling. This tentative conclusion will nevertheless need to be confirmed by plugging tests on the Pericles test loop at the CEA's Grenoble Nuclear Research Center.

### b) Cooling of the spectrum-varying fertile rods

When a fertile rod is inserted into the RCVS core, the energy it releases is evacuated by radiation to its guide tube and the rod rapidly reaches thermal equilibrium with its environment. It then follows the temperature evolution of the surrounding fissile rods, with a temperature difference that can attain several tens of degrees centigrade.

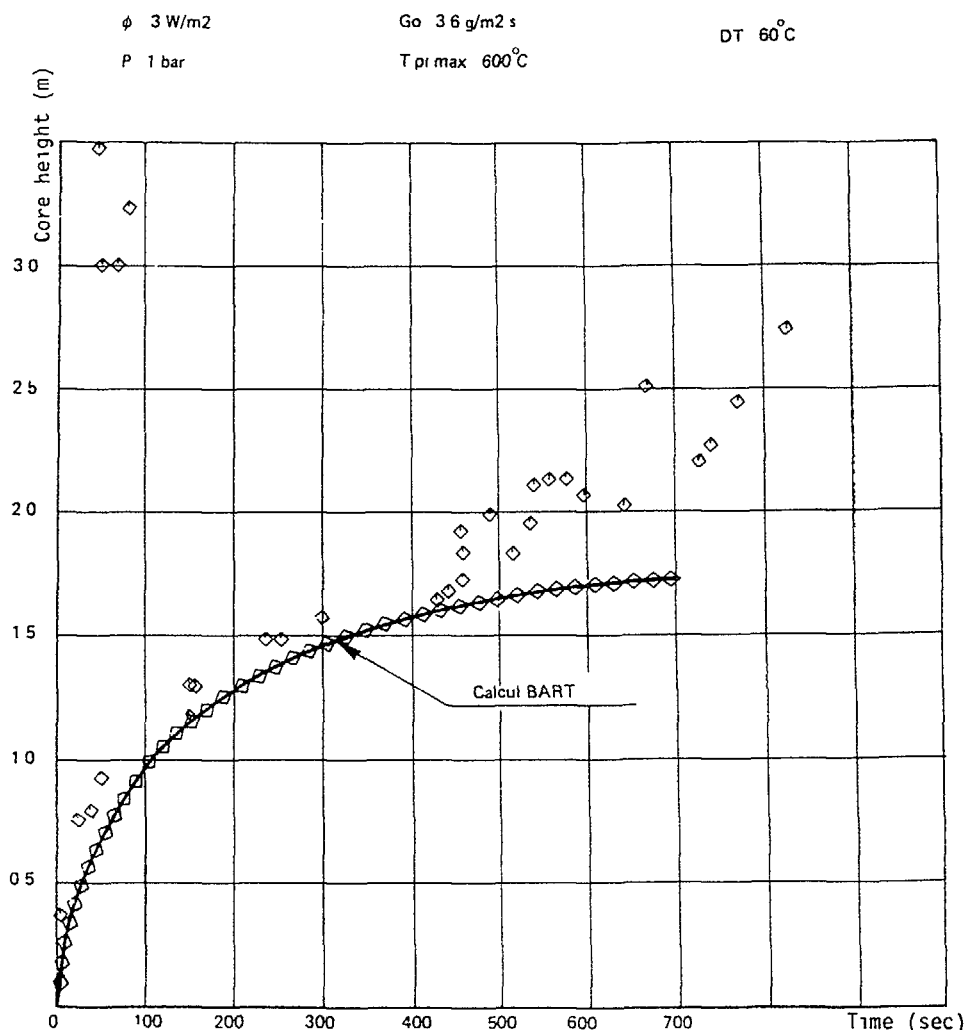


FIG. 3 Result of RCVS core reflooding tests on CEA's Echo B loop

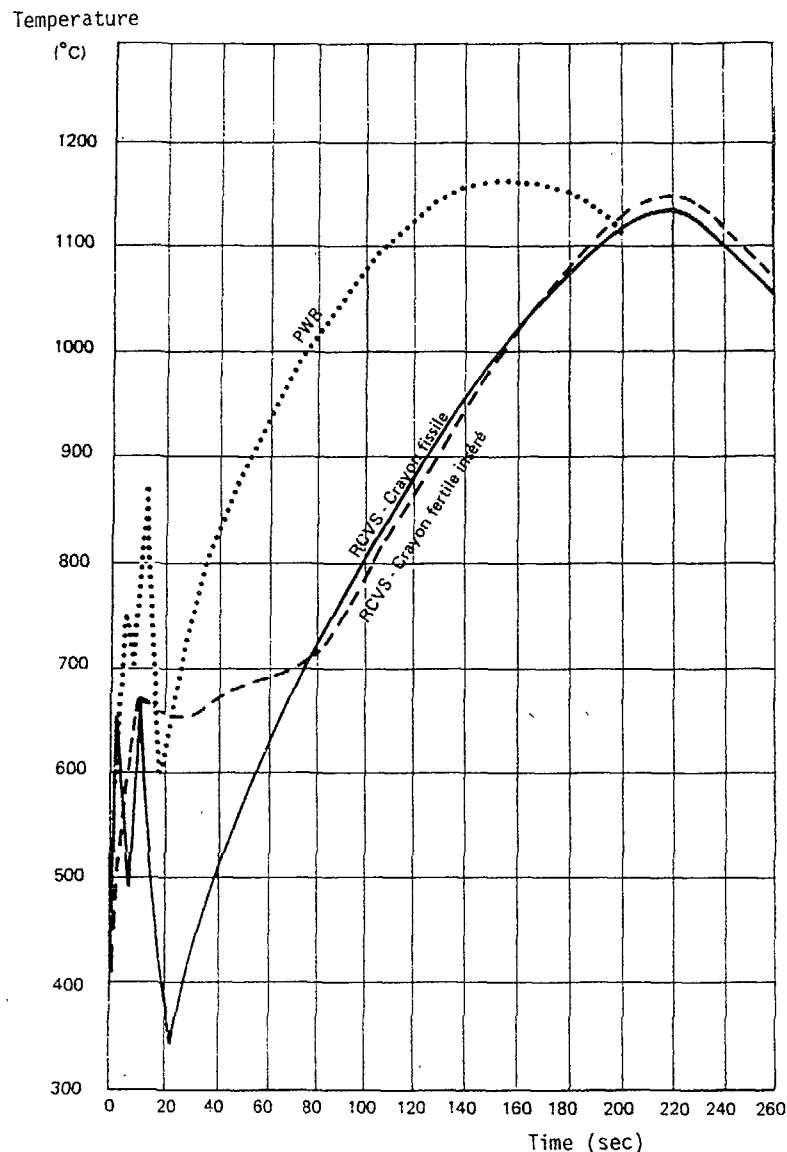


FIG. 4. Evolution of the maximum temperatures of the RCVS fissile and fertile rod cladding in case of LOCA.

In the withdrawn position and in case of a LOCA, once the rod is withdrawn its cooling poses a particular problem. Part of the rod is no longer immersed in the reactor coolant, in view of its position at the end of the transient. The behavior of the fertile rods thus was the subject of a special analysis, taking into account the different possibilities for evacuating the energy it releases.

The least-cooled part of the rod is the part situated in the reactor vessel dome, the rest of the rod being either in the upper plenum and in the RCC guide tube, which is cooled by the steam current leaving the core, or in the baseplate of the inverted-hat upper reactor internals, which have high thermal inertia and which are also being cooled by the steam flow.

The behavior of the fertile rods was analyzed taking into account the evacuation of their energy only through the reactor vessel and the baseplate of the inverted-hat upper internals. A computation was made for the most pessimistic case, that of the six clusters in the ring of fuel assemblies at the center of the core, including the residual power of the other fertile rods assumed to have all been withdrawn from the core. The evolution of the cladding temperature found shows that the maximum temperature reached is 450°C, and that the temperature drops below 400°C after five hours. The thickness of the resulting zirconium layer is on the order of several micrometers (Figure 5).

#### Steam-Line Break Accident

The RCVS behavior in case of a steam line break differs considerably from that of a conventional PWR. This is because the RCVS has a large reserve of negative reactivity immediately available, thanks to its larger number of neutron-absorbing control rod clusters. This enables ensuring core subcriticality down to intermediate shutdown (180°C) without using soluble boron.

For this reason, the steam-line break accident is not a design-basis accident for the RCVS.

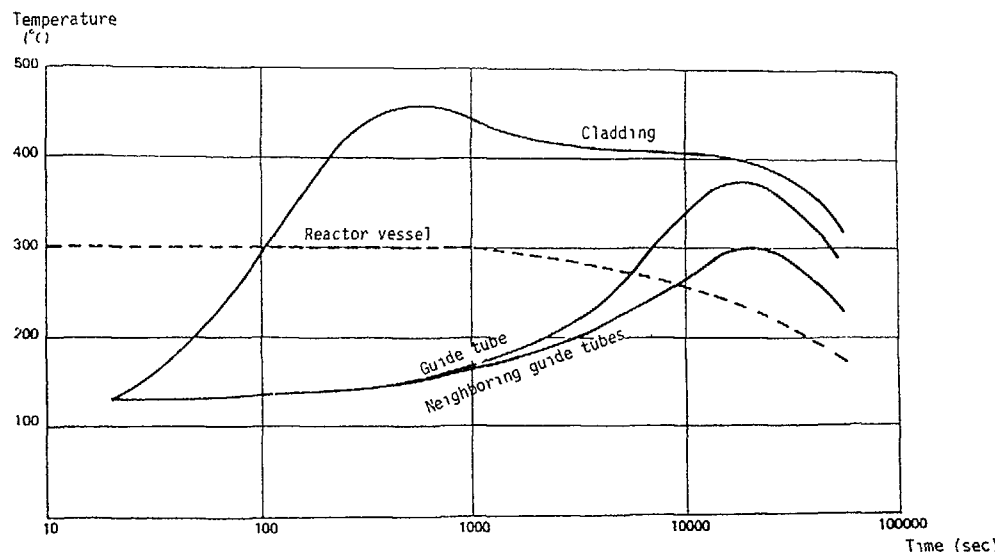


FIG. 5. Evolution of the cladding temperature of withdrawn fertile rods in a RCVS in case of LOCA.

#### Rod Ejection Accident

The design condition for the RCVS with a uranium or plutonium core was determined by the same method as the one used for PWRs. This method consists of determining by statistical computation the ejected reactivity and the hot channel factor in the post-ejection configuration. This computation is made using a hexagonal code, for a complete core. It is assumed that the hot channel factor and the axial power distribution remain constant throughout the transient, which is a conservative assumption. The neutron kinetics are then computed using a special-purpose model, to determine the evolution of power with time, and from these two results the evolution of the fuel temperature at the hot spot is deduced.

The most penalizing case is that of the uranium core. The accumulated energy and thus the maximum temperature depend mainly on the Doppler feedback coefficient, for a given reactivity, and the value of this coefficient is  $-2.6 \text{ pcm}^{\circ}\text{C}$  for the U core versus  $-3.6 \text{ pcm}^{\circ}\text{C}$  for the Pu core. This effect is due

to hardening of the neutron energy spectrum. The effects of the decreased neutron life and of the fraction of delayed neutrons are more than compensated for by the increase in the Doppler coefficient. As the ejected reactivity at reduced power is the same as at high power, it is the latter case that is the most penalizing. The results obtained are given in Figure 6.

The maximum temperature attained in the most penalizing case is  $2575^{\circ}\text{C}$ , so there is no fuel meltdown. The maximum stored energy is  $529 \text{ J/g}$ , which is less than the allowable maximum energy of  $836 \text{ J/g}$ .

The rod-ejection accident criteria are therefore amply respected, despite the adoption of highly pessimistic hypotheses for the analysis. The situation of the RCVS appears to be a little more severe than it is for the 1300 MWe class "P4" design for such an accident, but the difference is barely significant in view of the present uncertainties in evaluating the accident parameters.

#### Core Voiding Risk (Pu Core)

In case the quantity of coolant water in the core is reduced for very low densities, the neutron spectrum becomes a fast spectrum. Under these conditions, the even-numbered Pu isotopes become particularly fissile, which can lead to increased reactivity.

An analysis of the reactivity variation was carried out, taking the enrichment in fissile plutonium as the main variable. Whereas for low void fractions the reactivity is monotonously decreasing, for high void fractions it goes through a minimum and then increases. When the entire core is concerned, this increase is nevertheless partially compensated for by increased neutron leakage, related to the length of slowing. These phenomena lead to taking into account two types of limits:

- 1) In case of a LOCA, once it has been voided the core must be subcritical, which imposes a maximum core enrichment of about 7.5%.
- 2) In case of a local accident (plugging, control rod ejection), the reactivity at all points of the voided core must be at most equal to the value of

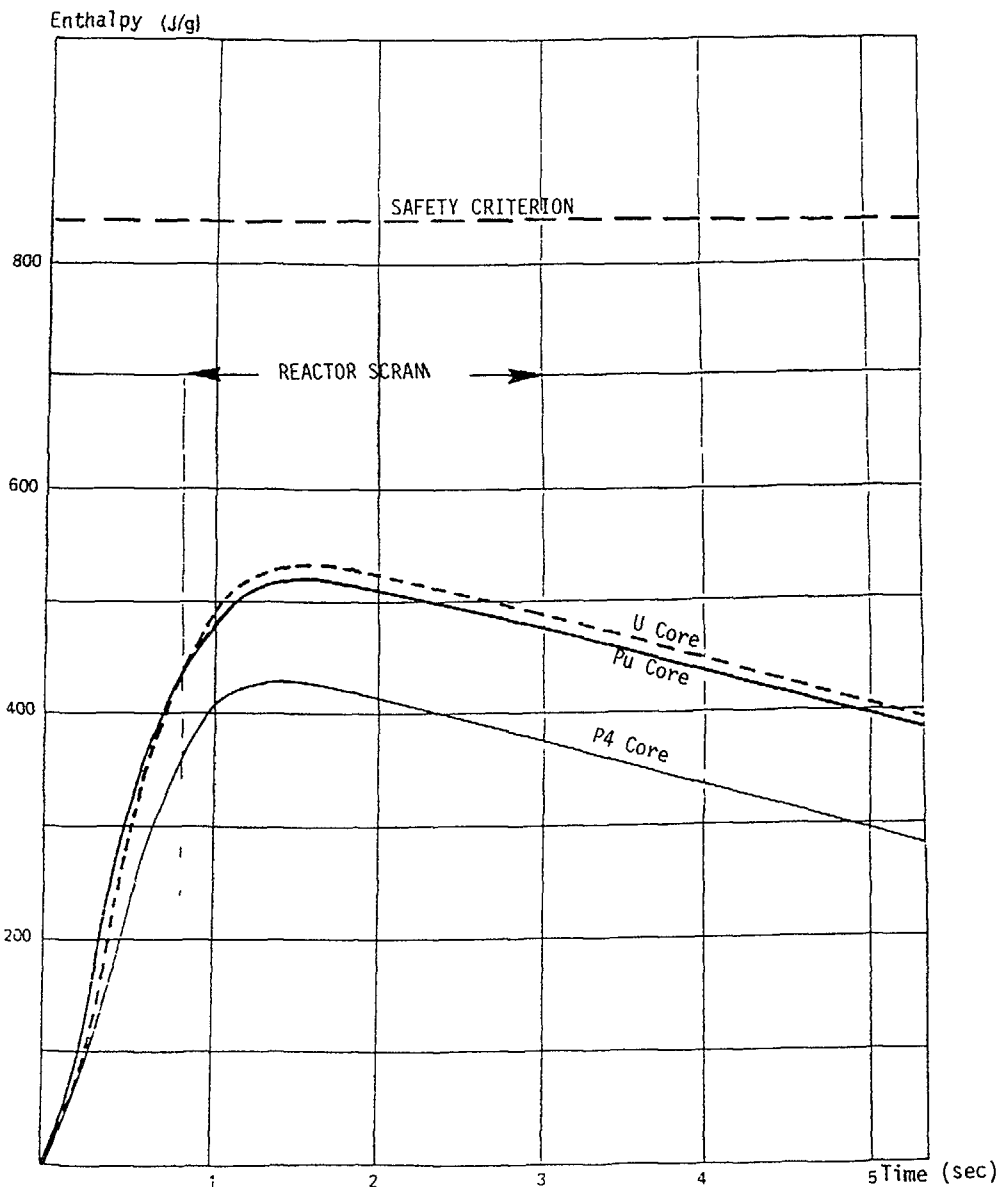


FIG. 6 Fuel enthalpy variation during a control rod injection transient

the reactivity at the same point under normal conditions. This necessitates a more constraining enrichment limit than the one above (about 6.8 %).

The analysis and results summarized above are supported by the following tests, carried out by the CEA in cooperation with EDF and Framatome, which are discussed in another presentation:

- The Erasme criticality experiment,
- DNB tests, and
- Core reflooding tests

#### COMPARING THE RCVS AND CURRENT PWR MODELS

If one now wants to compare the RCVS to other types of PWRs from the standpoint of the plutonium user, this comparison must take into account several different criteria:

- Economic factors,
- Strategy of fissile material use,
- Safety, and
- Control effectiveness.

#### ECONOMIC FACTORS

For an all-plutonium core, the cycle cost is a decreasing function of the discharge burnup (see Figure 7). There is no optimum, as there is in the case of an uranium core.

Figure 8 shows the dependence of the cycle cost on the moderator ratio. As can be seen, this is a decreasing function for a first recycling, increasing for the second recycling, but in any event the dependence is small.

If the cost of plutonium is reduced, so is the difference between the various possible solutions.

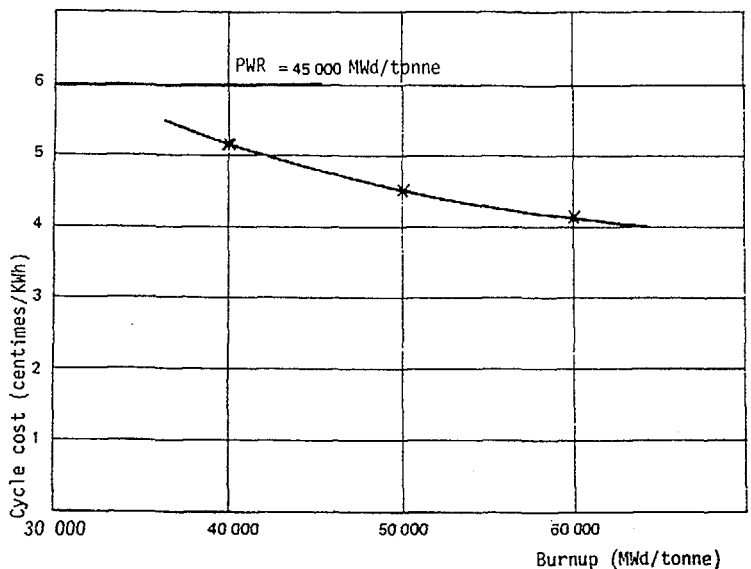


FIG. 7. Cycle cost as a function of discharge burnup.

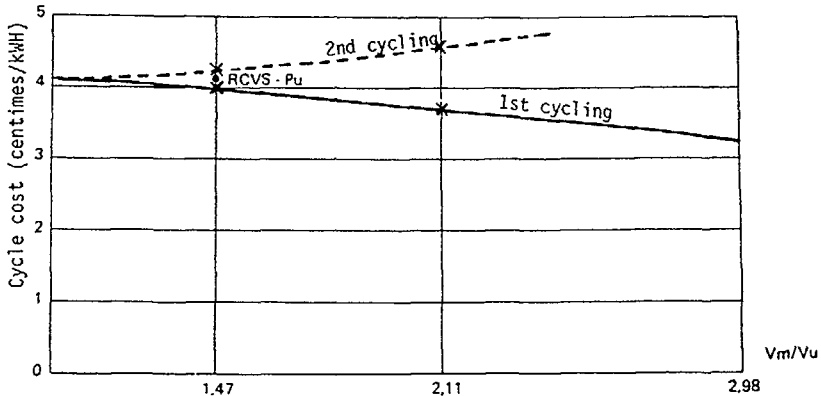


FIG. 8. Influence of the moderator ratio on the cycle cost.

In conclusion, economic analysis at the plane of a single reactor shows the advantages of increasing the burnup, but it does not give any major motivation for the choice of the type of core to use.

#### STRATEGY OF FISSILE MATERIAL USE

The use of plutonium in a pressurized water reactor necessitates a quantitative analysis (mass or plutonium enrichment) and a qualitative analysis (isotopic composition of the Pu) over time, the qualitative aspect being particularly important in case of multiple recycling.

At present, the plutonium is produced by PWRs using enriched uranium as their fuel. The quality of this plutonium does not greatly depend on the burnup, as shown by the following table.

Table 8. Isotopic composition of the Pu produced by a PWR, as a function of the discharge burnup of the fuel.

| Burnup           | Pu <sup>239</sup> | Pu <sup>240</sup> | Pu <sup>241</sup> | Pu <sup>242</sup> |
|------------------|-------------------|-------------------|-------------------|-------------------|
| 33 000 MWD/tonne | 58.3              | 22.8              | 13.8              | 5.1               |
| 45 000 MWD/tonne | 55.8              | 23.0              | 14.8              | 6.4               |
| 60 000 MWD/tonne | 52.4              | 23.6              | 15.7              | 8.3               |

The behavior of this type of plutonium, in a light water fuel assembly array, is mainly influenced by the moderator ratio. Starting from the plutonium recovered from PWR fuel with a discharge burnup of 45 000 MWD/tonne (see below), the qualitative evolution of the plutonium, as a function of the moderator ratio and for a burnup of 60 000 MWD/tonne, is given by the following table, for two cycles.

Table 9 Evolution of Pu fuel in an RCVS as a function of the moderator ratio

| Vm/Vu                    | Cycle no | % Pu <sup>239</sup> | % Pu <sup>240</sup> | % Pu <sup>241</sup> | % Pu <sup>242</sup> |
|--------------------------|----------|---------------------|---------------------|---------------------|---------------------|
| 1.16                     | 1        | 51.5                | 26.4                | 15.4                | 6.7                 |
|                          | 2*       | 47.4                | 28.7                | 16.0                | 7.9                 |
| 1.47                     | 1        | 46.3                | 27.7                | 17.7                | 8.3                 |
|                          | 2*       | 40.4                | 30.0                | 18.2                | 11.4                |
| Standard<br>PWR<br>Array | 1        | 37.1                | 31.3                | 19.2                | 12.4                |
|                          | 2**      | 29.8                | 33.0                | 18.8                | 18.4                |
| 2.98                     | 1***     | 30.4                | 40.0                | 11.7                | 17.9                |

Notes \* Equilibrium Pu attained, \*\* Equilibrium Pu not attained,  
 \*\*\* No recycling possible

Figure 9 gives the initial total Pu and fissile Pu enrichments for the first two cycles, as a function of the moderator ratio. This figure and Table 9 show that, for a given burnup (60 000 MWD/tonne in this case), a high moderator ratio leads to a low initial enrichment requirement, but causes appreciable degradation of the plutonium. Inversely, the lower the moderator ratio, the better the isotopic quality of the plutonium is conserved.

The final destination of the plutonium being to serve as fast breeder reactor (FBR) fuel, we have analyzed the mass of Pu consumed, expressed in FBR-equivalent Pu<sup>239</sup>, for different types of use:

- An all-Pu PWR, for different moderator ratios,
- An RCVS, with or without radial blankets, and
- Storage

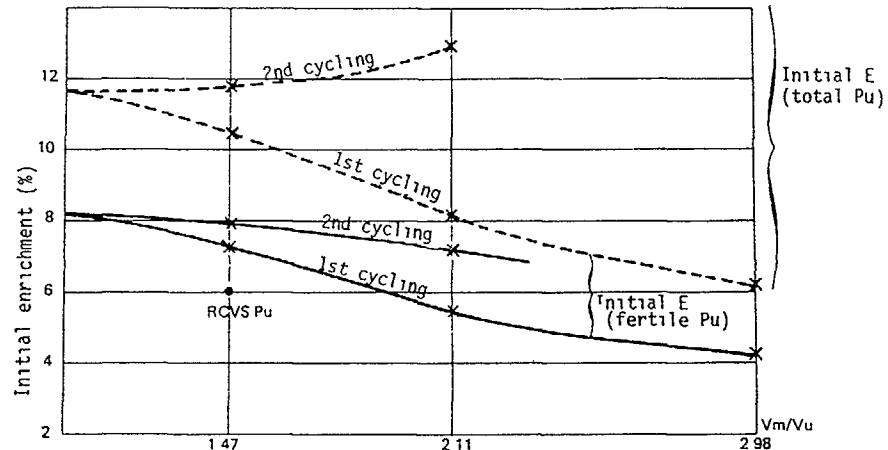


FIG 9 Initial enrichment as a function of the moderator ratio

For the purposes of this comparison, the RCVS can, schematically, be considered to be a fuel assembly array with a moderator ratio of 1.47, subject to spectrum variation, and profiting or not from the addition of radial blankets.

In the case of storage, the evolution results from the transformation of Pu<sup>241</sup> into Am<sup>241</sup>.

The main variable is the duration of use, between the initial production of the plutonium and its loading into an FBR, multiple recycling (per array type) being taken into account.

Figure 10 presents the main results of this analysis. One can see the advantages of a low moderator ratio. In addition, it can be noted that the spectrum variation, on one hand, and the radial blankets, on the other, enable compensating for the penalizing effects due to a looser array.

The energy produced as a function of the loss of Pu during this lapse of time was also taken into account. The results obtained are expressed in terms of the energy produced (in TWh) per tonne of the plutonium consumed.

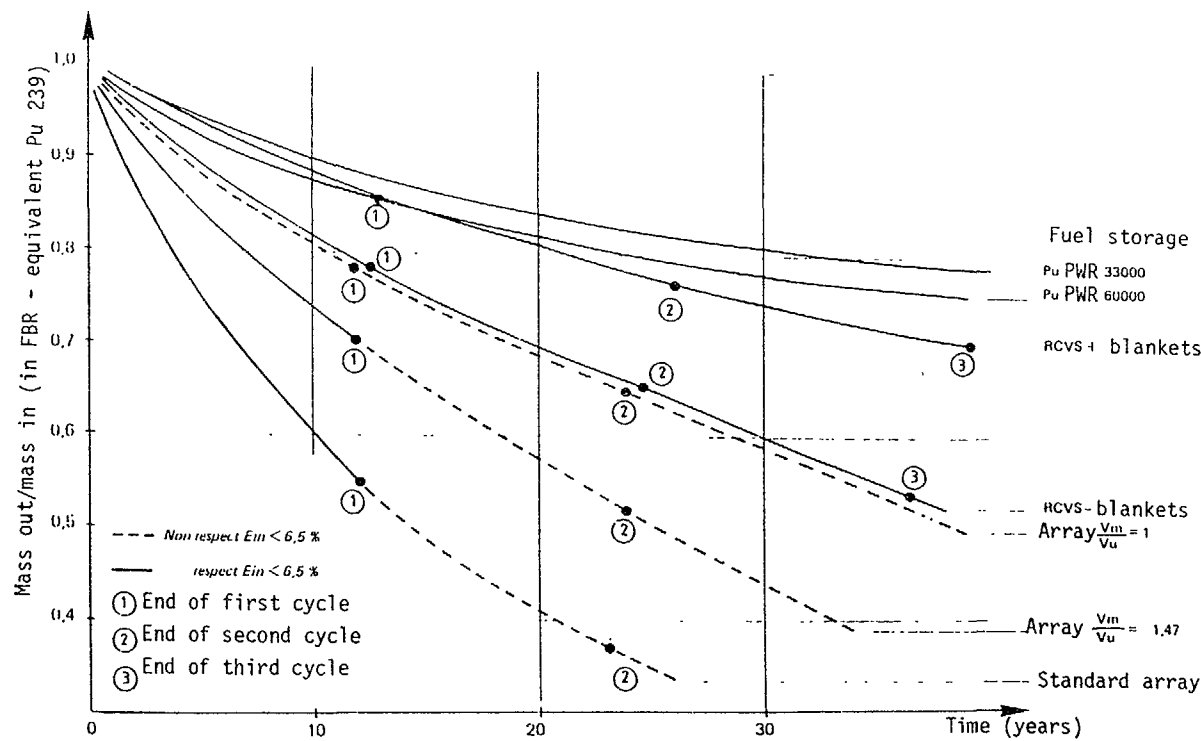


FIG. 10. Pu evolution in all Pu PWR (discharge burnup 60 000 MWd/t).

- RCVS: 59 TWh
- RCVS without blankets: 34 TWh
- PWR with  $V_m/V_u = 1$ : 27 TWh
- PWR with  $V_m/V_u = 1.47$ : 20 TWh, and
- PWR with standard array: 17 TWh.

All of these analyses show the advantages of using a low moderator ratio, in the absence of any other determining criteria, and axial blankets.

#### CONTROL EFFECTIVENESS CRITERIA

The use of soluble boron enriched in  $B^{10}$  and control rod clusters for reactor control was analyzed under the assumption that the criteria that define the necessary negative reactivity margins are the same as those for a current PWR. The boron enrichment and the number of control rod drive mechanisms necessary are given in the next table.

Table 10 Reactivity control of a Pu-fueled PWR

| $V_{M}/V_{U}$                            | 0.6        | 1.13      | RCVS with<br>fert rods<br>inserted* | 1.47      | Standard  |
|--|------------|-----------|-------------------------------------|-----------|-----------|
| Worth of natural soluble boron (pcm/ppm) |            |           |                                     |           |           |
| • hot                                    | -0.73      | -1.35     | -1.51                               | -1.83     | -2.40     |
| • cold                                   | 1.25       | -2.29     | -2.57                               | -3.12     | -4.10     |
| Enrichment of soluble boron (1)          | ??         | 90 %      | 76 %                                | 63 %      | 48 %      |
| No. of fuel assemblies                   | 199        | 199       | 199                                 | 199       | 205       |
| No. of CRDMs (2)                         | 131<br>(3) | 85<br>(3) | 73<br>(3)                           | 79<br>(3) | 89<br>(4) |

## Notes

- \* Without elimination of soluble boron but with compensation RCCAs
- 1 The soluble boron compensates for the burnup and provides the same reactivity margin at cold shutdown (concentration 200' ppm)
- 2 With reactor control by compensation RCCAs
- 3 With 36  $B^{10}$ C-enriched rods for the shutdown RCCAs
- 4 With 24  $B^{10}$ C-enriched rods for the shutdown RCCAs

These results must be weighted, because they result from estimations made on the basis of RCVS analyses. Therefore, they can only be considered as orders of magnitude. Nevertheless, the following tendencies can be noted:

- Without eliminating the use of soluble boron, all of these reactors necessitate the use of enriched boron. Under these conditions, this use will result in extra costs, which will be all the higher as the treatment systems become more sophisticated to reduce the boron losses.
- All of these all-plutonium reactors with tighter arrays than those of standard PWRs imply the use of such a large number of control rod drive mechanisms that the conventional latch-arm type can no longer be used, because of its size. Therefore more-compact mechanisms will be necessary.

- With moderator ratios of less than 1.1, reactivity control using conventional means is delicate.

## SUMMARY OF THE RCVS/PWR COMPARISON

From the economic viewpoint, reactors using plutonium fuel appear to be advantageous. This advantage increases if one can at the same time push the burnup and increase the number of reactors of this type and, subsequently, increase the conversion factor. The problems posed by reactivity control using conventional means make it necessary to keep the moderator ratio at 1 or above. In the range of moderator ratios considered possible, the array must be chosen as a function of an optimized tradeoff between the burnup and the conversion factor.

It is possible to further improve this tradeoff if one can, by other means than the moderator ratio, reduce the initial enrichment and increase the conversion factor. This is why we have been led to analyze the advantages of using as tight an array as possible, along with spectral variation RCCs and blankets (the quantification of these advantages are given in the Mass Balance paragraph on p. 31).

The analyses carried out show that with a burnup of 60 000 Mwd/tonne the reactor obtained could respect the fissile-plutonium enrichment limits related to the current state of research. The spectrum variation, which enables varying the moderator ratio between 1.16 and 1.47, presents in fact the advantage of enabling the use of an enrichment lower than that of an array having a  $V_{M}/V_{U}$  of 1.47, while at the same time leading to a conversion factor on the same order as that of an array having a  $V_{M}/V_{U}$  of about 1.

For this, the spectrum-variation RCCs must necessarily contain fertile rods. The use of water-displacement RCCs would reduce the initial enrichment gain by a factor of 2.5 (see the following table) and would increase the plutonium consumption by a factor of 2.

Table 11. Gain on initial enrichment as a function of the nature of the spectral-variation RCCAs.

| Burnup |           |           |
|--------|-----------|-----------|
| :      | 45 000    | 60 000    |
| :      | MWd/tonne | MWd/tonne |
| :      |           |           |
| :      | 0.12 %    | 0.20 %    |
| :      |           |           |
| :      | 0.30 %    | 0.50 %    |
| :      |           |           |

With recycled plutonium, the gain is even greater.

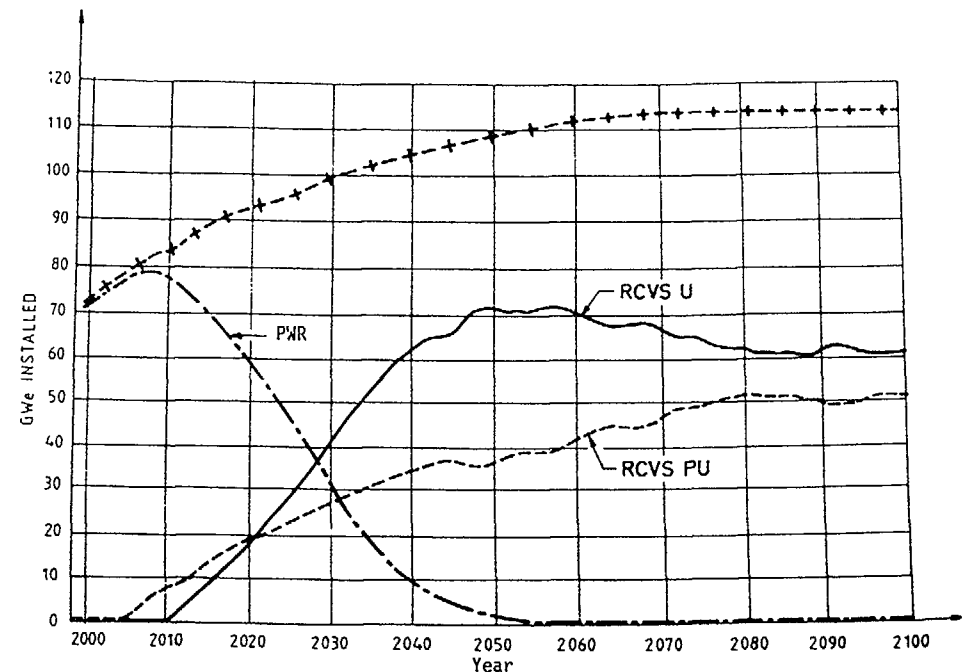


FIG. 11. Penetration possibilities of the RCVS into the French nuclear power unit population.

## CONCLUSION

The feasibility of the RCVS convertible spectral shift reactor concept seems to have been essentially demonstrated, and the initial goals appear to have practically been attained. In the next phase, more detailed analyses will be performed, to confirm certain key points of this feasibility and obtain more precise information about the probable reactor performances, by reducing the present uncertainties. This additional concept-proving work will be part of EDF's REP 2000 program.

To illustrate the advantages of integrating the RCVS into an existing reactor population, an analysis was made of the possibility of its penetration into the French population, starting in 2005, taking into account Pu availability and the present plans for replacing the existing PWR units (see Figure 11). This analysis showed that the extent of penetration of RCVS units using plutonium fuel could be up to 45 %, and that the use of the convertible spectral shift technology would enable cutting the consumption of natural uranium by some 50 %.

## ANALYSIS OF VVER CHARACTERISTICS WITH TIGHT LATTICE AND MOX FUEL

V. PSHENIN, I. LEVINA, A. SUSLOV,  
A. GAGARINSKII, A. LAZARENKO,  
D. MACHOV, L. KOBZAR, V SEMENOV,  
N ALEKSEEV

I.V. Kurchatov Institute of Atomic Energy,  
Moscow,  
Union of Soviet Socialist Republics

### Abstract

The use of tight pitch lattice and MOX fuel is one of the ways to improve fuel utilization in VVERs. The presented report is devoted to an analysis of main neutron-physical and thermohydraulic problems connected with such core design. In order to achieve the needed accuracy of tight pitch lattices burnup calculations it is necessary to provide a high accuracy of reaction rates calculations in the resonance energy range and therefore the cross sections of the used Pu, Am, Cm isotopes and fission products should be reliable. For such calculations the UNIRASOS-2 and SAPFIR codes are used at the Kurchatov Institute. The "second" equivalence theorem with specially selected parameters and generalized subgroup approach are used for resonance treatment in these codes. MCU code package calculations have been used for their validation. This code package is based on the Monte-Carlo method with a detailed description of cross section energy dependence in the energy range of resolved resonances. A comparison of MCU, UNIRASOS and SAPFIR calculations with the results of precision calculations, results of benchmark problems on tight lattices burnup solutions and measured data obtained at the PROTEUS critical assembly, has shown that the obtained accuracy of these codes is satisfactory for practical purposes. However, in order to estimate the reliability of void reactivity coefficient calculations under low moderator density, it is necessary to perform special investigations. For two dimensional pin power distribution calculations, the 4-group code PERMAK, in which both diffusion and nodal type balance equations are realized, has been used.

### 1. INTRODUCTION

Fuel reprocessing and plutonium recycling is one of the ways to improve fuel utilization in VVERs. It has been shown in Ref.1 that direct substitution - the simplest route of plutonium introducing into VVER-1000 fuel cycle provides reducing of specific natural uranium spending per Mwt el year by 2 times. Further increasing of uranium utilization efficiency can be achieved under using of tight pitch lattices and MOX fuel. This paper presents results of preliminary analysis of main neutron-physical and thermohydraulic characteristics of VVER (VVER-M) with such lattices

A short description of codes used for calculations and some results of their verification obtained using comparision calculated data with benchmark problems solutions and measured data are also presented in this paper.

### 2 METHODS AND CODES FOR CALCULATIONS OF LATTICE NEUTRON-PHYSICAL CHARACTERISTICS

Neutron physics of VVER with tight pitch lattices and MOX fuel differs significantly from physics of today VVERs. It is known that in order to achieve needed accuracy of tight lattices burnup calculations it is necessary to provide high precision of reaction rate calculations in the resonance energy range and reliability of used cross sections libraries for Pu, Am, Cm isotopes and fission products. Short description of codes which have been used for core characteristics analysis are given below. These codes are part of code package for VVERs core neutron physical calculations. More detailed description of this code package is given in Ref.2.

MCU code package [3] is used for neutron transport calculations by Monte-Carlo method. In the energy range of  $10.5 \text{ Mev} \leq E \leq 10 \text{ Kev}$  collision calculations are usually performed using 11-group model and well known ABBN [4] cross sections library. More detailed group structure (18 or 52 groups) and special library can be used in the energy range of  $10.5 \text{ Mev} \leq E \leq 100 \text{ Kev}$ . In the energy range of unresolved resonances subgroup method [5] is usually applied. In the energy range of resolved resonances using of subgroup method or detailed descriptions of cross sections energy dependence on a base of LIPAR [3] - estimated resonance parameters library data is possible. In practice the second approach is usually applied. In thermal energy range ( $E \leq 1.0 \text{ eV}$ ) 40-group representation of cross sections is used. Continuous changing of neutron energy is also taken into account in this energy interval. Scattering cross sections are calculated in consideration of chemical binding and thermal motion of nucleus on a base of KORT [3] library data.

Code package SAPFIR [6] is assigned for semiprecision fuel lattice burnup calculations. In the energy range  $10.0 \text{ Kev} \leq E \leq 10.5 \text{ Mev}$  in this code package 11-group approach and corresponding data from ABBN-TR (an extended version of ABBN) library are used. In the resonance energy range a generalized subgroup method [6] is applied. Subgroup parameters from ABBN for unresolved resonances and generalized subgroup parameters obtained on the basis of LIPAR data for resolved resonances are used in SAPFIR. In this code package there are also special modules for detailed calculations (some thousands energy points) of resonance absorption by resolved resonances. Thermal spectrum calculations are carried out using 40-groups approach. Spatial distributions of group and subgroup fluxes are calculated using first collision probabilities method.

Codes UNIRASOS-2 and RAFORIN are assigned for design fuel cell and supercell burnup calculations. These codes are modules of code TVS which is used for fuel assembly burnup calculations.

Energy region  $4.65 \text{ Kev} \leq E \leq 10.5 \text{ Mev}$  is subdivided in this codes in two groups. Micro cross-sections of the most important nuclides are represented in this codes as a function of some parameters determining detailed neutron spectrum in mentioned above energy range. Corresponding approximation formulas have been obtained using SAPFIR modules and ABBN data. It has been shown that this approach provides satisfactory accuracy of calculations. The resonance energy range ( $4.65 \text{ Kev} \leq E \leq 0.625 \text{ eV}$ ) is subdivided in this codes into 12 groups. Calculations of U235, U236, U238, Pu239 - Pu242 shielded cross-sections are performed in this codes using second equivalence theorem with specially selected parameters. An effect of heavy nuclides resonances overlapping are taken into account using correction suggested in Ref.7. Neutron spectrum in resonance energy range

is calculated using continuous slowing down theory methods [8]. Thermal neutron spectrum calculation is carried out using differential thermalization model (in UNIRASOS-2) and 24-groups model (in RAFOPI) on a basis of KORT data. For spatial fluxes distributions in this codes first collision probabilities method and method of surface pseudosources [9] are applied. Under burnup calculations changing of 19 heavy nuclides (from Th232 to Cm244) and 95 fission products concentrations are taken into account.

Control rods efficiency and rod by rod power distributions calculations were performed using four-groups code PERMAK [10]. In this code both standard diffusion approach and nodal type balance equation [11-12] are realized. For estimation of three-dimensional power distribution nodal simulator BIPR-8 was employed.

For a verification of mentioned above design spectral codes results of a comparison of calculated data with data obtained using MCU and SAPFIR code packages, measured data, data on spent fuel isotopic content were used. Some results of such comparisons are given in tables 1-3 and fig. 1-4. In table 1 results of calculations for NB-lattices suggested as a calculational benchmark in Ref.13 are given. Results of solution of benchmark problems on tight pitch lattices burnup are presented in fig 1-4. Tables 2 and 3 demonstrate results of comparison measured and calculated data for BAPL [15] and PROTEUS [16] critical assemblies.

The results of design codes verification allowed to make a conclusion that accuracy of lattice characteristics is satisfactory for practical purposes. But calculation of void reactivity coefficient under low moderator density is still a problem to be solved. Making Pu239, Am, Cm isotopes and fission products cross sections more accurate, taking into account effects of some fission products cross sections selfshielding and overlapping of their resonances with resonances of heavy isotopes are also needed.

### 3. CORE DESIGN AND RESULTS OF MAIN NEUTRON-PHYSICS CHARACTERISTICS ANALYSIS

Going over to using closely packed plutonium enriched lattices put some problems connected with significant increasing of friction pressure drop and choosing of spacers type. Necessity of increasing enrichment up to 8-8.5% can moreover lead to positive value of void reactivity coefficient. This circumstances determined choosing lesser than in today VVERs core length and greater than in APWR [18] moderator/fuel volume ratio. Harder than in today VVERs neutron spectrum provides a possibility of using steel as fuel clad material without appreciable falling of neutron balance.

Two different design of fuel assembly have been examined - with grids and helical fins as a spacer. Isotopic contents of Pu in fresh fuel is similar to that in VVER-1000 with three years fuel cycle after a burnup of 40 Mwd/t and fuel reprocessing duration of 1-3 years. Am241 has been neglected. Table 4 shows VVER-M core parameters in comparison with APWR parameters presented in Ref.18. Main core neutron physical characteristics obtained using UNIRASOS-2 code are given in Tabl.5. This table contains the following values:  $K_{inf}$  at BOC and EOC, final burnups depending on Pu239 and Pu241 concentrations at the BOC and average conversion ratio (CR). Final burnups have been obtained for a case of three reloading per cycle using known approximate formula.

$$M = 2 M / (1 + 1/3) \quad (1)$$

where  $M$  is determined from the following correlation

$$\frac{1}{K_{inf}(M)} = \frac{n}{K_{inf}} \quad (2)$$

TABLE 1 RESULTS OF CALCULATIONS FOR NB LATTICES

| Lattice | Parameter              | Code name, deviation from results given in Ref. 13 (%) |               |         |      |            |
|---------|------------------------|--|---------------|---------|------|------------|
|         |                        | M.C.<br>[12]   | EPRI-<br>CELL | CASMO-3 | MCU  | UNIRASOS-2 |
| NB-1    | $K_{\infty}$<br>$\rho$ | 1.147  | -0.2          | -0.2    | 0.1  | -0.3       |
|         | $\delta^{25}$          | 1.363  | -0.2          | -1.5    | 0.3  | 2.5        |
|         | $\delta^{28}$          | 0.0803   | 1.4           | 2.2     | 0.6  | 0.7        |
|         | $\delta^{28}$          | 0.0722   | -2.4          | 1.9     | -2.7 | -0.1       |
|         | MCR                    | 0.798  | -0.3          | -1.6    | 0.4  | 0.0        |
| NB-2    | $K_{\infty}$<br>$\rho$ | 1.175  | -0.4          | -       | 0.2  | 0.7        |
|         | $\delta^{25}$          | 2.612  | 0.0           | -       | -1.4 | 0.2        |
|         | $\delta^{28}$          | 0.151  | 0.7           | -       | -0.7 | -0.7       |
|         | $\delta^{28}$          | 0.297  | 0.0           | -       | -7.6 | -2.1       |
|         | MCR                    | 2.148  | 0.0           | -       | -1.3 | -1.3       |
| NB-4    | $K_{\infty}$<br>$\rho$ | 1.342  | -0.1          | -0.2    | 0.1  | 0.5        |
|         | $\delta^{25}$          | 2.654  | -0.8          | 0.8     | -0.4 | -2.1       |
|         | $\delta^{28}$          | 0.159  | -1.3          | -0.1    | -1.7 | -6.0       |
|         | $\delta^{28}$          | 0.062  | -0.8          | 3.0     | -0.8 | -3.1       |
|         | MCR                    | 0.549  | -0.2          | -1.3    | -0.1 | -2.2       |
| NB-5    | $K_{\infty}$<br>$\rho$ | 1.146  | -0.3          | -       | 0.3  | -0.9       |
|         | $\delta^{25}$          | 8.503  | 0.4           | -       | -0.1 | 1.0        |
|         | $\delta^{28}$          | 0.548  | 0.4           | -       | -0.3 | -2.8       |
|         | $\delta^{28}$          | 0.133  | -0.8          | -       | -2.5 | -5.5       |
|         | MCR                    | 1.006  | 0.0           | -       | -0.2 | -0.3       |

TABLE 2. COMPARISON OF CALCULATED AND MEASURED DATA FOR BAPL LATTICES

| Lattice | Param         | value        | Measured Deviation from measurement (%) |            |         |         |       |            |
|---------|---------------|--------------|---|------------|---------|---------|-------|------------|
|         |               |              | WYSYST-CG-M                             | RABAB-OZMA | CASMO-3 | WIMS-D4 | CU    | UNIRASOS-2 |
| BAPL-1  | Keff          | 1 000        | 0 1                                     | 0 1        | 0 1     | -0 4    | -0 3  | -0 2       |
|         | $\delta_{28}$ | 1 390(0 010) | 2 1                                     | 1 7        | -0 7    | -7 7    | -4    | 2 3        |
|         | $\delta_{25}$ | 0 084(0 002) | 0 1                                     | 1 0        | 0 1     | 5 3     | -0 8  | -1 7       |
|         | $\delta_{28}$ | 0 078(0 004) | 0 6                                     | -2 4       | -0 5    | 1 0     | -2    | -5 1       |
|         | MCR           | -            | 0 813                                   | 0 810      | -       | 0 770   | 0 813 | 0 808      |
| BAPL-2  | Keff          | 1 000        | 0 0                                     | 0 1        | -       | -0 4    | 0 1   | -0 1       |
|         | $\delta_{28}$ | 1 120(0 011) | -                                       | 4 6        | 2 8     | -4 7    | 2 7   | 5 1        |
|         | $\delta_{25}$ | 0 068(0 001) | -                                       | 1 6        | 1 0     | 5 9     | -2 1  | -1 2       |
|         | $\delta_{28}$ | 0 070(0 004) | -                                       | -7 0       | -4 6    | 5 4     | -5 7  | -8 9       |
|         | MCR           | -            | -                                       | 0 737      | -       | 0 707   | 0 735 | 0 736      |
| BAPL-3  | Keff          | 1 000        | 0 1                                     | 0 2        | -       | -1 0    | 0 2   | 0 3        |
|         | $\delta_{28}$ | 0 906(0 020) | -                                       | 0 4        | 0 0     | -7 3    | -0 6  | 1 2        |
|         | $\delta_{25}$ | 0 052(0 001) | -                                       | 2 1        | 1 5     | 6 5     | -1 5  | -1 0       |
|         | $\delta_{28}$ | 0 057(0 003) | -                                       | -6 3       | 3 8     | -4 0    | -3 6  | -7 3       |
|         | MCR           | -            | -                                       | 0 657      | -       | 0 637   | 0 656 | 0 654      |

- - - data is absent in available literature

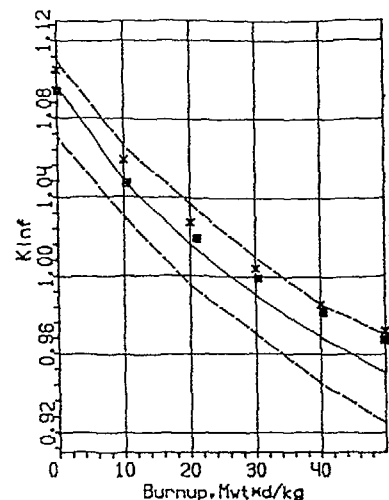
TABLE 3. COMPARISON OF CALCULATED AND MEASURED DATA FOR PROTEUS CRITICAL ASSEMBLY (phase I, core 1, x = 6%)

| Param | Measured value<br>(err %) | Code name calculation/measurement |        |        |         |          |         |        |       |       |            |
|-------|---------------------------|-----------------------------------|--------|--------|---------|----------|---------|--------|-------|-------|------------|
|       |                           | WIMS-Std/WI 8-81                  | GRUCAH | KARBUS | SPECTRA | EPRI-CPM | SRAC/J2 | HELIOS | HX    | BOXER | UNI-ASOS-2 |
| F5/F9 | 0 988 (2 0)               | -                                 | -      | -      | -       | -        | 1 016   | 1 002  | 0 964 | 1 011 | 1 013      |
| C8/F9 | 0 0691 (2 2)              | 1 002                             | 0 951  | 1 042  | 1 005   | 0 983    | 0 933   | 0 967  | 0 964 | 1 036 | 0 997      |
| F8/F9 | 0 00987(2 5)              | 0 974                             | 0 992  | 0 979  | 0 999   | 0 941    | 1 003   | 1 010  | 0 993 | 1 113 | 0 973      |
| F1/F9 | 1 780 (4 5)               | -                                 | -      | -      | -       | -        | 1 033   | 0 953  | 0 970 | 0 889 | 0 974      |
| Kinf  | 1 045 (1 1)               | 0 986                             | 1 009  | 0 995  | 0 992   | 1 001    | 1 012   | 1 005  | 0 996 | -     | 1 001      |
| Z     | -2                        | -                                 | -      | -      | -       | -        | -       | -      | -     | -     | -          |
| Bz    | (7 2+0 4)m                | -                                 | -      | -      | -       | -        | -       | -      | -     | -     | -          |
| Bx    | (1 3+2 0)m                | -                                 | -      | -      | -       | -        | -       | -      | -     | -     | -          |
| B     | * 2                       | -                                 | -      | -      | -       | -        | -       | -      | -     | -     | -          |
| M     | 53 0cm                    | -                                 | -      | -      | -       | -        | -       | -      | -     | -     | 55 0       |

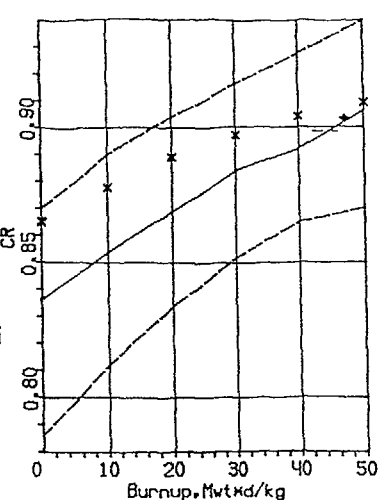
\* - calculated value used in Ref 16 for determination of Kinf

- - - data is absent in available literature

Calculated data obtained using WIMS-Std WIMS 81 GRUCAH KARBUS SPECTRA EPRI-CPM SRAC/J2 HELIOS HX, BOXER have been taken from Ref 16-17

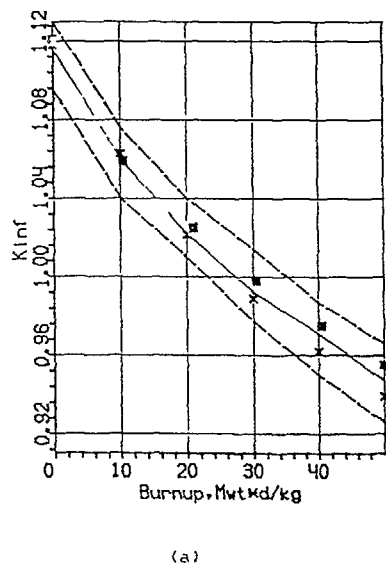


(a)

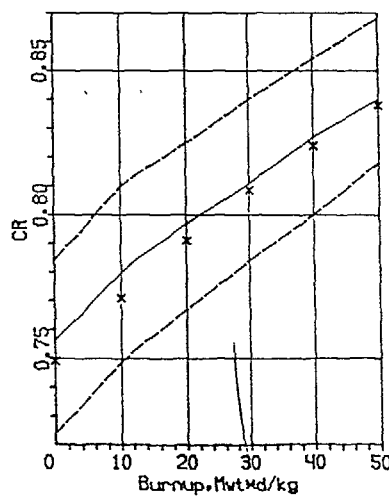


(b)

Fig. 1.  $K_{inf}$  and CR as a function of burnup.  $V_m/V_f=0.6$ ,  $\xi=8.0\%$   
 ---, - - - extreme and average results from [14].  
 x, ■ - UNIRASOS-2 and SAFFIR results.

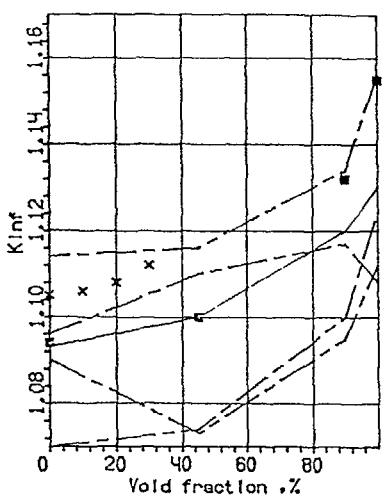


(a)

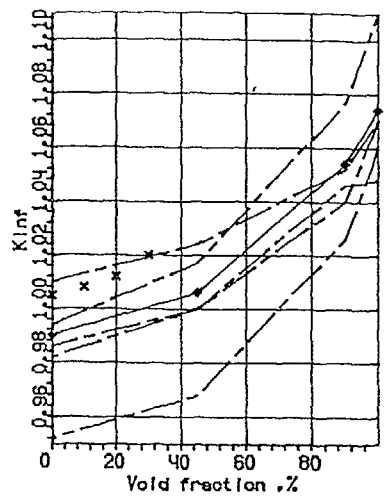


(b)

Fig. 2.  $K_{inf}$  and CR as a function of burnup.  $V_m/V_f=1.1$ ,  $\xi=7\%$   
 ---, - - - extreme and average results from [14].  
 x, ■ - UNIRASOS-2 and SAFFIR results.

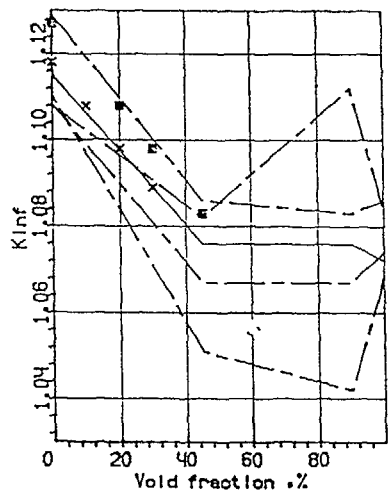


(a)

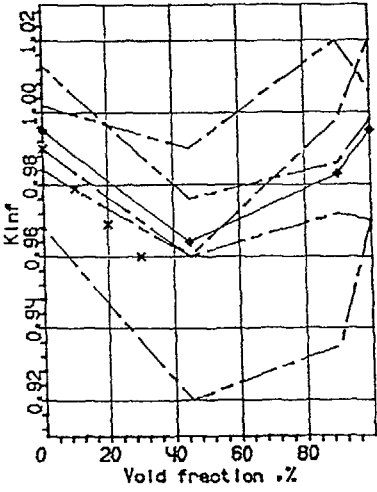


(b)

Fig. 3.  $K_{inf}$  as a function of moderator void fraction.  $V_m/V_f=0.6$   
 $W=0.0$  (a), 30.0 Gvt d/t (b). Designation the same as on Fig. 1



(a)



(b)

Fig. 4.  $K_{inf}$  as a function of moderator void fraction.  $V_m/V_f=1.1$   
 $W=0.0$  (a), 30.0 Gvt d/t (b).

TABLE 4 BASIC PARAMETERS OF VVER WITH TIGHTER PITCH PLUTONIUM ENRICHED LATTICE

| Core, elementary cell and fuel assembly parameters. | Reactor type         |                  |
|---|----------------------|------------------|
|   | VVER-M               | AP'R(18)         |
| Core equivalent diameter (cm)                       | 3.94                 | 3.70             |
| Core active length (cm)                             | 2.5                  | 2.23             |
| Heavy metal inventory (t)                           | 112                  | 121.5            |
| Thermal power (MW)                                  | 5250                 | 3782             |
| Average power density (kW/L)                        | 170                  | 151              |
| Average heavy metal specific power (W/gHHD)         | 46.9                 | 31.0             |
| System pressure (bar)                               | 157                  | 158              |
| System flow rate (kg/s)                             | 25000                | 16500            |
| Coolant temperature core-inlet/outlet (C)           | 292/327              | 286/326          |
| Number of assemblies                                | 253                  | 236              |
| Number of cells in assembly                         | 469                  | 469              |
| Number of guide tube for control rods               | 24                   | 24               |
| Control rods material                               | B <sub>4</sub> C     | B <sub>4</sub> C |
| Canning diameter (cm)                               | 0.90                 | 0.95             |
| Canning material, cladding thickness (cm)           | St. 0.055<br>(0.04)  | St. 0.04         |
| Pin pitch (cm)                                      | 1.06                 | 1.05             |
| Spacers   | Hel. fins<br>(grids) | Hel. fins        |
| Fuel assembly moderator/fuel volume ratio           | 0.785                | 0.53             |
| Fuel assembly steel / fuel volume ratio             | 0.413                | 0.25             |
| Reload enrichment (%)                               | 8.3                  | 7.5              |
| Average burnup (Gwd/t)                              | 41.0*                | 45.0             |
| Conversion ratio                                    | 0.80                 | 0.95             |

\* - obtained for case of cladding thickness - 0.04 cm.

TABLE 5. RESULTS OF VVER-M FUEL LATTICES BURNUP CALCULATIONS

| Lattice parameter           |                  | Result of calculation |       |       |       |       |       |       |        |       |
|-----------------------------|------------------|-----------------------|-------|-------|-------|-------|-------|-------|--------|-------|
| $h$ (cm)                    |                  | 1.09                  |       |       |       |       |       |       |        |       |
| $\omega_f / \omega_m$       |                  | 0.79                  |       |       |       |       |       |       |        |       |
| $\rho_{Pu,fis}^o$ (g)       |                  | 7.2                   | 8.0   | 8.5   | 8.5   | 8.5   | 8.0   | 3.0   | 3.0    | 3.0   |
| $T_f$ (°C)                  |                  | 1200                  | 1200  | 1200  | 1000  | 1000  | 1200  | 1200  | 1200   | 1200  |
| $\omega_{steel} / \omega_f$ |                  | 0.413                 | 0.413 | 0.413 | 0.413 | 0.336 | 0.413 | 0.333 | 0.333  | 0.333 |
| $K_\infty^{BOC}$            |                  | 1.106                 | 1.134 | 1.152 | 1.159 | 1.169 | 1.139 | 1.149 | 1.159  | *     |
| $K_\infty^n = 1.05$         | $H$ (Gwd/t)      | 15                    | 24    | 30    | 32    | 35    | 25    | 29    | 30     |       |
|                             | $K_\infty^{EOC}$ | 1.028                 | 1.020 | 1.015 | 1.013 | 1.011 | 1.020 | 1.014 | 1.014  | *     |
|                             | CR               | 0.843                 | 0.816 | 0.799 | 0.793 | 0.789 | 0.795 | 0.792 | 0.777* |       |
| $K_\infty^n = 1.03$         | $H$ (Gwd/t)      | 22                    | 32    | 39    | 40    | 43    | 33    | 36    | 38     | *     |
|                             | $K_\infty^{EOC}$ | 1.002                 | 0.995 | 0.990 | 0.990 | 0.990 | 0.994 | 0.992 | 0.993* |       |
|                             | CR               | 0.849                 | 0.824 | 0.809 | 0.801 | 0.797 | 0.801 | 0.798 | 0.786  | *     |

Correlation (2) allows to take into account a leakage Data of Tabl 4  
<sup>n</sup>  
correspond two different Kinf values - 1.03 and 1.05 Analysis of Tabl 4 data makes it possible to conclude that.

- needed Pu239, Pu241 enrichment to provide fuel load life time 7000 full power hours is changing from 8.2 to 8.5 % in dependence of lattice pitch, leakage, volume steel fraction, and other characteristics Average conversion ratio is in excess of 0.8;

- obtained burnup characteristics are less optimistic than given in Ref 18 characteristics of APWR. It can be explained by greater moderator/fuel volume ratio and volume steel fraction, distinctions of used codes and data libraries;

- possible unaccuracy of final burnup apparently don't exceed 20 - 25%.

A comparision of effective specific natural uranium spending for reloading of VVER-1000 with three-years open fuel cycle and described here advanced VVER shows that using of tight plutonium enriched lattices provides reducing of this value more than 4 times Such comparision with VVER-1000 with closed fuel cycle shows that in this case reducing of uranium spending is about 2.7 times

It should be noted that given in Tabl. 5 characteristics have been obtained under supposition that Am241 is absent in fresh fuel and fuel is homogeneous mixture of uranium and plutonium dioxide. Taking into account of Am241 and PuO<sub>2</sub> grains availability can lead to small reducing of final

burnup. Increasing of fuel reprocessing duration because of Pu241 decay also leads to reducing of final burnup (~ 5.0% per each three years).

The results of reactivity coefficients calculations at some burnup points and boron concentrations for 8% enriched lattice obtained using UNIRASOS-2 code are presented in Tabl. 6. Data of this table shows that critical boron concentration in tighter lattice is significantly greater than in today VVERs lattices. Such boron concentrations lead to positive reactivity changing under moderator density reducing. At zero boron concentration void reactivity coefficient changes sign. Data of Tabl. 6 allow to make a conclusion that using of liquid boron for compensation of total reactivity excess for burnup is undesirable because it can led to zero or slight positive void reactivity coefficient at BOC. Therefore application of IFBA type burnable absorbers for partial reactivity excess compensation can be necessary.

It should be mentioned that taking into account real flux distribution in the core can a little change given reactivity coefficients. It is necessary also to analyse behaviour of void reactivity coefficient under moderator density changing from 1.0 to 0.0 g/cm<sup>3</sup>. An absence of corresponding experimental data in our opinion does not allow to guarantee now sufficient accuracy of such calculations.

To determine power peaking factor and control rods worth two dimensional fine mesh calculations have been performed using PERMAK code for core containing fuel assemblies with enrichment - 7.5, 8.0 and 8.5%. It has been shown that power peaking factor for this core don't exceed needed value. But it is seen that fuel pin power peaking factor in tighter lattice is greater than in VVERs lattices. Calculations have also shown that in order to provide undercriticality of fresh core at cold state without liquid boron by B4C control rods it is necessary to enrich boron by B10 up to 90%

Preliminary calculations of three dimensional fuel assembly power distributions have been performed using BIPR-8 nodal simulator

TABLE 6 RESULTS OF REACTIVITY COEFFICIENT CALCULATIONS

| Lattice parameters                                     | Core state parameters  |                        |                        |                        |                        |                         |  |  |
|--|------------------------|------------------------|------------------------|------------------------|------------------------|-------------------------|--|--|
|  | W = 0.0 %              | W = 0.0 %              | W = 100 %              | T <sub>f</sub> = 293°K | T <sub>f</sub> = 593°K | T <sub>f</sub> = 1200°K | γ <sub>m</sub> = 1.00g/cm <sup>3</sup> | γ <sub>m</sub> = 0.71g/cm <sup>3</sup> |
|  | T <sub>m</sub> = 293°K | T <sub>m</sub> = 593°K | T <sub>m</sub> = 593°K | T <sub>m</sub> = 293°K | T <sub>m</sub> = 593°K | T <sub>m</sub> = 593°K  | T <sub>m</sub> = 593°K                 | T <sub>m</sub> = 593°K                 |
|  | M=0 Gvd/t              | M=0                    | M=32                   |                        |                        |                         |  |  |
| C <sub>B</sub> <sup>nat</sup> g/kgH <sub>2</sub> O     | 22.50                  | 0.00                   | 30.10                  | 0.00                   | 23.85                  | 0.00                    | 0.00                                   | 0.00                                   |
| Keff   | 1.0000                 | 1.1985                 | 1.0000                 | 1.1553                 | 1.0000                 | 1.1183                  | 0.9878                                 |  |
| ∂ρ/∂CB · 10 <sup>-3</sup> kg/g                         | -6.375                 | -14.930                | -3.939                 | -7.856                 | -4.010                 | -6.866                  | -5.119                                 |  |
| ∂ρ/∂T <sub>f</sub> 10 <sup>-5</sup> °K <sup>-1</sup>   | 0.000                  | 0.000                  | -2.592                 | -3.840                 | -2.442                 | -3.220                  | -2.594                                 |  |
| ∂ρ/∂γ <sub>m</sub> 10 <sup>-1</sup> cm <sup>3</sup> /g | -1.365                 | 1.073                  | -1.714                 | 0.863                  | -1.347                 | 0.701                   | 0.764                                  |  |
| ∂ρ/∂T <sub>m</sub> 10 <sup>-5</sup> °K <sup>-1</sup>   | 1.680                  | -0.840                 | 0.380                  | -0.560                 | 0.360                  | -0.240                  | -0.056                                 |  |

It has been shown that under choosen core parameters it is possible to provide needed value power of peaking factor. It is worth to mention that in this case disagreements of calculated by fine mesh code PERAK and BIPR-8 two dimensional fuel assembly power distributions are greater than usually observed for VVER-1000 cores

#### 4 THE OHYDRAULICS PROBLEMS AND SAFETY ASPECTS

VVER 'i' reactors have two special features closely packed rod bundles and helical fins as a spacer. These features affect the fuel assemblies hydraulic resistance and critical heat flux (CHF). Thus for the proper thermohydraulic calculation of VVER-M it is necessary to create two new correlations.

##### 4.1 Hydraulic Resistance Calculations

Here the basic principles of the hydraulic resistance correlation are discussed. Experimental data on hydraulic resistance obtained for channels with cross section of complicated form (for example for fuel assemblies)

show that measured hydraulic resistance coefficient differs from calculated value if the classic correlation for round tubes is used. Such an error may be eliminated through multiplication of the coefficient obtained from classic correlation by factor

For a fuel assembly  $\lambda/\lambda_r$  factor may be obtained according to ideas of Ref. 19. In accordance with method suggested in [19] the channel cross section is divided onto elementary subchannels. For typical subchannels the values of  $\lambda/\lambda_r$  ratio were calculated in [19]. As  $\lambda/\lambda_r$  factor for the channel in whole the weighted average is taken with subchannel area as a weight.

Helical fins change the bundle's geometry. So the axial alteration of the subchannel's configuration causes difficulties in taking into account of helical fin effects. Thus  $\lambda/\lambda_r$  ratio estimations were performed for smooth bundles (without taking fins into consideration) with length-averaged values of cross section, hydraulic diameter and wetted perimeter. Helical fins effect is treated by introduction of local pressure loss coefficient.

Calculations of these effective local pressure losses were performed basing on the method from paper Ref. 20. This method was recommended for situated on channel walls arbitrarily formed lugs. The method takes into account tightening of the channel due to small rod-to-rod gaps and for angle of incidence between the lug surface and the direction of flow. Thus method is relatively universal for various spacing elements geometry.

Traditional honey type spacer grids were also considered in one of the variants of core design. In that case the local hydraulic losses were calculated using method described in [21].

#### 4.2 CHF calculations

IAE correlation [22, 23] for CHF prediction is based on a wide set of experimental data and may be used for fuel assemblies of different type. So IAE correlation has been chosen as the base formula for tight lattice bundles CHF predictions improvement.

The IAE correlation is

$$q(z) = \frac{f_1(P) d_{tr}^{1/3} (q_w d_{tr})^{1/5} [A - 0.286(q_w) d_{tr} x(z) f_2(P)]^{2/5} \lambda^{1/5}}{345 (1 + 0.282 B(z))}, \text{ W/m}^2,$$

$$f_1(P) = [1 + 0.7 e^{-1.4(1 - \frac{P}{P_c})^2}] \frac{r}{V(M)}^{1/5} [g(ga')^{1/3} \lambda']^{1/3}$$

$$f_2(P) = \left(\frac{V'}{G}\right)^{1/5}$$

$$A = 0.3 + \frac{0.7}{1 + \frac{0.0133}{Fr^{0.5}} \frac{V}{V'}}$$

$$B(z) = \int_z^z \frac{q(z')}{q(z)} dz'$$

|       |          |  |
|-------|----------|--|
| where | $d$      | - heated diameter, m,                                      |
|       | $P$      | - pressure, bar,   |
|       | $x$      | - quality,   |
|       | $q_w$    | - mass velocity, kg/m <sup>2</sup> s,                      |
|       | $v$      | - specific volume, m <sup>3</sup> /kg,                     |
|       | $q$      | - heat flux, W/m <sup>2</sup> ,                            |
|       | $z$      | - axial coordinate, m,                                     |
|       | $r$      | = 1" - 1',   |
|       | $r$      | - specific heat of evaporation, J/kg,                      |
|       | $i$      | - specific enthalpy, J/kg,                                 |
|       | $g$      | - gravity-forced acceleration, m <sup>2</sup> /s           |
|       | $a$      | - temperature conductivity coefficient, m <sup>4</sup> /s, |
|       | $\nu$    | - kinematic viscosity, m <sup>2</sup> /s,                  |
|       | $\mu$    | - dynamic viscosity, kg/m s,                               |
|       | $\sigma$ | - surface tension, kg/s,                                   |
|       | $Fr$     | - Frud criterion,  |
|       | $\rho$   | - density, kg/m <sup>3</sup> .                             |

Indexes ' and " refer to saturated water and vapour properties. The IAE correlation validity needs to be proved by assessment of bundle tightness and helical fins influences on CHF.

The preliminary analysis of helical fins influence was carried out basing on published experimental CHF data, obtained on wire-wrapped bundles. Among them there were experimental data from Ref. 24, 25. It should be noted that in Ref. 24 the following conclusions have been made:

- in the case of unique direction of fins on each rod the wire wrap does not affects CHF at all,
- in the case of opposite directions of fins on the neighbouring rods CHF decreases by 25-30 %.

These conclusions have been made for the case of one fin per rod. Data from [24] were also analysed using IAE correlation. The results showed the lack of the helical fins influence on CHF. The paper [25] presents two pairs of test sections. Each pair of sections has identical geometries, but in the first section of pair wire wrap is used and in the second grid spacers are used. The sections of the first pair are squares without corners (21 heated rod in square lattice). The sections of the second pair are of hexagonal form (19 heated rods in hexagonal lattice). In spite of the differences in spacing elements the sections of each pair have equal cross sections. So the direct comparison of measured CHFs in both sections of pair may be performed at least for regimes with equal pressures, mass flow rates and inlet coolant temperatures. Such comparison gives the following results. Let  $q_{w1}$  and  $q_{w2}$  - local critical heat fluxes for the wire-wrapped section and section with grids accordingly. Then for the square sections  $q_{w1}/q_{w2} = 0.84 - 0.90$ , for hexagonal sections  $q_{w1}/q_{w2} = 1.05 - 1.15$ .

On a basis of performed analysis the following conclusion have been made - until CHF experiments will be done it is not expedient to install into the correlation any correcting factor taking into account an influence of wire wrap.

It is very difficult to take into account a tightness of rods lattices because of a small quantity of experimental data for tight lattice bundles. For a preliminary analysis data from Ref. 26-28 have been used. Calculations based on IAE CHF correlation have showed a satisfactory accordance with experiment. Nevertheless the attempts of making of IAE correlation more precise have been undertaken. A constant  $d=0.011$  (m) was installed into the correlation instead of a heat diameter  $d$ . This constant corresponds approximately to the heat diameter of VVER-1000 rod bundle.

After that different correcting factors have been installed and every factor was a monotone function of S/D where S - pitch of a rod lattice, D - outer rod diameter. Unfortunately the absence of the own CHF data for tight lattices and the small quantity of published data does not permit to choose groundedly a shape of such function and to optimize its coefficients. So the original IAE correlation [22,23] was used in calculations.

#### 4.3 Stationary Thermo-Hydraulic Calculations

Stationary calculations for NPP with VVER-m have been performed using MOCT-7-EC code [29]. This code is suitable for performing of stationary and transient analysis of VVER-type NPP. The following main components of NPP were considered: core channels, upper and lower plenum, primary loops, pressurizer, primary and secondary sides of steam generators, main steam collector. Automatic control system and primary pumps were also taken into account. The following parameters were calculated: heat power, pressures in loops, in pressurizer in steam generators and main steam collector, mass flow rates in primary loops and core channels, coolant specific enthalpies, fuel and cladding temperatures, wall and SG tubes temperatures rotation velocities of primary pumps, SG and pressurizer water levels.

The changes taking into account the above-stated pressure losses calculation method were installed into the code MOCT-7-EC. Three parallel channels were considered in the core: the hottest subchannel formed by three neighbouring rods, the most loaded fuel assembly and the rest of the core.

The following conditions have been analyzed by MOCT-7-EC code:

1. the nominal conditions (the values of the main parameters were taken from the table 4);
2. the conditions with deviations of the main parameters (the power is 102 % of the nominal power, the pressure is the nominal pressure minus 3 bar, the core inlet coolant temperature is 2 C below of the nominal temperature);
3. the conditions with deviations of hydraulic characteristics of primary loops (loop pressure drop equals the nominal drop times 1.10);
4. the conditions with deviations of hydraulic characteristics of primary pumps (the pump head equals the nominal head minus 0.245 bar);
5. the conditions with combination of these unfavourable deviations.

Calculations were performed for both variants of fuel assembly design: with helical finned rods and with grid spacers. The relative power radial and axial distributions obtained from neutron-physical calculations were used under this calculations.

The calculations results show that under all conditions except the case with the worst combination of deviations the mean coolant temperature in the exit of the most loaded fuel assembly does not reach the saturation temperature. Under the worst conditions the quality in the exit of the hottest bundle equals 0.004. The maximal fuel temperature does not exceed 1950 C for all cases. The calculations results are in whole slightly more favourable for the variant of core with grid spacers.

For CHF calculations the original IAE correlation was used. The minimum CHF-ratio under the worst conditions equals 1.20 in consideration of engineer coefficients. This low CHF-ratio may be explained by correlation features. For example when quality equals 0 the correlation has the form  $q=C*d$ . Such significant reducing of VVER-M bundle heat diameter in comparison with VVER-1000 causes significant decreasing of calculated CHF-ratio. Obviously CHF experiments for tight lattice bundles and further IAE correlation improvement are needed.

Thus the preliminary results of VVER-M NPP thermo-hydraulic calculations show that it is possible to satisfy safety requirements under chosen core design but more detailed thermo-hydraulic analysis are needed. For such analysis subchannel thermo-hydraulic code VEVERKA [30] can be used.

#### 5 CONCLUSION

Preliminary analysis of neutron-physical and thermohydraulic problems of VVER with tight lattice and plutonium enriched fuel have showed that

- it is possible to achieve average conversion ratio in excess of 0.8 final burnup 41 Gvt d/t using tighter pitch lattice ( $V_m/V_f=0.79$ ) and plutonium enrichment ~8.3%;
  - natural uranium utilization in VVER-M in comparison with reactor of VVER-1000 type is improved by factor 4-4.5;
  - VVER-M design can satisfy the main safety requirements.
- In our opinion the following problems are most important now:
- further improving and verification of the codes to provide needed accuracy of calculations;
  - analysis of void reactivity coefficient at different core states
  - optimization of reactor control system consisting of control rods, burnable absorbers of IFBA type and probably boron regulation system;

For codes verification special experimental investigations are planned to perform in Kurchatov Institute. CHF and pressure drop tests will be performed soon using two sections - with helical fins (first stage) and grids as a spacers (second stage).

Studying of plutonium enriched lattices will be performed at special critical assembly. Measurements will start with case of wide lattice ( $V_m/V_f=1.8 \pm 5\%$ ) and then tight pitch lattices will be studied. Special activity on making cross-sections of some heavy isotopes and most important fission products more precise are also planned.

#### ACKNOWLEDGEMENTS

The authors are pleased to express their gratitude to A. Novikov, L. Maiorov, M. Judkevich and V. Tebin for useful advices and fruitful discussions.

#### REFERENCES

- 1 I.K. Levina, V.N. Proselkov et al.  
Physical and Technical Aspects of Using Pu in VVERs  
IAEA Technical Committee Meeting on Recycling of Plutonium and Uranium  
in Water Reactor Fuels. Cadarache, November 1989.
- 2 A.N. Novikov, V.V. Pshenin et al.  
Problems of VVERs In-core Fuel Management.  
IAEA 622-I3-TC-676.3
- 3 Л.В. Майоров, М.С. Жукевич  
Нейтронно-физические константы в расчетах реакторов на тепловых нейтронах  
Энергоатомиздат, 1988

- 4 Л.П. Абагян и др  
Групповые константы для расчета ядерных реакторов Энергоатомиздат, 1981
- 5 С.М. Николаев и др.  
Метод подгрупп для учета резонансной структуры сечений в нейтронных расчетах Атомная энергия, 1970, т. 29, вып. 1
- 6 V.V. Tebin.  
A Generalized Subgroup Approach to Calculating Resonance Absorption of Neutrons in Nuclear Reactors.  
IAEA-Tecdoc-491.
7. J.R. Askew.  
The calculation of Resonance Captures in Few-Group Approximation.  
AEEW-R 489, 1966.
- 8 Y. Yamamuro, T. Sekiya.  
Wigner Continous Slowing Down for the Fast Neutron Spectrum.  
Nucl. Sci. Eng., V.63, 213(1971).
9. Н.И. Лалетин.  
Метод поверхностных псевдоисточников для решения уравнения переноса нейронов (Gn-приближение). Препринт ИАЭ-1374. Москва, 1967.
10. М.П. Лизоркин.  
Аннотация программы ПЕРМАК-У.  
Вопросы атомной науки и техники, Сер. Физика и техника ядерных реакторов, вып. 4, 1988.
11. Н.И. Лалетин  
Об уравнениях гетерогенного реактора  
Вопросы атомной науки и техники, Сер. Физика и техника ядерных реакторов, вып. 5(18), 1981.
12. В.В. Пшенин, А.Н. Новиков, И.И. Сурначева.  
Анализ возможностей повышения точности мелкосеточных расчетов ВВЭР на примере решения модельных задач в плоской геометрии  
Вопросы атомной науки и техники. Сер. Физика и техника ядерных реакторов. вып. 4, 1988
13. M.Z. Williams et al.  
Analysis of Thermal Reactor Benchmarks with Design Codes Based on ENDF/B-V Data. Nucl. Techn., 71(7), 386(1985).
14. Y. Ishiguro. Resonance Absorption and Coolant Void Reactivity Coefficient in Tighter Pitch Lattices. IAEA Advisory Group Meeting on Nuclear Data for Calculation of Thermal Reactor Reactivity Coefficient. Vienna, 1987.
15. Thermal Reactor Benchmark Compilation. CSEWC Data Testing Subcommittee. June 1974.
16. R. Chawla et al.  
Reactivity and Reaction Rate Ratio Changes with Moderator Voidage in a Light Water High Converter Reactor Lattice. Nucl. Techn., v.67, 360(1984).
17. M. Yamamoto.  
Validation of HELIOS-HX Code for High Conversion Light Water Reactor Analysis. Nucl. Techn., V.80, 240(1988).
18. W. Oldekop et al.  
General Features of Advanced Pressurized Water Reactors with Improved Fuel Utilization. Nucl. Techn., V.59, 212(1982).
19. М.Х. Ибрагимов, Л.Л. Кобзарь  
Расчет коэффициента гидравлического сопротивления и профиля скорости в трубах с регулярной шероховатостью. Атомная энергия т. 37, вып. 4, 1974
20. М.Х. Ибрагимов, И.А. Ксупов, Л.Л. Кобзарь, В.И. Субботин.  
Расчет коэффициентов гидравлического сопротивления при турбулентном течении жидкости в каналах некруглого поперечного сечения Атомная энергия, т.23, вып. 4, 1967.
21. В.К. Иванов, Л.Л. Кобзарь  
Расчет гидравлического сопротивления пучков стержней с решетками интенсификаторами теплообмена. Атомная энергия, т.49, вып.3, 1980.
22. Й. Котрнох, Л.Л. Кобзарь и др.  
Исследование кризиса теплоотдачи в пучках стержней на 'Большом Водяном Стенде ЭЭМ "Шкода" Семинар "Теплофизика-88", Варшава 1988.
23. В.А. Еноградов и др  
Исследование гидравлического сопротивления, паросодержания и кризиса теплоотдачи в моделях тепловыделяющих сборок реактора типа БК-500 и АСТ-500. В сб. Вопросы атомной науки и техники, Серия "Физика и техника ядерных реакторов". стр 7-16. вып 6. 1973
24. P.V. Macbeth.  
Burn-out Analysis. Part 5: Examination of Published World Data for Rod Bundles. AEEW-R358, 1964.
25. L.S. Tong et al.  
Critical Heat Flux (DNB) in Square and Triangular Array Rod Bundles. JSME Semi-International Symposium, Tokyo, September, 1967.
26. K.J. Coeling.  
Critical Heat Flux and Pressure Drop Tests with Vertical Upflow of Water in a 20-rod Bundle of 0.695-inch Diameter Rods. (CLWR Development Program), WAPD-TM-1155, 1977.

27. B. W. Le Tourneau.

Critical Heat Flux and Pressure Drop Tests with Parallel Upflow of High Pressure Water in Bundles of Twenty 3/4-inch Rods.  
Nucl. Sci. and ENG., v. 54, p. 214, 1974.

28. B. W. Le Tourneau.

Critical Heat Flux and Pressure Drop Tests with Parallel Upflow of High Pressure Water in Bundles of Twenty 0.25 and 0.28 inch Diameter Rods (LWR Development Program), WAPD-TM-1013, 1975.

29. А И Мъсенков, А И Суслов

Программа MOST-7-EC Препринт ИАЭ-3975/5, 1984

30. Я Коштялек, Я Волмут

Расчетная программа BEBERKA для анализа по ячейкам теплогидравлических и нейтронно-физических характеристик ядерных реакторов  
Семинар "Теплофизика-82". Прага, 1982

## THE CONCEPT OF AXIALLY HETEROGENEOUS HIGH CONVERSION LIGHT WATER REACTORS

Y. ISHIGURO, Y. MURAO, S. YASUKAWA,  
T. IWAMURA, K. OKUMURA, O. SATO  
Japan Atomic Energy Research Institute,  
Tokai-mura, Naka-gun, Ibaraki-ken,  
Japan

### Abstract

A new concept of an axially heterogeneous high conversion light water reactor(HCLWR) is proposed to improve the natural uranium utilization. It consists of a top blanket, an upper core, an inner blanket, a lower core and a bottom blanket for axial direction. From the neutron physics and thermohydraulics analyses, it is found that the potential problems of the HCLWRs such as a positive void coefficient and severe heat removal can be settled by this concept. The effect of the HCLWR installation on long-term fuel cycle is also evaluated.

---

### I Introduction

Recently, much work has been performed to determine the feasibility of high conversion light water reactor(HCLWR)<sup>(1)</sup> whose core consists of a tight lattice of mixed-oxide(MOX) plutonium fuel rods. It aims to improve the natural uranium utilization without major changes from a current LWR plant system. The positive void coefficient have however been one of the most critical problems in neutron physics aspect to achieve both high conversion and high burnup<sup>(2)</sup>. It is caused by the use of the tight fuel rod lattice and highly enriched plutonium fuel<sup>(3)</sup>. From a thermohydraulic aspect, moreover, the tight lattice pitch makes it difficult to maintain sufficiently safe heat removal during normal operation and loss-of-coolant accident(LOCA).<sup>(4)</sup>

A concept of the HCLWR with a flat core and axial blankets was proposed at Japan Atomic Energy Research Institute(JAERI) to achieve both high conversion and high burnup, while maintaining a negative void coefficient.<sup>(5)</sup> By this concept, the positive void coefficient can be reduced by the neutron leakage to the axial direction. The leakage neutrons can be utilized in the axial blankets to enhance the conversion ratio. One of the most direct ways to apply the concept of the flat-core is its use in a small- or intermediate-scale( $\leq$ 400MW-electric) LWR. It is, however, difficult to apply the flat-core to a current-scale LWR plant because of too short active core height. As an extension, two such flat cores with axial blankets can be stacked to construct a reactor with an inner blanket as shown in Fig.1, which provides a thermal output consistent with a conventional 3-loop pressurized water reactor(PWR). It is called "double-flat-core HCLWR" at JAERI.

In order to grasp the overall neutron physics characteristics of such an HCLWR, preliminary survey calculations were made on the basis of a one-dimensional core burnup calculation, changing fundamental design parameters such as moderator-to-fuel volume ratio, core height, inner blanket thickness and so on.<sup>(6)</sup> A preliminary feasibility study was also performed from thermohydraulic and safety aspects using available thermohydraulic correlations.<sup>(7),(8)</sup> It was found that the double-flat-core HCLWR was highly feasible; there is a sufficient margin in the critical heat flux, core pressure drop comparable with conventional PWRs, and a fairly low peak clad temperature in LOCA situation.

Based on the survey results, more concrete design parameters were determined for a reference HCLWR with the double-flat-core. In the present paper, the design work performed for the reference HCLWR will be described on the neutron physics and thermohydraulic aspects. Descriptions will be given also for the evaluated result for the fuel cycle strategy using the HCLWR.

## II. Reference Core; HCLWR-JDF1

Figure 2 shows the fuel rod structure of the double-flat-core HCLWR, which consists of top blanket, upper core, inner blanket, lower core and bottom blanket for its axial direction. The fuel pellet of the active core parts is made of plutonium MOX with 0.2wt% depleted UO<sub>2</sub>, while the blanket

pellet is made of depleted UO<sub>2</sub>. The fissile plutonium enrichment of the MOX fuel for the equilibrium cycle is 10wt%, which was determined to obtain the discharge burnup of more than 40000MWd/t by a preliminary analysis based on a one-dimensional core burnup calculation assuming four batches refueling.

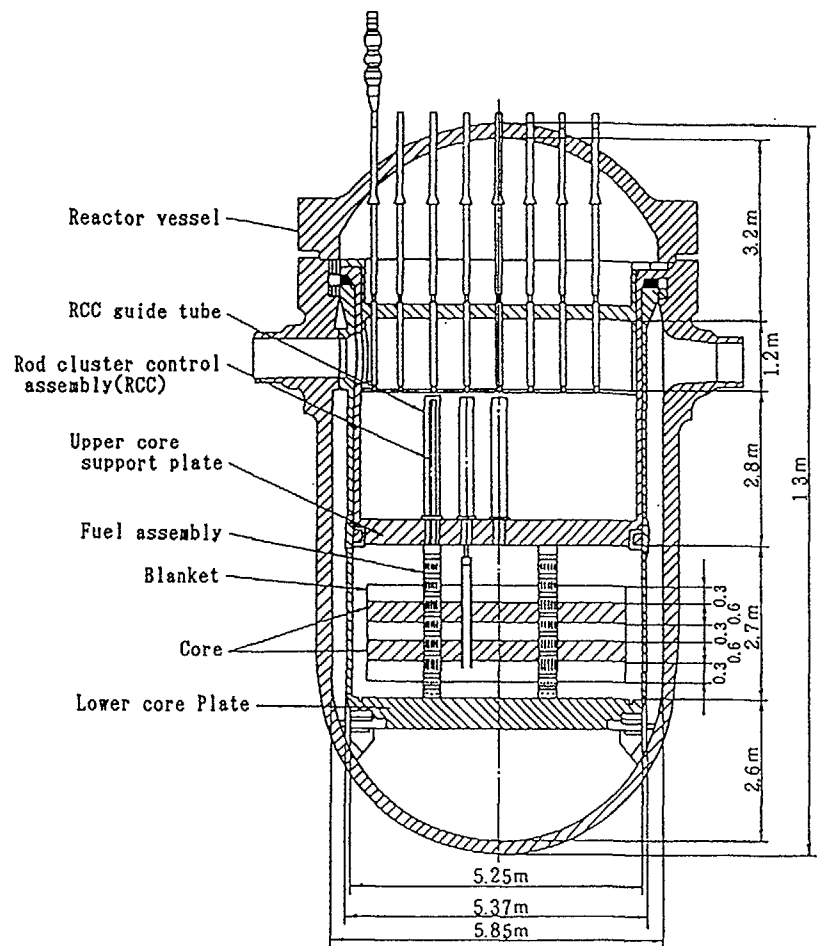


Fig.1 Reactor internals of an axial heterogeneous HCLWR (HCLWR-JDF1).

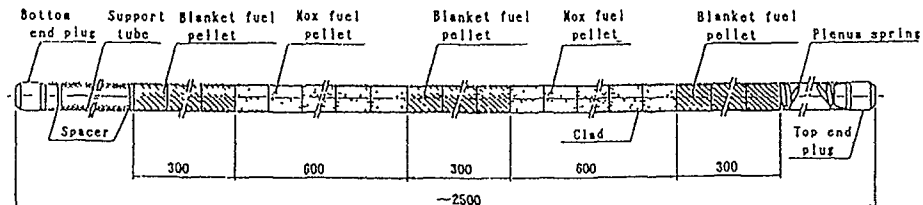


Fig.2 Fuel rod structure.

The core height and blanket thickness was also determined based on the parametric survey results, which compromised the balance among allowable linear heat rating, obtainable burnup and conversion ratio

The horizontal cross section of the fuel assembly is shown in Fig.3 and its specifications are shown in Table 1. The fuel assembly contains 372 fuel rods, 24 thimbles for control elements and one detective tube. The cladding of the fuel rod is 0.57mm-thick Zircaloy tube with 9.5mm-o.d., which has been widely used in current PWRs. The lattice pitch of 11.7mm corresponds to the moderator-to-fuel volume ratio of 1.06 at the condition that all con-

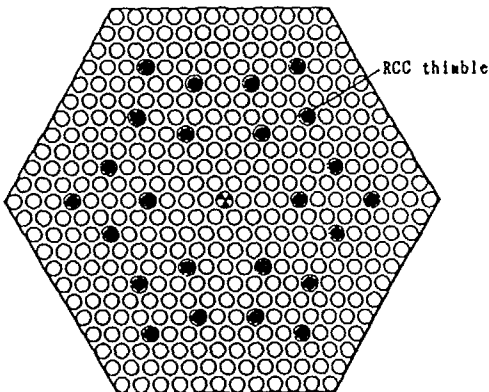


Fig.3 Horizontal fuel assembly cross section.

Table 1 Specifications of HCLWR-JDF1

|  |                          |
|--|--------------------------|
| Thermal output (MW)  | 2432                     |
| Electric power (MW)  | 810                      |
| Equivalent core diameter (m)                                       | 4.37 [4.80]*             |
| Unit core height (m)   | 0.6                      |
| Top and bottom blankets thickness (m)                              | 0.3                      |
| Inner blanket thickness (m)  | 0.3                      |
| Number of fuel cycles  | 4 [6]                    |
| Number of fuel assemblies(FA)                                      | 313 [66]                 |
| Fuel assembly pitch (mm)   | 235.4                    |
| Number of fuel rod per FA  | 372 [397]                |
| Number of rod cluster(RCC) thimbles per FA                         | 24 [0]                   |
| Fuel rod outer diameter (mm)                                       | 9.5 [9.8]                |
| Fuel rod pitch (mm)  | 11.7                     |
| $V_m/V_f$  | 1.06 [0.79]              |
| Spacer type  | Grid                     |
| Fuel cladding material   | Zircaloy                 |
| Blanket material   | Depleted UO <sub>2</sub> |
| Cladding thickness (mm)  | 0.57                     |
| RCC thimble outer diameter (mm)                                    | 11.0                     |
| B <sub>4</sub> C(90% <sup>10</sup> B) absorber outer diameter (mm) | 7.52                     |
| Number of RCCs   | 85                       |
| Initial core Pu' enrichment (wt%)                                  | 5.2 / 6.6 / 8.1 / 10.0   |
| Equilibrium core Pu' enrichment (wt%)                              | 10.0                     |
| Initial Pu' loading inventory (tonne)                              | 4.9                      |

\*[ ] : Values for radial blanket.

trol elements are withdrawn. In such a volume ratio, the chemical shim using soluble boron is effective for excess reactivity control. A honeycombed grid spacer is used to support the fuel rods with the gap of 2.2mm between the rods. The radial blanket assembly without guide thimble contains 397 depleted UO<sub>2</sub> rods whose outer diameter is 10.1mm, while the lattice pitch is the same as that of the core assembly. Thus, the moderator-to-fuel volume ratio of the radial blanket assembly is somewhat smaller( $=0.79$ ) to enhance the conversion ratio.

The reference HCLWR can provide the electric power of 800-MW consistent with the output of current 3-loop PWRs. Figure 4 shows the horizontal cross section of the HCLWR, which consists of four core zones with different burnup degree and a layer of radial blanket assemblies. The radial blanket is effective not only to increase the conversion ratio but also to protect the reactor vessel from hard neutron exposure.

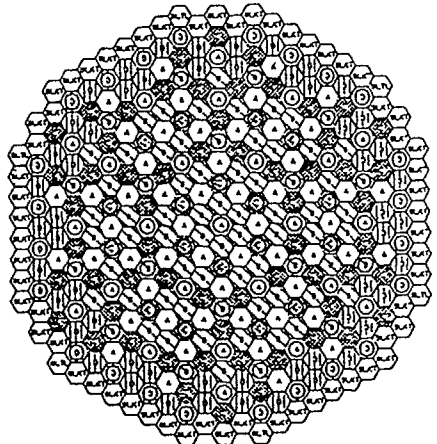


Fig.4 Horizontal core cross section.  
(A~D:Fuel, BLKT:Blanket, O:RCC)

As seen from Fig.1, the core diameter, hence the diameter of the pressure vessel is considerably larger, as compared with conventional PWRs. A pressure vessel corresponding to such a reactor is not difficult to be constructed using the state-of-arts technology. To decrease the radial core size while maintaining the same linear heat rating, it is necessary to enlarge the upper and lower core height or to remove the radial blanket. This means, however, to reduce the merits of the flat-core such as high conversion, negative void coefficient and thermohydraulic safety.

#### 4.1 Three-dimensional Core Burnup Calculation

The spatial dependent burnup calculation was performed with the three-dimensional diffusion code COREBN, which is an auxiliary program of the SRAC code<sup>(9)</sup> generated on the basis of the CITATION code<sup>(10)</sup>. The calculation was made, with the ( $\Delta$ -Z) meshing option, up to the equilibrium cycle on the basis of an optimized fuel shuffling and refueling. A six energy group structure (5 fast + 1 thermal groups) was employed for the diffusion calculation. The burnup duration estimated by the diffusion code was corrected considering the transport effect due to the short active core height,

which was evaluated by the one-dimensional transport calculation using the ANISN code<sup>(11)</sup>. The collapsed effective cross sections with burnup dependence were beforehand prepared by the collision probability routine of the SRAC code. A four-batches refueling was assumed here to estimate the burnup related quantities, such as the discharge burnup, conversion ratio and so on.

These results are collectively listed in Table 2. It will be seen that a considerably high value is obtainable for the average conversion ratio( $=0.83$ ) along burnup, the fissile plutonium inventory ratio( $=0.86$ ) and discharge burnup( $=42.5\text{GWd/tonne}$ ). Here, the burnup corresponds to the power generation in the active cores alone. The contribution to the power generation in the blanket regions is about 20% of the whole power generation at the end of the equilibrium cycle. If this power generation in the blanket regions is taken into account, the effective burnup per the active parts of the loaded fuel inventory is about  $56\text{GWd/tonne}$ . From these results, the power generation per net consumption of fissile material as a balance between conversion and depletion is estimated to be 2.2 times as large as that of the current PWR whose discharge burnup and fissile material inventory ratio are  $33\text{GWd/t}$  and

Table 2. Core Burnup Calculation Results

|  |                   |
|--|-------------------|
| Discharge burnup (GWd/tonne)                 |                   |
| Core / Axial blanket / Radial blanket        | 42.5 / 10.1 / 4.9 |
| Cycle length (Full-power days)               | 380               |
| Average conversion ratio                     | 0.83              |
| Fissile Pu inventory ratio                   | 0.86              |
| Average Linear heat rating at BOC/EOC (W/mm) |                   |
| Core   | 11.4 / 10.9       |
| Axial blanket                                | 0.21 / 0.28       |
| Radial blanket                               | 0.13 / 0.13       |
| Fractional power generation at BOC/EOC (%)   |                   |
| Core   | 84.7 / 80.9       |
| Axial blanket                                | 3.5 / 3.5         |
| Radial blanket                               | 11.8 / 15.6       |
| Radial power form factor; $\max(F_r)^*$      | 1.48              |
| Axial power form factor; $\max(F_z)$         | 1.22              |
| Hot channel factor; $\max(F_r \times F_z)^*$ | 1.80              |
| Void coefficient at BOC/EOC (pcm/%void)      | -61.1 / -97.3     |
| Excess reactivity in cold condition (pcm)    | 9640              |
| Chemical shim worth (cold) (pcm/ppm-nat.B)   | -1.96             |
| B <sub>4</sub> C control rod worth (cold)    | -7280             |
| Most reactive one-rod stuck reactivity (pcm) | 247               |

\*Including hot channel factor inside of assembly(1.06).

0.45, respectively. There are, however, about three times number of fuel rods in HCLWR-JDF1, as compared with the PWR of the same thermal output. This means higher reprocessing and fabrication cost for the double-flat-core HCLWR, though natural uranium utilization can be successfully improved.

Figure 5 shows the moderator void reactivity characteristics of HCLWR-JDF1. The excess reactivities at the beginning of the initial cycle and the equilibrium cycle are controlled by soluble boron. It is seen that a sufficiently negative void reactivity coefficient (-60~100pcm/%void) can be maintained through burnup in hot full power condition.

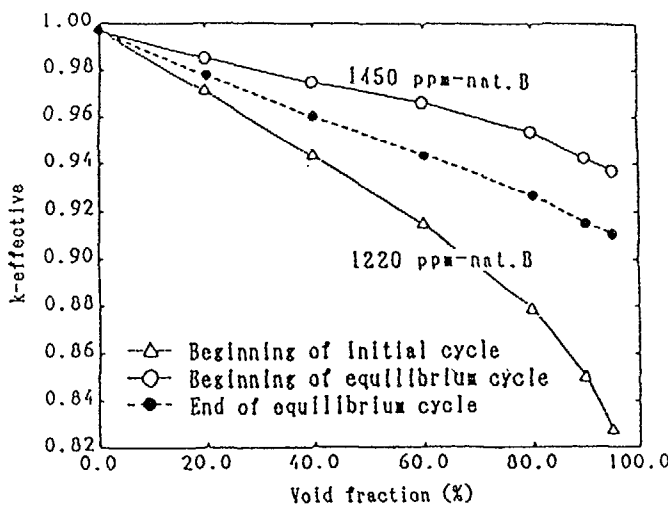


Fig.5  $k_{\text{eff}}$  variation versus void fraction.

To clear up the applicability of the chemical shim to the reactivity control in the states of cold shutdown and fuel exchange, the reactivity worths of the soluble boron and  $\text{B}_4\text{C}$  control rod with  $^{10}\text{B}$  enriched up to 90% were computed in the cold condition. As shown in Table 2, the excess reactivity is very small in HCLWR-JDF1, while the chemical shim worth is also small about one fifth of that in a conventional PWR. In the cold state, the following two conditions are requested for the chemical shim: 1) a sub-criticality of  $5\Delta k/k$  in one-rod stuck condition for cold shutdown, 2) a

sub-criticality of  $5\Delta k/k$  with all control rods insertion for fuel exchange. The concentrations of the soluble boron satisfying the above two conditions are 1800ppm-nat.B for the cold shutdown and 3800ppm-nat.B for the fuel exchange. These concentrations are less than the limit ( $\sim 4000\text{ppm}$ ) of boron solution in cold moderator. Thus, the conventional reactivity control system can be applied to HCLWR-JDF1 without major changes.

## H. Thermal Hydraulic Characteristics

In order to evaluate a thermal-hydraulic feasibility of the double-flat-core HCLWR, experimental and analytical studies have been performed.

### H.1 Experiments

Experiments for critical heat flux (CHF), bundle pressure drop, fluid mixing between subchannels, fuel rod vibration and reflood core cooling have been conducted to understand phenomena peculiar to a tight lattice core and to develop analytical models.

The CHF experiments were performed using 4 or 7-rod bundles arranged in a triangular lattice with a pitch-to-diameter ratio (p/d) of 1.126 or 1.2 under 4.0MPa water flow. Evaluating existing CHF correlations, it was found that KFK correlation<sup>(12)</sup> coupled with the subchannel code COBRA-N-I<sup>(13)</sup> analyses agreed fairly well with the experimental results. A turbulent mixing coefficient, which is the most sensitive parameter in the subchannel analyses, was determined by the fluid mixing experiments.

The bundle pressure drop and fuel rod vibration were measured in 6x6 rod bundles with various p/d's and spacer types under atmospheric pressure. For the rod bundles with the spiral wire or integral spiral rib spacer, Reheme's correlation<sup>(14)</sup> could be used to predict the pressure drop. On the other hand, a new evaluation method was developed to predict the pressure drop for a rod bundle with the grid spacers. It was also found that the vibration of fuel rod under operating condition is negligibly small for the integrity of fuel rod assembly.

The reflood experiments showed that the double-flat-core is cooled more rapidly than a conventional LWR configuration mainly due to its short core length. It was also confirmed that the present reflood cooling model<sup>(15)</sup> predicts the cladding temperature conservatively.

## II.2 Evaluation of DNBR and Pressure Drop under Operational Condition

The minimum allowable DNBR (departure from nucleate boiling ratio) for the HCLWR configuration was evaluated to be 1.28 based on the criterion that no fuel rod in the core experiences DNB with 95% probability at 95% confidence level. The estimated minimum DNBR for the present design under the steady-state condition was 1.66, which is larger than the DNBR criterion.

The bundle pressure drop of the core estimated with the proposed method was much smaller than 100KPa, which is the core pressure drop in a current PWR.

Therefore, it is concluded that large thermal-hydraulic margin is assured under the operational condition in the present design.

## II.3 Safety Analysis under Accident Conditions

The present HCLWR design should meet the same safety criteria for licensing as the current LWR. In the framework of the safety analyses, the following accidents were considered: 1) Primary coolant pump trip, 2) Locked rotor of one out of three primary coolant pumps, 3) Large break loss of coolant accident (LOCA), 4) Small break LOCA with instrumentation pipe break at the bottom of pressure vessel, and 5) Anticipated transient without scram (ATWS) initiated by station blackout. A best estimate code J-TRAC was used for the system transient calculations with conservative assumptions for the initial conditions. The radial and axial peaking factors and various reactivity coefficients were determined by the neutronic calculations.

The first two accidents are considered to be most severe cases with respect to the DNBR. As shown in Figs.6 and 7, the evaluated minimum DNBR's for those two accidents are 1.56 and 1.34, respectively, and above the DNBR criterion. That is, the present design is acceptable from a point of view of the DNBR.

As shown in Figs.8 and 9, the peak cladding temperatures (PCT's) during the large and small break LOCA's are 1172K and 1265K, respectively, and lower than the licensing limit of 1473K. The small axial peaking factor and large pressure vessel volume contribute to the lower PCT in the present design as compared with the current PWR.

Figure 10 shows that the maximum pressure at the pressurizer during the station blackout ATWS was 18.7MPa, which is lower than the licensing limit of 20.6MPa.

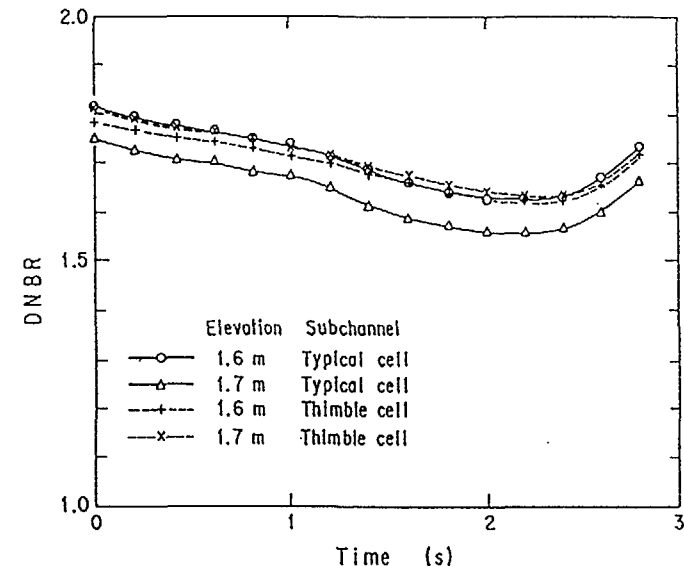


Fig.6 DNBR analysis results for pump trip accident.

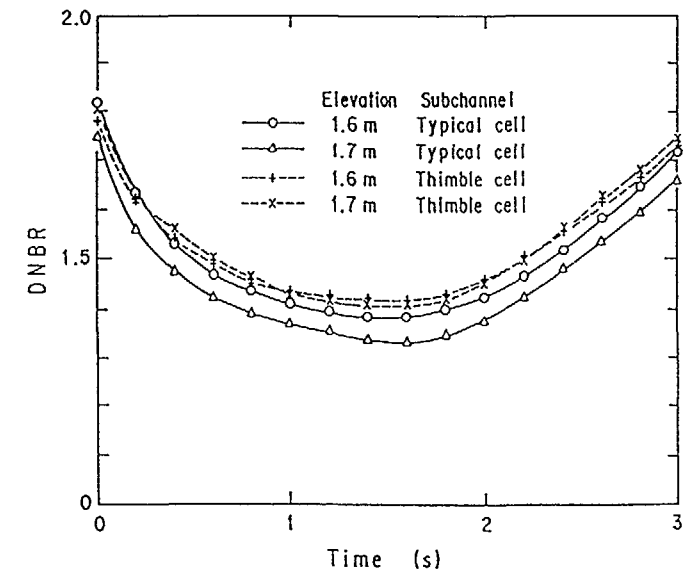
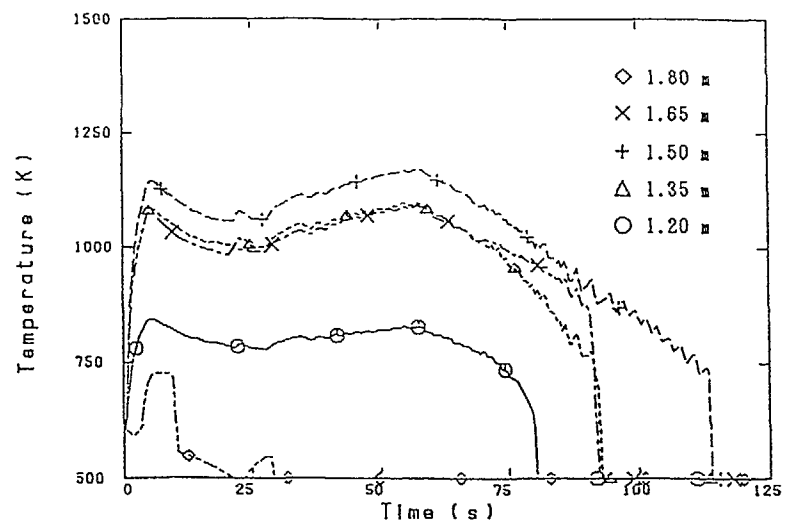
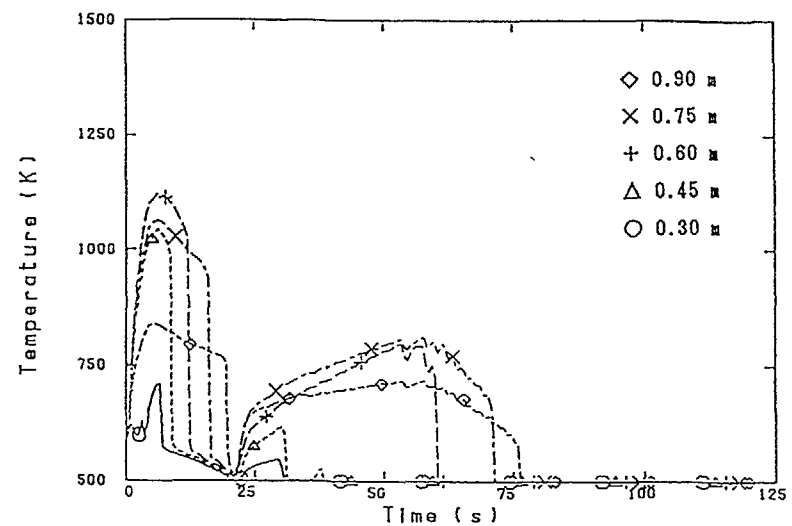


Fig.7 DNBR analysis results for locked rotor accident.

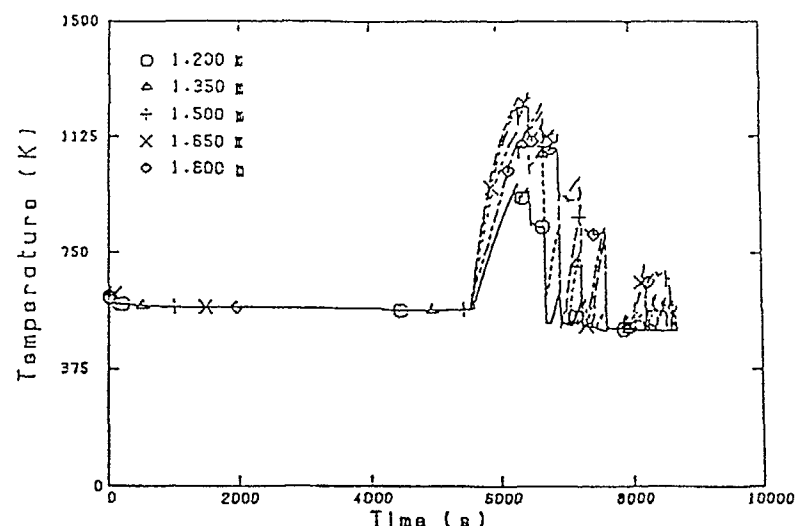


(a) Upper-core

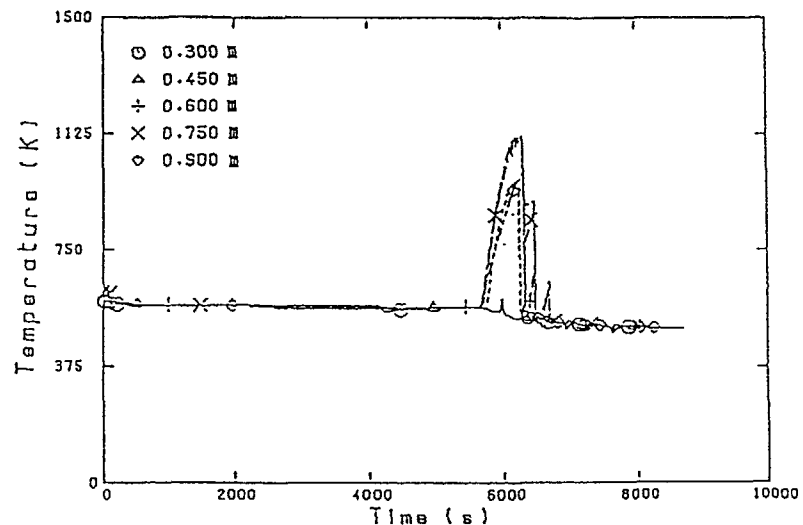


(b) Lower-core

Fig.8 Cladding temperatures during large break LOCA.



(a) Upper-core



(b) Lower-core

Fig.9 Cladding temperatures during small break LOCA.

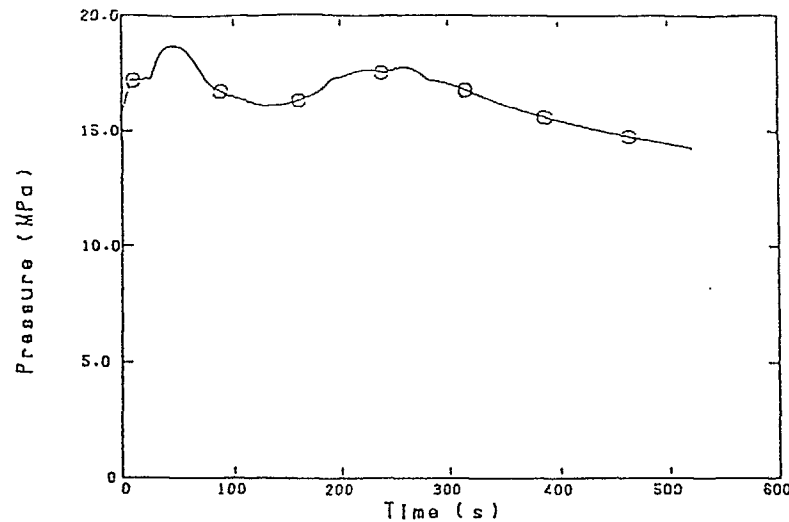


Fig.10 Pressure at pressurizer during station blackout ATWS.

#### V. Effect of HCLWR Installation on Long-Term Fuel Cycle

##### V.1 Methodology and Assumptions

The power reactor strategy and nuclear fuel cycle optimizer JALTES-III<sup>(16)</sup> has been used for the evaluation of HCLWR installation in a long-term nuclear power system. This optimizer can decide the optimal configuration of nuclear power capacity with linear programming method, where a discounted system cost or a cumulative natural uranium requirement is utilized as an objective function.

The time period studied in this analysis covers 130 years starting from 1970 to 2100. The nuclear power capacity over this time period is assumed to be 53.3GWe in 2000, 107GWe in 2030, which are based on the utility long-term plan. Beyond 2030, an additional 1GWe/year is assumed and total capacity reaches to 177GWe in 2100.

Only LWR, HCLWR, and LMFBR(liquid metal cooled fast breeder reactor) are considered in this study. The LWR is assumed introduceable in whole time period without imposing any capacity constrain, while their cores are swit-

ched to more advanced one (A-LWR) from 1995. For LMFBR, its commercial operation is assumed to start in 2030, and its capacity growth is limited within 1GWe/year for initial five years after its introduction.

Three types of HCLWR are considered as references. The first type, HCR-1, which has been designed at JAERI, employs the HCLWR-J2S core<sup>(17)</sup> which takes rather lower fissile plutonium inventory and attain higher fuel burnup but lower conversion ratio. The second type, HCR-2, employs the HCLWR-JDF1 core designed also at JAERI, which takes rather higher fissile plutonium inventory. The third type, HCR-U, is not fuelled by plutonium but by enriched uranium. The purpose of introducing this type of HCLWR is to make the reactor power system respond flexibly to plutonium fuel balance through switching to HCR-U from HCR-1 and/or HCR-2 in case of plutonium shortage.

Assumptions made on fuel cycle processes as well as on cost parameters are summarized in Table 3, where natural uranium price is assumed to be

Table 3. Assumption on Fuel Cycle Processes and Cost Parameters

| Lead time and lagged time                |   | Process loss               |                                |
|--|---|----------------------------|--------------------------------|
| Uranium procurement→Uranium enrichment   | 0yr                                     | Uranium enrichment         | 2.0%                           |
| Uranium enrichment →Fuel fabrication     | 1                                       | Fuel fabrication           | 1.5%                           |
| Fuel fabrication →Reactor in-loading     | 1                                       | Reprocessing               | 2.0%                           |
| <sup>235</sup> U concentration           |   |                            |                                |
| Reactor off-loading→Reactor re-loading   | 4                                       | Natural uranium            | 0.711%                         |
| Reactor off-loading→Spent fuel reprocess | 2                                       | Tail assay                 | 0.250%                         |
| Economic parameters                      |   |                            |                                |
| 1) Long-term discount rate :             | 6%/yr.                                  | 2) Natural uranium price : | 1% increase from 1990          |
| 3) Separative work price :               | 130\$/kgSWU in 1985, 70\$/kgSWU in 2000 | 4) Reactor related cost :  | ↓ (ratio to LWR)               |
| Reactor type                             | Capital cost                            | O&M cost                   | Fuel fabri.cost                |
| FBR                                      | 1.20                                    | 1.07                       | MOX 8.0<br>UO <sub>2</sub> 1.0 |
| HCLWR                                    | 1.05                                    | 1.00                       | MOX 3.0<br>UO <sub>2</sub> 1.0 |

deflated by 1% per year from 1990 in the reference case and by 2% for a sensitivity analysis. The cost ratio of FBR capital cost to that of LWR is assumed 1.2 and for HCLWR it is assumed 1.05.

## W.2 Analytical Results and Discussion

Analytical results are categorized as the following four groups; the first group denoted by case 1 is the case where only LWRs are installed, the second group being the combined system of LWRs and FBRs denoted by case 2A and 2B, the third group consisting of LWRs and HCLWRs indicated by case 31 and 32, and the fourth group of the combined system of LWRs, HCLWRs, and FBRs. The last group is further divided into two cases 41A and 41B or cases 42A and 42B depending on whether the HCLWRs are the type HCR-1 or HCR-2. For each of the above cases, the system optimization is made from

the viewpoint of cumulative natural uranium minimization or discounted system cost minimization. Main results are summarized in Table 4.

### (i) LWR-FBR System(Case 2A and 2B)

The FBRs can be introduced from the year assigned technically feasible, i.e., 2030 for the case 2A and 2050 for the case 2B in the case of minimizing natural uranium consumption. As plutonium becomes insufficient in the case 2A, A-LWRs are additionally installed even after the introduction of FBR. For the case 2B, there is no additional installation of LWRs after FBR introduction and no plutonium shortage happens. The cumulative natural uranium requirement of the case 2A is 0.91Mton and of the case 2B 1.30Mton, which results in 58% and 40% reduction, respectively, compared with the case LWR installation only, as shown in Fig.11. The separative works are much reduced by the magnitude of 0.012Mton/year (2028) in the case 2A and 0.014Mton/year (2052).

Table 4. Fuel Cycle Activities in the Case of Natural Uranium Minimization

| Case   | Index<br>Reactor configuration<br>FBR introduction timing | 1<br>L<br>-                               | 2A<br>L - F<br>2030                            | 2B<br>L - F<br>2050                            | 31<br>L - H<br>-                                    | 32<br>L - H<br>-                             | 41A<br>L - F - H<br>2030                          | 41B<br>L - F - H<br>2050                                 | 42A<br>L - F - II<br>2030                              | 42B<br>L - F - II<br>2050                              |
|--|---|---|--|--|---|--|---|--|--|--|
| Cumulative capacity<br>(GWe)   | LWR<br>FBR<br>HCLWR(Pu)<br>HCLWR(Pu/U)                    | 418.1<br>-<br>-<br>-                      | 147.7<br>270.4<br>-<br>-                       | 208.1<br>210.0<br>-<br>-                       | 318.1<br>-<br>102.0<br>-                            | 327.6<br>-<br>90.5<br>-                      | 106.3<br>254.9<br>20.5<br>36.2                    | 143.5<br>175.8<br>45.7<br>53.0                           | 114.5<br>240.8<br>35.1<br>27.6                         | 161.1<br>195.5<br>31.3<br>30.1                         |
| Cumulative system cost<br>(10 <sup>8</sup> \$)                               | Discounted<br>Nondiscounted                               | 108.73<br>2,559.57                        | 108.67<br>2,505.91                             | 108.77<br>2,504.97                             | 108.69<br>2,522.52                                  | 108.98<br>2,547.74                           | 109.15<br>2,520.03                                | 108.85<br>2,519.93                                       | 109.18<br>2,521.92                                     | 108.94<br>2,524.18                                     |
| Natural uranium requirement<br>(10 <sup>4</sup> ton,10 <sup>3</sup> ton/yr.) | Cumulative<br>Yearly maximum(year)                        | 2.18<br>29.3(2100)                        | 0.91<br>17.4(2025)                             | 1.29<br>20.2(2047)                             | 1.66<br>21.6(2084)                                  | 1.71<br>22.0(2097)                           | 0.82<br>17.5(2025)                                | 1.10<br>20.2(2047)                                       | 0.84<br>17.1(2028)                                     | 1.12<br>16.8(2028)                                     |
| Separative work<br>(10 <sup>4</sup> tonSWU,10 <sup>3</sup> tonSWU/yr.)       | Cumulative<br>Yearly maximum(year)                        | 1.53<br>20.4(2097)                        | 0.65<br>12.0(2028)                             | 0.92<br>14.3(2052)                             | 1.17<br>15.2(2100)                                  | 1.20<br>15.2(2100)                           | 0.58<br>11.4(2025)                                | 0.78<br>13.1(2047)                                       | 0.59<br>11.3(2028)                                     | 0.80<br>12.6(2047)                                     |
| Reprocessing requirement<br>(ton/yr.)  | LWR<br>FBR<br>HCLWR(Pu)<br>HCLWR(Pu/U)                    | 3,556(2100)<br>- (- )<br>- (- )<br>- (- ) | 2,074(2027)<br>2,449(2100)<br>- (- )<br>- (- ) | 2,524(2056)<br>2,450(2100)<br>- (- )<br>- (- ) | 2,636(2098)<br>1,684(2100)<br>1,598(2086)<br>- (- ) | 2,749(2100)<br>- (- )<br>404(2081)<br>- (- ) | 1,659(2020)<br>2,258(2100)<br>568(2088)<br>- (- ) | 2,074(2074)<br>2,237(2100)<br>1,030(2099)<br>1,510(2060) | 1,755(2021)<br>2,048(2096)<br>687(2076)<br>2,000(2071) | 2,004(2027)<br>2,410(2100)<br>687(2076)<br>1,352(2061) |
| Fissile plutonium build up<br>(ton)  | 2050<br>2100<br>Maximum(year)                             | 628<br>1,562<br>1,562(2100)               | 281<br>363<br>363(2100)                        | 619<br>312<br>646(2053)                        | 0<br>8<br>104(2012)                                 | 0<br>0<br>66(1998)                           | 179<br>171<br>220(2033)                           | 219<br>34<br>320(2053)                                   | 171<br>64<br>234(2033)                                 | 171<br>17<br>267(2053)                                 |

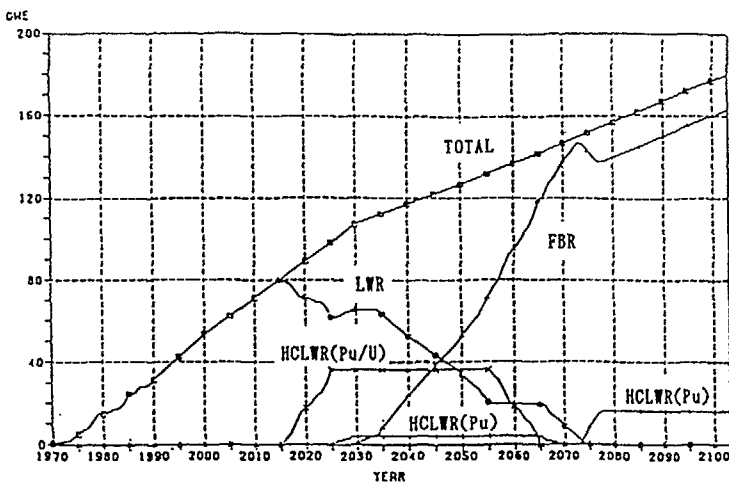


Fig.11 Capacity configuration in the case of natural uranium minimization.

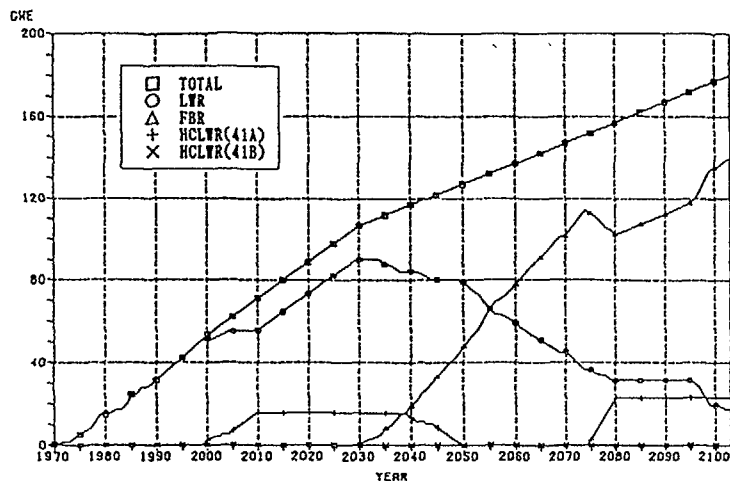


Fig.12 Capacity configuration in the case of discounted system cost minimization (2%/yr increase of natural uranium price).

For the case of minimizing discounted system cost, the FBR introduction delays 30 years later than the technically feasible timing, and its initial introduction is 2061 for the case 2A and 2B. Because of the late FBR introduction, the cumulative natural uranium requirement increases to the level 1.51Mton, which is a 30% reduction from the case 1.

#### (ii) LWR-HCLWR-FBR

The HCLWR(Pu/U)(of which the fuel is switched to  $\text{UO}_2$  in 2026) is introduced in 2016 instead of its technically feasible timing 2000, and the HCLWR(Pu)(Pu utilization in whole life time) in 2026 in the case 41A of minimizing cumulative natural uranium requirement as shown in Fig.11. Those HCLWRs continue their installation till 2070 when plutonium surplus becomes zero. As plutonium balance is loosened, the HCLWR(Pu) is installed again. The case 41B takes also the same pattern of installation as the case 41A except for 20 years late introduction of the HCLWRs.

Cumulative natural uranium requirement, as shown in Fig. 11, is 0.83Mton in the case 41A and 1.11Mton in the case 41B, which are by 9% and 15% reduction, respectively, from the case LWR-FBR. Separative work is also reduced a little, but the requirements of fuel fabrication as well as of spent fuel reprocessing somewhat increase because of rather higher specific inventory of the HCLWRs.

In the case of minimizing discounted system cost, no FBR is allowed to be introduced in the system for both the cases 41A and 41B. The reason why such results are obtained is due to the fact that FBRs can serve as cost saving through excess plutonium utilization in the cases 2A and 2B, instead of using high price natural uranium in LWRs, while the HCLWRs can serve the same role as FBRs in the cases 41A and 41B owing to its low capital cost. As a sensitivity analysis, we analyze the effect of natural uranium price increase in the case 41A. Even under the minimization of discounted system cost, the HCLWR(Pu) can be introduced from its technically feasible year 2000, as shown in Fig.13, and it can coexist with FBR after the FBR introduction, complementing the economical disadvantage of FBR. Cumulative natural uranium requirement of this case is in the level of 1Mton, which is of course a little higher than the case 41A of minimizing natural uranium.

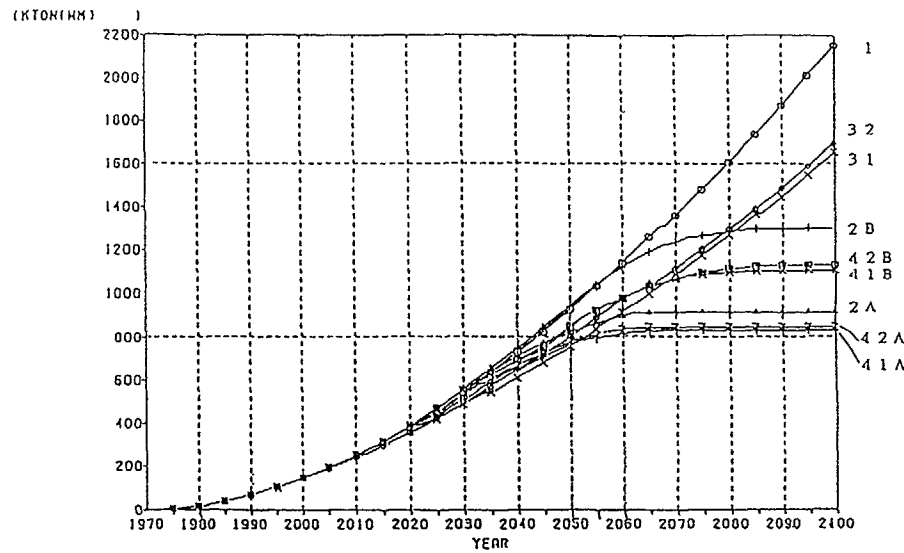


Fig.13 Cumulative natural uranium requirement in the case of natural uranium minimization.

#### V. Conclusions

A new concept of a double-flat-core HCLWR was proposed and the feasibility study has been performed with respect to its neutron physics aspects. A three-dimensional core burnup calculation was carried out to grasp detailed core characteristics of such an HCLWR.

As a result, it was shown that considerably high burnup and high conversion ratio were obtainable while maintaining a negative void coefficient and also that chemical shim using soluble boron was effective for the excess reactivity control. The design of the double-flat-core HCLWR is feasible from a thermal hydraulic point of view.

From the studies made on the long term fuel cycle adopting the HCLWRs, we can conclude the followings: (1) The HCLWR can contribute not only to the saving of natural uranium consumption but also to the improvement of nuclear power economy in the long-term, especially in the system of FBR installation. (2) To enhance the proper characteristics of the HCLWR above stated, its fissile plutonium inventory must be furthermore lowered.

#### References

- (1) Edlund,M.C.: *Trans.Am.Nucl.Soc.*, 24, 508 (1976).
- (2) Okumura,K., Ishiguro,Y., Doi,E.: *JAERI-M* 88-129, (in Japanese) (1988).
- (3) Okumura,K., Nishina,K.: *Nucl.Sci.Eng.*, 102, 381 (1988).
- (4) Oldekop,W., et al.: *Nucl.Technol.*, 59, 212 (1982).
- (5) Ishiguro,Y., Okumura,K.: *ibid.*, 84, 331 (1989).
- (6) Okumura,K., Ishiguro,Y., Akie,H.: *Proc. Int.Conf. on the Physics of Reactors: Operation, Design and Computation*, Marseille (1990).
- (7) Sugimoto,J., et al.: *JAERI-M* 89-002 (1989).
- (8) Iwamura,K., et al.: *JAERI-M* 89-004, (in Japanese) (1989).
- (9) Tsuchihashi,K., et al.: *JAERI-1302*, (1986).
- (10) Fowler,T.B., Vondy,D.R., Cunningham,G.W.: *ORNL-TM-2496*, (1969).
- (11) Engle Jr.,W.W.: A User Manual for ANISN, A One Dimensional Discrete Ordinates Transport Code with Anisotropic Scattering. K-1693, Oak Ridge National Laboratory, (1967).
- (12) Dalle Donne,M. et al.: *Nucl.Technol.*, 71,111 (1985).
- (13) Wheeler,C.L., et al.: COBRA-IV-I : An Interim Version of COBRA for Thermal-Hydraulic Analysis of Rod Bundle Nuclear Fuel Elements and Cores, BNWL-1962 (1976).
- (14) Rehme,K.: *Nucl.Technol.*, 17, 15 (1973).
- (15) Murao,Y.: *JAERI-M* 83-032, (in Japanese) (1983).
- (16) Yasukawa,S., Sato,O.: Optimization Program JALTES-II for Long-Term Fuel Cycle Analysis. The Report to the Nuclear Material Control Center of Japan, (1986).
- (17) Okumura,K., et al.: to be published in *JAERI-M*

## IMPROVED FUEL UTILIZATION WITH A SLIGHTLY ENRICHED SPECTRAL SHIFT REACTOR

J.C. LEE, W.R. MARTIN

Department of Nuclear Engineering,

University of Michigan,

Ann Arbor, Michigan

M.C. EDLUND

Department of Mechanical Engineering,

Virginia Polytechnic Institute and

State University,

Blacksburg, Virginia

United States of America

### Abstract

The slightly-enriched spectral shift reactor (SESSR) utilizes conventional light water reactor fuel arranged in a moderately-tight lattice with spectral shift control rods (SSCRs) which displace water when inserted. The SSCRs are inserted in the beginning of the cycle, hardening the spectrum and increasing the production of fissile plutonium. The SSCRs are withdrawn later in the cycle, softening the spectrum and depleting the plutonium. Recycling of plutonium is not necessary, avoiding difficulties such as a tendency for a positive moderator temperature coefficient of reactivity and regulatory concerns associated with plutonium recycle in the United States. Preliminary fuel cycle calculations, including equilibrium core analyses, have shown that the use of spectral shift control can result in ~ 15-25% increases in fuel cycle length. This *spectral shift advantage* tends to decrease with tighter lattices, leading to the conclusion a hexagonal lattice may not be necessary to achieve satisfactory fuel cycle performance.

### INTRODUCTION

An advanced converter reactor (ACR) utilizing an open fuel cycle with slightly-enriched uranium fuel (~ 1.5 - 3.5 w/o) in a conventional pressurized water reactor (PWR) configuration is investigated. The SESSR uses a semi-tight lattice with inert mechanical SSCRs which displace water to enhance production of fissile plutonium in a relatively hard spectrum early in the cycle. The plutonium is then burned *in situ* in a soft spectrum later in the cycle, when the SSCRs are withdrawn. Most of the recent ACR designs<sup>1,2</sup> use high fissile loading (6-8 w/o) in closed fuel cycles, resulting in significant perturbations to PWR characteristics. We present preliminary nuclear and thermal-hydraulic calculations which indicate the SESSR offers the benefits of substantially increased fuel cycle lengths and increased uranium utilization, while

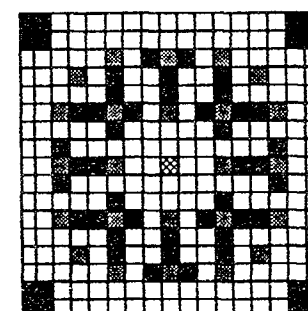
retaining the proven safety characteristics of PWR technology. We present a brief description of the methods used for neutronic and thermal-hydraulic analysis of the SESSR designs as well as results of our calculations for a range of SESSR designs and comparisons with a typical PWR design. In addition, a preliminary comparison is made between the SESSR and an ACR lattice with recycled plutonium, with plutonium loadings in the range ~ 6-8%.

### ANALYSIS METHODS

The CPM-2 assembly collision probability code<sup>3</sup> generates few-group macroscopic cross sections, which are used in global neutronic calculations with a modified version of the 2DB diffusion-depletion code.<sup>4</sup> Batch core and equilibrium core fuel cycle analyses are performed with a simple cycling model. Steady-state, single-channel thermal-hydraulic analyses are performed to obtain pressure drops, flow rates, temperature drops, and other parameters. A later section discusses our efforts to verify the applicability of the neutronics methods for SESSR configurations.

### REFERENCE SESSR DESIGN

Our preliminary SESSR design is based on a typical PWR (17x17) assembly design but with a relatively tighter lattice spacing and SSCRs in many of the lattice locations. The tighter lattice results in a high fuel-to-moderator volume ratio (F/M) when SSCRs are inserted and, for our reference design, a F/M equivalent to a typical PWR when the SSCRs are withdrawn. Specifically, the pitch and number of SSCRs for the reference design were determined on the basis that the end-of-cycle (EOC) F/M, after the SSCRs are withdrawn, was the same as a typical PWR case (~0.54). Therefore, the F/M for the reference SESSR (11.20 mm pitch) ranges from 0.81 at beginning-of-cycle (BOC) (with SSCRs inserted) to 0.54 at EOC (SSCRs withdrawn). Figure 1 illustrates the reference SESSR assembly configuration that is being examined and Table I contains core parameters for the reference SESSR design as well as parameters for two typical PWR configurations<sup>5,6</sup> that have been used for comparison with the SESSR designs in this paper.



- Fuel Rod
- Spectral Shift Control Rod (SSCR)
- Control Rod (CR) or SSCR
- Instrument Tube

#### Assembly Dimensions (mm)

|                         |        |
|-------------------------|--------|
| Fuel Radius             | 4.102  |
| Clad Inner Radius       | 4.178  |
| Clad Outer Radius       | 4.750  |
| Pin Cell Pitch          | 11.201 |
| Guide Tube Inner Radius | 5.169  |
| Guide Tube Outer Radius | 5.601  |

Spectral Shift Assembly: 208 Fuel Rods, 80 SSCRs

Control Assembly: 208 Fuel Rods, 56 SSCRs, 24 CRs

#### Fuel to Moderator Ratio

|                          |       |
|--------------------------|-------|
| Spectral Shift Assembly: |       |
| SSCRs In                 | 0.812 |
| SSCRs Out                | 0.540 |
| Control Assembly:        | 0.707 |

Figure 1. 17x17 SESSR Reference Assembly

An SESSR assembly can be used as either a spectral shift control (SSC) assembly, with 80 SSCRs connected to a spider assembly, or as a control assembly, with 24 control rods connected to a spider assembly and 56 SSCRs not connected. The core consists of 269 assemblies in a three-enrichment (1.5, 2.0, and 2.5 w/o  $^{235}\text{U}$ ) pattern with ~1/3 being control assemblies.

Preliminary BOC core calculations yield a critical soluble boron concentration of 1130 ppm with boron worth of 9 pcm/ppm ( $1 \text{ pcm} = 10^{-5} \Delta k/k$ ) and a moderator temperature coefficient (MTC) of -18 pcm/K, all at hot zero power (HZP). To accommodate the tight lattice spacing, coolant flow rate and inlet temperature are reduced to 13.9 Mg/s and 562 K, respectively, from 18.9 Mg/s and 573 K for Bellefonte. This yields a core pressure drop of 0.13 MPa and core average temperature rise of 44 K for the SESSR compared to 0.12 MPa and 31 K for Bellefonte. As expected, the tighter lattice results in an increased pressure drop and moderator temperature rise in order to attain the same power rating.

Table I. Selected Core Parameters

|                           | SESSR | Millstone-3 | Bellefonte |
|---------------------------|-------|-------------|------------|
| <b>Active Core</b>        |       |             |            |
| Diameter (m)              | 3.59  | 3.37        | 3.52       |
| Height (m)                | 3.66  | 3.66        | 3.63       |
| <b>Fuel Assembly</b>      |       |             |            |
| Number in core            | 269   | 193         | 205        |
| Rod Array                 | 17x17 | 17x17       | 17x17      |
| Rods/Assembly             | 208   | 264         | 264        |
| Rod Pitch (mm)            | 11.20 | 12.60       | 12.75      |
| Assembly Pitch (mm)       | 191.4 | 214.0       | 216.8      |
| CR/SSCR Tube ID (mm)      | 10.34 | 11.43       | 10.92      |
| CR/SSCR Tube OD (mm)      | 11.20 | 12.24       | 11.81      |
| Number of SSCR/CR         | 80    | 24          | 24         |
| 56/24                     |       |             |            |
| Fuel Rods in Core         | 55952 | 50952       | 54120      |
| <b>Enrichment (w/o)</b>   |       |             |            |
| Region 1                  | 1.5   | 2.4         |            |
| Region 2                  | 2.0   | 2.9         |            |
| Region 3                  | 2.5   | 3.4         | average    |
| <b>Thermal-Hydraulics</b> |       |             |            |
| Core Thermal Power (MWt)  | 3618  | 3411        | 3618       |
| Linear Heat Rate (kW/m)   | 17.7  | 17.8        | 18.3       |
| System Pressure (MPa)     | 15.51 | 15.51       | 15.51      |
| Coolant Flow Rate (Mg/s)  | 13.86 | 17.64       | 18.90      |
| Inlet Temperature (K)     | 562   | 565         | 573        |
| Core Temperature Rise (K) | 44    | 35          | 31         |
| Core Pressure Drop (MPa)  | 0.13  | 0.17        | 0.12       |

In the current design, relatively high radial peaking factors may accompany SSCR withdrawal. When SSCRs are withdrawn from assemblies, the positive reactivity introduced by local spectrum softening can cause significant increases in the overall radial peaking factor. The magnitude of this increase depends on the arrangement of SSCRs within assemblies, on the position of the assembly in the core, and on the amount of time the SSCRs have been inserted. This sensitivity of the radial power distribution to SSCR withdrawal sequence indicates the need for an optimal SSCR management strategy. Initial parametric studies have

shown that intra-assembly radial power peaking can be substantially reduced using a more optimum SSCR arrangement than that shown in Figure 1. Further optimization of intra-assembly and global radial power distributions will be the subject of future studies.

## FUEL CYCLE CALCULATIONS

### Batch Core Analyses

Figure 2 shows the burnup-dependent reactivity and principal fissile nuclide inventory for a 2.5 w/o reference SESSR assembly. The curves representing SSCRs withdrawn at BOC, with a F/M of 0.54, closely approximate a conventional PWR assembly of the same enrichment (with no burnable poison rods). The difference  $\Delta k$  between the  $k_{\infty}$  curves in Figure 2, with SSCRs inserted and withdrawn at various burnups, is an approximate measure of the SSC advantage over a typical PWR. With SSCRs inserted, the  $^{235}\text{U}$  depletion rate is slightly decreased and the  $^{239}\text{Pu}$  production rate is substantially increased due to the hardened spectrum. This results in an increased cycle length compared to a conventional PWR by 15 - 25%, depending on enrichment and choice of BOC and EOC F/Ms, as discussed in more detail in the following sections.

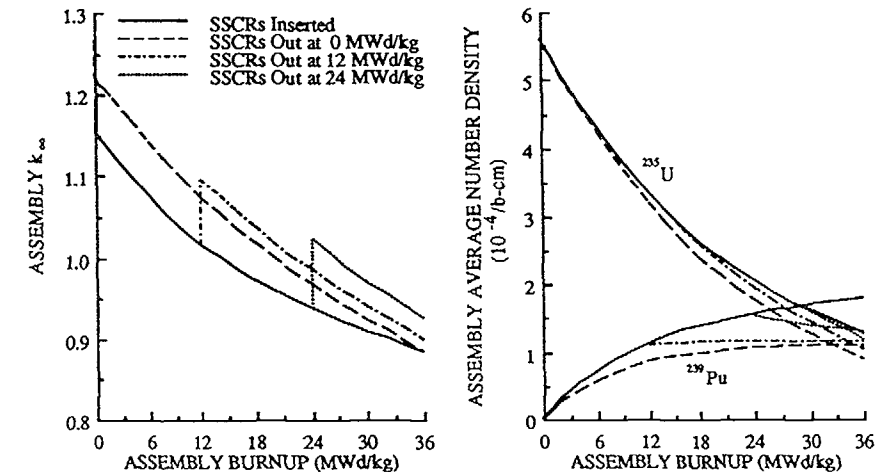


Figure 2. Assembly  $k_{\infty}$  and Fissile Nuclide Inventory versus Assembly Burnup for a 2.5 w/o Spectral Shift Assembly

The CYCLE code was developed to estimate the SESSR cycle length from  $k_{\infty}$  curves such as those illustrated in Figure 2. The CYCLE code applies a fraction of the burnup-dependent SSC  $\Delta k$  as needed to maintain  $k_{\infty}$  above a given cutoff point, which was chosen as 1.020 for all of the work described here. This approximates the reactivity behavior of a reactor, where the SSCRs are withdrawn from only a few assemblies at a given time. A batch-core cycle length of ~21.1 MWd/kg is obtained for our SESSR design which compares with ~17.8 MWd/kg obtained from the curve with SSCRs withdrawn at BOC, an approximation to a typical PWR. This corresponds to an increase of 18.5% in cycle length. Equilibrium cores show a slightly lower percentage increase. To demonstrate the predictive ability of CYCLE, a

comparison between depletion results from the CYCLE code and explicit burnup calculations performed using the CPM-2 code is given in Figure 3, which shows reasonable agreement between the two codes.

The fuel cycle analyses demonstrate an interesting tradeoff between the objective to harden the spectrum through SSCR insertion and the need to maintain criticality through SSCR withdrawal. The SSCRs represent a source of positive reactivity and are withdrawn to balance the negative reactivity due to fuel depletion. On the other hand, production of plutonium is maximized with the SSCRs inserted, therefore the longer one can refrain from withdrawing the SSCRs, the greater the cycle length for a given core/SSCR configuration. The need to maintain a critical reactor may, however, force the withdrawal of SSCRs early in the cycle offsetting some of the potential advantages of the SESSR.

Batch core fuel cycle calculations were performed for several SESSR assembly configurations to examine the effect on cycle length due to changes in enrichment, number of SSCRs, F/M ratio and fuel pin diameter, and effect of burnable poison. These results are discussed in the following paragraphs.

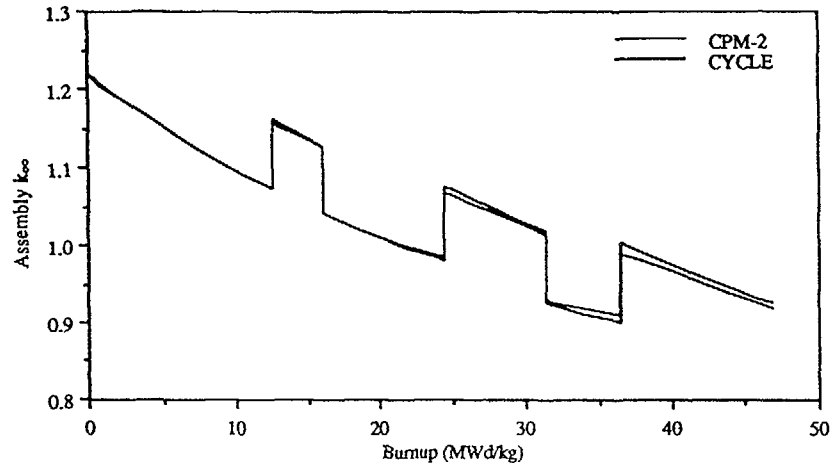


Figure 3. Comparison of CPM-2 and CYCLE Depletion Results for Equilibrium SESSR Cycle with 3.5 w/o Feed

**Effect of Enrichment:** Table II summarizes the results of analyses of several different enrichments for the reference SESSR assembly design (11.20 mm pitch, 80 SSCRs). The cycle length comparisons in Table II include percentage increases in cycle length for each fuel design for SSCRs "in" versus SSCRs "out". This may be viewed as the *spectral shift advantage* for a specific fuel design. The percentage increases in cycle length for each case versus a typical PWR assembly<sup>6</sup> are also tabulated. Finally, the energy extracted per kg of uranium mined is also tabulated to show the effect of the spectral shift designs on uranium utilization. The following comments pertain to the results tabulated in Table II:

(1) For the reference SESSR design, the cycle lengths are typically increased by 15-22%, relative to the reference PWR, through the use of spectral shift control for a wide range of enrichments (1.5 - 3.5 w/o). The spectral shift advantage is fairly insensitive to enrichment. A

slight decrease is noted with increasing enrichment. This occurs because high enrichment assemblies already have a relatively hard spectrum compared with lower enrichment assemblies. Thus, the relative effect of withdrawing SSCRs in a high enrichment assembly is less than in a low enrichment assembly. This tends to offset the longer SSCR insertion time possible in high enrichment assemblies.

(2) There is a steady trend to increase uranium utilization with increasing enrichment, although the effect appears to be levelling off even at 3.5 w/o fuel. Thus, both increased cycle lengths and increased uranium utilization are obtained with higher enrichment fuel, although of course there will be increased costs associated with enriching services, which have not been evaluated to date.

Table II. Effect of Enrichment on Cycle Length and Fuel Utilization  
(Pin Cell Pitch = 11.20 mm, 80 SSCRs, F/M = 0.81 to 0.54)

| Enrichment<br>(w/o $^{235}\text{U}$ ) | Cycle Length (MWd/kg U) |       |                    | % Increase<br>Due to<br>Spectral<br>Shift | % Increase<br>Relative to<br>Reference<br>PWR |
|---------------------------------------|-------------------------|-------|--------------------|---|---|
|                                       | Reference<br>PWR        | SESSR | SESSR<br>SSCRs Out |   |   |
| 1.5                                   | 6.4                     | 7.8   | 6.7                | 16.4                                      | 21.9  |
| 2.0                                   | 12.4                    | 15.1  | 12.6               | 19.8                                      | 21.8  |
| 2.5                                   | 17.8                    | 21.1  | 17.8               | 18.5                                      | 18.5  |
| 3.0                                   | 22.7                    | 26.5  | 22.6               | 17.3                                      | 16.7  |
| 3.5                                   | 27.3                    | 31.6  | 27.1               | 16.6                                      | 15.8  |

| Enrichment<br>(w/o $^{235}\text{U}$ ) | Fuel Utilization (MWd/kg U mined) |       |                    | % Increase<br>Due to<br>Spectral<br>Shift | % Increase<br>Relative to<br>3.0 w/o<br>PWR* |
|---------------------------------------|-----------------------------------|-------|--------------------|---|--|
|                                       | Reference<br>PWR                  | SESSR | SESSR<br>SSCRs Out |   |  |
| 1.5                                   | 2.46                              | 3.00  | 2.58               | 16.4                                      | -31.3  |
| 2.0                                   | 3.44                              | 4.19  | 3.50               | 19.8                                      | -0.3   |
| 2.5                                   | 3.87                              | 4.59  | 3.87               | 18.5                                      | 11.5   |
| 3.0                                   | 4.05*                             | 4.73  | 4.04               | 17.3                                      | 16.7   |
| 3.5                                   | 4.14                              | 4.79  | 4.11               | 16.6                                      | 19.3   |

**Effect of Fuel to Moderator Ratio:** Preliminary parametric studies were performed using various 2.5 w/o SESSR assemblies with the same fuel rod design. The primary parameters were BOC F/M and EOC F/M. The desired F/Ms determine the number of SSCRs and pin cell pitch. The SSCR guide tubes are assumed to have an outer diameter equal to the pitch. A simple thermal-hydraulic analysis was performed to obtain the assembly pressure drop and fuel rod power density, assuming a constant total core flow rate and height. Depletion analyses were performed using the CPM-2 code and the results transmitted to the CYCLE code, which was used to determine the batch cycle length. Equilibrium cycle lengths were determined for a few configurations, which are discussed in the next section. A large number of different combinations of BOC and EOC F/Ms were analyzed and the results are tabulated in Table III and shown graphically in a contour plot in Figure 4. The contour lines on this plot represent contours of equal cycle length increase. The other lines are constant BOC  $k_{\infty}$  and assembly pressure drop lines. The points represent the cases in Table III. When examining Figure 4, it should be kept in mind that the neutronic parameters held constant for these cases were fuel rod

diameter and enrichment, hence as shown in Table III, the number of fuel rods is changing as well as the pitch and number of SSCRs. The following observations are made regarding the results in Table III and Figure 4.

(1) Our reference design point (Case 5 in Table III) yields 21.1 MWd/kgU with a spectral shift advantage of 18.5%. Keeping the EOC F/M the same and changing the BOC F/M (by increasing the number of SSCRs, Cases 1 and 2) results in essentially no change in the spectral shift advantage. This is seen graphically in Figure 4 where the contours level out in this region of the parameter space.

(2) The spectral shift advantage increases as one moves vertically down the contour plot from our reference design point, but the pressure drop also increases quickly, which poses thermal-hydraulic and safety concerns. However, if one moves down and to the left, following an "isobar" (in pressure drop), the spectral shift advantage increases by nearly 34%, but the corresponding increase in cycle length is only 8%, due to the poor cycle length for these lattices with the SSCRs withdrawn. However, a 8% increase in cycle length is not negligible and these configurations will be examined in more detail. One disadvantage to this change is that the number of fuel rods decreases as one moves down the isobars, resulting in an increase in the linear power density. Another potential disadvantage is the increased BOC  $k_{\infty}$ . This must be compensated for by using increased soluble boron or perhaps reactivity shims. These issues are currently under investigation.

**Use of Mixed Oxide Fuels:** Two SESSR designs using mixed plutonium-uranium oxide (MOX) fuel were investigated. The MOX designs used an initial plutonium concentration of 6.0 w/o total plutonium in the total fuel heavy metal (HM) content. The initial plutonium

Table III. Effect of Fuel to Moderator Ratios on Cycle Length for 2.5 w/o Assemblies

| Case | Fuel to Moderator Ratio |                       | Number of SSCRs | Pin Cell Pitch (mm) | Pressure Drop (MPa) | Number of Fuel Rods in Core | Cycle Length (MWd/kg U) |                 | % Increase Due to Spectral Shift |
|------|-------------------------|-----------------------|-----------------|---------------------|---------------------|-----------------------------|-------------------------|-----------------|----------------------------------|
|      | SSCRs Inserted (BOC)    | SSCRs Withdrawn (EOC) |                 |                     |                     |                             | SESSR                   | SESSR SSCRs Out |                                  |
| 1    | 0.900                   | 0.540                 | 96              | 10.82               | 0.17                | 56256                       | 21.2                    | 17.8            | 19.1                             |
| 2    | 0.850                   | 0.540                 | 88              | 11.02               | 0.14                | 55400                       | 21.2                    | 17.8            | 19.1                             |
| 3    | 0.850                   | 0.495                 | 104             | 10.89               | 0.18                | 50068                       | 22.0                    | 17.9            | 22.9                             |
| 4    | 0.850                   | 0.463                 | 116             | 10.77               | 0.21                | 50396                       | 22.3                    | 17.9            | 24.6                             |
| 5    | 0.812*                  | 0.543*                | 80*             | 11.20*              | 0.11*               | 55952                       | 21.1*                   | 17.8*           | 18.5*                            |
| 6    | 0.813                   | 0.499                 | 96              | 11.07               | 0.14                | 53184                       | 22.0                    | 17.9            | 22.9                             |
| 7    | 0.812                   | 0.457                 | 112             | 10.93               | 0.18                | 48752                       | 22.5                    | 17.9            | 25.7                             |
| 8    | 0.813                   | 0.417                 | 128             | 10.76               | 0.24                | 46880                       | 23.1                    | 18.1            | 27.6                             |
| 9    | 0.700                   | 0.498                 | 72              | 11.68               | 0.08                | 52056                       | 21.5                    | 18.3            | 17.5                             |
| 10   | 0.700                   | 0.460                 | 88              | 10.56               | 0.10                | 49000                       | 22.1                    | 18.2            | 21.4                             |
| 11   | 0.700                   | 0.423                 | 104             | 11.42               | 0.11                | 48024                       | 22.7                    | 18.2            | 24.7                             |
| 12   | 0.580                   | 0.462                 | 52              | 12.43               | 0.05                | 52156                       | 21.1                    | 18.7            | 17.1                             |
| 13   | 0.580                   | 0.422                 | 72              | 12.29               | 0.06                | 47736                       | 21.9                    | 18.7            | 17.1                             |

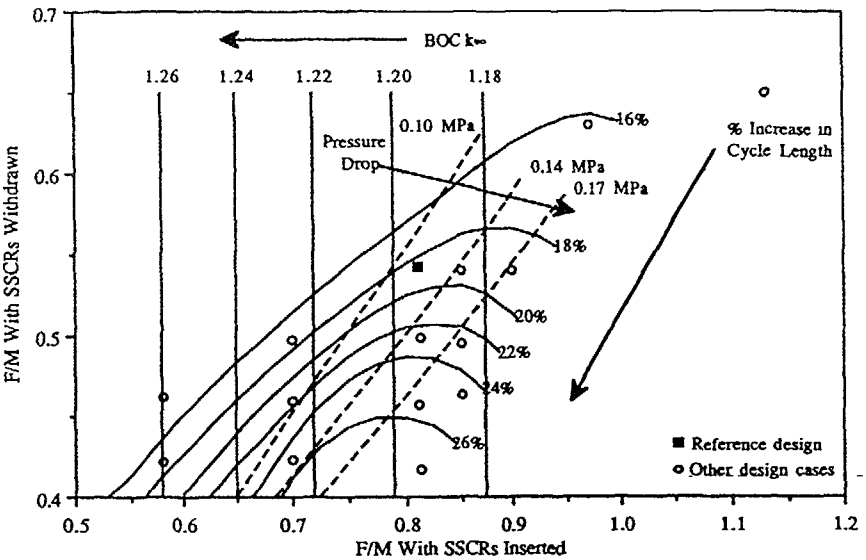


Figure 4. Cycle Length Increase, BOC  $k_{\infty}$ , and Assembly Pressure Drop for Several 2.5 w/o SESSR Assembly Configurations as a Function of F/M.

isotopes were typical of that of discharged conventional light water reactor (LWR) fuel. Table IV summarizes the cycle lengths, spectral shift advantages, fissile inventory ratios and conversion ratios for the two MOX designs and equivalent uranium oxide designs. The conventional uranium oxide designs used 3.5 w/o enriched uranium. The conversion ratios given are the ranges of instantaneous conversion ratios with SSCRs inserted over the first 24 MWd/kg HM burnup. Although the higher F/M cases for both the conventional uranium and the MOX designs show higher conversion and fissile inventory ratios, this is achieved at the expense of decreasing the spectral shift advantage. Because the SESSR utilizes an open fuel cycle, increased cycle length is preferred over a higher conversion ratio.

Table IV. Comparison of Mixed Oxide and Conventional Fuel Designs.

| Fuel to Moderator Ratio | Cycle Length (MWd/kg HM) |                            |           |       |                 | % Increase Due to Spectral Shift | Fissile Inventory Ratio | Conversion Ratio |
|-------------------------|--------------------------|----------------------------|-----------|-------|-----------------|----------------------------------|-------------------------|------------------|
|                         | SSCRs Inserted (BOC)     | SSCRs Withdrawn (EOC)      | Fuel Type | SESSR | SESSR SSCRs Out |                                  |                         |                  |
| 0.812                   | 0.543                    | $\text{UO}_2$              |           | 31.6  | 27.1            | 16.6                             | 0.53                    | 0.56 - 0.75      |
| 1.13                    | 0.65                     | $\text{UO}_2$              |           | 27.3  | 24.0            | 13.8                             | 0.65                    | 0.68 - 0.86      |
| 0.812                   | 0.543                    | $\text{PuO}_2/\text{UO}_2$ |           | 33.2  | 27.6            | 20.2                             | 0.74                    | 0.78 - 0.86      |
| 1.13                    | 0.65                     | $\text{PuO}_2/\text{UO}_2$ |           | 24.9  | 22.1            | 12.5                             | 0.84                    | 0.92 - 0.95      |

**BOC Reactivity Parameters:** Table V summarizes the BOC HZP assembly  $k_{\infty}$ , critical boron concentrations, and MTCs for the reference SESSR design and several alternatives. One SESSR design with burnable poison loaded into the SSCRs was analyzed and the results are included in Table V. The poison loading was chosen to allow it to burn out by EOC and the resultant cycle length was essentially unchanged from the design without burnable poison. Thus, the initial cycle for the SESSR could include poisoned SSCRs to reduce BOC reactivity while maintaining a negative MTC with negligible effect on cycle length. An additional design with thin fuel rods was also analyzed. The number of SSCRs and the pitch were chosen to yield a F/M range comparable to the reference design. The effect was a decrease in cycle length, and there does not appear to be a neutronic advantage for this particular design. The thermal/hydraulic characteristics of this design are also changed. The MOX designs described in the previous section are also analyzed. The results show that the reactivity parameters for the MOX designs remain acceptable for incorporation into an otherwise conventional PWR, although soluble boron enriched in  $^{10}B$  may be required.

Table V. BOC Reactivity Parameters

- Case 1: Pin Cell Pitch = 11.20 mm, Fuel Rod Diameter = 9.50 mm, Unshimmed SSCRs
- Case 2: Pin Cell Pitch = 11.20 mm, Fuel Rod Diameter = 9.50 mm, Shimmed SSCRs
- Case 3: Pin Cell Pitch = 8.36 mm, Fuel Rod Diameter = 7.24 mm, Unshimmed SSCRs
- Case 4: Pin Cell Pitch = 11.20 mm, Fuel Rod Diameter = 9.50 mm, Unshimmed SSCRs
- Case 5: Pin Cell Pitch = 9.91 mm, Fuel Rod Diameter = 9.50 mm, Unshimmed SSCRs

| Case | Fuel Type    | Enrichment<br>(w/o $^{235}U$ or<br>w/o Pu in HM) | No Boron<br>HFP-BOC<br>$k_{\infty}$<br>(SSCR's In) | HZP-BOC<br>Critical Boron<br>Concentration<br>(ppmB) | HZP-BOC<br>MTC<br>(pcm/K) |
|------|--------------|--|--|--|---------------------------|
| 1    | $UO_2$       | 1.5  | 1.0718   | 780  | -11.3                     |
|      |              | 2.0  | 1.1455   | 1760   | -1.7                      |
|      |              | 2.5  | 1.1957   | 2760   | +4.8                      |
|      |              | 3.0  | 1.2322   | 3690   | +9.1                      |
|      |              | 3.5  | 1.2602   | 4550   | +12.7                     |
| 2    | $UO_2$       | 3.5  | 1.0932   | 2160   | -9.1                      |
| 3    | $UO_2$       | 2.0  | 1.1223   | 1540   | -6.7                      |
| 4    | $PuO_2/UO_2$ | 6.0  | 1.0920   | 5180   | -8.5                      |
| 5    | $PuO_2/UO_2$ | 6.0  | 1.0284   | 2730   | -17.3                     |

#### Equilibrium Core Analyses

Equilibrium core analyses have also been performed with the CYCLE code for several of the batch core configurations discussed above. The equilibrium cycle methodology is based on the assumption of equal-power sharing among the three enrichment zones, and a linear dependence of SSC  $\Delta k$  between actual SSCR withdrawal times. Reinsertion of SSCRs is also allowed with this method, which complicates the  $\Delta k$  interpolation procedure due to the fact that the linear interpolation must account for previous SSCR residence time as well as the time for SSCR withdrawal in the current cycle. In our simple cycling study, an effective value of the cumulative SSCR residence time is used to represent SSCR reinsertion effects. Table VI summarizes the equilibrium core cycle lengths for a number of different SESSR designs in addition to the reference design. The ratio of the cycle length of the equilibrium cycle to that of the batch cycle  $\sim 2n/(n+1) = 1.5$  with three enrichment zones, i.e.,  $n=3$ , for both feed enrichments and with or without spectral shifting, is summarized in Table VI. The relative advantage of spectral shifting for the equilibrium cycles is  $\sim 15\%$  and is essentially insensitive to feed enrichment, similar to the observation made for batch cycles in Table II.

Table VI. Equilibrium and Batch Cycle Burnup

(Pin Cell Pitch = 11.20 mm, 80 SSCRs, F/M = 0.81 - 0.54)

| Enrichment<br>(w/o $^{235}U$ ) | Equilibrium Cycle<br>Discharge Burnup<br>(MWd/kg U) |                       | Ratio of Equilibrium<br>Discharge Burnup to<br>Batch Burnup |                       | % Increase<br>Due to<br>Spectral<br>Shift |
|--------------------------------|---|-----------------------|---|-----------------------|---|
|                                | SESSR   | SESSR<br>SSCRs<br>Out | SESSR   | SESSR<br>SSCRs<br>Out |   |
| 2.5                            | 31.7  | 27.5                  | 1.50  | 1.54                  | 15.3                                      |
| 3.5                            | 48.3  | 42.0                  | 1.53  | 1.55                  | 15.0                                      |

#### VERIFICATION OF NEUTRONIC METHODS

The adequacy of thermal spectrum LWR neutronics codes for analysis of harder spectrum tight lattice configurations must be evaluated. We have used the UMLEO and CPM-2 codes for unit-cell and unit-assembly SESSR analyses. UMLEO is a substantially revised version of the LEOPARD infinite medium spectrum code,<sup>7</sup> which performs thermal and fast spectrum calculations for a unit cell with an explicit non-lattice region to accommodate non-unit cell regions (water holes, gaps, etc.) in a fuel assembly. CPM-2 is a transport theory code utilizing collision probability (CP) methods to analyze typical PWR and boiling water reactor (BWR) assemblies. The accuracy of these codes in handling various material heterogeneities (thermal and epithermal) for spectra characteristic of a tight lattice needs to be established.

#### Comparison with the VIM Monte Carlo Code

We have initiated preliminary efforts to compare the UMLEO and CPM-2 codes with the VIM code.<sup>8</sup> VIM is a continuous-energy Monte Carlo code used for neutronic analysis of thermal as well as fast spectrum reactors. The cross section library utilized in VIM is based on ENDF/B Versions 4 and 5. Our VIM calculations typically used 90,000 histories for each case and hence are subject to non-negligible statistical fluctuations, which are noted in the tabulated results. We present in Table VII preliminary comparisons of the infinite multiplication factor  $k_{\infty}$  from the three codes for typical SESSR pin cells and for an idealized 4x4 SESSR assembly shown in Figure 5. The pin cell calculations used an isothermal pin cell at a temperature of 300 K, while the 4x4 lattice calculations used a temperature of 1000 K for the fuel and 300 K for the clad and moderator. Initial comparisons between CPM-2 and VIM yielded marginal results, with differences ranging from 1% to 2%. In an effort to correct this, the number of spatial mesh points within the fuel region used by the CPM-2 code was increased. This improved the agreement between CPM-2 and VIM substantially, with differences of less than 0.7%. The pin cell calculations shown below used the increased number of mesh points, whereas the 4x4 lattice calculations did not. The UMLEO results seem to have no trend, perhaps indicative of cancellation of errors due to the many approximations inherent in the infinite medium approach of UMLEO.

The 4x4 assembly configuration corresponds to F/M ratios of 0.80 with a water-filled central tube (corresponding to the SSCR withdrawn) and 1.20 with the central tube voided (SSCR inserted). For the UMLEO simulation, an effort was made to represent as accurately as possible the non-lattice compositions and peaking factors calculated by the CPM-2 code. The assembly  $k_{\infty}$  comparisons indicate marginally acceptable CPM-2 results (less than 1.7%) and somewhat worse UMLEO results. We expect to see improved results for the CPM-2 cases with an increased number of mesh points for the fuel region as observed for the pin cell cases.

Table VII. Comparison of the CPM-2, UMLEO, and VIM Computer Codes

| Comparison of $k_{\infty}$ for pin-cell calculations |                   |       |       |           |           |
|--|-------------------|-------|-------|-----------|-----------|
| 2.0 w/o $^{235}\text{U}$                             |                   |       |       |           |           |
| F/M  | VIM               | UMLEO | CPM-2 | UMLEO/VIM | CPM-2/VIM |
| 0.50   | $1.248 \pm 0.003$ | 1.265 | 1.240 | 1.014     | 0.994     |
| 0.70   | $1.201 \pm 0.003$ | 1.219 | 1.195 | 1.015     | 0.995     |
| 1.00   | $1.134 \pm 0.002$ | 1.146 | 1.126 | 1.011     | 0.993     |
| 1.30   | $1.071 \pm 0.002$ | 1.079 | 1.066 | 1.007     | 0.995     |

| Comparison of $k_{\infty}$ for idealized 4x4 lattice calculations |                   |       |       |           |           |
|---|-------------------|-------|-------|-----------|-----------|
| 2.5 w/o $^{235}\text{U}$  |                   |       |       |           |           |
| F/M   | VIM               | UMLEO | CPM-2 | UMLEO/VIM | CPM-2/VIM |
| 0.50  | $1.304 \pm 0.003$ | 1.323 | 1.299 | 1.015     | 0.996     |
| 0.70  | $1.252 \pm 0.002$ | 1.270 | 1.247 | 1.014     | 0.996     |
| 1.00  | $1.177 \pm 0.002$ | 1.191 | 1.173 | 1.012     | 0.997     |
| 1.30  | $1.113 \pm 0.002$ | 1.121 | 1.111 | 1.005     | 0.998     |

| Comparison of $k_{\infty}$ for idealized 4x4 lattice calculations |                   |       |           |           |       |
|---|-------------------|-------|-----------|-----------|-------|
| F/M   |                   |       |           |           |       |
| VIM   | UMLEO             | CPM-2 | UMLEO/VIM | CPM-2/VIM |       |
| 0.80  | $1.201 \pm 0.002$ | 1.236 | 1.214     | 1.029     | 1.011 |
| 1.20  | $1.089 \pm 0.003$ | 1.108 | 1.108     | 1.017     | 1.017 |

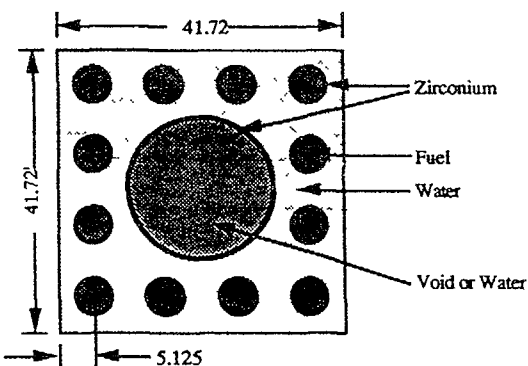


Figure 5. Idealized 4x4 Lattice for Assembly-level Comparison (Dimensions in mm)

#### Simulation of Proteus Critical Experiments

Efforts to benchmark CPM-2 have included simulation of the tight-lattice PROTEUS critical experiments. The series of light-water high-conversion reactor (LWHCR) critical experiments performed in the PROTEUS zero power facility (Wurenlingen, Switzerland) were designed to provide critical benchmarks for the evaluation of LWR physics codes applied to tight-pitch LWHCR lattices. Original analysis of the six Phase I test cores, sponsored by EPRI, was performed using the EPRI-CPM computer code.<sup>9</sup> Preliminary analyses were

performed for our study using CPM-2 (a successor to EPRI-CPM) to reproduce, as closely as possible, the published calculational results. Reaction rates, reaction rate ratios, and two-rod heterogeneity factors calculated using CPM-2 agree with the published EPRI-CPM results within < 0.42% for  $^{238}\text{U}$  fission and < 0.20% for all other reaction rates ( $^{238}\text{U}$  capture,  $^{239}\text{Pu}$  fission, and  $^{241}\text{Pu}$  fission).

#### SUMMARY

Our preliminary design analysis indicates the feasibility of SESSR designs that can yield substantial improvement in fuel utilization in open fuel cycles with acceptable nuclear and thermal-hydraulic characteristics. The SESSR design results in an increase (compared to typical PWR at the same enrichment) in cycle length for both batch and equilibrium cores in the range of 15-22%, and this increase is observed over a large range of core parameter variations. It appears that the EOC spectrum is a crucial factor in obtaining increased cycle lengths, and should be made relatively soft. The BOC moderator temperature coefficients are acceptable, although further increases in enrichment may necessitate the use of burnable poison in the SSCRs to reduce the MTC at BOC. Although the relatively high radial power peaking factors place thermal-hydraulic and safety restrictions on the SESSR design, further core design optimization is expected to reduce the radial power peaking to acceptable levels. Validation of our neutronic methodology for tight lattices is in progress along with development of optimal SSCR management strategy. The efforts we have taken to date to validate our lattice physics codes through cross-comparisons and simulation of the PROTEUS criticals data indicate the need for further validation, optimization, and development of the neutronic methodology for tight-lattice SESSR analysis.

#### ACKNOWLEDGMENTS

This work was performed under the auspices of the U.S. Department of Energy, Grant DE-FG07-88ER12809.

#### REFERENCES

1. W. Oldekop, H. Berger, and W. Zeggel, *Nuclear Technology* **59**, 212 (1982).
2. Y. Ronen and M. J. Leibson, *Nuclear Technology* **80**, 216 (1988).
3. D. B. Jones, "ARMP-02 Documentation, Part II, Chapter 6 -- CPM-2 Computer Code Manual," EPRI NP-4574-CCM, Part II, Ch. 6, Volumes 1, 2, and 3, Electric Power Research Institute (1987).
4. W. W. Little, Jr. and R. W. Hardie, "2DB - User's Manual - Revision I," BNWL-831 Rev. 1, Battelle Pacific Northwest Laboratory (1969).
5. "Babcock & Wilcox Standard Safety Analysis Report," B-SAR-205, Babcock & Wilcox Fuel Company (1976).

6. "Millstone Nuclear Power Station Unit 3 Final Safety Analysis Report," U.S. Nuclear Regulatory Commission Docket Number 50-423, Amendment 13 (1985).
7. R. F. Barry, "LEOPARD - A Spectrum Dependent Non-Spatial Depletion Code for the IBM-7094," WCAP-3269-26, Westinghouse Electric Corporation (1963).
8. L. J. Milton and R. E. Prael, "A User's Manual for the Monte Carlo Code, VIM," FRA Technical Memorandum No. 84, Applied Physics Division, Argonne National Laboratory (1976).
9. E. Hettergott, R. Chawla, and K. Gmür, "Analysis of Test Lattice Experiments in the Light Water High-Conversion Reactor PROTEUS," EPRI-NP-3190, Electric Power Research Institute (1983).

## PRELIMINARY PHYSICS DESIGN OF ADVANCED HEAVY WATER REACTORS (AHWRs)

K. BALAKRISHNAN, A. KAKODKAR  
Bhabha Atomic Research Centre,  
Bombay, India

### Abstract

The Indian PHWR, based on the CANDU type reactor, is by now a commercial system in India, and it would now be logical to think in terms of an advanced heavy water reactor (AHWR). Preliminary studies are being carried out on a system which can take advantage of a lot of the experience gained and infrastructure developed for the PHWR. The proposed system envisages a pressure tube type of heavy water reactor with vertical channels using boiling light water as coolant. Keeping in mind India's thorium reserves, the system has been tailored to work on the thorium  $U^{233}$  cycle. Since the coolant is light water, a breeding or self sustaining cycle is unlikely. However, our aim would be to make it self sustaining in  $U^{233}$  with minimum consumption of Plutonium.

With boiling light water as coolant, it is important to avoid a positive void coefficient or reactivity. We have attempted to achieve this in the following way :

The major part of the reactor core will consist of thorium oxide clusters in pressure tubes arranged in a lattice. The thorium will be enriched with  $U^{233}$ . The  $U^{233}$  content will be so chosen that the system will be self-sustaining in  $U^{233}$  with a discharge burnup in the region of 20,000 Mwd/T. A lattice of this kind will not be sufficiently reactive to make the reactor critical. Criticality will be achieved by a small number of driver zones distributed in the core. These driver zones are plutonium-uranium mixed oxide pins contained in pressure tubes cooled by boiling light water. Each driver zone is sufficiently large that the neutron spectrum inside it is determined largely by the boiling light water which is therefore, effectively functioning as both coolant and moderator. The coolant circuit of the thorium zone and this driver zone are tightly coupled thermohydraulically so that the void conditions in both are exactly the same. The bottom zone will be having a positive void coefficient of reactivity. But the voiding of the driver zone will result in the removal of the moderating medium thus hardening the neutron spectrum so as to reduce the reactivity. The combined effect of both on the reactor core should be a negative void coefficient. This is achieved by proper optimisation.

One important parameter is the fraction of power produced in the driver zone. The contention is to maximise the power obtained from the thorium zone. The preliminary design, presented here, produces 80% of the power in the thorium zone. These calculations have been made using the WIMS 69 group cross section library.

## 1. INTRODUCTION

India's nuclear power program has been conceived of as evolving in three phases. The first phase will consist of Candu type PHWR's, the second phase will be fast breeders, and the third phase will be primarily intended for utilising our vast deposits of thorium. The first phase is now well under way with five PHWR units operating, three nearly completed, and a large number of further units already sanctioned. For the second phase, a test fast breeder is operating and the design of a prototype fast breeder is well advanced. As such, it is time to start thinking about the reactor system that should be deployed in the third phase.

Since this phase is to be based on thorium, the choice of a heavy water reactor in the light of its excellent fuel utilisation characteristics and the flexibility it provides in adopting different fuelling strategies is obvious for this role. Further, in the Indian context, it would be a small extension of a technology well assimilated in our infrastructure.

## 2. CHARACTERISTICS OF THE PRESENT PHWR SYSTEM

Having decided to start from the existing PHWR system, and improve upon it if possible, let us note some of the desirable characteristics of the present design :

1. Presence of a large inventory of low temperature heavy water moderator inside the reactor as well as the presence of a large inventory of water in the reactor vault along with their own cooling systems. These systems have the potential for providing diverse means of core decay heat removal under severe accident conditions.
2. Availability of diverse shutdown systems assures a very high degree of reliability for shutdown function.
3. Since the moderator is at low pressure, the reactivity adjustment devices do not have to operate in a high pressure environment; thus precluding the possibility of accidental ejection from the core.
4. On account of the availability of on-power fuelling, the core can function with low excess reactivity.

5. Large containment volume practically rules out any threat to the structural integrity of the containment in case of a severe accident.

### 3. ADVANTAGES OF THE PRESSURE TUBE CONCEPT

Apart from these, the pressure tube concept itself offers scope for a number of additional improvements :

(a) The tube construction along with the availability of onpower refuelling machine could in principle facilitate inservice inspection of the internal pressure boundary of the reactor for (i) detection of any volumetric defects; (ii) detection of any changes in terms of displacement of supports; (iii) taking small material samples to check possibilities of degradation in the material of the pressure tube on account of environmental effects. Further , this system can also be extended to a variety of maintenance tasks connected with the reactor core.

(b) Possibility of shop assembled coolant channels which would enable achieving far greater quality control as well as a speedier construction. The design of these channels along with technology for replacement of channels could also enable a longer life for the PHWR.

(c) The channel construction with on power refuelling feature provides a much greater flexibility in adopting different refuelling schemes.

These factors influence us to retain the pressure tube concept for our advanced reactor.

### 4. REQUIREMENTS TO BE SATISFIED BY THE ADVANCED REACTOR SYSTEM

As already mentioned, we are looking for a system suited to thorium utilisation. We also like to retain all the desirable features of PHWR and of the pressure tube construction as described earlier. We also like to look for low capital costs and low operating costs.

One of the main short-comings of the PHWR is the leakage of heavy water from the PHT system. This is both an economic penalty and a source of high man-rem expenditure due to tritium activity. Use of boiling light water coolant will save the capital cost of the heavy water inventory by about 30%, reduce the D<sub>2</sub>O make up requirements by 90%; eliminate the need for having extreme leak tightness in all the seals and valves of the PHT, thus saving on cost; eliminate the tritium problem, thus saving on man-rem expenditure; enable the use of direct cycle, thus doing away with the steam generator and saving on cost. The major disadvantage of light water coolant is the positive void

coefficient. This can pose a safety problem, even more so when the coolant is two phase.

The SGHWR of UK had solved this problem by making the coolant act as part moderator. This necessitated enriching the fuel to compensate for the loss in reactivity due to the relatively hard spectrum. In India, since we lack enrichment facilities, this will have to be done by adding plutonium. The PHWR spectrum is a very undesirable spectrum for Pu-239, which has a comparatively high capture to fission ratio in this spectrum.

The other constraint we imposed on the AHWR design is that it should be suitable for serving as the work horse of our third phase, which is to operate on thorium fuel. Thorium reactors have to be initiated by external fissile material anyway, and in the Indian context this has per force to be plutonium. We thus have an incentive for designing a heavy water reactor in which Pu will be positioned in a favourable spectrum.

In short then, the requirements are :

- (a) use of boiling light water as coolant
- (b) Avoidance of positive coolant void coefficient.
- (c) Placing the plutonium fuel in a favourable spectrum.

## 5. THE PHYSICS DESIGN : A QUALITATIVE DESCRIPTION

Given the above requirements, the design is almost self evident. There have to be two distinct regions, with

different spectra. The seed and blanket concept immediately suggests itself. The blanket region in this case will differ from the commonly understood blanket region in that it will not be made of pure fertile material.

The blanket region will be similar to an ordinary PHWR lattice - but the coolant will be boiling light water and the fuel will be thorium, suitably enriched with U<sup>233</sup>. The enrichment will be so adjusted that the thorium fuel will be self-sustaining in U<sup>233</sup>. The burnup of the outer region will be adjusted according to the fuel performance capability. For a start, it is being taken as 20,000 Mwd/T. As fuel development proceeds and better performance fuels become available, the burnup could be increased to any level. The thorium lattice will naturally be subcritical. The seeds will act as driver zones.

The seed will be made of a lattice of (U,Pu) MOX pins. Each seed region will be sufficiently large that the spectrum in the seed will be decided by the seed alone. Boiling light water will act as coolant-moderator in this region. The spectrum can be made hard to favour Pu<sup>239</sup>. In the outer pins of the seed however, the spectrum will get softened by the presence of D<sub>2</sub>O outside so we can expect power peaking in these pins. This is avoided by using lower enrichment in the peripheral pins.

The thorium region with its soft spectrum will be having a positive void coefficient. But the composite core

can be designed to have a negative void coefficient. This is done by having the coolant of the blanket region and the coolant-moderator of the seed region in one single primary heat transport (PHT) circuit, and ensuring that the thermal hydraulic coupling is sufficiently strong that the void conditions in the seed and the blanket will be the same. The void coefficient of the seed will be negative. This has to be ensured by properly adjusting the enrichment and the VF/VH<sub>2</sub>O ratio. With proper thermohydraulic coupling, the composite core will have negative void coefficient.

## 6. CALCULATIONAL METHOD

Lattice calculations were made using the WIMS 69 groups library and the same group structure; but an Indian lattice code was used. It solves the integral transport equation in one dimensional cylindrical geometry in 69 energy groups. The cell is divided into a number of concentric cylindrical regions. The regions are connected through interface currents. The collision rate in group  $\ell$  and region j can be written as

$$c_{ij} = S_{\ell j} P_{vv} + J_o^j P_{ov} + J_i^j P_{iv} \quad (1)$$

where

$S_{\ell j}$  = source in group  $\ell$  and region j

$J_o^j$  = total current into region j in group  $\ell$  through the outer surface

$\ell_j$  = total current into region j in group  $\ell$  through the inner surface

$P_{vv}$  = No of collisions a neutron born in group  $\ell$  and region j undergoes while still inside the group  $\ell$  and region j

$P_{ov}$  = No of collisions which a neutron in group  $\ell$  entering region j through its outer surface undergoes while remaining in group  $\ell$  and region j.

$P_{iv}$  = No of collision which a neutron in group  $\ell$  entering region j through its inner surface undergoes while remaining in group  $\ell$  and region j.

The following equations hold for the interface current

$$J_i^j = S_{\ell, j+1} P_{vi} + J_i^{j-1} * P_{io} + J_o^{j-1} P_{oo} \quad (2)$$

$$J_o^j = S_{\ell, j+1} P_{vi} + J_i^{j+1} P_{ii} + J_o^{j+1} P_{oi} \quad (3)$$

Where  $P_{ii}$ ,  $P_{io}$  etc. have interpretations similar to that of  $P_{iv}$  and  $P_{ov}$  given above.

This set of three equations (1)-(3) are solved to obtain the 69 group fluxes in all regions. These fluxes are used to homogenise the cell and collapse the cross-sections into four groups.

The core calculations have been made using four group diffusion theory. The four group diffusion equations are solved by the finite difference method. The requirement of a small mesh size has made it necessary to restrict our study to a 2-D analysis with quarter core symmetry.

## RESULTS

For a start, a parametric study was carried out varying the following quantities:

- (a) Fissile plutonium content in the various pins in the driver zone
- (b) size of the driver zone

- (c) Number of driver zones
- (d) Fuel-to-coolant ratio in the driver zone
- (e) Positioning of the driver zone in the core
- (f) Thorium cluster design

The total power has been calculated assuming fuel design limits. Results are shown in Table 1. We can see that it possible to reconcile the conflicting demands of negative void coefficient, acceptable power distribution and reasonably low plutonium consumption.

More details are shown in Table 2 for one of the cases in Table 1. Fig. 1 shows a schematic of the reactor and Fig 2 shows the layout of the core.

TABLE - 1  
RESULTS OF THE SURVEY CALCULATIONS

| Case | $K_{eff}$ | Total Power MW (th) | Fraction of Power from Seed | Void Coefficient mk/% void | Yearly Plutonium Consumption (Kg fissile) |
|------|-----------|---------------------|-----------------------------|----------------------------|---|
| 1.   | 1.010     | 750                 | 14.6                        | -1.44                      | 39.1                                      |
| 2.   | 1.026     | 779                 | 16.5                        | -0.81                      | 48.0                                      |
| 3.   | 1.026     | 789                 | 16.5                        | -0.81                      | 45.4                                      |
| 4.   | 1.026     | 756                 | 16.5                        | -0.60                      | 44.5                                      |
| 5.   | 1.030     | 659                 | 18.0                        | -0.96                      | 42.4                                      |
| 6.   | 1.010     | 750                 | 9.3                         | -0.90                      | 24.9                                      |
| 7.   | 1.015     | 750                 | 10.0                        | -0.87                      | 26.7                                      |

T A B L E - 2  
DETAILED DESCRIPTION OF ONE CASE

|  |   |  |
|--|---|--|
| ① Reactor Power  | = | 750 MW(th)   |
| ① Number of channels                                       | = | 306  |
| ① Lattice pitch  | = | 20.0 cms square  |
| ① Number of driver zones                                   | = | 7  |
| ① Positions  | = | 1 at core centre   |
| ① Number of lattice positions removed for each driver zone | = | 6 symmetrically placed at $60^\circ$ one from the next, and at an approximate distance of 160 cms from core centre |
| ① VM within the driver zone = YF                           | = | 1.54   |
| ① The thorium fuel   | = | 19 rod cluster   |
| ① Coolant density  | = | 0.45 g/cc  |
| ① $K_{eff}$  | = | 1.010  |
| ① Power in seed region                                     | = | 14.6%  |
| ① Void coefficient   | = | - 1.44 mW/% void   |
| ① $U^{233}$ content in thorium                             | = | 1.3%   |
| ① Number of MOX pins in each seed                          | = | 216  |
| ① In core plutonium inventory                              | = | 176 kg (fissile)   |
| ① Discharge burnup of the thorium fuel                     | = | 20,000 Mwd/T   |
| ① Calandria radius   | = | 300 cms  |

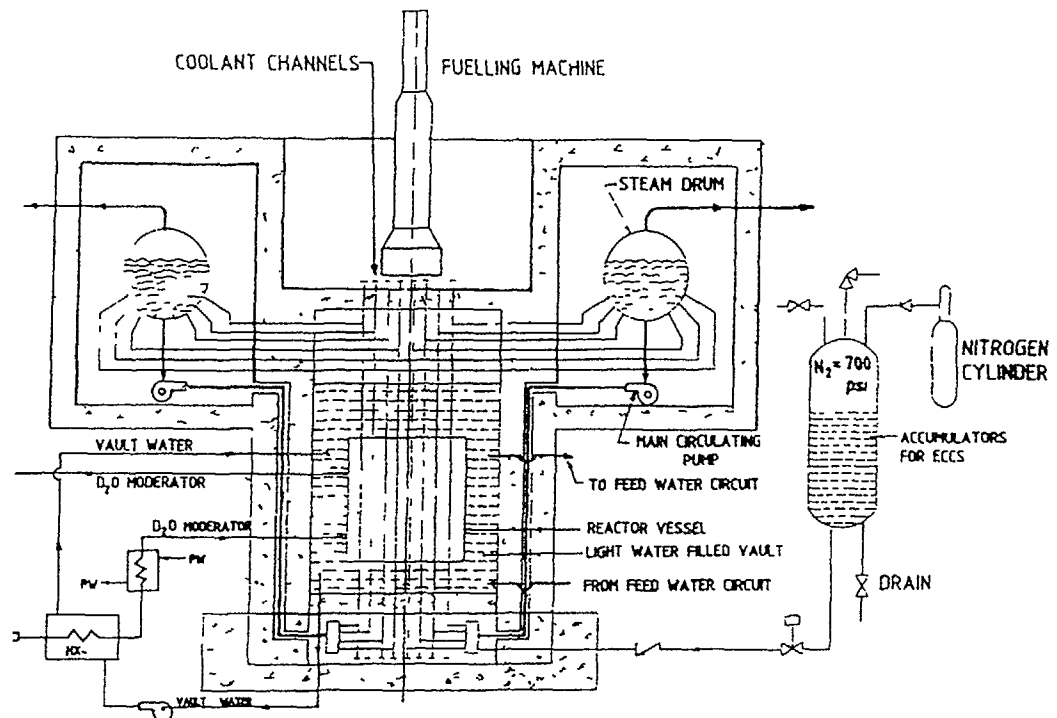


FIG 1. Advanced heavy water reactor (schematic)

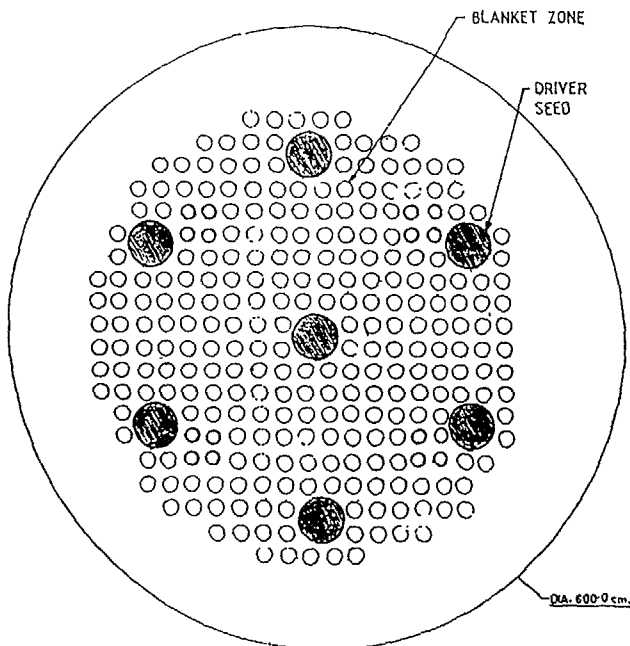


FIG. 2. Lattice layout.

## 8. CONCLUSIONS

Clearly the design can be optimised still further. But sufficient data has been generated to establish the feasibility of the concept. Work is continuing on both the reactor physics and engineering aspects.

## ACKNOWLEDGEMENTS

The authors wish to thank Dr. P.K. Iyengar, Chairman AEC, for the great encouragement he gave during the course of this work. We also wish to acknowledge helpful discussions with M.L. Dhavan, H.P. Vyas and K. Anantaraman.

## FUEL CYCLE COST EVALUATION OF A HCPWR

H. HISHIDA, R. SHIMADA  
Mitsubishi Atomic Power Industries, Inc.,  
Tokyo, Japan

### Abstract

Utilization of Pu<sub>f</sub> in terms of a thermal recycling reactors, a HCPWR and a FBR is taken into consideration and the contribution to the saving in the annual natural uranium consumption as well as the related average fuel cycle cost over all nuclear power plants in operation is compared under the condition of limited Pu<sub>f</sub> supply.

HCPWR's introduced in advance of the commencement of introducing FBR's contribute toward the lowering in the annual natural uranium procurement and facilitate the increase in the rate of annual introducible number of FBR plants. A HCPWR without blanket fuel assemblies becomes competitive in fuel cycle cost to the conventional light water reactors by the sacrifice of conversion ratio by 0.05. A HCPWR provided with a flexible core in V<sub>m</sub>/V<sub>f</sub> ratio, which is achieved simply by replacing the type of fuel assemblies, is recommendable to meet the economic and strategic demands on Pu<sub>f</sub> utilization.

---

### 1. Introduction

A high conversion PWR (HCPWR) is generally aimed at better fuel utilization by means of maintaining the higher rate of Pu production within a core with fertile blanket assemblies.<sup>1,2,3,4</sup> So long as attention is focused at Pu<sub>f</sub> generation from a single high conversion PWR, a core with the higher conversion ratio naturally yields the more Pu<sub>f</sub> generation, which corresponds to the better saving in the natural uranium procurement. Generally speaking, the conversion ratio may be raised to a certain extent by tightening the fuel rod lattice configuration to shift incore neutron spectrum to the higher energy side, however the amount of Pu<sub>f</sub> to be loaded in a core consequently increases while the possible burnup decreases due to the difficulty in reactivity control. Therefore, under the condition of limited Pu<sub>f</sub> annual supply such as in the case that Pu<sub>f</sub> is

---

A part of this work was done under a joint research contract between an electric utilities group of Kansai, Hokkaido, Tokyo, Chubu, Shikoku, Kyushu and Japan Atomic Power, and Mitsubishi Heavy Industries, Ltd.

available due only to the spent fuel from domestic nuclear power plants, a core design with the higher conversion ratio does not always correspond to the less uranium consumption if evaluated on the basis of the whole domestic nuclear power plants in operation

In this paper, discussion is given on the amount of annual natural uranium saving and the average fuel cycle cost (FCC) evaluated over the whole nuclear power plants in operation equipped with different types of nuclear reactors in a given closed region where Pu<sup>f</sup> is only internally recycled. Four types of nuclear reactors are taken into consideration conventional LWR's, advanced LWR's, HCPWR's and FBR's. Depending on the Pu<sup>f</sup> availability, a MOX fueled core of a HCPWR may be replaced with a UO<sub>2</sub> core of different moderator to fuel volume ratio (V<sub>m</sub>/V<sub>f</sub> ratio) which is optimized with respect to the overall uranium saving, while a conventional LWR or an advanced LWR may be equipped with either a normal UO<sub>2</sub> core or a 1/3 thermal Pu recycling core. Discussion is based on the following assumptions

1) Operation of any FBR's once started up must not be suspended within the plant life due to the shortage in Pu<sup>f</sup> supply. Therefore, in case that Pu<sup>f</sup> shortage is expected, MOX fueled cores of the highest Pu<sup>f</sup> inventory except FBR's are to be replaced with UO<sub>2</sub> fueled cores in advance and the discharged MOX fuel is to be reprocessed for refueling FBR's in operation

2) Refueling of reactors except FBR's is so managed that cores with higher conversion characteristics have the priority of being loaded with MOX fuel as long as surplus Pu<sup>f</sup> is available, while the rest of them are kept loaded with UO<sub>2</sub> fuel. On the other hand, if Pu<sup>f</sup> supply is insufficient, MOX fueled cores should be converted to UO<sub>2</sub> fueled cores in refueling

3) The amount of MOX fuel laid outside reactor cores is to be minimized so that the utilization of Pu<sup>f</sup> may be maximized

In the following sections, relations are formulated among the amount of annual Pu<sup>f</sup> supply at year t in the form of readily loadable MOX fuel assemblies estimated based on the amount of previously discharged fuel and the capability of fuel reprocessing facilities, the amount of Pu<sup>f</sup> demand for nuclear power plants in operation and in startup, and the allowable numbers of different type of plants. Results of evaluation on a few typical cases are also shown

## 2. Numerical Formulation on Fissile Utilization

### 2.1 Specification of nuclear power plants under consideration

In order to specify the type of reactors equipped either with UO<sub>2</sub> or MOX fueled cores, a set of subscripts (i, ξ) are employed in the following notations, where i = 1, 2, 3 and 4 indicate a conventional LWR, an advanced LWR, a HCPWR and a FBR while ξ = u and p correspond to a UO<sub>2</sub> fueled core and a MOX fueled core, respectively. A 1/3 Pu thermal recycling core is classified as a MOX fueled core

Let N<sub>i,ξ</sub>(t), n<sub>i,ξ</sub>(t) and m<sub>i,ξ</sub>(t) denote the number of nuclear power plants of type (i, ξ) in operation at year t in the closed region under consideration, removed out of N<sub>i,ξ</sub>(t) at the end of year t and newly added into N<sub>i,ξ</sub>(t) at the beginning of year t, respectively. As mentioned in the introduction, a FBR with UO<sub>2</sub> fueled core is not considered in the present discussion, that is, N<sub>4,u</sub>(t) = 0

Nuclear plants being removed out of N<sub>i,ξ</sub>(t) rise in several measures and the number of removed plants (i, ξ) due to each different measure is denoted as follows

n<sup>S</sup><sub>i,ξ</sub>(t) number of plants (i, ξ) scheduled to be decommissioned after the plant life t<sub>e</sub> at the end of year t,

n<sup>D</sup><sub>i,p</sub>(t) (i ≤ 3) number of MOX fueled plants whose entire cores are discharged in replacement with UO<sub>2</sub> fueled cores for Pu<sup>f</sup> supply at the end of year t,

n<sup>R</sup><sub>i,u</sub>(t) (i ≤ 3) number of UO<sub>2</sub> fueled plants whose cores are to be converted to MOX fueled cores in refueling due to surplus Pu<sup>f</sup> supply at the end of year t,

n<sup>R</sup><sub>i,p</sub>(t) (i ≤ 3) number of MOX fueled plants whose cores are to be converted to UO<sub>2</sub> fueled cores in refueling due to insufficient Pu<sup>f</sup> supply at the end of year t

On the other hand, nuclear plants being added to N<sub>i,ξ</sub>(t) are expressed as follows

m<sup>S</sup><sub>i,ξ</sub>(t) number of plants (i, ξ) scheduled to be newly started up to replace decommissioned plants n<sup>S</sup><sub>i,ξ</sub>(t-1) and to meet the growth in power demand at the beginning of year t,

m<sup>D</sup><sub>i,u</sub>(t) (i ≤ 3) number of UO<sub>2</sub> fueled plants created by replacing n<sup>D</sup><sub>i,p</sub>(t-1) MOX fueled cores, which have been taken out for Pu<sup>f</sup> supply, with UO<sub>2</sub> fueled cores at the beginning of year t,

m<sup>R</sup><sub>i,p</sub>(t) (i ≤ 3) number of MOX fueled plants created by replacing n<sup>R</sup><sub>i,u</sub>(t-1) UO<sub>2</sub> fueled cores with MOX fueled cores in refueling due to surplus Pu<sup>f</sup> supply at the beginning of year t,

m<sup>R</sup><sub>i,u</sub>(t) (i ≤ 3) number of UO<sub>2</sub> fueled plants created by replacing n<sup>R</sup><sub>i,p</sub>(t-1) MOX fueled cores with UO<sub>2</sub> fueled cores in refueling due to insufficient Pu<sup>f</sup> supply at the beginning of year t

Among those specified nuclear power plants, the following relations hold

$$m_{i,u}^D(t) = n_{i,p}^D(t-1) \quad \text{for } 1 \leq i \leq 3, \quad (1)$$

$$m_{i,p}^R(t) = n_{i,u}^R(t-1) \quad \text{for } 1 \leq i \leq 3, \quad (2a)$$

$$m_{i,u}^R(t) = n_{i,p}^R(t-1) \quad \text{for } 1 \leq i \leq 3, \quad (2b)$$

$$m_{i,p}^S(t-t_e) + m_{i,u}^S(t-t_e) = n_{i,p}^S(t) + n_{i,u}^S(t) \quad \text{for } t \geq t_e, \quad (3)$$

Increment in the number of plants in operation at year  $t$

$$= \sum_{i=1}^4 \left\{ m_{i,p}^S(t) + m_{i,u}^S(t) - n_{i,p}^S(t-1) - n_{i,u}^S(t-1) \right\}, \quad (4)$$

$$m_{i,p}^D(t) = n_{i,u}^D(t-1) = 0 \quad \text{by assumption} \quad (5)$$

All the initially proposed values of  $m_{i,\xi}^S(t)$  should be specified

## 2.2 Supply and demand of Pu<sup>f</sup>

In order to make the evaluation on supply and demand of Pu<sup>f</sup> at year  $t$ , all nuclear power plants with different electrical output are normalized to be of 1000 MWe. The amount of Pu<sup>f</sup> and metallic uranium to be loaded to or discharged from a UO<sub>2</sub> fueled core ( $i, u$ ) or a MOX fueled core ( $i, p$ ) so normalized are designated as in Table 1

Table 1 Fissile Balance Normalized for a 1000 MWe Core ( $i, \xi$ )

| Core                             | Loading or Discharge | Fissile in Unit of Pu <sup>f</sup> | Enrichment (%)   | Amount (fissile)                                 |
|----------------------------------|----------------------|------------------------------------|------------------|--|
| Initial Core ( $i, \xi$ )        | loading              | metallic U Pu <sup>f</sup>         | $E_{i,u}^I$<br>- | $U_{i,\xi}^I$ (ton)<br>$P_{i,\xi}^I$ (ton)       |
|                                  | discharge            | metallic U Pu <sup>f</sup>         | $E_{i,u}^D$<br>- | $U_{i,\xi}^D$ (ton)<br>$P_{i,\xi}^D$ (ton)       |
| Equilibrium Core ( $i, \xi$ )    | loading              | metallic U Pu <sup>f</sup>         | $E_{i,u}$<br>-   | $U_{i,\xi}$ (ton/year)<br>$P_{i,\xi}$ (ton/year) |
|                                  | discharge            | metallic U Pu <sup>f</sup>         | $E_{i,u}$<br>-   | $U_{i,\xi}$ (ton/year)<br>$P_{i,\xi}$ (ton/year) |
| Decommissioned Core ( $i, \xi$ ) | discharge            | metallic U Pu <sup>f</sup>         | $E_{i,u}^D$<br>- | $U_{i,\xi}^D$ (ton)<br>$P_{i,\xi}^D$ (ton)       |

As defined in sec 2.1,  $N_{i,\xi}(t)$  represents the number of nuclear power plants equipped with cores ( $i, \xi$ ) at year  $t$ , then

the number of plants with the initial cores ( $i, \xi$ ) at year  $t$

$$= N_{i,\xi}(t) - \left\{ N_{i,\xi}(t-1) - n_{i,\xi}(t-1) \right\} = m_{i,\xi}(t), \quad (6)$$

and

$$\begin{aligned} & \text{the number of plants with the equilibrium cores} (i, \xi) \text{ at year } t \\ & = N_{i,\xi}(t-1) - n_{i,\xi}(t-1), \end{aligned} \quad (7)$$

where  $m_{i,\xi}(t)$  and  $n_{i,\xi}(t)$  are defined such that

$$m_{i,\xi}(t) \equiv m_{i,\xi}^S(t) + m_{i,\xi}^D(t) + m_{i,\xi}^R(t), \quad (8a)$$

and

$$n_{i,\xi}(t) \equiv n_{i,\xi}^S(t) + n_{i,\xi}^D(t) + n_{i,\xi}^R(t) \quad (8b)$$

The amount of Pu<sup>f</sup> available  $S_p(t)$  in the form of readily loadable fuel assemblies at the beginning of year  $t$  is given by the following expression

$$\begin{aligned} S_p(t) &= \sum_{i=1}^4 \sum_{\xi} m_{i,\xi}(t-\tau_{i,\xi}) P_{i,\xi}^I + \sum_{i=1}^4 \sum_{\xi} \left\{ N_{i,\xi}(t-\tau_{i,\xi}-1) - n_{i,\xi}(t-\tau_{i,\xi}-1) \right\} P_{i,\xi} \\ &+ \sum_{i=1}^4 \sum_{\xi} \left\{ n_{i,\xi}^D(t-\tau_{i,\xi}) + n_{i,\xi}^S(t-\tau_{i,\xi}) \right\} P_{i,\xi}^D + \sum_{i=1}^3 \sum_{\xi} n_{i,\xi}^R(t-\tau_{i,\xi}) P_{i,\xi} \end{aligned} \quad (9)$$

when  $\tau_{i,\xi}$  is the time required to reprocess and fabricate the spent fuel from core ( $i, \xi$ ) and the summation on  $\xi$  appeared in expression (9) represents  $\sum_{\xi} n_{i,\xi}(t) \equiv n_{i,u}(t) + n_{i,p}(t)$

On the other hand, the amount of Pu<sup>f</sup> needed  $Q_p(t)$  in the form of readily loadable fuel assemblies at the beginning of year  $t$  is expressed with the definitions of  $Q_{i,p}(t)$  and  $Q_{i,p}^I(t)$  as follows

$$Q_p(t) \equiv \sum_{i=1}^4 \left\{ Q_{i,p}^I(t) + Q_{i,p}(t) + m_{i,p}^R(t) P_{i,p} \right\}, \quad (10)$$

$$Q_{i,p}^I(t) \equiv m_{i,p}^S(t) P_{i,p}^I, \quad (11a)$$

and

$$Q_{i,p}(t) \equiv \left\{ N_{i,p}(t-1) - n_{i,p}(t-1) \right\} P_{i,p} \quad (11b)$$

$S_p(t)$  is not equal to  $Q_p(t)$  in general and the allowable numbers of different type of nuclear power plants are mutually adjusted so that the assumptions stated in the introduction may be realized

### 2.3 Determination of permissible $m_{i,\xi}(t)$

In this section, logical procedures to determine  $m_{i,\xi}(t)$  are discussed

- 1) In case that the following relation (12) is satisfied

$$S_p(t) > Q_{4,p}(t) + Q_{4,p}^I(t), \quad (12)$$

the supply of PuF in the form of readily loadable MOX fuel assemblies at the beginning of year  $t$  exceeds the necessary amount for refueling and initial loading of FBR plants. The surplus PuF is used to replace some possible number of UO<sub>2</sub> fueled cores of HCPWR or LWR plants by MOX fueled cores as shown in Diagram 1 based on the following sequential conditions

$$S_p(t) - Q_{4,p}(t) - Q_{4,p}^I(t) > Q_{3,p}(t) + Q_{3,p}^I(t), \quad (13)$$

$$S_p(t) - \sum_{i=3}^4 \{ Q_{i,p}(t) + Q_{i,p}^I(t) \} > Q_{2,p}(t) + Q_{2,p}^I(t), \quad (14)$$

and

$$S_p(t) - \sum_{i=2}^4 \{ Q_{i,p}(t) + Q_{i,p}^I(t) \} > Q_{1,p}(t) + Q_{1,p}^I(t) \quad (15)$$

- 2) If relation (12) is not satisfied, then MOX fueled cores ( $i, p$ ) with  $i = 2$  or  $3$  within the core life  $t_c$  are to be decommissioned  $\tau_{i,p}$  years in advance to increase the amount of PuF supply at year  $t$ , where the following relation must hold

$$N_{i,p}(t - \tau_{i,p}) - n_{i,p}^D(t - \tau_{i,p}) \geq 0 \quad \text{with } i = 2 \text{ or } 3 \quad (16)$$

- 3) In case relation (12) is not yet satisfied for  $n_{i,p}^D(t - \tau_{i,p}) = N_{i,p}(t - \tau_{i,p})$ , then some or all of FBR plants being scheduled to start up newly at the beginning of year  $t$ , i.e.  $m_{4,p}^S(t)$ , are to be replaced by the identical number of nuclear plants equipped with UO<sub>2</sub> fueled cores  $m_{i,u}^S(t)$  with  $i = 2$  or  $3$ . Balance in the supply and the demand of PuF should be recalculated starting at year  $t - \tau_{i,p}$ .

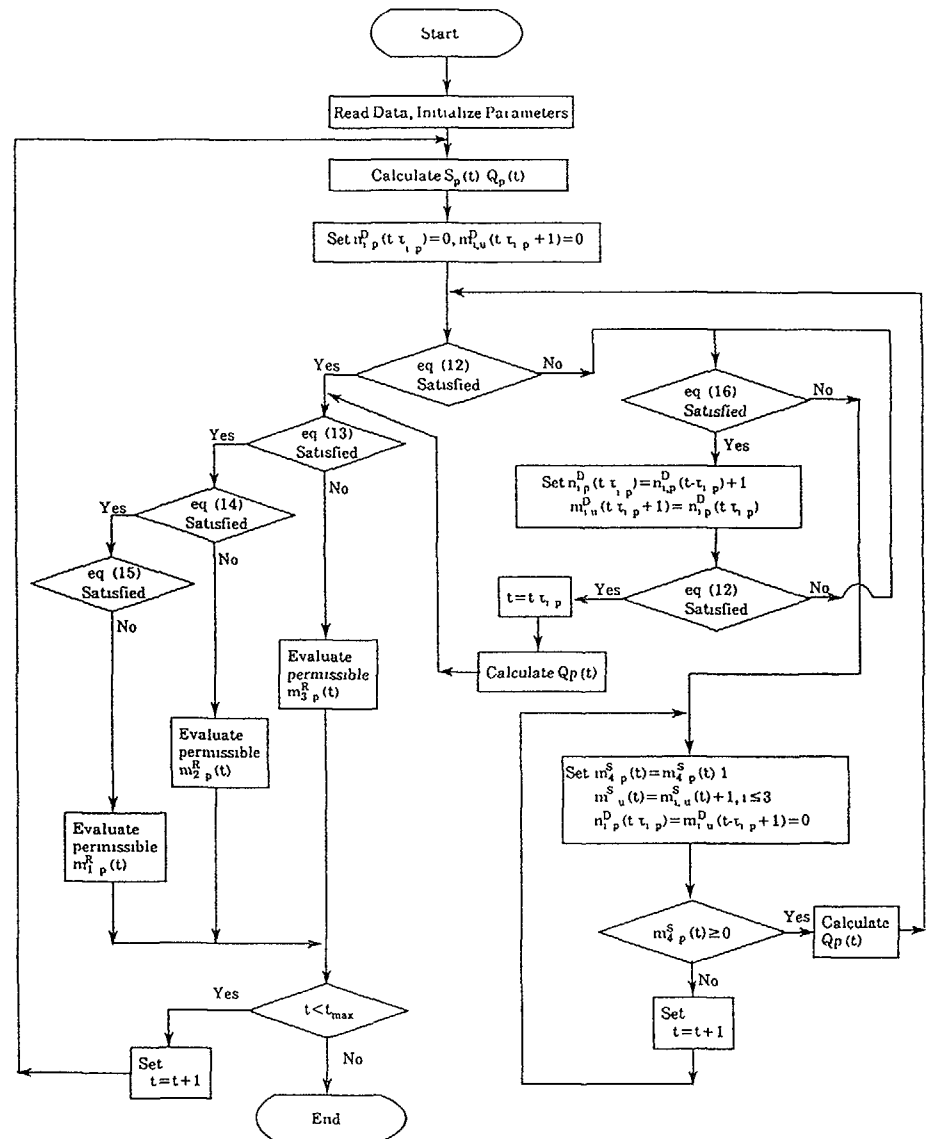


Diagram 1 Logical procedures to determine  $m_{i,\xi}(t)$

4) Through the previously mentioned procedure 3), the amount of Pu<sup>f</sup> supply for refueling FBR plants in operation at the beginning of year t may still be insufficient, then the number of FBR plants being scheduled to start up newly in the preceding year,  $mS_{4,p}(t-1)$  is to be reduced so as to satisfy relation (12) and the corresponding number of nuclear plants equipped with UO<sub>2</sub> fueled cores,  $mS_{1,u}(t-1)$  with  $i = 2$  or 3, replace the reduced number of FBR plants

#### 2.4 Annual uranium demand

The amount of U<sup>235</sup> needed  $Q_u(t)$  in the form of readily loadable fuel assemblies at the beginning of year t is expressed with the definitions of  $Q_{i,u}(t)$  and  $Q_{i,u}^I(t)$  as follows

$$Q_u(t) = \sum_{i=1}^3 \left\{ Q_{i,u}^I(t) + \sum_{\xi} Q_{i,\xi}(t) + m_{i,u}^R U_{i,u} E_{i,u} \right\}, \quad (17)$$

$$Q_{i,u}^I(t) = \left\{ m_{i,u}^S(t) + m_{i,u}^D(t) \right\} U_{i,u}^I E_{i,u}^I, \quad (18a)$$

and

$$Q_{i,\xi}(t) = \left\{ N_{i,\xi}(t-1) - n_{i,\xi}(t-1) \right\} U_{i,\xi} E_{i,\xi}, \quad (18b)$$

where  $n_{i,u}(t)$  is expressed from expressions (5) and (8b) as follows

$$n_{i,u}(t) = n_{i,u}^S(t) + n_{i,u}^R(t) \quad (18c)$$

The summation on  $\xi$  appeared in expression (17) represents  $\sum_{\xi} Q_{i,\xi}(t) = Q_{i,u}(t) + Q_{i,p}(t)$

#### 3. Averaged Fuel Cycle Cost and Natural Uranium Saving Evaluation

To calculate future costs for the nuclear fuel cycle,

- 1) costs for various component stages of the fuel cycle,
- 2) the required lead or lag time for each component operation in the fuel cycle,
- 3) reactor charge and discharge mass flow data, and
- 4) interest and inflation rates

should be provided. Costs for various component stages include cost of natural uranium, cost of conversion, cost of enrichment, cost of fabrication, cost of transportation, cost of reprocessing with disposal of waste, and cost of plutonium in case of MOX fuel

In the following examples, for the uranium fuel cycle, unit cost for each component under the current practice among utilities is employed. For the fabrication cost and the reprocessing cost of MOX fuel cycle, the following factors are multiplied to the corresponding unit costs of uranium fuel cycle

$$\frac{\text{MOX fuel fabrication cost}}{\text{UO}_2 \text{ fuel fabrication cost}} = 2.4$$

$$\frac{\text{MOX fuel reprocessing cost including waste disposal}}{\text{UO}_2 \text{ fuel reprocessing cost including waste disposal}} = 1.3$$

For the interest and the inflation, the following rates are employed throughout the term of evaluation, however fluctuation in these rates may easily be taken into evaluation

interest rate = 5%/annum,

inflation rate = 2%/annum

The lead or the lag time for each component is illustrated in Table 2. Let  $C_i(t)$ ,  $M_i(t)$ ,  $r$  and  $t_i$  be the unit cost of component i of the fuel cycle, the mass under consideration in the component i

Table 2 Lead and Lag Time for Each Component Operation in Fuel Cycle

| Process Component    | enrichment                             | fabrication      | new fuel transportation and storage | spent fuel transportation and interim storage | reprocessing   |
|----------------------|--|------------------|-------------------------------------|---|--|
| Time (year)          | $t_3$                                  | $t_2$            | $t_1$                               | $t$   | $t_4$  |
| Payment and Credit   |  |                  | new fuel loading                    | spent fuel discharge                          |  |
| UO <sub>2</sub> fuel | uranium cost including conversion cost | enrichment cost  | fabrication cost                    | transportation and interim storage cost       | reprocessing and waste disposal cost<br>Pu, U credit |
| MOX fuel             | Pu cost                                | fabrication cost |                                     | transportation and interim storage cost       | reprocessing and waste disposal cost<br>Pu credit    |

In the present analyses, parameters  $t_a$  are set as follows

|               | for UO <sub>2</sub> fuel | for MOX fuel (year) |
|---------------|--------------------------|---------------------|
| $t_2 - t_3 =$ | 0.5                      | —                   |
| $t_1 - t_2 =$ | 1.0                      | 1.5                 |
| $t - t_1 =$   | 0.5                      | 0.5                 |
| $t_4 - t =$   | 1.0                      | 2.0                 |
| $t_5 - t_4 =$ | 1.0                      | 2.0                 |

at  $t_i$ , interest rate and lead time or lag time of the component  $i$  with respect to  $t$  as defined in Table 2, respectively. Then, the amount to be recovered  $A_i(t)$  as being included within the leveled power rate at  $t$  corresponding to the payment for component  $i$  of the fuel cycle made at  $t_i$  is written as follows

$$A_i(t) = C_i(t_i) M_i(t_i) (1 + r)^{t_i - t}$$

where  $C_i(t_i)$  may be correlated to  $C_i(t_0)$  in terms of inflation rate  $f$  and the base date of monetary unit  $t_0$  as

$$C_i(t_i) = C_i(t_0) (1 + f)^{t_i - t_0}$$

The method employed in the present evaluation of FCC is principally based on a NEA/OECD report<sup>5</sup>

Annual charge and discharge mass flow data for each type of a nuclear power plant have been provided based on the corresponding core nuclear design<sup>4</sup>

### 3.1 FCC evaluated on single plant basis

Comparison of FCC among different types of power plants normalized for thermal output of 1000 MWe and average discharge burnup of 45,000 MWd/t is given in Fig. 1 where the FCC of the conventional LWR with UO<sub>2</sub> fuel, example 8, is chosen as the reference and the contribution of each component to the individual FCC is shown

Here, the cost of natural uranium and plutonium fissile is assumed to be \$40/lb U<sub>3</sub>O<sub>8</sub> and \$15/g Pu, respectively. Example 3 corresponds to FCC of the HCPWR<sup>4</sup> whose blanket assemblies and fertile rods are replaced by MOX fuel assemblies and water displacer rods, respectively so as to lower the power density and to achieve 4 batch loading. The FCC is lowered appreciably at the sacrifice of average conversion ratio by 0.05

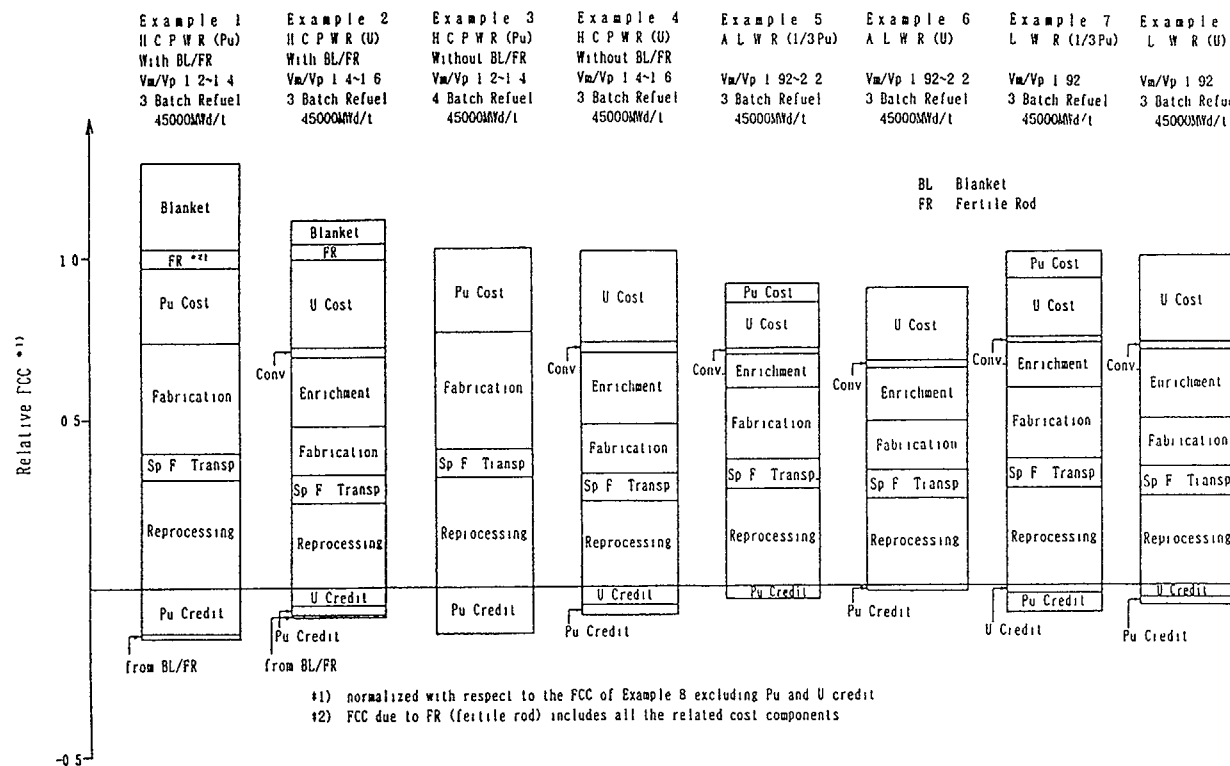


Fig. 1 Plantwise FCC of a different type of nuclear power plant

### 3.2 Natural uranium saving

Comparison of cumulative natural uranium procurement associated with Pu utilization by different types of nuclear power plants is shown in Fig. 2 where feasible number of FBR plants with breeding ratio of 1.2 are assumed to be introduced beyond year 2030 in each evaluation case. The power growth beyond year 2000 is assumed to be 1500 MWe per annum based on the expected GNP expansion with 53 LWR power plants, each of 1000 MWe power output, being in operation at year 2000. The annual supply of Pu<sup>f</sup> is based on the recycling of spent fuel only from the domestic plants in operation or being decommissioned.

In Fig. 2, evaluation cases 1 and 2 correspond to the non-Pu<sup>f</sup>-utilization and the 1/3 thermal Pu recycling of a conventional LWR cited as examples 5 in Fig. 1 until the introduction of FBR's at year 2030, respectively. Evaluation case 3 corresponds to the introduction of the normal HCPWR's each with a MOX fueled core of Vm/Vf = 1.4 cited as example 1 in Fig. 1, where under Pu<sup>f</sup> shortage, a HCPWR with UO<sub>2</sub> fueled core of Vm/Vf = 1.6 cited as example 2 in Fig. 1 is to be introduced in place of a normal HCPWR until the introduction of FBR's at year 2030. In evaluation cases 3 and 2, entire MOX fuel assemblies of a HCPWR core or a 1/3 thermal Pu<sup>f</sup> recycling core may be discharged and replaced by UO<sub>2</sub> fuel assemblies with Vm/Vf = 1.6 or by

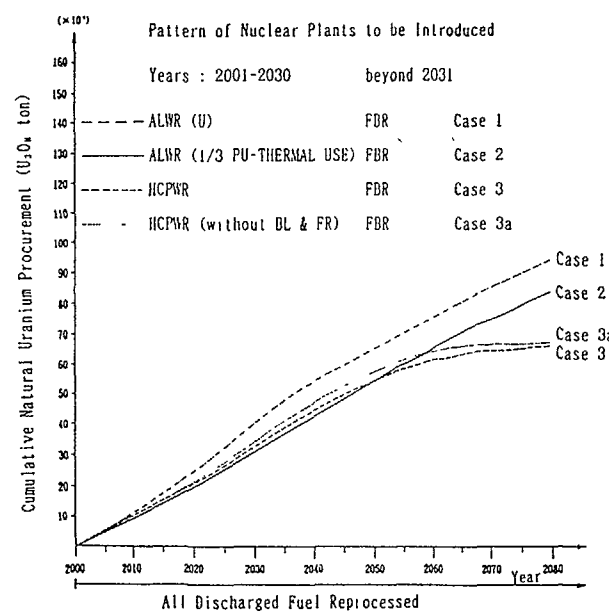


Fig. 2 Cumulative natural uranium procurement

UO<sub>2</sub> fuel assemblies of a LWR, respectively to bring the discharged fuel assemblies into reprocessing for providing necessary Pu<sup>f</sup> for FBR's to be newly introduced and to be refueled in case Pu<sup>f</sup> shortage is expected.

The difference in uranium saving between evaluation case 2 and case 3 is mainly due to that in evaluation case 3, approximately twice as much Pu<sup>f</sup> is reserved in HCPWR cores as in evaluation case 2 at the commencement of introducing FBR's and the higher rate of Pu<sup>f</sup> productivity in UO<sub>2</sub> fueled HCPWR cores of Vm/Vf = 1.6 which replace normal HCPWR cores when the supply of Pu<sup>f</sup> is not sufficient as mentioned above.

Evaluation case 3a corresponds to case 3 where HCPWR's, cited as example 3 in Fig. 1, whose blanket fuel assemblies and fertile rod clusters are replaced by MOX fuel assemblies and water displacer rods clusters, respectively are introduced under the same condition as of evaluation case 3.

### 3.3 Averaged fuel cycle cost over nuclear power plants in operation

Under the same assumptions adopted in the previous natural uranium saving analyses, the corresponding averaged fuel cycle cost to evaluation cases 1, 2, 3 and 3a is shown in Fig. 3. Due to the advantage in fabrication cost and reprocessing cost associated with UO<sub>2</sub> fuel, the averaged

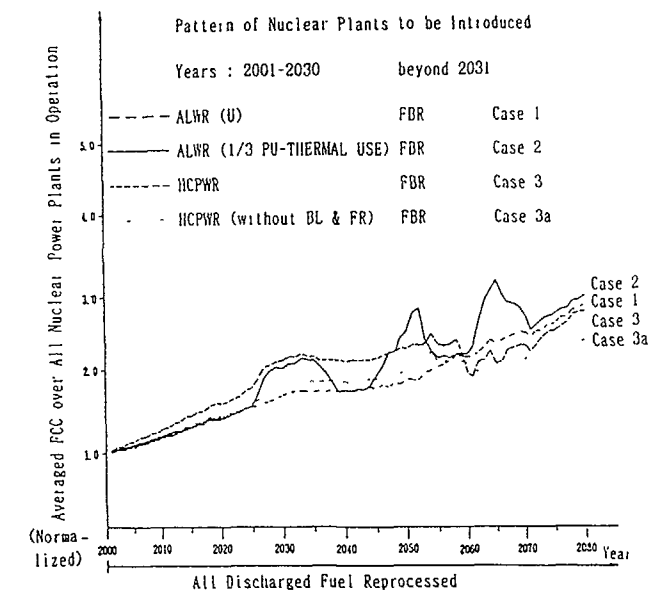


Fig. 3 Averaged FCC over all nuclear power plants in operation

fuel cycle cost in evaluation case 1 is the lowest until the contribution of fissile breeding from FBR plants to the reduction in fuel cycle cost in evaluation cases 3 and 3a becomes of dominating factor, which is seen appreciable around years 2055 ~ 2060. Temporary rise in fuel cycle cost appeared in evaluation cases 2, 3 and 3a beyond year 2025 is due mainly to the increase in reprocessing cost for MOX fuel assemblies discharged from the cores, which are replaced by UO<sub>2</sub> fuel assemblies, to make up the shortage in Pu<sup>f</sup> supply for FBR's to be newly introduced and to be refueled.

Numbers of different nuclear plants in operation in evaluation cases 1, 2 and 3 with 3a are shown in Figures 4, 5 and 6, respectively.

#### 4. Summary

Results of fuel cycle cost analyses are widely influenced by costs for various component stages of the fuel cycle. Due to the expected fluctuation in future economic as well as strategic trends, any economic feasibility evaluation on a HCPWR does not give definite conclusion reliable in future under various assumptions including ambiguity factors as previously mentioned. Evaluations with stress on either the optimum utilization of natural uranium resource or fuel cycle cost give the different features of a HCPWR. However, the following qualitative conclusions are withdrawn from the present analyses:

- 1) Reduction in annual natural uranium procurement is possible by introducing HCPWR's in place of conventional LWR's. In case that the continuous introduction of FBR's is commenced,

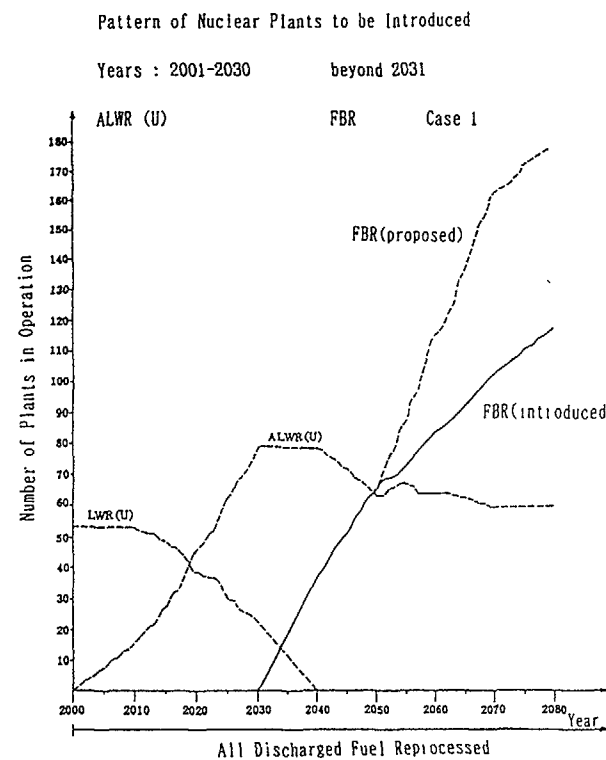


Fig. 4 Number of different type of plants in operation, Case 1

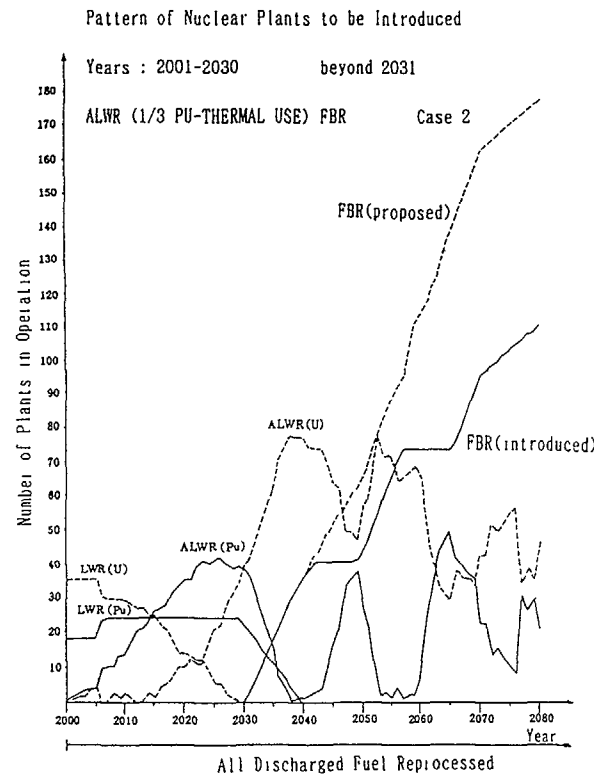


Fig. 5 Number of different type of plants in operation, Case 2

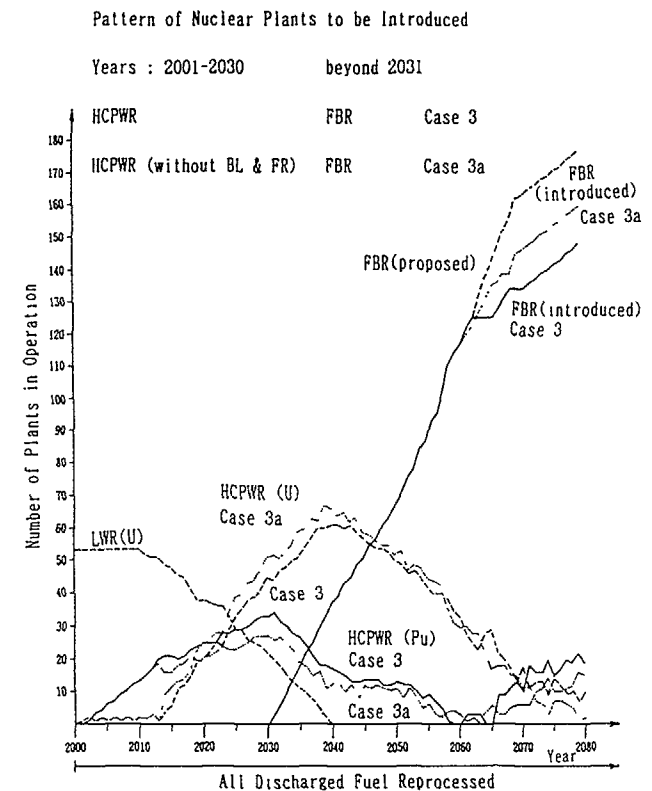


Fig. 6 Number of different type of plants in operation, Cases 3 and 3a

existing HCPWR cores may discharge MOX fuel to supply Pu<sub>f</sub> required to feed into FBR's being newly introduced and to refuel those in operation afterward which facilitates the rate of the annual increase in the number of FBR plants to result in the saving of the natural uranium consumption as well as the lowering of the long term fuel cycle cost averaged over all the nuclear power plants in operation

2) Under the low cost of natural uranium, the average fuel cost of a nuclear power plants system including HCPWR's cited as example 1 in Fig 1, which corresponds to the present evaluation case 3, is not competitive to that of a system consisting only of LWR's in a short term comparison However, a system including HCPWR's whose blanket fuel assemblies and fertile rods are replaced with MOX fuel assemblies and water displacer rods respectively, cited as example 3 in Fig 1, which corresponds to the present evaluation case 3a is competitive

3) A nuclear power plants system including thermal Pu<sub>f</sub> recycling reactors cited as example 5 in Fig 1, which corresponds to the evaluation case 2, consumes more Pu<sub>f</sub> than that including HCPWR's so that, for a short term evaluation, the former system lowers the natural uranium consumption in comparison with the system consisting only of LWR's However, its contribution toward the increase in the number of introducible FBR plants is smaller than that including HCPWR's due to the less amount of incore Pu<sub>f</sub> storage, and the advantage associated with FBR's in average fuel cycle cost as well as natural uranium saving cannot be expected so much as in the case of HCPWR's in long term evaluation

4) Extension of plant life is presently expected and to meet the fluctuation in economic and strategic trends during the plant life, the core of a HCPWR should be provided with flexibility in transition of core configuration between a semi tight lattice of  $V_m/V_f = 1.4$  corresponding to higher conversion ratio and a loose lattice of  $V_m/V_f = 2.0 \sim 2.2$  corresponding to low FCC without replacing any core components except for fuel assemblies A HCPWR with such flexibility may exhibit its most favourable scope under various economic and strategic demands including FCC and natural uranium saving on every particular occasion, which a conventional LWR plant cannot

Research works associated with the realization of such flexibility are under progress

#### REFERENCES

- 1 T Umeoka, et al ,Nucl Tech 80(1988)29
- 2 E Saji, et al , Nucl Tech 80(1988)18
- 3 A Iizuka, et al , Int Reactor Phys Conf ,Jackson Hole (1988) III 107
- 4 H Hishida, et al , IAEA Tech Comm on Tech and Economic Aspects of High Converters, 622 I3 TC 700/2 4, (1990)
- 5 NEA "The Economics of the Nucl Fuel Cycle" NEA/OECD (1985)

## A CONCEPTUAL CORE DESIGN OF A PLUTONIUM GENERATION BOILING WATER REACTOR

R TAKEDA, M AOYAMA, Y ISHII,  
O YOKOMIZO, K ISHII, N SADAOKA,  
S. UCHIKAWA  
Energy Research Laboratory,  
Hitachi Ltd,  
Moriyama-cho, Hitachi-shi, Ibaraki-ken,  
Japan

#### Abstract

A design concept for a plutonium generation BWR (PGBR) is proposed, in which the effective moderator-to-fuel volume ratio less than 0.3 is realized in the design concept of the BWR with a closely packed hexagonal lattice and a higher core exit quality of coolant to achieve 1.0 of plutonium generation ratio. Three kinds of PGBR core designs are evaluated from the view points of nuclear, thermal hydraulic, mechanical, and safety performance. Evaluations show that the proposed designs are feasible, and that the PGBR concept has a potential of realizing a new recycle system in which plutonium and other actinide are confined to only nuclear reactors and reprocessing plants.

#### INTRODUCTION

In studies on high conversion light water reactors, it is recognized that a higher conversion ratio close to 1.0 is required to achieve an greater improvement on natural uranium utilization by a factor of 5-10 compared with current LWRs<sup>1-4</sup>. The authors has proposed a concept of plutonium generation boiling water reactor (PGBR)<sup>5-6</sup> having 1.0 of plutonium generation ratio, which means that the amount of fissile plutonium obtained from reprocessing of discharged fuel is almost the same as that of new loaded fuel, thereby enabling to continue to operate commercial reactors at rated power in plutonium recycling by compensating only natural uranium.

This paper deals with conceptual design studies on three kinds of PGBR cores.

## MAIN FEATURES OF PLUTONIUM GENERATION BWR

On the basis of neutron balance, a CR can be written by

$$CR = \alpha \times (1 + \beta) - (1 + \gamma), \quad (1)$$

where,

$$\alpha = \left( \frac{\nu \Sigma_f}{\Sigma_a} \right)^{25+49+41}, \quad \beta = \left( \frac{(\nu-1) \Sigma_f^{28+40+42}}{\nu \Sigma_f^{25+49+41}} \right), \quad \gamma = \frac{\Sigma_a^M}{\Sigma_a^{25+49+41}}$$

The  $\alpha$ -factor represents the ratio of the number of neutrons produced by fission to that of neutrons absorbed in fissile materials. The  $(1+\beta)$ -factor corresponds to the additional contribution by fast fission of fertile materials, and  $\Sigma_a^M$  represents the parasitic neutron capture rate of fission products, transplutonium elements, structure materials, and so on.

Figure 1 shows the relation between the effective moderator-to-fuel volume ratio and the factors included in expression (1). The effective moderator-to-fuel volume ratio is defined as a moderator-to-fuel volume ratio taking into account the moderator voidage effect such as boiling. The  $\alpha$  and  $\beta$ -factors increase as the effective moderator-to-fuel volume ratio decreases, in particular, this tendency of the  $\beta$ -factor is remarkable in the range of the low effective moderator-to-fuel volume ratio. This is caused by the increase in  $\nu$  value. The  $\gamma$ -factor including  $\Sigma_a^M$  has a value of about 0.3, and decreases with the effective moderator-to-fuel volume ratio. To realize the CR close to 1.0, the utilization of fast fission of fertile materials is essential, and the first term in expression (1) must be more than 2.3. This means that the moderator-to-fuel volume ratio must be less than 0.3.

Under the practical constraint of a rod-to-rod clearance of more than 1mm, such a low effective moderator-to-fuel volume ratio can be realized in boiling water reactor (BWR) due to void generation in fuel bundles.

Figure 2 shows the relation between the effective moderator-to-fuel volume ratio and fissile Pu enrichment and conversion ratio

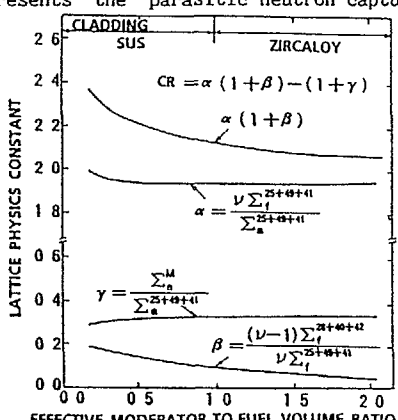


Fig.1. Relation between the effective moderator-to-fuel volume ratio and the lattice physics constants

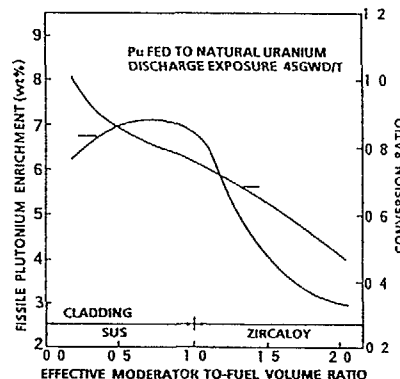


Fig.2. Relation between the effective moderator-to-fuel volume ratio and fissile Pu enrichment and conversion ratio

required Pu-fissile enrichment and CR, which is evaluated under a typical operating condition of a cycle exposure of 9GWd/t and a discharge exposure of 45GWd/t. In case of less than 0.3 of effective moderator-to-fuel volume ratio, the required plutonium enrichment fed to natural uranium is reduced less than 6.5 percent due to increase in  $\beta$ -values as well as  $\alpha$ -values of fissile plutonium isotopes following decrease in parasitic absorption rates of fission products and structure materials. This causes the void coefficient on PGBR to be improved to the same levels as those of a number of heavy-moderator commercial nuclear reactors in operation, which has a possibility to make void coefficient zero by adapting the flattened core. It must be emphasized in characteristics of PGBR in safety that excess reactivity during operation cycle is about one tenth and doppler coefficient is more than 50% larger in comparison with those of the current BWR because of little change in the number densities of fissile plutonium and the large portion of neutron absorptions in resonance energy region.

## CONCEPTUAL DESIGN OF PLUTONIUM GENERATION BWR

To confirm the feasibility of the plutonium generation BWR, three kind of designs have been investigated. Basic design parameters are summarized in TABLE I.

TABLE I  
Specifications of Plutonium Generation BWR

| Parameter                                  | PGBR-I | PGBR-II | PGBR-III |
|--|--------|---------|----------|
| Electric power (MW)                        | 600    | 900     | 900      |
| Dome pressure (MPa)                        | 7.2    | 7.2     | 7.2      |
| Coolant flow rate ( $10^4$ t/h)            | 1.04   | 2.25    | 2.19     |
| Core active length (m)                     | 2.00   | 2.00    | 1.35     |
| Core outer diameter (m)                    | 4.9    | 4.7     | 5.3      |
| Number of fuel bundle                      | 601    | 601     | 781      |
| Number of fuel rods per bundle             | 151    | 151     | 151      |
| Fuel rod outer diameter (mm)               | 12.3   | 11.8    | 11.8     |
| Fuel rod-to-rod clearance (mm)             | 1.5    | 1.3     | 1.3      |
| Moderator-to-fuel volume ratio             | 0.53   | 0.50    | 0.50     |
| Specific power (kw/kg)                     | 10.7   | 17.5    | 20.0     |
| Average power density (kw/l)               | 51.4   | 85.1    | 97.0     |
| Average linear heat generation rate (kw/m) | 9.9    | 14.9    | 17.0     |
| Core outlet quality (%)                    | 40     | 27      | 28       |
| Core average void fraction (%)             | 56     | 51      | 51       |

PGBR-I is a 600 MWe prototype reactor having the same power density as those of current BWRs, and some results of core performances were presented in Ref 6

PGBR-II is a 900 MWe commercial reactor of which fissile plutonium inventory per unit power is minimized in order to start up a 900 MWe commercial PGBR by using fissile plutonium obtained from reprocessing of discharged fuels corresponding to 80GWe-Year electric power production of the current BWR.

PGBR-III was designed to make void coefficient zero by shortening the height of the core from 2.0m of PGBR-I and II to 1.35m in considering that people are sensitive for void coefficients of which signs have no intrinsic problem as far as its absolute values are small.

In these designs, the effective moderator-to-fuel volume ratio of less than 0.3 can be realized by the closely packed hexagonal lattice with the rod-to-rod clearance of 1.3~1.5mm and the core averaged void fraction more than 50%.

#### Fuel Bundle Design

The PGBR fuel bundle consists of 151 fuel rods, 18 control rod guide thimbles, 5 (or 4) spacers, a hexagonal channel box and upper and lower tie plates. Stainless-steel (SUS) is chosen for fuel cladding and channel materials instead of Zircaloy in the current BWRs. Stainless steel is considerably stronger than Zircaloy, so thinner stainless steel is sufficient to suppress the deformation of fuel cladding and channel box during operation.

Main specifications of fuel bundle design are summarized in TABLE II. These specifications enable the fuel bundle to keep within the design limit both mechanically and thermal-hydraulically. The key design concepts include the ring cell type spacer, thin channel box and narrow channel box gap. In the ring cell type spacer one cell is overlapped with neighboring cells each other because of narrow fuel rods gap. Inconel is adopted as spacer material. The thin channel box and narrow channel box gap are accomplished by reducing the pressure difference

TABLE II  
Specifications of Fuel Bundles in PGBR

| Parameter                      | PGBR-I                 | PGBR-II | PGBR-III |
|--------------------------------|------------------------|---------|----------|
| Bundle geometry                | Hexagonal Lattice      |         |          |
| Bundle pitch (cm)              | 18.34                  | 17.46   | 17.46    |
| Number of fuel rods            | 151                    | 151     | 151      |
| Number of control rods         | 18                     | 18      | 18       |
| Channel water gap (mm)         | 0.8                    | 0.8     | 0.8      |
| Channel box thickness (mm)     | 0.95                   | 0.95    | 0.95     |
| Fuel rod outer diameter (mm)   | 12.3                   | 11.8    | 11.8     |
| Fuel rod-to-rod clearance (mm) | 1.5                    | 1.3     | 1.3      |
| Cladding and channel materials | Stainless-steel        |         |          |
| Pellet diameter (mm)           | 11.3                   | 10.8    | 10.8     |
| Space type / material          | Ring cell type/Inconel |         |          |

between channel box inside and outside by maintaining the constant flow in a channel box gap

#### Design of Reactor Internals

The control rod assembly consists of cluster type rods and has one rod drive for three fuel bundles. Figure 3 shows a cross section of fuel bundle and control rod assembly. Each control rod is equipped with a follower in its upper region. The control rods are inserted to the fuel bundles from the lower part of the core.

An upper core plate connected with the upper shroud is set on the top of all fuel bundles. This configuration prevents the fuel bundles from rising by the hydraulic lift force caused by upward coolant flow

The steam driers and separators of PGBR are designed as the same as that of the current BWR.

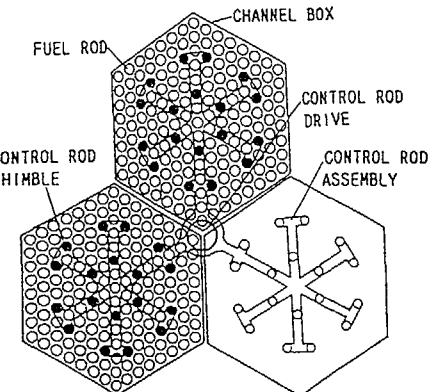


Fig.3. Cross section of fuel bundle and control rod assembly

#### PERFORMANCE EVALUATION

##### Calculation methods

One of the remarkable features of the plutonium generation BWR is that the effective moderator-to-fuel volume ratio is smaller than in current BWRs, so that the calculation method for microscopic epithermal cross sections and the nuclear data library for resonance energy range have an important role in nuclear characteristic evaluation. In particular, evaluations of burnup characteristics for the resonance-dominated neutron spectrum have some uncertainty. For precise numerical evaluation of fuel bundle designs, the VMONT<sup>7</sup>, in which a vectorized Monte Carlo neutron transport method is coupled with the burnup calculation, has been developed. The applicability of the VMONT code to tight lattice configurations was confirmed using the PROTEUS experimental data<sup>8</sup>.

For thermal hydraulic analysis, the critical power correlation for the tight lattice configuration gains increasingly in importance. So, the modified CISE critical power correlation<sup>9</sup>, which is based on the critical quality-boiling length correlation developed by CISE<sup>10</sup>, has been developed and verified using data from the experiment for the critical power of the closely packed lattice bundles. The proposed correlation can reproduce the experimental data within a standard deviation error of 9%<sup>9</sup>.

The transient behavior of a BWR involves a complex interplay between the inherent system thermal-hydraulics and neutronics and the active components. The transient behaviors in the reactor vessel were evaluated by a lumped-region model for in-reactor component thermal hydraulics coupled with a point reactor neutron kinetics model, followed by one-dimensional single channel analysis to estimate flow transient in a fuel

bundle More precise analyses by a three dimensional nodal kinetic code<sup>11</sup> are now in preparation. The modified CISE critical power correlation was used for thermal margin calculations.

#### Core performance

Performances of the proposed three designs of the plutonium generation BWR are summarized in TABLE III. In the study, the average exposure of discharged fuel bundles and the operational cycle were assumed to be 45GWd/t and 12 months respectively.

Figure 4 shows comparison of the core averaged axial void distributions of PGBR-II with that of current BWRs. The steam void is generated at a lower part of core than the current BWR designs due to the PGBR design concept of a higher outlet coolant quality. As a result, the core averaged void fraction is 51% for the PGBR-II and the effective moderator-to-fuel volume ratio less than 0.3 is realized. The required enrichments of fissile plutonium fed to natural uranium for discharged exposure of 45GWd/t are 6.5% for PGBR-I and II, 7.0% for PGBR-III. Evaluation confirms that the proposed designs have the plutonium generation ratios of ~1.0, which means that consumption of fissile plutonium is equal to generation of fissile plutonium.

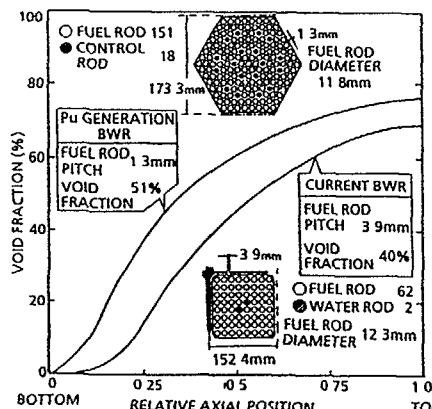


Fig.4. Comparison of fuel bundle configurations and axial distributions of void fraction

TABLE III  
Core Performance of Plutonium Generation BWR

| Parameter                         | PGBR-I | PGBR-II | PGBR-III |
|-----------------------------------|--------|---------|----------|
| Discharge exposure (GWd/t)        | 45     | 45      | 45       |
| Operational cycle length (months) | 12     | 12      | 12       |
| Pu-fissile enrichment* (w/o)      | 6.5    | 6.5     | 7.0      |
| Plutonium fissile inventory (t)   | 10.9   | 10.0    | 9.4      |
| Plutonium generation ratio**      | 1.02   | 1.02    | 1.0      |
| Maximum linear heat rate (kW/m)   | 18     | 27      | 30       |
| Minimum critical power ratio      | >1.3   | >1.3    | >1.3     |

\* The fissile plutonium is fed to the natural uranium.

\*\* Plutonium Generation Ratio  

$$= \frac{\text{Pu-fissile amount in discharged fuel}}{\text{Pu-fissile amount in new fuel}}$$

Thermal margin was evaluated using the modified CISC critical power correlation and the proposed designs are confirmed capable of having minimum critical power ratio (MCPR) of more than 1.3

#### Transient and Safety Analysis

The proposed designs of the plutonium generation BWR have negative reactivity power coefficients. The typical transients were analysed and the ΔMCPR, that is, decrease in thermal margin during transients was evaluated. On the evaluation, the characteristics of the active components in PGBR were assumed to have those of the ABWR's<sup>12</sup>. For example, internal pumps are utilized as recirculation pumps instead of jet pumps in the current BWRs.

Figure 5 shows the results of transient analyses. The maximal ΔMCPR of the PGBR-I is 0.13, which is nearly the same as the current BWR's. The PGBR-II has an increasing power density compared with the PGBR-I. Though the maximal ΔMCPR of the PGBR-II is 0.21, which is larger than the currents BWR's, boiling transient will not occur and the fuel integrity can be maintained because of the MCPR more than 1.3 in the rated power normal operation. Thermal margin of the PGBR-III is improved compared with the PGBR-II by improving a void reactivity coefficients and decreasing the bundle power.

In all cases, the maximum heat flux and the maximum vessel pressure during transients were confirmed to be maintained below the limiting values of the current BWRs.

From the safety aspects, a HPCS line break accident, which seems to be the most severe loss-of-coolant accident for the PGBRs, was also analysed. Analyses showed that the peak cladding temperature in LOCA is 550°C for the PGBR-II, which is less than the limiting value (1200°C) of the current BWRs.

#### ACTINIDE TRANSMUTATION

The design concept of the plutonium generation BWR seems to play an important role from a view point of storage of long-life actinide elements. In the second phase of PGBR development divided into two phase other actinide elements as well as plutonium are recycled together taking one step forward from only plutonium recycling in the first phases. Figure 6 shows that accumulation of neptunium-237 of which half life is about

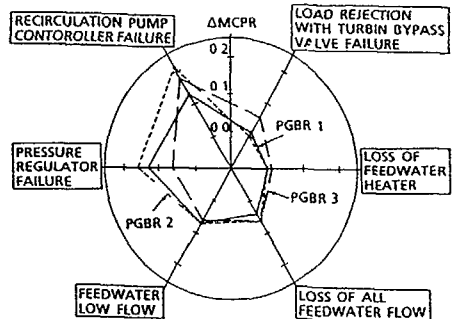


Fig.5. Thermal margin during typical transients

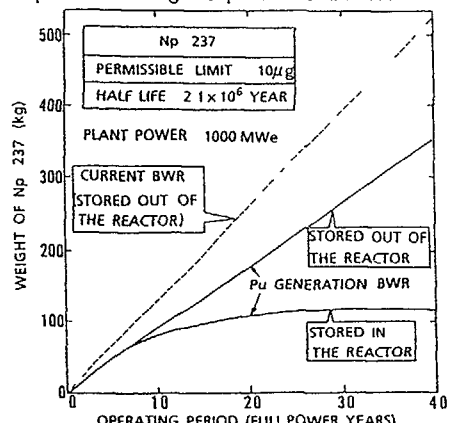


Fig.6. Accumulation of Np-237

$2 \times 10^6$  year becomes equilibrium at the amount of 120kg per 1GWe PGBR core. This result means that equilibrium state of neptunium between production rates and consumption rates is kept in PGBR under the condition that 120kg of neptunium-237 generated in current BWRs is fed to the plutonium-enriched natural uranium fuel bundles in the initial core of 1GWe PGBR, and a new recycle system can be realized with light water reactor technology, in which plutonium and other actinides are confined to only nuclear reactors and reprocessing plants.

#### CONCLUSION

The design concept of a plutonium generation BWR was proposed, which has a potential for achieving a plutonium generation ratio close to 1.0 and better natural uranium utilization by a factor of 5~10 compared with current LWRs. To achieve a higher conversion ratio, the effective moderator-to-fuel volume ratio of less than 0.3 was realized in the BWR by using a closely packed hexagonal lattice with the rod-to-rod clearance of 1.3~1.5mm and a higher core average void fraction of more than 50%. Numerical evaluation for three kinds of designs for BWRs with electric power of 600MW and 900MW showed that the proposed designs are feasible from nuclear, thermal-hydraulic and safety aspects, and that the concept has another potential of realizing a new recycle system in which plutonium and other actinide are confined to only nuclear reactors and reprocessing plants.

#### REFERENCES

1. M. C. EDLUND, "High Conversion Ratio Plutonium Recycle in Pressurized Water Reactors," *Ann. Nucl. Energy*, **2**, 801 (1975)
2. W. OLDEKOP et al., "General Features of Advanced Pressurized Water Reactors with Improved Fuel Utilization," *Nucl. Technol.*, **59**, 212 (1982)
3. V. G. RODRIGUES, "Untersuchungen zum Hochkonvertierenden Siedewasserreaktor," PhD Thesis, Hannover University, (1983)
4. R. TAKEDA and M. AOYAMA, "Natural Uranium Utilization and the Role of HCR in the New Generation LWR," Preprint 1986 Fall Meeting At. Energy Soc. Japan, F-8 (1986)
5. R. TAKEDA et al., "Study on Plutonium Generation BWR Core," Preprint 1987 Fall Meeting At. Energy Soc. Japan, D-4 (1987) (in Japanese)
6. R. TAKEDA et al., "A Conceptual Core Design of Plutonium Generation Boiling Water Reactor", Proc. of the 1988 International Reactor Physics Conf. Vol. III, 119 (1988)
7. H. MARUYAMA et al., "A Monte Carlo Method with Pseudo Scattering for Neutron Transport Analysis," in Proceedings of International Topical Meeting on Advances in Reactor Physics, Mathematics and Computation, Paris (Apr. 1987)
8. Y. MORIMOTO et al., "Development of Vectorized Monte Carlo Nuclear Analysis Program VMONT(3) -Analysis of Tight Lattice Cell-," Preprint 1987 Fall Meeting At. Energy Soc. Japan, D-60 (1987) (in Japanese)
9. T. MATSUMOTO et al., "Development of Critical Power Correlation for Tight Lattice Fuel Assembly," Preprint 1987 Annu. Meeting At. Energy Soc. Japan, E-40 (1987) (in Japanese)
10. S. BERTOLETTI et al., "Heat Transfer Crisis with Steam-Water Mixtures," *Energia Nucleare*, **12**, 121 (1965)
11. Y. Bessho et al., "Development Program Based on Nodal Expansion Method," submitted to ANS 1990 Annual Meeting, (1990)
12. S. A. HUCIK et al., "Outline of the Advanced Boiling Water Reactor (ABWR)," Proc. of Second International Topical Meeting on Nuclear Power Plant Thermal Hydraulics and Operations, 4-10, (1986)

## STEAM-WATER POWER REACTOR CONCEPT

P.N. ALEKSEEV, E.I. GRISHANIN, Yu.A. ZVERKOV,  
V.V. KUZNETSOV, A.G. MOROZOV, V.V. ORLOV,  
I.S. SLESAREV, V.A. STUKALOV, S.A. SUBBOTIN,  
T.D. SHCHEPETINA, L.N. FALKOVSKIY  
I.V. Kurchatov Institute of Atomic Energy,  
Moscow,  
Union of Soviet Socialist Republics

### Abstract

The work considers a steam-water power reactor (SWPR) concept aimed at the improvement and development of thermal light-water reactors. The basic features of the proposed concept are reported along with the results of some development efforts.

---

The analysis of the present-day trends in the nuclear power development indicates that the rate of growth of the total capacity of nuclear power plants (NPPs) decreases in many countries [1]. The deceleration of nuclear power progress and the recent serious NPP accidents arouse interest for the development of a new generation of NPPs to improve cardinally

- the NPP safety, in particular, with respect to severe accidents
- the NPP economy and
- the efficiency of fuel utilization

and to extend the scope of NPP use in the nuclear power industry.

The preference will be seemingly given to the NPP development efforts which ensure the solution of at least one of the above problems.

The priority development in the world nuclear power engineering has been given by now to the light-water thermal reactors (VVER, PWR and BWR). Moreover, the developed machine-building base and tested

technology can favour the dominant role of LWRs in the nuclear power engineering in the nearest future.

At the same time the up-to-date LWR designs are characterized by some significant shortcomings. Among them are:

- relatively large reactivity margins in the core;
- poor protection against the LOCA type accidents, sensitivity to the accidents with coolant circulation break;
- low efficiency of fuel utilization;
- low thermodynamics parameters;
- low-grade heat limiting the sphere of LWR usefulness.

Nevertheless, the highest, at present, economy of the LWR-based NPPs resulting from the water technology cheapness and availability and the large experience in the LWR development and operation is a powerful incentive to the efforts on improving the nuclear reactors of this type. Therefore, the development of such reactor concepts is urgent as could employ the LWR up-to-date technology and industrial infrastructure and satisfy the present-day requirements to a larger degree.

In authors' opinion, the essential reduction in coolant density in turning to the steam-water cooling of the reactor is one possible way of the LWR improvement and development.

The idea of using steam as a coolant is not original; it was discussed as early as at the first Geneva conference on peaceful use of atomic energy [2].

The realizability of a low-cost reactor loop using the commercial components and technology has aroused interest for steam-cooled reactors (SFR) [3]. The development works on SFRs as an alternative of sodium breeders were carried out rather actively in the sixties in some countries (USA, FRG and others). However, without any advantage gained over the sodium breeders the SFR concept did not

reach completeness and the SFR development works had been terminated by the seventies in all countries. Moreover, the negative attitude to SFRs was promoted by the unsufficient confidence in ensuring the NPP safety accounted for the large void effect of reactivity and by the lack of any substantiation for the workability of the fuel elements at coolant pressures of up to 18.0 MPa and cladding operating temperatures of up to 650 °C.

For the period elapsing from the seventies the requirements to NPPs have changed; the experience has been gained in the fuel element operation in fast reactors at high temperatures and fluences; new structural materials have been developed. All these together with the water technology attractiveness have revitalized the interest to the reactor steam cooling concept [4, 5, 6].

This work proposes the concept of a pressure vessel power reactor cooled with steam-water mixture (steam-water power reactor - SWPR) and reports the basic results of the development works.

#### STEAM-WATER POWER REACTOR CONCEPT

The use of steam-water mixture for the reactor cooling is a key feature of the concept [7].

The utilization of heat of water-steam phase transition reduces considerably the weight consumption of coolant and ensures an efficient heat transfer at a small degree of coolant heating (~10-50 °C), an outlet steam temperature of 360-400 °C and a pressure of 10.0-16.0 MPa. The efficient heat transfer permits cladding operation temperatures of 450-500 °C to be reached and low-swelling ferritic-martensitic steels to be used as a cladding material. The relatively high steam parameters at the reactor outlet allow the efficiency of the steam-turbine cycle to be increased up to 35-37 % and the area of SWPR use to be potentially extended.

It is possible to avoid the core dryout choosing the parameters of steam-water mixture (the operation with post dryout parameters of coolant). The experimental study of the fuel assembly thermohydraulics confirms the realizability of a required efficiency of heat transfer using steam-water mixture with an inlet void fraction  $x_{in} \sim 0.35-0.40$  at a pressure of 16.0 MPa.

#### TECHNICAL ASPECTS OF THE SWPR CONCEPT

The engineered features of the SWPR concept are based on the experience in the design and operation of the VVER-type pressure-vessel reactors and the BN-type fast reactors (LMFBRs).

The SWPR design as a vessel type reactor one (see Fig. 1) presupposes to use the VVER vessel designed for a pressure of up to 18.0 MPa. The loop arrangement of the primary circuit presupposes the presence of a main circulator, steam generators and reservoirs of the emergency core cooling system in each loop. The fuel element and assembly designs are similar to those for the fast reactors of the BN-type. The NPP has two circuits (in principle, it is possible to use the one-circuit NPP layout). The primary equipment is disposed within the containment.

The steam-water mixture preparation and distribution system asks for the original solutions and their substantiation. The steam recirculation through the reactor could be realized by steam blowers with a separate circuit as well as water-jet circulators (jet pumps) built in the reactor vessel. The steam-water mixture is prepared in the first case in special nozzle mixers set at the fuel assembly inlet, in the second case - directly in the jet pumps. The water is fed into the reactor by the main circulator (see Fig. 2).

The analysis and optimization of above principles are beyond the scope of this paper. It should be noted that some experimental

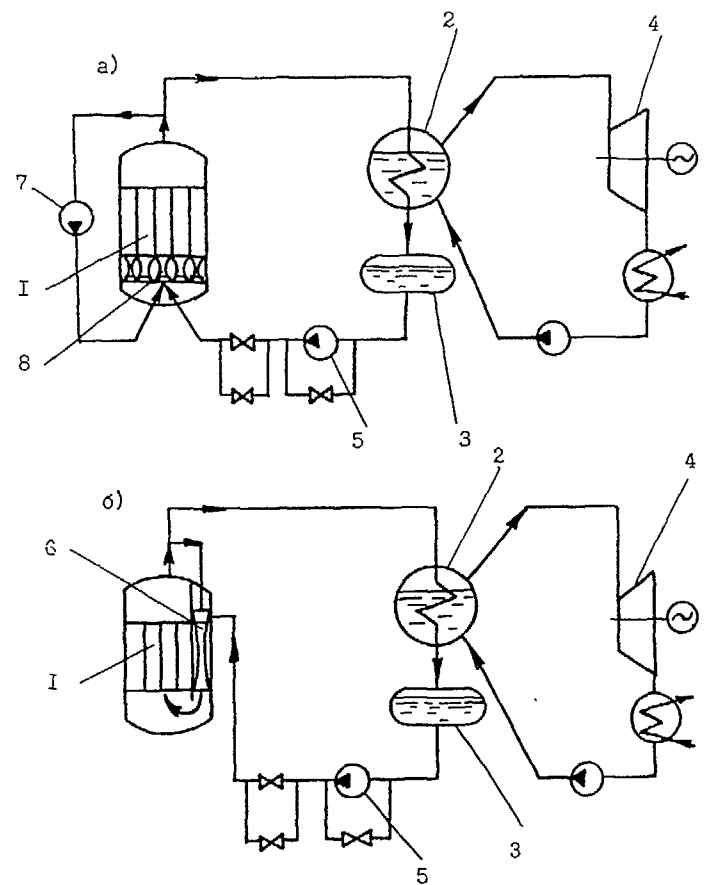


Fig. 1. Diagram of heat circuits at NPP with SWPR for the versions of steam recirculation by steam blowers (a) and by jet pumps (b):

1 - core; 2 - steam generator; 3 - buffer hydroaccumulator;  
 4 - turbine generator; 5 - MCP; 6 - jet pump;  
 7 - steam blower; 8 - steam-water mixer (SWM)

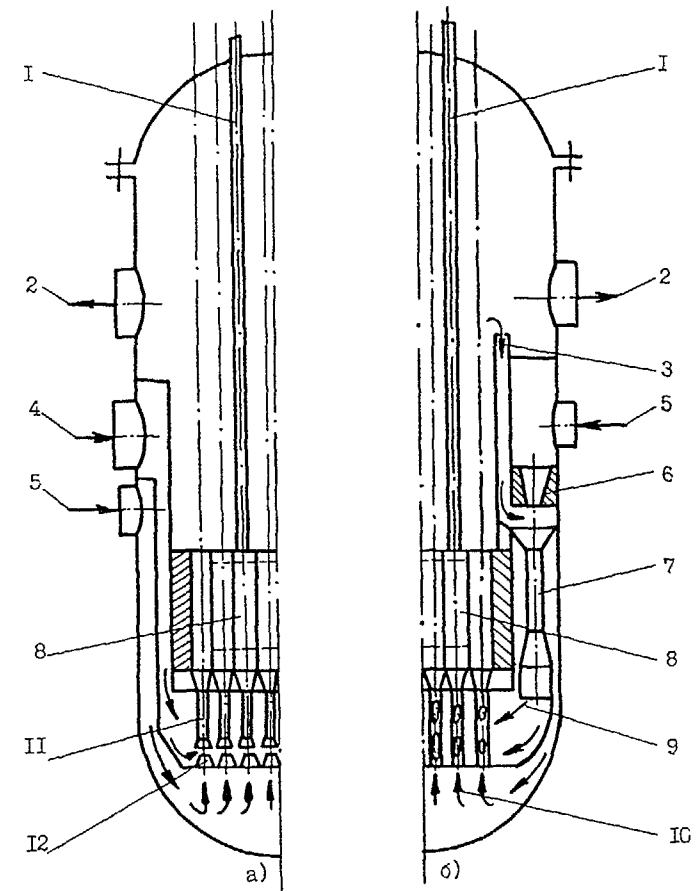


Fig. 2. Schematic diagram of SWPR for the versions of steam recirculation by steam blowers (a) and by jet pumps (b):

1 - shield pipe unit with control and safety system; 2 - steam withdrawal; 3 - steam to the suction side of jet pumps; 4 - steam addition from steam blowers; 5 - water addition from MCP; 6 - water-spraying nozzle; 7 - jet pump; 8 - core; 9 - steam-water mixture addition to fuel assemblies; 10 - addition of water with low flow rate; 11 - steam-water mixer (SWM); 12 - SWM water-spraying nozzles

investigations which have been made give confidence in the solvability of the arising problems.

The preliminary economical analysis of the complex of the used engineering principles by bringing into comparison the main functional components of the VVER- and SWPR-based NPPs on their specific consumption of materials showed that the unit capital costs of their construction are comparable. Moreover, the higher power density of the SWPR equipment permits the reactor vessel height and the overall dimensions of steam generators to be decreased. The considerable reduction of the required flow rate of the primary water makes it possible to minimize the piping diameters. There is no necessity in pressurizers and a liquid boron control system. All the above are good reasons to expect an additional reduction in the capital component of the SWPR cost at the expense of decreasing the specific consumption of materials in the primary equipment and the constructions.

#### POTENTIAL OF THE SWPR NUCLEAR SAFETY

In developing the SWPR concept the goal was set to increase the reactor safety potential in comparison with the VVER reactors. The nuclear safety of the SWPR concept is based mainly on the inherent physical features of the reactor which are attained by a proper choice (see Figs. 3-6) of

- the composition and size of the core, shields and their components;
- the parameters of steam-water mixture;
- the core power density;
- the isotope compositions of the charged fuel and the refuelling strategy.

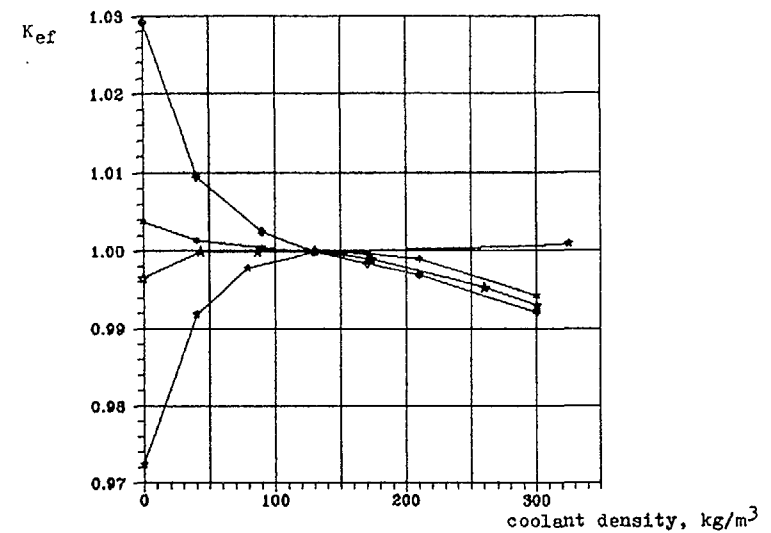


Fig. 3.  $K_{ef}$  vs coolant density for various SWPR versions

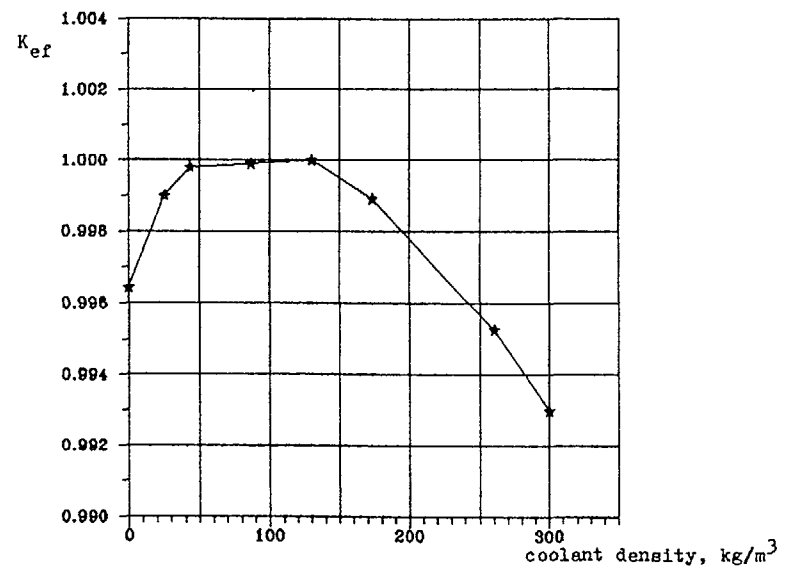


Fig. 4. Optimal dependence of  $K_{ef}$  on coolant density for SWPR

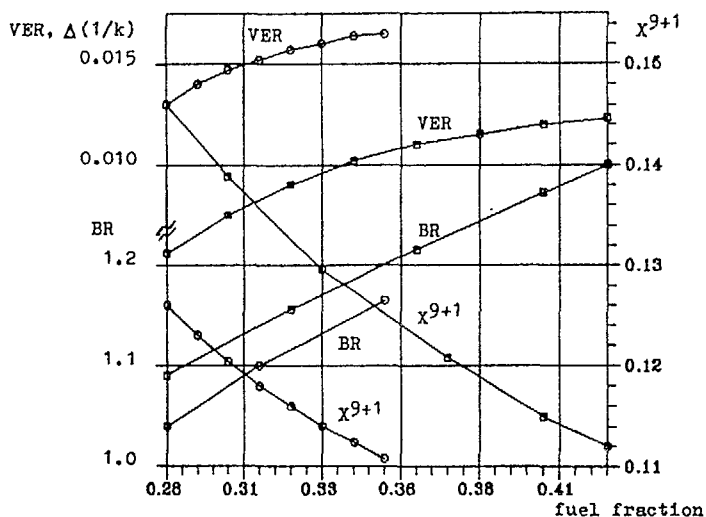


Fig. 5. Void effect of reactivity (VER), breeding ratio (BR) and critical fuel enrichment ( $X^{9+1}$ ) vs fuel fraction in SWPR core at blanket thickness of 25 cm:

○ -  $H_{core} \cdot D_{core} = 1.5 \cdot 3$  m;  
□ -  $H_{core} \cdot D_{core} = 1.0 \cdot 3$  m

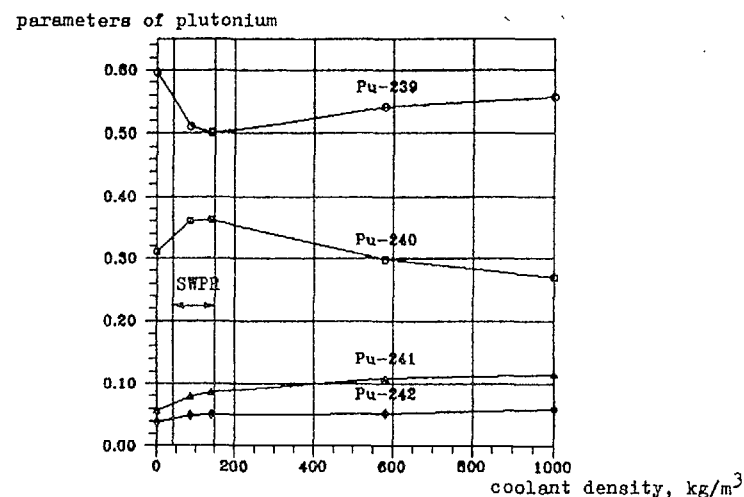


Fig. 6. Parameters of equilibrium isotopic composition of plutonium in SWPR core vs working coolant density

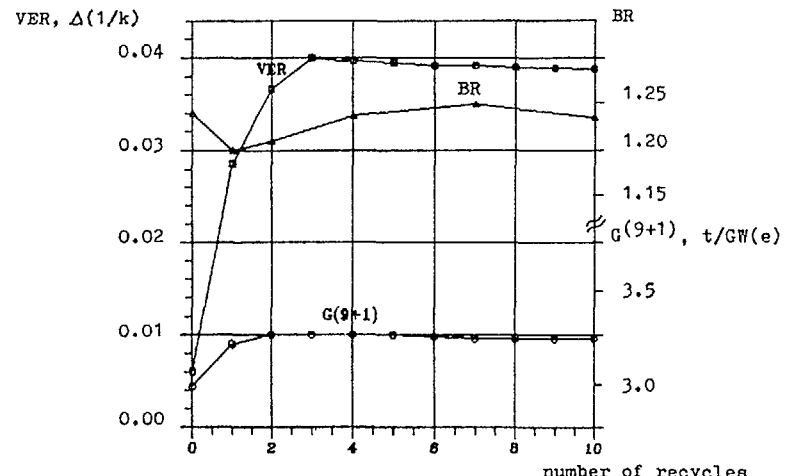


Fig. 7. Void effect of reactivity (VER), breeding ratio (BR) and average loading of nuclear fuel ( $G^{(9+1)}$ ) to SWPR core vs number of fuel recycles

It should be noted that the changeability of the SWPR coolant density in a wide range gives a greater freedom in "designing" the reactivity effects determining the reactor safety:

- the non-positive void coefficient;
- the required reactor subcriticality in flooding and whereby the realization of an additional shutdown system;
- the minimum reactivity margins for fuel burnup.

Then the effective multiplication factor versus the collant density depending on the contribution of neutron leakage from the reactor to the reactivity balance could correspond to one of the curves in Fig. 3. The form of curve corresponding to one of the SWPR versions (see Fig. 4) is more preferable.

As noted the reactor flooding with water in the SWPR case is an independent system of reactivity handling and ensures the residual heat removal. The flooded reactor cannot be put into the critical

state by means of control rods. To do it the coolant should be converted to the steam-water state (for example, at the cost of pump energy).

The features of the SWPR neutron spectrum ensure the low sensitivity of reactivity to the coolant temperature variations (which excludes the accidents with "cold" loop connection) and eliminate the problems connected with the xenon poisoning and "iodine pit" effects.

The use of steel claddings with their high corrosive stability and strength excludes the fast chemical reactions between the coolant and the structural components.

#### NEUTRON-PHYSICAL CHARACTERISTICS AND EFFICIENCY OF FUEL UTILIZATION

The SWPR reactor is characterized by a fast-resonance energy spectrum similar, to a large extent, to that of the conventional fast reactors (see Fig. 8). The higher fraction of neutrons in the range of high ( $E_n > 0.8$  MeV) and resonance ( $E_n < 20-50$  keV) energies is characteristic of the SWPR spectrum.

The fast-resonance nature of the neutron spectrum and the essential change of the coolant density in the reactor are responsible for the close connection of the neutron-physical and thermohydraulic characteristics and require to calculate in detail the space-energy distribution of neutrons over the whole range of energies with the aim of the correct allowance for:

- the heterogeneous and transport effects;
- the Doppler effect;
- the change of the isotope composition during the fuel operating period.

The consideration of the above effects is of special significance in analyzing the transient and accident conditions.

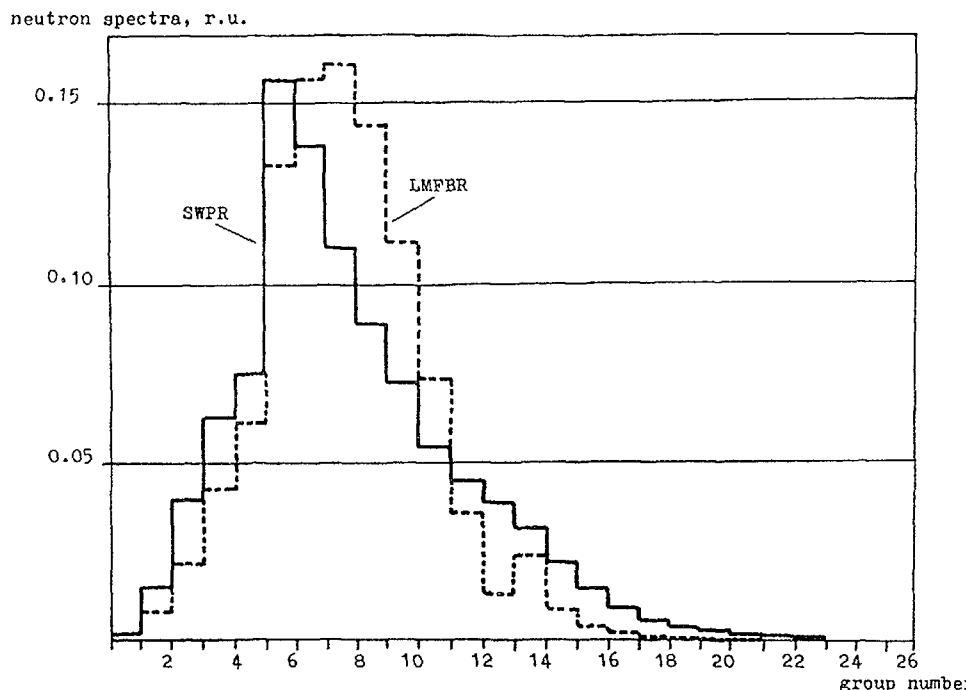


Fig. 8. Comparison of 26 group neutron energy spectra in the cores of liquid metal fast reactor (LMFBR) and SWPR

The SWPR performance depends to a considerable degree on the fuel element pitch, coolant density and fraction of the parasitic capture of neutrons in the core (see Figs. 4-6). The features of the SWPR energy spectrum create conditions for the nuclear fuel breeding with  $BR > 1$  allowing the reactor operation under self-sustaining conditions. In this case the maximum fuel burnup attains about 7-10 %. The high level of breeding in the SWPR core ensures the low reactivity margins (~1-2 %) for fuel burnup.

The investigations have demonstrated a strong dependence of the void effect of reactivity on the isotope composition of plutonium in the fuel charge and on the dynamics of its change (see Fig. 7). The

isotopic composition of plutonium with the highest Pu-241 content and the lowest Pu-240 and Pu-242 content is more preferable for decreasing the void effect of reactivity. However, in the SWPR reactor the Pu-241 content in the equilibrium isotope composition is low (about 6-7 %) offering the additional requirements for the choice of the isotope composition of the charged fuel, the strategy and duration of its irradiation in the reactor.

Table 1. Comparison of the main physical characteristics of VVER and different versions of SWPR

| Characteristic   | VVER                    | SWPR                | SWPR                 | SWPR                  |
|--|-------------------------|---------------------|----------------------|-----------------------|
| Electrical power, MW   | 1000                    | 1000                | 1000                 | 840                   |
| Thermal power, MW  | 3000                    | 2700                | 2700                 | 2270                  |
| Fuel   | UO <sub>2</sub>         | UO <sub>2</sub>     | (U+Pu)O <sub>2</sub> | (U+Pu)O <sub>2</sub>  |
| Core height/diameter, m  | 3.53*3.12               | 1.5*2.7             | 1.5*2.7              | 0.8*3.0               |
| Fuel element diam., mm   | 9.1*0.55                | 9.0*0.55            | 9.0*0.55             | 6.0*0.3               |
| Relative pitch of fuel lattice                                   | 1.40                    | 1.11                | 1.11                 | 1.20                  |
| Maximum fuel cladding temperature (without overheat factors), °C | 350                     | 450                 | 450                  | 500                   |
| Maximum rod linear heat rate, kW/m                               | 45.0                    | 48.5                | 48.5                 | 30.0                  |
| Average fuel enrichment, %                                       | 4.4**                   | 14.0                | 11.9*                | 12.3*                 |
| Maximum fuel burnup, %   | 4.1**                   | 10.0                | 10.0                 | 7.0                   |
| Specific fuel loading, t/GW(e)                                   | 2.1                     | 3.7                 | 3.6***               | 2.9                   |
| Reactor lifetime, eff. yrs.                                      | 2.4                     | 2.1                 | 2.2                  | 1.1                   |
| Breeding ratio   | - core                  | -                   | 0.61                 | 0.90                  |
|  | - reactor               | 0.5                 | 0.75                 | 1.10                  |
| 0.82   |                         |                     |                      | 0.92                  |
| Void effect of reactivity, % Δk/k                                | < 0                     | -0.8                | -0.4                 | -0.5                  |
| Burnup reactivity margin, % Δk/k                                 | 10-12                   | 2.0                 | 1.5                  | 1.5                   |
| Power coefficient of reactivity, (Δk/k)/MW(th)                   | -(5-7)*10 <sup>-5</sup> | -5*10 <sup>-6</sup> | -4*10 <sup>-6</sup>  | -3.5*10 <sup>-6</sup> |

\* - for fissile plutonium isotopes (<sup>239</sup>Pu + <sup>241</sup>Pu);

\*\* - average fuel burnup;

\*\*\* - core contains a fraction of solid moderator ( $\epsilon_{mod} \approx 0.075$ )

#### BASIC RESULTS OF DEVELOPMENT WORKS

Some versions of the reactor installation investigated have a capacity ranged from 500 to 1500 MWe and various parameters of steam-water mixture (differing in void fraction, pressure) at the core inlet. The versions were analyzed in a complex way - with allowance for the parameters of safety, breeding and the thermohydraulic characteristics. The results of the development works have demonstrated the possibility of ensuring a high level of safety for the power units of various unit capacity. Tables 1, 2 summarize the basic characteristics of some of the SWPR versions in comparison

Table 2. Comparison of the main thermal and technical parameters of VVER and various versions of SWPR

| Parameter                                 | VVER            | SWPR            | SWPR                 | SWPR                 |
|---|-----------------|-----------------|----------------------|----------------------|
| Electrical power, MW                      | 1000            | 1000            | 1000                 | 840                  |
| Thermal power, MW                         | 3000            | 2700            | 2700                 | 2270                 |
| Number of loops                           | 4               | 2               | 2                    | 2                    |
| Fuel                                      | UO <sub>2</sub> | UO <sub>2</sub> | (U+Pu)O <sub>2</sub> | (U+Pu)O <sub>2</sub> |
| <u>Reactor coolant parameters:</u>        |                 |                 |                      |                      |
| Pressure, MPa                             | 16.0            | 16.0            | 16.0                 | 10.0                 |
| Temperature, °C                           |                 |                 |                      |                      |
| - inlet                                   | 289             | 348             | 348                  | 310                  |
| - outlet                                  | 322             | 360             | 360                  | 380                  |
| Average density, kg/m <sup>3</sup>        | 714             | 130             | 130                  | 50                   |
| Flow rate, kg/s                           | 16600           | 3740            | 3740                 | 5080                 |
| - including steam                         |                 |                 |                      |                      |
| Inlet mass steam content, %               | -               | 1540            | 1540                 | 4600                 |
| Pressure losses in the circuit, MPa       | 0.60            | 0.65            | 0.65                 | 0.70                 |
| Power consumption for pumping, MW         | 20.0            | 10.0            | 10.0                 | 43.0                 |
| - including steam pumping                 |                 |                 |                      |                      |
| <u>Parameters of steam turbine cycle:</u> |                 |                 |                      |                      |
| Pressure, MPa                             | 6.3             | 9.4             | 9.4                  | 9.0                  |
| Temperature, °C                           | 279             | 340             | 340                  | 360                  |
| Efficiency, %                             | 33.3            | ~37.0           | ~37.0                | ~37.0                |

with the VVER-1000 reactor. The presented SWPR characteristics should be considered to be preliminary and to require the additional development efforts, optimization and experimental substantiation.

#### CONCLUSION

With the aim of improvement and development of light-water thermal reactors the present work offers a steam-water power reactor concept.

The concept considered is directed to the development of a high-safety reactor, which is ensured at the cost of:

- decreasing the reactivity margin for fuel burnup;
- introducing an additional independent system of reactivity handling (the reactor flooding with water);
- managing the accident situations due to an unauthorized subcooling of the coolant;
- increasing the stability margins of the core materials (giving zirconium up);
- neglecting the problems connected with xenon poisoning.

The features of the SWPR fast-resonance energy spectrum of neutrons are responsible for a high efficiency of fuel utilization (up to the conditions of nuclear fuel self-supply) and a reduced reactor throughput of fuel.

The use of the present-day LWR technology and machine-building base ensures the capital costs of the SWPR-based NPP construction comparable with those for the LWR-based NPP. The possibility of decreasing the specific expenditure of materials in the primary circuit and structures owing to a high-efficiency heat transfer makes it possible to expect the reduction in the capital component of the SWPR-based NPP cost. The SWPR-based NPP could be designed to operate both under condensation conditions and as a NHPP.

The preliminary results of the investigations showed the principal solvability of the basic problems arising in the implementation of the SWPR concept. This makes it possible to make a conclusion about the reality and promising future of the proposed concept and the usefulness of its further detailed development.

#### REFERENCES

1. Blix H. IAEA today. "Energy: economics, engineering, ecology" 1985, № 9, pp. 2-12.
2. Power Reactors. - In book: Proceedings of the International conference on peaceful use of atomic energy (8-20 August 1955, Geneva). - Moscow: Gosenergoizdat, 1958, v. 3.
3. Kalafati D.D., Petrov S.I., Ignat'ev V.V. Designing of NPPs with Steam-Cooled Reactors: Review. - Teploenergetika, 1972, № 3, pp. 88-92.
4. Analysis of the Breeding Properties of Steam-Cooled Fast Reactors: Preprint/D.D.Kalafati, I.S.Slesarev, V.A.Stukalov, T.D.Shchepetina. - Moscow: IAE, 1984, № 3996/4.
5. Prospects in the Improvement Breeding in the Steam-Cooled Reactors with the Heterogeneous Core: Preprint/D.D.Kalafati, A.G.Morozov, I.S.Slesarev, T.D.Shchepetina. - Moscow: IAE, 1984, № 3997/4.
6. Schultz M.A., Edlund M.C. A New Steam-Cooled Reactor. - Nuclear Science and Engineering, 1985, v. 90, pp. 391-399.
7. Inventor's certificate № 776334 (USSR). Method of Fast-Reactor Core Cooling/V.V.Orlov, E.I.Grishanin, V.M.Murogov, et al. - Bulletin of inventions, 1986, № 7.

## HIGH CONVERSION THORIUM FUEL ALTERNATIVES FOR CANDU REACTORS

D. SERGHIUTA, V. RAICA,  
D. GAMULESCU, E. NICHITA

Institute for Nuclear Power Reactors,  
Pitesti, Romania

### Abstract

The good neutron economy and the use of on-power refueling allow the CANDU reactor a wide variety of fuels and fuel cycles to be adapted to with no need of major alterations in the standard core design.

A wide variety of thorium fuel cycles can be implemented in the CANDU reactor. These may be classified as (a) cycles without reprocessing, using separate fissile and fertile channels or separate fissile and fertile bundles, and (b) cycles with reprocessing or thorium conventional cycles, based on U-233 recycle and concurrently requiring an external fissile source such as enriched uranium or plutonium. Just on the line stands the self sustaining thorium cycle which, once the equilibrium is reached, no longer requires fissile addition from outside.

With regard to the SSET (Self Sustaining Equilibrium Thorium) cycle the main problems reside in obtaining appropriate discharge burnup from the economic point of view and conversion rates to account for the through-cycle losses at the foreseeable technological performance of the reprocessing facilities.

Three possible solutions of using thorium fuel in the CANDU reactor are examined in the paper:

- the use of different enrichment fueling zones,
- the use of a thorium blanket instead of the D2O reflector, and
- the use of metallic thorium fuel.

The above solutions emerged from the need of obtaining high conversion rates and from that of keeping the main core parameters within the operational limits of the standard CANDU reactor.

### 1. Introduction

The good neutron economy and the use of on-power refueling allow the CANDU reactor a wide variety of fuels and fuel cycles to be adapted to with no need of major alterations in the standard core design.

Implementing the thorium fuel cycle in CANDU in the SSET (Self Sustaining Equilibrium Thorium) alternative offers a really

attractive long-term possibility of maintaining the installed nuclear power in CANDU type reactors for long, with no need of fissile addition from outside.

However, thorium fuel cycle implementation involves the problem of its initiation and support, since U-233 can only be obtained by irradiating thorium in nuclear reactors. In view of overriding this difficulty a series of transition fuel cycles have been proposed to connect the natural uranium fueled reactors with the U233-Th fueled ones.

The primary scope of the transition cycles consists in continuously satisfying the energy demand while building up a stock of fissile material (Pu 239 and/or U233), necessary for initiating and sustaining the thorium cycles.

Various chains of fuel cycles of this kind are presented in detail in the numerous papers on the subject matter (/1/,/2/,/3/). The SSET cycle implementation is finally being considered in all of those cases as an alternative of great interest for the thermal reactors and particularly for the CANDU reactors, provided the uranium cost increases.

The SSET cycle implementation rises at present specific technological difficulties related to the fuel cycle requirements, i.e.U233 reprocessing and highly radioactive fuel fabrication and handling. The economic aspects can hardly be estimated now as no practical basis exists for cost evaluation of the technological processes involved.

The effects of SSET cycle implementation in a CANDU based nuclear power system are presented in the paper together with some ways of reaching the equilibrium in the SSET cycle and the alternatives of increasing the discharge burnup obtainable from a standard CANDU reactor working in the SSET cycle.

### 2. Aspects of the SSET cycle implementation in a nuclear power system with CANDU reactors

A nuclear power system developing exclusively on a CANDU reactor basis on a Fischer-Pry type logistics curve was considered for analyzing the effects of the SSET cycle implementation. A fifty-year time interval was considered, the installed nuclear power reached at the end of the interval being 17.5 GW(e) with a mean growth period of 10 years. The system is initially developing on natural uranium fueled CANDU reactors. Three scenarios of the various alternatives studied are presented in the paper, as follows

- a) CANDU-U<sub>n</sub> + CANDU SSET
- b) CANDU-U<sub>n</sub> + CANDU (U,Pu)O<sub>2</sub> + CANDU SSET
- c) CANDU-U<sub>n</sub> + CANDU (Pu,Th)O<sub>2</sub> + CANDU SSET

The (U,Pu)O<sub>2</sub> fueled CANDU reactors work in the natural uranium-plutonium cycle with 0.2% fissile Pu doping in the charged fuel and without Pu recycle. The specific data are that given in reference /10/.

The ( $\text{Pu},\text{Th}$ )O<sub>2</sub> fueled CANDU reactors work in the once-through cycle, with no recycle, U<sub>233</sub> being stored for further use in SSET cycle reactors. The burnup is 30000 Mwd/tHE. The specific information regarding this kind of reactors and the ones operating in the SSET cycle were taken from reference /5/. Two alternatives were considered for the SSET reactors, characterized by different discharge burnups of 10000 and 14000 Mwd/tHE, respectively (further on denoted as SSET 10 and SSET 14).

In all of the cases it was considered that the first reactor being operated in an advanced fuel cycle becomes operational in the 20-th year of the scenario.

The penetration model developed by Fischer and Prv used in the FURST Canadian code /14/ was also used in our analyses. A discretisation technique was applied using a 600MW power unit. The model was included in a calculational package also utilizing the SCENARIOS code, developed at IAEA by W.Benette as a module for evaluating the materials requirements.

A lower limit of 8 years was imposed to the transition period for the reactors penetrating the system (the time interval elapsed since the first reactor was introduced up to the moment all the reactors of the kind completely penetrate the system).

### 2.1. Scenario "a"

The main parameters characterizing the first growth scenario (a) are presented in the following table

|                                 | SSET 10 | SSET 14 |
|---------------------------------|---------|---------|
| Natural uranium consumption (t) | 36400   | 27100   |
| Transition period (years)       | 17      | 14      |

Although this scenario conduced to the largest effects in the natural uranium requirements, the following aspects have to be pointed out here

- shifting the moment of introducing the first advanced reactor conduced to the reduction of the transition period, therefore a limiting time can be determined to obtain the same low value for the natural uranium consumption in the system.

- U<sub>233</sub> reprocessing requires a rapid growth of the U<sub>233</sub> reprocessing and fabrication capacities (it is practically shown that they ought to be available at the beginning of the year following the introduction of the first advanced reactor)

- large reprocessing capacities are needed, both for reprocessing the fuel discharged from the natural uranium fueled reactors and for and fabrication, with strong effects on the total costs in the system.

### 2.2. Scenario "b"

Introducing the ( $\text{L},\text{Pu}$ )O<sub>2</sub> CANDU reactors as an intermediate alternative allows the postponing of the SSET reactor introduction with effects upon the pressure induced by the need of the U<sub>233</sub> reprocessing and fabrication technologies.

Varying the natural uranium ratio consumed in ( $\text{L},\text{Pu}$ )O<sub>2</sub> CANDU reactors generated important effects upon the natural uranium consumption in the system, the transition period and the moment of introducing the SSET reactors. The main parameters characterizing this scenario are presented in the following table

|  | SSET 10 | SSET 14 |
|--|---------|---------|
| Natural uranium consumption(t)   | 38800   | 32100   |
| Year of introducing the first SSET reactor                                       | 33      | 30      |
| Year when ( $\text{L},\text{Pu}$ )O <sub>2</sub> CANDU reactors leave the system | 43      | 42      |

The values presented correspond to a natural uranium consumption in ( $\text{L},\text{Pu}$ )O<sub>2</sub> CANDU reactors of 30% from the minimum natural uranium quantity required by the system consumption.

By shifting the moment of ( $\text{L},\text{Pu}$ )O<sub>2</sub> CANDU reactors introduction cases are obtained when the implementation of this reactors is no longer possible. This occurs in all the cases when the moment of introduction corresponds to the moment when more than 50% of the natural uranium quantity has already been consumed. In this way the result suggested by M.Milgram / 1/ was numerically obtained.

The main conclusions of the study are outlined below

- the transition period decreases while increasing the natural uranium ratio assigned to the ( $\text{L},\text{Pu}$ )O<sub>2</sub> CANDU reactors. For a minimum length of time of 8 years, a maximum acceptable value of 0.5 results for this ratio.

- the moment of introducing the first SSET reactor is shifted while increasing the natural uranium ratio assigned to the ( $\text{L},\text{Pu}$ )O<sub>2</sub> CANDU reactors, because of the slower plutonium accumulation in the system

- the natural uranium requirement in the system increases with the ratio assigned to the ( $\text{L},\text{Pu}$ )O<sub>2</sub> CANDU reactors, due to the fact that those reactors produce a smaller amount of plutonium as compared to the natural uranium fueled ones

- the pressures are lowered upon the reprocessing of the uranium burned in natural uranium fueled CANDU reactors, as concerns the production capacities size, upon the U<sub>233</sub> reprocessing, as concerns the moment when the first capacity is to become available, and also upon the and fabrication, in the same way

### 2.3. Scenario "c"

As concerns the third scenario (c), the initially slower plutonium accumulation rate determined the moment of introducing the first advanced reactor to be shifted, this fact being also required by the burnup value in the SSET reactors.

The main specific parameters are listed below:

|   | SSET 10 | SSET 14 |
|---|---------|---------|
| Natural uranium consumption(t)                              | 41500   | 37600   |
| Year of introducing the first (Th,Pu)O <sub>2</sub> reactor | 23      | 22      |
| Year of introducing the first SSET reactor                  | 30      | 30      |
| Year when natural uranium CANDU reactors leave the system   | 43      | 40      |
| Year when (Th,Pu)O <sub>2</sub> reactors leave the system   | 44      | 42      |

This scenario was fund advantageous from the point of view of technological and economical aspects.

The technological and economical parameters characterizing this scenario are presented in the following tables:

|  | UN-Reference | Scenario a | Scenario c |
|--|--------------|------------|------------|
| Fuel cycle services cost (mil.\$)                | 1400         | 4900       | 4090       |
| Natural uranium consumption (t) (for - 50 years) | 69           | 400        | 34200      |
| Total natural uranium needed (t)                 | 105400       | 30400      | 34200      |

|                    | Nr.of plant | Year | Scenario a Capacity(t) | Year | Scenario c Capacity(t) |
|--------------------|-------------|------|------------------------|------|------------------------|
| Pu-reprocessing    | 1           | 17   | 1690                   | 17   | 600                    |
|                    | 2           | -    | -                      | 29   | 1150                   |
| U-233-reprocessing | 1           | 21   | 500                    | 29   | 840                    |
|                    | 2           | 31   | 910                    | 44   | 200                    |
|                    | 3           | 39   | 500                    | 53   | 840                    |
| L-Fuel Fabrication | 1           | 17   | 250                    | 17   | 450                    |
|                    | 2           | -    | -                      | 26   | 900                    |
| Y-Fuel Fabrication | 1           | 21   | 500                    | 34   | 840                    |
|                    | 2           | 31   | 910                    | 44   | 200                    |
|                    | 3           | 34   | 500                    | 47   | 840                    |
|                    | 4           | 44   | 910                    | -    | -                      |
|                    | 5           | 47   | 900                    | -    | -                      |

### 3. Establishing of the equilibrium conditions in the SSET cycle

#### 3.1 Evolution of the fuel isotope composition

The equilibrium isotope composition is reached by the fuel successively transiting the cycle.

The time interval characterized by a constant composition of the charged fuel is called a generation. The isotope composition of the charged fuel is the result of reprocessing the previous generation discharged fuel to which an adequate fissile amount is added in order to obtain the desired burnup.

Starting from the integrated multiplication factor concept, which allows the use of cell calculations, the following alternatives were examined:

1- The first generation includes four burnup variants of 10,15,20 and 30 Mwd/kgHE respectively, the following generations having a constant burnup value of 10 Mwd/kgHE.

2- The first two generations include the above mentioned variants, the following generations having the same burnup value of 10 Mwd/kgHE.

3- The first generation includes the four burnup variants, the following ones with a burnup of 10 Mwd/kgHE given only by the recycled uranium from each variant.

Reprocessing losses were considered, in amount of 2% for the first generations and of 0.5% for the generations corresponding to the end of the SSET cycle initiation period. The plutonium isotope composition used corresponds to that discharged from the CANDU reactor, i.e. /Pu 239/Pu 240/Pu 241/Pu 242/ in the

following amounts /0.675/0.264/0 048/0.014/. The cases described here only cover the numerous ways of initiating the SSET cycle in the sense they represent limiting cases for those alternatives, from the point of view of plutonium consumption.

The results we have come to show an increase in the plutonium amount required to obtain the prescribed burnup, as follows from 23.7 g/kgHE at a burnup value of 10 Mwd/kgHE to 34.6 g/kgHE at a burnup value of 30 Mwd/kgHE.

The plutonium amount added decreases rapidly from generation to generation, reaching a value of less than 2 g/kgHE in the fifth generation and decreasing after that in a slower manner to about 1 g/kgHE in the tenth generation.

The plutonium required by the higher generations decreases more rapidly in the case of the higher burnup alternatives, due to the faster accumulation of U 233 in this case.

The accumulated amount of uranium increases from 6.7 g/kgHE in the 10 Mwd/kgHE burnup case, to 10.4 g/kgHE for 20 Mwd/kghe, and to 12.5 g/kgHE for a burnup value of 30 Mwd/kgHE.

The differences become even more evident when distinct burnup values are maintained for two generations. Thus, values of 10.9 g/kgHE and 17.1 g/kgHE are obtained for burnups of 15 Mwd/kgHE and 30 Mwd/kgHE, respectively.

More than that, if a burnup level of 30 Mwd/kgHE is maintained for two generations, an amount of 14.3 g/kgHE of U 233 is reached, that is very close to the equilibrium value of 15 g/kgHE.

This value is reached in the 10 Mwd/kgHE alternative after 8 generations.

The third case corresponds to the assumption that all the uranium amount discharged in the first generation is used for equilibrium fuel fabrication. In this respect, the fissile contents providing for the equilibrium criticality to fissile contents discharged in each alternative ratio was evaluated. The values obtained for this ratio are presented below:

| Burnup (Mwd/kgHE) | 10    | 15    | 20    | 30    |
|-------------------|-------|-------|-------|-------|
| Ratio             | 2.320 | 1.803 | 1.551 | 1.318 |

Uranium composition evolution towards equilibrium shows the fact that practically the same final composition is reached in all the cases, in spite of the significantly different starting composition. It is to be pointed out that a fairly long time interval is needed to reach the equilibrium composition of the SSET cycle.

Due to the flux level effect, differences are obtained between the compositions resulted from the cell calculations and from core calculations. Still, the comparison made for the first generation showed insignificant differences let it is to be expected that those differences will increase as a result of the fuel repeatedly transiting the cycle.

That is the reason why the effective solution can only be obtained from complex core calculations.

### 3.2 Analysis of the alternatives of reaching the equilibrium

The scope of this analysis was that of determining the way by which the plutonium amount required for initiating the SSET cycle is affected by the external cycle parameters and the conditions of implementation in the power system.

Up to now, both the Canadian papers and the ones worked out at INPR treated the aspects concerning the thorium fuel cycles initiation in terms of fuel generations. This type of approach assumes a constant materials circulation speed, including that of fuel transiting the reactor, and, consequently, a constant burnup from generation to generation till the onset of equilibrium.

The plutonium amount required for initiating the SSET cycle is then determined as the sum of the addition quantities of plutonium from every generation.

In fact this condition is not required, the adequate one being that of conserving the reprocessed fissile amount passing from a generation to another.

Considering that the i-th generation is characterized by:

$\beta_i$  - burnup value

$\Delta t_i$  - generation period

$x_i$  - uranium contents of the charged fuel

$x_i'$  - " " " " discharged fuel

$y_i$  - plutonium contents of the charged fuel

$y_i'$  - " " " " discharged fuel

The condition of consuming the reprocessed material becomes:

$$\frac{\alpha P \Delta t_i}{B_i} x_i' (1-r) \geq \frac{\alpha P \Delta t_{i+1}}{B_{i+1}} x_{i+1}$$

P - fission power

$\alpha$  - capacity factor

r - reprocessing losses

Considering that the fissile amount charged in generation  $i+1$  represents a ratio  $\beta_{i+1}$  from that discharged in the previous generation,

$$x_{i+1}' = \beta_{i+1} x_i'$$

result that

$$\frac{\Delta t_i}{B_i} \geq \frac{\beta_{i+1} \Delta t_{i+1}}{B_{i+1} (1-r)}$$

Denoting by B and  $\Delta t$  the burnup and the generation period, respectively, for the n-th generation, assumed to be at equilibrium, we have

$$\Delta t_i > \frac{\beta_{i+1} \beta_{i+2} \dots \beta_n}{(1-r)^{n-i}} \beta_i \frac{\Delta t}{B}$$

A generation's plutonium consumption is.

$$\frac{\alpha P \Delta t_i}{B_i} (\gamma_i - (1-r)\gamma'_{i-1}) = \frac{\alpha P \Delta t_i}{B_i} \gamma''_i$$

where  $\gamma''_i$  - the addition plutonium amount.  
The total plutonium consumption becomes.

$$C = \sum_{i=1}^m \frac{\alpha P \Delta t_i}{B_i} \gamma''_i \geq \frac{\alpha P \Delta t}{B} \sum_{i=1}^m \frac{\prod_{k=i+1}^n \beta_k}{(1-r)^{n-i}} \gamma''_i$$

For  $\beta_1 = 1 - r$  all the reprocessed plutonium is charged, thus the plutonium consumption becoming:

$$C = \frac{\alpha P \Delta t}{B} \sum_{i=1}^m \gamma''_i$$

One can see that it is enough to minimize the addition amounts  $\gamma''_i$  for reducing the plutonium consumption, whatever the burnup is achieved.

For a generation period of 3 years the following values were obtained for the SSET cycle initiation in a CANDL-600 reactor:

|                           |                   |          |
|---------------------------|-------------------|----------|
| Every generation          | 10 Mwd/kgHE ..... | 8345 kg  |
| The first generation      | 15 Mwd/kgHE ..... | 8557 kg  |
| The first generation      | 20 Mwd/kgHE ..... | 8824 kg  |
| The first generation      | 30 Mwd/kgHE ..... | 9474 kg  |
| The first two generations | 15 Mwd/kgHE ..... | 8652 kg  |
| The first two generations | 20 Mwd/kgHE ..... | 9225 kg  |
| The first two generations | 30 Mwd/kgHE ..... | 10467 kg |

The differences resulted are not very large, if we take into account the fact that the effect of the external cycle parameters has a significant weight. Reducing the generation period to 2 years conduced to a decrease in the plutonium consumption of 35%, while raising the generation period to 4 years determines an increase in the plutonium consumption of 25%.

The required amount of plutonium is also directly affected by the reactor's performances.

The plutonium consumption is inversely proportional to the discharge burnup, thus increasing by a factor of two the burnup would reduce by 50% the plutonium consumption. Moreover, those alternatives have to be studied from the point of view of the conditions imposed to the external cycle, too. Utilizing a burnup value of 15 Mwd/kgHE conduces to a 40 % decrease in the reprocessing requirement in the first 5 years following the introduction of the thorium fuel cycles. This period can easily be extended to 9 years by imposing a 15 Mwd/kgHE burnup value for the first two generations. By utilizing a 30 Mwd/kgHE burnup a reduction by a factor of 3 of the reprocessed quantity can be obtained for as long as 9 to 18 years, depending on the way of imposing the burnup, to the first generation or to the first two generations.

Hence, the use of high burnup values significantly lowers the fuel cycle costs during the initial period of introducing the thorium fuel cycles.

This aspect is also supported by the annual fissile plutonium consumption values, that are decreasing from 1446 kg/year at 10 Mwd/kgHE to 735 kg/year at 30 Mwd/kgHE, and also by the reprocessing capacities required, that are decreasing in the same way: 368 t/year at 10 Mwd/kgHE to 187 t/year at 30 Mwd/kgHE.

In plutonium consumption the principal weight is hold by the first generation. Under those circumstances, the unavailability of the U-233 reprocessing and fabrication would have the effect of prolonging the first generation, with penalties in the plutonium consumption. The 30 Mwd/kgHE burnup alternative would allow a 12 years delay with only 8 % increase in plutonium consumption, thus becoming the most advantageous.

On the basis of the observations made above the following cycle alternative can be considered.

- Thorium + Plutonium fuel in the first generation
- U233 reprocessing and fabrication of fuel containing U233 in the equilibrium concentration
- Pu reprocessing and use of Thorium + Plutonium fuel with Plutonium addition to cope for the required burnup

The fissile plutonium consumption is in this case as follows.

| Burnup(Mwd/kgHE)        | 10   | 15   | 20   | 30   |
|-------------------------|------|------|------|------|
| Pu-fiss consumption(kg) | 8772 | 8093 | 7978 | 8700 |

Based on this results the 20 Mwd/kgHE burnup case is more advantageous due to the fact that it requires minimum reprocessing capacity and offers a great flexibility in all the variants for SSET implementation.

### 3.3 Power distributions

The essential requirement in core configuration design is to comply with the power restrictions (imposed by thermal-hydraulic conditions and fuel bundle behavior) as well as assuring satisfactory operational limits.

This requirement is fastidious if no changes in the reactor's constructive parameters are imposed or in the case of the transition period to the thorium fed core.

In this paper we have selected some results for power distributions for a CANDU Th-Pu core, corresponding to the initial period in a SSET cycle.

The primary scope of the analysis is to determine the way of complying with the power restrictions by the use of adequate refueling strategies.

The computation model is presented in reference /9/, and consists in coupling the cross-sections generating process with flux and power distributions calculations.

The computation algorithm assumes iterations on both the flux distribution and the macroscopic constants.

For this evaluations iterations on the discharge irradiation distribution were needed in order to obtain an adequate power distribution and also iterations on the amount of Pu-fiss required to assure the criticality and the burnup imposed.

The chosen case corresponding to the initial period is representative for both the power distribution (because of the high content in Pu-fiss and the strong differences between charged and discharged Pu-fiss concentration) and the Pu-fiss consumption (because of the rapid diminution of Pu-fiss amount added in the next generations).

Three burnup cases corresponding to 10, 15, and 20 MWd/kgHE were considered.

Starting from the standard CANDU case a core calculation model was constructed. The adjuster rods and the liquid zone control absorbers were detailed.

For the equilibrium core the obtained maximum bundle and channel powers are perceptibly smaller than those for the natural uranium core.

The maximum channel powers obtained are 6.33, 6.13 and 6.77 MW, corresponding to axial fueling schemes with 8, 4 and 2 bundles shifted, respectively.

The axial power distribution for the 20 MWd/kgHE burnup case presents two significant maximum values of 850 kW/bundle and 700 kW/bundle. The first bundle power maximum corresponds to the 2-nd position in the channel. This shape favors the heat transfer. From the point of view of bundle power restrictions the second bundle power maximum is significant.

The bundle power maximums are of 750 kW and 675 kW, respectively, for the 10 MWd/kgHE and the 15 MWd/kgHE burnup cases.

The asymmetry in the axial power distribution is typical to all the cases, but the difference between the two maximum values is small (100kW for the 15 MWd/kgHE burnup case and 50kW for the 10 MWd/kgHE burnup case).

This effect results from the superposition of the axial refueling scheme and the evolution with burnup of the flux to power ratio.

The high rate of the Pu-fiss consumption and the small rate of the U 233 accumulation give the explanation.

The inner to outer region burnup ratio is relatively large in all the cases, from 1.5 in the 10 MWd/kgHE burnup case, to 1.65 and 1.34 in the 15 and 20 MWd/kgHE burnup cases, respectively.

These solutions illustrate the possibility of complying with the power restrictions by the use of adequate refueling strategies.

Realistic solutions further require adjuster rods regrading in order to diminish the differences in the discharge burnups of the radial regions.

### 4. Solutions of increasing the burnup in the SSET reactor

As it has resulted from both the system analysis and the analysis of the ways of reaching the equilibrium, the discharge burnup is a parameter with important effects. Numerous solutions have been suggested for increasing the discharge burnup in the SSET reactor. The most important of them are presented below:

a.The use of metallic fuel allows a lowered flux level and, by this way, an improved neutron balance. Moreover, the absorptions in the structural materials, moderator and coolant are reduced as well. As a result a definitely higher reactivity excess is obtained as compared to the oxide fuel case for the same initial fissile content.

b.Replacing the radial reflector by pure thorium channels(blanket) is a way of using the neutrons otherwise lost by radial leakages for fissile production and increasing the inventory ratio. Thus the initial fissile content of the fuel can be increased, the core inventory ratio decreasing as fissile is generated in the blanket.

c.The use of specific fueling schemes is a way of reducing the absorptions in U234 and increasing the U233 production by temporarily storing the irradiated fuel bundles and then reintroducing them in the core. While the fuel is out of core U233 is generated by Pa233 desintegration thus the fissile content being raised. The fact has a positive influence upon the neutron balance by increasing the multiplication factor, but simultaneously conduces to decrease of the inventory ratio.

The use of metallic fuel still enjoys a great interest. Results corresponding to oxide fuel and metallic fuel, equilibrium composition, are presented below. A 3-D calculation model was used, for a 7x7 supercell. The values presented correspond to the central channel, which simulates a average channel in the core.

As results from the following table, an important effect is obtained in the discharge burnup:

|   | Type of fuel   |       |       |                |       |       |
|---|----------------|-------|-------|----------------|-------|-------|
|   | Oxide          |       |       | Metallic       |       |       |
|   | Fueling scheme |       |       | Fueling scheme |       |       |
|   | 4              | 6     | 8     | 4              | 6     | 8     |
| Burnup<br>(Mwd/kgHE)                        | 10.24          | 10.46 | 10.52 | 15.08          | 14.67 | 14.79 |
| Discharge<br>burnup<br>uniformity<br>factor | 0.95           | 0.90  | 0.84  | 0.95           | 0.90  | 0.84  |
| Conversion<br>rate                          | 1.034          | 1.034 | 1.034 | 1.034          | 1.034 | 1.034 |
| Maximum<br>bundle<br>power(kw)              | 484            | 505   | 496   | 474            | 496   | 496   |

The results obtained show that the same features are obtained, as concerns the power distributions and the conversion rates, for the two types of fuel.

Under those circumstances, the use of metallic fuel becomes really attractive with regard to its effect upon the burnup achieved.

### 5. Conclusions

Implementing the thorium cycles in the CANDU reactor, especially in the SSET alternative, represents a solution of great interest for a long-term plan of assuring the fuel for the CANDU reactors, in the situation the natural fissile resources are gradually exhausting.

For a system developing on a CANDU reactor basis and disposing of low natural uranium resources, with a loose access to the international uranium market, introducing the SSET cycle allows it to cope with the energy demands with low uranium resources. However, this advantage is counterbalanced by the need of rapidly developing the complex technologies required by this fuel cycle. Those technologies have not yet exited the laboratory stage and they are not expected to be finished up in the near future.

The use of transition fuel cycles allows the energy demand to be satisfied economically and the moment when the complex technologies required by the fuel cycle are needed to be postponed. Although this solution conduced to penalties in the

natural uranium amount needed, the solution is on the whole economically advantageous due to the reduced size of the reprocessing and fuel fabrication capacities required.

There are numerous ways of initiating the SSET cycle.

From the fissile plutonium consumption point of view, the lowest consumption is given by the constant fuel speed of transiting the cycle alternative, but the differences are relatively small, of 2% to 25%.

The high burnup alternatives need low reprocessing capacities, thus being advantageous from both the point of view of fuel cost and of conditions imposed to the external fuel cycle.

As concerns the thorium fuel utilisation in the CANDU reactor, solutions were found to comply with the power restrictions by the use of adequate refueling strategies.

An important parameter is the discharge burnup. An attractive solution of increasing the burnup is that of using metallic fuel, which would also allow a higher speed of the fuel transiting the cycle, especially due to the possibility of using more efficient reprocessing technologies. However, the use of this type of fuel rises numerous technological and physics problems that have not yet been dealt with.

For the near future we consider the use of slightly enriched uranium in CANDU, as the solution of interest from the economic point of view, in the first place.

Numerous studies have been carried out at INPR on the subject, part of the results obtained being also presented in reference /9/.

### REFERENCES

- /1/ M.S. Milgram "Thorium Fuel Cycles in CANDU Reactors - A Review", AECL-8236
- /2/ \* \* \* "Research and Development Activities in Canada on CANDU Reactors", TM in Vienna, 1984
- /3/ \* \* \* "Advanced Heavy Water Reactors", TM in Vienna, 1984
- /4/ H. Hatton "Users Guide to the Computer Program FURST (Future Reactor Strategies)", AECL-7226
- /5/ \* \* \* "Data Base for a CANDU-PHW Operating on the Thorium Cycle", INFCE/WG8/DCC4 and also AECL-6595
- /6/ I. Griffiths "Reactor Physics and Economic Aspects of the CANDU Reactor System", AECL-7615

- /7/ E. Critoph "Prospects for Self-Sufficient Equilibrium Thorium Cycles in CANDU Reactors", AECL-5501
- /8/ M.S. Milgram W.S. Walker "Some Physics Problems in the Design of Thorium Fueled CANDU Reactors", AECL-5561
- /9/ D. Serghiuta V. Raica D. Gamulescu E. Nichita "Some Physics Aspects of the In-Core Fuel Management Analysis for the CANDU-PHW Type Reactors", 622-I3-TC-676.3, Vienna, 1989
- /10/ D. Serghiuta V. Raica L. Nicolescu "Advanced Fuel Cycles on PHW Reactors - Physics Aspects", National Conference on Energetics, nov. 1986 (in romanian)

Next page(s) left blank

HIGH CONVERSION REACTOR (HCR) DESIGNS  
(Session 2)

Chairman

**B. KUCZERA**  
Germany

## GENERAL ADVANTAGES OF HEXAGONAL FUEL ASSEMBLIES

H. MOLDASCHL, P.J. RAU, I. RUMMEL  
Siemens AG,  
Unternehmensbereich KWU,  
Erlangen, Federal Republic of Germany

### Abstract

Since several years Siemens KWU is developing a High Conversion Reactor in cooperation with the Swiss PSI, KfK and the Technical University of Braunschweig. An HCR requires a tight lattice which is easier to accomplish in a triangular pitch as compared to a square one. The triangular pitch leads to a hexagonal fuel assembly.

Beyond the potential of tightening the lattice, there are other advantages of hexagonal fuel assemblies which are valid also for moderation ratios in the range of conventional PWRs:

- the cylindrical core barrel can be filled to a higher degree with hexagons than with square elements. Apart from being able to incorporate more fuel - if so desired - there is the important aspect that the better approximation of the cylindrical geometry by hexagons leads to a larger minimum distance between the peripheral fuel assemblies and the RPV and thus to lower maximum neutron fluence at the RPV. Furthermore, there is larger space to install an effective reflector which again reduces the fluence.

A suitable combination of these measures may lead to an increase of the maximum life time of the RPV.

Additionally, the reflector reduces neutron leakage leading to higher fuel utilization.

- a hexagonal fuel assembly has 6 neighbours, a square one only 4. Thus there is a stronger coupling between fresh and spent fuel which allows
  - o greater flexibility for optimizing fuel management
  - o a flatter power distribution which in turn results in a better fuel utilization because of an improved burn-up distribution
- a hexagonal fuel assembly has a more symmetrical coolant sub-channel than a square one, resulting in better coolability and/or margin.

- a hexagonal fuel assembly has an increased stiffness compared to a square one, which may potentially be beneficial in case of accidents, e.g. LOCA.

The major current disadvantage is that some of the important design codes have to be adapted to the hexagonal geometry.

### 1. Introduction

Since several years Siemens KWU has been developing a Pressurized Water High Converter Reactor (PWHCR) in a joint cooperation with Karlsruhe Nuclear Research Center, Paul Scherrer Institute Wurenlingen and Technical University of Braunschweig / 1 /. A PWHCR is designed to improve the fuel utilization, to enhance fuel autarky and to decrease energy cost, while using the standard design as far as possible.

The fuel utilization can be improved by increasing the effective conversion rate ("recovery rate"), which is the ratio of the discharged amount of fissile material to the inloaded one. An increase of the recovery rate can be performed by hardening the neutron spectrum and this can be achieved by insertion of plutonium and/or by reduction of the amount of coolant in the fuel rod lattice, e.g. by reduction of the volumetric moderation ratio VMF.

For the above mentioned process of spectrum hardening the reduction of the number of hydrogen atoms per fissile material's atom is relevant, what can be performed in several ways, e. g. using D<sub>2</sub>O, spectral shift rods or - in case of BWRs - by increasing the amount of steam. The fundamental and most often practised way is to tighten the lattice, either by reducing the pitch or increasing the outside diameter of the fuel rods, or both. However, spectral shift rods for example are additionally under discussion.

Hexagons are widespread - tried and tested and one of the basic construction elements of nature, Fig. 1 and, one example, / 2 /. Everybody instinctively feels that a triangle could meet our goal - namely tightening a fuel rod lattice - much better than a square shaped configuration and therefore all people in the community of PWHCR-designers have been dealing with a triangular lattice. Nevertheless one should quantify the advantages of hexagonal lattices compared to square-shaped at the same moderation ratio.

### 2. Topology and Symmetry

Why should a hexagonal geometry be better than a square? Squares are a well proven topology - at least in modern architecture. Of course, since a long time nature uses hexagons

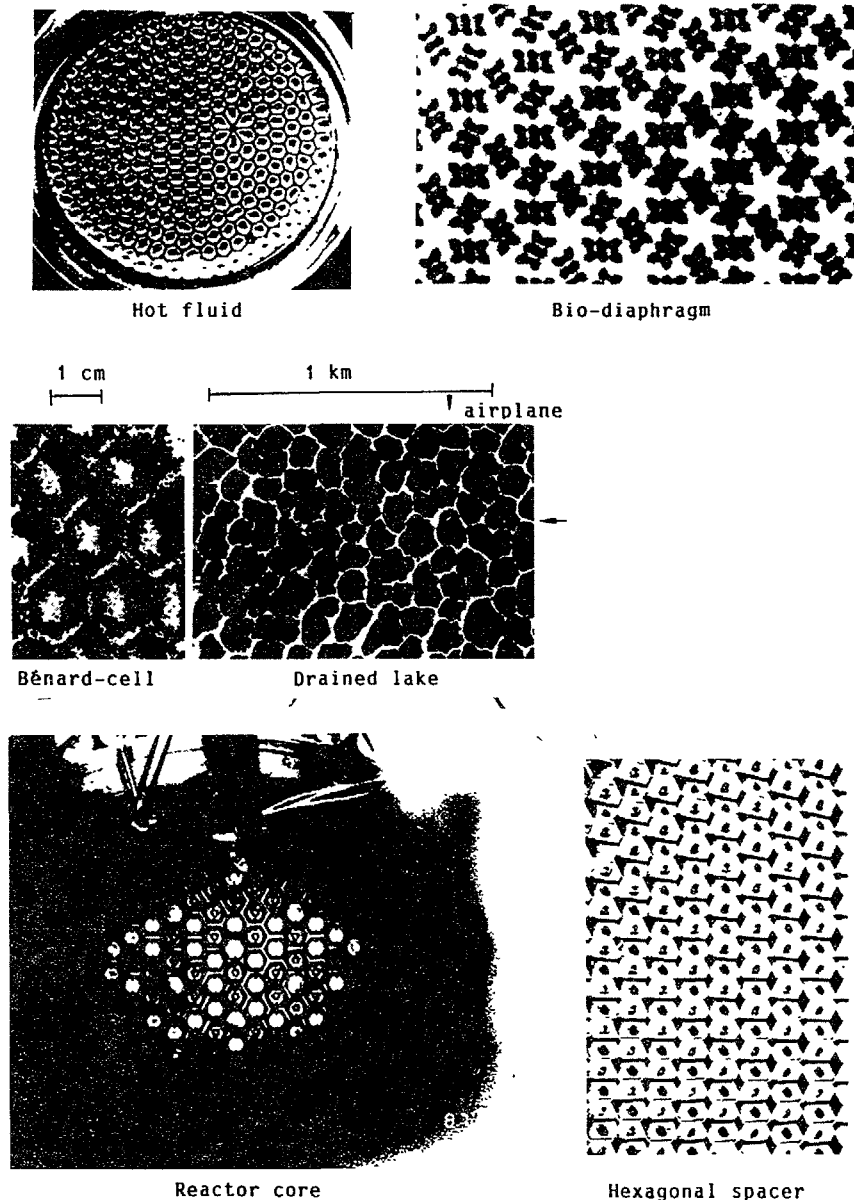


FIG. 1. Hexagonal structures.

(Fig. 1): their symmetry will not only ask questions to somebody dealing with, but it offers a lot of advantages by

- the high area-perimeter ratio
- the small symmetry angles
- the small average distance of the peripheral points to the central point
- the high density of nodes

All these features are related one to the other - they have the same origin. Nevertheless they will lead to different consequences in a reactor. Now we will analyse in detail.

### 3. The Advantages of a Triangular Fuel Rod Array

#### 3.1 Coolant Channel Heat Removal Capability

Fig. 2 shows a square and a triagonal coolant subchannel: in the square geometry (the left one) we find 8 subchannels with an identical coolant velocity profile ( $2\hat{y}$ ) which is repeated every  $45^\circ$ . The right figure, the hexagonal geometry, shows a topology, where the velocity symmetry is repeated every  $30^\circ$ .

The current profile determines the energy amount, which can be transported from the rod into the coolant, since it determines the biggest whirls possible which crucially influence mixing effects.

Dependent on the angle  $\alpha$  of the profile  $2\hat{y}$  we get:

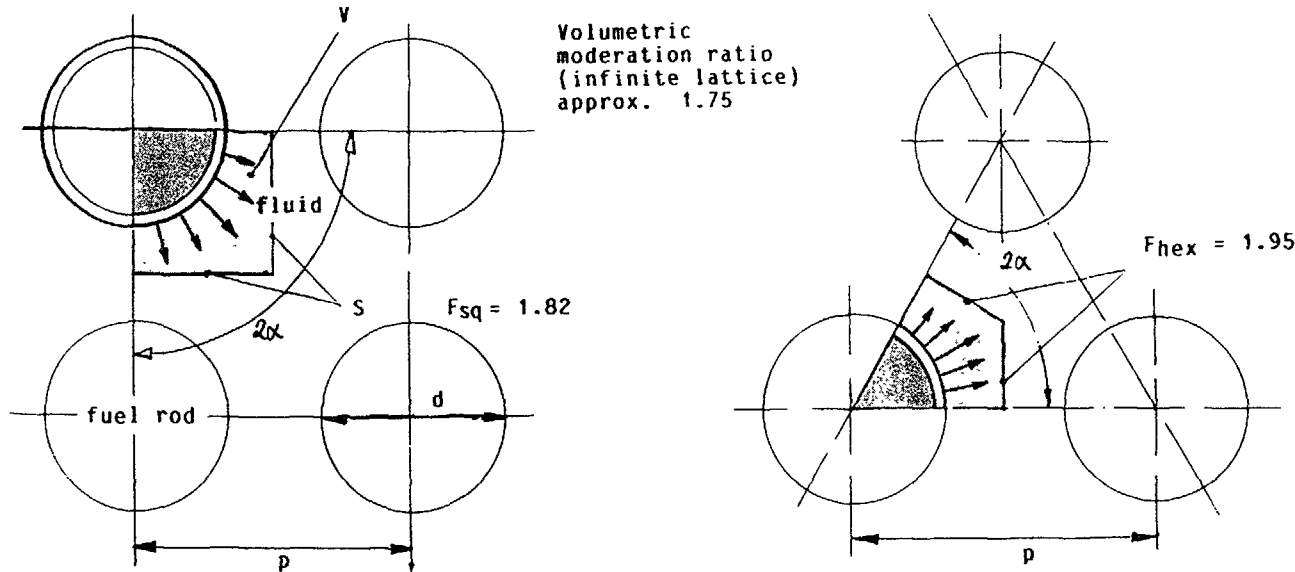
$$\hat{y} = \frac{p}{2 \cos \alpha} - \frac{d}{2}$$

Since the variation of  $\cos \alpha$  is greater in the square geometry ( $0 \leq \alpha \leq 45^\circ$ ) than in the triangle ( $0 \leq \alpha \leq 30^\circ$ ), the relative variations of the current velocity in the triangle lie between 1 and 1.15, while the variation range in the square lattice is between 1 and 1.41. The result is a much more regular current profile in the triangular lattice, which naturally favours heat removal. This is quantitatively valid for an undisturbed flow and it holds qualitatively also for a flow pattern disturbed by spacers.

Since heat removal depends on the mass of coolant in the surrounding of the fuel rod on one hand, and on the other hand depends on the circumferential shape of the coolant channel, one can quantify the "quality" of a coolant channel in a simple way by defining a mathematical measure  $F$  for the average lateral distance concerning heat removal in the coolant channel:

$$F = V/S$$

(V - adjacent volume part of the subchannel, S - enclosing surface)



The average distance  $F$  from the rod to the fluid is a function of subchannel symmetry:  $F = \frac{V}{S}$  / cm /

$$V_{sq} = \left[ p^2 - \frac{d^2}{4} \right] \frac{1}{4}$$

$$S_{sq} = p$$

(V - adjacent volume part  
S - enclosing surface)

$$V_{hex} = \left[ p^2 \frac{\sqrt{3}}{4} - \frac{d^2 \pi}{8} \right] \cdot \frac{1}{3}$$

$$S_{hex} = \frac{p}{\sqrt{3}}$$

FIG. 2. Subchannel symmetry F.

Regarding the same moderation ratio, diameter and cladding for both geometries we can calculate the relation between the pitches

$$p_{hex}^2 = \frac{2}{\sqrt{3}} \quad p_{sq}^2$$

and thus for F results

$$\frac{F_{hex}}{F_{sq}} = \sqrt{\frac{2}{\sqrt{3}}} \approx 1.075$$

where hex indicates hexagonal and sq square geometry.

For a VMF of  $\sim 1.75$  one gets (Fig. 2)  $F_{hex} = 1.95$  and  $F_{sq} = 1.82$ , which shows a remarkable advantage of the hexagonal channel form.

### 3.2 Potential for Tightening the Lattice

If one looks on the potential of tightening the lattice (Fig.3) one should compare the moderation ratio of the two different topologies at the same minimum fuel rod distance. The figure shows the volumetric moderation ratio VMF for square and hexagonal lattices and the outside diameter of the fuel rod as a function of the lattice pitch. One can realize that for a

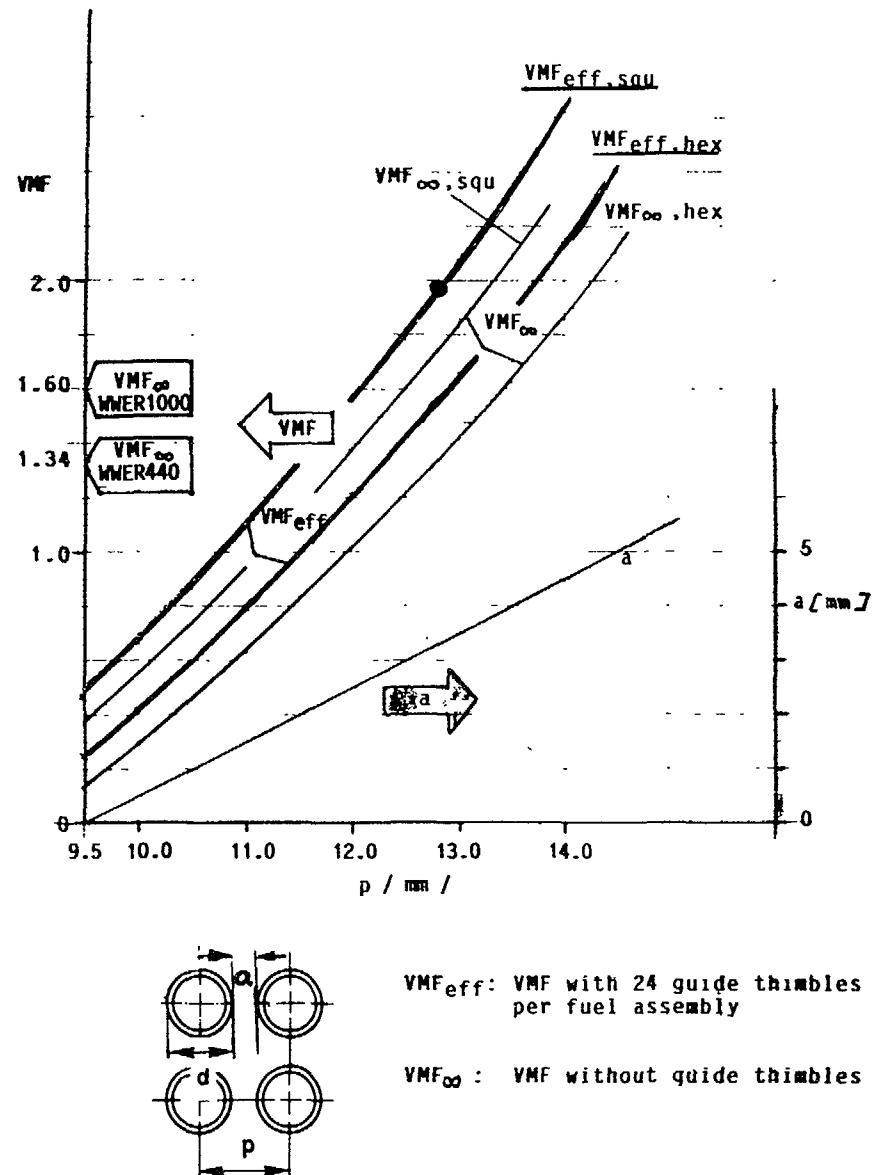


FIG. 3. Volumetric moderation ratio VMF for square and triangular fuel rod lattices as a function of the pitch  $p$ .

typical lattice with  $\text{VMF} = 2$  the minimum distance of the rods in a triangular lattice is about 1 mm larger than the minimum distance in a square lattice with the same VMF.

$p = 12.8 \text{ mm}$  and an outside diameter  $d = 9.5 \text{ mm}$  result in a minimum rod distance of 3.3 mm. The moderation ratios for these parameters are

$$\begin{aligned}\text{VMF}_{\infty, \text{hex}} &= 1.32 \text{ and } \text{VMF}_{\infty, \text{squ}} = 1.72 \text{ and} \\ \text{VMF}_{\infty, \text{hex}}/\text{VMF}_{\infty, \text{squ}} &= 0.77\end{aligned}$$

thus the potential of tightening the lattice using the triangular lattice will be of about 23 % higher than with the square lattice.

#### 4. The Reason for and the Advantages of Hexagonal Fuel Assemblies

If one arranges triangular sets of fuel rods to ensembles, one will recognize, that due to symmetry conditions only two macroscopic structures, i. e. fuel assemblies, arise:

the triangle and the hexagon.

Nobody will earnestly deal with other combinations of 6 triangles (Fig. 4) instead of the totally symmetric hexagon like the "church", the "comb" or the "boomerang", which have a creative look for mathematicians solely, but are somehow crazy in connection with core topologies.

##### 4.1 Degree of Filling

Due to the ideal circumferential form of the hexagon, a better degree of filling of the core barrel can be expected than with the square. So one should be able to insert more fuel assemblies at a given maximum radius of the core (Fig. 5) and thus could gain a smaller average linear heat rate or a larger integral power at the same linear heat rate or a smaller pressure vessel fluence at the same linear heat rate and at the same power as for the square-lattice core.

A lower average linear heat rate is important at least in three ways:

- it will decrease the amount of oxid layer development at the outside of the cladding and thus favour the goal of a higher reload burnup
- it results at the same time in increased safety margins for several kinds of accidents

- and last not least it leads to a smaller pressure vessel (RPV) fluence.

On the other hand RPV fluence depends also on the distance of the outermost point of the active core to the RPV. Thus we can define a function A to quantify the filling degree of the core barrel:

$$A = 1/(q'^3 \cdot R_{\max}) \quad (q' - \text{average linear heat rate}, R_{\max} - \text{distance of the outermost fuel rod from the core center})$$

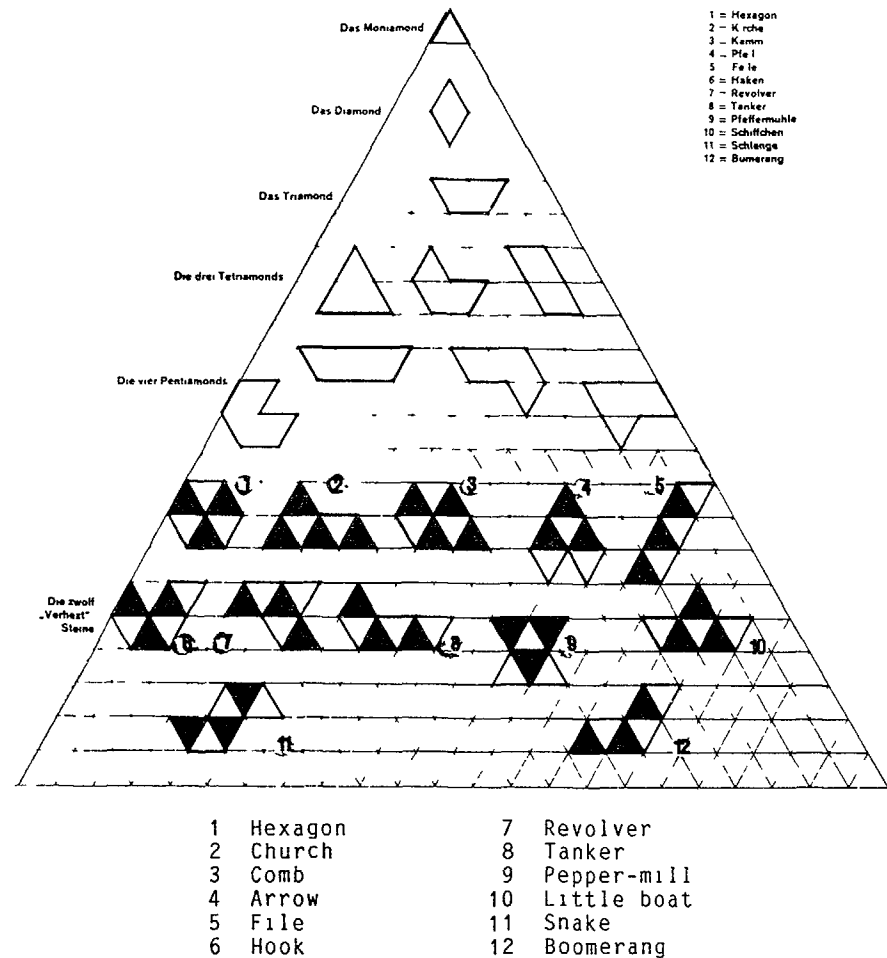


FIG. 4. Different triangular topologies.

$$A_r = \frac{\frac{1}{q'^3 \cdot R_{\max}}}{1} = \frac{A}{A_m}$$

*q'^3(a) R<sub>max,cell</sub>*

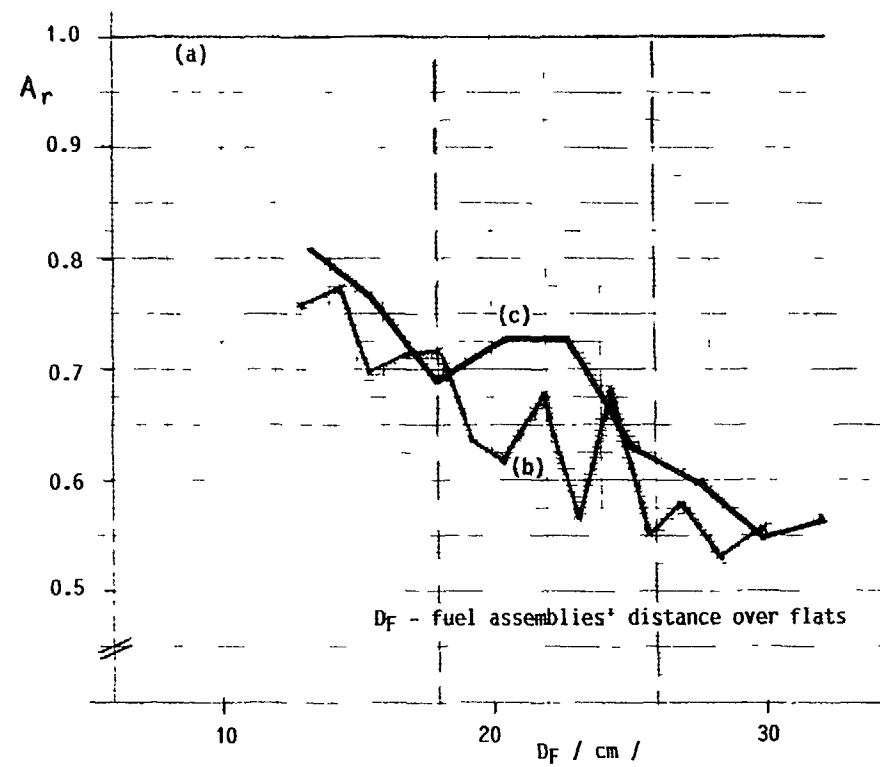
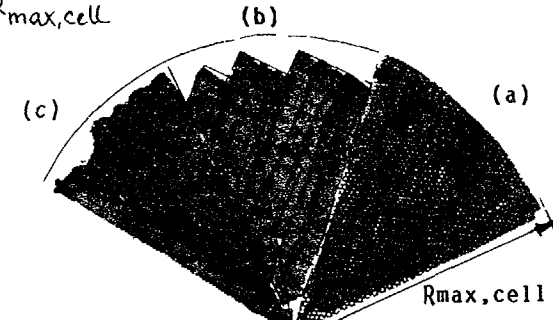


FIG. 5. Degree of filling.

The maximum value  $A_m$  of  $A$  can - only theoretically - be gained by filling the available "core volume" with cells. The figure shows in principle the three different degrees of filling with pure cells (a), squares (b) and hexagons (c). The worth  $A_r$  of the relative filling degree, i.e. the value  $A$  normalized to  $A_m$  as a function of fuel assemblies' (FA) size (= distance over flats  $D_F$ ) is shown by the curves below. It is clear that smaller fuel assemblies will result in a better degree of filling and thus larger  $A$ , which results in a general decrease of the curves for squares and for hexagons with increasing FA size. The decrease is not monotoneous, since somewhat like quantum numbers exist for squares as well as for hexagons. However, in the interesting range of FA sizes - it is the range between the dashed lines - the average  $A_{hex}$  is almost 10 % better than the  $A_{squ}$ .

#### 4.2 Neutronic Zone Coupling

The hexagonal topology of a core will have additional advantages concerning the neutronic coupling between fresh and spent fuel assemblies:

One can easily recognize that a hexagon has 6 "real" neighbours, a square only 4. To quantify the physical essence of this fact, one can deal simply with an infinite lattice configuration (Fig. 6), which of course is representative for the real configuration in a reactor. For example we will discuss a 3 batch refuelling cycle and thus relative BOC-burnup values of the batches of 0, 1/3 and 2/3. The coupling strength  $C$  can be defined as the average burnup gradient in the given configuration:

$$C = (1/V) \sum_i (\Delta B / \Delta x)_i$$

For the square lattice there are two symmetrical possibilities (a) and (b) to arrange the burnup values 1/3 and 2/3 around the fresh assembly. The resulting  $C$ 's - normalized to the volume of the square - are what could be qualitatively expected:

$$C(a) = 0.402 \text{ and } C(b) = 0.451.$$

Each other arrangement of those fuel assemblies would result in  $C < C(b)$ .

For the equivalent hexagonal topology we get

$$C(hex) = 0.577, \text{ which is more than 25 \% higher than } C(b).$$

Due to better neutronic coupling of fuel assemblies in a hexagonal pattern one can expect for the same VMF-value of fuel assemblies a decisively better fuel utilization on one hand, and on the other hand a flatter power distribution than in a pattern of square-type FAs, which follows from the better neutron economy.

Measure for coupling strength;

$$C = \frac{1}{V} \sum_i \left( \frac{\Delta B}{\Delta x} \right)_i$$

$\Delta B$  - burnup difference  
 $\Delta x$  - distance  
 $V$  - Volume of neighbours  
of  $B_0$

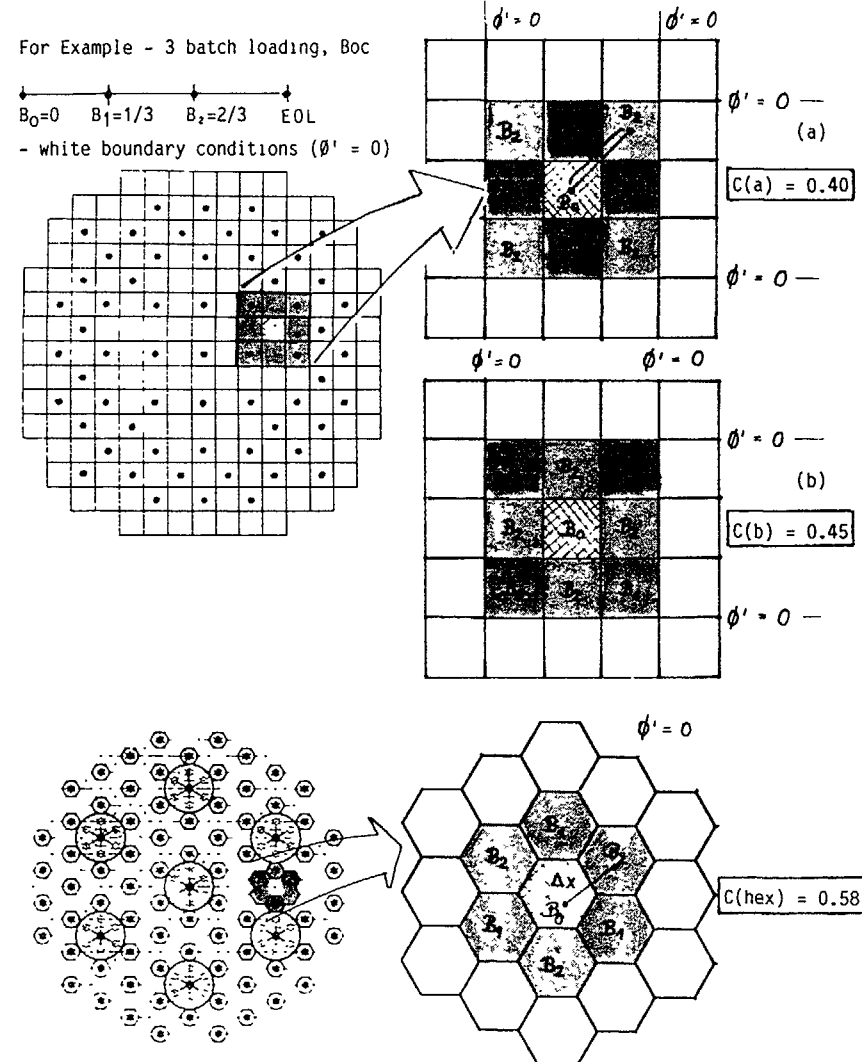


FIG. 6. Neutronic zone coupling in square and hexagonal lattices.

### 4.3 Relative Density of Control Assemblies

Hexagonally shaped fuel assemblies will lead to an advantageous arrangement of RPV lid penetrations and thus in a higher relative density of control assemblies (CA) in the core (Fig. 7). One can simply calculate the CA density  $D_{CA}$ :

$$D_{CA,squ} = 1/d^2$$

$$D_{CA,hex} = (2/\sqrt{3})/d^2 = 1.155/d^2, \quad (d - \text{central distance of RPV lid penetrations})$$

which means 15 % more control assemblies in a hexagonal array with identical  $d$ .

### 4.4 Rigidity of the Spacer

A measure  $R$  for rigidity is given by

$$R = N/S^2 \quad (N - \text{number of ligaments connected to a node}, S - \text{length of those ligaments})$$

if each ligament is treated to be fixed only on one side.

To get some information about the ratio of the rigidity between a hexagon and a square spacer, one must compare these two types at the same volumetric moderation ratio. The moderation ratio for the square lattice is given by

$$VMF_{squ} = (S_{squ}^2 - V_C - V_F)/V_F$$

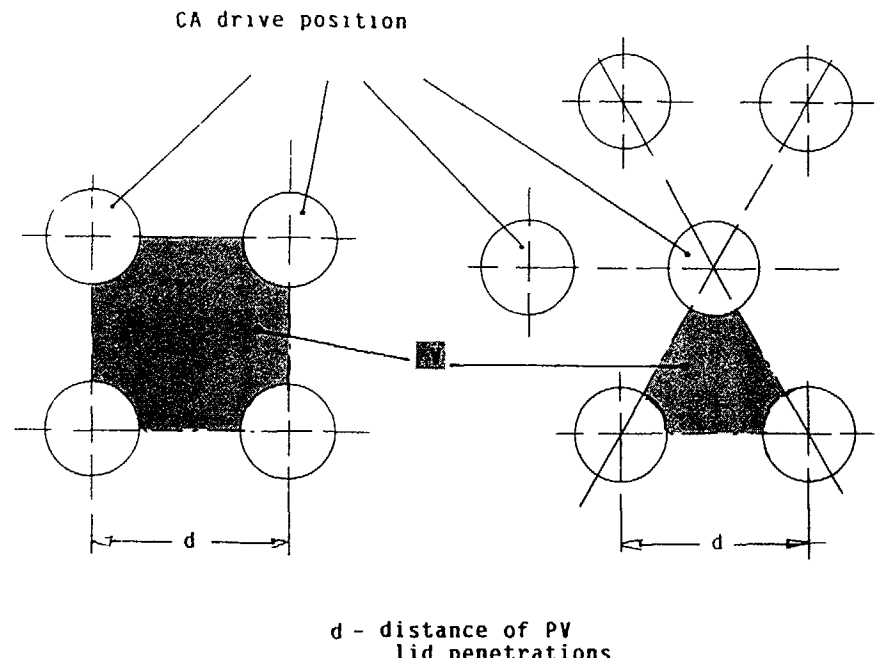
for the triangular lattice

$$VMF_{hex} = (\rho_{hex}^2 \cdot \sqrt{3}/2 - V_C - V_F)/V_F = (S_{hex}^2 \cdot 3 \cdot \sqrt{3}/2 - V_C - V_F)/V_F$$

$V_C$  - cladding volume,  $V_F$  - fuel volume,  $\rho_{hex}$  - pitch of the hexagonal lattice

If the lengths of the ligaments of a square FA are defined as  $S_{squ}$ , then those of a hexagonal FA, namely  $S_{hex}$  with the same VMF are given by the equations above for the VMF's:

$$S_{hex} = S_{squ} \cdot \sqrt{2/(3\sqrt{3})}$$



$N_{CA}$  - number of penetrations per area unit

$$N_{CA} = \frac{4}{d^2}$$

$D_{CA}$  - CA penetration density

square lattice

$$V = d^2$$

$$N_{CA} = 4 \cdot \frac{1}{4} = 1$$

$$D_{CA} = \frac{1}{d^2}$$

hexagonal lattice

$$V = d^2 \frac{\sqrt{3}}{4}$$

$$N_{CA} = 3 \cdot \frac{1}{6} = \frac{1}{2}$$

$$D_{CA} = \frac{1.155}{d^2}$$

FIG. 7. Specific control assembly (CA) density

116 It should be mentioned here, that this ratio does not depend on the volume of the fuel or the cladding.

If all other characteristics of the ligaments are identical, one gets for the case

$$VMF_{hex} = VMF_{squ}$$

$$R_{squ} = 4/S_{squ}^2 \quad \text{and} \quad R_{hex} = 9\sqrt{3}/2 / S_{squ}^2 = 7.79/S_{squ}^2$$

and thus

$$R_{hex}/R_{squ} = 1.95.$$

## 5. Summary

All advantages of hexagons result from their comparatively higher symmetry!

One can summarize the general advantages of the hexagonal structure mentioned above in the following table:

### Advantages compared to the square geometry

- |   |              |
|---|--------------|
| 1. Higher subchannel symmetry                   | >> 8 %       |
| 2. Larger adaptation potential toward lower VMF | 23 %         |
| 3. Lower linear heat rate and RPV fluence       | 6-9 %        |
| 4. Better neutronic zone coupling               | > 28 %       |
| 5. Higher specific control assembly density     | approx. 15 % |
| 6. Higher fuel assembly deformation resistance  | approx. 95 % |

Those advantages definitely result in

- a lower linear heat rate or a smaller RPV fluence or a higher net power
- a smaller neutron leakage
- a better power distribution
- a better fuel utilization
- better cooling conditions
- a larger control assembly worth
- larger deformation resistance to external forces
- larger optimization margins

and thus have certain impacts given in the following table:

| Impact of ---><br>on | 1 | 2 | 3 | 4 | 5 | 6 |
|----------------------|---|---|---|---|---|---|
| Safety margins       | * | * | * | * | * | * |
| Availability         | * | * | * | * | * | * |
| Energy cost          | * | * | * | * | * | * |
| Fuel utilization     | * | * | * | * | * | * |

## REFERENCES

- / 1 / H. Moldaschl, R. Brogli, B. Kuczera  
Status and Prospects of the Cooperative KWU High  
Converter Development 1989  
ICENES 1989, Karlsruhe 3-6 July
- / 2 / D. Weaire  
Magnetic froth  
Physics World, November 1989

# NUCLEAR CORE DESIGN STUDIES FOR A TIGHT LATTICE PWR

G.J. SCHLOSSER, H.-D. BERGER,  
M. SCHATZ, K. THIEME  
Siemens AG,  
Unternehmensbereich KWU,  
Erlangen, Federal Republic of Germany

## Abstract

One measure to improve fuel utilization in light water reactors is to increase the conversion ratio in a tight, hexagonal  $\text{PuO}_2/\text{UO}_2$  mixed oxide fuel pin lattice. The PWHCR (pressurized water high converter reactor) is the Siemens/KWU approach towards this kind of tight lattice reactor, with the main characteristics of the actual concept being zirconium-clad fuel rods and an average moderator-to-fuel volume ratio of 1.2. In a recent study, concerning the nuclear core design for the PWHCR, mainly the questions related to the fuel assembly design, the reactivity control system and fuel management strategies have been addressed. Results of these investigations essentially confirmed the concept of the tight lattice PWR to be technically feasible.

## 1. INTRODUCTION

In the Federal Republic of Germany the commercial utilization of  $\text{PuO}_2/\text{UO}_2$  mixed oxide fuel (MOX) in Light Water Reactors (LWR) started as early as in 1972. Until recently more than 50,000 mixed oxide fuel rods in some 400 MOX fuel assemblies have been inserted in pressurised and boiling water reactors (PWR and BWR, respectively), with the maximum number of MOX fuel assemblies in one core load, licensed today, being 50 % [1]. With the accumulation of significant amounts of plutonium from reprocessed LWR-fuel on the one hand and the considerable delay of the commercial introduction of fast breeder reactors on the other, the question of an optimized utilization of plutonium in LWR has become of prime importance.

The evolutionary step of a Pu-burner, i.e. a current-day design PWR fueled 100 % with MOX fuel assemblies is just one step in this direction. Real optimization of plutonium use in light water reactors calls for special MOX fuel elements as well as appropriate core designs. Depending on the basic incentive of such an optimization process, i.e. whether to burn the Pu in order to avoid further accumulation or to conserve this material - both in quantity and quality - for future use, this will lead to either higher or lower moderated fuel pin lattices, respectively, as compared to current day design values.

The tight lattice PWR, the nuclear core design studies of which are subject of this paper, is the Siemens/KWU approach towards an optimization of the latter type. This reactor concept is aimed at improved plutonium utilization by means of increased conversion ratio. This is achieved by decreasing the relative moderator content within a hexagonal lattice arrangement. Studies of a very tight lattice with an average moderator-to-fuel volume ratio ( $V_{\text{Mod}}/V_{\text{Fuel}}$ ) of as low as 0.5 demonstrated the potential for improved fuel utilization of this concept. The technical feasibility of this particular design (especially questions related to neutron-physics and thermal-hydraulics under LOCA conditions), however, could not yet been demonstrated to a satisfactory extent. Therefore a less ambitious design with a  $V_{\text{Mod}}/V_{\text{Fuel}}$  of about 1.2 and a build-in flexibility, allowing to switch to tighter lattice configurations if desired (cf. Reference [2]), was selected for detailed nuclear core design studies. The current paper will summarize results of these investigations.

## 2. METHODS AND CODES USED

Tightening the fuel pin lattice in a light water reactor results in a shift of the neutron spectrum into the epithermal energy range, with increased resonance absorptions - mainly in the fertile nuclides  $^{238}\text{U}$  and  $^{240}\text{Pu}$  - leading to increased conversion and improved fuel utilization. The bulk of neutron physics codes and data sets employed for the analysis of these lattices, however, has originally been designed for either thermal or fast neutron energy spectra. Thus the selection and testing of suitable calculational tools for tight pitch lattices formed an important part of these investigations.

In a first phase of calculations two different code systems, viz. the BWR code package BPSA and a fast reactor design code, have been used. While it was felt that BPSA is able to describe the physics of tight lattice reactors at normal operational conditions fairly accurate, its applicability for the prediction of the overall void coefficient  $\alpha_v$  (0 to 100 % void) - a crucial safety parameter for the MOX-fueled high conversion reactor - has not yet been qualified. For the fast reactor code, as expected, the opposite is true - reliable results for voided lattices on the one hand and insufficient accuracy for moderated states on the other. Although it was thus possible to study special effects or transitions using one or the other code, none of the tools alone could be employed for an entire core design study.

With more and more experimental data from the PROTEUS-LWHCR programme [3] - part of a joint PSI/KfK/Siemens high converter collaboration - becoming available and the results of the NEACRP burnup benchmark [4] being published, the final evaluation of appropriate code systems could be based on a broad and comprehensive set of experimental and theoretical results. For the design studies presented hereafter it was decided to use two different tools, viz. the CASMO-3 code and the Monte Carlo code KMC, for both of which the comparison with experimental and theoretical results yielded acceptable accuracies. As an example, Figure 1 presents CASMO-3 results for one of the NEACRP benchmark problems in comparison with the mean values of 16 solutions of other codes. With an average deviation from the mean of -0.7 % in the multiplication constant and -1.3 % in the conversion ratio, the CASMO-3 based results may be considered to be conservative.

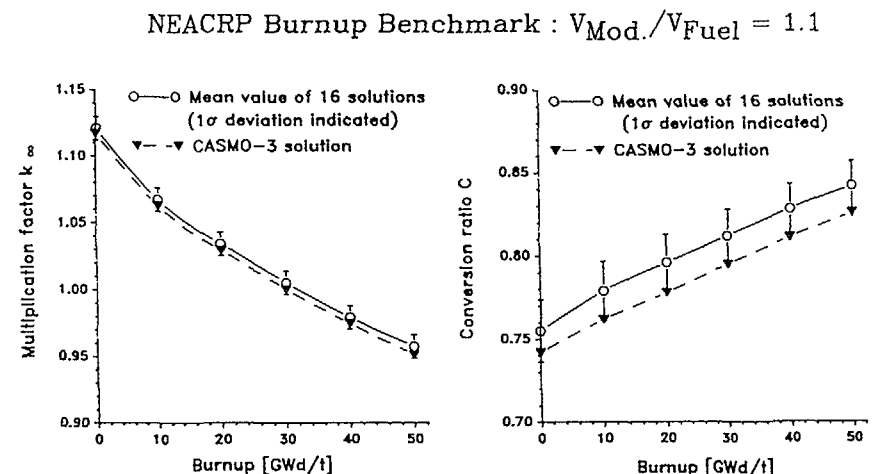


Fig. 1: Comparison of CASMO-3 results for the burnup-dependence of the infinite multiplication factor and conversion ratio with the mean results of 16 other solutions for the second NEACRP burnup benchmark problem

While CASMO-3, mainly due to the missing hexagonal geometry option, was used just as a cross-section generating module for two- and three-dimensional reactor calculations, the excellent geometry capabilities of the Monte Carlo tool KMC were employed for detailed studies of special local effects including rod cluster control investigations. The multidimensional reactor calculations were performed using the HEXNOD/HEXMED code package, details of which will be presented in [5].

### 3. GENERAL CORE DESIGN CHARACTERISTICS

The tight lattice PWR, referred to as PWHCR (pressurized water high converter reactor) hereafter, consists of 349 hexagonal fuel assemblies surrounded by heavy steel reflector elements to reduce radiation damage to the reactor pressure vessel, a current day design type RPV. The thermal power of 3765 MW is identical to the Siemens/KWU CONVOY reactors. Due to the tighter lattice arrangement, allowing almost 50 % more rods to fit into the core than in the CONVOY type, and an only moderate reduction of the active height to 300 cm, the linear heat rate could be lowered by some 12 % to a core averaged value of 146 W/cm. The mixed-oxide fuel is clad in Zircaloy-4 canning of an outer diameter of 9.5 mm with Inconel grid-type spacers.

Some basic design parameters of the PWHCR are compared with those of a "conventional" plutonium fueled PWR (Pu-Burner) and the very tight PWR core design mentioned before and labeled KHCR in Table I.

TABLE I  
General Core Characteristics of Different Plutonium-burning Light Water Reactor Concepts

|                       | Pu-Burner | PWHCR     | KHCR      |
|-----------------------|-----------|-----------|-----------|
| Thermal Power MW      | 3765      | 3765      | 3612      |
| No. Fuel Assemblies   | 193       | 349       | 349       |
| Active Height cm      | 390       | 300       | 200       |
| Assembly Design       | quadratic | hexagonal | hexagonal |
| V Mod/V Fuel          | 1.93      | 1.19      | 0.53      |
| Fuel Rods/Assembly    | 300       | 247       | 313       |
| Guide Tubes/Assembly  | 24        | 24        | 12        |
| Cladding Material     | Zry-4     | Zry-4     | SS        |
| Linear Heat Rate W/cm | 167       | 146       | 165       |

As Table I reveals, pursuing the PWHCR concept, in several respects, means steering a middle course between the obvious solution of a Pu-Burner and the ultimate goal of a real high converting PWR. The choice of the PWHCR lattice in fact is a compromise resulting from the consideration of the following three problem areas : plutonium utilization, void characteristics and reactivity control. A rough summary of the assessment of individual pros and cons of different concepts is presented in Table II.

TABLE II  
Assessment of the Main Pros and Cons of Different Plutonium-burning LWR Concepts

|                      | Pu-Burner                                 | PWHCR  | KHCR   |
|----------------------|---|--|--|
| Pu-Utilization       | poor                                      | well   | excellent                                    |
|                      | - low C<br>- degradation of<br>Pu-quality | - higher C<br>- conservation of<br>Pu-quality  | - large C<br>- improvement of<br>Pu-quality  |
| Void Characteristics | good                                      | reasonable                                     | questionable                                 |
|                      | - similar to U-PWR                        | - sufficiently negative $\alpha_v$             | - positive $\alpha_v$ at high Pu<br>contents |
| Controllability      | feasible                                  | feasible                                       | complicated                                  |
|                      | - standard PWR systems<br>to be improved  | - new RCC-system<br>backed by soluble<br>boron | - RCC only<br>- FBR type of control          |

### 4. NUCLEAR DESIGN

Results of the core design study will be presented in the following sections for :

- (i) fuel assembly and control element (RCC)
- (ii) beginning of life (BOL) core
- (iii) equilibrium core and fuel management strategies.

#### 4.1 FUEL ASSEMBLY AND RCC ELEMENT

The hexagonal PWHCR fuel element comprises 271 rod-positions, 24 of which are occupied by control rod guide tubes (see Reference [2] for details). The local arrangement of the guide tubes within the assembly - the final result of an iterative process between neutron physical and mechanical reactor design - is indicated in the 30° section plot shown in Figure 2. The distribution of local pin power values in an unrodded assembly, the main information provided by Figure 2, shows the maximum value to be located in the fuel assembly's edge position. This power peak of 1.15 appears just small enough to avoid special technical measures (e.g. local reduction of fissile contents).

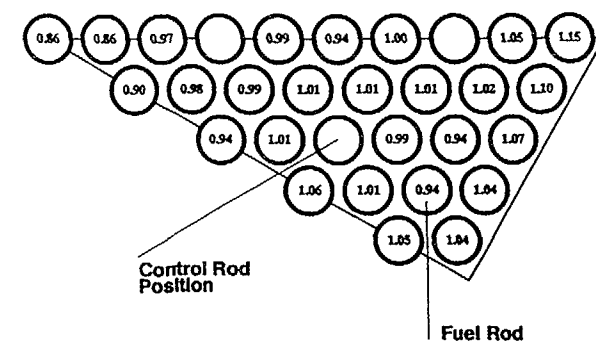


Fig. 2 : Local power distribution in a PWHCR fuel assembly without control rods (8 %  $P_{fiss}$ , 1/12 representation, KMC)

The PWHCR control rods contain boron carbide with enriched  $^{10}\text{B}$  content. The effect of increasing the concentration is demonstrated in Figure 3, where the reactivity equivalent of one control element is plotted versus the fissile plutonium content of the fuel assembly for two distinctive  $^{10}\text{B}$  enrichments.

This figure reveals, that there is only a relatively small reactivity benefit in doubling the  $^{10}\text{B}$  enrichment from 45 % to 90 %. Nevertheless, concentrations in the order of the latter quantity probably have to be considered for at least some of the RCC elements to meet the reactivity demands of the PWHCR. Current estimates for the RCC systems reactivity requirements are based on the following reactivity control philosophy :

- compensation of excess reactivity by means of the RCC-system
- shut down from any hot, full power condition by the RCC-system
- additional use of soluble boron for long term cold subcriticality.

Potential benefits resulting from the use of soluble boron for partial compensation of the excess at begin of cycle will be discussed in chapter 4.3.

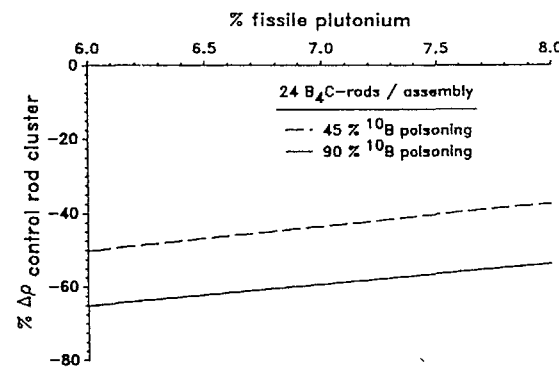


Fig. 3 : Reactivity worths of  $\text{B}_4\text{C}$  RCC elements as function of the fissile plutonium concentration and  $^{10}\text{B}$  enrichment (one rodded assembly, reflective boundary condition, KMC)

#### 4.2 THE BOL CORE

The loading pattern for the first core (beginning-of-live, BOL) has been evaluated according to the following criteria :

- limitation of BOL excess reactivity with respect to the BOC value of an equilibrium cycle in order to avoid oversizing the reactivity control system on the one hand and restrict BOL cycle length on the other
- minimizing of the assembly peak power factors (maximum value  $\leq 1.3$ ):

The relatively simple 3-zone loading scheme presented in Figure 4 fulfills the above mentioned requirements. With 193 fuel assemblies (FA) having a fissile Pu content of only 4.5 % located in the centre, 48 FA with 5.6 %  $\text{Pu}_{\text{fiss}}$  in the middle and 108 FA with the reload enrichment of 8.0 %  $\text{Pu}_{\text{fiss}}$  at the periphery, the average fissile plutonium concentration of the BOL core yields 5.73 %; the associated excess reactivity amounts to 6.2 %. According to the first criterion an even lower BOL reactivity could be considered beneficial. For the time being, however, no vital need was seen for further optimization of the first core loading related e.g. to a partial low leakage loading, fissile Pu contents and cycle length.

As regards the macroscopic power shape of the unpoisoned core the assembly power distribution (axially averaged) presented in Figure 4 shows a very flat profile with the peak value being as low as 1.19, which remains almost constant during exposure with only minor shifts in the local power production.

As mentioned before reactivity control of the PWHCR is based predominantly on the use of rod cluster control elements with  $^{10}\text{B}$  enriched  $\text{B}_4\text{C}$  as absorber material. Accordingly, as compared to common PWR, the number of FA containing control rod clusters has to be significantly increased (approximately 125 instead of 61). Limitations resulting from the mechanical design of pressure vessel and control rod drive mechanics, however, do only permit a maximum number of about 85 control drives to penetrate the reactor pressure vessel closure head. To overcome this problem, an RCC design with 78 single driven control elements and 7 "super"-clusters, each consisting of 7 control elements assembled and linked to one common drive mechanism, was proposed (cf. Figure 5).

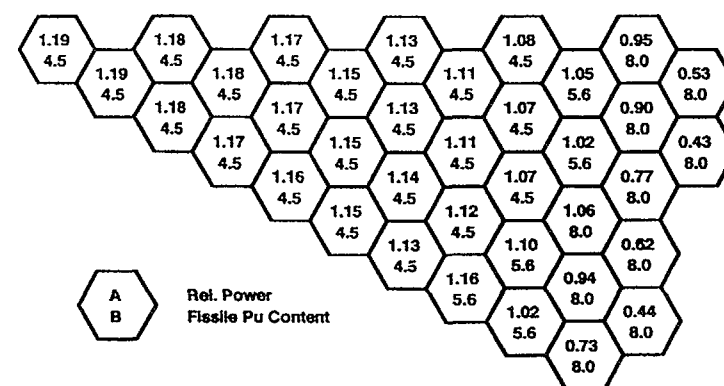


Fig. 4 : Axially averaged power distribution and initial fissile plutonium contents for the PWHCR beginning of live (BOL) core

Based on detailed investigations of the control rod worths and associated power distributions for different patterns of inserted RCC elements - the three basic ones being presented in Figure 5 - the following conclusions can be made :

- single RCC elements (SRE) are used for control of short term reactivity changes as well as for compensation of the major portion of the burnup swing
- excess reactivity compensation by SRE will be performed in a BWR type control rod sequence
- super-cluster RCC elements are used for shutdown purposes only.

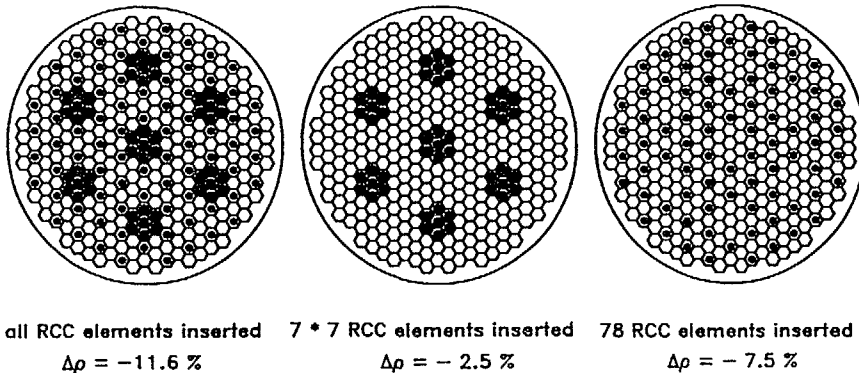


Fig. 5 : Reactivity worth of different insertion patterns of the PWHCR control rod system for BOL core conditions (45 %  $^{10}\text{B}$ , 24  $\text{B}_4\text{C}$ -rods/control assembly, HEXNOD)

It should be mentioned, however, that the RCC design presented here does not yet meet all demands of the PWHCR nuclear core design. Especially problems originating from the simultaneous movement of the super cluster RCC elements, e.g. those related to the stuck-rod reactivity of such RCC ensembles, need further investigations. Studies considering patterns of RCC elements with different  $^{10}\text{B}$  enrichments - lower  $^{10}\text{B}$  content in super cluster RCC to decrease stuck-rod reactivity accompanied by significantly higher (upto 90 %)  $^{10}\text{B}$  enrichments of those single RCC elements not required for excess reactivity compensation - have currently been initiated. Results of these additional studies will either confirm the technical feasibility of the current RCC design or ultimately force a mechanical solution for the subdivision of the super clusters under accidental conditions.

#### 4.3 EQUILIBRIUM CORE

Starting with the BOL core presented in Figure 4 calculations for the transition into the equilibrium cycle were performed in 2-dimensional geometry with the HEXMED code [5]. Establishment of the equilibrium core was based on the following boundary conditions and fuel cycle strategy :

- reload assemblies containing 8 % fissile plutonium mixed oxide fuel ( $\text{Pu}_{\text{fiss}}/\text{Pu}_{\text{tot}} = 0.67$ , tails uranium with 0.2 %  $^{235}\text{U}$  as carrier material)
- fixed reload quantity of 72 fuel assemblies
- partial low leakage loading scheme.

The burnup calculations were performed for unpoisoned core conditions with the effect of axial leakage taken into account in a simplified way by defining EOC at  $k_{\text{eff}} = 1.005$ . The transition of the PWHCR core into the equilibrium, which already in the fifth cycle is almost established, is demonstrated in Figure 6.

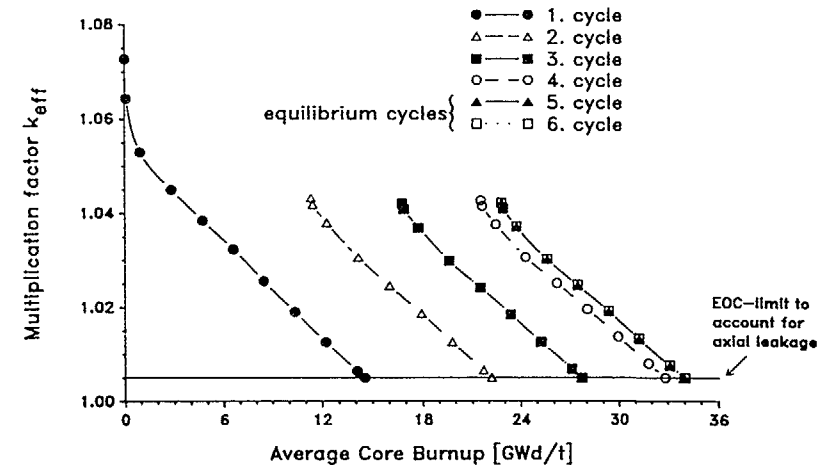


Fig. 6 : Multiplication factor  $k_{\text{eff}}$  as function of average core burnup during transition of the PWHCR core into the equilibrium cycle (partial low leakage loading, HEXMED)

As mentioned before the task of compensating excess reactivity has originally been assigned completely to the rod cluster control system. With respect to the assembly power distribution, on the other hand, a combination of RCC elements and soluble boron in the moderator appears advantageous. In doing so, however, limitations set forth by the void coefficient have carefully to be considered. Results of additional core studies, related to soluble boron worth and void effects, indicate the following reactivity control partitioning to be feasible :

- use of soluble boron for compensation of up to 65 % of the BOL and upto 30 % of the equilibrium cycle BOC excess reactivity, which results in an
- almost constant number of RCC elements inserted at BOC for all cycles (approximately 30 RCC elements required).

Power distribution, local arrangement and FA burnup values are presented in Figures 7 for the beginning and 8 for the end of the (unpoisoned) equilibrium cycle, respectively. With assembly peak power values of 1.27 (BOC) and 1.24 (EOC) a very flat and stable power distribution is achieved. Although compensation of BOC excess reactivity by means of soluble boron (approximately 1000 ppm) and single RCC elements naturally increases power peaking factors, the resulting values (based on preliminary calculations) in the order of 1.50 don't cause major problems for core thermal-hydraulics.

As regards the fuel assembly burnup values, Figures 7 and 8 indicate a certain potential for further optimization, e.g. by considering a full instead of partial low leakage scheme, the main advantage of which is seen in a more uniform discharge burnup distribution. In this context it has to be stated that the fuel management strategy as employed in these calculations is not considered as final. Further studies, addressing the topics mentioned above, are necessary and have already been initiated.

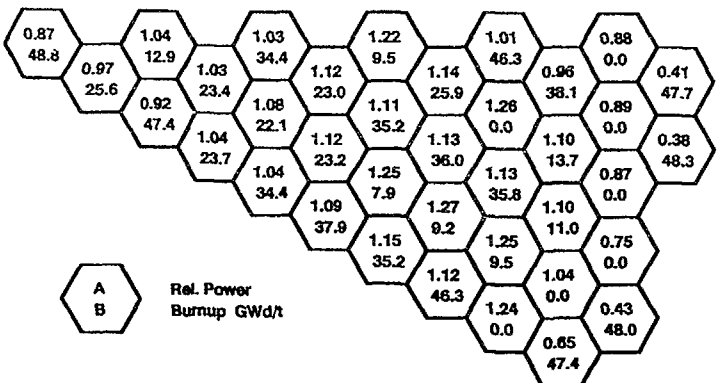


Fig. 7 : Power and burnup distribution of PWHCR core at begin of the equilibrium cycle (partial low leakage loading, HEXMED)

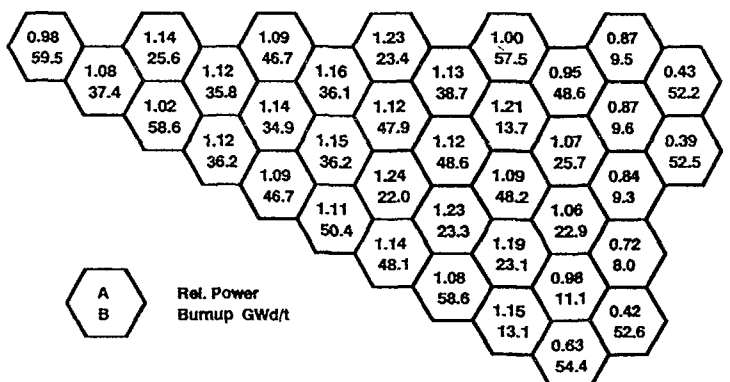


Fig. 8 : Power and burnup distribution of PWHCR core at end of the equilibrium cycle (partial low leakage loading, HEXMED)

The main characteristics of the PWHCR equilibrium core being presented here are summarized in Table III. With a length of 358 full power days (fpd) this equilibrium cycle does not fit too well into the normal annual reloading scheme. For a better coincidence of the reload quantity or the reload enrichment has to be reduced; additional advantages of the latter measure being an even better void behaviour on the one hand and an improved conservation factor on the other.

TABLE III  
Equilibrium Fuel Cycle Characteristics of the PWHCR

|  |            |
|--|------------|
| BOC Excess Reactivity (including Xe)                         | 3.5 %      |
| Mean Cycle Length  | 358 fpd    |
| Cycle Burnup   | 11.2 GWd/t |
| Average Discharge Burnup                                     | 53.7 GWd/t |
| Conversion Ratio (EOC)                                       | 0.78       |
| Conservation Factor CF<br>(unloaded/loaded fissile contents) | 0.74       |

For the assessment of conversion properties of a particular core design the integral quantity conservation factor CF - defined as ratio of unloaded to loaded fissile mass - is considered to be more representative than the commonly used conversion ratio, which due to its nuclide density dependence varies with exposure.

The fuel composition for 8 %  $\text{Pu}_{\text{fiss}}$  containing PWHCR assemblies at BOL and EOL is given in Table IV. While the absolute amount of fissile material decreases according to CF by 26 %, the associated changes in the plutonium isotopes - especially the increasing relative content of  $^{241}\text{Pu}$  - demonstrates what was previously called the conservation of plutonium quality.

TABLE IV  
Fuel Composition [g/kg<sub>fresh fuel</sub>] of PWHCR Assemblies  
of 8 %  $\text{Pu}_{\text{fiss}}$  at BOL and EOL

| Nuclide           | 0.0 GWd/t | 53.7 GWd/t |
|-------------------|-----------|------------|
| $^{235}\text{U}$  | 1.8       | 1.0        |
| $^{238}\text{U}$  | 878.8     | 841.6      |
| $^{239}\text{Pu}$ | 68.1      | 45.3       |
| $^{240}\text{Pu}$ | 32.2      | 29.1       |
| $^{241}\text{Pu}$ | 11.9      | 14.0       |
| $^{242}\text{Pu}$ | 7.2       | 5.7        |
| $^{241}\text{Am}$ | 0.0       | 1.7        |
| $^{243}\text{Am}$ | 0.0       | 3.3        |
| $^{244}\text{Cm}$ | 0.0       | 1.5        |

## 5. CONCLUSIONS

This paper summarized results of a recent study concerning the nuclear core design of high converting tight lattice PWR. The results obtained so far permit to draw the following conclusions :

- from a neutron-physical point of view the concept of the PWHCR appears to be technically feasible
- average discharge burnups in the order of 55 GWd/t can be attained within the limits set by the void coefficient
- reactivity control can be based almost exclusively on the use of RCC elements; with respect to power peaking, however, a combination of solid and dissolved absorbers is seen to be advantageous.

Further topics, which so far have only preliminarily been addressed in our investigations are the possibility of employing burnable absorbers, the impact of changes in the available plutonium quality and consequences resulting from the initial  $^{241}\text{Am}$  content. For the final design of the high conversion Pu-burning tight lattice PWR these aspects have carefully to be taken into account. While, especially the use of burnable absorbers provides a potential for further core optimization, questions related to the initial mixed oxide composition may cause additional problems. In general, however, the tight lattice pressurized water reactor seems to have a good potential for entering future worlds nuclear energy market.

## REFERENCES

- [1] KREBS, W.D., SCHLOSSER, G.J., "Status of fuel assembly design and core management experience with MOX fuel in the FRG for Siemens/KWU type LWRs", IAEA Technical Committee Meeting on Recycling of Plutonium and Uranium in Water Reactor Fuels, Cadarache, France (1989).
- [2] GOETZMANN, C.A., MÄRKI, H., MOLDASCHL, H., "Rationale for PWHCR development strategy", IAEA Technical Committee Meeting on Technical and Economical Aspects of High Converters, Nürnberg, FRG (1990).
- [3] CHAWLA, R., BERGER, H.-D., HAGER, H., SEILER, R., "The PROTEUS phase II experiments as data base for LWHCR physics validation", IAEA Technical Committee Meeting on Technical and Economical Aspects of High Converters, Nürnberg, FRG (1990).
- [4] AKIE, H., ISHIGURO, Y., TAKANO, H., "Summary report on the international comparison of NEACRP burnup Benchmark calculations for high conversion light water reactor lattices", NEACRP-L-309, JAERI-M 88-200 (1988).
- [5] WAGNER, M., "HEXNOD and HEXMED - Nodal reactor codes for the design of high converter reactors", IAEA Technical Committee Meeting on Technical and Economical Aspects of High Converters, Nürnberg, FRG (1990).

## NEUTRON PHYSICS AND THERMOHYDRAULICS DESIGN OF A REFERENCE HIGH CONVERSION PWR

C.H.M. BROEDERS, M. DALLE DONNE  
Kernforschungszentrum Karlsruhe GmbH,  
Karlsruhe, Federal Republic of Germany

### Abstract

The neutron physics and thermohydraulic design work for a reference High Conversion PWR core is presented. The fuel is  $(\text{Pu},\text{U})\text{O}_2$  and the coolant / moderator is light water. The core dimensions should be such as to allow a replacement of the core of a KWU 1300 MWe PWR with only minor changes in the internals of the reactor pressure vessel

The fuel rods are 3.5 m long and have a diameter of 9.5 mm. The cladding is made up of Zircaloy. The rods are placed in 349 hexagonal open fuel elements and they are arranged in triangular arrays with a pitch of 11.8 mm ( $p/d = 1.242$ ). This results in a water to fuel volume ratio of 0.94 and 1.23 for the unit fuel cell and for the whole core respectively. The fuel rods are supported by spacers grids. The control and shut-down system is based on a KWU design. The total core heat output is 3765 MWth, the same as for a 1300 MWe PWR, resulting in a rod linear rating of 125 W/cm, considerably smaller than in a PWR. The core pressure drop of 2 bar can be obtained by the standard PWR main water pumps. The minimum safety margin against critical heat flux, considering all hot spot factors and a plant overpower factor of 12%, is 36%, i.e. an acceptable value.

The burnup calculations have been performed for a six batch fuel element cycle, for a cycle duration of 320 full power days. The plutonium feed enrichment is 8%, where the plutonium vector corresponds to plutonium discharged from a PWR and a 10 yr ex-core time. Reactivity control during burn-up is obtained by boron dissolved in the water. During the equilibrium cycle the void coefficient is between -5% and -7%, while the reactivity variation between the core full power water density of 0.7 g/cm<sup>3</sup> and 0.5 g/cm<sup>3</sup> is about the same as for a PWR, so that no problems should be expected for a ATWS. The fuel utilization ratio is about 0.8 and a discharge burnup of 50000 - 52000 MWd/t is achieved.

## I INTRODUCTION

Since 1979, the Karlsruhe Nuclear Research Center (KfK) has been involved in the design and assessment of an advanced pressurized water reactor (APWR), sometimes also called High Conversion PWR (HCPWR) that is being developed with the idea of improving uranium utilization. This work is carried out in collaboration with Kraftwerk Union (KWU), the University of Braunschweig, and the Paul Scherrer Institut in Wurenlingen. The investigations have been restricted to the uranium / plutonium fuel cycle and to light water as coolant / moderator. The idea is to replace the core of a KWU 1300 MW (electric) pressurized water reactor (PWR) with a high-converting core with only minor changes in the internals of the reactor pressure vessel (RPV). Two types of core have been studied: a homogeneous, where all fuel elements have a similar form, and a heterogeneous, where there are two kinds of fuel elements: the "seed" and the "blanket" elements.<sup>1/</sup> The fuel in the seed elements has a higher plutonium enrichment. The seed elements' main function is to produce power and neutrons, while the function of the blanket, with a considerably lower plutonium enrichment, is mainly that of breeding plutonium. In the KfK reference designs, the fuel rods of the homogeneous reactor are spaced by six spiral ribs, while for the heterogeneous reactor the seed rods are supported by grid spacers and the blanket rods by six spiral ribs.<sup>1/</sup>

A realistic assessment of the potential of this type of reactor must include an evaluation of the safety. It is clear that, to be licensed, this reactor must have the same safety standards as the PWR. It was therefore decided to investigate within the present program a large loss-of-coolant-accident (LOCA) and an anticipated transient without scram (ATWS), both for the homogeneous and the heterogeneous type of APWR. The chosen large LOCA was the one considered as the Design Basis Accident for a PWR, that is an accident caused by the sudden guillotine break of the main water pipe in one of the four primary loops at a position between the main water pump and the RPV. The ATWS was investigated especially to assess the importance of the water density reactivity coefficient, which is expected to be less negative than in a PWR, especially in an APWR with a very tight fuel rod lattice. Of the various ATWS considered in the FRG the one was selected which is believed to have the worst consequences for the APWR, namely the station blackout together with the failure to scram the reactor.

The calculations of the blow-down phase of the LOCA and the ATWS calculations were performed with the computer code RELAPS/MOD1, properly modified to account for the different geometries present in the APWR cores<sup>2/</sup>, while the reflood phase was modelled with the code FLUT FDWR (FDWR = Fortgeschrittener Druckwasser Reaktor, i.e. APWR)<sup>3/</sup>, a modified version of the code FLUT, originally developed at GRS-Garching<sup>4/</sup>, as it was discovered that RELAPS / MOD1, as well as RELAPS / MOD2, was not well suited to model the reflood phase for an APWR geometry.

The calculations were performed for two homogeneous reactors, one with a very tight fuel rod lattice ( $p/d = 1.123$ ) and a second with a less tight lattice ( $p/d = 1.2$ ), as well as for a heterogeneous APWR. Table I shows the most important results of these calculations as compared with the relative data for a PWR, calculated by us with the same procedures. From the Table is evident that both the homogeneous reactor with  $p/d = 1.123$  and the heterogeneous reactor are not acceptable from a safety point of view, however for different reasons. The homogeneous APWR with  $p/d = 1.123$  is not acceptable safe because the maximum coolant pressure reached during the investigated ATWS is too high. The main reason for this is that the water density reactivity coefficient is not sufficiently negative. The heterogeneous APWR is not acceptable because the maximum hot spot fuel rod cladding temperature in the seed region during the LOCA is too high.

Only the homogeneous APWR with  $p/d = 1.2$  appears to be acceptably safe on the base of the mentioned safety analysis. However, with this reactor only an average discharge burnup of 31000 MWd/t is achievable.<sup>1/</sup> This kind of burnup is considered today too small for a reactor with relatively expensive fuel, especially because already the present development of the PWR strives to obtain higher burnups than that. The reason for this limitation is the relatively low plutonium enrichment assumed for this reactor (7.4%). With a higher enrichment it is possible to achieve higher burn-ups, however the water density reactivity coefficient becomes less negative and this may have bad safety implications. To obviate this difficulty we decided to enlarge the fuel rod lattice even more to have a sufficiently negative water density coefficient at the higher plutonium enrichment. In the present paper we describe the new reference APWR and show its main data and characteristics.

TABLE I Main Results of the Safety Investigations of Ref. /2/ and /3/

| Reactor  | Maximum fuel rod cladding temperature during LOCA (°C) | Maximum coolant pressure in the reactor vessel during ATWS (bar) |
|--|--|--|
| Reference PWR  | 1040   | 180  |
| Homogeneous APWR<br>with wide fuel rod lattice<br>(p/d=1.20) | 1120   | 182  |
| with tight fuel rod lattice (p/d=1.123)                      | 1100   | >230   |
| Heterogeneous APWR<br>seed                                   | 1285   |  |
| blanket  | 975  | 215  |

## II CHOICE OF THE REFERENCE APWR CORE GEOMETRY

Due to the tighter lattice, a APWR core has a larger number of fuel rods than in a usual PWR, furthermore the horizontal cross section of a fuel element is not square but rather hexagonal to accomodate the triangular array of the fuel rods and to give a better filling of the space available inside the core barrel. Thus, the choice of the size of fuel element cross section is not a simple problem and it is mainly dictated by the design and number of the control / shut down rod mechanisms and by the space available above the core and in the upper lid of the core vessel. It was therefore decided to choose the size of the element suggested by KWU and compatible with the control / shut down rod system designed by KWU /5/. This is characterized by a distance between the flats of the hexagonal fuel element of 198.25 mm. Originally the KWU proposal was to have a fuel rod diameter of 9.5 mm, a rod pitch of 10.67 mm and therefore a very tight lattice of p/d = 1.123. Subsequently, after the KfK work described in Ref /2/ and /3/, the possibility of enlarging the lattice was left open by varying the fuel rod diameter down to 8.5 mm, the solution with 8.5 mm being the reference one /5/. Lately, after a KWU-KfK thorough comparison of the advantages and disadvantages from a neutronic and thermohydraulic viewpoint of the two types of fuel rods,

KWU accepted the KfK proposal of using a fuel rod of 9.5 mm, mainly due to the extra cost and time required by the development of a new kind of rod with 8.5 mm in diameter, 9.5 mm being the diameter of the fuel rod of the latest standard KWU PWR.

TABLE II Geometrical Data of the PWR and the Reference APWR Design

|   | PWR*<br>(Triang.<br>Lattice) | Ref. APWR  |
|---|------------------------------|------------|
| Equivalent core diameter (cm)                       | 360.5                        | 388.9      |
| Active core height (cm)                             | 390                          | 350        |
| Number of fuel elements in the core                 | 189                          | 349        |
| Distance between the flats of the fuel element (mm) | 249.7                        | 198.25     |
| Number of control rod guide tubes per fuel element  | 24                           | 24         |
| Number of fuel rods per fuel element                | 307                          | 247        |
| Total number of fuel rods                           | 58023                        | 86203      |
| Cladding material                                   | Zircaloy 4                   | Zircaloy 4 |
| Fuel rod outer diameter (mm)                        | 9.5                          | 9.5        |
| Cladding thickness (mm)                             | 0.64                         | 0.64       |
| Fuel rod pitch (mm)                                 | 13.6                         | 11.8       |
| p/d ratio   | 1.432                        | 1.242      |
| Spacer type   | grid                         | grid       |
| Axial distance of the spacer grids (mm)             | 548                          | 380        |
| Water-to-fuel volume ratio in the core**            | 1.95                         | 1.23       |

\*PWR with triangular fuel rod lattice having the same water volume fraction and the same core equivalent diameter of the standard German PWR of 1300 MWe (KONVOI).

\*\* With all control and shut-down rods withdrawn from the core.

Fig 1 shows a cross section of the fuel element with the rod arrangement proposed by KfK and now accepted by KWU /6/. To cope with the large rod diameter of 9.5 mm, the outer row of rods has been eliminated resulting in a rod pitch of 11.8 mm and a p/d ratio of 1.242. The rod cladding is made of Zircaloy, with a thickness of 0.64 mm as in the PWR. The choice of Zircaloy, rather than steel as in the previous designs, has been taken in view of the fact that with a

larger p/d ratio, the neutron spectrum is softer and Zircaloy offers considerable advantages over steel from a neutronic viewpoint. The rods are supported by 40 mm high Nimonic grid spacers. The design of the grid has been performed by KWU /7/. The axial distance of the grids is about 400 mm and it has been determined by the condition, that the ratio of the maximum rod lateral displacement caused by a load proportional to the axial pressure drop per unit length of the core height divided by the minimum distance of the rods p-d is the same as for the PWR.

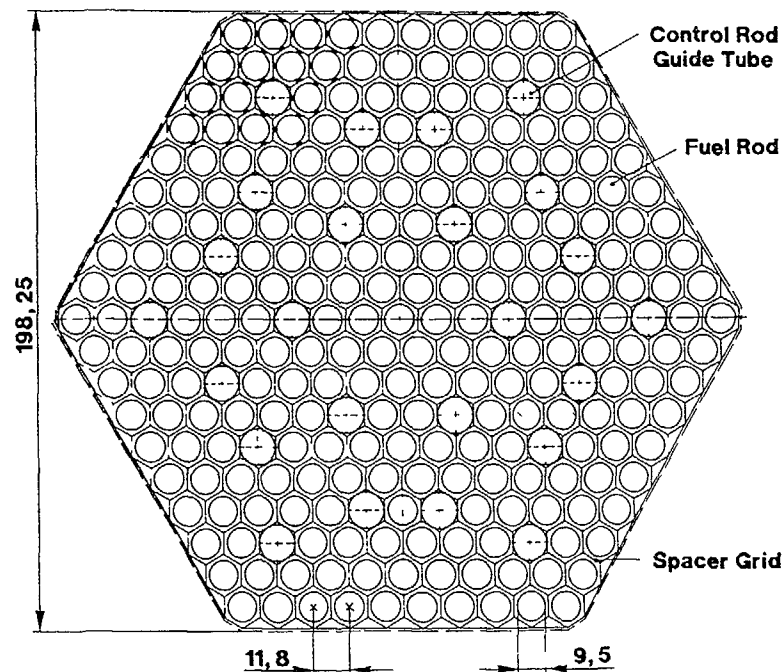


Fig.1 Cross section of the fuel element (dimensions in millimeters).

Fig.1 shows the position of 24 control rod guide tubes in the fuel element, the number of which has been assessed by preliminary neutron physics calculations /8/. The fuel element has no shroud. No tie-rods are required, as the grids are fixed to the control rod guide tubes /7/.

Fig.2 shows the cross section of the proposed arrangement of the fuel elements within the core barrel of a standard German PWR of 1300 MWe. This arrangement is compatible with the KWU design of the control / shut-down rod system /6/. There are 349 fuel elements and 85 drive mechanisms for the control / shut-down systems. Of these, 7 drive mechanisms are connected to 7 fuel elements each and serve only for shut-down purposes. The other 78 are each connected to one fuel element only.

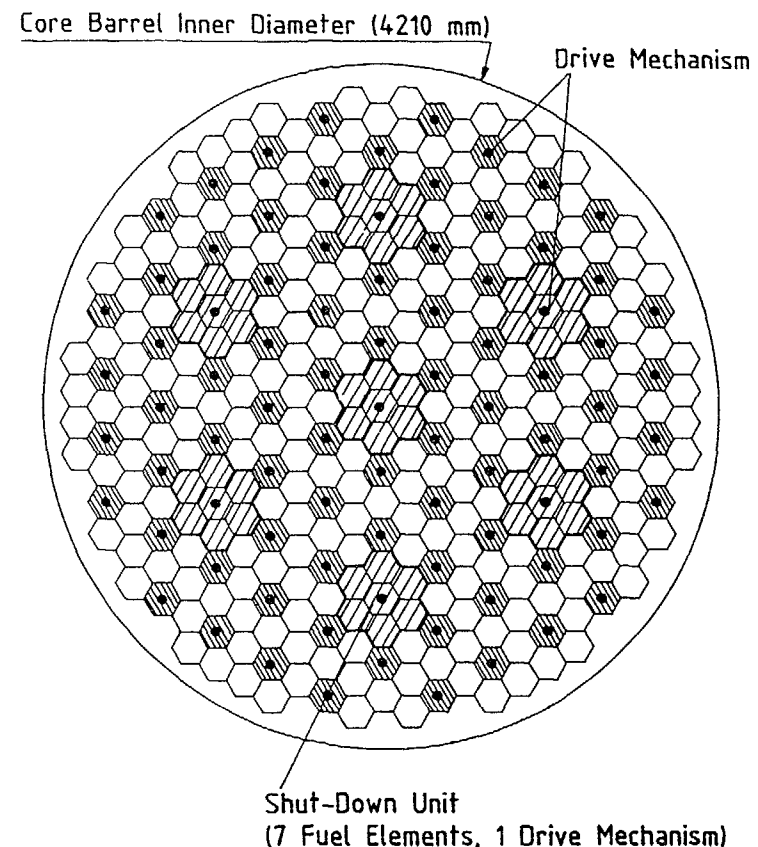


Fig.2 Core cross section compatible with KWU design of the control / shut-down system.

### III THERMOHYDRAULIC OPTIMISATION AND DETERMINATION OF THE CORE HEIGHT

In the previous chapter the choice of the core cross section was illustrated. However the core height is not yet fixed. For this we performed a thermohydraulic parametric study, because the core height plays a determining role on the thermohydraulics aspects of the core design (core power density, core pressure drop). The calculations were performed with the computer code HADA-2 developed at KfK /9-11/. They were performed with the constant values of the neutron flux axial and radial form factors of  $F_{ax} = 1.45$  and  $F_{rad} = 1.43$  which

TABLE III Thermohydraulic Data of the PWR and of the Reference APWR Design

|   | PWR*<br>(Triang. Lattice) | Ref. APWR |
|---|---------------------------|-----------|
| Core thermal output ( $MW_{th}$ )   | 3765                      | 3765      |
| Plant net electrical power (MWe)  | 1300                      | 1300      |
| Pumping power for primary circuit water (MWe)                               | 21.9                      | 22.8      |
| Primary circuit total water mass flow (kg/sec)                              | 19044                     | 18360     |
| Water temperature at core inlet ( $^{\circ}C$ )                             | 291.4                     | 291.2     |
| Water temperature at core outlet ( $^{\circ}C$ )                            | 325.9                     | 326.8     |
| Water pressure at core outlet (bar)   | 158.3                     | 158.3     |
| Secondary circuit saturated vapor pressure (bar)                            | 64.5                      | 64.5      |
| Average nominal rod linear rating (W/cm)                                    | 166.4                     | 124.8     |
| Average heat flux at fuel rod surface (W/cm <sup>2</sup> )                  | 55.7                      | 41.5      |
| Average volumetric core power density (W/cm <sup>3</sup> )                  | 103.9                     | 90.5      |
| Power hot channel factor $F_q$  | 2.1                       | 1.93**    |
| Water enthalpy rise hot channel factor $F_{\Delta H}$                       | 1.6                       | 1.58**    |
| Maximum plant overload factor $F_{OP}$                                      | 1.12                      | 1.12      |
| DNBR, ratio between CHF and maximum hot channel heat flux for $F_{OP}=1.12$ | 1.46***                   | 1.36***   |
| Average water velocity in the core (m/s)                                    | 4.38                      | 4.55      |
| Spacer pressure drop coefficient  | 1.03                      | 1.16      |
| Core pressure drop (bar)  | 1.16                      | 2.02      |
| Total pressure in water primary circuit (bar)                               | 6.45                      | 6.95      |

\* PWR with triangular fuel rod lattice having the same water volume fraction and the same core equivalent diameter of the standard German PWR of 1300 MWe (KONVOI)

\*\* The flow of the coolant water at the fuel element outer border is separately accounted for.

\*\*\* Calculated with the Dalle Donne-Hame critical heat flux correlation.

were assessed by preliminary neutronic calculations, and with the values of the power hot channel factor and of the water enthalpy rise hot channel factor of  $F_q = 2.3$  and  $F_{\Delta H} = 1.65$  respectively, which resulted from these neutron flux form factors. As usual a plant overload factor of  $F_{OP} = 1.12$  was applied /9,10/

Fig. 3 shows the main results of these calculations. The chosen range of core height  $H$  was 230-390 cm. In all the cases it was possible to obtain the standard PWR net electrical power of 1300 MWe. Obviously the average fuel rod linear rating  $q_l$  decreases with  $H$  being the core power and the number of fuel rods constant. As expected, the core pressure drop  $\Delta p$  increases linearly with  $H$ . Even with the highest values of  $H$ , it appears to be acceptable for the standard PWR main water pumps. The DNBR, minimum ratio between the Critical Heat Flux and the maximum hot channel heat flux for a plant overload factor of  $F_{OP} = 1.12$ , was calculated using the Dalle Donne Hame Critical Heat Flux correlation, which was developed especially for tight triangular rod lattices ( $p/d = 1.02 - 1.36$ ) /12/. Fig. 3 shows the values of DNBR calculated with the WSC-2 correlation valid for higher values of  $p/d$  /13/ as well, as the present core configuration ( $p/d = 1.242$ ) is rather on the higher edge of the validity field of the Dalle Donne Hame correlation,

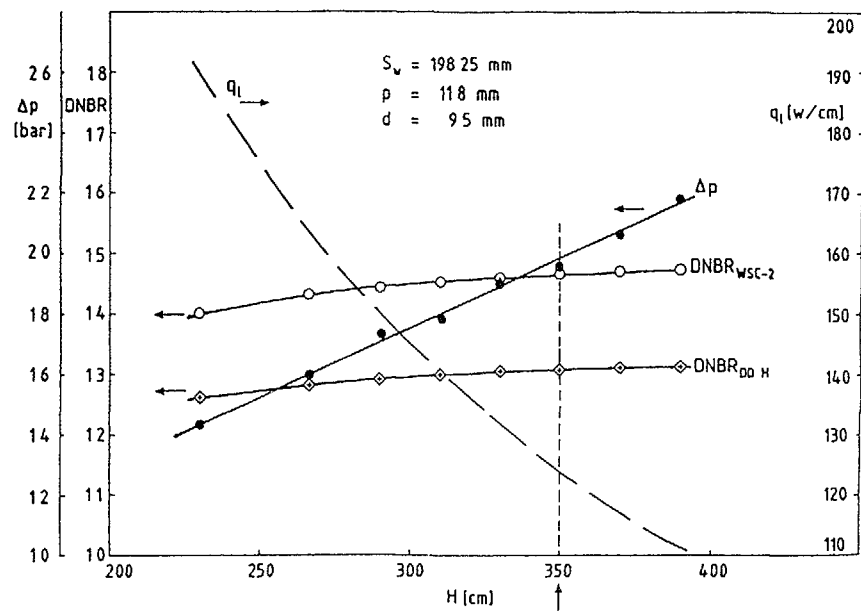


Fig. 3 Main results of the thermohydraulic parametric calculations.

which might be slightly too pessimistic. For  $H > 310$  cm even the DNBR values according to Dalle Donne Hame are equal or above 1.30 which is generally considered the minimum acceptable value.

The result of this thermohydraulic parametric study is that the range of core height 310 to 390 cm is acceptable. The decision on the exact height was therefore taken on the base of a further consideration. It is generally recognized in Germany that long in-core residence times of fuel rods with Zircaloy claddings require relatively low heat fluxes at the clad surface and low rod linear ratings. The present reference APWR core will remain in operation for a very long time (see next chapter), therefore after consultation with KWU, the relatively high value of  $H$  equal to 350 cm was chosen, which allows the relatively low value of rod linear rating of about 125 W/cm.

#### IV NEUTRON PHYSICS CALCULATIONS

The neutron physics calculations for the new design have been performed with the calculational procedures described in a separate contribution to this meeting /14/. At variance with our previous investigations, we did not analyse a "Begin of Life" (BOL)-Core with different enrichment zones, but an equilibrium core with fixed enrichment for the fresh fuel assemblies was considered. For the choice of the reload pattern we had the following boundary conditions:

- low power rating ( $\sim 125$  W/cm)
- high burnup ( $> 50000$  MWd/Thm))
- restricted enrichment due to the voiding problem

From practical considerations by KWU a cycle time of 300-320 fuel power days was required /15/. The conditions mentioned above could be met by a design with the following characteristics:

- enrichment for equilibrium fuel assemblies = 8% Pu<sub>fis</sub>
- cycle time  $\approx 320$  full power days
- reload of  $\approx 1/6$ th of the core after each cycle

The whole core calculations were performed with 4 energy groups. Table IV shows the boundaries within the WIMS 69 energy group scheme.

TABLE IV Coarse group structure for reactor calculations

| Coarse Group | WIMS Group | Energy Range      |
|--------------|------------|-------------------|
| 1            | 1 - 5      | 0.821 - 10 MeV    |
| 2            | 6 - 14     | 9.118 - 821 keV   |
| 3            | 15 - 25    | 15.968 - 9118 keV |
| 4            | 26 - 69    | 0 - 15.968 keV    |

#### IV. 1 Applied nuclear data

The 4-group HXSLIB library (see ref /14/) has been created on the basis of a 1989 nuclear library. It contains the required nuclear group constants for the following parameters:

- Fuel temperature 300, 920 and 2100 K
- Moderator and can temperature 573 K
- B<sup>10</sup> concentration in the coolant 0, 500, 1000, 2000 and 4000 ppm
- Burnup of the fuel 0, 10, 20, 30, 40, 50, 60 and 70 GWd/Thm
- Fuel assembly data for 24 control rod positions, filled with coolant (H<sub>2</sub>O) or B<sub>4</sub>C with 60% B<sup>10</sup> enrichment
- Water density ratios  $\rho/\rho_N = 0.01, 0.1, 0.3, 0.5, 0.7, 0.8, 0.9, 1$  and 1.1

#### IV.2 The fuel assembly shuffling

For the fuel assembly shuffling a quite simple model was chosen. After each cycle  $\approx 1/6$ th of the assemblies is removed from the core and replaced by fresh ones with 8% Pu fissile. The available fuel assemblies for the new cycle are arranged in a way, that the burnup for the fuel assembly positions is in a predefined order,

being determined by two-dimensional exploratory calculations. The code ARCOSE /14/ enables succeeding cycle calculations with an arbitrary number of micro time steps pro cycle, both in two- and three-dimensional geometry

#### IV.3 Results for the equilibrium Core

Mainly three-dimensional four group diffusion calculations have been performed with the nodal code HEXNODK, being developed from the KWU-code HEXNOD /16/. The geometry model contained 16 axial planes for a 30° - sector of the core. The axial reflectors were approximated by 30 cm zones at the top and the bottom of the model, containing the fuel-lattice without fuel (density 0 g/cm<sup>3</sup>). The radial reflector was approximated by 1 ring of fuel assemblies at the outer boundary of the core, containing a mixture of 50% SS and 50% H<sub>2</sub>O.

The initial burnup distribution in the core was estimated from two-dimensional HEXNODK calculations. With the code ARCOSE eight cycles were calculated with ten micro time steps each cycle. At each micro time step a criticality search by change of the B<sub>10</sub> content in the coolant was performed. Using the same shuffling scheme after each reactor cycle a stable power and burnup distribution in the core could be obtained after about six cycles.

With the help of the restart-options of the code ARCOSE the most important characteristics of the final equilibrium core could be determined.

The figures 4-10 show some results, obtained from the ARCOSE-plotting interface.

Fig. 4 gives the axial burnup profile of selected fuel assemblies from each charge of the core filling. In fig. 5 the burnups of the 37 fuel assemblies of a 30° sector of the core are plotted for the begin and the end of the equilibrium core. Fig. 6 shows the axial distribution of the power ratings in representative fuel assemblies (FA) after 1 to 6 in-core cycles. The value F<sub>ax</sub> is the axial form factor, changing from 1.15 at the end of the first in-core cycle to about 1.10 at the end of the in-core time. Fig. 7 shows the behavior of the axial power rating during the first in-core cycle. The axial form factor decreases from 1.29 to 1.15, the axial power flattening being caused by the higher burnup in the core center. The main numerical results are summarized in Table V. The data for the reference PWR have been taken from reference /1/.

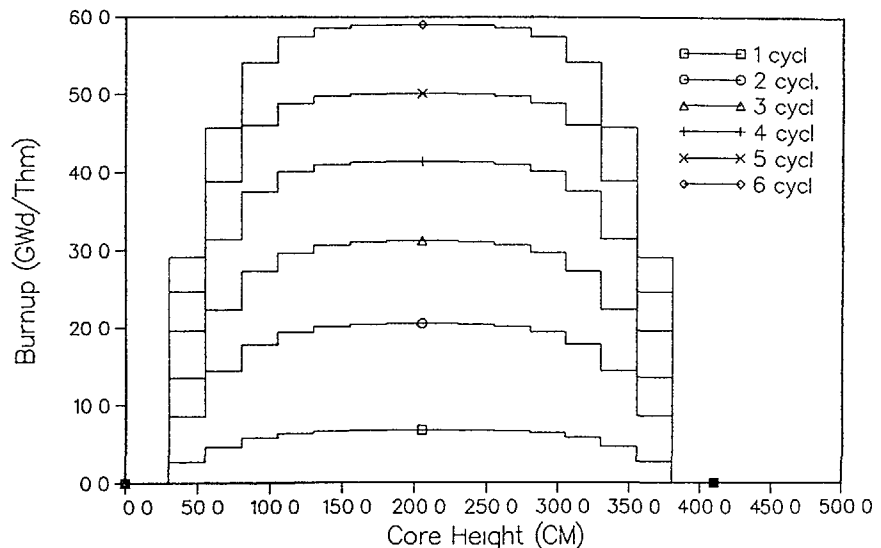


FIG. 4 KfK HCLWR Design, Equilibrium Core, Axial Burnup/Charge

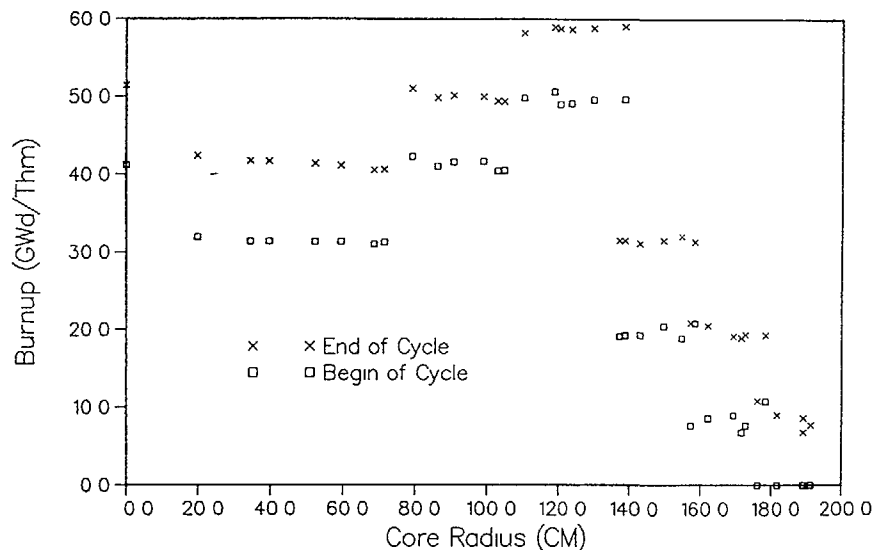


FIG. 5 KfK HCLWR Design, Equilibrium Core, Core Center Burnup

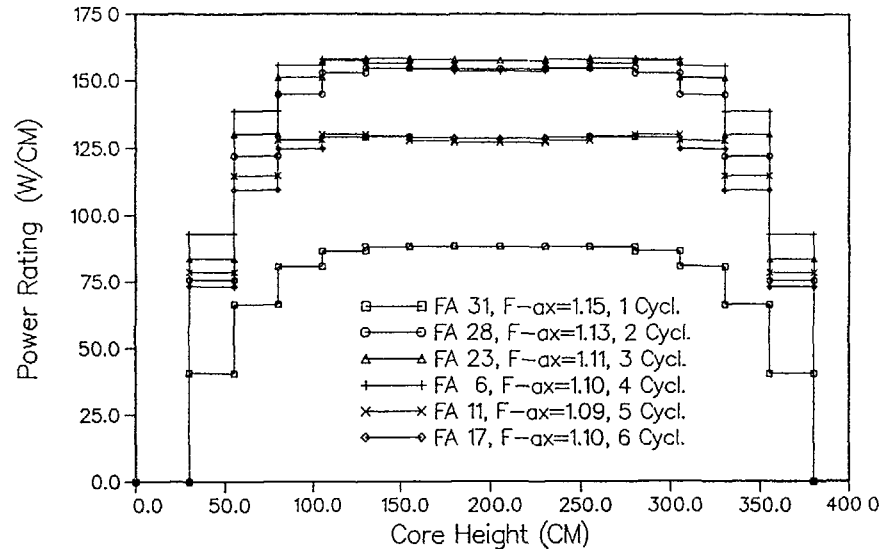


FIG. 6. KfK HCLWR Design, Equilibrium Core, Power Rating EOC

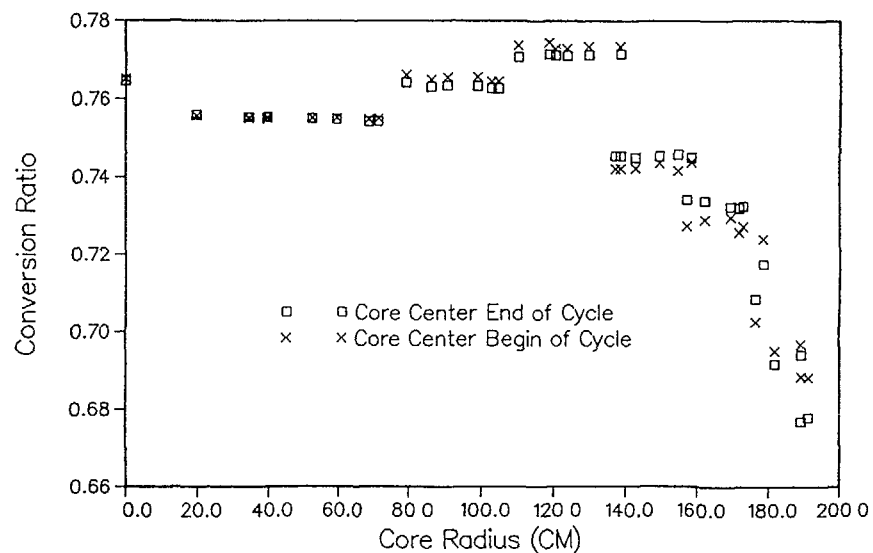


FIG. 7. KfK HCLWR Design, Equilibrium Core, FA Conversion Ratios

For the conversion ratio the mean core value is given. Fig. 8 shows the conversion ratios for the fuel assemblies in the core. Depending on the number of cycle corelife the fuel assembly conversion ratio varies between 0.68 and 0.77.

Another important parameter for the fuel utilization is the conservation factor, defined as the ratio of the fissile inventory after burnup to the initial fissile fuel inventory. Fig. 9 shows the behaviour of the conservation factor from the basic cell calculation for the equilibrium fuel lattice with 8% Pu<sub>141</sub>. For discharge burnup values slightly above 50000 MWd/Thm, a conservation factor near 0.8 may be obtained. The axial and radial power form factors vary slightly between begin and end of cycle. In the worst case (BOC) they are 1.3 and 1.4 respectively. These values were calculated for the fuel assembly power ratings. Variations within the fuel assemblies are not yet taken into account. The Doppler coefficient was determined by k<sub>eff</sub> core calculations for three mean fuel temperatures 300, 920 and 2100 K, assuming the Doppler temperature formula dK/dT = A/T<sup>x</sup>.

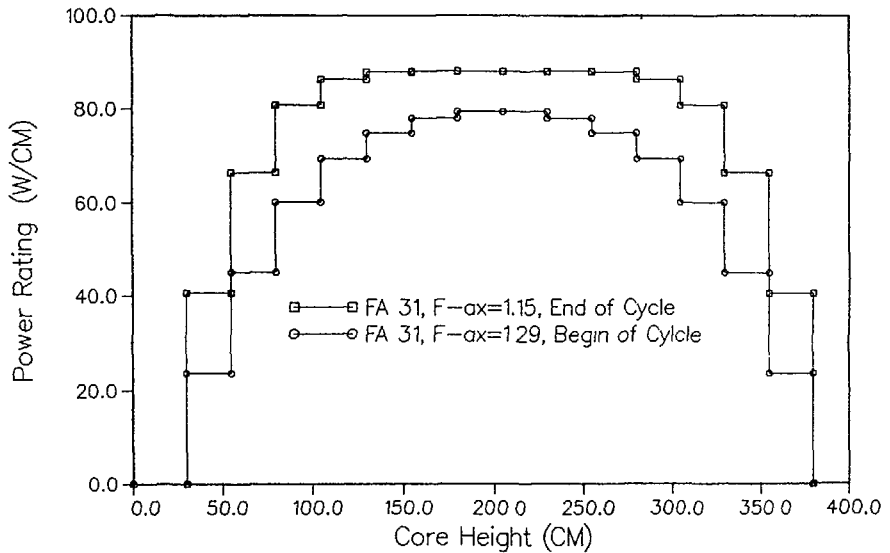


FIG. 8. KfK HCLWR Design, Equilibrium Core, Fresh Fuel Assembly

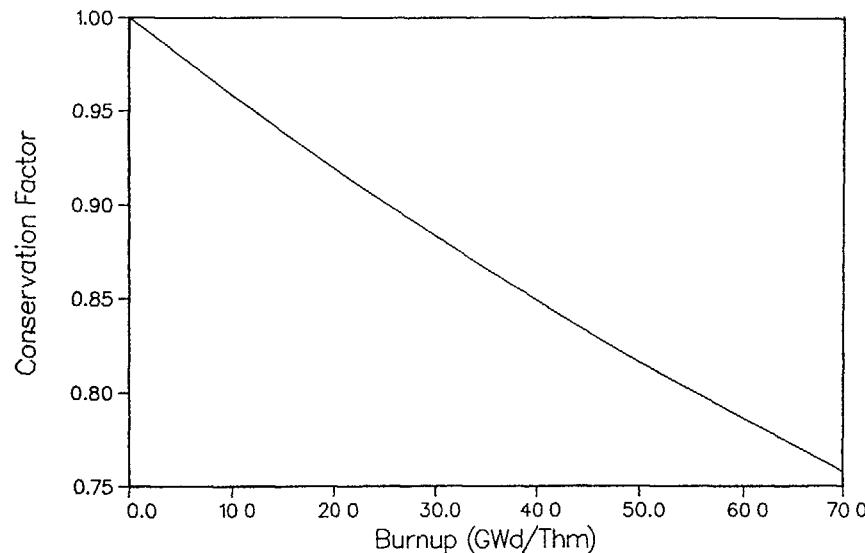


FIG. 9 KfK HCLWR Design, 8% Pu-fis Cell Calculations

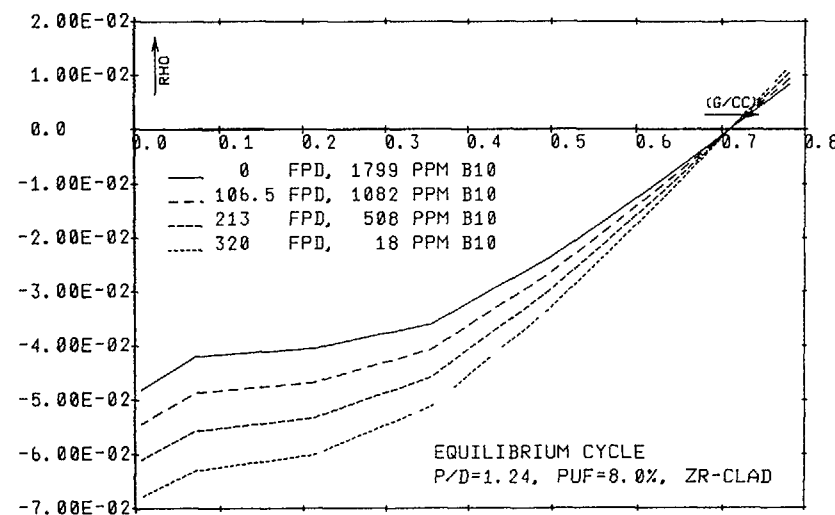


FIG. 10 KfK HCLWR DESIGN, K-EFF AS A FUNCTION OF WATERDENSITY

For the void calculations the critical B<sub>10</sub> concentration was searched for 4 time steps within the reactor cycle 0, 106.5, 213 and 320 fpd. For these reactor conditions full core calculations were performed for 9 water densities

$$\rho/\rho_N = 0.01, 0.1, 0.3, 0.5, 0.7, 0.8, 0.9, 1 \text{ and } 1.1$$

Fig 10 shows the resulting curves. In the range of water density (0.5 – 0.7 g/cm<sup>3</sup>) of interest for the ATWS Station Blackout with Failure to Scram the water reactivity coefficient is about the same as for the PWR (see Table V)

TABLE V: Neutron Physics Data of PWR and KfK APWR Design

|  | Ref. PWR                | KfK APWR                          |
|--|-------------------------|-----------------------------------|
| Plutonium reactor<br>(Pu <sup>238</sup> , Pu <sup>239</sup> , Pu <sup>240</sup> , Pu <sup>241</sup> , Pu <sup>242</sup><br>wt/%) | -                       | 1.94, 56.63, 25.24, 9.87,<br>6.32 |
| Uranium reactor<br>(U <sup>235</sup> , U <sup>238</sup><br>wt/%)   | 3.2, 96.8               | 0.2, 99.8                         |
| Reload fissile (%)   | 3.2                     | 8.0                               |
| Total fuel inventory (THM)   | 103.5                   | 137*                              |
| Total fissile inventory  | 2.57                    | 11.2*                             |
| Conversion ratio   | 0.55                    | ≈ 0.74                            |
| Utilisation factor   | -                       | 0.8                               |
| ΔK/fpd   | -3.10 <sup>-4</sup>     | -0.83 × 10 <sup>-4</sup>          |
| Number of fuel cycles  | 3                       | 6                                 |
| Fuel cycle duration (fpd)  | 360                     | 320                               |
| Discharge burnup (MWd/THM)   | 33000–35000             | 50000–52000                       |
| Axial power factor   | 1.3–1.2                 | 1.3–1.1                           |
| Radial power factor  | 1.5–1.3                 | 1.4–1.3                           |
| Global power factor  | -                       | 1.75–1.37                         |
| Doppler coefficient BOL, 900 K   | -2.1 × 10 <sup>-5</sup> | -2.8 × 10 <sup>-5</sup>           |
| Total void reactivity at BOC   | -                       | -5 × 10 <sup>-2</sup>             |
| Water density coefficient $\frac{dk}{dp}$ at BOC   | +10 × 10 <sup>-2</sup>  | +11 × 10 <sup>-2</sup>            |

\* Fresh load

## V CONCLUSIONS

The present KfK reference design of the High Conversion PWR has a fuel rod lattice less tight than in previous KfK studies. This is due to the wish to reach higher fuel burn-ups and still maintain a sufficiently negative reactivity void coefficient.

The fuel rods are 3.5 m long and have a diameter of 9.5 mm, like in the modern PWR's. The cladding is made up of Zircaloy. The rods are arranged in triangular arrays with a pitch of 11.8 mm ( $p/d = 1.242$ ). This results in a water to fuel volume ratio of 1.23 for the whole core. The fuel rods are supported by spacer grids.

The thermohydraulic characteristics of the presented HCPWR are similar to those of the modern German PWR's. The core thermal output and the net electrical power are the same. The higher core pressure drop of 2 bar can be achieved by the standard PWR main water pumps. The average fuel rating of 125 W/cm has been chosen to cope with the very long in-core time life (6x320 f.p.d.). The minimum safety margin against critical heat flux, considering all hot spot factors and a plant overpower factor of 12%, is 36%, i.e. an acceptable value.

The burnup calculations have been performed for a six batch fuel element cycle, for a cycle duration of 320 full power days. The plutonium feed enrichment is 8%, where the plutonium vector corresponds to plutonium discharged from a PWR and a 10 yr ex-core time. Reactivity control during burn-up is obtained by boron dissolved in the water. During the equilibrium cycle the void coefficient is between -5% and -7%, while the reactivity variation between the core full power water density of 0.7 g/cm<sup>3</sup> and 0.5 g/cm<sup>3</sup> is about the same as for a PWR, so that no problems should be expected for a ATWS. The fuel utilization ratio is about 0.8 and a discharge burnup of 50000-52000 MWd/t is achieved.

## REFERENCES

- 1 C H M BROEDERS and M DALLE DONNE, "Conceptual Design of a (Pu,U)O<sub>2</sub> Core with a Tight Fuel Rod Lattice for an Advanced Pressurized Light Water Reactor", *Nucl Technol*, 71, 82 (1985)
- 2 M DALLE DONNE and C FERRERO, "Loss-of Coolant Accident and Anticipated Transient Without Scram Calculations for Homogeneous and Heterogeneous Advanced Pressurized Water Reactors," *Nucl Technol*, 80, 133 (1988)
- 3 M CIGARINI and M DALLE DONNE, "The Reflooding Phase after a Loss-of-Coolant Accident in an Advanced Pressurized Water Reactor", *Nucl Technol*, 84, 33 (1989)
- 4 V TESCHENDORFF, "The Two Fluid Code FLUT for LOCA Reflood Analysis," presented at Workshop International Atomic Energy Agency Program in Uses of Computer Codes for Safety Analysis, Varna, Bulgaria (May 1984)
- 5 H AMM and H MOLDASCHL, "ATWS Parameterstudie zu einem Reaktorkern mit engem Brennstabgitter", Proc Jahrestagung Kerntechnik '89, Dusseldorf, FRG, May 9-11, 1989, p 195, Deutsches Atomforum, Bonn (1989)
- 6 H MOLDASCHL, R BROGLI and B KUCZERA, "Status and Prospects of the Cooperative KWU High Converter Development 1989", Proc 5th Int Conf Emerging Nuclear Energy Systems, Karlsruhe, July 3-6, 1989, p 25, World Scientific (1989)
- 7 P RAU, Kraftwerk Union, Private communication, 1989
- 8 C H M BROEDERS, Kernforschungszentrum Karlsruhe, Unpublished, 1989
- 9 M DALLE DONNE, W HAME, "HADA, A FORTRAN-IV Program for the Thermohydraulic Design of An Advanced Pressurized Light Water Reactor with a Tight Fuel Rod Lattice," KfK 3904, EUR 7996E (1985)
- 10 M CIGARINI, M DALLE DONNE, "Thermohydraulic Optimization of Homogeneous and Heterogeneous Advanced Pressurized Water Reactor", *Nucl Technol*, 80, 107 (1988)
- 11 T MORI, M CIGARINI and M DALLE DONNE, "HADA-2 (Modified Version of HADA) A FORTRAN-IV Program for the Thermohydraulic Design of an Advanced Pressurized Light Water Reactor with a Tight Fuel Rod Lattice". KfK 4663, EUR 11395EN (1989)
- 12 M DALLE DONNE and W HAME, "Critical Heat Flux Correlation for Triangular Array Rod Bundles with Tight Lattices, Including the Spiral Spacer Effect," *Nucl Technol*, 71, 111 (1985)

- 13. R.W. BOWRING, "WSC-2, A Subchannel Dryout Correlation for Water-Cooled Clusters over the Pressure Range 3.4-15.9 MPa," AEEW-R983, U.K. Atomic Energy Authority (1979).
- /14/ C.H.M. BROEDERS, "Development of Calculational Procedures for the Neutron Physics Design of Advanced Reactors", This meeting
- /15/ G. SCHLOSSER, Private communication, KWU, 1989.
- /16/ M.R. WAGNER, "Three-dimensional Nodal Diffusion and Transport Theory Methods for Hexagonal-Z Geometry", NSE 103, p. 377 (1989).

## **PRESENT STATUS OF DESIGN STUDIES ON A HCPWR WITH SEMI-TIGHT CORE CONFIGURATION**

H. HISHIDA, T. KONDO

Mitsubishi Atomic Power Industries, Inc.,  
Tokyo, Japan

### **Abstract**

Design studies of a high conversion PWR (HCPWR) plant have been performed in which the nuclear characteristics associated with the transition between a semi-tight MOX core and a loose UO<sub>2</sub> core, power capability of the core with respect to V<sub>m</sub>/V<sub>f</sub> ratio, mechanical integrity of fuel assemblies as well as spectral shift rods within a guide tube under flow-induced vibration in reactor's upper plenum region, and safety assessment on some of the typical non-LOCA's were evaluated.

Technical feasibility of a HCPWR with a semi-tight latticed core is verified whose associated fuel cycle cost may be reducible to the competitive level with respect to an advanced LWR.

Further design studies related to the realization of core flexibility with the V<sub>m</sub>/V<sub>f</sub> ratio ranging between 1.4 and 2.2 are under progress.

### **1. Introduction**

Feasibility of a HCPWR with semi-tight latticed core provided with fertile rods for spectral shift control, whose moderator to fuel volume ratio (V<sub>m</sub>/V<sub>f</sub>) is 1.4 when the spectral shift rods are withdrawn, has been improved considerably<sup>1,2,3,4</sup> and the design objectives are fulfilled satisfactory. The expected contribution of introducing HCPWR's to the cumulative natural uranium procurement has been verified although slight increase in fuel cycle cost (FCC) in comparison with that of the conventional LWR due to blanket fuel assemblies was left as one of the related R & D objectives<sup>4</sup>. In fact, it is quite possible that the FCC may be lowered at least to the competitive level with respect to the conventional LWR by means of replacing blanket fuel assemblies of the reference HCPWR core by normal MOX fuel assemblies with least increase in natural uranium consumption rate<sup>5</sup>.

This work was done under a joint research contract between an electric utilities group of Kansai, Hokkaido, Tokyo, Chubu, Shikoku, Kyushu and Japan Atomic Power, and Mitsubishi Heavy Industries, Ltd.

The reference HCPWR core design has such flexibility that it may be operated with UO<sub>2</sub> fuel assemblies of Vm/Vf ratio being 1.6 without affecting the power capability of the core in accordance with the change in annual Pu<sup>f</sup> supply rate and the related economic trends. The transition schemes are discussed and verified in nuclear and thermohydraulic design studies. Further studies on the transition capability between a semi-tight MOX core of Vm/Vf ratio being 1.4 and a loose UO<sub>2</sub> core of Vm/Vf ratio being 2.2 are under progress.

As to the mechanical integrity of the core structure provided with spectral shift mechanism, flow induced vibration tests of spectral shift rods in the upper core region were performed and the integrity was verified.

Safety analyses related to several cases of non LOCA were performed and the integrity of the core was verified. For the safety assessment under a large break LOCA, readers may refer to the previously published paper<sup>4</sup>.

## 2. Nuclear Design

The core specification and the horizontal core cross section are shown in Table I and Fig. 1, respectively. One third of the fuel assemblies are provided with control rod clusters and the rest of them are provided with spectral shift rods filled with fertile material. Nuclear parameters such as moderator temperature coefficient, moderator density coefficient, Doppler power coefficient and kinetics parameters were evaluated in connection with non-LOCA analyses. These parameters are shown in Table II. Ejection rod worth were evaluated for the cases with the spectral shift rods being totally inserted and withdrawn, which turned out to be smaller than those corresponding to the conventional PWR plants due to the hardening of incore neutron spectrum as shown in Table III.

Nuclear characteristics associated with the transition between a semi tight MOX core and a loose UO<sub>2</sub> core were investigated. In a case of replacing a reference HCPWR core by UO<sub>2</sub> fuel assemblies with Vm/Vf ratio of 1.6, which corresponds to the minimum natural uranium consumption, radial blanket assemblies may be replaced by UO<sub>2</sub> fuel assemblies either by one-batch or three-batch scheme. The variation in nuclear peaking factors F<sub>XY</sub> for the both scheme is small with respect to the burnup as shown in Fig. 2 and Fig. 3, which verify the feasibility of such transition schemes.

Table I Core Specifications

|   | IIC 9<br>Reference HCPWR | UO <sub>2</sub> Replaced<br>Core |
|---|--------------------------|----------------------------------|
| Number of assembly                            |                          |                                  |
| Core  | 199                      | 253                              |
| Blanket                                       | 54                       | 0                                |
| Active core height (m)                        | 3.5                      | ←                                |
| Axial blanket (mm)                            | 250<br>at both ends      | ←                                |
| Vm/Vf   |                          |                                  |
| Core (fertile rods in/out)                    | 1.21/1.40                | 1.43/1.60                        |
| Blanket                                       | 0.8                      |                                  |
| Number of fuel rods in an assembly            | 342                      | 318                              |
| Number of rod thimbles in an assembly         | 42                       | ←                                |
| Control rods <sup>1)</sup>                    | 30                       | ←                                |
| Fertile rods for spectral shift <sup>2)</sup> | 42                       | ←                                |
| Number of water rods in an assembly           | 12                       | 36                               |
| Fuel rod diameter (mm)                        | 9.5                      | ←                                |
| Fuel rod                                      |                          |                                  |
| Pitch (mm)                                    | 12.0                     | ←                                |
| Gap (mm)                                      | 2.5                      | ←                                |
| Fuel rod spacing                              | Grid                     | ←                                |
| Assembly pitch (mm)                           | 243                      | ←                                |
| Pu <sup>f</sup> /235U enrichment (wt %)       | 6.2 (Pu <sup>f</sup> )   | 4.4 (235U)                       |
| Discharge burnup (MWd/t)                      | 45000                    | ←                                |
| Average conversion ratio                      | 0.85                     | 0.66                             |
| Electrical output (MWe)                       | 1355                     | 1380                             |
| Average core linear heat rate (KW/m)          | 15.3                     | 13.5                             |
| Primary coolant temperature                   |                          |                                  |
| Inlet (°C)                                    | 294                      | 295                              |
| Outlet (°C)                                   | 329                      | 330                              |
| Primary coolant flow rate (m <sup>3</sup> /h) | 89200                    | 92800                            |

1) Equipped with one third of the fuel assemblies

2) Equipped with two thirds of the fuel assemblies

3) Increment by blanket is 0.055

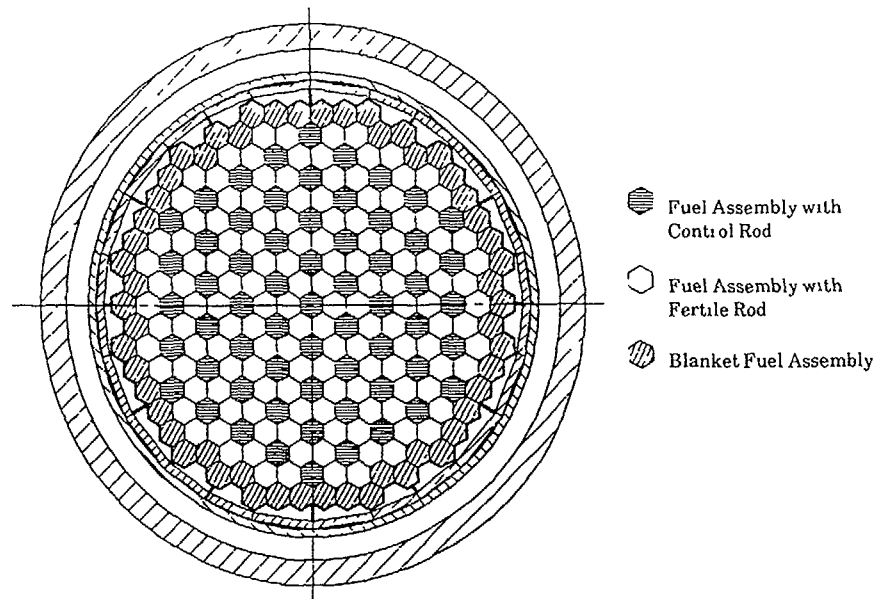


Fig 1 Horizontal Core Cross-Section

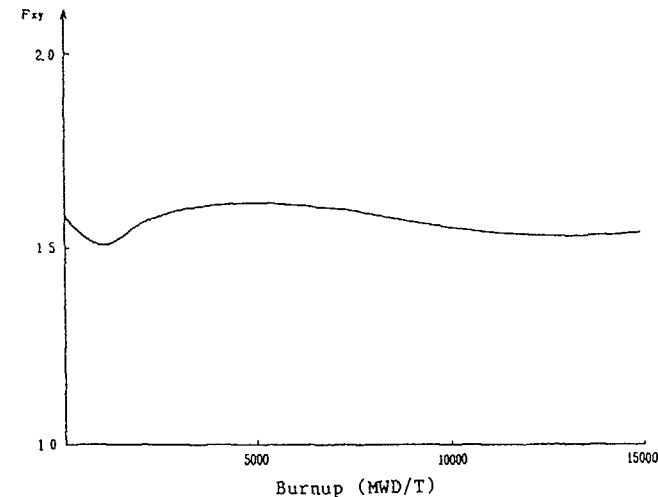
Table II Nuclear Parameters for non LOCA Analyses

| Coefficients         | Unit                                    | HCPWR        |
|----------------------|---|--------------|
| Mod Temp Coeff       | $10^{-5} (\Delta k/k)/^{\circ}\text{C}$ | -94 ~ 0      |
| Mod Density Coeff    | $10^{-5} (\Delta k/k)/(g/cm^3)$         | 0 ~ 0 42     |
| Doppler Power Coeff  | $10^{-5} (\Delta k/k)/(\%P)$            | -21 5 ~ -7 5 |
| $\beta_{\text{eff}}$ | (%)                                     |              |
| Max Value            |   | 0 75         |
| Min Value            |   | 0 39         |
| $\epsilon^*$         | ( $\mu\text{sec}$ )                     |              |
| Max Value            |   | 20           |
| Min Value            |   | 2 7          |

Table III Control Rod Cluster Ejection Analyses

|     |     | Added Reactivity<br>(% $\Delta k/k$ ) | $F_Q$ |
|-----|-----|---------------------------------------|-------|
| BOV | HFP | 0 18                                  | 6 11  |
|     | HZP | 0 38                                  | 11 50 |
| EOV | HFP | 0 28                                  | 6 63  |
|     | HZP | 0 50                                  | 19 90 |
| BOF | HFP | 0 22                                  | 5 48  |
|     | HZP | 0 44                                  | 17 17 |
| EOF | HFP | 0 27                                  | 6 17  |
|     | HZP | 0 49                                  | 18 58 |

BOV Beginning of Voidage  
 EOV End of Voidage  
 BOF Beginning of Flooding  
 EOF End of Flooding  
 HFP Hot Full Power  
 HZP Hot Zero Power

Fig 2 Burnup Dependency of  $F_{XY}$  (one batch scheme)

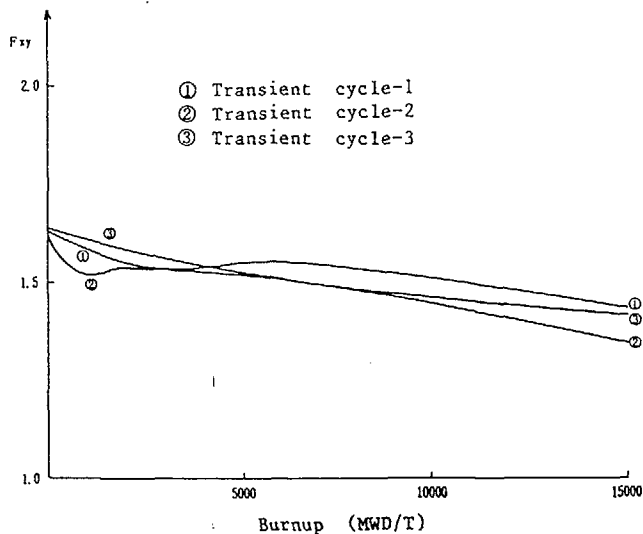


Fig. 3 Burnup Dependency of  $F_{XY}$  (three-batch scheme)

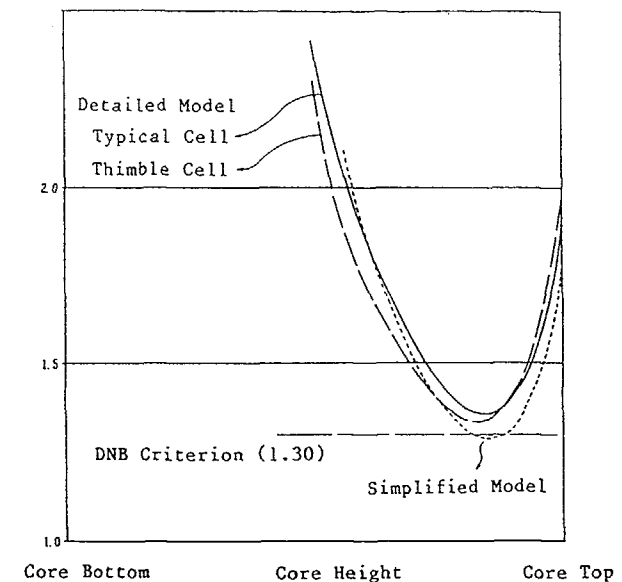


Fig. 4 Axial Variation of DNBR

### 3. Thermal and Hydraulic Design

Based on DNB tests under the plant operating conditions, EPRI-1 correlation was slightly modified and was applied to hot channel analyses of the reference HCPWR core. Fig. 4 shows the axial variation in DNBR along the hottest channel, where the minimum DNBR is greater than the design critical value of 1.3 under the nominal power output.

Fig. 5 shows the power capability of the core with respect to its  $V_m/V_f$  ratio, which may be shifted by means of either replacing fuel rods with water rods successively or decreasing the fuel rod diameter keeping the lattice configuration unchanged. The results shown in Fig. 5 was evaluated based on the former means, which verifies that the HCPWR plant under discussion may be operated with either a MOX fueled core of  $V_m/V_f$  ratio 1.4 corresponding to high conversion core characteristics or a  $UO_2$  fueled core of  $V_m/V_f$  ratio 2.2 corresponding to low FCC under the current uranium market price. Whether such core transition based on the conventional multi-batch refueling scheme is possible without affecting power capability is under investigation.

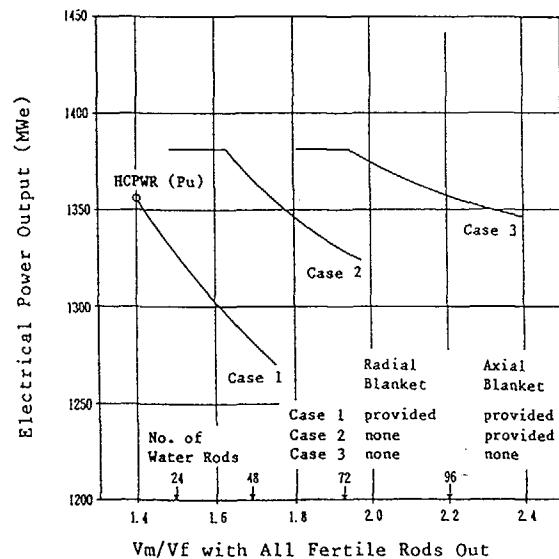


Fig. 5 Dependency of Electrical Power Output from  $UO_2$  - Fueled Core on  $V_m/V_f$  Ratio

#### 4. Fuel Assemblies

The structure and the cross-sectional view of the HCPWR fuel assembly are shown in Fig. 6a and Fig. 6b, respectively. Integrity of a fuel rod throughout its life is verified based on the evaluation of such parameters as fuel temperature, internal pressure, clad stress and strain, clad oxidation and hydrogen absorption rate.

The effect of the coolant jet momentum flux in the vicinity of the fuel-blanket boundary interface was evaluated not being appreciable to cause the instable vibration of fuel assemblies on the boundary.

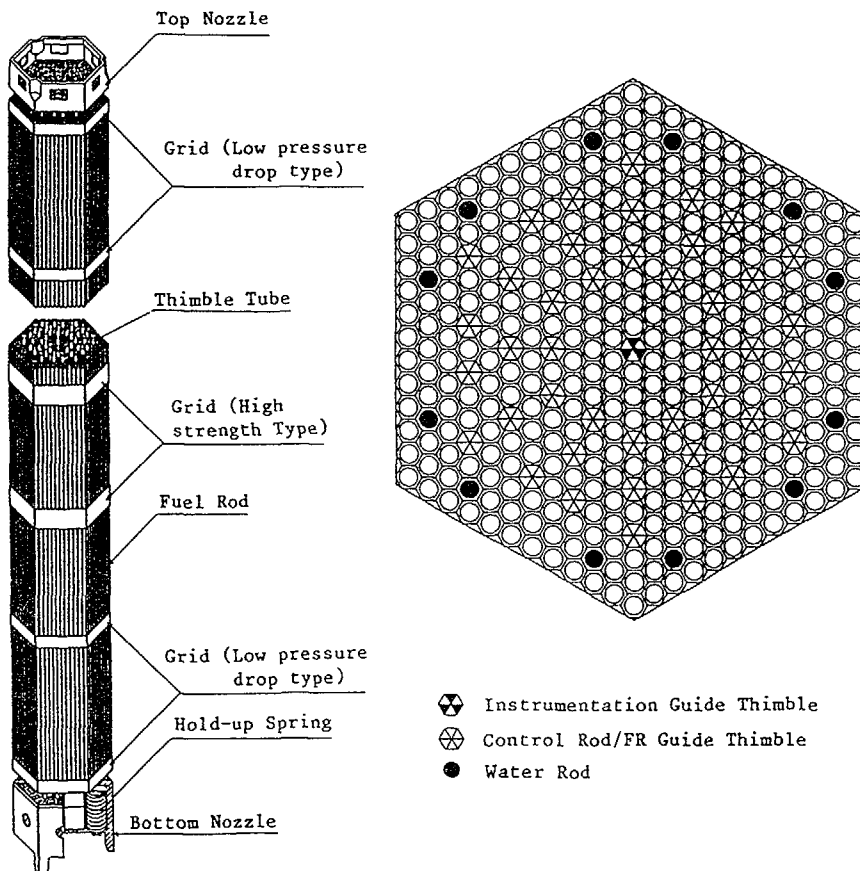


Fig. 6a Fuel Assembly Structure

Fig. 6b Fuel Assembly Cross-Section

#### 5. Reactor Internals

Reactor Internals of the reference HCPWR design is shown in Fig. 7. To secure the integrity of spectral shift rods within a guide tube under flow-induced vibration in the upper plenum region, flow tests were performed, where the maximum value of rod acceleration under the

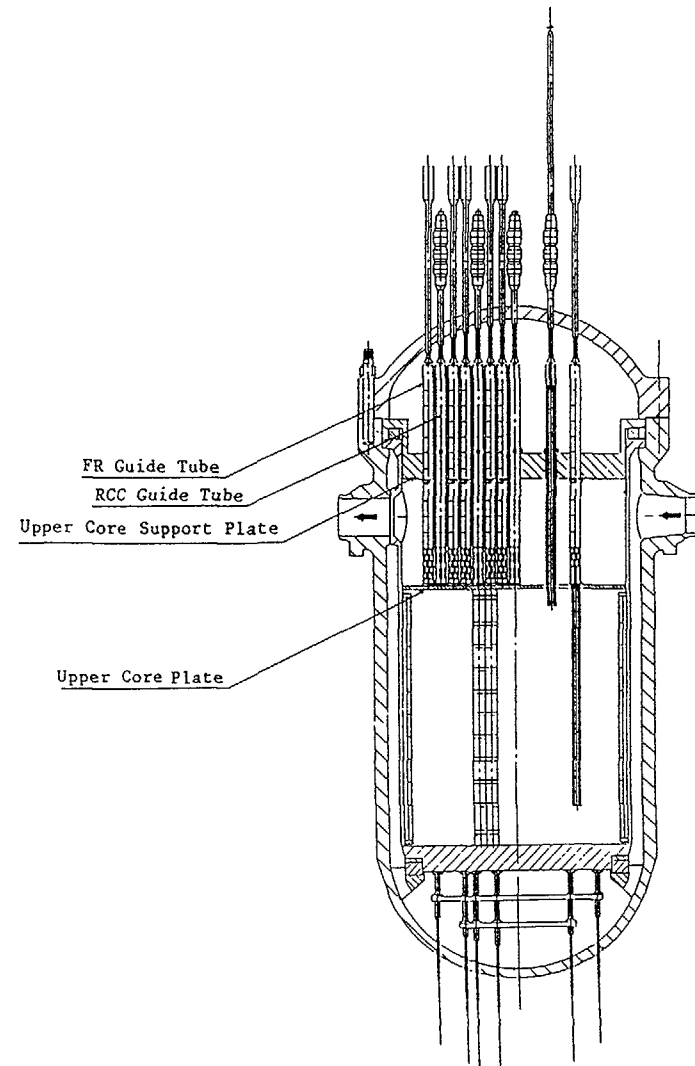


Fig. 7 Reactor Internals

mechanical design flow was of the order of 0.2G and no resonant vibration of any rods was observed. Fig. 8 shows a guide tube with coolant flow holes for a fertile rods cluster. The maximum coolant flow velocity across the guide tube bundle was evaluated to be 14.0 m/sec and the flow-induced characteristics are summarized in Table IV.

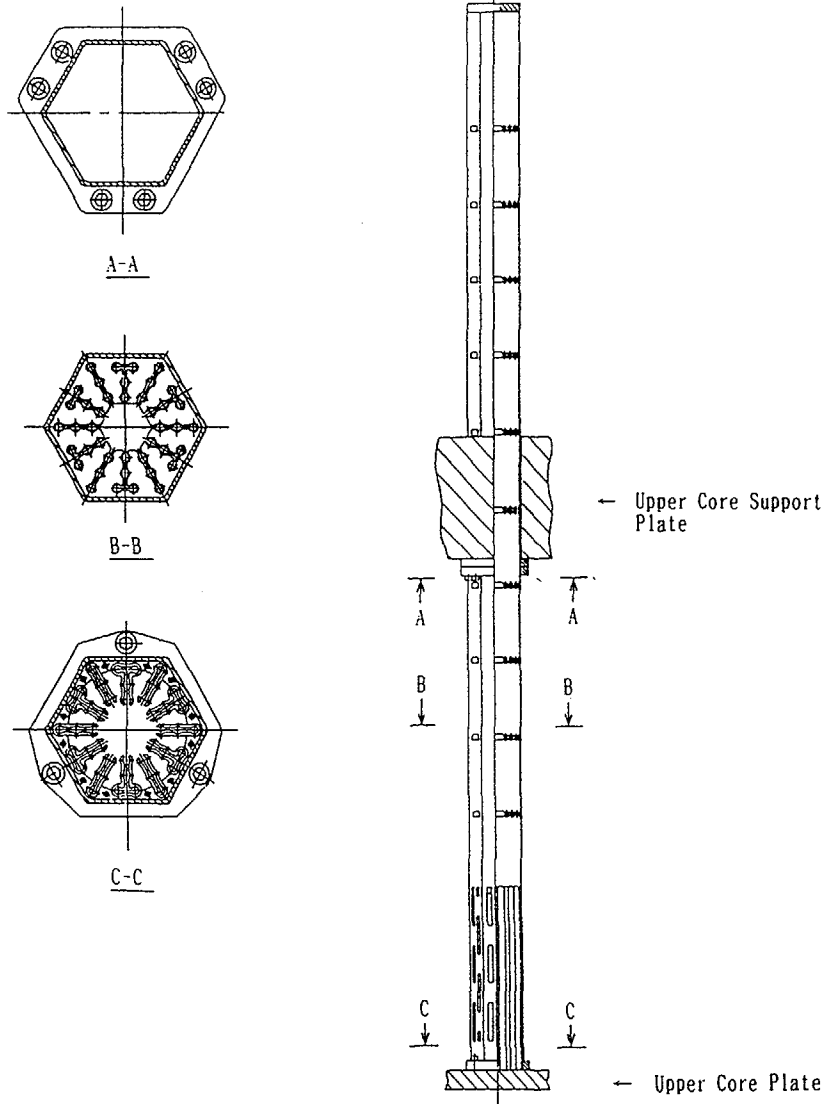


Fig. 8 Guide Thimble for Fertile Rods Cluster — Cross Flow Type

Table IV Flow Induced Vibration of Fertile Rods

| Flow Characteristics        |                                      | CR Guide Tube | FR Guide Tube |
|-----------------------------|--------------------------------------|---------------|---------------|
| Vortex<br>Shedding          | Characteristic<br>Frequency          | 71.8 Hz       | 160.0 Hz      |
|                             | KARMAN Vortex<br>Frequency           | 28.5 Hz       | 35.0 Hz       |
| Fluidelastic<br>Instability | Max. Flow Velocity<br>in Tube Bundle | 11.4 m/sec    | 14.0 m/sec    |
|                             | Critical Flow<br>Velocity            | 18.3 m/sec    | 43.3 m/sec    |

The maximum stress values expected to appear in the core support structures were evaluated to be sufficiently lower than the corresponding permissible values.

## 6. Safety Assessment

The peak clad temperature in a LOCA was found to be of a few tens of degrees centigrade lower than that of the conventional PWR as reported in the previous paper<sup>4</sup>. In the followings, some of the typical non-LOCA's are evaluated, which include (1) loss of main feed water to steam generators, (2) complete loss of primary coolant flow, and (3) control rod ejection. These accidents are chosen since the HCPWR core characteristics affect the natural convection flow rate through the core, the DNBR, the incore neutron energy spectrum, the power distribution and the fuel melting temperature.

Figures 9, 10, and 11 show the results of these accident analyses. In Fig. 10, the value of the minimum DNBR is slightly lower than that of the conventional PWR. However this can be settled by improvement of DNBR accuracy as well as slight modification of the plant design. In Figures 9 and 11, each parameter transient is almost the same as that of the conventional PWR. Therefore, the safety design criteria are satisfied in these typical cases.

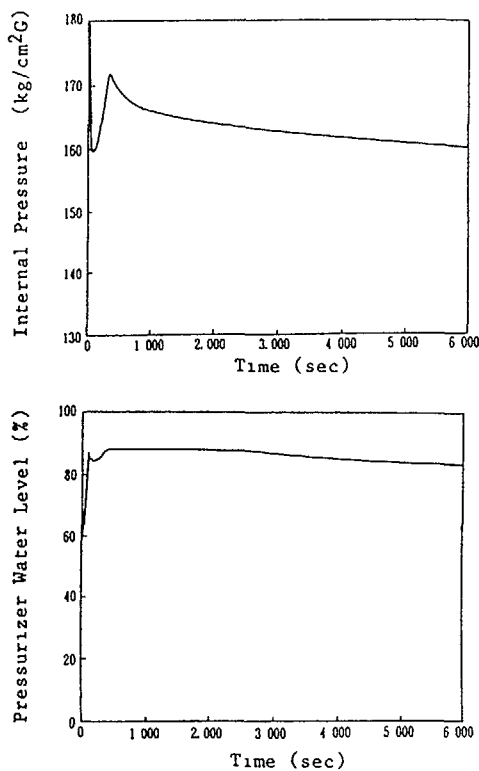


Fig 9 Loss of Main Feed Water to SG Analysis

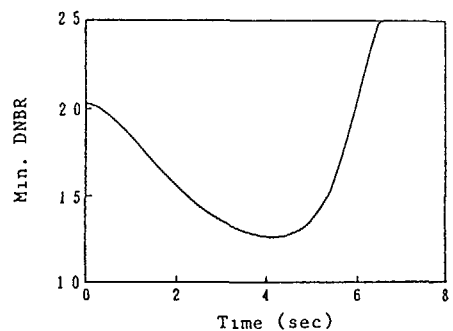


Fig 10 Complete Loss of Primary Coolant Flow Analysis

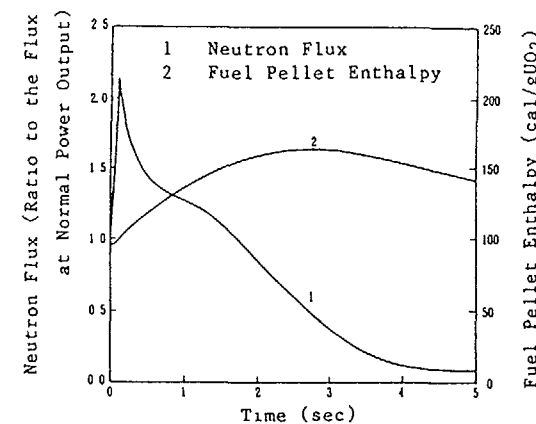


Fig 11 Control Rod Clusters Ejection Analysis at Hot Full Power (Beginning of Cycle)

## 7. Summary

Technical feasibility of a HCPWR with a semi tight latticed core employing a spectral shift scheme has been verified and the design objectives are fulfilled satisfactory

The optimum value of the core V<sub>m</sub>/V<sub>f</sub> ratio is found roughly between 1.1 and 1.4 when the design feasibility is discussed within the proven LWR plant technology with the expected FCC being competitive to that of LWR plants, since burnup is not attainable high enough due to the difficulty associated with excess reactivity control in case of a tight latticed core

A HCPWR provided with a flexible core of transition capability between a semi tight MOX fueled core of V<sub>m</sub>/V<sub>f</sub> = 1.4 corresponding to high conversion core characteristics and a loose UO<sub>2</sub> fueled core of V<sub>m</sub>/V<sub>f</sub> = 2.2 corresponding to low FCC under the current uranium market price by interchanging only fuel assemblies is desirable to meet adequately the change in economic or strategic trends throughout the plant life. Studies on appropriate transition schemes are under progress

## REFERENCES

- 1 T Umeoka, et al , Nucl Tech 80 (1988) 29
- 2 E Saji, et al , Nucl Tech 80 (1988) 18
- 3 Y Matsuoka, et al , Int Topical Meeting on Advances in Reactor Phys , Math and Comp , Paris (1987) 243
- 4 A Iizuka, et al , Int Reactor Phys Conf , Jackson Hole (1988) III-107
- 5 H Hishida, et al , IAEA Tech Comm on Tech and Economic Aspects of High Converters, 622 I3 TC 700/1 8 (1990)

# CRITICAL POWER CHARACTERISTICS OF A HIGH CONVERSION BOILING WATER REACTOR

K. ARAI, S. TSUNOYAMA, S. YOKOBORI

Toshiba Corporation,  
Kawasaki

K. YOSHIMURA  
Toshiba Corporation,  
Yokohama

Japan

## Abstract

A high conversion boiling water reactor (HCBWR) is a concept for improving uranium utilization by reducing the moderator/fuel (H/HM) ratio. This is achieved with a tight pitch fuel lattice and boiling water. A BWR offers an advantage wherein the vapor in a reactor core has an effect of reducing the H/HM ratio. Consequently, a BWR is expected to achieve a high conversion ratio with a less tight fuel lattice, compared with a pressurized water reactor. We have made analytical and experimental studies on the critical power characteristics in a fuel rod bundle with a narrow gap, under BWR conditions.

The existing correlations to predict critical heat flux (CHF) for a tight lattice are based on the so-called local condition hypothesis. This hypothesis is valid to describe phenomena under high-pressure and high-flow conditions. In the BWR conditions, on the other hand, an integral approach is employed, since upstream history in a nonuniform heat flux profile is quite important. The upstream history strongly depends on flow regime and, thus, quality.

Therefore, a critical quality-type correlation for a tight-spaced triangular lattice has been developed, based on the Biassi correlation. This correlation is a critical quality-boiling length ( $X_c-L_b$ ) type correlation, based on published experimental boiling transition data which were derived from triangular arrays of rod clusters.

Further, the lattice tightening effect on the critical power characteristics was studied, using a simple shaped experimental apparatus, an annulus tube. Comparisons of the prediction results with the critical power data obtained were also carried out for steady state conditions and transient conditions. From these comparisons, it is considered that the present correlation is applicable to the critical power prediction in a tightly-spaced triangular fuel lattice.

Using the present correlation, we have estimated the critical power characteristics of a HCBWR, under abnormal transient conditions.

## 1. Introduction

The concept of a high conversion light water reactor has recently become of great concern, due to delays in fast breeder reactor development program (Barré et al., 1988; Brogli et al., 1988; Märkl et al., 1988; Saji et al., 1988). The concept is improving uranium utilization by reducing the moderator/fuel (H/HM) ratio, which is achieved with a tight pitch fuel lattice and boiling water.

A boiling water reactor (BWR) offers an advantage wherein the vapor in the reactor core has an effect of reducing the H/HM ratio. Consequently, the BWR is expected to achieve a high conversion ratio with a less tight fuel lattice, compared to a pressurized water reactor (PWR). For this reason, we have carried out a feasibility study on the high conversion BWR (HCBWR).

From the thermal hydraulics design viewpoint, the prediction of boiling transition is primarily important. Critical heat flux (CHF) correlations or critical power correlations are therefore required for triangular fuel bundles with tight spacing. Some CHF correlations have already been developed for triangular tight lattices. These are based on the so-called local conditions hypothesis, which is valid when the rapid deterioration of heat transfer occurs in a low-quality or subcooled region. In the BWR condition, however, boiling transition is primarily due to high-quality film dryout on the heated surface. Thus, an integral concept is valid, since the upstream history is quite important. The applicability of these CHF correlations to the BWR condition has not been clarified. A boiling transition correlation, based on the integral concept, was therefore studied, which is valid to estimate the critical power for a closely spaced triangular fuel bundle.

Using boiling transition (BT) data, obtained with triangular arrays of fuel bundles at the Bettis Atomic Power Laboratory, the validity of the existing CHF correlation under BWR conditions was investigated. A critical quality-boiling-length-type correlation for triangular fuel lattices with narrow gap, based on the Biassi correlation, was developed, based on the Bettis data.

To investigate the critical power dependence on the rod clearance in a BWR operating condition, critical power tests have been carried out on annulus tubes. The present correlation has been tested with these test data, both for steady state and transient conditions.

Using the present correlation, the critical power characteristics of a HCBWR has been estimated for abnormal operating transients.

## 2. Existing CHF Correlation for a Tight Lattice

Among the CHF correlations for tight lattices, the KfK (Kernforschungs-zentrum Karlsruhe) correlation has been extensively used (Dalle Donne, 1985). Its validity under the BWR condition was investigated. Most of its data base was obtained for higher pressures than that in the BWR condition. The pressure of the BWR is about 7MPa while the KfK correlation is expected to be valid near 15MPa. The extrapolation to the lower pressure has not yet been tested.

The pressure dependence in the KfK correlation has been compared with the data base for the correlation. The test data were obtained with a triangular array of rod clusters, consisting of twenty rods, arranged as shown in Fig 1. The rods were 7 mm in outside diameter and had a 1.37 m heated length. The rod pitch was 8.6 mm.

Figure 2 shows the ratios for the predicted CHF to the measured CHF ( $q''_{\text{CHF,calc}} / q''_{\text{CHF,exp}}$ ) versus mass velocity at 13.8 MPa, 11.0 MPa, 8.3 MPa and 5.5 MPa. It is clearly seen that the KfK correlation was conservative for the BWR condition and agreed reasonably well with test data near Pressurized Water Reactor (PWR) conditions. Consequently, it is concluded that the correlation is not appropriate for predicting boiling transition in BWR's.

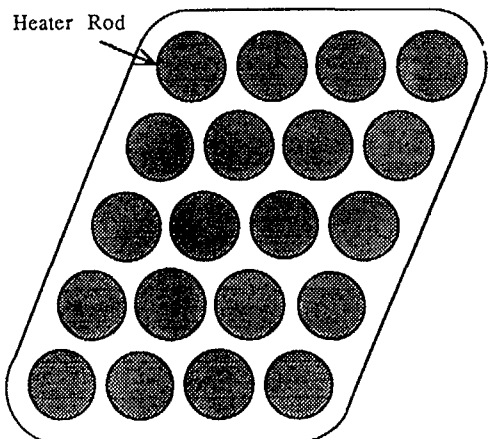


FIGURE 1 Bundle cross section (Letourneau et al , 1975)

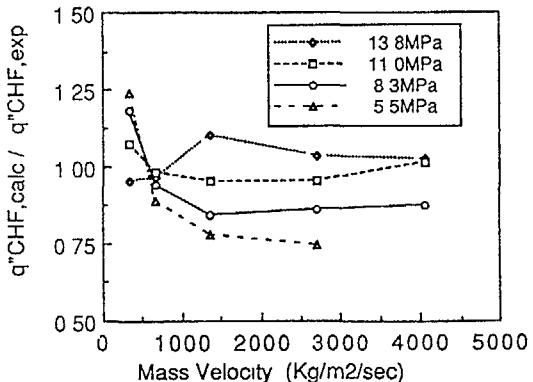


FIGURE 2 Ratio of predicted critical heat flux values to those measured as a function of mass velocity

### 3 Critical Power Correlation for a Tight Pitch Fuel Lattice

In fuel bundles, a boiling transition occurs in the high quality annular flow regime. Under these hydrodynamic conditions, the boiling transition is primarily attributed to dryout of the liquid film on the fuel rod surface. The film dryout is governed by evaporation, by entrainment from the film, and by deposition of droplets from the steam core.

It is well known that the integral concept is appropriate for the high quality boiling transition (Lahey and Moody, 1977). Some correlations, based on the integral concept, have been developed for predicting the boiling transition under BWR conditions (General Electric Co , 1973, Bertoletti et al , 1965). These correlations predict the critical power (i.e., the bundle power at the boiling transition point) in terms of critical quality and boiling length.

To estimate the critical power in a tight pitch fuel lattice under the BWR condition, critical-quality-type correlations for the triangular fuel bundle with narrow gap were studied. Experiments in tight pitch triangular fuel lattices, conducted at Bettis Atomic Power Laboratory (Letourneau et al , 1975), were a part of the light water breeder reactor development program carried out with 20-rod bundles arranged in a 5x4 triangular array, as shown in Fig 1. The BT data were obtained with two rod arrays with different degrees of lattice tightness. The rods in the two arrays were of either 6.4 mm or 7.1 mm outside diameter, and the rod pitch was 8.6 mm for the both arrays. The spacing between rods was maintained by four spacer grids. The fuel bundle geometry and the experimental conditions are summarized in Table 1.

TABLE 1 Summary of bundle geometry and experimental conditions

|  |                                |
|--|--------------------------------|
| Number of Rods                                 | 20                             |
| Rod Arrangement                                | 5 x 4 triangular array (Fig 1) |
| Number of Rod Bundles                          | 2                              |
| Rod Diameter (mm)                              | 6.4 and 7.1                    |
| Rod Pitch (mm)                                 | 8.6                            |
| Pitch to Diameter Ratio (same for both bundle) | 1.36 and 1.21                  |
| Infinite Array Hydraulic Diameter (mm)         | 6.6 and 4.6                    |
| Heated Length (m)                              | 1.37                           |
| Heat Flux Distribution                         | uniform                        |
| Pressure (MPa)                                 | 5.5 and 8.3                    |
| Mass Velocity (kg/m <sup>2</sup> /sec)         | 340 - 4000                     |
| Inlet Subcooling (kJ/kg)                       | 200 - 930                      |
| Average Exit Quality                           | 0.06 - 0.70                    |

Figure 3 shows the data obtained with the two different rod arrays, whose rod pitch-to-diameter ratios (P/D) were 1.36 and 1.21. It is observed that there is no significant difference between data for these two ratios, with similar inlet subcoolings. This indicates that the rod spacing effect on critical power may be captured by the critical quality type correlation.

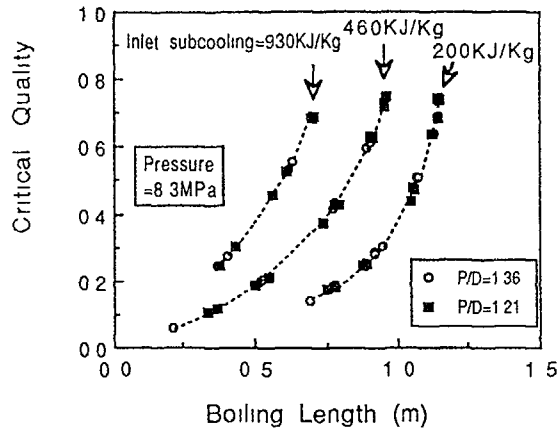


FIGURE 3 20-rod bundle test data (Letourneau et al , 1975) compared on the basis of equilibrium boiling length

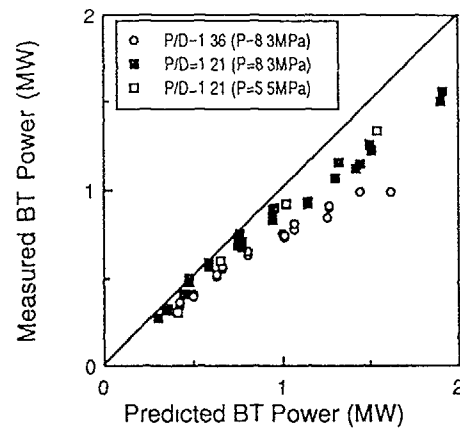


FIGURE 4 Comparison of measured BT power data with CISE (Bertozetti et al , 1965) prediction

As part of this study, the two versions of the critical quality type correlation were examined, versus the Bettis data (Letourneau et al , 1975) as shown in Fig 3. The first is the CISE correlation (Bertozetti et al , 1965), and second is the Biasi critical quality correlation (Biasi et al , 1967, Phillips et al , 1981). The Biasi correlation is based on a broad data base and has been used in TRAC-BD1(Taylor et al , 1984), which is an advanced best estimate computer program for BWR transient analysis, developed at the Idaho National Engineering Laboratory.

Figures 4 and 5 show comparisons of these correlations with the experimental data. From these figures, the following observations may be made,

- 1 Compared with the Biasi prediction, the CISE prediction shows a larger scatter,
- 2 For the CISE correlation, the deviations between the predicted and measured powers for the rod array, whose P/D is 1.36, are larger than those for the other array

This indicates that the CISE correlation cannot describe the rod spacing effect properly

In the Biasi prediction (Fig 5), the deviations for the two arrays are comparable. The Biasi correlation may capture the rod spacing effect rather well, even though it is inadequate to predict the critical quality for the tight pitch triangular fuel lattice

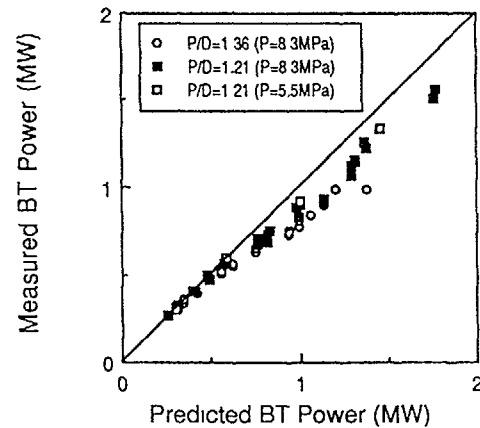


FIGURE 5 Comparison of measured BT power data with Biasi (Biasi et al , 1967, Phillips et al , 1981) prediction

Based on the above observations, the Biasi correlation seemed preferable for this study, but it is necessary to modify the correlation for tight pitch triangular arrays. This modification was undertaken based on the Bettis data, and is compared with the original in Table 2. A parity plot is shown in Fig. 6.

It is seen that the modified correlation yields a better fit to the data, compared with the unmodified correlation shown in Fig. 5. The mean error in the predictions of the present correlation is -0.3%, and the standard deviation is 4.9%.

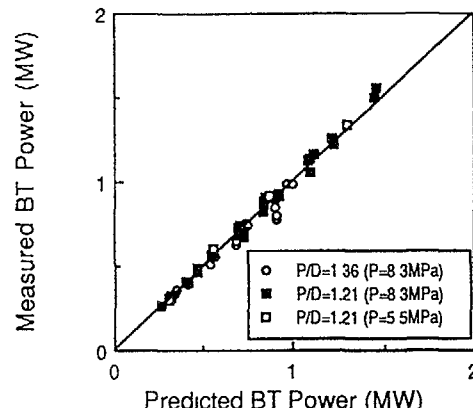


FIGURE 6 Comparison of measured BT power data with modified Biasi prediction.

#### 4 Test of the Correlation with Annulus Tube Test Data

To confirm the validity of the present critical power correlation, critical power tests were carried out and results were compared with the predictions. The experiments were performed with an electrically heated rod enclosed by a thin-walled tube, which forms a coolant annulus (Fig. 7). The test section consisted of a heated inner rod with a 2.3 m heated length, an unheated outer tube, and spacing elements. The geometrical details of the annulus tube, and the experimental conditions are listed in Table 3.

Three inner rods with different diameters were used, in order to simulate three triangular arrays with different rod spacings. The diameter of the inner rod was determined so that the annulus tube has the same heated equivalent diameter ( $4A_x/P_h$ ) as that of the triangular array of the rod cluster which was to be modeled. Table 4 shows the relationship between the inner rod diameter of the annulus tube and the rod clearance (or the rod spacing) for the triangular, 10.9-mm diameter rod array. The fuel rod diameter for the HCBWR we have studied is 10.9-mm, as described in the next section. On the basis of equal heated equivalent diameters between the annulus tube and rod array, it is possible to determine the dependence between critical

TABLE 2 Original Biasi critical quality correlation (Phillips et al, 1981) and modified correlation

$$\begin{aligned}
 A_1 &= 10 \\
 B_1 &= b_1 G^{m_1} D_h^{n_1} h_{fg} / h(p) \\
 X_{c1} &= \frac{A_1 L_B}{B_1 + L_B} \frac{P_h}{P_w} R_f^{-1/2} \\
 A_2 &= a_2 f(p)/G^{m_2} \\
 B_2 &= b_2 G^{m_3} D_h^{n_1} h_{fg} \\
 X_{c2} &= \frac{A_2 L_B}{B_2 + L_B} \frac{P_h}{P_w} R_f^{-1/2} \\
 h(p) &= -1.159 + 0.149p \{\exp(0.019p)\} + 8.99p/(10+p^2) \\
 f(p) &= 0.7249 + 0.099p \{\exp(-0.032p)\} \\
 p &= 10^{-5} P
 \end{aligned}$$

#### Original Biasi

$$\begin{aligned}
 100 < G < 300 & , X_c = X_{c1} \\
 300 < G & , X_c = \text{Max}(X_{c1}, X_{c2}) \\
 m_1 = 1.6 & \quad m_2 = 1/6 \quad m_3 = 7/6
 \end{aligned}$$

$$D_h > 0.01 ; n_1 = 1.4 \quad b_1 = 1.048 \times 10^{-8}$$

$$a_2 = 1.468 \quad b_2 = 5.707 \times 10^{-8}$$

$$D_h < 0.01 ; n_1 = 1.6 \quad b_1 = 2.633 \times 10^{-8}$$

$$a_2 = 1.468 \quad b_2 = 1.434 \times 10^{-7}$$

#### Modified Biasi

$$300 < G < 2000 , X_c = X_{c1}$$

$$2000 < G , X_c = \text{Max}(X_{c1}, X_{c2})$$

$$m_1 = 1.7 \quad m_2 = 0.15 \quad m_3 = 1.27$$

$$n_1 = 1.5 \quad b_1 = 1.320 \times 10^{-8}$$

$$a_2 = 1.413 \quad b_2 = 7.132 \times 10^{-8}$$

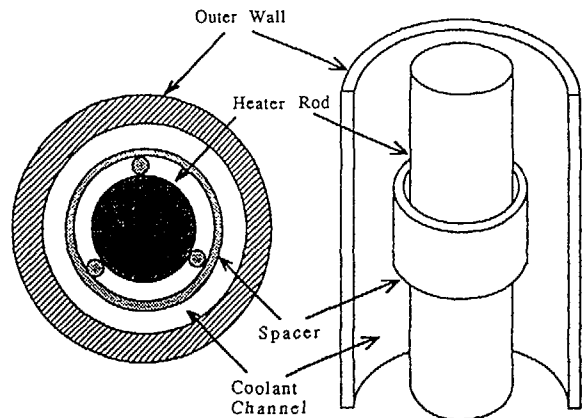


FIGURE 7 Schematic of the heated section of the annulus tube  
(Yokobori et al., 1987)

TABLE 3 Geometrical details of annulus tube  
and experimental conditions

|                                     |                          |                  |
|-------------------------------------|--------------------------|------------------|
| Inner Rod Diameter                  | (mm)                     | 13.2, 13.6, 14.3 |
| Inner Diameter of<br>the Outer Tube | (mm)                     | 17.0             |
| Heated Length                       | (m)                      | 2.3              |
| Axial Peaking Factor                |                          | 1.5              |
| Pressure                            | (MPa)                    | 7.0              |
| Mass Velocity                       | (Kg/m <sup>2</sup> /sec) | 830 - 1390       |
| Inlet Subcooling                    | (KJ/Kg)                  | 23 - 70          |

power and rod clearance from annulus tube test data. From comparisons of the present correlation with the annulus tube data, the rod clearance dependence of the correlation, derived from the Bettis rod bundle data, were verified. Details of the test facility and the test results were reported by Yokobori et al. (1987).

#### 4.1 Critical Power Under Steady State Conditions

Figure 8 shows the critical quality data obtained on three annulus tubes. The converted clearance in the figure denotes the rod clearance for a triangular array, which is to be modeled by the annulus tube. The converted rod clearances correspond to the inner rod diameters of the annulus tubes, as shown in Table 4. The same trend can be seen as in the Bettis data; that is, the  $X_c$ - $L_B$  lines are similar, for three converted clearances, when the inlet subcoolings are the same.

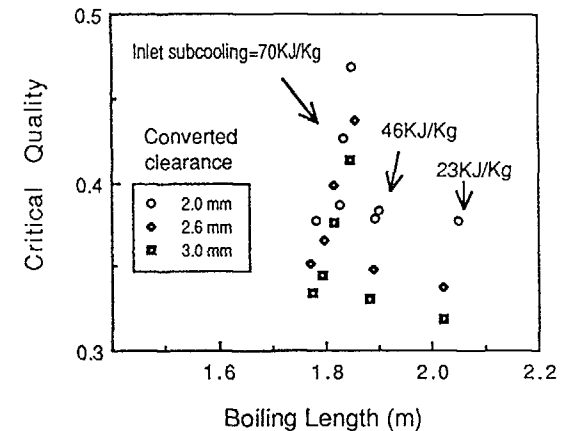


FIGURE 8 Annulus tube test data compared on the basis of equilibrium boiling length.

TABLE 4 Relationship between inner rod diameter of the annulus and rod clearance for a triangular array of 10.9-mm diameter rods, having identical heated equivalent diameters

| Diameter (mm) | Clearance (mm) | Diameter=10.9mm |     |     |
|---------------|----------------|-----------------|-----|-----|
|               |                | 3.0             | 2.6 | 2.0 |
| 14.3          |                |                 |     | O   |
| 13.6          |                |                 | O   |     |
| 13.2          | O              |                 |     |     |

Comparisons of the predictions with data taken from the annulus tubes are shown in Figs 9 and 10. Figure 9 shows that the rod clearance effects are well predicted by the present correlation. The slope of the critical power versus the rod clearance curve becomes smaller with increasing rod clearance. This trend is well captured by the prediction which accurately represents the annular data obtained (Fig. 10).

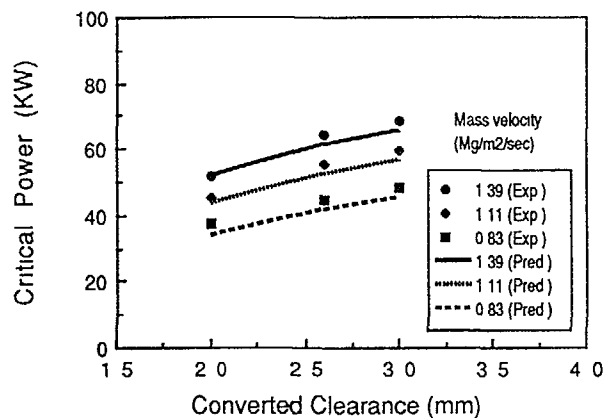


FIGURE 9 Comparison of measured critical power dependence on rod clearance with modified Biassi prediction

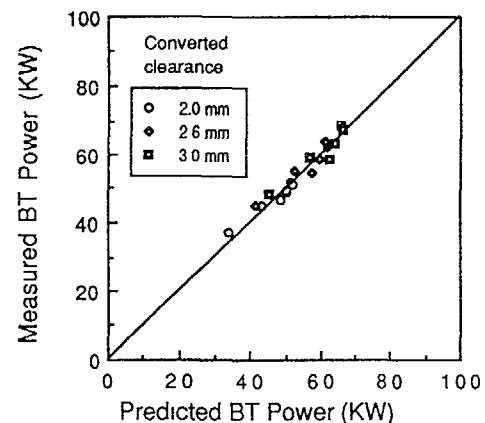


FIGURE 10 Comparison of annulus tube BT power data with modified Biassi prediction

#### 4.2 Critical Power Under Transient Conditions

In the transient tests, the inlet mass flow decreased to about 60 % of the initial flow in two seconds, typical of a BWR flow coastdown under a recirculation pump trip condition (Fig. 11). The rod power, pressure and inlet subcooling were held constant throughout the mass flow transient. The times to boiling transition under the flow decay were measured at several power levels between 52KW and 68KW. The tests were conducted using two annulus tubes, which simulated triangular rod arrays with 2.6mm rod clearance and 2.0mm clearance. The transient test conditions are summarized in Table 5.

A one-dimensional, transient, thermal hydraulic model (General Electric Co., 1978) incorporating the modified correlation, was used to analyze the annulus tube data. Both transient flow and precalculated transient equilibrium boiling length were specified in order to obtain critical power predictions. In both cases, the time to boiling transition was conservatively predicted (Fig. 12).

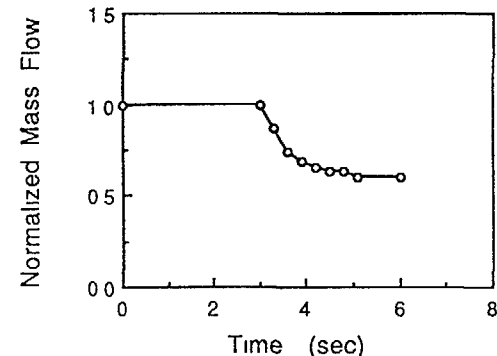


FIGURE 11 A typical flow decay curve

TABLE 5 Transient test conditions

|                                   |               |
|-----------------------------------|---------------|
| Inner Rod Diameter (mm)           | 13.6 and 14.3 |
| Pressure (MPa)                    | 7.0           |
| Initial Mass Velocity (Kg/m²/sec) | 1390          |
| Inlet Subcooling (KJ/Kg)          | 70            |
| Rod Power (KW)                    | 52 - 68       |

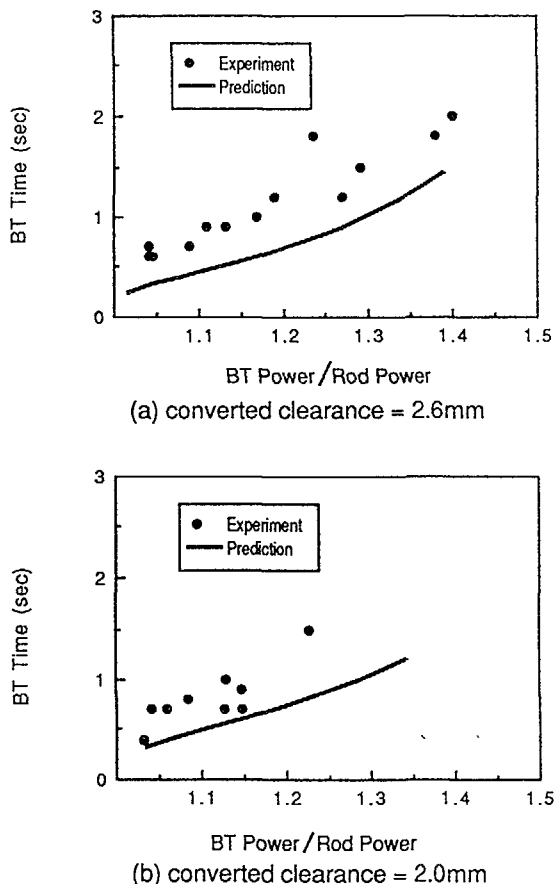


FIGURE 12 Measured versus predicted time to boiling transition

##### 5. Estimation of HCBWR Critical Power Characteristics

The critical power characteristics of a HCBWR have been estimated, using the present correlation. The major data of the HCBWR is listed in Table 6. An assembly spectrum code for HCLWR hexagonal lattice, HELIOS.HX (Yamamoto et al., 1988) was used to estimate the nuclear characteristics. 247 fuel rods and 24 guide tubes, arranged in a triangular array, are contained in a channel box (Fig. 13) and 499 fuel assemblies constitute the reactor core. Fuel rod diameter is 10.9-mm and rod pitch is 12.9-mm. A 2-mm rod gap is maintained by four grid spacers. The water-to-fuel volume ratio is 1.0 and the average conversion ratio of 0.85 is achieved. In the 1350-MWe BWR, the fuel rod diameter is 12.3-mm and the rod gap is 4-mm.

Table 6 HCBWR Major Data

|  |                          |                   |
|--|--------------------------|-------------------|
| Core Thermal Power                               | (MW)                     | 3926              |
| Electric Power                                   | (MW)                     | 1350              |
| Number of Fuel Assembly                          |                          | 499               |
| Number of Fuel Rod per Assembly                  |                          | 247               |
| Number of Guide Tube per Assembly                |                          | 24                |
| Fuel Rod Arrangement                             |                          | triangular array  |
| Fuel Rod Diameter                                | (mm)                     | 10.9              |
| Fuel Rod Pitch                                   | (mm)                     | 12.9              |
| Fuel Rod Length                                  | (m)                      | 2.3               |
| Water-to-Fuel Volume Ratio<br>(Assembly Average) |                          | 1.0               |
| Average Linear Heat Rate                         | (KW/ft)                  | 4.3               |
| Power Density                                    | (KW/L)                   | 83                |
| Axial Peaking Factor                             |                          | 1.23              |
| Radial Peaking Factor                            |                          | 1.50              |
| Pu Enrichment                                    | (%)                      | 7.4               |
| Average Conversion Ratio                         |                          | 0.85              |
| Pressure   | (MPa)                    | 7.1               |
| Recirculation Flow                               | (Kg/hr)                  | $5.2 \times 10^7$ |
| Core Average Mass Velocity                       | (Kg/m <sup>2</sup> /sec) | $1.8 \times 10^3$ |
| Inlet Subcooling                                 | (KJ/Kg)                  | 57                |
| Core Average Exit Quality                        |                          | 0.14              |
| Core Pressure Drop                               | (KPa)                    | 240               |

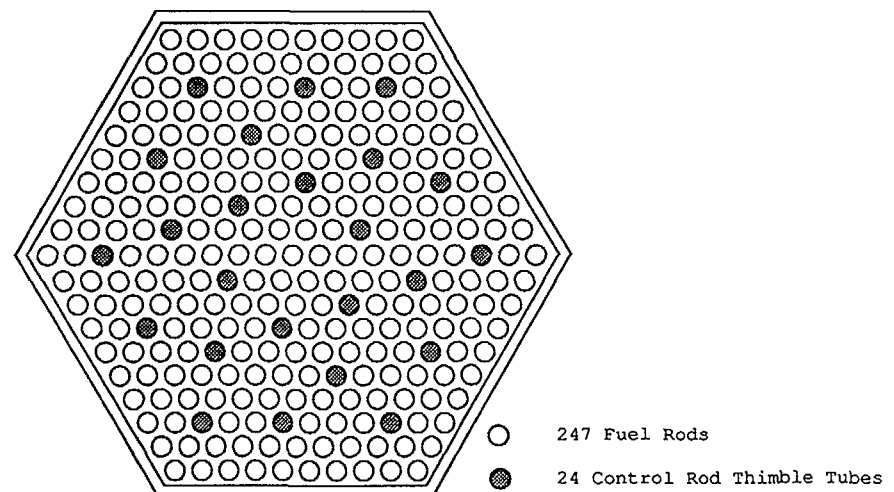


FIGURE 13 HCBWR fuel assembly

Compared to the 1350-MWe BWR plant, the active core length is reduced to about 60% and the recirculation flow is reduced to 90%, to decrease the core pressure drop. The core pressure drop is 240Kpa which is about 30% higher than that of the current BWR plant, due to the packed rod array. However the same recirculation pump can be used in the HCBWR plant as in the 1350-MWe BWR, because of the reduced recirculation flow. The pressure and inlet subcooling are the same as in the current BWR.

The channel-wise power and flow rate were calculated by using LOGOS HX (Tsukui et al., 1987), which is a three-dimensional nuclear-thermal-hydraulic coupled code for HCBWRs. Using the flow rate and power, the critical power ratio (CPR) was estimated for the highest power channel by the present correlation. The calculation results are presented in Table 7. Sufficient margin is predicted for the normal operating condition.

Table 7 Thermal-hydraulic condition for the highest power channel

|  |      |
|--|------|
| Channel Power (MW)                     | 11.8 |
| Mass Velocity (Kg/m <sup>2</sup> /sec) | 1320 |
| Minimum Critical Power Ratio           | 1.38 |

To estimate the HCBWR critical power characteristics under transient conditions, two typical transient phenomena were simulated, using the BWR licensing code REDY for calculating the plant transient behavior and the one-dimensional, transient, thermal hydraulic model incorporating the present correlation for calculating the critical power characteristics. The transient phenomena were load rejection without turbine bypass and feedwater heater cut. The neutron kinetics parameters and reactivity coefficients were estimated using HELIOS HX.

In the case of load rejection without turbine bypass, the reactor pressure increases due to the rapid closure of the main steam control valve, so the vapor in the pressure vessel collapses. This results in the neutron flux increase due to the positive void reactivity feedback. The feedwater heater cut leads to the feedwater temperature decrease and the consequent increase of the core inlet subcooling. Hence this phenomena causes the power rise.

The calculation results are summarized in Table 8, compared with the 1350-MWe BWR plant calculation results. It is seen that the HCBWR shows a comparable transient behavior with that for the 1350-MWe BWR plant. The reduction in the minimum critical power ratio ( $\Delta MCPR$ ) for the load rejection is larger in the HCBWR than that in the 1350-MWe BWR. It is considered that, in the HCBWR, the larger flow resistance caused the faster flow coast down after the recirculation pump trip and this resulted in the larger  $\Delta MCPR$ . The reduction is, however, acceptable considering that the HCBWR has the sufficient margin in the normal operating condition, as shown in Table 7.

Table 8 Calculation results for operational transients

| Reactor      | Transients     | $\Delta MCPR^*$ | Pressure Peak Value | Heat Flux Peak Value |
|--------------|----------------|-----------------|---------------------|----------------------|
| HCBWR        | Load Rejection | 0.14            | 8.4 MPa             | 100% of rated value  |
|              | Heater Cut     | 0.12            | 7.3 MPa             | 115% of rated value  |
| 1350-MWe BWR | Load Rejection | 0.07            | 8.4 MPa             | 100% of rated value  |
|              | Heater Cut     | 0.12            | 7.3 MPa             | 118% of rated value  |

\*  $\Delta MCPR$  = reduction in the minimum critical power ratio  
 $\Delta MCPR$  was calculated by using the present correlation for HCBWR and the licensing correlation (GEXL) for 1350-MWe BWR

## 6 Conclusions

A critical power correlation for boiling transition was obtained by modifying the Biassi critical quality correlation, and compared both with existing tight-spaced triangular-pitch rod bundle data and new annulus tube data. The correlation predicts the steady state data base with mean and standard deviations of -0.3% and 4.9% respectively, and accurately predicts spacing and rod-clearance effects for the two geometries. Times to boiling transition were conservatively predicted when the correlation was incorporated in a one-dimensional, transient, thermal hydraulic model.

Using the present correlation, the critical power characteristics for the HCBWR were predicted for the typical transient phenomena. The predicted results were comparable with the transient behavior for the 1350-MWe BWR plant. The reductions in the minimum critical power ratio for the transients in the HCBWR were acceptable, considering that the HCBWR has the sufficient margin in the normal operating condition.

Nomenclature

A see TABLE 2

A<sub>x</sub> cross sectional flow area (m<sup>2</sup>)

B see TABLE 2

D<sub>h</sub> hydraulic diameter (m)

G mass velocity (Kg/m<sup>2</sup>/sec)

h<sub>fg</sub> latent heat of evaporation (J/Kg)

H<sub>sub</sub> inlet subcooling (J/Kg)

L<sub>B</sub> boiling length (m)

P pressure (Pa)

P/D pitch-to-diameter ratio

P<sub>h</sub> heated perimeter (m)

P<sub>w</sub> wetted perimeter (m)

q<sup>c</sup>CHF critical heat flux (W/m<sup>2</sup>)

R<sub>f</sub> local peaking factor

x<sub>c</sub> critical quality

Subscripts

exp. experimental

calc. calculated

Brogli, R. H., Goetzmann, C. A. and Kuczera, B. J. 1988, Research And Development Efforts For The Light Water High Conversion Reactor, Nuclear Technology, Vol.80.

Dalle Donne, M. and Hame, W. 1985, Critical Heat Flux Correlation For Triangular Arrays of Rod Bundles with Tight Lattices, including The Spiral Spacer Effect, Nuclear Technology, Vol.71.

General Electric Company 1973, General Electric BWR Thermal Analysis Basis (GETAB): Data, Correlation and Design Application, NEDO-10958.

General Electric Company 1978, Qualification Of The One-Dimensional Core Transient Model For Boiling Water Reactors, Vol.1, NEDO-24154.

Lahey, R. T. and Moody, F. J. 1977, The Thermal-Hydraulics of a Boiling Water Nuclear Reactor, ANS.

Letourneau, B. W., Peterson, A. C., Coeling, K. J., Gavin, M. E. and Green, S. J. 1975, Critical Heat Flux and Pressure Drop Tests with Parallel Upflow of High Pressure Water in Bundles of Twenty 0.25- and 0.28-inch Diameter Rods, WAPD-TM-1013.

Märkl, H., Goetzmann, C. A. and Moldaschl, H. 1988, KWU's High Conversion Reactor Concept-An Economical Evolution Of Modern Pressurized Water Reactor Technology Toward Improved Uranium Ore Utilization, Nuclear Technology, Vol.80.

Phillips, R. E., Shumway, R. W. and Chu, K. H. 1981, Improvements to the Prediction of Boiling Transition in BWR Transient Calculation, Proceedings of the 20th ASME/AICHE National Heat Transfer Conference, Milwaukee, Wisconsin.

Saji, E., Akiyama, Y., Kono, N., Namba, K., Hori, K., Umeoka, T. and Kono, T. 1988, Feasibility Studies On High Conversion Pressurized Water Reactors With Semitight Core Configurations, Nuclear Technology, Vol.80.

Taylor, D. D., Shumway, R. W., Singer, G. L. and Mohr, C. M. 1984, TRAC-BD1/MOD1: An Advanced Best Estimate Computer Program For Boiling Water Reactor Transient Analysis, Vol.1, NUREG/CR-3633.

Tsuiki, M., Sakurada, K. and Yoshida, H. 1987, LOGOS.HX: A Core Simulator for High Conversion Boiling Water Reactors, NAIG Annual Review.

Yamamoto, M., Sakurada, K., Mizuta, H. and Makino, K. 1988, Validation Of The HELIOS.HX Code For High Conversion Light Water Reactor Lattice Analysis, Nuclear Technology, Vol.80.

Yokobori, S., Kato, K., Nagasaka, H. and Yoshimura, K. 1987, Characteristics of Boiling Transition of Tight Lattice Rod Assembly, Proceedings of the 24th National Heat Transfer Symposium of Japan, C223, May (in Japanese).

REFERENCES

Barré, B., Gambier, G. and Golinelli, C. 1988, Development Trends For Future French Pressurized Water Reactors, Nuclear Technology, Vol.80.

Bertolletti, S., Gaspari, G. P., Lombardi, C., Peterlongo, M., Silvestri, M. and Tacconi, F. A. 1965, Heat Transfer Crisis with Steam-Water Mixtures, Energia Nucleare, 12, 3.

Biasi, L., Clerici, G. C., Garribi, S., Sala, R. and Tozzi, A. 1967, Studies on Burnout: Part 3, Energia Nucleare, 14, 9.

## MECHANICAL DESIGN ASPECTS OF KWU'S PWHCR

W. MEIER, P.J. RAU, D. UMLAUFT

Siemens AG,  
Unternehmensbereich KWU,  
Erlangen, Federal Republic of Germany

### Abstract

Two features of the HCR define the main design areas:  
the triangular pitch of the fuel bundle and the higher density of control assemblies.

The triangular pitch requires a novel spacer design. Several solutions have been identified. A honey comb grid assembled from bent straps was selected for further detailed development. The main features of these spacers are:

- uniform wall thickness
- low pressure drop and
- adequate rigidity.

In order to obtain specimens for thermohydraulic tests and manufacturing experiences about 50 spacers were built to present.

The higher control assembly (CA) density necessary to compensate reactivity in a harder neutron spectrum requires to join at seven positions seven spiders to one "super RCC" and to one CA drive. This is necessary since the dimensions of the magnetic jack mechanism does not allow to equip two adjacent assemblies with individual drives. Due to the fact that part of reactivity will be compensated by CA a safety mechanism is required which prevents any rod ejection failure.

Furthermore, an adequate coolant flow path especially for the central fuel assembly at a "super RCC position", must be provided.

A safety mechanism which unlatches drive and control element if the upward motion is larger than a regular step has been designed. The function was demonstrated. The required flow path from the central element into the plenum can be provided by a novel control rod guide structure. A template encloses the complete assembly of seven control rod spiders. The flow area and guide path are separated such that the coolant flow cannot induce adverse vibrations. This structure is extended almost directly from the fuel rod bundle into the upper plenum. The remaining flow path is sufficient. The guide structure itself is latched at the assembly in order to prevent mismatch between the upper guide and the assembly internal guide tubes.

### 1 Introduction

As mentioned in /1/ the development of the PWHCR<sup>1)</sup> at SIEMENS is embedded in a cooperation with the Karlsruhe Nuclear Research Center, the Paul Scherrer Institute Wuerenlingen and the Technical University of Braunschweig.

Part of the SIEMENS-contribution was the mechanical design of the key components of the PWHCR.

A number of requirements formulated from

- reactor physics
- thermohydraulics
- structural analysis
- accident analysis

define an aim which has to be met by the designer under consideration of:

- experience and standards
- codes and guidelines
- cost and time schedules

Thus the designer has to strive in a hostile environment to find areas of compatibility between the competing requirements. Two features of the PWHCR determine the main field of design work. They are the triangular pitch of fuel rods and the higher density of control assemblies.

The triangular pitch requires a novel spacer design, paragraph 2. The higher control assembly density necessary to compensate reactivity in a harder neutron spectrum requires to join at seven positions seven control rod spiders to one entity and handle such a super RCC with one drive. This uncommon arrangement is necessary since the element cross section is smaller than that of the drive mechanism. The introduction of said super RCCs complicates the

<sup>1)</sup> Pressurized Water High Converter Reactor

drainage of the coolant out of the protection tube. The investigation of this fact lead to a novel and advantageous design of the control rod guide structure. See paragraph 3.

Due to the fact, that part of the reactivity will be compensated by control assemblies, a safety mechanism is required which prevents any rod from ejection failure, this mechanism is described in paragraph 4.

## 2 Spacer design

A number of different spacer design concepts have been investigated under certain criteria.

Table 1  
Criteria for spacer selection

- 
- availability of manufacturing technology
  - radial and axial rigidity
  - time for preparation of manufacturing
  - manufacturing time for test specimens
  - potential of low pressure drop
  - variability
  - low parasitic absorption
  - acceptable costs
- 

As the most promising concept a spacer design was selected which is based on bent metal strips which can be produced easily in small quantities by simple tools at comparable low cost. In order to reduce the cross section of the grid structure, and to symmetrize the radial rigidity half of the original wall thickness of the straps is removed by milling or ECM in that regions where two adjacent straps are in contact (see fig. 1). Thus a honey comb grid of uniform wall thickness assembled from metal straps was realized.

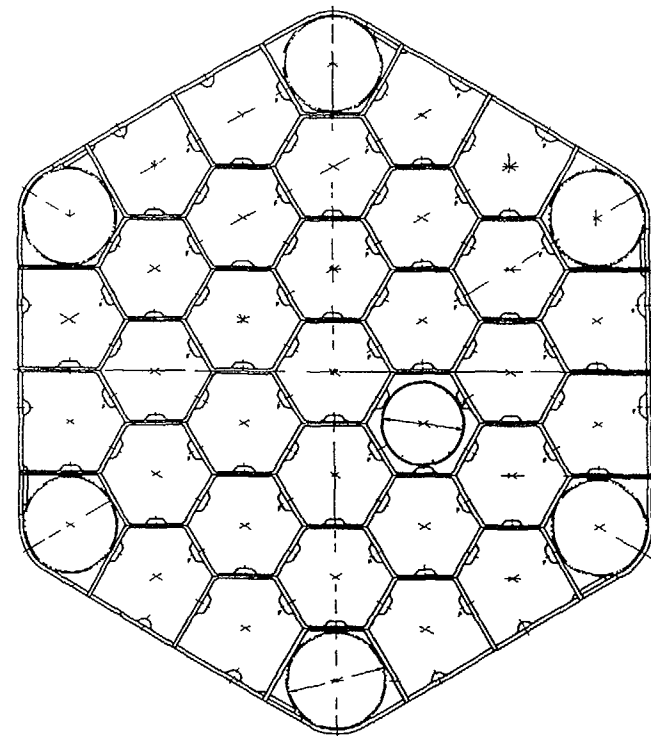
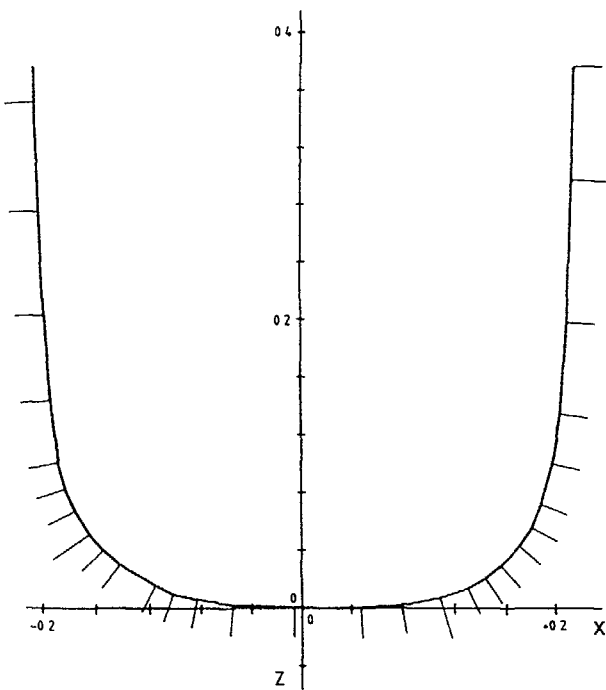


Fig.1 Spacer Grid

In order to increase both, the axial and radial rigidity two adjacent straps are welded together at the contact surfaces by spot welding.

The lateral bearing of the rod is achieved by two 120° spaced thimbles of elliptic cross section and a leave spring in opposition of the thimbles. For the test specimen this spring has been simplified and shaped like a coffin-lid. To fulfill the criteria of low pressure drop the edges of the straps are removed. (See fig. 2)



**Fig.2 Spacer Edges Removed by ECM**

To present more than 50 spacer grids of different geometry and number of cells have been produced at SIEMENS. All these grids will be used for thermohydraulic and safety test purposes. Fig. 3 shows one of these spacers manufactured at SIEMENS Workshops.

### 3 Super RCC and CR - Guide Structure

The number of feasible control rod drives is given by the triangular pattern of the fuel elements and the assembly diameter of the drive mechanism. Thus in the case of the PWHCR 86 CRDs evenly distributed are realistic. Since the number of control assemblies (CA), requested from reactor physics is about 50 % higher than the feasible number of drives, a grouping of control assemblies

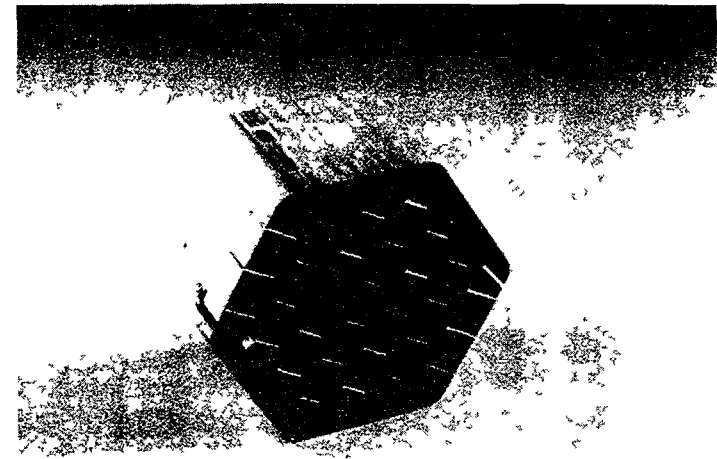


**Fig.3 Spacer Grid**

is necessary. An advantageous distribution of the control assemblies and drive positions are shown in fig. 4, which shows in the centre of the core a super RCC, built by a group of seven individual CAs. Furthermore six additional Super RCCs are distributed in a triangular pitch of six element cross sections over the core, forming a hexagon which is pointing with one corner to the symmetry axis of two adjacent exit nozzles of the RPV. On the basis of fuel rod diameter, pitch, fuel element design, control rod number and distribution over the element cross section the design of a super spider was relatively easy, but problems arise from the guide structure which has to guarantee a reliable insertion of the super RCC in the core under normal and adverse conditions and which protects the control rod from vibration, induced from any forced flow of coolant out of the central fuel assembly of such a super RCC arrangement. To solve this problems a control rod guide structure was designed which has the following features

- it envelopes the complete control assembly from the rod support grid plate of the fuel assembly upward to the tip of coolant exit slots located in the bottom section of the protection tube

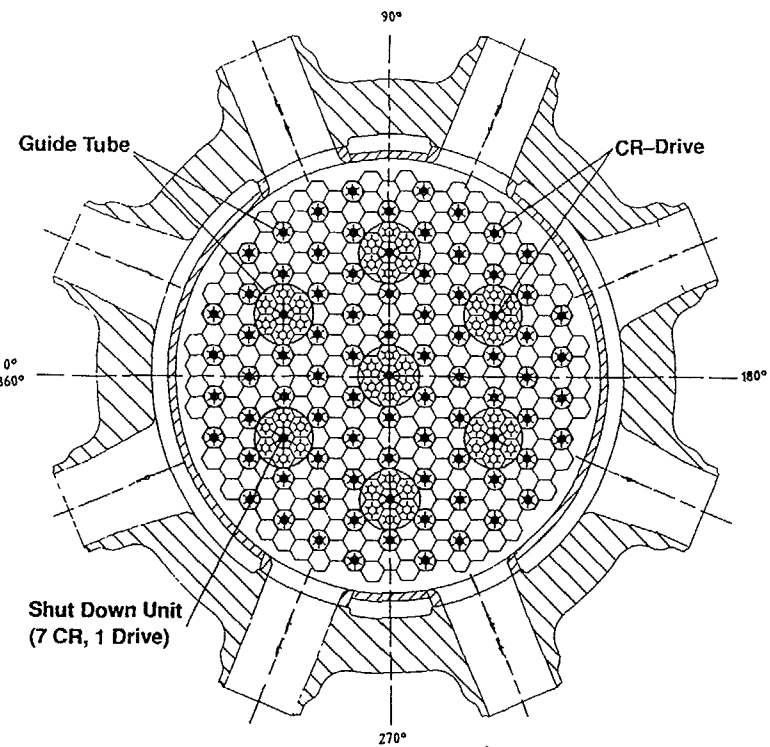


Fig.4 Control Element Distribution

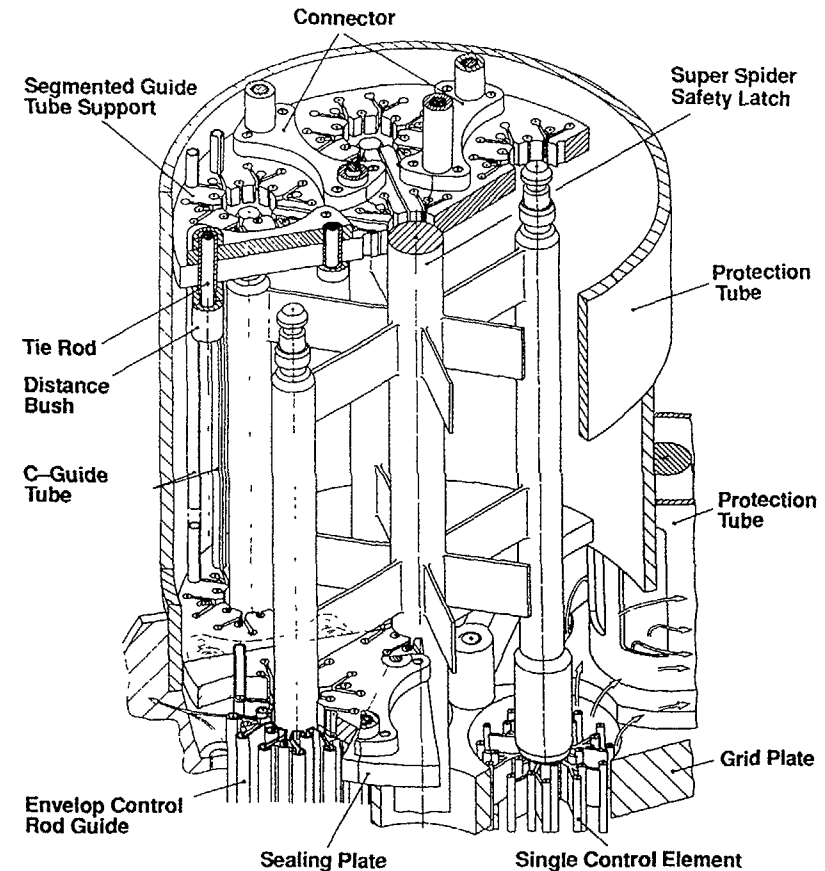


Fig.5 Control Element Guide Structure

- separation of the areas of control guide and coolant flow over the axial area mentioned above
- engaged with and locked at the fuel element exit nozzle during reactor operation
- can be removed with the upper RPV internals since it is held with play by axial keys in the protection tube.

Fig. 5 shows an artist view of a super RCC in the guide structure. Fig. 6 shows the profile tube which acts as a CR-guide and that protects the control rods completely from radial coolant flow. Since the guide structure is engaged and locked at the outlet nozzle of the fuel assembly a missaglignement between the guide tubes in the fuel assembly and the upper guide structure can be avoided. Thus it is expected that a reliable insertion of the control elements even under adverse conditions can be achieved.

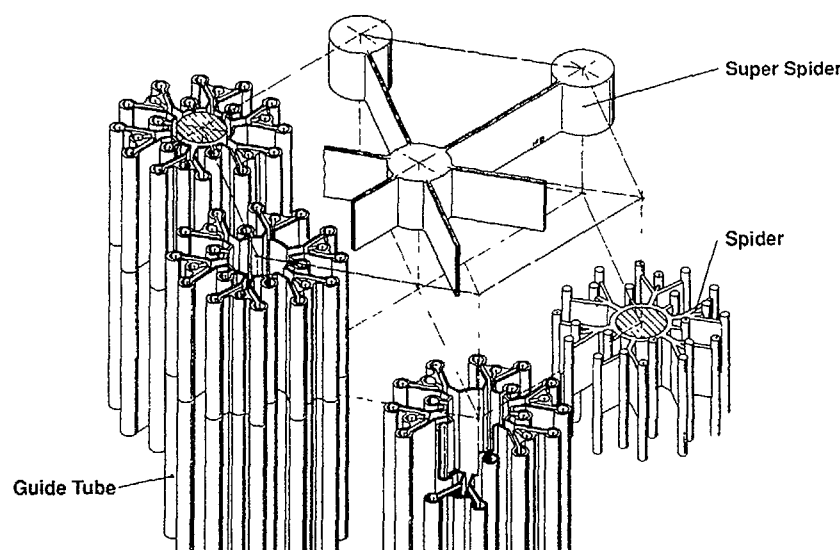


Fig.6 Guide Tube

#### 4 Control Rod Ejection Lock

As mentioned above, part of the reactivity of the PWHCR is compensated by control assemblies, thus at nominal power control rods are fully inserted. A rupture of the pressure tube of the drive of such a control rod would entail a rapid ejection of the control assemblies. A device is needed in order to avoid a rod ejection transient. Since the acceleration during a regular step is about four times higher than during ejection, it was rather difficult to find an adequate and reliable solution. The key idea to solve the problem was to install a spring between drive shaft and spider. Thus the acceleration during a regular step could be reduced below that one during an ejection. By limiting the stroke of said spring to about 1.2 times a step length a second spring in series with the first one is compressed if the motion exceeds the limit. This second elastic member e.g. a package of belleville washers below the coupling between shaft and spider allow a relative motion between the hub and the lock of the latch coupling if this coup-

ling is builtin upside down compared to the standard PWR CR-coupling. This motion unlocks the latches, the spider and the shaft separate and since the weight of the control assembly is slightly higher than the buoyancy, the control assembly drops into its shutdown position in the core, while the shaft will be ejected with increased velocity until its lower thickend endsection is stopped at the insertion funnel of the penetration. Fig. 7 shows at the left the ejection lock during reactor operation. The release situation during ejection and during handling at the right side. Fig. 8 shows the super spider with the ejection lock in the upper region

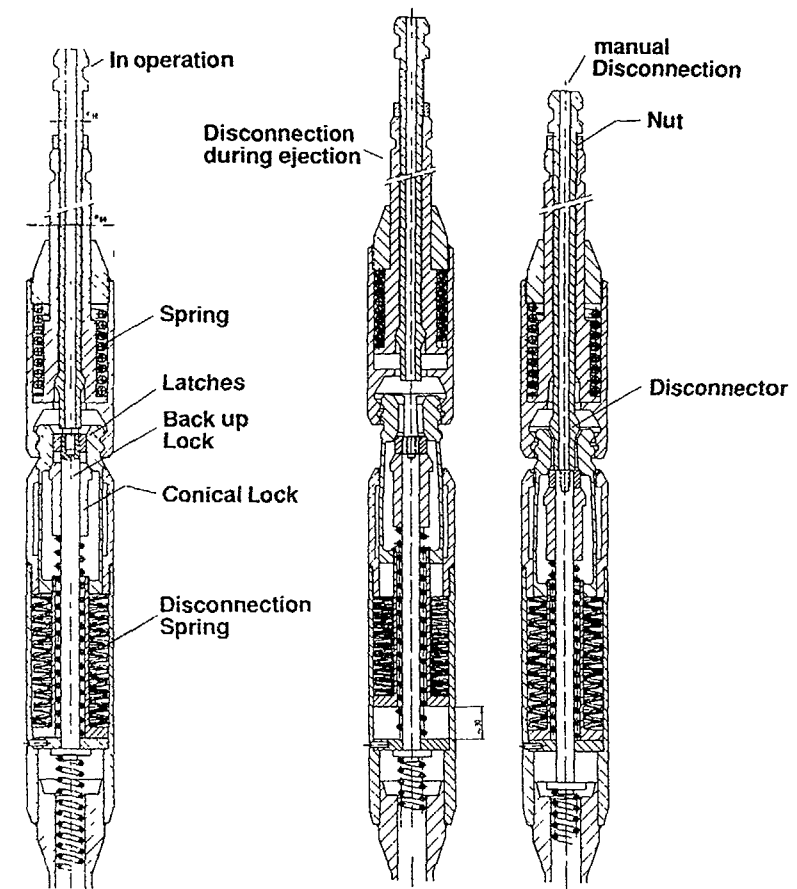


Fig.7 Ejection Lock

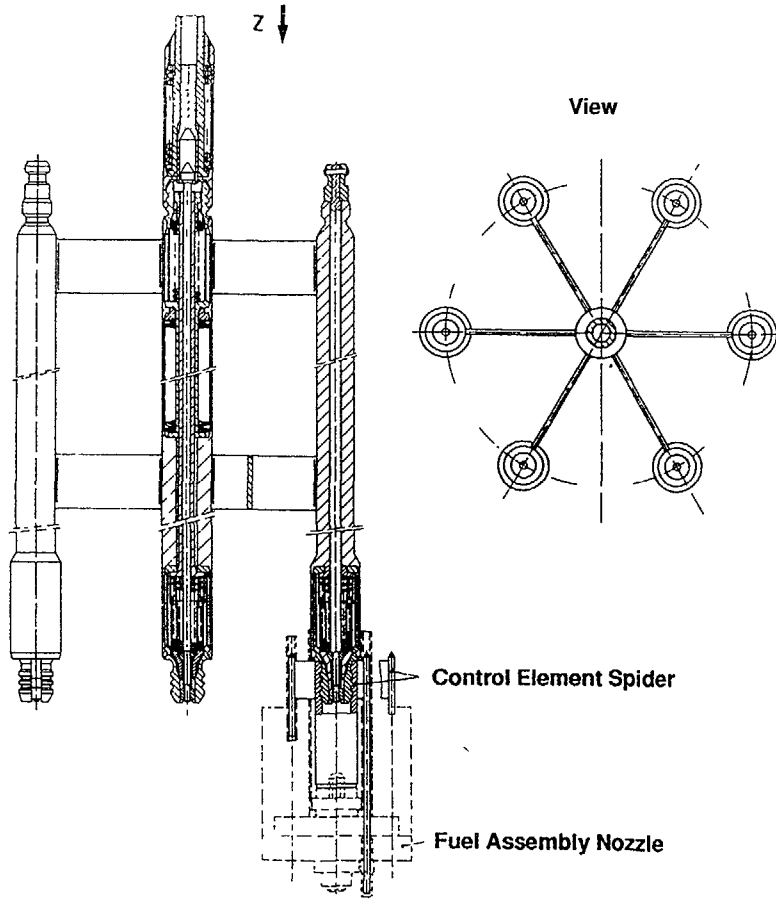


Fig.8 Super Spider

of the central hub. At the lower end of the seven hubs modified standard latch coupling are located which connect seven individual spiders with the super RCC.

A function model of this ejection lock was built at SIEMENS Erlangen and its function was demonstrated.

## 5 Conclusions

The development work of the PWHCR initiated noval solution which can be elements of advanced PWRs, or even lead to improvements of the existing PWR.

- A spacer grid with triangular pitch, uniform wall-thickness adequate rigidity and low pressure drop was designed. More than 50 grids mainly for hydraulic tests were manufactured at SIEMENS workshops
- A noval control rod guide structure which reliably prevents from failure during control rod insertion was designed for a seven control assembly Super RCC
- A control element ejection lock was designed. The function of which was demonstrated with success.

The money spent into mechanical design lead to an adequate equivalent in noval but feasible and useful solutions.

## BIBLIOGRAPHY

- /1/ H. Moldaschl et al  
 General Advantages of Hexagonal Fuel Assemblies  
 IAEA Technical Committee Meeting on Technical and Economic  
 Aspects of Higher Converters. Nuremberg March 26 - 29, 1990
- /2/ H. Moldaschl  
 Status and Prospects of Cooperative KWU High Converter  
 Development 1989  
 ICENES 1989

## RADIATION FIELD IN THE REFLECTOR AND RPV REGION OF THE HIGH CONVERTER REACTOR DESIGNED BY SIEMENS AG

W. HOFMANN, J. KOBAN

Siemens AG,

Unternehmensbereich KWU,

Erlangen, Federal Republic of Germany

### Abstract

The core of the 3765 MW<sub>th</sub> high converter designed by Siemens AG in cooperation with Paul Scherrer Institut (PSI, Switzerland), Kernforschungszentrum Karlsruhe (KFK, Germany) and the Technical University of Braunschweig (Germany) is characterized by the hexagonal geometry of the fuel assemblies. This was one reason among others to investigate an alternative reflector construction instead of the usual shroud. The result was a bulk steel reflector perforated with bore holes to allow the flow of cooling water for heat removal from gamma radiation absorption in the reflector. A preliminary optimization of the number, diameter, and positions of the bore holes was performed to guarantee that the maximum temperature in the steel reflector is lower than 400° C. The gamma heating in the reflector ranges from 12 W/cm<sup>3</sup> to 1 W/cm<sup>3</sup> in the core midplane which indicates a steep radial gradient. Therefore it is necessary to locate most of the bore holes along the core edge. The preliminary analysis showed that there are no significant difficulties which could prevent use of this kind of reflector.

The second point for analysis was the RPV fluence. The calculations showed that the RPV diameter of the 3765 MW<sub>th</sub> PWR class designed by Siemens AG can be retained without any significant increase in the maximum EOL-fluence due to fast neutrons. This result was obtained in spite of the larger core diameter of the high converter because of the steel reflector and the hexagonal geometry of the core. An additional effect of the steel reflector was the neutron spectral shift so that for identical fast fluence values less primary damage in the RPV is caused by the high converter. In any case the EOL fluence  $E > 1 \text{ MeV}$  is lower than the fluence limit of  $1 \text{ E}19 \text{ cm}^{-2}$  for 32 full power years given in the German "RSK-Leitlinien für Druckwasserreaktoren" (Reactor Safety Commission Guide-lines for PWR).

### 1 Introduction

The core of the 3765 MW<sub>th</sub> high converter designed by Siemens AG in cooperation with Paul Scherrer Institut (PSI, Switzerland), Kernforschungszentrum Karlsruhe (KFK, Germany) and the Technical University of Braunschweig (Germany) is characterized by the hexagonal geometry of the fuel assemblies. A new reflector for this geometry had to be developed. An optimization of a combined steel-water zone had to be found to guarantee that the maximum temperature in the steel reflector is lower than 400° C. In order to obtain the amount of gamma heating in the reflector material, the gamma radiation field in this region had to be calculated by means of a neutron and gamma transport code.

Another point for analysis was the reactor pressure vessel fluence due to fast neutrons. According to the German "RSK-Leitlinien für Druckwasserreaktoren" (Reactor Safety Commission Guidelines for PWR) the RPV fluence after a period of 32 full power years must be lower than the fluence limit of  $1 \text{ E}19 \text{ cm}^{-2}$ . Neutron transport calculations were performed to get information about the radiation field in the RPV region, depending on the effect of the reflector construction.

### 2 Description of the reactor core and reflector geometries

The reactor core geometry of a standard PWR (KONVOI) designed by Siemens AG with the same thermal power output of 3765 MW<sub>th</sub> is represented in Figure 1. The 193 fuel assemblies for this type of reactor geometry are square, and therefore the core outline of a standard PWR is not circular. Because of the varying shielding thickness outside the standard PWR core a strong variation in the azimuthal flux distribution along the inner surface of the RPV is observed. In addition, the radiation field in the region of the PWR reflector shows a rapidly varying distribution of the gamma radiation inside the

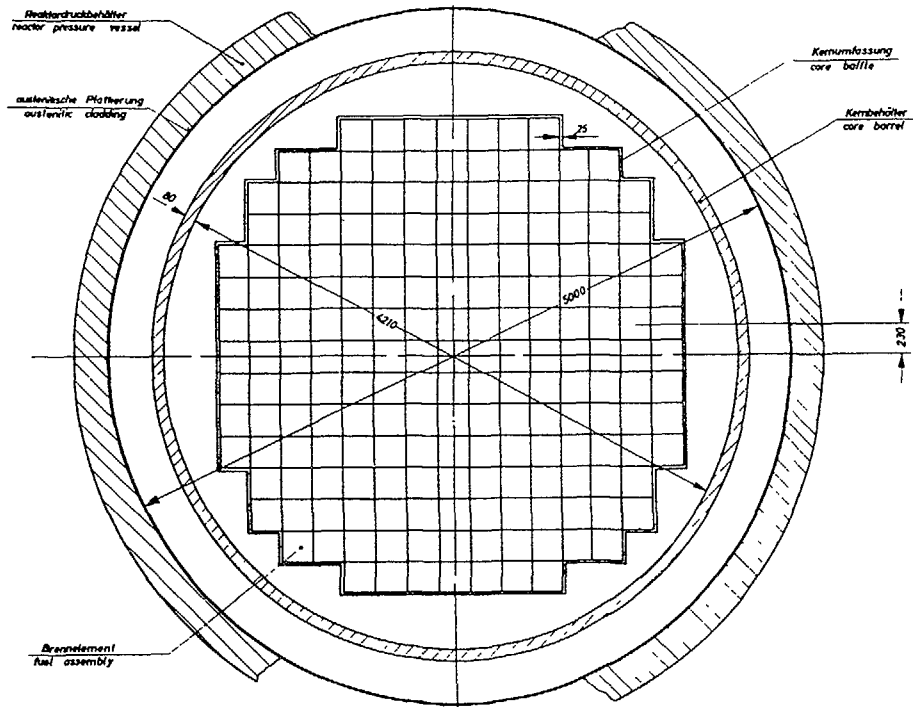


Figure 1

Reactor core geometry of the 3765 MW<sub>th</sub> standard PWR (KONVOI) designed by Siemens AG

core baffle, which leads to great differences in the azimuthal distribution of the gamma heating in the core baffle material.

The reactor core of the high converter designed by Siemens AG consists of 349 hexagonal fuel assemblies, which are arranged in a symmetrical form in relation to an angle of 30°. Due to the small pitch of these fuel assemblies a rather circular core outline (Figure 2) could be achieved, resulting in an almost uniform shielding thickness in the region outside the reactor core. Because of these slight changes in the shield thickness a rather uniform azimuthal flux distribution along the inner surface of the RPV is expected.

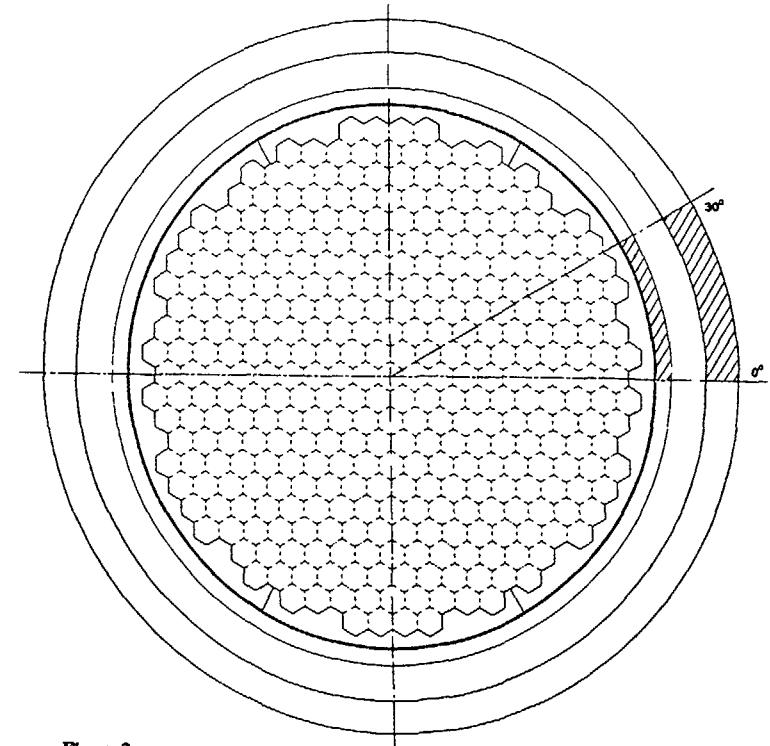
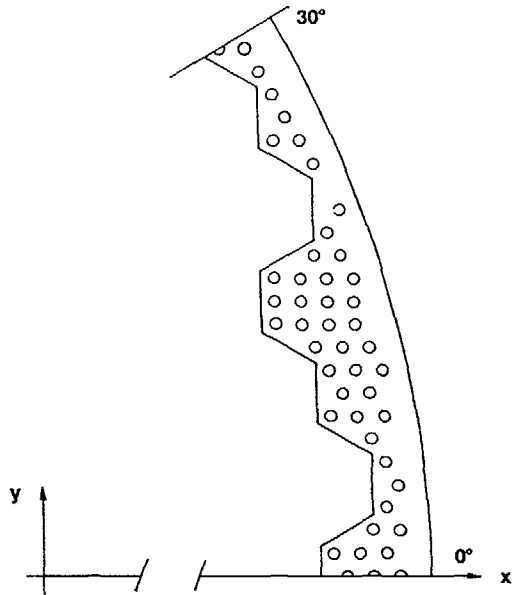


Figure 2

Reactor core geometry of the 3765 MW<sub>th</sub> high converter designed by Siemens AG

The reflector of the high converter is composed of bulk steel segments perforated with bore holes to allow the flow of cooling water for heat removal from gamma radiation absorption in the reflector. In order to guarantee that the maximum temperature in the steel reflector of the high converter is lower than 400° C, an optimized combination of the bore hole diameter, the bore hole positions and the number of bore holes had to be found. Because of the great height of the reflector segments the bore hole diameter could not be chosen arbitrarily small for manufacturing. The preliminary optimized bore hole combination for the steel reflector is represented in Figure 3.



**Figure 3**  
High converter steel reflector segment with bore holes for the flow of cooling water

One advantage of this type of reflector geometry with bulk steel segments outside the high converter core is that the reflection of fast neutrons back into the core is better than the reflection in the case of a standard PWR with the usual core baffle. Another advantage is that there is no possibility for baffle jetting due to gamma heating gradients in the reflector material. Thus the damage of single fuel rods along the core edge can be avoided. The third advantage of the bulk steel reflector is that the slowing down of the very fast neutrons is more effective than in the usual reflector of a standard PWR. This results in a lower fast neutron fluence at the RPV.

### 3 Method of calculation for the radiation field outside the core

For the calculation of the neutron and gamma radiation field outside the high converter core we used one and two dimensional transport codes solving the Boltzmann transport equation by the method of discrete ordinates. For the one dimensional problems the ANISN code, and for the two dimensional problems the DOT code was used.

The microscopic neutron and gamma cross sections were taken from the 120 group coupled neutron and gamma library EURLIB 4, which is based on ENDF/B4. The order of Legendre expansion of the cross sections was P3, and for the directional quadrature we used S8. The original 120 group library was condensed by means of the ANISN code, yielding a 54 group coupled neutron and gamma library for the two dimensional calculations with DOT.

The local neutron source in the reactor core was calculated from the power density distribution for an initial core, using the following equation:

$$s = p * f * n$$

where

s ..... number of source neutrons per unit volume

p ..... power density

f ..... number of fissions per unit energy

n ..... number of neutrons produced per fission

The input data for the power density distribution are shown in Figure 4, and for the resulting neutron source distribution a 3d-picture is given in Figure 5.

These data are valid for a high converter with the lattice parameter  $p/d$  = pitch/diameter = 1.24. The average enrichment is 5.7 %  $P_{ufiss}$  and the enrichment steps are 4.5 %, 5.6 % and 8.0 %  $P_{ufiss}$ .

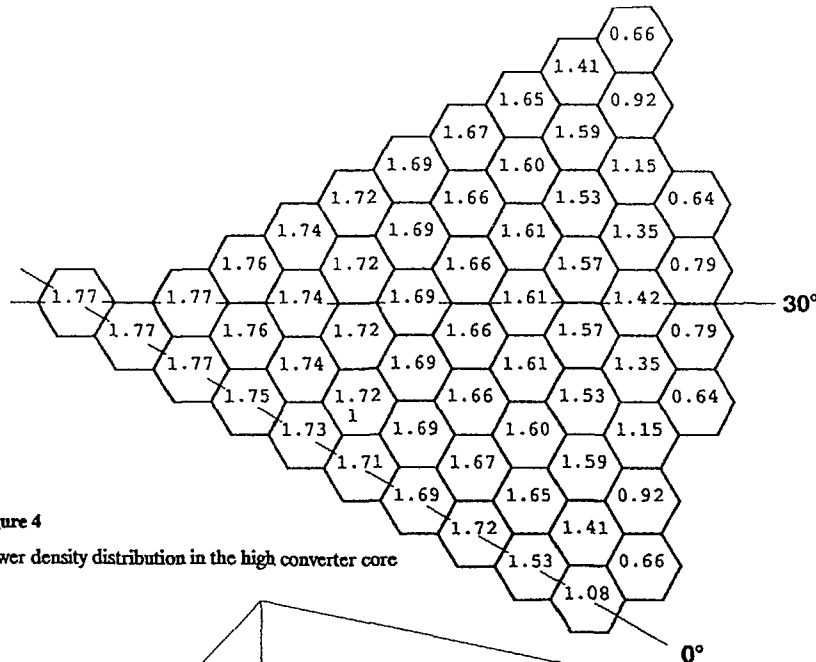


Figure 4

Power density distribution in the high converter core

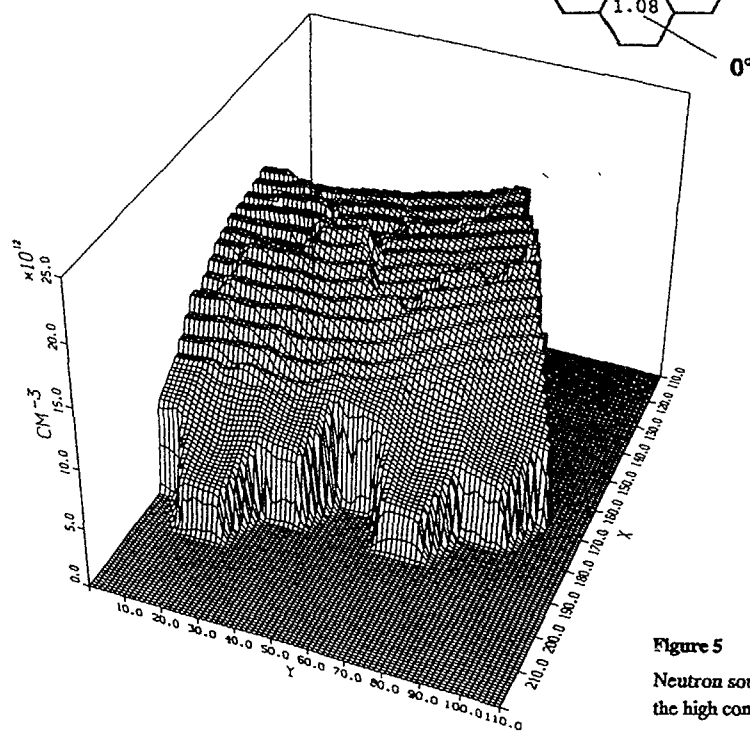


Figure 5

Neutron source distribution in the high converter core

#### 4 Gamma heating in the reflector of the high converter

The analysis of the gamma radiation field in the region of the high converter reflector yielded the gamma heating distribution inside the reflector material. The gamma radiation in this region is caused by gamma particles leaving the core and by gamma production due to neutron absorption reactions. A 3d-picture of the gamma heating in the reflector with the bore hole configuration in Figure 3 is shown in Figure 6.

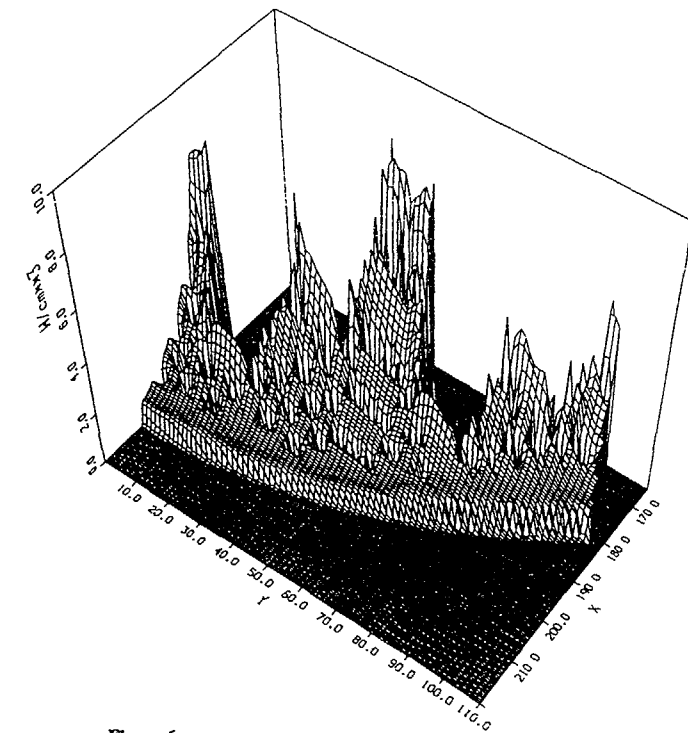


Figure 6

Distribution of the gamma heating in the high converter reflector

The gamma heating values are decreasing from the core edge to the outer parts of the reflector. The maximum value of the gamma heating is  $12 \text{ W/cm}^3$ . This maximum is located at one of the offset corners of the core, at the axial level of the core

mid plane. The gamma heating distribution at the reflector edge along the core barrel is very uniform, and the maximum value is about  $2 \text{ W/cm}^3$ .

The minimum value of the gamma heating is lower than the maximum by 3 orders of magnitude. The position of the minimum is at the upper end of the reflector segment.

The bore holes in the reflector of the high converter are located to allow the flow of cooling water for heat removal in the vicinity of the maximum gamma heating values. This guarantees that the maximum temperature in the reflector steel segments is lower than  $400^\circ \text{ C}$ .

A further optimization of the bore hole arrangement would possibly improve the heat removal and thus the temperature distribution in the reflector. But for the actual design of the reflector there are no gamma heating or temperature problems which could prohibit this construction.

### 5 Reactor pressure vessel fluence

For a standard  $3765 \text{ MW}_{\text{th}}$  PWR (KONVOI) designed by Siemens AG the reactor pressure vessel maximum fluence due to fast neutrons after a period of 32 full power years is  $5 \text{ E}18 \text{ cm}^{-2}$ .

The RPV diameter of this type of reactor is 5 m, which is the same value as for the high converter. However, the core and the reflector geometries of both reactor types are very different (see Figures 1 and 2). The core cross section of the high converter is larger than the core cross section for the standard PWR, but the core outline is more circular in the case of the high converter. Based on the large steel components in the high converter reflector the negative effect of the larger core cross section on the RPV fluence is partly compensated, because there are a lot of inelastic neutron

scatterings in the steel reflector. That means that the fast neutrons, reaching this steel region, are scattered down into the energy range from about 1 to 2 MeV. In the succeeding water zone outside the reflector and the core barrel, these neutrons are scattered down to energies below 1 MeV. Therefore many of the neutrons, reaching the RPV of the high converter, don't have enough energy for an essential contribution to the steel embrittlement.

The calculated maximum RPV fluence for the high converter is  $7.5 \text{ E}18 \text{ cm}^{-2}$  and therefore only 50 % higher than the fluence of the standard PWR.

The result of the RPV fluence calculation for both reactor types is represented in Figure 7, showing the different azimuthal distributions of the fluence due to neutrons with energy values larger than 1 MeV.

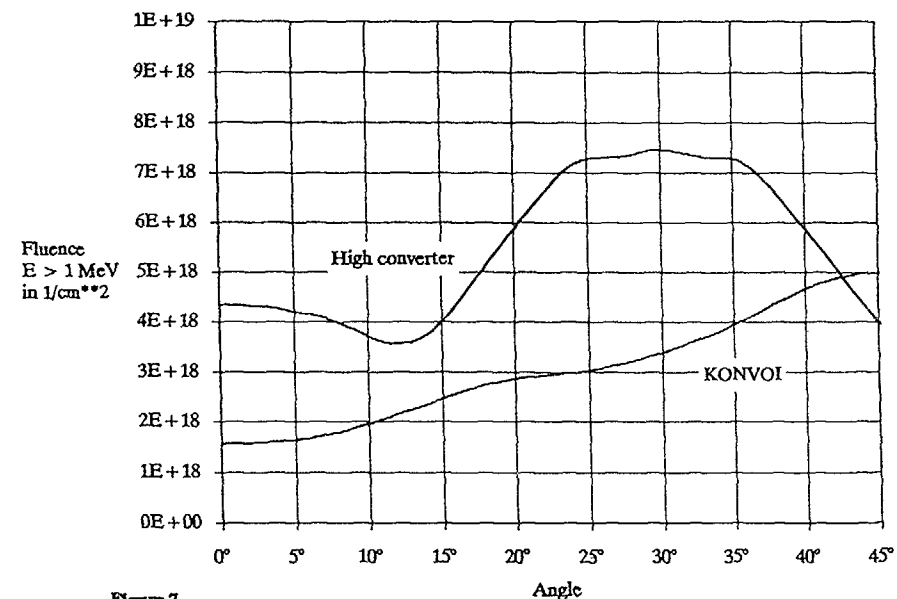


Figure 7

Azimuthal distribution of the neutron fluence due to fast neutrons along the inner RPV surface of the high converter and the standard PWR (KONVOI)  $3765 \text{ MW}_{\text{th}}$

The curves represent the distribution along the inner surface of the RPV at the level of the axial maximum. The factor between the maximum and minimum values is lower in the case of the high converter, due to the more circular core outline of this geometry. For both reactor types the fluence values are lower than the fluence limit of  $1 \text{ E}19 \text{ cm}^{-2}$  given in the German "RSK-Leitlinien für Druckwasserreaktoren" (Reactor Safety Commission Guide-lines for PWR).

Because of the bulk steel reflector and the thicker core barrel there is a different spectrum in the RPV of the high converter compared with the spectrum in the RPV of the standard PWR. The differences in the neutron spectra can be shown in terms of displacements per atom (dpa). In Table 1 the contributions of different neutron energy ranges to the total dpa values are listed for both reactor types.

**Table 1**

Contribution of different neutron energy ranges to the number of displacements per atom (dpa) in the RPV of the high converter and the standard PWR 3765 MW<sub>th</sub>

| Neutron Energy         | High converter             |       | Standard PWR (KONVOI)      |       |
|------------------------|----------------------------|-------|----------------------------|-------|
|                        | dpa                        | %     | dpa                        | %     |
| $E > 3 \text{ MeV}$    | $3.66 \text{ E-12 s}^{-1}$ | 31 %  | $5.34 \text{ E-12 s}^{-1}$ | 45 %  |
| $E > 1 \text{ MeV}$    | $8.04 \text{ E-12 s}^{-1}$ | 68 %  | $9.24 \text{ E-12 s}^{-1}$ | 78 %  |
| $E > 0.1 \text{ MeV}$  | $1.11 \text{ E-11 s}^{-1}$ | 94 %  | $1.14 \text{ E-11 s}^{-1}$ | 97 %  |
| $E > 0.414 \text{ eV}$ | $1.14 \text{ E-11 s}^{-1}$ | 97 %  | $1.17 \text{ E-11 s}^{-1}$ | 99 %  |
| Total                  | $1.18 \text{ E-11 s}^{-1}$ | 100 % | $1.18 \text{ E-11 s}^{-1}$ | 100 % |

Concerning the total dpa values the neutron radiation field in the RPV of the high converter causes the same effect as the neutron radiation field of the standard PWR. But, as can be seen from Table 1, neutron energies above 1 MeV contribute much less to the dpa's in the case of the high converter. Due to the different energy spectrum the fluence  $E > 1 \text{ MeV}$  of

$7.5 \text{ E}18 \text{ cm}^{-2}$  standing for the high converter produces the same total dpa value as  $5.0 \text{ E}18 \text{ cm}^{-2}$  calculated for the standard PWR. From this point of view the existing differences between the RPV fluences for both reactor types are even less important.

## 6 Conclusion

The analysis of the radiation field in the reflector and the RPV of the high converter leads to the following conclusions:

- For the actual design of the high converter reflector, composed of bulk steel segments with bore holes, there are no gamma heating or temperature problems which could prohibit this construction. A further optimization is possible.
- Concerning the RPV fluence the high converter shows approximately the same value as the standard PWR. Consequently, from this point of view the same RPV could be used for the high converter.

CODES AND DATA BASES  
(Session 3)

**Chairman**

**J.N. NIGON**  
France

# DEVELOPMENT OF CALCULATIONAL PROCEDURES FOR THE NEUTRON PHYSICS DESIGN OF ADVANCED REACTORS

C.H.M. BROEDERS

Kernforschungszentrum Karlsruhe GmbH,  
Karlsruhe, Federal Republic of Germany

## Abstract

The Nuclear Reactor Center Karlsruhe has been involved with the development of Light Water Tight Lattice Reactors (LWTLR) since more than ten years. A considerable amount of thermohydraulic and nuclear physics code development has been performed during this time. The present paper describes main aspects of the neutron physics calculational tools. From the neutron physics point of view, two different tasks have to be adapted for LWTLR- calculations:

- + determination of mean cross section sets within the hexagonal fuel assemblies (FA).
- + determination of the characteristics of LWR cores with hexagonal FA.

All developments for the neutron physics design of LWTLR have been performed within the established system for Fast Breeder Reactor (FBR) calculations at KfK, KAPROS, using a various number of available options for FBR- work. The present status of the calculational tools for LWTLR- investigations will be described, especially the features of a new developed KAPROS- procedure ARCOSI: Advanced Reactor COre SImulator, including:

- + Preparation of the ARCOSI- library HXSLIB, containing burnup dependant cross section sets for FA with control rod positions containing control rod material or waterholes and with borated water in the moderator region of the pin cells. Also, data for different coolant densities and pin cell temperatures may be processed.
- + Simulation of equilibrium core calculations, including critical reactivity search by waterboration control and simple FA- management. Threedimensional full core calculations are performed with the KAPROS version of the hexagonal nodal code HEXNOD, developed by Wagner, KWU.
- + Powerful interfaces for interactive graphical analysis of results.

## 1 Introduction.

After the proposal of Edlund [1] in the year 1975, to improve uranium utilization with the help of tight lattice light water reactors with  $(Pu, U)O_2$  mixed oxyde (MOX) fuel, the nuclear research center Karlsruhe started a small project to investigate the future potential of such a reactor concept. The basic idea was to modify the core of a modern german pressurized water reactor (PWR) and to keep all other components unchanged as far as possible. In close cooperation with a number of other groups all main aspects of the core replacement for a Kraftwerkunion (KWU) PWR have been studied. The main results have been published, eg. in special issues of "Nuclear Technology" [2,3]. The present paper describes the development of the calculational procedures for the neutron physics investigations related to this advanced reactor project. The main characteristics of the neutronic calculations of these "Advanced Pressurized Water Reactors" (APWR) are:

- Relatively tight triangular lattices in hexagonal fuel assemblies.
- MOX fuel with plutonium as basic fissile material.
- Reactor control by means of enriched  $B^{10}$ . Two alternative methods for inserting the control material into the reactor have been considered:
  1. Control rods within the fuel assembly.
  2. Boration of the coolant water.

The first task of these APWR investigations was the assessment of available calculational tools for the description of tight water moderated lattices with MOX fuel. In close cooperation between KfK, KWU and the University of Braunschweig (TUBS), benchmark investigations were performed to validate available codes and libraries for APWR calculations. The main findings from these investigations were [4]:

- Available experiments for tight water moderated  $UO_2$  lattices from the ZPR-7 program could be recalculated satisfactorily, both with data and methods for fast reactor calculations and with codes, mainly developed for thermal reactor design, eg. the WIMS/D code [5].
- The results for the calculation of a theoretical tight water moderated MOX lattice showed significant deviations, especially in the case of voidage.
- No experiments were available for tight water moderated MOX lattices.

The most important recommendation from these investigations was, to perform relevant experiments with representative MOX fuel in tight lattices. They have been performed meanwhile in several laboratories in Switzerland, W.-Germany, France and Japan. Unfortunately, most of the experimental results are not yet available because of restricted distribution. A careful analysis of the results for the theoretical MOX benchmark lead to the following conclusions:

- It is necessary to apply cell calculation methods for these tight lattices.
- The 69 group WIMS/D energy group scheme seemed to be adequate.
- The available WIMS/D data libraries were not well suited for APWR work, especially for voided configurations.

On the basis of these results new calculational procedures for the description of tight water moderated lattices with MOX fuel have been developed. They will be described in section 2.

A second field of basic calculations is the description of the burnup behaviour of the fuel. For this task it was possible to cooperate with another project being in progress at KfK. It was intended to establish a computer code system capable to perform most of the calculations for the nuclear fuel cycle for different reactor types. All APWR code developments were integrated within this fuel cycle project. In section 3 some characteristics of the burnup calculations will be described.

The main objective of the KfK APWR investigations was to analyze the potential of the advanced MOX fuel in a modern PWR as designed by Siemens/KWU. Two main problems arise during whole core calculations:

- Description of realistic fuel assemblies.
- Realistic description of the whole reactor core.

Starting from cell calculations for regular infinite lattices, specific irregularities in this lattice have also to be taken into account. Typical irregularities may be grid spacers, fuel assembly bandages and coolant in the edges of the fuel assembly. Moreover in some designs control rod positions within the fuel assembly, filled with control rods or with other materials, have to be considered. In a first stage these effects were treated in a very crude way. The latest investigations show a more detailed treatment. In section 4 the

development for the description of the fuel assemblies will be described in more detail.

During preliminary whole core calculations only crude approximations for the fuel assemblies were used. Therefore the applied reactor geometries were also quite crude: one- and twodimensional (R-Z) models with smeared fuel zones. The latest calculations have been performed with more accurate geometrical representation. In section 5 the developments for the theoretical investigation of the whole reactor will be described in more detail, especially a new method for the description of the long-time behaviour of the core, including fuel burnup, reactor control and fuel management.

## 2 Calculation of infinite fuel arrays.

For the calculation of infinite fuel arrays two aspects must be considered:

- Calculational programs.
- Data libraries.

The combination of the calculational procedures together with the applied data libraries must be verified for the intended application.

### 2.1 Calculational procedures.

When the APWR investigations were started, good experience was available in calculating fast reactors and only some experience in calculating thermal systems. Furthermore, the spectrum in an APWR was expected to be somewhere between those of fast and thermal reactors. At first the investigations were started using standard fast reactor methods. However, already the first recalculations of tight light water moderated  $UO_2$  lattices showed that heterogeneity corrections, similar to those used in codes for thermal reactors, had to be applied. Simple approximations for the treatment of the spatial selfshielding were introduced. Within the frame of the selfshielding tabulations for fast reactor calculations (narrow-resonance approximation NRA), the Dancoff-corrected volume-to-surface modification of the background cross section  $\sigma_0$  is performed:

$$\sigma'_0 = \sigma_0 + \frac{(1 - C)4V}{S} \quad (1)$$

In a first approach this modification was performed within the standard calculational procedure for homogenized fast reactor zones: the program GRUCAL [6] was modified to a special version GRUCAH. With appropriate group constant sets, GRUCAH gives quite good results for tight light water moderated lattices with  $UO_2$  fuel. However, detailed investigations for APWR MOX lattices showed the need to apply more accurate cell calculations, as commonly used in calculational procedures for thermal reactors.

So the next step was to establish another procedure for cell calculations. For this purpose three tasks must be performed:

1. Preparation of adequate group cross sections in the cell-zones.
2. Calculation of space- and groupdependant neutron fluxes in the cell.
3. Calculation of cellhomogenized group constants for succeeding reactor calculations.

The first task, group constant calculations, is performed with a second modified version of the basic code GRUCAL: GRUCEL. Using the same principles as in GRUCAH, spatial resonance selfshielding is taken into account by the Dancoff-corrected volume-to-surface modification.

The second task, cell flux calculations, needs a solution based on transport theory. In a first approach we applied the fast breeder reactor (FBR) code ONETRA [7,8], part of the established FBR codesystem KAPROS [9], for onedimensional  $S_n$  calculations. After the successful establishment of an own KAPROS procedure for APWR and PWR cell calculations, a second faster transport theory program, based on first flight collision probability methods (CPM) was taken from WIMS and adapted to the KAPROS program system: WEKCPM.

For the third task, cell homogenization, a new program was written: ONEHOM.

Having established the cell calculational procedure, described above, a number of refinements had to be introduced. The most important ones are:

- Introduction of material dependant fission spectrum matrices. The first KEDAK based 69 group libraries contained only one fission spectrum for all fissile materials. These data were updated with materialde-

pendant fission spectrum matrices from JEF-1.1, calculated with the Karlsruhe version of NJOY [10]. A special module CHICOR was written to calculate the material composition dependant fission spectrum iteratively.

- Improvement of the calculation of the resonance cross sections. Alternatively to the standard selfshielding calculations on the basis of selfshielding factor tabulations and modified  $\sigma_0$  (see formula (1)) interpolations, a more accurate method has been made available on the basis of the program RESAB-II [11], developed at the University of Stuttgart. RESABK solves the transport equation in the resonance region by first flight collision probability methods in a very fine energy resolution of constant lethargy width. The fine energy mesh fluxes are used to calculate the effective shielded cross sections directly.
- Introduction of a critical buckling search procedure for use together with the collision probabiltiy code WEKCPM.

All options discussed above can be selected in the KAPROS procedure KARBUS by input. For the preparation of the atom number densities in the cell zones and in the homogenized cell, two modules are available with different ways to define the lattice specifications:

1. Module NDCALC with more global input data, like moderator-to-fuel volumes, plutonium fissile enrichment etc.
2. Module NDWIMS with input specifications similar to the WIMS/D input. Numberdensities and geometry data must be given in detail.

During the PROTEUS evaluation work [12] the FBR cell code KAPER4 [13] has been modified to enable 69 group calculations, including upscattering.

The results of the calculations for the infinite arrays can be stored in the KAPROS-own data archives for use in succeeding steps, eg. in fuel assembly calculations.

## 2.2 Data libraries.

The first APWR investigations at KfK were performed with modified FBR methods, using the standard KfK FBR library KFKINR [17] with the 26 energy group scheme of the Russian ABBN group constant set. Together with

an early version of the GRUCAH code, good agreement could be obtained for the recalculation of tight light water lattices (see for example reference [4]). However, analysis showed a coding error in the GRUCAH version. After correction disagreement with more advanced calculational methods was observed and 26 group APWR calculations were stopped.

For LWR and APWR investigations, a new group constant library with the 69 energy group scheme of the WIMS/D code and the features of the FBR libraries was established. In this way the advantages of the libraries for thermal and fast reactors were combined, eg.:

- Adequate energy group structure at lower energies.
- Storage of material dependant spectra of fission neutrons.
- Detailed description of degradation processes at high energies (elastic scattering, inelastic scattering,  $(n,2n)$  and  $(n,3n)$  processes).

The group constant sets, described here, were calculated from the Karlsruhe nuclear data library KEDAK-4 [14] with the standard group constant generation code MIGROS-3 [15]. The data for the fission products (most of them not available on KEDAK-4) were provided by ECN Petten, mainly based on ENDF/B-V [16]. The generation of a consistent 69 energy group library with the structure of the FBR libraries for about 100 materials, including fission products, was a quite laborious task. During the development activities a few versions were fixed for applications, like recalculation of PROTEUS experiments and design investigations. The most important intermediate library versions, reported in the literature, are:

- The 1985 versions G69HOT and G69COLD, mentioned in reference [18]. On these libraries the WIMS convention, to apply resonance tabulations only in the groups 15 - 27 (4eV - 9118 eV), was maintained. The problem of the temperature dependence of the cross sections and upscatter matrices below 4 eV was solved by the use of two separate libraries for cold (experiments) and hot (reactor design) lattices (assignment KARBUS-85). However, the selfshielding of the large absorption resonance of  $Pu^{242}$  at 2.67 eV is neglected in this way. This error was recognized during the succeeding analysis of PROTEUS experiments and of the results for the NEACRP HCLWR burnup benchmark.
- For the treatment of the NEACRP HCLWR burnup benchmark, two improved libraries were prepared: G69CT005 and G69HT005 (assi-

gnment KARBUS-88). The essential improvements were:

- Material dependant fission spectra.
- Selfshielding factors for the 2.67 eV resonance of  $Pu^{242}$ .
- Consistent group constants for the fission products from JEF-1.1.
- In the course of 1989, temperature and  $\sigma_0$  dependant group constants were introduced below 4 eV. Together with the earlier introduced temperature dependant upscatter matrices, now all temperatures may be calculated with the same library: G69NV003 (assignment KARBUS-89).

During the analysis of the results of the NEACRP HCLWR burnup benchmark, the weighting spectrum for the calculation of the quite broad WIMS groups above 4 eV played an important role. Some codes enable corrections for the calculation of the removal cross sections from the coarse groups with changing slowing down power, eg. during the lattice voiding. For this reason we started in the beginning of 1990 with a further assessment of this problem. Some possible solutions are:

- Creation of separate group constant libraries for different stages of a reactor system (eg. normal and voided condition).
- Introduction of a formalisms for the improved calculation of the removal cross sections. Examples are the so called "REMO" correction in the KfK FBR codesystem [19] and some features of the AARE system at PSI Würenlingen [20].
- Generation of a new energy group scheme with narrow energy groups. Again examples may be found in the KfK FBR and in the AARE system.

As a next step a new fine energy group system was introduced. At the present time a preliminary library with 334 energy groups is being developed. The structure is based on an extension of the 69 group WIMS scheme:

- WIMS energy groups below 4 eV. This choice enables the transfer of the upscatter matrices from the 69 group to the 334 group system. A disadvantage is the fact, that the important absorption resonance of  $Pu^{242}$  at 2.67 eV is not resolved and lies near a group boundary.

- Above 4 eV, a lethargy width  $\Delta u \approx 0.05$  has been chosen with all WIMS 69 group boundaries included. Moreover, the large absorption resonance of  $U^{238}$  at 6.7 eV is resolved in more detail.

Until now, a KEDAK-4 version with 334 groups has been realized, containing all important materials for the calculation of the investigated fresh core benchmarks: G334V002, being as consistent as possible with the 69 group library G69NV005. The differences between the G69NV003 and G69NV005 libraries are mainly some changes for  $Pu^{239}$  below 10 eV (see section 2.3.1) and introduction of selfshielding factors for oxygen in the high energy region. The next section will show some preliminary results of these developments.

### 2.3 Validation investigations.

The validation of the calculational procedures was one of the main tasks of our neutron physics APWR investigations. Because of the possible problems with the reactivity of voided APWR lattices, it is necessary to analyze problems with a wide variety of neutron spectra. At the beginning, a common benchmark project in collaboration between KfK, KWU and TUBS was organized (see section 1). The results are reported in reference [4] and will not be discussed here. Furthermore, a large number of FBR problems, mainly experiments, were used for validation work (see f.e. reference [18]). In a later stage of the project new validation benchmarks became available for us:

- The NEACRP HCLWR burnup benchmark exercise, proposed by Ishiguro et al. [21,22].
- The APWR experiments at KfK, Karlsruhe (SNEAK) and PSI, Würenlingen (PROTEUS).

Concerning the participation in the NEACRP HCLWR benchmark, the next section will give some recent information. The analysis of new APWR experiments is presented in a separate paper to this meeting [12], only some results obtained with the newest group constant libraries will be discussed here.

#### 2.3.1 Results for the NEACRP HCLWR burnup benchmark.

The international NEACRP HCLWR burnup benchmark exercise, proposed by Ishiguro et al. [21], was a very useful activity for the validation work. Together with some findings from the PROTEUS evaluations, the HCLWR benchmark investigations gave the hint to analyze the treatment of  $Pu^{242}$

in more detail; the KfK calculational procedures seemed to overestimate the capture in this fuel isotope. As already mentioned above, the error was found in the treatment of the absorption resonance of  $Pu^{242}$  at 2.67 eV. Similar like the treatment of this resonance in the original WIMS code, no resonance shielding tabulations were applied below 4 eV. Finally, the KfK contributions to the NEACRP HCLWR benchmark contained solutions with and without this error. Here some results for the voiding behaviour at begin of cycle (BOC) will be discussed. In the figures 1 and 3,  $k_\infty$  values are shown for the NEACRP HCLWR burnup benchmark case 2, a wider lattice with moderator-to-fuel volume ratio  $V_m/V_f = 1.1$ , 7 %  $Pu_{fis}$  and Zr cladding, obtained with some of the libraries discussed before. The  $k_\infty$  values are plotted as a function of the lattice voiding. Void 0 means normal waterdensity, void 100 % means a totally voided lattice. Additionally to the benchmark mean values and the KfK solution of summer 1989, four KfK results are given:

- G334V002, new 334 energy group library (see section 2.2).
- G69NV005, 69 energy group library consistent with G334V002.
- G69EV003, 69 energy group library, used for our last design calculations [23].
- G69HOT, 69 energy group library, used for the calculations in reference [18].

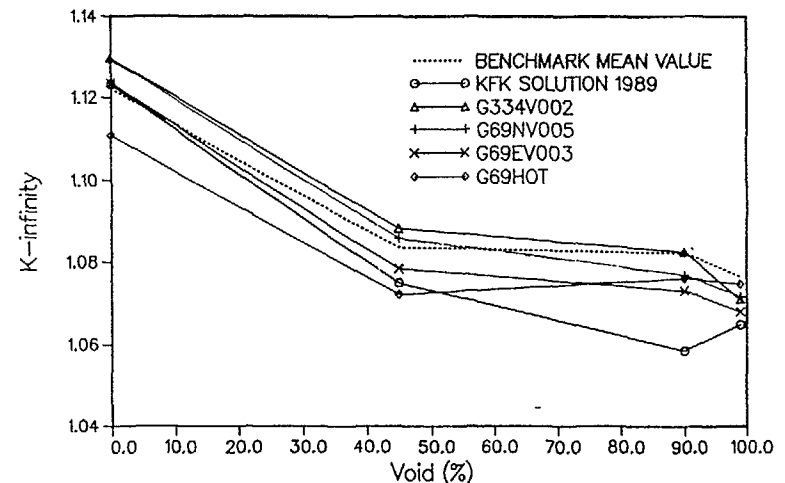


FIG. 1. NEACRP HCLWR burnup benchmark case 2, BOC (standard libraries).

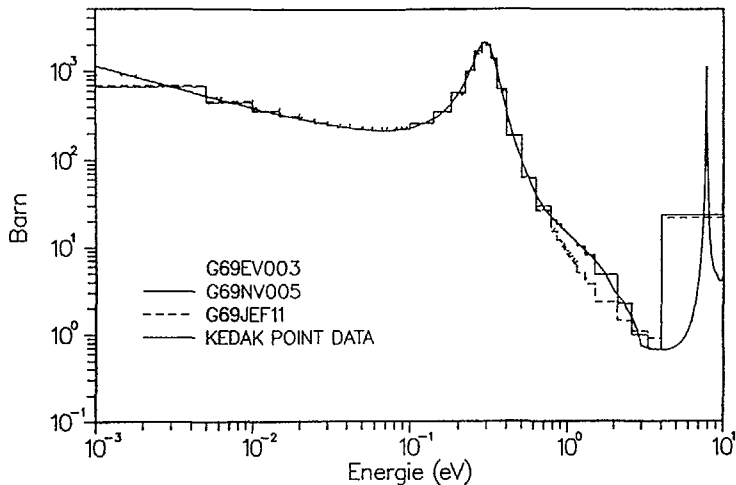
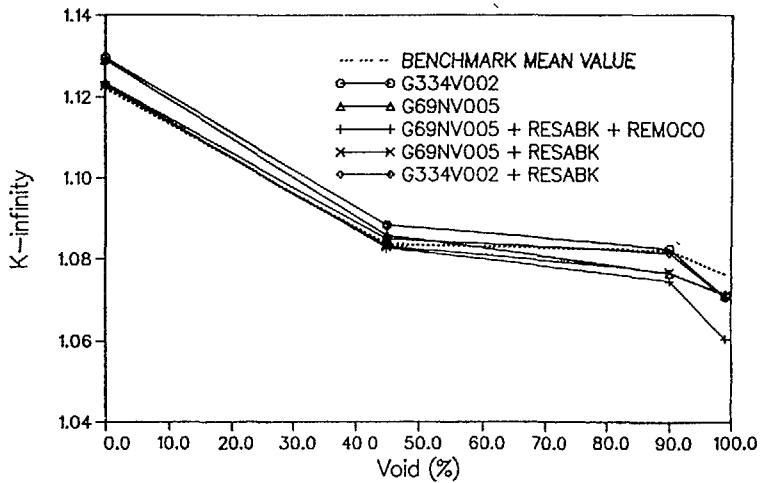
FIG. 2. Comparison of data for  $^{239}\text{Pu}$  SCAPT.

FIG. 3. NEACRP HCLWR burnup benchmark case 2, BOC (improved libraries).

The large effect of the  $\text{Pu}^{242}$  absorption resonance at 2.67 eV may be observed for the library G69HOT at void 0: this value lies  $\approx 1\%$  below the mean value. The discrepantly trend of the KfK solution 1989 for void changes from 90 to 99 % compared to the benchmark mean values has disappeared for the newer solutions, both with 69 and 334 groups. The reason is not completely clear.

A remarkable difference occurs for the normal lattice (void=0) between the curves for the new libraries G334V002 / G69NV005 and the other ones. This behaviour could be identified as a data inconsistency for  $\text{Pu}^{239}$  on the KEDAK-4 library, as shown in figure 2. Here the capture cross section of  $\text{Pu}^{239}$  is plotted from the pointwise KEDAK-4 data and from three group constant libraries: G69NV005, G69EV003 based on KEDAK-4 and G69JEF11, based on the JEF-1.1 file. Quite large deviations can be observed between the KEDAK-4 results in the low energy region. The G69NV005 data is calculated from pointwise data on KEDAK-4, whereas the G69EV003 data is calculated from resonance parameters. The JEF-1.1 data is given for comparison and lies somewhat closer to the resonance data from KEDAK-4.

The figure 3 shows some results for the same lattice, obtained with alternative calculational procedures for the data libraries G334V002 and G69NV005. Two special codes are applied:

- RESABK. This code calculates improved cross sections in the resolved resonance energy region (see section 2.1). The RESABK calculations were performed in the energy region 0.25 - 148.7 eV.
- REMOCO. This code calculates effective 69 group cross sections from group cross sections and cell fluxes, obtained with an 334 energy group structure. The results of figure 3 have been calculated with a preliminary version of the program in the energy region 148.7 eV to 10 MeV.

For void=0 the effect of the improved cross section calculation in the thermal region can be observed clearly: for both libraries G334V002 and G69NV005 a  $k_\infty$  decrease of  $\approx 0.8\%$  may be observed. For the dry lattices, the effect of the RESABK calculations is small. Here the REMOCO effect is significant: a decrease of  $k_\infty$  of about  $\approx 1\%$ . These first results indicate a significant sensitivity of the description of the high energy slowing down processes. A careful assessment of this problem possibly will reduce the spread of calculational results for dry MOX lattices, as observed during the PROTEUS evaluations [12]. We plan to start such an assessment in the near future on the basis of the JEF-2 nuclear data library.

### 2.3.2 Results for PROTEUS HCLWR experiments.

In this section some preliminary results are presented for the recalculation of the PROTEUS Phase-II experiments 7-9 ( $p/d=1.12$ ) and 13-15 ( $p/d=1.26$ ), using the newest calculational programs and the data libraries G334V002 with 334 groups and the corresponding 69 group library G69NV005 (see above). Figure 4 shows  $k_{\infty}$  values and figure 5 the very important reaction ratio of captures in  $U^{238}$  to fissions in  $Pu^{239}$ , C8/F9. The same representation as in reference [12] is used. A remarkable result is the strong overestimation of C8/F9 at low moderation values, especially with the fine group library. In order to investigate this behaviour, the high energy data of  $U^{238}$  capture were analyzed. Figure 6 shows these data in the energy region 10 KeV to 10 MeV from pointwise data representations on the basic nuclear libraries KEDAK-4, JEF-1.1 and a preliminary version of JEF-2. We can observe relevant differences in three energy ranges with different trends between the libraries: below 40 KeV, 40 KeV - 1 MeV and above 1 MeV.

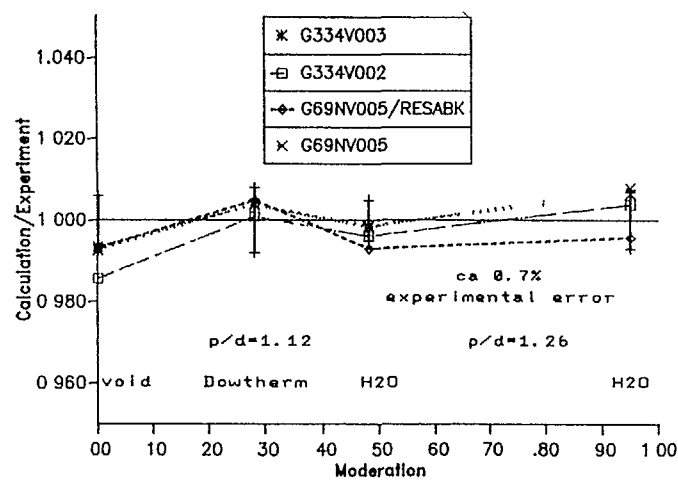


FIG. 4. C/E of  $k_{\infty}$  for PROTEUS experiments.

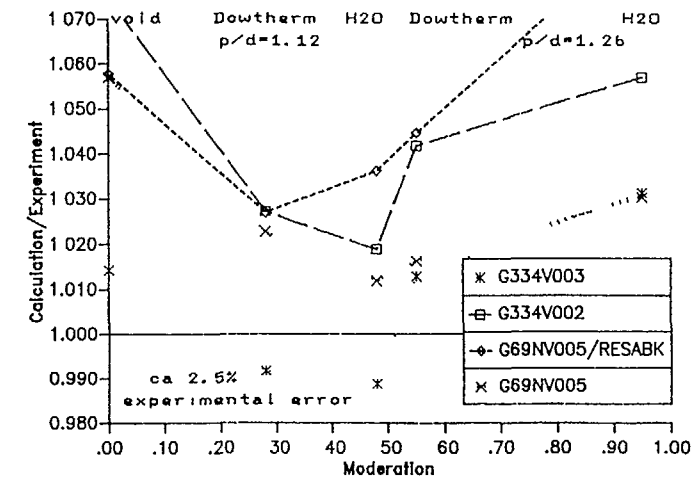


FIG. 5. C/E of C8/F9 for PROTEUS experiments.

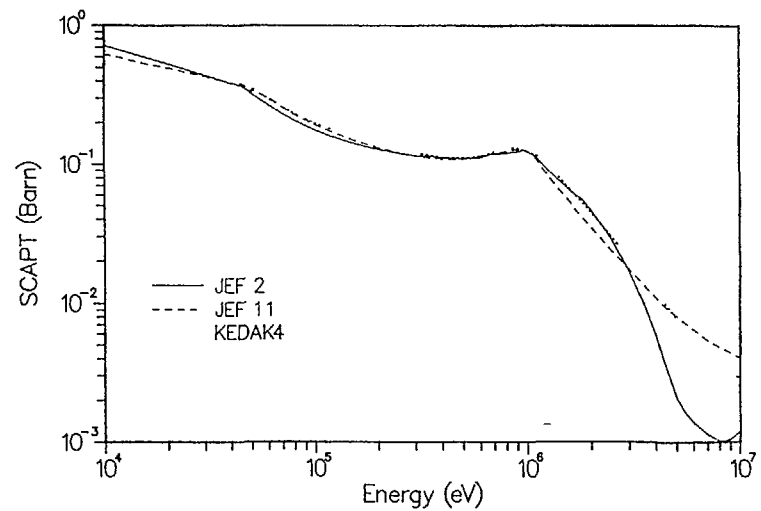


FIG. 6. Comparison of data for  $^{238}\text{U}$ , SCAPT.

The influence of the differences between KEDAK-4 and JEF-1.1 was investigated in more detail. All data of  $U^{238}$  above 10 KeV on the KEDAK-4 based library G334V002 were replaced by data, calculated from JEF-1.1 with the KfK version of NJOY [10]. This test library is identified as G334V003. The G334V003 results in the figures 4 and 5 show a significant improvement in the C/E values, both for  $k_{\infty}$  and for C8/F9. The fourth curve in the figures 4 and 5 is obtained with the library G69NV005, using the module RESABK for improved calculation of the resonance cross sections in the energy region 0.25 eV to 148.7 eV. The  $k_{\infty}$  values are lower, compared to the standard solution, but within the experimental error. The C8/F9 values increase significantly with increasing moderation and are obviously overestimated. These results are obtained on the basis of the KEDAK-4 library data and must be analyzed in more detail. We plan to perform these investigations on the basis of the final JEF-2 library, taking care to use consistent data for the different codes.

### 3 Burnup calculations.

As mentioned in section 1, the burnup calculational procedures for APWR investigations could be imbedded within the KfK project for the development of a code system to describe the problems of the nuclear fuel cycle of all common reactor types [24].

#### 3.1 Calculational programs and libraries.

A careful analysis of available procedures for fuel cycle analysis led to the decision to establish an improved version of the ORNL depletion program ORIGEN [25] as the basic module within the standard code system KAPROS [9]. Some arguments for this choice were:

- The good experience with the code ORIGEN during the development of the improved KfK version KORIGEN [26].
- The information for the transitions between isotopes is defined on code-own libraries, containing data for nearly all interesting isotopes.
- “Feedback” transitions (production of own precursors) can be handled ( $\alpha$ - decay).

On the basis of the KORIGEN code, a new KAPROS module was developed, BURNUP [27], with the following characteristics:

- The ORIGEN data libraries with the information for the transition matrix for the isotope transmutations have been reordered, resulting in more efficient calculations (shorter loops over precursors).
- The ORIGEN data library for fission products has been extended with yields of maximal 15 fissile isotopes instead of 5 before.
- The number of macro burnup timesteps is not restricted by the code. Only the capacity of the resources of the computer is restrictive.
- Up to 10 micro timesteps pro macro timestep can be calculated. This ORIGEN restriction is not modified. For the micro timesteps constant power or constant neutron flux can be selected by input. Intermediate micro timesteps with zero power (or flux) are not allowed.
- The required data for neutron induced transitions is automatically retrieved from preceding neutron physics calculations, if available on a standard data interface for system dependant group cross sections. The required microscopic onegroup cross sections can be prepared in any arbitrary way. If no data from a preceding calculation is available for an isotope, the data of the BURNUP libraries is applied.

The procedure KARBUS, mentioned before, is the main code for the automated application of BURNUP. The main characteristics of this procedure are:

- Number density and geometry data can be provided with the help of the codes NDCALC (global zone specifications) and NDWIMS (detailed specifications) as described in section 2.1. All informations needed in the subsequent programs are generated in these modules.
- Macroscopic group constants for reactor zones can be calculated in different routes, selectable by input:
  - Standard or modified FBR methods with the codes GRUCAL or GRUCAH.
  - Cell calculations in a onedimensional “Wigner-Seitz” model, using the codes GRUCEL, WEKCPM/ONETRA and ONEHOM, as described in section 2.1.

If several reactor zones are calculated in one KARBUS run, mixing of these routes can be applied, eg. for fuel and reflector zones.

- Improvement of macroscopic group constant data by more sophisticated methods may be applied, f.e.:
  - Iterative calculation of the mean fission spectrum in a reactor zone containing several fissionable isotopes (module CHICOR).
  - Direct calculation of effective group cross sections in the energy region with resolved cross section resonances (module RESABK).
  - Direct calculation of effective group cross sections in the 69 WIMS energy group structure from 334 fine group calculations (preliminary module REMOCO).
- Global reactor calculations may be performed, if required. The procedure KARBUS enables both cell burnup calculations and detailed whole reactor burnup calculations. The weighting spectra for the determination of the onegroup depletion data are taken from the last flux calculation performed, i.e.:
  1. The flux in the corresponding zone of the global reactor model if a global reactor calculation has been performed.
  2. The flux in the fuel zone of the "Wigner-Seitz" cell if no global reactor calculation has been performed and the macroscopic group constant calculation was performed with a cell calculation.
  3. The flux of a fundamental mode calculation for the homogenized reactor zone in the case of application of the codes GRUCAL or GRUCAH for the macroscopic group constant generation. A constant zero buckling is applied for subcritical reactor zones, otherwise a critical buckling search is performed.

For the **global reactor calculations** the following programs may be selected:

- For twodimensional diffusion calculations, mainly in (R-Z) geometry, the KfK code DIXY [28]. Evaluations are performed by DIXY modules and by a special module DXPODA.
- For threedimensional diffusion calculations, the KfK code D3E [29]. Evaluations are performed with the module AUDI3 [30].

- For onedimensional transport calculations (eg. for shielding problems), the  $S_n$  code ONETRA, mentioned before.
- The calculation of onegroup data is performed in the module COLLUP.
- The burnup calculations are performed with the module BURNUP.
- The archivation of relevant results on standard KAPROS archives is automatized. Depending on the complexity of the problem, the amount of archived data may be controlled by input.

### 3.2 Validation investigations.

At the beginning of the APWR investigations at KfK, the reactivity loss during burnup was quite uncertain. As pointed out in reference [31], publications in the years 1981 to 1983 claimed differences in the reactivity loss per full power day by a factor of two for comparable systems. Consequently, the calculational procedures for fuel burnup investigations also have been validated with the help of benchmark problems and of reactor experiments, as far as available. Here two activities will be discussed to some extend:

1. Participation in the NEACRP HCLWR burnup benchmark, already discussed in section 2.3.1 for the BOC voiding behaviour. Figure 7 shows a comparison for the benchmark case 2 with  $V_m/V_f = 1.1$  for the old library G69HOT (no  $Pu^{242}$  2.67 eV shielding) and a newer one G69HT005 with corrected  $Pu^{242}$  data with the mean values of all benchmark solutions as reported in reference [22] (the G69HOT results are excluded). We can observe good agreement between the G69HT005 and the mean results.
2. Analysis of the results of the "Isotope Correlation Experiment" ICE, performed in the PWR at Obrigheim in W.-Germany, reported in reference [32]. This experiment also was analyzed for the KORIGEN verification work [26]. For the ICE experiment five fuel assemblies were irradiated in the Obrigheim PWR for an in-core time of 1316 days, reaching about 30 GWd/Thm. From each fuel assembly two batches were prepared for analysis in a number of international laboratories. The reference [32] summarizes the results of these investigations. For the KARBUS cell burnup calculations the life history of the fuel was discretized into 29 macro time steps, containing a variable number of

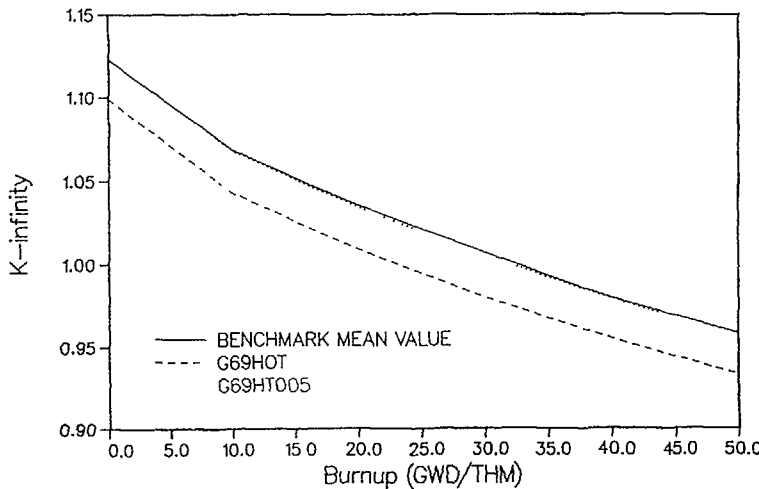
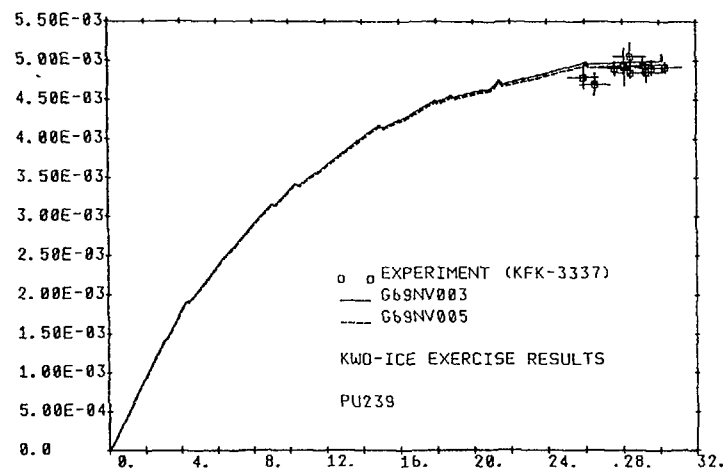
FIG. 7. NEACRP HCLWR burnup benchmark case 2,  $V_m/V_f = 1.1$ .

FIG. 8. Atoms/IMA as a function of burnup (GWd/Thm).

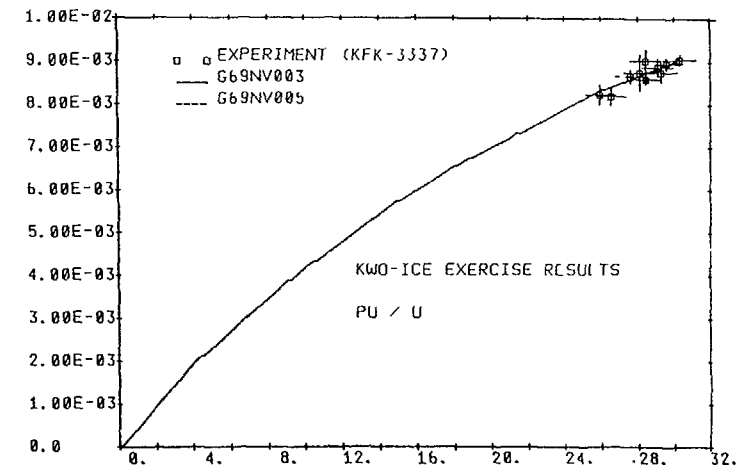


FIG. 9. Atom ratios as a function of burnup (GWd/Thm).

micro time steps. The total number of time steps was 53, including 365 days cooling time after reactor life. The boron concentration was changed after every macro time step on the basis of informations about the reactor control from the manufacturer [33].

The results of the KARBUS cell burnup calculations show quite good agreement with the experimental data, especially for the main fuel isotopes, being important for the reactor criticality. Figures 8 and 9 show the build-up of  $Pu^{239}$  and the ratio  $Pu/U$  in the  $UO_2$  fueled Obrigheim PWR, calculated with the libraries G69NV003 and G69NV005, using standard calculation methods. The agreement is satisfactory.

These results for the NEACRP burnup benchmark and the ICE experiment give good confidence for APWR burnup investigations with our procedures.

#### 4 Fuel assembly modelling.

The first whole core investigations utilized crude models for the fuel assemblies. Usually, the assembly materials not belonging to the infinite lattice, were approximated by admixtures to this lattice. In reference [34] a systematic investigation of this problem may be found. An important advantage of this fuel assembly model is the possibility to perform burnup calculations

for these modified infinite lattices within whole core investigations, using the whole core spectra for the onegroup calculation for the depletion. However, the problem is more complicated in the case that the fuel assembly contains rod positions to be used for reactor control. Here more detailed fuel assembly models are necessary. The calculation of a hexagonal fuel assembly, containing a number of control rod positions with absorber or follower material is not simple. In reference [35] a comparative study for this problem has been performed. Three alternative transport theory based methods have been compared:

1. Two-step cell calculation:

- Cell calculation for the infinite fuel array, followed by a
- Supercell calculation for a control rod position, filled with absorber or follower, surrounded by the homogenized fuel data from the preceding cell calculation and other fuel assembly components.

For the cell calculations collision probability methods are used.

2. Use of a twodimensional multigroup collision probability method.

3. Twodimensional continuous energy Monte Carlo calculations. Both last methods enable an exact modelling of the fuel assembly.

The result of these investigations is that the simplified first two-step method is accurate enough for exploratory investigations. The two-step method has the tendency to overestimate the control rod worths with increasing  $B^{10}$  enrichment, but the maximum deviation from the direct methods is rather small (about 5 % at 90 %  $B^{10}$  enrichment).

These results give a justification for our first more detailed fuel assembly calculations. A two-step procedure has been established, similar to the approach in reference [35]. The supercell model for these calculations is shown in figure 10. The surrounding of the control rod is represented in detail. The outer radius of the fuel is determined by the number of control rods within the fuel assembly. The outer zone represents spacer materials and additional water at the fuel assembly edges. The two calculational steps are:

1. Infinite lattice calculations with GRUCEL, WEKCPM and ONEHOM.
2. Supercell calculations with ONETRA.

With this calculational model, fuel assembly calculations have been performed for absorber and follower configurations for different burnup stages,

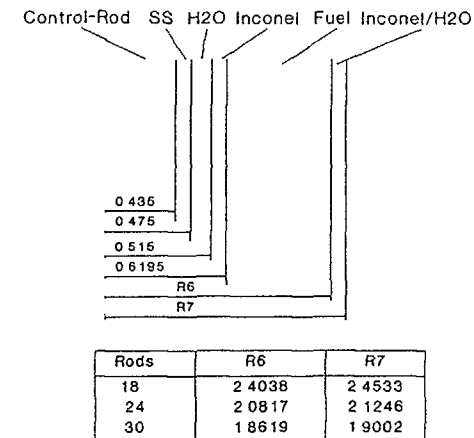


FIG. 10. One dimensional supercell model of APWR fuel assembly.

different temperatures, different  $B^{10}$  concentrations in the coolant and different coolant densities. In this way a data base for whole core analysis has been created.

It is also intended to validate the onedimensional supercell procedure with the model of figure 10. However, at the present time at KfK there is no adequate code available for the calculation of a hexagonal APWR fuel assembly with single control rod positions.

## 5 Whole core calculations.

In order to reliably estimate the characteristics of an advanced reactor, it is necessary to perform whole core calculations. The required refinement of these core calculations depends on the refined description of the core internals. At the beginning of our APWR investigations, we applied rather crude approximations for the fuel assemblies. Consequently, it was justified to apply less detailed models for the core calculations. As described in section 3.1, the procedure KARBUS enables the combination of macroscopic cross section calculation, global reactor calculation and burnup calculation within one computer run. The main restriction is the relatively poor approximation for the description of the fuel assemblies: additive materials are treated as admixtures of the basic infinite lattice cell. Most of the core investigations,

we have performed until now, are based on these principles. In reference [31] first cycle core calculations have been presented for two reactor types, a homogeneous core with a single fuel assembly type and a heterogeneous core with two assembly types (seed, blanket). These calculations have been performed with the procedure KARBUS, using the  $(R, Z)$  option of the code DIXY for the homogeneous core and the  $(\Delta, Z)$  option of the D3E/AUDI3 route for the heterogeneous core.

For more complicated multi cycle calculations with fuel management new calculational procedures have been developed on the basis of precalculated cell or fuel assembly burnup data. In reference [34] this principle has been applied with some simplifications for the determination of the cross sections at arbitrary burnup stages: on the basis of cell burnup calculations with a rather fine burnup mesh, the most reasonable values from this burnup tables were taken. In the meantime a new module XSPROC has been developed for the interpolation of these burnup dependant cross sections.

Starting from the experience during the investigations of reference [34] new procedures have been developed for the more complicated multi-cycle calculations:

1. A new data library has been created, containing cell or fuel assembly data for the most important fuel parameters:

- Fuel, clad and moderator temperatures.
- Moderator density.
- Moderator  $B^{10}$  concentration.
- Fuel burnup.
- Control rod specification (number of rods, rods in/out).

On the basis of the results of preceding cell or fuel assembly burnup calculations, stored on standard KAPROS archives, the new program CXSLIB creates a library HXSLIB, containing the data needed for core calculations.

2. A corresponding KAPROS procedure for the organisation of reactor calculations, starting from the HXSLIB library: ARCOSE, Advanced Reactor COre SEimulator, with the following features:

- The whole core calculations are performed with the nodal code HEXNODK, being developed on the basis of the KWU code

HEXNOD [36]. Only minor changes have been made for the implementation in the KAPROS system and for the representation of the results.

- The preparation of the burnup dependant cross sections in the reactor zones is based on the interpolation of HXSLIB library burnup data.
- A criticality search by change of the  $B^{10}$  concentration of the moderator can be performed, using interpolated cross sections from the HXSLIB library.
- The preparation of the burnup pattern in a threedimensional core model can be started from a twodimensional precalculation.
- The arbitrary insertion of an arbitrary number of fuel assemblies with control rods is allowed for a threedimensional core model. Also fuel assembly clusters can be handled. Until now, an automatized change of control rod insertions is not yet realized.
- An arbitrary number of time steps within one core cycle is allowed. A criticality search is performed after each timestep.
- Fuel assembly shuffling can be performed after each core cycle. The present version enables two shuffling strategies:
  - The fuel assemblies are shuffled in a fixed pattern ("absolute addressing").
  - The fuel assemblies are shuffled in a predefined order with respect to the burnup ("relative addressing").
- An arbitrary number of succeeding fuel cycles, using the same fuel assembly shuffling strategy, is allowed. The number of whole core calculations is only restricted by the computer resources (eg. computing time, storage requirements). For the investigations of reference [23] 7 cycles were completed with 10 micro timesteps each.

The 8th macro timestep was terminated, because the ARCOSE graphic interface file could not be extended any more (computer restriction).

- Restart options are available for several purposes, like:
  - Calculation of succeeding cycles.
  - Parameter variations, as temperature, boration, waterdensity.

- All relevant results are stored with a special format on a graphics interface file. A DISSPLA based interactive plotting procedure at KfK enables the direct representation of these results [37].

Figure 11 shows a flowchart for the stages of neutron physics calculations, as realized at the present time. The archives 1 and 2 are standard KAPROS archives. Figure 12 is a typical plot, directly produced from the ARCOSSI interface file with the program PLY. The axial power rating of fuel assembly nr. 2 is given. Every curve is identified uniquely with information about cycle,  $k_{eff}$  of the core, full power days in the cycle,  $B^{10}$  content in the water, axial form factor and fuel assembly identification. The differences between the 6th and 7th cycle are small.

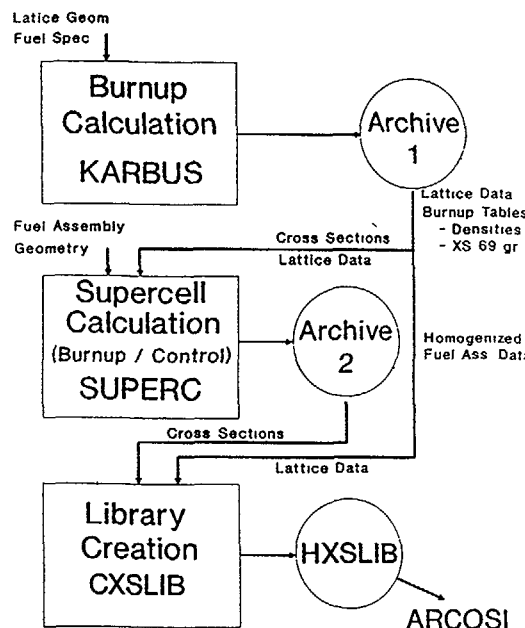


FIG. 11. Calculation scheme, normal case.

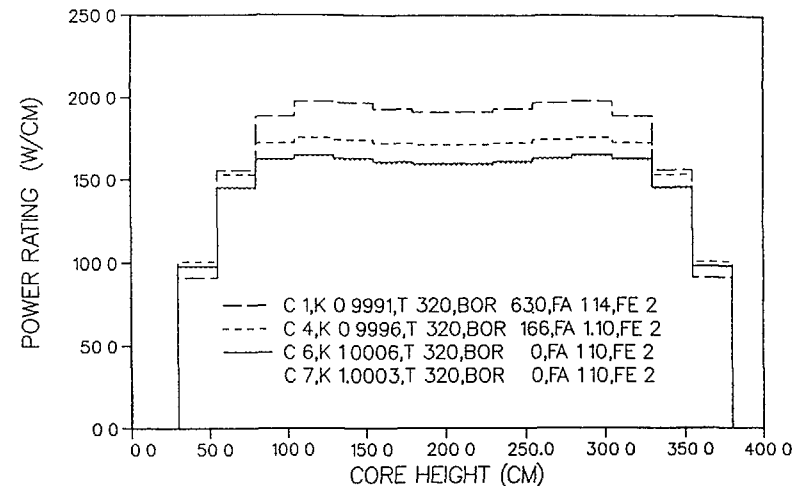


FIG. 12. KfK HCLWR design, power rating for cycles 1, 4, 6, 7.

## 6 Summary.

The present paper gives an overview of the developments at KfK during the past 10 years, related to the neutronics investigations of a tight lattice high converting PWR (the so-called Advanced Pressurized Water Reactor APWR). The principal objective of these investigations was the reliable prediction of the neutronic longterm behaviour of an APWR core for all coolant conditions (voiding problem). Systematic developments of data libraries and calculational procedures and improvement of the models for the description of the APWR cores enable at present reliable exploratory longterm investigations for an advanced PWR core with the following characteristics:

- hexagonal fuel assemblies and
- reactor control by water boration or control rods in selected fuel assemblies.

The applied data and methods are validated satisfactorily for the range of core parameters of interest at present.

In the near future consistent data libraries for different calculational procedures, described above, will be established on the basis of a reliable modern basic nuclear data file, probably JEF-2.

## References

- [1] M.C. Edlund "High Conversion Ratio Plutonium Recycle Pressurized Water Reactors"  
Annals of Nuclear Energy 2, 801 (1975)
- [2] Special Issue "Prof. Wirtz"  
Nuclear Technology Vol. 71, No. 1 (1985)
- [3] Special Issues on "Advanced Light Water Reactors"  
Nuclear Technology Vol. 80, No. 1,2 (1988)
- [4] H.D. Berger, A.W. Rowe, C. Broeders, M. Schatz "Überprüfung der Berechnungsverfahren für enge Reaktorgitter von Fortschritten Druckwasserreaktoren (FDWR) an experimentellen Anordnungen"  
KFK 3389 / IfRR K 8212 (1982)
- [5] J.R. Askew, F.J. Fayers, P.B. Kemshell "A General Description of the Lattice Code WIMS"  
Journal of British Nuclear Energy Society, 5,564 (1966)
- [6] D. Woll "GRUCAL, Ein Programmsystem zur Berechnung makroskopischer Gruppenkonstanten"  
KFK 2108 (1975)
- [7] V. Brandl  
"User Manual for the KAPROS Module ONETRA (based on ONE-TRAN, a one-dimensional SN Code by T.R. Hill, LASL, USA)"  
Internal KfK report, PB01.02.04P41A (1980)
- [8] T.R. Hill  
"ONETRAN, A Discrete Ordinates Finite Element Code for the Solution of the One-Dimensional Multigroup Transport Equation"  
LA-5990, Los Alamos National Laboratory (1975)
- [9] H. Bachmann, G. Buckel, W. Hoebel, S. Kleinheins "The Modular System KAPROS for Efficient Management of Complex Reactor Calculations"  
Proc. Conf. Computational Methods in Nuclear Energy, Charleston, CONF-750413 (1975)
- [10] B. Krieg, I. Broeders "The KfK-Version of the Neutron and Photon Cross Section Generation Code NJOY:Implementation, Verification and Modification of the Code"  
JEF-DOC 194 (1985)
- [11] B. Riik, R. Rühle "RESAB-II, Ein Programm zur Berechnung von Gruppenkonstanten im Resonanzbereich nach der Stoßwahrscheinlichkeitsmethode"  
IKE Bericht Nr. 3.3-6.1209 (1972)
- [12] R. Böhme, J. Axmann, C.H.M. Broeders, S. Pelloni, M. Schatz "Improvements in the Prediction of LWHCR Lattice Parameters"  
This Meeting
- [13] R. Böhme, E.A. Fischer "The Fast Reactor Cell Code KAPER4"  
KfK 4435 (1988)
- [14] B. Goel, B. Krieg "Status of the Nuclear Data Library KEDAK4"  
KfK 3838 (1984)
- [15] I. Broeders, B. Krieg "MIGROS-3: A Code for the Generation of Group Constants for Reactor Calculations from Neutron Nuclear Data in KEDAK Format"  
KFK 2388 (1977)
- [16] H. Gruppelaar  
Private Communication (1982)
- [17] E. Kiehaber "The KFKINR-Set of Group Constants; Nuclear Data Basis and first Results to the Recalculation of Fast Zero Power Reactors"  
KFK 1572 (1972)
- [18] C.H.M. Broeders "Neutron Physics Investigations for Advanced Pressurized Water Reactors"  
Nuclear Technology Vol.71, p.96 (1985).
- [19] I. Broeders "Status of and Further Activities on Processing Codes for Coarse Groups (MIGROS-2) and Fine Groups (FIDAS)"  
Seminar on Nuclear Data Processing Codes. Ispra 5-7 December 1973.  
EACRP-U-52, NEA Newsletter No 16.

- [20] S. Pelloni, J. Stepanek, P. Vontobel "Analysis of PROTEUS Phase II Experiments Performed Using the AARE Modular System and JEF-Based Libraries"  
NSE 103, p 247 (1989)
- [21] Y. Ishiguro, H. Akie, H. Takano "Proposal of Benchmarks on Data and Methods to Calculate Reactor Characteristics in High Conversion Light Water Reactors"  
NEACRP-A-789 (1986)
- [22] H. Akie, Y. Ishiguro, H. Takano "Summary Report on the International Comparison of NEACRP Burnup Benchmark Calculations for High Conversion Light Water Reactor Lattices"  
NEACRP-L-309 (1988)
- [23] C.H.M. Broeders, M. Dalle Donne "Neutronphysics and Thermohydraulics Design of a Reference High Conversion PWR"  
This Meeting
- [24] C.H.M. Broeders  
"Überlegungen zur Gestaltung eines Programmsystems für Untersuchungen zum nuklearen Brennstoffkreislauf"  
Internal KfK report, PB01.05.07P81B (1982)
- [25] M.J. Bell "ORIGEN- The ORNL Isotope Generation and Depletion Code"  
ORNL-4628 UC-32 (1973)
- [26] U. Fischer, H.W. Wiese "Verbesserte konsistente Berechnung des nuklearen Inventars abgebrannter DWR-Brennstoffe auf der Basis von Zell-Abbrand-Verfahren mit KORIGEN"  
KfK 3014 (1983)
- [27] E. Stein, E. Wiegner, C. Broeders "Kurzbeschreibung des KAPROS-Moduls BURNUP"  
Internal KfK report, PB 01.05.07P81D (1982)
- [28] W. Hoebel  
"Numerical Methods Used in the Two-Dimensional Diffusion Program DIXY"  
Fast Elliptic Solvers, U. Schumann, Ed., Advanced Publications (1977)
- [29] B. Stehle  
"Code Abstract for D3D and D3E"  
Proceedings ANS Topical Meeting Advances in Reactor Computations, p. 209, American Nuclear Society (1983)
- [30] G. Willerding  
"AUDI3, ein Programm für Störungsrechnung 1. Ordnung und andere Auswertungen der Ergebnisse von 3-dimensionalen Multi-Gruppen Difusionsrechnungen"  
Internal KfK report, PB 01.02.04 P81G (1982)
- [31] C.H.M. Broeders, M. Dalle Donne "Conceptual Design of a  $(Pu, U)O_2$  Core with a Tight Fuel Rod Lattice for an Advanced Pressurized Light Water Reactor"  
Nuclear Technology Vol.71, p.82 (1985).
- [32] L. Koch, S. Schoof, editors "The Isotope Correlation Experiment ICE" ESARDA 2/81, EUR 7766 EN, KfK3337 (1981).
- [33] H.W. Wiese "KARBUS Input Data for KWO Cell Burnup Calculation"  
Private communication (1990)
- [34] B. Klüver "Ganzcore-Abbrandrechnungen für einen fortgeschrittenen Druckwasserreaktor mit dem Programmsystem KARBUS"  
Technische Universität Braunschweig, K8804 (1988)
- [35] K. Okumura, Y. Ishiguro, K. Tsuchihashi "Calculational Methods of Control Rod Worth for High Conversion Light Water Reactor"  
Journal of Nuclear Science and Technology, Vol. 25, p.318 (1988)
- [36] M.R. Wagner "Three-Dimensional Nodal Diffusion and Transport Theory Methods for Hexagonal-Z Geometry"  
NSE 103,4 p 377 (1989)
- [37] E. Stein "PLY: Graphics for PLOTEASY curves. SPF-Procedure at the KfK Computing Center"  
Private communication (1989)

## HEXNOD AND HEXMED, NODAL REACTOR CODES FOR THE DESIGN OF HIGH CONVERTER REACTORS

M.R. WAGNER, W. FRANCIS<sup>†</sup>

Siemens AG,  
Unternehmensbereich KWU,  
Erlangen, Federal Republic of Germany

### Abstract

The purpose of the paper is to describe the nodal reactor codes HEXNOD and HEXMED which are used for high converter reactors at SIEMENS/KWU. HEXNOD is a three-dimensional nodal diffusion and transport theory program for reactors with hexagonal-z geometry. The code is based on advanced hexagonal nodal methods for solving global diffusion theory and nodal transport problems for fast reactors and light water high converter reactors (LWHCR). The methods have a high accuracy and efficiency for 3D fast reactor benchmark problems. The present paper gives similar benchmark results for epithermal and thermal reactor systems. The numerical results for HTGR and thermal reactor benchmark problems of the Soviet PWR types VVER-440 and VVER-1000 show that HEXNOD, with one single node per assembly, is as accurate as conventional finite difference computer codes using a mesh of 96 triangles per hexagon. The computing times of HEXNOD are extremely small and allow to perform 3D calculations routinely with reliable results at very small costs. On the basis of HEXNOD the hexagonal nodal reactor burnup program HEXMED has been developed for LWHCR design calculations, allowing 4 to 10 energy groups. HEXMED is a microscopic burnup program. Based on a library of microscopic cross sections the nuclide depletion equations for multi-branched nuclide chains are solved nodewise with the local assembly spectrum.

Main operational features of HEXMED are:

- flexible control of time stepping
- refueling operator for the removal, shuffling and loading of fresh fuel assemblies
- movement of control rods in bank configuration
- criticality search with control banks in discrete axial steps
- criticality search with soluble boron
- computation of the axial variation of moderator temperatures and densities.

### 1 Introduction

This paper describes the 3D nodal reactor codes HEXNOD and HEXMED for hexagonal -z geometry which are presently used at SIEMENS/KWU as the basic computer programs for PWHCR core design calculations. Section 2 describes the static 3D multigroup program HEXNOD which is based on advanced nodal diffusion and nodal transport theory methods. These methods are very powerful both with respect to accuracy and computational efficiency, as

has been demonstrated in a recent publication for a number of fast reactor benchmark problems. In a second step the nodal 3D reactor burnup program HEXMED was developed which is based on the HEXNOD neutronics module. Section 3 describes the basic features and various computational options of the code HEXMED. Finally, in sections 4 and 5 numerical results are presented which demonstrate the accuracy of both programs for the epithermal spectrum reactor HTGR and for thermal reactors of the Soviet PWR type WWER-440. From the results described in sections 4 and 5 it is concluded that the codes HEXNOD/HEXMED are very powerful tools for PWHCR core design and fuel management calculations. Applications of HEXMED are described in a companion paper of this meeting.

### 2 HEXNOD - Static 3D Nodal Diffusion and Transport Theory Program for Hexagonal -z Geometry

Due to the tight lattice the fuel subassemblies of pressurized water high converter reactors (PWHCR) are hexagonal which requires that computer codes for the design of the PWHCR must describe exactly the hexagonal geometry of the reactor core. Therefore, hexagonal nodal methods and computer codes have been developed at Siemens/KWU in close analogy to the Cartesian geometry advanced nodal methods /1-3/. These methods were originally pioneered by KWU in the 1970's /4-6/ which have become, by now, the standard computational tools for fuel management calculations for conventional LWR's, at KWU and many other vendors and utilities.

The first step was the development of three-dimensional nodal diffusion and transport theory methods for hexagonal -z geometry which were then implemented in the static nodal reactor code HEXNOD. The newly developed nodal methods are described in a recent publication /7/. Nodal methods for hexagonal geometry are also very useful for fast reactor applications. Therefore, the accuracy and the efficiency of both the nodal diffusion theory (DT) and the nodal transport theory (NT) methods in HEXNOD, have been tested for several mathematical fast reactor benchmark problems. This work was done in cooperation with Kernforschungszentrum Karlsruhe (KFK) and INTERATOM. The results have been described in some detail in the above mentioned paper /7/. It was shown that for these fast reactor problems the computational errors of the diffusion theory option of HEXNOD are considerably smaller than those of conventional finite difference diffusion theory codes using a radial mesh of 54 triangles per hexagon. The computing time of HEXNOD is about a factor of 25 smaller than for FDM calculations of comparable accuracy. It was also shown /7/ that HEXNOD allows to solve three-dimensional global fast reactor problems in transport approximation with very small computing costs. Because of the lack of three-dimensional discrete ordinate codes the accuracy of the nodal transport option of HEXNOD was demonstrated in corresponding 2D fast reactor problems by comparing with the triangular mesh  $S_N$  code TWOHEX.

The results /7/ show that the errors relative to the  $S_N$  reference solution are of the same order as those of corresponding nodal diffusion theory calculations relative to the diffusion theory reference solution, while the computing time increases only by about 50 %. Finally, a direct verification of the transport theory option of HEXNOD for the extremely difficult three-dimensional KNK benchmark problem was obtained by comparison with Monte Carlo calculations with remarkably good results /7/.

The application of HEXNOD to light-water reactors presents a new problem class. The hexagonal fuel assemblies of the PWHCR are considerably larger, in terms of mean free paths, than for fast reactors. Hence, it was considered necessary to verify the accuracy of the code explicitly by comparing with existing benchmark solutions for epithermal and thermal reactor systems. This is shown in sections 4 and 5 of this paper. Before we come to the discussion of the computational results a description of the hexagonal nodal reactor burnup code HEXMED is given in the next section.

### 3 HEXMED - 3D Nodal Reactor Fuel Management Program for Hexagonal -z Geometry

On the basis of the HEXNOD neutronics module the reactor burnup program HEXMED was developed for use in PWHCR design calculations. In the following the basic features and various computational options of HEXMED are briefly described:

1. HEXMED is used, typically, with 4 to 8 energy groups. Except for some small number of local storage fields dynamic storage allocation is used so that the upper limit of energy groups is more or less arbitrary.
2. HEXMED is a microscopic reactor burnup program. Based on a precomputed library of microscopic cross sections the nuclide depletion equations are solved nodewise to compute the average isotopic nuclide densities corresponding to the local burnup of each node. The isotopic reaction rates are calculated according to the local spectrum so that history effects are explicitly taken into account.
3. Multi-branched nuclide depletion chains are defined via user input at execution time. The method of integration of the depletion equations allows for nuclide coupling, such as  $\alpha$ -n or n-2n reactions, which lead back to predecessors in the depletion chains.
4. At each time point the user can choose to solve either for k-effective or for the critical concentration of soluble boron. For static problems HEXMED allows also to solve adjoint eigenvalue or fixed source problems.
5. Control rods of several different types are represented in terms of control rod banks which may be inserted at any time point in several configurations. In 3D calculations a criticality search with control rods can be performed in discrete steps according to the axial mesh used in the calculation.
6. The time stepping procedure of HEXMED allows to redefine the operational code options and parameters at every time point during the reactor burnup calculation.
7. At the end of a reactor cycle a reload operation is performed. Fuel assemblies may be discharged from the core or shuffled into other locations. Finally fresh fuel is loaded into the empty core positions.

8. HEXMED uses a simple model for computing the axial and radial variation of the moderator density and the fuel temperature, similar to the corresponding approximation in the nodal fuel management code MEDIUM /2/ for Cartesian geometry.
9. Presently preparations are being made to include the representation of space-dependent neutronic feedback effects such as local Doppler and Xe distribution as well as the computation of various reactivity and temperature coefficients.
10. The HEXNOD neutronics module in HEXMED allows to utilize this program also for assembly transport calculations. A DP<sub>1</sub> approximation is used at the interfaces of the hexagonal nodes which, in this case represent homogenized pin cells.

Summarizing, the code HEXMED is an accurate, flexible and very efficient reactor burnup program and a valuable tool for fuel management calculations in hexagonal geometry for several types of reactors, not limited to the tight lattice PWHCR. Some applications of HEXMED are described in a companion paper /8/ of this meeting.

### 4 Numerical Calculations for HTGR Benchmark Problems

This section describes results of benchmark calculations with HEXNOD which have been carried out in order to investigate the error of the nodal diffusion theory approximation for the high temperature gas-cooled reactor (HTGR). This is an epithermal spectrum reactor and in this respect similar to the PWHCR. The numerical results of HEXNOD are compared with well-established reference solutions for 2D and 3D benchmark problems that were published in the literature.

The three-dimensional HTGR Benchmark Problem was initially defined by Steinke /10/ and the complete problem specification, including a set of 4-group macroscopic cross sections, is given in the Benchmark Problem Book ANL-7416 /11/, supplement 2. It represents a 60-degree sector of an HTGR with a half-inserted central rod and a ring of six fully inserted control rods (full core). A 2D companion problem is also defined which corresponds to a horizontal plane through the upper rodded half of the core. For both problems a number of solutions are given in ANL-7416, Suppl. 2 and 3, and elsewhere /12,13/. This allows a meaningful comparison of the accuracy of various computational methods for this type of problem.

#### 4.1 Two-Dimensional HTGR Problems

Table 1 gives a summary of computational results for the 2D HTGR problem. The table shows the eigenvalues obtained with finite difference, finite element and a number of different nodal methods. The errors relative to the most accurate reference solution which was obtained by Gado and Schmidt /11/ with the FEM code DIFGEN /14/, using 18 triangular finite elements of second order, are given in column 4 of Table 1. Also shown

**Table 1**  
**2D HTGR Benchmark Problem (7 Rods)**  
**Comparison of Computational Results**

| Code        | Mesh                | k-effective | $\epsilon_k(\%)$ | $\text{Max} \epsilon_p(\%) $ | CP-Time<br>sec | Computer    |
|-------------|---------------------|-------------|------------------|------------------------------|----------------|-------------|
| VENTURE     | $6\Delta$           | 1.12028     | 0.182            | n.a.                         | 19             | IBM 360/91  |
|             | $24\Delta$          | 1.11891     | 0.059            | n.a.                         | 59             | /195        |
|             | $54\Delta$          | 1.11860     | 0.031            | n.a.                         | 173            | /195        |
|             | $\infty$            | 1.11835     | 0.009            | n.a.                         |                |             |
| BUGTRI      | $6\Delta$           | 1.11672     | - 0.137          | 8.28                         | 115            | Univac 1108 |
|             | $24\Delta$          | 1.11777     | - 0.043          | 2.07                         | 796            |             |
|             | $96\Delta$          | 1.11815     | - 0.009          | 0.48                         | 9654           |             |
|             | Extrapolated        | 1.11828     | - 0.003          |                              |                |             |
| DIFGEN      | $18\Delta$ , 1.ord. | 1.11633     | - 0.172          | 4.03                         | 8.2            | CRAY-1      |
|             | $6\Delta$ , 2.ord.  | 1.11820     | - 0.005          | 0.07                         | 9.6            |             |
|             | $18\Delta$ , 2.ord. | 1.11825     | Reference        |                              | 49.5           |             |
| SIXTUS-2    | 1                   | 1.11917     | 0.082            | 1.42                         | 100            | CYBER 720   |
| HEXAN       | 1                   | 1.11888     | 0.055            | 1.02                         | 537            | EC-1040     |
| DIF3D-Nodal | 1                   | 1.11857     | 0.029            | 1.6                          | 700            | IBM 3033    |
| HEXNOD      | 1                   | 1.11819     | 0.005            | 0.35                         | 3.33           | CYBER 176   |

n. a. not available

are the maximum errors of the power density of the hexagonal subassemblies, if available. It is seen from Table 1 that the conventional finite difference diffusion theory programs VENTURE /15/ and BUGTRI /16/ require a radial mesh of at least 54 triangles per hexagon to obtain an accuracy of about  $3 \cdot 10^{-4}$  in k-efficteve and to reduce the maximum error of the assembly powers to below 2 %. On the other hand, the errors of HEXNOD are nearly one order of magnitude smaller, even though a mesh of one single node per hexagon is used. Compared to the code VENTURE the computing time of HEXNOD is about a factor of 50 smaller. HEXNOD compares also favourably with the other nodal codes HEXAN /17/ and DIF3D-Nodal /18/.

Gado /12/ has also published results with DIFGEN for a number of related 2D problems with several different control rod configurations, Table 2. This allows to determine the accuracy with which HEXNOD computes the rod worths of these configurations. It is seen from the data given in the lower half of Table 2 that the relative errors of  $\Delta p$  for all three rodded configurations are equal to or less than 0.12 % in absolute value which is very satisfactory.

#### 4.2 Three-Dimensional HTGR Benchmark Problem

A similar comparison of computational results for the 3D HTGR Benchmark Problem is presented in Table 3. Except for HEXNOD, the data shown in this table are taken from references /11/ and /13/. Again, results are given for finite difference, finite element and nodal calculations. The errors quoted in Table 3 are relative to the DIFGEN second order finite element calculation which is considered as the reference solution. The best finite difference solution still has an eigenvalue error of  $3 \cdot 10^{-4}$  and the error of the axially integrated assembly powers is about 2 %. Results of the same order of accuracy are obtained with the nodal option /18/ of the code DIF3D. However, some caution may be indicated, because the agreement between the best FDM and FEM solutions is not as good as for the corresponding two-dimensional problem, Table 1. Nevertheless, one finds that HEXNOD with 16 axial layers agrees with the DIFGEN reference solution within the same error band as was shown in Table 1 for the 2D case. The computing time of HEXNOD is considerably less than 1 min on the CDC 990 computer.

#### 5 Benchmark Calculations for Thermal Reactors

A second series of numerical calculations is described in this section. These calculations refer to thermal reactors of the Soviet PWR type WWER-440 for which two- and three-dimensional benchmark problems have been defined by Grundmann /19/.

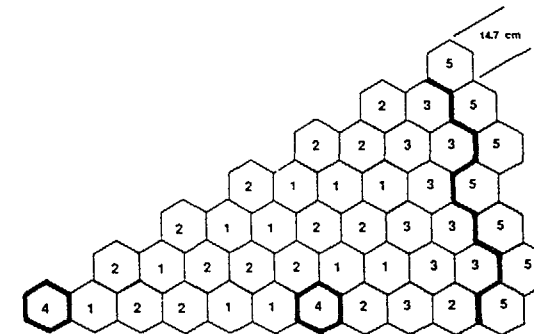
The first test case is a two-dimensional two-group model problem which represents a 30-degree sector of the reactor WWER-440. The geometry and the material distribution are shown in Fig. 1. The core contains fuel of three different enrichments, 7 control rods (full core), and one row of hexagonal reflector assemblies. Vacuum boundary conditions are assumed at the outer boundary. Fig. 1 also shows the geometry of a corresponding 3D

**Table 2**  
**2D HTGR Benchmark with Control Rods**

| Code    | Mesh          | k-effective |         |                            |         |               | Max. node power Pmax |        |        |            |              |
|---------|---------------|-------------|---------|----------------------------|---------|---------------|----------------------|--------|--------|------------|--------------|
|         |               | 0           | 6       | 7                          | 37      | control rods  | 0                    | 6      | 7      | 37         | control rods |
| VENTURE | 6Δ            | 1.17539     | 1.13343 | 1.12028                    | -       | n.a.          | n.a.                 | n.a.   | -      |            |              |
| DIFGEN  | 6Δ , 1. order | 1.17538     | 1.12987 | 1.11605                    | 0.91646 | 1.6160        | 1.9786               | 1.2847 | 1.7640 |            |              |
|         | 6Δ , 2. order | 1.17545     | 1.13169 | 1.11820                    | 0.92825 | 1.6180        | 1.9718               | 1.3041 | 1.7681 |            |              |
| HEXNOD  | 1             | 1.17541     | 1.13170 | 1.11819                    | 0.92806 | 1.6199        | 1.9760               | 1.3041 | 1.7708 |            |              |
|         |               | Rod Worth   |         | $-\Delta p \times 10^{-2}$ |         | CP Time (sec) |                      |        |        | Computer   |              |
| VENTURE | 6Δ            | -           | 3.150   | 4.185                      |         | 20.4          | 22.8                 | 18.6   |        | IBM 360/91 |              |
| DIFGEN  | 6Δ , 1. order | -           | 3.427   | 4.523                      | 24.037  | 1.2           | 1.2                  | 0.9    | 1.1    | CRAY-1     |              |
|         | 6Δ , 2. order | -           | 3.290   | 4.356                      | 22.656  | 7.6           | 8.7                  | 7.3    | 7.5    |            |              |
| HEXNOD  | 1             | -           | 3.286   | 4.354                      | 22.676  | 3.4           | 3.5                  | 3.5    | 3.1    | CYBER 176  |              |

Table 3  
3D HTGR Benchmark Problem  
Comparison of Computational Results

| Code                | Mesh<br>rad./ax. | k-effective | $\varepsilon_k$ (%) | Max/ $\varepsilon_p$ (%)/ | CP-Time<br>sec | Computer  |
|---------------------|------------------|-------------|---------------------|---------------------------|----------------|-----------|
| VENTURE             | 6 $\Delta$ / 8   | 1.09069     | 0.063               | 17.                       | 131            | IBM 3033  |
|                     | /16              | 1.09063     | 0.058               | 10.                       | 234            |           |
| DIF3D-FDM           | 6 $\Delta$ / 8   | 1.09069     | 0.063               | 17.                       | 45             | IBM 3033  |
|                     | /16              | 1.09063     | 0.058               | 10.                       | 85             |           |
|                     | /32              | 1.09137     | 0.126               | 6.                        | 162            |           |
|                     | 24 $\Delta$ /64  | 1.09033     | 0.030               | n. a.                     | 2471           |           |
| DIF3D-NODAL         | 1 / 8            | 1.08992     | - 0.007             | 3.0                       | 47             | IBM 3033  |
|                     | /16              | 1.09028     | 0.026               | 2.0                       | 114            |           |
|                     | /32              | 1.09032     | 0.029               | 2.0                       | 230            |           |
| DIFGEN,<br>1. order | 6 $\Delta$ / 8   | 1.09130     | 0.119               | n.a.                      | 29.2           | CRAY-1    |
|                     | 6 $\Delta$ / 8   | 1.09000     | Reference           | -                         | 425.6          |           |
| HEXNOD              | 1 / 8            | 1.09013     | 0.012               | 0.42                      | 32.4           | CYBER 990 |
|                     | /16              | 1.09006     | 0.005               | 0.40                      | 38.5           |           |



2D Test Problem WWER-440 with Control Rods.  
Material assignments of a 30-degree sector.  
This map corresponds to the upper core half  
of the 3D WWER-440 test problem (below)

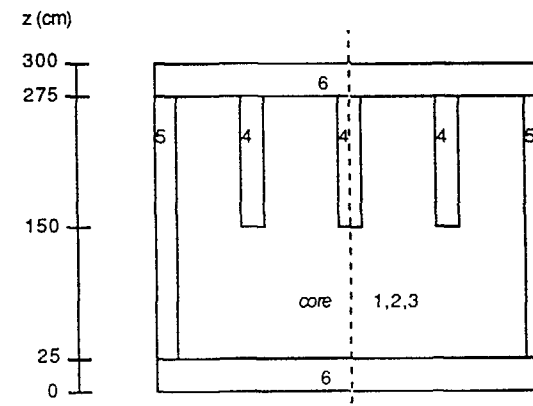


Fig. 1 Axial Geometry of the 3D Test Problem WWER-440.

Note: In the lower core half the control rods  
are replaced by fuel of type 2.

test problem WWER-440 with the control rods inserted to the core midplane. In the lower core half the control rods are replaced by fuel of type 2. The complete specification of the test problems WWER-440 was given by Grundmann /19/. This reference also presents numerical results which have been obtained by several authors with a number of finite difference and nodal codes. Some of these results are reproduced in Tables 4 and 5 and in Fig. 2.

Table 4 compares the eigenvalues as obtained with the corner mesh FDM code MNATA /19/ with increasingly refined radial meshes. An accurate reference solution for the nodewise power distribution of the 2D WWER-440 problem is shown in Fig. 2. This reference solution was obtained /19/ by extrapolating the results of MNATA with 6, 24, 54 and 96 triangles per hexagon. The extrapolated eigenvalue of MNATA is given in Table 4. It is seen from this table that all nodal codes compute the eigenvalue with an error of about  $5 \cdot 10^{-4}$  or better. This error is smaller than that of the FDM calculation with the finest spatial mesh of 96 triangles per hexagon. The maximum error of the power distribution is also much smaller than that of the fine mesh calculation. This is shown in more detail in Fig. 2 where the nodewise errors of the subassembly powers of HEXNOD/KWU and MNATA (96  $\Delta$ /hex) are compared.

In Table 5 some results are given for the 3D test problem WWER-440. Unfortunately, no reference solution of sufficient accuracy is known, other than those of the nodal codes HEXNOD23 and HEXNOD/KWU. The solution of the corner mesh FDM code OSCAR /19/ with a radial mesh of 54  $\Delta$ /hex and an axial mesh of 5 and 10 cm is not nearly accurate enough to be considered as reference solution. From the data in Table 5 it can be estimated that the true eigenvalue is about 1.0120. The k-effective of the nodal codes HEXNOD23 /19/ and HEXNOD/KWU are close to this value and agree with each other within  $1.5 \times 10^{-4}$ . Incidentally, it should be noted that HEXNOD and HEXNOD23 are different codes. The nodal methods of HEXNOD are based on the transverse integration procedure /5-7/ for all spatial directions whereas HEXNOD23 uses, in radial direction, a two-dimensional expansion in terms of Bessel and trigonometric functions, by replacing the hexagon by an equivalent cylinder.

**Table 4**  
2D Test Problem WWER-440  
Comparison of Computational Results

| Code           | Mesh/<br>Hexagon | k-eff    | $\epsilon_k$ (%) | Max  $\epsilon_p$ (%) | Comput.<br>Time<br>(sec) | Computer  |
|----------------|------------------|----------|------------------|-----------------------|--------------------------|-----------|
| MNATA          | 6 $\Delta$       | 1.016364 | 0.657            | 28.9                  | 64                       | BESM-6    |
|                | 24 $\Delta$      | 1.012119 | 0.237            | 11.5                  | 162                      |           |
|                | 54 $\Delta$      | 1.010899 | 0.116            | 5.9                   | 358                      |           |
|                | 96 $\Delta$      | 1.010418 | 0.068            | 3.5                   | 686                      |           |
| Extrapol.      | $\infty$         | 1.009730 | Reference        | -                     |                          |           |
| HEXAN          | 1                | 1.010267 | 0.053            | 1.2                   | 150                      | EC-1040   |
| HEXNOD 23      | 1                | 1.010252 | 0.051            | 1.2                   | 13                       | EC-1055   |
| HEXNOD/<br>KWU | 1                | 1.009901 | 0.017            | 0.7                   | 0.9                      | CYBER 176 |

**Table 5**  
3D Test Problem WWER-440

| Code       | Mesh/<br>Hexagon | Axial<br>Mesh<br>(cm) | k-eff   | Comput.<br>Time<br>(sec) | Computer  |
|------------|------------------|-----------------------|---------|--------------------------|-----------|
| OSCAR      | 6 $\Delta$       | 25.0                  | 1.0169  | 251                      | BESM-6    |
|            | 24 $\Delta$      | 12.5                  | 1.0133  | 1415                     |           |
|            | 54 $\Delta$      | 5.0/10.0              | 1.0124  | 6000                     |           |
| HEXNOD 23  | 1                | 25.0                  | 1.01172 | 305                      | EC-1055   |
|            | 1                | 12.5                  | 1.01164 | 783                      |           |
|            | 1                | 6.25                  | 1.01164 | 1750                     |           |
| HEXNOD/KWU | 1                | 25.0                  | 1.01157 | 11                       | CYBER 990 |
|            | 1                | 12.5                  | 1.01156 | 15                       |           |

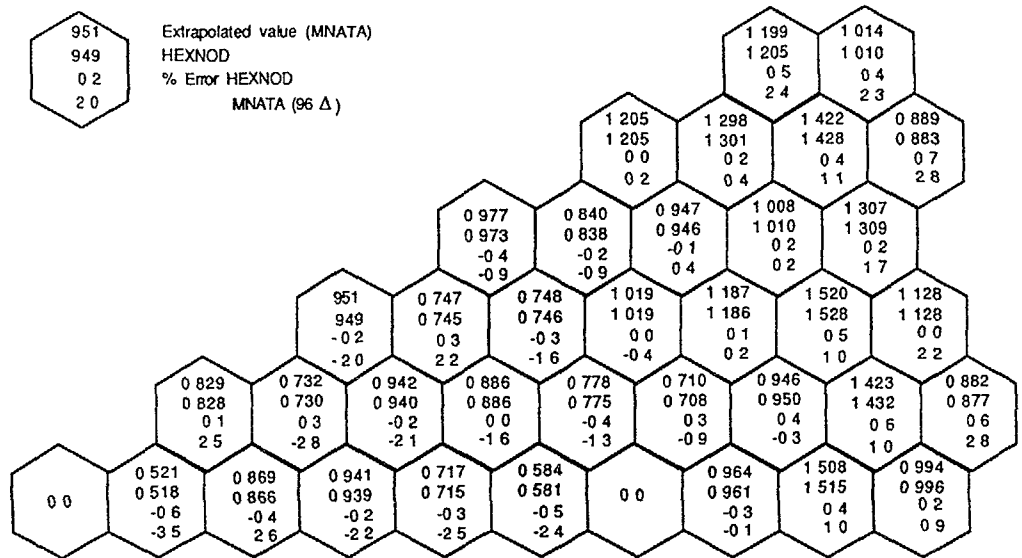


Fig. 2

Normalized power density of 2-D test case WWER-440 with control rods  
Comparison of HEXNOD with reference solution (extrapolated values of  
MNATA calculations)

## 6 Conclusions

The results of the numerical calculations described in sections 4 and 5 demonstrate clearly the extremely high accuracy and computational efficiency of the advanced nodal methods for hexagonal geometry for epithermal and thermal reactor systems. From this it also becomes clear that three-dimensional fuel management calculations with FDM codes are impractical and that the use of modern nodal or finite element codes is mandatory.

## References

1. H. Finnemann et al., Atomkernenergie, 30, 123 (1977)
2. M. R. Wagner et al., Atomkernenergie, 30 129 (1977)
3. K. Koebke et al., "Principles and Application of Advanced Nodal Reactor Analysis Methods", Proc. Topl. Mtg. on Reactor Physics and Shielding, Chicago, Illinois, Sept. 17-19, 1984, Vol. 1, p. 134
4. M. R. Wagner, Trans. Am. Nucl. Soc., 18, 152 (1974)
5. F. Bennewitz et al., "Solution of the Multidimensional Neutron Diffusion Equation by Nodal Expansion", Proc. Conf. on Comput. Methods in Nucl. Eng., Charleston, South Carolina, April 15-17, 1975, Vol. 1, p. 99
6. J. J. Dorning, "Modern Coarse-Mesh Methods - A Development of the 70's", Proc. Conf. Comput. Methods in Nucl. Eng., Williamsburg, Virginia, April 23-25, 1979, Vol. 3, p. 1
7. M. R. Wagner, Nucl. Sc. Eng., 103, 377 (1989)
8. G. J. Schlosser et al., "Nuclear Core Design Studies for a Tight Lattice PWR", IAEA Technical Committee Meeting on Technical and Economical Aspects of High Converters, Nurnberg (1990)
9. M. R. Wagner, "A Nodal Discrete-ordinates Method for the Numerical Solution of the Multidimensional Transport Equation", Proc. Conf. Comput. Methods in Nucl. Eng., Williamsburg, Virginia, April 23-25, 1979, Vol. 4, p. 117
10. R. G. Steinke et al., Trans. Am. Nucl. Soc., 23, 209 (1976)
11. "Benchmark Problem Book", ANL-7416, Suppl. 2 and 3
12. J. Gado, "Solution of 2D and 3D Hexagonal Geometry Benchmark Problems by using the Finite Element Diffusion Code DIFGEN", IKE 4-121, Institut für Kernenergetik und Energiesysteme, Universität Stuttgart (1986)
13. J. Gado and F. Schmidt, Ann. of Nucl. Energy, 14, No. 2, p. 83 (1987)
14. F. Schmidt, et. al., "DIFGEN-Ein Programmepaket zur Lösung der Diffusionsgleichung mit der Methode der Finiten Elemente", IKE 4-75, Institut für Kernenergetik und Energiesysteme, Universität Stuttgart (1978)
15. D. R. Vondy et al., "The Bold Venture Computation System for Nuclear Reactor Core Analysis", Version III, ORNL-5711, Oak Ridge National Laboratory, USA (1981)
16. J. P. Dorsey et al., "BUG-2/BUGTRI, Two Dimensional Multigroup Burnup Codes for Rectangular and Hexagonal Geometry", GA-8272, Gulf General Atomic Inc., (1969)
17. M. Makai, "HEXAN-A Hexagonal Nodal Code for Solving the Diffusion Equation", KFKI-1982-47, Central Research Institute for Physics, Budapest, Hungary (1982)
18. R. D. Lawrence, "The DIF3D Nodal Neutronics Option for Two- and Three-Dimensional Diffusion Theory Calculations in Hexagonal Geometry", ANL-83-1, Argonne National Laboratory, USA (1983)
19. U. Grundmann, "HEXNOD 23 - A Two- and Three-Dimensional Nodal Code for Neutron Flux Calculation of Thermal Reactors with Hexagonal Geometry", ZfK-557, Zentralinstitut für Kernforschung Rossendorf, GDR (1985).

# UO<sub>2</sub>-PuO<sub>2</sub> CRITICALITY ANALYSIS BASED ON A COUPLED SYSTEM NJOY/AMPX-II/HAMMER-TECHNION

A. DOS SANTOS, C.R. FERREIRA,  
M.A. RODRIGUES FERNANDES  
Instituto de Pesquisas Energéticas e Nucleares,  
São Paulo, Brazil

## Abstract

The proposed calculational methodology to analyze critical experiments shows that with the available computer codes and nuclear data files, one can obtain reasonable good agreement between calculated and experimental integral parameters. The analysis of the thermal UO<sub>2</sub>-PuO<sub>2</sub> critical experiments shows that there appears to be a tendency for the k-eff calculated with the four group cross sections of HAMMER-TECHNION to be overestimated for experiments with lattice spacing close to the optimum pitch and to be underestimated as the pitch is decreased. The XSDRNPM diffusion coefficients are too high and consequently the CITATION k-effs are underestimated. The analysis of the thermal systems indicates the good quality of the nuclear data of U-238 of JENDL-2. The PROTEUS lattice analysis confirms this fact since the C/E value of the two-rod heterogeneity factor C8 is in reasonable good agreement. The PROTEUS calculated value of k- $\infty$  is in excellent agreement. The PROTEUS lattice analysis also indicates that the average fission cross section of Pu-239 of JENDL-2 might be overestimated.

## INTRODUCTION

The analysis of critical experiments and also of their related spectral indices has always been recognized as one the most important aspects in the nuclear reactor technology. The adequacy of the nuclear data files for use in reactor applications and also the performance of the mathematical methods used in the nuclear reactor codes can both be verified on the basis of benchmark experiments. It is necessary that such analysis be made using up-to-date nuclear data files and nuclear reactor codes with well established mathematical methods which introduce errors smaller than the uncertainties due to the basic nuclear data themselves. The purpose of this work is to present a procedure to analyze critical experiments and also their related spectral indices based on the coupling among two of the most popular nuclear data pre-processing systems : NJOY<sup>1</sup> and AMPX-II<sup>2</sup> and the HAMMER-TECHNION<sup>3</sup> computer code.

The proposed methodology combines the accurate nuclear data pre-processing capability of NJOY as demonstrated in the IAEA Verification Pre-Processing Code Project<sup>4</sup>, the actinide resonance mutual shielding capability of ROLAIDS module of AMPX-II which might be considered of benchmark quality and the few-groups cross section capabilities of the XSDRNPM module of AMPX-II and that of the HAMMER-TECHNION computer code. The final set of few-groups cross section is input into the CITATION<sup>5</sup> code to make the whole criticality analysis.

The methodology in development at IPEN/CNEN/SP has been applied in criticality analysis of fast systems<sup>6</sup>, thermal systems<sup>7</sup> and in the generation of multigroup fission product cross sections to be used in the coupled HAMMER-TECHNION/CINDER-2 system<sup>8</sup>.

At this time, the calculational methodology will be applied to critical experiments of UO<sub>2</sub>-PuO<sub>2</sub> available in the open literature and also to the light water high converter reactor (LWHCR) test lattices in the PROTEUS reactor<sup>9</sup>. The basic nuclear data utilized in this work will be provided by processing the ENDF/B-IV and JENDL-2 nuclear data files.

From the nuclear data pre-processing, actinide resonance mutual shielding and cross section weighting capability points of view, the proposed methodology has the desired features that fulfill the thermal and fast reactor system requirements and therefore it can be applied in an LWHCR environment as well.

## THE CALCULATIONAL METHODOLOGY

The calculational methodology is shown in Figure 1 . The calculational strategy starts with the ENDF/B-IV or JENDL-2 nuclear data file and with the NJOY nuclear data pre-processing system.

Basically, the following steps are executed in the NJOY processing path : MODER is used to convert between ENDF/B standard mode and the NJOY blocked binary mode . RECONR is used to reconstruct resonance cross sections from resonance parameters and to reconstruct cross sections from ENDF/B nonlinear interpolation schemes. The output is written as a pointwise-ENDF tape (PENDF) with all cross sections on an unionized grid suitable for linear interpolation to within a specified tolerance . BROADR is used to Doppler-broaden and thin cross sections in PENDF format starting from piecewise linear cross sections in PENDF format . UNRESR is used to compute effective pointwise self-shielded unresolved cross sections in the unresolved energy range. THERMR is used to generate scattering cross sections and point-to-point kernels in the thermal range for free scatterers or for bound scatterers when ENDF/B scattering functions<sup>10</sup> are available . The final results are added to an existing PENDF tape . GROUPR is used to transform the PENDF tape into multigroups cross sections for a given weighting function and for a given multigroup structure. This is the NJOY processing path . Before going into the AMPX-II processing path, some details will be given for the NJOY calculations . In all calculations, the fractional tolerance used by RECONR, BROADR, and THERMR has been set to 0.005, 0.002, and 0.001 respectively. The thermal cross sections and the thermal scattering kernels were calculated at 300K for all nuclides but Hydrogen bound in water which the thermal scattering kernel was calculated at 293K . Free atom scattering kernels have been calculated by THERMR for all nuclides with an exception made to Hydrogen bound in water for which the thermal scattering kernel was calculated using the ENDF/B scattering function S( $\alpha, \beta$ ).

Multigroup cross sections libraries have been generated in the standard HAMMER-TECHNION energy structure and also in a special multigroup structure for the XSDRNPM module. The XSDRNPM multigroup structure utilized in this work combines the HAMMER-TECHNION structure up to group 49 and the remainder were taken from the EPRI-CELL<sup>11</sup> thermal structure. Therefore a total of 85 multigroups was used in the XSDRNPM calculations with a maximum energy for thermal treatment of 1.855 eV . A third order of anisotropy was specified for all nuclides in the XSDRNPM library .

Two types of files are transferred to the AMPX-II system : the PENDF tape produced by BROADR which will serve as the pointwise cross section library for the ROLAIDS module calculations and the output of GROUPR which will be transformed

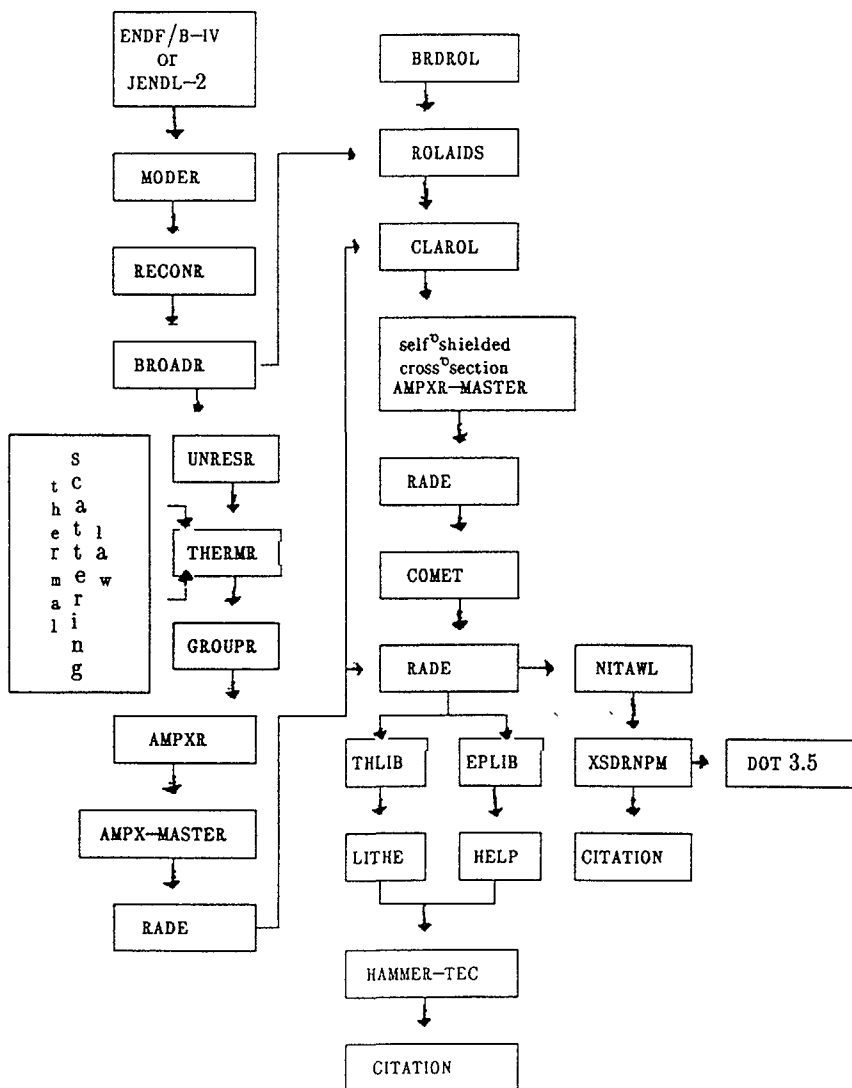


Figure 1 – The Calculational Methodology

into the MASTER library of AMPX-II. For these purposes two new modules have been added to the NJOY system : AMPXR<sup>12</sup> and BRDROL<sup>13</sup>. AMPXR transforms the output of GROUPR into the MASTER library of AMPX-II and BRDROL reads the PENDF tape produced by BROADR and writes a file in a format suitable for the ROLAIDS calculations.

With the MASTER and the ROLAIDS libraries, the AMPX-II processing path can be executed in a straightforward fashion. The AMPX-II processing path starts with the ROLAIDS module. Given material composition by region and problem geometry, ROLAIDS calculates effective multigroup self-shielded cross sections by region in the resolved energy range for all nuclides that takes part in the problem. The ROLAIDS module has the capability, as will be shown in this work, to calculate effective self-shielded cross sections subdividing the pellet region in a set of subzonas with homogeneous nuclide densities but with different sets of self-shielded cross sections. CLAROL reads the self-shielded cross sections produced by ROLAIDS and then replaces them in the MASTER library. RADE checks the consistency of the self-shielded MASTER library, and if any inconsistency in the total cross section or in the normalization of the scattering matrices is found, COMET does the job to fix that. The second RADE is executed to verify whether the COMET task was successfully performed. In this point the MASTER library library is ready to be formated in the WORKING library for the XSDRNPM calculations or in a format suitable for the LITHE<sup>14</sup> and HELP<sup>15</sup> programs. These last two programs write the thermal and epithermal HAMMER-TECHNION binary tapes. The WORKING library for XSDRNPM is written by the NITAWL module of AMPX-II and the input files for the LITHE and HELP is made by two modified versions of the NITAWL module denominated THLIB<sup>16</sup> and EPLIB<sup>17</sup>. Therefore, the XSDRNPM and the HAMMER-TECHNION can be executed to produce the few-groups cross sections to be used in the CITATION code.

#### ANALYSIS OF THE THERMAL UO<sub>2</sub>-PuO<sub>2</sub> CRITICAL EXPERIMENTS

Several room-temperatures UO<sub>2</sub>-PuO<sub>2</sub> approach-to-critical experiments have been conducted in the Critical Approach Facility<sup>18</sup> under the Plutonium Utilization Program (PUP)<sup>19</sup> and these experiments have been chosen to serve as benchmark tests of the calculational methodology as well as of the nuclear data utilized in this work. These clean approach-to-critical experiments consisted of a core region composed of UO<sub>2</sub>-PuO<sub>2</sub> fuel pins and water moderator surrounded by a water reflector. The lattice covered a broad range of water-to-rod volume fractions and PuO<sub>2</sub> weighting fraction varied from 1.5 to 4.0 wt%. The reactor model assumed for all calculations is a two-region right circular cylinder consisting of a homogeneous core and a water reflector. The core radius R<sub>c</sub> is determined from the measured critical number of rods N<sub>c</sub>, by conserving volume and the physical height of the fuel region is taken from the active part of the fuel rod. Few-group cross sections for the core and reflector have been produced by HAMMER-TECHNION and XSDRNPM in the four group standard HAMMER-TECHNION neutron energy structure and then input into the two-region CITATION diffusion theory calculations of the core-reflector geometry. The CITATION calculations of the effective multiplication factor have been performed with four group cross sections arising from two distinct sets of nuclear data as shown in Table I

TABLE I  
Nuclear Data Sets For The Criticality Analysis Calculations –

| SET 1   |      |           | SET 2   |      |           |
|---------|------|-----------|---------|------|-----------|
| Nuclide | I.D. | Library   | Nuclide | I.D. | Library   |
| U-238   | 2925 | JENDL-2   | U-238   | 2925 | JENDL-2   |
| U-235   | 1261 | ENDF/B-IV | U-235   | 2923 | JENDL-2   |
| Pu-239  | 1264 | ENDF/B-IV | Pu-239  | 2943 | JENDL-2   |
| Pu-240  | 1265 | ENDF/B-IV | Pu-240  | 2944 | JENDL-2   |
| Pu-241  | 1266 | ENDF/B-IV | Pu-241  | 2945 | JENDL-2   |
| Pu-242  | 1161 | ENDF/B-IV | Pu-242  | 2946 | JENDL-2   |
| Zirc-2  | 1284 | ENDF/B-IV | Zirc-2  | 1284 | ENDF/B-IV |
| O-16    | 1276 | ENDF/B-IV | O-16    | 1276 | ENDF/B-IV |
| H-1     | 1269 | ENDF/B-IV | H-1     | 1269 | ENDF/B-IV |

No attempt has been made in this work to use the U-238 from ENDF/B-IV due to the well known fact that the ENDF/B-IV overpredicts the U-238 epithermal captures and consequently underpredicts the critical eigenvalues of low-enriched, H<sub>2</sub>O-moderator benchmark lattices.<sup>15-16</sup>

Due to the sophisticated mathematical techniques used by the ROLAIDS and the XSDRNPM modules of AMPX-II which require a considerable amount of computer time, only two experiments of Ref.13 are analyzed in this work . The lattice specifications and the relevant experimental results of the experiments analyzed in this work are shown in Table II. The experiments chosen used UO<sub>2</sub>-2wt%PuO<sub>2</sub> and with 8%wt content of Pu-240. Further details can be found in Ref.13 .

TABLE II  
Lattice Specifications and Experimental Results

| Case | Buck m- <sup>2</sup> | Pitch (in) | Cri.Rad (cm) | No.rods Criti. | H <sub>2</sub> O/Rod Vol.Ratio | H/Pu Atom Rat |
|------|----------------------|------------|--------------|----------------|--------------------------------|---------------|
| 1    | 93.70                | 0.800      | 19.0759      | 319.7          | 1.211                          | 238           |
| 2    | 101.30               | 1.050      | 17.2694      | 152.1          | 2.808                          | 554           |

The criticality analysis was performed by first executing the ROLAIDS module of AMPX-II for the appropriate unit cell configuration . A cylindrized unit cell configuration consisting of a pellet region, a cladding region and a moderator region was utilized in all ROLAIDS calculations. The pellet region was further subdivided in a set of 10 equal area zones in order to be able to obtain actinide self-shielded cross sections across the pellet radius. As a result, the epithermal multigroup calculations of the HAMMER-TECHNION and that of the XSDRNPM characterize the pellet region as made of uniform composition but with distinct sets of multigroup cross section in each zone . The pellet region mesh intervals in ROLAIDS was set to one by zone and kept equal in XSDRNPM and in HAMMER-TECHNION . The ROLAIDS slowing-down calculations were performed in the resolved neutron energy region spanning the interval 5.53 keV – 0.625 eV using a total of 62915 energy points.

The fundamental quantity describing the shielding effects due to the resonances on the multigroup effective cross sections is the self-shielding factor<sup>17</sup> defined as the ratio of the multigroup self-shielded cross section to its corresponding infinite dilution value . The self-shielding factor is commonly interpreted as a measure of how much the group cross section of a nuclide is reduced from its infinite dilution value due to the presence of resonances belonging to this nuclide in the group under consideration.

However when interference of resonances belonging to different nuclides is important, the resonance shielding effect on the multigroup cross sections of a nuclide might not be of a resonance belonging to this nuclide. Instead, the resonance shielding effect is the combined effects due to the resonances belonging of all nuclides on the multigroup cross section of a nuclide under consideration. It turns out that depending on the epithermal neutron spectra behavior the multigroup effective cross section of a nuclide might have values higher than its infinite dilution value. Tables III, IV and V show examples of the multigroup self-shielding factors as a function of the pellet zone number for U-238, U-235 and Pu-239 respectively .

TABLE III  
Self-Shielding Factors for U-238 in case 1 using Nuclear Data Set 1 in group 44 (8.351 eV – 6.476 eV)

| Pellet Zone | Self-Shielding Factors (n,gamma) |
|-------------|----------------------------------|
| 1           | 2.15356 – 02                     |
| 2           | 2.25454 – 02                     |
| 3           | 2.37030 – 02                     |
| 4           | 2.51168 – 02                     |
| 5           | 2.69109 – 02                     |
| 6           | 2.92977 – 02                     |
| 7           | 3.27056 – 02                     |
| 8           | 3.82370 – 02                     |
| 9           | 5.04600 – 02                     |
| 10          | 1.45222 – 01                     |

$\sigma_{n,\gamma}^{\infty} = 5.01371 + 02 \text{ barns}$

$$\sigma_{n,\gamma}^{\infty} = \text{infinite dilution } (n,\gamma) \text{ group cross section}$$

Tables III, IV and V show all kinds of resonance shielding characteristics discussed above . Due to the high concentration of U-238 and also to its pronounced resonance located at 6.67 eV, U-238 dominates the neutron spectra in this group and therefore its multigroup cross sections are severely reduced from the corresponding infinite dilution value. This is mostly the resonance shielding effect of a resonance belonging to U-238 on itself. On the other side, the U-235 and Pu-239 multigroup cross sections are shielded mainly by this resonance of U-238 and the final effect on their multigroup cross sections depends on their cross section shape and also on the neutron spectra shape calculated by ROLAIDS . The final results illustrated in Table IV and V show that the self-shielding factors can be higher than 1.0 and thus showing some features of the resonance interference effect. Besides that, Tables III, IV and V show that the self-shielding factors depend on the radial pellet zone number with U-238 showing the strong variation. The U-238 self-shielding factors are basically flat in the inner zones while close to the periphery of the pellet they show a sharp increase. Basically the

TABLE IV  
Self-Shielding Factors for U-235 in case 1 using Nuclear  
Data Set 1 in group 44 ( 8.351 eV - 6.476 eV )

| Zona   | Self-Shielding Factors |             |
|--|------------------------|-------------|
|  | (n,gamma)              | (n,fission) |
| 1  | 0.84636                | 0.97202     |
| 2  | 0.86715                | 0.98191     |
| 3  | 0.87800                | 0.99001     |
| 4  | 0.88854                | 0.99743     |
| 5  | 0.89908                | 1.00440     |
| 6  | 0.90971                | 1.01085     |
| 7  | 0.92043                | 1.01660     |
| 8  | 0.93118                | 1.02132     |
| 9  | 0.94164                | 1.02760     |
| 10   | 0.94777                | 1.01747     |
| $\sigma_{n,\gamma}^{\infty} = 17.46458 + 01 \text{ barns}$ |                        |             |
| $\sigma_{n,f}^{\infty} = 14.18717 + 01 \text{ barns}$      |                        |             |

TABLE V  
Self-Shielding Factors for Pu-239 in case 1 using Nuclear  
Data Set 1 in group 44 ( 8.351 eV - 6.476 eV )

| Zona  | Self-Shielding Factors |             |
|---|------------------------|-------------|
|   | (n,gamma)              | (n,fission) |
| 1   | 1.13552                | 1.11966     |
| 2   | 1.14467                | 1.12871     |
| 3   | 1.15071                | 1.13476     |
| 4   | 1.15520                | 1.13934     |
| 5   | 1.15831                | 1.14260     |
| 6   | 1.15975                | 1.14430     |
| 7   | 1.15929                | 1.14422     |
| 8   | 1.15595                | 1.14146     |
| 9   | 1.14756                | 1.13396     |
| 10  | 1.12099                | 1.10954     |
| $\sigma_{n,\gamma}^{\infty} = 7.44360 + 01$ |                        |             |
| $\sigma_{n,f}^{\infty} = 8.83578 + 01$      |                        |             |

$\sigma_{n,\gamma}^{\infty}$  = infinite dilution (n,γ) group cross section  
 $\sigma_{n,f}^{\infty}$  = infinite dilution (n,f) group cross section

radial behavior of the U-238 self-shielding factor is due to the spatial self-shielding effect since the inner zones do not feel the heterogeneity effect due to cladding and moderator as much as the outer zones do. The features discussed above for the self-shielding factor behavior were also found in several other groups.

The AMPX-II MASTER multigroup library obtained by replacing the self-shielded multigroup cross sections calculated by ROLAIDS were then written in a WORKING library for XSDRNPM and in a binary epithermal tape for HAMMER-TECHNION. The unit cell HAMMER-TECHNION and XSDRNPM spectral calculations were performed keeping whenever was possible the same problem specification. Therefore, 10 mesh was used in the pellet region, i.e., one for each pellet zone specified in ROLAIDS; 1 mesh in the cladding and 5 in the moderator. The HAMMER-TECHNION spectral calculations assume that the heterogeneous effect inherent in the unit cell (advantage/disadvantage factors) and leakage to be independents. The unit cell multigroup calculations are made as though the lattice were infinity with zero net flow of neutrons across its outer boundary. Leakage is subsequently taken into account for the homogenized unit cell by means of the Fourier transform method<sup>14</sup>. A B-1 method was specified in the whole analysis of this work. Finally, the HAMMER-TECHNION unit cell analysis were performed by using the U-235 and Pu-239 fission spectra consecutively.

The XSDRNPM unit cell analysis kept whenever was possible the same steps followed by HAMMER-TECHNION. Therefore, the XSDRNPM multigroup calculations were made in two steps. A multigroup unit cell analysis assuming an infinite array of repetitive unit cells followed by a leakage treatment for the homogenized unit cell. The first step is straightforwardly performed by specifying the white boundary condition at the outer boundary of the cylindrized unit cell. The leakage treatment for the homogenized unit cell is made in the assymptotic reactor theory procedure.

The XSDRNPM solution of the transport equation is made in an infinite isolated cylinder whose radius is obtained from the experimental buckling. A small correction due to the extrapolated distance ( $\sim 2.0 \text{ cm}$ ) is also applied in the cylinder radius in to order to make the transport treatment of XSDRNPM simulates the same leakage of the HAMMER-TECHNION B-1 method. A vacuum boundary condition is specified at the outer boundary. The few-group cross sections to be used in CITATION are obtained from this last step. A final consideration about the unit cell XSDRNPM multigroup analysis regards the diffusion coefficient to the used in CITATION.

The diffusion coefficients are obtained from the current-weighted transport cross section based on the inseatter approximation. From the mathematical point of view this is the limiting case of the HAMMER-TECHNION B-1 based diffusion coefficients for small  $B/\alpha_t$ ; where B is the square root of the Buckling and  $\alpha_t$  is the current-weighted total cross section. The few-groups water reflector cross sections used in CITATION were computed by HAMMER-TECHNION and by XSDRNPM in the following ways: the HAMMER-TECHNION reflector cross sections were averaged over a neutron spectrum calculated for fission neutrons slowing down and thermalizing in an infinite medium of water; the XDRNPM reflector cross sections were averaged over a neutron spectrum calculated in a one-dimensional two-region (core-reflector) cylindrical representation of the radial direction of the reactor model. From the view point of preserving the leakage, the XSDRNPM reflector cross sections are more representative than that of the HAMMER-TECHNION. It is illustrative to compare the  $k_{\infty}$  calculated by XSDRNPM and by HAMMER-TECHNION before discussing the CITATION results. The  $k_{\infty}$  results are shown in Table VI.

As shown in Table VI, all  $k_{\infty}$  calculated by XSDRNPM are sistematically higher than the corresponding HAMMER-TECHNION values. The Pu-239 fission spectrum is harder than that of U-235 and this aspects is reflected in the HAMMER-TECHNION  $k_{\infty}$  results.

TABLE VI  
Comparison of  $k_{\text{eff}}$  calculated by XSDRNPM and HAMMER-TECHNION

|       | Nuclear Data Set 1                |                      |                      | Nuclear Data Set 2   |                      |         |
|-------|-----------------------------------|----------------------|----------------------|----------------------|----------------------|---------|
|       | H-TEC <sup>a</sup><br>$\chi^{25}$ | H-TEC<br>$\chi^{49}$ | XSDRNPM <sup>d</sup> | H-TEC<br>$\chi^{25}$ | H-TEC<br>$\chi^{49}$ | XSDRNPM |
| Cas 1 | 1.3403                            | 1.34359              | 1.34925              | 1.34198              | 1.34523              | 1.35065 |
| Cas 2 | 1.3797                            | 1.38005              | 1.38179              | 1.38145              | 1.38309              | 1.38423 |

a) H-TEC stands for HAMMER-TECHNION

b)  $\chi^{25}$  stands for U-235 fission spectra

c)  $\chi^{49}$  stands for Pu-239 fission spectra

d) S8 - P3

Cas stands for Case

The use of the Pu-239 fission spectrum representation in the HAMMER-TECHNION compared to that of U-235 increases the fast fission rate and consequently the  $k_{\text{eff}}$  assumes higher values. On the other side, the use of the Pu-239 fission spectrum increases the leakage of the reactor system and the final effect on the effective multiplication factor will depend on the competition between fast fission and leakage effects.

Table VII summarizes the effective multiplication factors calculated by CITATION. Table VII also shows for comparison purposes the effective multiplication factors calculated by DOT-3.5 using the XSDRNPM four-group cross sections.

TABLE VII  
Effective Multiplication Factor  
Calculated by CITATION and DOT-3.5

|                  | Nuclear Data Set 1 |         | Nuclear Data Set 2 |          |         |
|------------------|--------------------|---------|--------------------|----------|---------|
|                  | CASE1              | CASE2   | CASE1              | CASE2    |         |
| H-TEC/CITATION   | $\chi^{25}$        | 0.99555 | 1.00349            | 0.996569 | 1.00453 |
|                  | $\chi^{49}$        | 0.99272 | 0.99829            | 0.993538 | 0.99888 |
| XSDRNPM/CITATION | 0.98945            | 0.98852 | 0.98920            | 0.99028  |         |
| XSDRNPM/DOT-3.5  | 1.0074             | —       | —                  | —        |         |

The lattices chosen to serve as benchmark tests of the calculational methodology proposed in this work were selected to try to study any possible trend of the calculational methodology when the pitch is tightened. The 1.050-in.-pitch lattice corresponds to a lattice close to the optimum pitch; i.e., the lattice pitch that corresponds to a maximum  $k_{\text{eff}}$  for a given fuel pin and cladding specifications. As shown in Table VII, there appears to be a tendency for the HAMMER-TECHNION/CITATION way path calculations to overestimate the  $k_{\text{eff}}$

of the 1.050-in.-pitch lattice (close to the optimum pitch) and to underestimate the  $k_{\text{eff}}$  as the lattice pitch is decreased. The  $k_{\text{eff}}$  calculated with the Pu-239 fission spectrum representation in HAMMER-TECHNION is systematically lower than that of the U-235 fission spectrum representation. Basically, this is the leakage effect due to the utilization of a harder fission spectrum representation. In the cases studied in this work leakage is more important than the fast fission events because the lattices chosen correspond to high leakage lattices. The XSDRNPM/CITATION way calculational path  $k_{\text{eff}}$ s there not appear to show the HAMMER-TECHNION/CITATION tendency. Instead, the  $k_{\text{eff}}$ s calculated by the XSDRNPM/CITATION way calculational path show nearly a constant bias with the  $k_{\text{eff}}$  being systematically underestimated.

Referring back to the  $k_{\infty}$  shown in Table VI, it may be noticed that the  $k_{\infty}$  calculated by the HAMMER-TECHNION show the same tendency of the  $k_{\text{eff}}$  when compared to the corresponding values of the XSDRNPM. The difference between the  $k_{\infty}$  calculated by XSDRNPM and by HAMMER-TECHNION increases as the lattice pitch decreases.

Therefore, at least part of the  $k_{\text{eff}}$  HAMMER-TECHNION/CITATION tendency resides on the main hypothesis assumed by HAMMER-TECHNION in the homogenization of the unit cell.

The  $k_{\text{eff}}$ s calculated by the XSDRNPM/CITATION way calculational path are well below of the experimental values. The main reason resides on the way that the diffusion coefficients are calculated. The XSDRNPM diffusion coefficients are good approximations for small  $B/\rho_t$ . The lattices studied in this work are high leakage system and consequently with large bucklings and it turns out that the XSDRNPM diffusion coefficients for the core and reflector being too high compared to that of HAMMER-TECHNION. The calculation with DOT 3.5 confirms this fact since it provides nearly a correct solution of the neutron transport in the reactor model. Therefore, it might be worthwhile to implement a B1-based diffusion coefficient in the XSDRNPM module of AMPX-II.

#### ANALYSIS OF THE PROTEUS LWHCR CORE 1

The zero energy facility, PROTEUS) is characterized by a tight hexagonal pitch and a hard neutron spectrum. This high-conversion lattice exhibits strong self-shielding of the U-238 resonances, mutual resonance interference effects due to the resonances of the Uranium and Plutonium isotopes and therefore provides a difficult test of the methods and nuclear data utilized in the epithermal calculations. Furthermore, the test lattice was constructed as a 1:1 mixture of two different types of fuel rods. Namely, these were 6.70-mm-diam rods of 15%  $\text{PuO}_2/\text{UO}_2$  and depleted  $\text{UO}_2$ , canned in steel tubes of 8.22-mm o.d. The two rod types were arranged in a such a way that they form an alternate parallel rows of hexagonal cells with 9.00-mm pitch providing a volumetric fuel/moderator of  $\sim 2.0$ . Further details of the PROTEUS - LWHCR cores and also nuclide densities for the two types of fuel rods can be found in Ref.19. The intention here is to analyze the PROTEUS LWHCR core 1; i.e., the one having water as moderator.

There are two levels of difficult in the analyse of the PROTEUS lattice. The first difficult arises from the fact that the lattice contains two types of fuel rods forming an alternate parallel rows of hexagonal cells, what makes the cell analysis model extremely difficult. The second difficult arises from the neutron physics point of view. This type of lattice exhibits neutron spectrum characteristics that are common to both thermal and fast reactor systems. Therefore, the PROTEUS lattice will provide a difficult test not only to the methods and nuclear data of this work but also to the cell model utilized to represent the fuel rod in the lattice.

The approach utilized here is to make use of a super-cell representation for each type of fuel rod. Referring to the Fig.3 of Ref.19, one may notice that each type of fuel rod is surrounded by two rods of the same type and four rods of the second type and therefore it might be a good idea to try to represent each hexagonal cell by a cylindrized super-cell conserving the 4/3 : 1/3 mixture of the two different rods. This will be the super-cell model approach utilized in this work. The super-cell depleted UO<sub>2</sub> will contain the following regions : a) the depleted UO<sub>2</sub> fuel rod at the center, b) the steel cladding, c) the moderator belonging to its individual cell, d) the moderator belonging to the surrounding cells, e) the steel cladding belonging to the surrounding rods and f) a homogenized region consisting of a mixture in a proportion of 2/3 of the UO<sub>2</sub>/PuO<sub>2</sub> rod and 1/3 of the depleted UO<sub>2</sub> rod. The whole superzone area was kept equal to twice the area of the individual cell type so that the outer region has the area equal to the first region ( individual fuel rod ). Furthermore from the symmetry of the cylindrization the third and fourth region has the same area and also the second and fifth has the same area. The UO<sub>2</sub>/PuO<sub>2</sub> supercell contains the UO<sub>2</sub>/PuO<sub>2</sub> fuel rod as the first region and in the last region a mixture of the 2/3 of the depleted UO<sub>2</sub> fuel rod and 1/3 of the UO<sub>2</sub>/PuO<sub>2</sub> fuel rod. The remaining regions were kept the same.

The cylindrized super-cell representations of the PROTEUS lattice will try to take into account the two-rod heterogeneity effect so that in the mutual shielding and also in the neutron transport calculations for each fuel rod type, the effect of the surrounding fuel rod will be taken into consideration.

The PROTEUS lattice analysis will be performed in an infinite medium basis. The cylindrized super-cell containing depleted UO<sub>2</sub> at the center will have its first three regions homogenized in the super-cell by conserving the reaction rates. The same approach will be done for the UO<sub>2</sub>/PuO<sub>2</sub> supercell. The infinite medium representation of the PROTEUS lattice will be the superposition of the homogenizations mentioned above for the two super-cell types.

The PROTEUS lattice analysis was performed by first executing the ROLAIDS module of AMPX-II for each type of super-cell representation. As before, the fuel pellet was further subdivided in a set of 7 equal area zone in order to be able to obtain actinide self-shielded cross sections across the pellet radius. The number of pellet zones has been reduced here due to the large number of regions utilized in the ROLAIDS slowing-down calculations. A total of 53,256 energy points spanning the neutron energy interval 5.53 keV–0.625 eV was utilized in the ROLAIDS calculations. The PROTEUS lattice analysis was performed by using a single set of nuclear data, the actinide nuclear data from JENDL-2 and the remainder from ENDF/B-IV. The nuclide densities for each fuel rod type, cladding and moderator were taken from Ref.19. A small amount of Pu-239 and Pu-241 (1.0E-30 atom/barn-cm) was included in the depleted UO<sub>2</sub> fuel rod in order to be able to calculate self-shielded Pu-239 and Pu-241 cross sections averaged in the depleted UO<sub>2</sub> fuel rod neutron spectrum.

The self-shielding factors calculated by ROLAIDS for the PROTEUS lattice basically follow the same characteristics already discussed in the last session.

The neutron transport equation inside of each supercell type was solved by XSDRNPM. The reason of the choice of XSDRNPM is that this module of AMPX-II solves the neutron transport equation using the SN-method<sup>20</sup> for any order of anisotropy and consequently has the desired features that fulfill the thermal and fast reactors requirements. A S8-P3 calculations were performed in the whole XSDRNPM analysis. The multigroup cross sections of the nuclides belonging to the first three regions of each super cell were then homogenized by XSDRNPM in the whole area of the super cell and finally a homogeneous medium spectral calculations for the superposed system was also performed by XSDRNPM to obtain k- $\omega$  and related actinide reaction rate ratios.

Consider the two-rod heterogeneity factors, defined as the ratio of a given reaction rate ( per atom ) in the depleted UO<sub>2</sub> rod to the same reaction rate in the 15%

PuO<sub>2</sub>/UO<sub>2</sub> rod. The two-rod heterogeneity factors provide a difficult test for the accuracy of two-rod modeling, data and methods employed in this work. Tables VIII compares experimental and calculational results for these factors and also shows for comparison purposes corresponding calculational results obtained by Chawla et al.<sup>21</sup>

TABLES VIII  
Comparisons of Two-Rod Heterogeneity Factors  
(Values for UO<sub>2</sub> rod, relative to these in PuO<sub>2</sub>/UO<sub>2</sub>)

| Reaction Rate | Experiment <sup>a</sup> | Calculation         |                       |                    |           |
|---------------|-------------------------|---------------------|-----------------------|--------------------|-----------|
|               |                         | WIMS-D <sup>‡</sup> | EPRI-CPM <sup>‡</sup> | BOXER <sup>‡</sup> | THIS WORK |
| C8            | 0.986 ± 1.0             | 0.929               | 0.916                 | 0.976              | 0.959     |
| F8            | 0.942 ± 0.8             | 0.934               | 0.945                 | 0.974              | 0.966     |
| F5            | 1.265 ± 1.2             | 1.278               | 1.257                 | 1.239              | 1.174     |
| F9            | 1.918 ± 1.4             | 2.154               | —                     | 1.899              | 1.653     |

<sup>a</sup> Errors are in percent.

<sup>‡</sup> Results taken from Ref.19

As shown in Table VIII, the agreement in the C8 and F8 calculated by the calculational methodology, nuclear data and model used in this work and experimental results is quite reasonable. The value of C8 which is probably the most difficult parameter to calculate in the PROTEUS lattice agrees within 3.5%. For F5 and F9, however, the calculational results are well outside of the experimental errors. From the view point of the neutron balance, the neutron captures in U-238 and fissions in Pu-239 are the most important neutron reactions that occur in the PROTEUS lattice. U-235 contributes with a small amount in the total neutron absorption and therefore the fact that F5 calculated result is not in good agreement has little impact in the analysis of the PROTEUS lattice. The fact that F9 is underpredicted indicates that the average fission cross section of Pu-239 of JENDL-2 might be overestimated. This point will be clear in the next Table.

Table IX compares experimental and calculational results for the core-center values of C8/F9, F8/F9, F5/F9 and F1/F9, as well as for k- $\omega$ . Each reaction rate ratio has been considered per atom as defined by Chawla et al.<sup>21</sup>. Also shown in Table IX for comparison purposes are the corresponding calculational results obtained by Chawla et al.<sup>21</sup>.

Table IX shows that all reaction rate ratios are systematically underpredicted, and thus indicates that the fission cross sections of Pu-239 of JENDL-2 might be overestimated. The fact that the fission cross section of Pu-239 of JENDL-2 is overestimated is quite clear from the value of F8/F9 since Takano<sup>22</sup> in his analysis of JENDL-2 concluded that the fission cross section of U-238 is overestimated. This aspect is somehow shown in Table VIII for the value of F8.

The calculated value of k- $\omega$  shown in Table IX is in excellent agreement with the experimental results and within the experimental errors. The fact that the calculated value of k- $\omega$  be a little bit higher than the experimental value might be credited to the overestimated value of the fission rates of Pu-239.

TABLE IX  
Comparisons of Experimental and Calculated Ratios  
for Reaction Rates and  $k_{\text{eff}}$  Occurring  
in the PROTEUS Core 1

| Parameter                 | Experiment <sup>a</sup><br>(PROTEUS) | C/E         |               |           |
|---------------------------|--------------------------------------|-------------|---------------|-----------|
|                           |                                      | WIMS-D<br>† | EPRI-CPM<br>† | THIS WORK |
| C8/F9                     | 0.0691 ± 2.2                         | 1.002       | 0.933         | 0.946     |
| F8/F9                     | 0.00987 ± 2.5                        | 0.974       | 1.003         | 0.980     |
| F5/F9                     | 0.988 ± 2.0                          | 1.096       | 1.016         | 0.944     |
| F1/F9                     | 1.78 ± 4.5                           | 1.096       | 1.033         | 0.943     |
| $k_{\omega}$ <sup>b</sup> | 1.045 ± 1.1                          | 0.990       | 1.012         | 1.008     |

<sup>a</sup> Errors are in percent

<sup>b</sup> Defined as the ratio of productions to absorptions in the fundamental mode spectrum.

† Results taken from Ref.19.

## CONCLUSIONS

It has been shown that the calculational methodology proposed in this work to analyze critical experiments can produce excellent results and due to its nuclear data processing resources, actinide resonance mutual shielding and cross section weighting capabilities it can be applied to analyze thermal and fast reactor systems and therefore it can be applied in the neutron physics analysis of an LWHCR as well. Besides that, the calculational methodology can even be used to produce standard mathematical results to serve as numerical benchmarks for checking the accuracy of some approximations commonly employed in several lattice codes. A typical example of such approximations is the utilization of the isolated resonance model (e.g. Bondarenko method, Nordheim method) to calculate the multigroup self-shielded cross sections.

The analysis of the thermal UO<sub>2</sub>-PuO<sub>2</sub> critical experiments shows that there are still some improvements that might be worthwhile to implement in the calculational methodology. The implementation of the B1-based diffusion coefficients into the XSDRNPM module of AMPX-II can improve the k-eff calculated by CITATION. The k-eff calculated by using the HAMMER-TECHNION four group cross sections might be considered of reasonable quality and somehow indicates the good quality of the nuclear data of U-238 of JENDL-2.

The analysis of the PROTEUS core 1 experiments confirm the good quality of U-238 of JENDL-2 and show that the averaged fission cross of Pu-239 of JENDL-2 might be overestimated. In the analysis performed in this work, the major fissile nuclide is Pu-239 and the results obtained in the thermal experimental shows that the k-eff calculated with Pu-239 of JENDL-2 is always higher than that of ENDF/B-IV. This conclusion might give an indication that the use of Pu-239 of ENDF/B-IV in the analysis of PROTEUS lattice could have been a better choice for the calculations of the reaction rate ratios and even for  $k_{\omega}$ . Therefore, it is left as a suggestion to repeat the PROTEUS analysis by replacing the nuclear data of Pu-239 of JENDL-2 by that of ENDF/B-IV.

## REFERENCES

1. R.E. MACFARLANE, R.J. BERRET, D.W. MUIR, and R.M. BOICOURT, "The NJOY Nuclear Data Processing System Users Manual," LA-7584-M(ENDF-272),(1978).
2. N.M. GREENE, R.J. FORD III, et al., "AMPX-II: A Modular Code System For Generating Coupled Multigroup Neutron Gamma Libraries from Data in ENDF format," PSR-63,Oak Ridge,Tennessee (1978).
3. J. BARHEN, W. ROTHESTEIN and E. TAVIV,"The HAMMER Code System,"(Technion-Israel Inst. of Tech. Haifa, Dept of Nuclear Engineering), EPRI-NP-656,(1978).
4. D.E.CULLEN,"Report on the IAEA Cross Section Processing Code Verification Project," INDC(NDS)-170/NI,(1985).
5. T.B. FOWLER, D.R. VONDY, G.W. CUNNING, "Nuclear Reactor Core Analysis Code CITATION," ORNL-TN-2406, Rev.2, (1971).
6. C.R. FERREIRA e A. SANTOS, "Análise de Criticalidade Utilizando-se os Sistemas NJOY,AMPX-II e KENO-IV," 215,1, Anais do VII Encontro Nacional de Física de Reatores e Termohidráulica, Recife,PE, Brasil,(abril 1989).
7. A. SANTOS e C.R. FERREIRA, "Elaboração de uma Interface AMPX-II / HAMMER-TECHNION," To be published at 3º CGEN, Rio de Janeiro, Brasil (1990)
8. A. SANTOS and A.Y. ABE,"Burn-up physics in a Coupled HAMMER-TECHNION/CINDER-2 System and ENDF/B-V Aggregate Fission Product Thermal Cross Section Validation," to be published at the proceedings of Physor 90 to be held at Marseille, France (April,1990).
9. R. CHAWLA, K.GMÜR, H. HAGER, E. HETTERGOTT, J.M.PARATTE, R.SEILER, and D. STAHEL, " Comparisons of Calculated and Measured Parameters for a Pu-Fueled LWHCR Lattice," EIR - Bericht Nr.463, Swiss Federal Institute for Reactor Research , (1982) .
10. J.U. KOPPEL and D.H. HOUSTON, " Reference Manual for ENDF Thermal Neutron Scattering Data," General Atomic Report GA-8774 revised and reissued as ENDF-269 by the National Nuclear Data Center, Brookhaven National laboratory, (1978) .
11. "Advanced Recycle Methodology Program System Documentation,"EPRI-CCM-3 RP 118-1, Part II.1, Eletric Power Research Institute,(Sept-1977).
12. A. SANTOS e E.M. LOPEZ," AMPXR e BRDROL : Dois Novos Módulos Para o Sistema NJOY, " to be published at IPEN/CNEN/SP.
13. V.O. UOTINEN, et.al., "Lattices of Plutonium-Enriched Rods in Light Water-Part I : Experimental Results," Nuclear Technology,15,257 (Aug.1972).
14. F.G. DAWSON," Program Analysis and Plans, Plutonium Utilization Programs," BNWL-298,Pacific Northwest Laboratories,(1966).

15. W.ROTHENSTEIN," Thermal Reactor Lattice Analysis Using ENDF/B-IV Data with Monte Carlo Resonance Reaction Rates," BNL-20446, Brookhaven National Laboratory,(1975); see also Nucl.Sci.Eng.,59,337,(1976) .
16. J.HARDY and D.R. FINCH,"Analysis of U-235 – U-238 Thermal Reactor Benchmarks – Consistency and Interpretation, " Proc. Symp. Nuclear Data Problems for Thermal Reactor Applications, Brookhaven National Laboratory, (May-1978), EPRI-NP-1098, (May-1978) .
17. I.I. BONDARENKO, ed., " Group Constants for Nuclear Reactor Calculations," Consultants Bureau ( New York, New York, 1964 ).
18. H. BOHL, et al., " MUFT-4 Fast Neutron Spectrum Code for the IBM-704," WAPD-TM-72, WAPD,(July-1957).
19. R.CHAWLA, et.al., "Reactivity and Reaction Rate Changes With Moderator Voidage in a Light Water High Converter Reactor Lattice," Nuclear Technology , 67, 360 , (1984) .
20. C.E. LEE, "The Discrete SN Approximation to Transport Theory," LA-2595, (1962).
21. TAKANO, et al., "The Benchmark Testes on JENDL-2," JAERI-M-83-202, (Nov.1983)

## HEXTIME: A HEXAGONAL SPACE-TIME KINETICS CODE FOR THE ANALYSIS OF PWHCR TRANSIENTS

H. FINNEMANN, R. BÖHM,  
J. HÜSKEN, R. MÜLLER  
Siemens AG,  
Unternehmensbereich KWU,  
Erlangen, Federal Republic of Germany

J. MACKIEWICZ  
Institute of Atomic Energy,  
Otwock-Swierk, Poland

### Abstract

The integrated program system HEXTIME features a neutronics model for solving the time-dependent few-group diffusion equation in hexagonal-z geometry coupled with an advanced version of the well-known thermal-hydraulics code COBRA-III. Combined with an accurate and efficient pin power reconstruction module the program is thus capable of performing not only global neutronics/thermal-hydraulics calculations but also to evaluate important safety-related parameters like DNB ratios and centerline fuel temperatures.

The basic neutronics equations implemented in HEXTIME are essentially the same as those developed for the steady-state code HEXNOD. Therefore, in this paper only the differences to the static formulation are discussed in more detail. Time-integration is based on a fully implicit Euler method in combination with an exponential transformation technique to reduce truncation errors. The reconstruction of pinwise power distributions relies on a hexagonal version of the weak element approximation method which has already been used successfully in Cartesian geometry.

The thermal-hydraulic part of the reactor calculation is based on the program COBRA III-C/P. It allows 3-dimensional steady-state and transient full-core as well as subchannel analyses to be performed. The capability to calculate crossflow effects is essential to achieve the high degree of spatial resolution and accuracy aimed at in the coupled system. The calculation procedure between neutronics and thermal hydraulics and of the related thermal margin and DNB evaluation methodology is therefore presented in some detail. A discussion of first results of a steam line break analysis completes this paper.

### 1 Introduction

With the advent of the high converter reactor ( PWHCR ) new calculation requirements have to be met due to its particular design features. The geometric layout of the fuel assemblies with their tighter hexagonal fuel rod lattice constitutes the basic difference in comparison with the PWR. It necessitates suitable adaptations of nodal methods available for Cartesian geometry. Besides, the resulting neutron spectrum is shifted towards higher energies and into the epithermal energy range. In order to correctly evaluate this effect, the neutronic equations must be treated allowing for more than two energy groups. With regard to thermal hydraulics, and apart from the need for hexagonal application of the corresponding equations, the narrow fuel rod pitch introduces the need for more

detailed safety-related analysis. Using an open-channel thermal-hydraulic model yields an improved description of core behaviour at far-off-nominal conditions with highly non-uniform power density distributions and/or low mass flow through the core e.g. under steam line break conditions.

The present paper gives an account of how these requirements are met by the new coupled neutron kinetics / thermal hydraulics program system HEXTIME for steady-state and transient calculation of PWHCRs. The underlying physical models and the safety evaluation methodology are presented.

The neutronic part of HEXTIME is based on the hexagonal code HEXNOD /1,2/ allowing for an arbitrary number of neutron energy groups. The steady-state and transient nodal methods applied in hexagonal geometry are similar to the corresponding Cartesian methods /3-6/. For a hexagonal prism (hexagonal node), however, three auxiliary one-dimensional diffusion equations for the transverse-averaged flux in the three directions perpendicular to the hexagon faces are needed.

The thermal-hydraulic part of HEXTIME makes use of the open-channel methods as implemented in COBRA III-C/P /9,10/. Coupling between subchannels is modeled for the net diversion cross-flow resulting from flow redistribution and for turbulent mixing without net mass exchange.

The time derivatives of the neutronic equations are approximated by a fully implicit differencing scheme rendering the solution procedure for the time-dependent problem similar to that for a static source problem. The fluid conservation equations are converted to a system of linear equations by a differencing scheme implicit both in space and time. Control of the overall coupled steady-state and transient iteration and calculation procedure includes examination of local truncation errors as well as of the behaviour of relative changes of the neutronic and thermal-hydraulic solutions between time steps.

## 2 Neutron Kinetics

### 2.1 Nodal Balance Equations

In this section the time-dependent nodal balance equations in hexagonal-z geometry are derived. These equations can be obtained by simply integrating the set of multi-group diffusion equations over the volume of a hexagonal prism, with radial and axial dimensions  $H_x$  and  $H_z$ , respectively (see Fig. below). The neutron diffusion equations are assumed to be given in P1-form:

$$\begin{aligned} & \left[ \frac{1}{v_g} \frac{d}{dt} + \Sigma_{ag} + \sum_{g'>g}^G \Sigma_{gg'} \right] \phi_g + \nabla J_g \\ &= \sum_{g'<g} \Sigma_{gg'} \phi_{g'} + \frac{1}{\lambda} \sum_{g'=1}^G \sum_{j=1}^J (1-\beta_j) \chi_{pg}^j v \Sigma_{fg'}^j \phi_{g'} \\ &+ \sum_{i=1}^I \chi_{dg}^i \lambda_i c_i + \chi_g^{\text{ext}} s \end{aligned} \quad (1a)$$

$$J_g = - D_g \nabla \phi_g \quad (1b)$$

$$\frac{dc_1}{dt} + \lambda_1 c_1 = \frac{1}{\lambda} \sum_{g'=1}^G \sum_{j=1}^J \beta_j^1 v \Sigma_{fg'}^j \phi_{g'}, \quad (2)$$

where  $\phi_g$  is the neutron flux in group  $g$ ,  $J_g$  the corresponding current and  $C_1$  the precursor concentration of precursor group 1. The notation is fairly standard and is repeated here for the convenience of the reader.

|                                      |  |
|--------------------------------------|--|
| $v_g$                                | neutron velocity, group $g$                                |
| $\Sigma_{ag}$                        | absorption cross section, group $g$                        |
| $\Sigma_{gg'}$                       | scattering cross section $g' \rightarrow g$                |
| $v \Sigma_{fg}^j$                    | $v$ - fission cross section of fissionable isotope $j$     |
| $D_g$                                | diffusion constant   |
| $s$                                  | constant external source                                   |
| $\chi_g^{\text{ext}}$                | external source spectrum                                   |
| $\beta_j^1 = \sum_{i=1}^I \beta_i^j$ | total yield of delayed neutrons of fissionable isotope $j$ |
| $\chi_{pg}^j$                        | prompt fission spectrum of fissionable isotope $j$         |
| $\chi_{dg}^i$                        | delayed fission spectrum of precursor group $i$            |
| $\lambda_i$                          | decay constant of precursor group $i$                      |
| $\lambda$                            | eigenvalue   |

The nodal balance equations are obtained by integrating the equations (1 a) and (2) over the volume and Fick's law (1 b) over the surfaces in x, u, v and z-direction of the hexagonal prism (see Fig.) The volume  $V_{\text{hex}}$  is given by

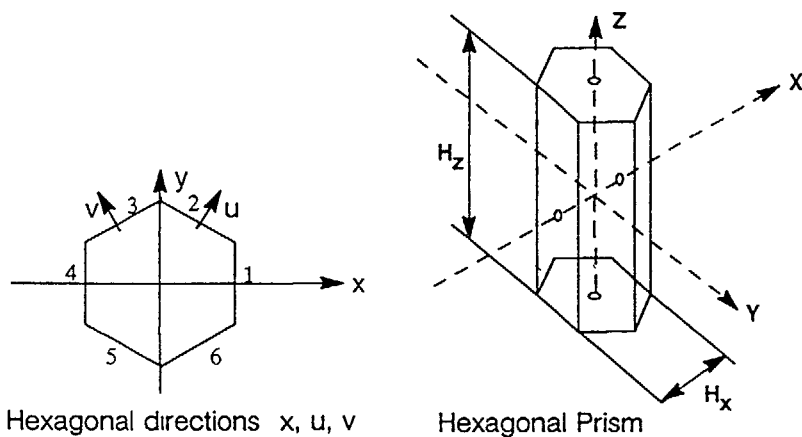
$$V_{\text{hex}} = H_z \int_{-H_x/2}^{H_x/2} dx \int_{-y_s(x)}^{y_s(x)} dy = \frac{\sqrt{3}}{2} H_x H_z$$

where

$$\frac{y_s(x)}{s} = \frac{H_x}{\sqrt{3}} \left( 1 - \frac{|x|}{H_x} \right)$$

$$-H_x/2 \leq x \leq H_x/2$$

describes the boundary of the hexagon.



The semi-discrete nodal balance equations then read

$$\left[ \frac{1}{v_g} \frac{d}{dt} + \sum_{g' > g}^G \sum_{g' > g} \bar{\phi}_{g'} \right] \bar{\phi}_g$$

$$+ \frac{2}{3} \frac{1}{H_x} \sum_{\substack{w=x,u,v \\ s=1,r}} \left( J_{gw}^{\text{out}} - J_{gw}^{\text{in}} \right)_s + \frac{1}{H_z} \sum_{s=1,r} \left( J_{gz}^{\text{out}} - J_{gz}^{\text{in}} \right)_s$$

$$= \sum_{g' < g} \sum_{g' > g} g g' \bar{\phi}_{g'} + \frac{1}{\lambda} \sum_{g'=1}^G \sum_{j=1}^J (1-\beta_j) \chi_{pg}^j v \sum_{g' > g} \bar{\phi}_{g'}$$

$$+ \sum_{i=1}^I \chi_{dg}^i \lambda_i \bar{C}_i + \chi_g^{\text{ext}} s$$

$$(J_{gx}^{\text{out}} - J_{gx}^{\text{in}})_s = - \frac{\text{sgn}(x)}{H_x / \sqrt{3}} \int_{-H_x/2}^{H_x/2} \frac{d}{dx} \left. \frac{d}{dy} \phi_g^z(x,y,t) \right|_{x=\pm H_x/2} dy$$

where  $\phi_g^z(x,y,t)$  is the z-averaged flux

Corresponding equations are valid for the u and v-direction  
For the z-direction we can write

$$(J_{gz}^{\text{out}} - J_{gz}^{\text{in}})_s = - \text{sgn}(z) \frac{d}{dz} \left. \psi_{gz}(z,t) \right|_{z=\pm H_z/2}$$

and the precursor equations read

$$\frac{d\bar{C}_i}{dt} + \lambda_i \bar{C}_i = \frac{1}{\lambda} \sum_{g'=1}^G \sum_{j=1}^J \beta_j \chi_{pg}^j v \sum_{g' > g} \bar{\phi}_{g'}$$

Obviously, in the above equations  $\bar{C}_i$  and  $\bar{\phi}_g$  are nodal average values, e.g.

$$\bar{\phi}_g(t) = \frac{2}{\sqrt{3} H_x^2 H_z} \int_{V_{\text{hex}}} \phi_g(x,y,z,t) dx dy dz$$

$\psi_{gz}(z,t)$  is the transverse-averaged flux in z-direction

$$\psi_{gz}(z,t) = \frac{2}{\sqrt{3} H_x^2} \int_{-H_x/2}^{H_x/2} dx \int_{-y_s(x)}^{y_s(x)} \phi_g(x,y,z,t) dy$$

The corresponding definitions in x u and v-direction are somewhat more involved

$$\psi_{gx}(x, t) = \frac{1}{2y_s(x)H_z} \int_{-y_s(x)}^{y_s(x)} dy \int_{-H_z/2}^{H_z/2} \phi_g(x, y, z, t) dz$$

For the spatial derivative of  $\psi_{gx}(x, t)$  we have

$$\begin{aligned} \frac{d}{dx} \psi_{gx}(x, t) &= \frac{1}{2y_s(x)} \int_{-y_s(x)}^{y_s(x)} \frac{d}{dx} \phi_g(x, y, t) dy \\ &\sim \frac{y'_s}{y_s} \left[ \psi_{gx}(x, t) - \frac{\phi_g(x, y_s, t) + \phi_g(x, -y_s, t)}{2} \right] \end{aligned}$$

The first term on the right-hand side (RHS) shows the typical form of an average gradient over the surface of a hexagon and is related to the difference of outgoing and incoming currents (3b). The other term is specific for hexagons. It is interesting to note that the term vanishes if the average flux in x-direction is equal to the arithmetic average of the corresponding fluxes on opposite surfaces. The terms can be evaluated by using local interpolation methods as discussed in section 2.4.

Since the derivative  $y'_s$  is given by

$$y'_s = -\frac{1}{\sqrt{3}} \operatorname{sgn}(x)$$

it shows a jump at  $x = 0$ . Thus the average of the derivative is zero over x.

Experience has shown /1/ that as a first approximation the contribution of the additional term which results from the variable integration limits can be neglected. A neglect of this term greatly facilitates the analysis. With this assumption hexagonal problems can be solved with the methods developed originally for Cartesian geometry /3-6/.

## 2.2 Transverse-Integrated Diffusion Equations

Using the approximations discussed in the previous section, the transverse-integrated diffusion equation in x (u,v) - direction can be written as follows

$$\begin{aligned} & \left[ \frac{1}{v_g} \frac{d}{dt} - D_g \frac{d^2}{dx^2} + \sum_{g'<g} \sum_g \psi_{g'x} \right] \psi_{gx} \\ &= \sum_{g'<g} \sum_g g g' \psi_{g'x} + \frac{1}{\lambda} \sum_{g'=1}^G \sum_{j=1}^J (1-\beta_j) x_{pg}^j v \sum_{fg'}^j \psi_{g'x} \\ &+ \sum_{i=1}^I x_{dg}^i \lambda_i \xi_{ix} - D_g L_{gx}(x) + x_g^{\text{ext}} s \end{aligned} \quad (5)$$

The  $\xi_{ix}$  are the one-dimensional precursor concentrations defined in analogy to  $\psi_{gx}$ . They obey the equations

$$\frac{d}{dt} \xi_{ix} + \lambda_i \xi_{ix} = \frac{1}{\lambda} \sum_{g'=1}^G \sum_{j=1}^J \beta_j^i v \sum_{fg'}^j \psi_{g'x} \quad (6)$$

$D_g L_{gx}(x)$  is the transverse leakage which has to be approximated during the solution process.

$$\begin{aligned} D_g L_{gx}(x) &= -\frac{D_g}{2y_s(x)H_z} \cdot \int_{-y_s(x)}^{y_s(x)} dy \int_{-H_z/2}^{H_z/2} dz \left( \frac{d^2}{dy^2} + \frac{d^2}{dz^2} \right) \phi_g(x, y, z, t) \\ &= D_g^L y_{gx}(x) + D_g^L z_{gx}(x) \end{aligned}$$

Since the y-currents are not known a simple consistent approximation as in Cartesian geometry is not possible. Thus the transverse-averaged diffusion equation is not fully consistent with the nodal balance equation. The consistency of the solution of this equation is obtained by explicitly requiring that the average of the 1-D flux is equal to the nodal average. The spatial dependence of the transverse leakage can be obtained by constructing a quadratic polynomial using information of the transverse leakage in adjacent boxes /1,3/.

In order to solve (3), (4) and (5), (6) two additional approximations are needed. The first concerns the time derivative of  $\psi_{gx}$ . This derivative is approximated by /5/

$$\frac{d\psi_{gx}}{dt} = \frac{1}{\bar{\phi}_g} \frac{d\bar{\phi}_g}{dt} \psi_{gx}$$

To reduce the truncation error  $\bar{\phi}_g(t)$  is exponentially transformed

$$\bar{\phi}_g(t) = e^{\omega(t-t_0)} T_g(t)$$

where  $\omega$  is the so-called frequency. The derivative is then given by

$$\frac{d\bar{\phi}_g}{dt} = \omega \bar{\phi}_g + e^{\omega(t-t_0)} \frac{dT_g(t)}{dt}$$

The frequency can be estimated during the iterative solution process /5/

Applying the implicit first order Euler formula we have

$$\frac{d\bar{\phi}_g}{dt} = \omega \bar{\phi}_g(t) + (\bar{\phi}(t) - e^{\omega\Delta t} \bar{\phi}(t_0)) / \Delta t \quad (7a)$$

$$\frac{1}{v_g} \frac{d\psi_{gx}}{dt} = \frac{1}{v_g \Delta t} (\omega \Delta t + 1 - \frac{\bar{\phi}(t_0)}{\bar{\phi}(t)} e^{\omega \Delta t}) \psi_{gx} \quad (7b)$$

$$\Delta t = t - t_0$$

The same approximation is assumed to be valid for the transverse-integrated precursor equations

$$\frac{d\zeta_{1x}}{dt} = \frac{1}{\bar{C}_1} \frac{d\bar{C}_1}{dt} \zeta_{1x}$$

It follows that

$$\zeta_{1x} = \frac{\sum_{g'=1}^G \sum_{j=1}^J \beta_1^j v \sum_{fg'}^j \psi_{g'x}}{\sum_{g'=1}^G \sum_{j=1}^J \beta_1^j v \sum_{fg'}^j \bar{\phi}_{g'}} \quad (8)$$

The solution of the precursor equation (4) can be written as

$$\begin{aligned} \bar{C}_1(t) &= \bar{C}_1(t_0) e^{-\lambda_1(t-t_0)} \\ &+ \frac{1}{\lambda} \sum_{g'} \sum_j \beta_1^j \int_{t_0}^t v \sum_{fg'}^j \bar{\phi}_{g'}(t') e^{\lambda_1(t'-t)} dt' \\ &= \bar{C}_1(t_0) e^{-\lambda_1(t-t_0)} \\ &+ \frac{1}{\lambda} \sum_{g'} \sum_j \beta_1^j \int_{t_0}^t v \sum_{fg'}^j e^{\omega(t'-t_0)} e^{\lambda_1(t'-t)} T_g(t') dt' \end{aligned}$$

By approximating  $T_g(t')$  by its arithmetic average one obtains

$$\begin{aligned} \bar{C}_1(t) &= \bar{C}_1(t_0) e^{-\lambda_1(t-t_0)} \\ &+ \frac{1}{\lambda} \sum_{g'} \sum_j \beta_1^j v \sum_{fg'}^j (\bar{\phi}_{g'}(t) + \bar{\phi}_{g'}(t_0) e^{\omega(t-t_0)}) / 2 \\ &\times \frac{1 - e^{-(\omega+\lambda_1)(t-t_0)}}{\omega+\lambda_1} \quad (9) \end{aligned}$$

The expression  $(\bar{\phi}_g(t) + e^{\omega(t-t_0)} \bar{\phi}_{g'}(t_0)) / 2$  can further be approximated by  $\bar{\phi}_{g'}(t)$ . The solution (9) is exact for purely exponential behaviour of the flux in  $(t_0, t)$ .

Given (7a) and (9) the solution of the nodal balance equation (3a) can be written

$$\begin{aligned} & \left[ \frac{1 + \omega \Delta t}{v_g \Delta t} + \Sigma_{ag} + \sum_{g'>g} \Sigma_{g'g} \right] \bar{\phi}_g \\ & + \frac{2}{3 H_x} \sum_{\substack{x_s \\ 6 \text{ faces}}} (J_g^{out} - J_g^{in}) x_s + \frac{1}{H_z} \sum_{s=1,r} (J_{gz}^{out} - J_{gz}^{in}) s \\ & = \sum_{g'<g} \Sigma_{gg'} \bar{\phi}_{g'}(t) + \frac{1}{\lambda} \sum_{g'} \sum_j x_{tg}^j v \Sigma_{fg'}^j \bar{\phi}_{g'}(t) + x_g^{ext} s \end{aligned} \quad (10)$$

$$\begin{aligned} & - \frac{1}{\lambda} \sum_i \sum_j \sum_{g'} x_{dg}^i \beta_i^j v \Sigma_{fg'}^j \bar{\phi}_{g'}(t) \frac{\omega + \lambda_i e^{-(\omega + \lambda_i) \Delta t}}{\omega + \lambda_i} \\ & + \frac{e^{\omega \Delta t}}{v_g \Delta t} \bar{\phi}_g(t_0) + \sum_{i=1}^I \lambda_i x_{dg}^i \bar{C}_i(t_0) e^{-\lambda_i \Delta t} \end{aligned}$$

where the transient part of the source has been surrounded by a rectangle and

$$x_{tg}^j = (1 - \beta_i^j) x_{pg}^j + \sum_i \beta_i^j x_{dg}^i$$

is the total fission spectrum. Using (7b, 8, 9) the equivalent one-dimensional diffusion equations (5) have the following form

$$\begin{aligned} & \sum_{rg} \psi_{gx} - D_g \frac{d^2}{dx^2} \psi_{gx} \\ & = \sum_{g'<g} \Sigma_{gg'} \psi_{g'x}(t) + \frac{1}{\lambda} \sum_{g'} \sum_j x_{tg}^j v \Sigma_{fg'}^j \psi_{g'x}(t) - D_g L_{gx}(x) \end{aligned}$$

$$\begin{aligned} & - \frac{1}{\lambda} \sum_i \sum_j \sum_{g'} x_{dg}^i \beta_i^j v \Sigma_{fg'}^j \psi_{g'x}(t) \frac{\omega + \lambda_i e^{-(\omega + \lambda_i) \Delta t}}{\omega + \lambda_i} \\ & + \sum_i \sum_j \sum_{g'} x_{dg}^i \beta_i^j v \Sigma_{fg'}^j \bar{C}_i(t_0) e^{-\lambda_i \Delta t} CQ_i \psi_{g'x}(t) \\ & + \frac{\bar{\phi}_g(t_0)}{\bar{\phi}_g(t)} \frac{e^{\omega \Delta t}}{v_g \Delta t} \psi_{gx} \end{aligned}$$

$$+ x_g^{ext} s = Q_g(x) - D_g L_{gx}(x) \quad (11)$$

where

$$CQ_i = 1 / \sum_g^G \sum_j^J \beta_i^j v \Sigma_{fg}^j \bar{\phi}_g(t)$$

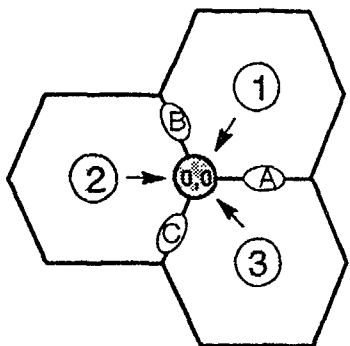
and an effective removal cross section has been defined by

$$\sum_{rg} = \frac{1 + \omega \Delta t}{v_g \Delta t} + \Sigma_{ag} + \sum_{g'>g} \Sigma_{g'g}$$

As indicated above equation (11) can be solved by various techniques. Here the semi-analytical procedure used in [1] and proven to be efficient and accurate is adopted. This method is based on the well-known fact that (11) can be solved analytically if the RHS is represented by a polynomial

## 2.4 Hexagonal Interpolation Scheme

Weak element approximations to elliptic differential equations /7/ can also be used for a posteriori interpolation. This was demonstrated earlier for Cartesian geometry /8/. The same method can be applied to hexagonal geometry. The first step is to construct corner values by the method of successive smoothing (MSS) /4/. Linearly extrapolated node values adjacent to the corner under consideration are averaged to get a smoothed flux estimate  $\phi_{\infty}$  (s. Fig.).



$$\phi_{\infty}^1 = \frac{2}{3} S_A + \frac{2}{3} S_B - \frac{1}{3} \phi^{-1}$$

$$\phi_{\infty}^2 = \frac{2}{3} S_B + \frac{2}{3} S_C - \frac{1}{3} \phi^{-2}$$

$$\phi_{\infty}^3 = \frac{2}{3} S_C + \frac{2}{3} S_A - \frac{1}{3} \phi^{-3}$$

$$\phi_{\infty} = \sum_{i=1}^3 w_i \phi_{\infty}^i$$

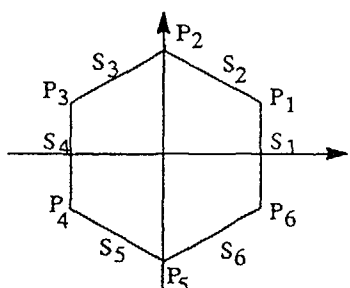
In the above formula  $S_A, B, C$  are average fluxes on the sides of three hexagons adjacent to point  $(0,0)$ . Arithmetic or diffusion coefficient weighting.

$$w_i = 1/3 \quad \text{or} \quad w_i = D_i / \sum D_i$$

have proven to yield sufficiently accurate results. Solutions  $\eta$  of the Helmholtz equation

$$\Delta \eta = \kappa^2 \eta \quad (12)$$

are then used to match point fluxes  $P_i$  and average flux values  $S_i$  on the boundary of the hexagon (s. Fig.). Though the proposed method is also applicable in three dimensions we assume that the intra-nodal flux distribution is separable in the axial and radial direction. Thus the interpolation problem is reduced to the solution of a two-dimensional inhomogeneous diffusion equation for each node



The buckling  $\kappa^2$  is given by the condition that the determinant of the corresponding multigroup system with  $\Delta \Phi$  replaced by  $\kappa^2 \Phi$  is zero.

If we denote the solutions of this algebraic equation by  $\kappa_g^2$  ( $g=1, \dots, G$ ) the flux solution is a linear combination of the corresponding  $\eta_g$

$$\phi_g = \sum_{g'=1}^G B_{gg'} \eta_{g'}, \quad g=1, \dots, G$$

where the  $B_{gg'}$  are the group coupling constants defined by the multigroup equation system.

For each group the function  $\eta$  is chosen as linear combination of elementary solutions of (12) as follows

$$\eta(x,y) = \sum_{j=1}^6 (c_j^+ \cosh \kappa \xi_j + c_j^- \sinh \kappa \xi_j), \quad \kappa^2 \geq 0$$

$$\eta(x,y) = \sum_{j=1}^6 (c_j^+ \cos \kappa \xi_j + c_j^- \sin \kappa \xi_j), \quad \kappa^2 < 0, \quad \kappa = \sqrt{-\kappa^2}$$

where

$$\xi_j = x \cos \alpha_j + y \sin \alpha_j \quad \text{and} \quad \alpha_j \text{ arbitrary.}$$

The  $c_j^\pm$  have to be determined by the boundary conditions.

The resulting interpolating flux functions fulfill the two-dimensional diffusion equation in the interior of the hexagon. Experience has shown /8/ that this approximation is superior to polynomial interpolation both with respect to accuracy and computational efficiency. This is especially true in case of steep flux gradients as they occur under off-nominal conditions. It should be noted that the procedure outlined is applicable for steady-state and transient problems. In time-dependent 3-D problems a buckling and a time absorption term have to be added to the removal cross section. For the precursors an approximation similar to that made in the derivation of the equivalent one-dimensional diffusion equation (8) can be used.

### 3 Thermal Hydraulics

The thermal-hydraulic part of the reactor calculation is based on the program COBRA III-C/P. It allows 3-dimensional steady-state and transient full-core as well as subchannel analyses to be performed. The capability to calculate crossflow effects is essential to achieve the high degree of spatial resolution and accuracy aimed at in the coupled neutronics - thermal hydraulics system HEXTIME.

Apart from structural modifications required for implementation into the coupled system all the original COBRA III-C/P features have been maintained. Geometry specification for the reactor core is flexible, relying on information about flow areas and lateral interconnections i.e. no particular coordinate system is defined. Both pressurised and boiling water reactors can be treated, the applications ranging from full-core to subchannel analyses. In the following, the underlying conservation equations will be given, based on the corresponding presentation in /11/.

The conservation equations of the two-phase flow are written for the mixture quantities in time-dependent, one-dimensional form. Separated slip flow is assumed in each subchannel, and the void fraction distribution is evaluated as a function of enthalpy, flow rate, heat flux and pressure. Fuel pin temperatures are calculated from the radial heat conduction equation, and the coupling to the coolant determining heat transfer dynamics is realized by appropriate models.

The conservation equations for mass, momentum and energy are basically one-dimensional in axial ( $x$ -) direction. However, lateral mixing between subchannels is accounted for by considering two types of crossflow. Diversion crossflow results from lateral pressure differences due e.g. to differing hydraulic conditions or to diverter vanes. It is superimposed by turbulent crossflow between adjacent subchannels with no net mass exchange but with contributions to energy and axial momentum balances. For simplicity's sake, the resulting basic conservation equations are written here for a subchannel  $i$  connected to only one adjacent subchannel  $j$ . In the general form all the crossflow-related terms (index  $ij$ ) have to be evaluated by summation over all the neighbouring subchannels. The equations read as follows (refer to Appendix 1 for a complete list of nomenclature).

The continuity equation

$$A_i \frac{\partial p_i}{\partial t} + \frac{\partial m_i}{\partial x} = -w_{ij}$$

states the mass balance taking into account the diversion crossflow  $w_{ij}$  per unit length. It is defined positive when flow is leaving the subchannel  $i$ . The turbulent crossflow does not appear because, as mentioned above, it does not constitute a net mass exchange.

On the left-hand side of the energy equation

$$\frac{1}{u''} \frac{\partial h_i}{\partial t} + \frac{\partial h_i}{\partial x} =$$

$$\frac{q'_i}{m_i} - (h_i - h_j) \frac{w'_{ij}}{m_i} - (t_i - t_j) \frac{c_{ij}}{m_i} + (h_i - h^*) \frac{w_{ij}}{m_i}$$

$u''$  represents an effective velocity for energy transport. On the right, turbulent crossflow  $w'_{ij}$  contributes through the difference in enthalpy between channels  $i$  and  $j$ . Similarly, the diversion crossflow  $w_{ij}$  carries an enthalpy  $h^*$  which needs to be defined. Thermal conduction due to temperature differences is accounted for by the third term, whereas the first one gives the heat transfer from the fuel rods ( $q'$  is the linear heat flux on the surface).

On the left-hand side of the axial momentum equation

$$\frac{1}{A_i} \frac{\partial m_i}{\partial t} - 2 u_i \frac{\partial p_i}{\partial t} + \frac{\partial p_i}{\partial x} =$$

$$- \left( \frac{m_i}{A_i} \right)^2 \left[ \frac{v_i f_i \Phi_i}{2 D_i} + \frac{k_i v'_i}{2 \Delta x} + A_i \frac{\partial}{\partial x} \left( \frac{v'_i}{A_i} \right) \right]$$

$$- p_i g_c \cos \Theta - \frac{f_T}{A_i} (u_i - u_j) w'_{ij} + \frac{1}{A_i} (2 u_i - u^*) w_{ij}$$

the axial pressure gradient and its transient components appear. Again, on the right-hand side turbulent and diversion crossflow contribute, due to differences in subchannel flow velocities  $u$  and crossflow velocity  $u^*$ , respectively. Besides, friction, spatial acceleration and elevation pressure drop terms are included.

The transverse momentum equation

$$\frac{\partial w_{ij}}{\partial t} + \frac{\partial (u^* w_{ij})}{\partial x} + \left( \frac{s}{l} \right) C_{ij} w_{ij} = \left( \frac{s}{l} \right) (p_i - p_j)$$

governs the momentum coupling between two adjacent subchannels. Crossflow temporal and spatial acceleration are supplemented by friction and pressure terms. Their relative importance against inertia terms is expressed by the transverse momentum parameter ( $s/l$ ).

In addition to these conservation equations, an equation of state expresses the two-phase fluid density in dependence of pressure, mixture enthalpy and flow rate. To complete the system of equations, a variety of correlations and models is provided for selection by the user. Included are correlations for single-phase friction factor and corresponding two-phase multiplier, spacer loss coefficient and bulk and subcooled boiling void fraction. With respect to crossflow calculation basically empirical models serve for determining forced as well as turbulent single- and two-phase mixing, and for specification of the parameters appearing in the transverse momentum equation.

The resulting system of partial differential equations is discretized in time and space and solved using a semi-explicit finite difference scheme. This scheme gives a boundary-value flow solution for both steady-state and transient cases. The boundary conditions to be specified are inlet enthal-

py and mass flow, and exit pressure. The solution procedure guarantees stability irrespective of space or time step size

The fuel rod model is based on the radial heat conduction equation i.e. axial heat conduction is ignored. After dividing the fuel rod and cladding into radial mesh cells, an implicit finite difference scheme is applied to achieve a numerical solution procedure which is stable for all time steps. The heat transfer coefficient is determined from correlations covering all the heat transfer regimes, and various critical heat flux correlations can be used in safety margin analyses.

#### 4 Coupling Neutron Kinetics and Thermal Hydraulics

In order to determine the nuclear reactor's behaviour as realistically as possible, two main aspects have to be taken into account. Firstly, it is obvious that the reactor core has to be treated by coupling neutron kinetics and thermal hydraulics, thereby modeling their respective feedback mechanisms. Secondly, appropriate boundary conditions for the core ( e.g. mass flow and enthalpy of coolant at the inlet, pressure ) must be specified. As HEXTIME treats only the reactor core, these boundary conditions are input based on steady-state operation data and, when calculating transients, are modified to reflect disturbances ( e.g. leaks ) assumed to be occurring in the primary circuits. The corresponding data must be provided by a plant or loop analysis program.

The calculation scheme of the coupled reactor core simulation system HEXTIME is shown in Fig. 1. First of all, input data are read and initialisations performed. In the coupled system, redundant data originally needed as input to each individual program have been eliminated. In particular, definition of the flow channels' arrangement in hexagonal geometry is input only once, based on the corresponding HEXNOD-T routines. An internal interface routine then generates all the information needed in COBRA ( e.g. neighbourhood relations, interconnections, gap widths ) automatically, which frees the user from tedious work.

In Fig. 1 the modules HEXNOD-T ( neutron kinetics ) and COBRA ( thermal hydraulics ) now represent the pure calculation parts of the formerly independent programs. The underlying equations have been described in the previous chapters. In the coupled system, their internal solution procedures have remained unchanged, i.e. suitable convergence criteria and iteration step limits can still be specified individually.

However, coupling of the modules introduces the need for an additional outer iteration loop which also contains the interface routines for updating cross sections and power density, in dependence of thermal-hydraulic conditions and nuclear fission rate, respectively. In the coupled system, the nodal power distribution is no longer an independent ( input ) parameter but changes according to the feedback affecting the nuclear cross sections. The steady-state solution is found by repeating the indicated calculation sequence until both the neutronic and the thermal-hydraulic solutions in two successive iterations meet a specified convergence criterion.

Any transient calculation will start from such an established convergent steady-state reactor core solution. Time-dependent changes can be specified as neutronic disturbances ( i.e. control rod movement ) and/or as variations in thermal-hydraulic boundary conditions ( inlet mass flow, inlet enthalpy, exit pressure ). Transient time step widths are determined by a control module after checking of local truncation errors as well as of the behaviour of relative changes of the neutronic and thermal-hydraulic solutions during time steps.

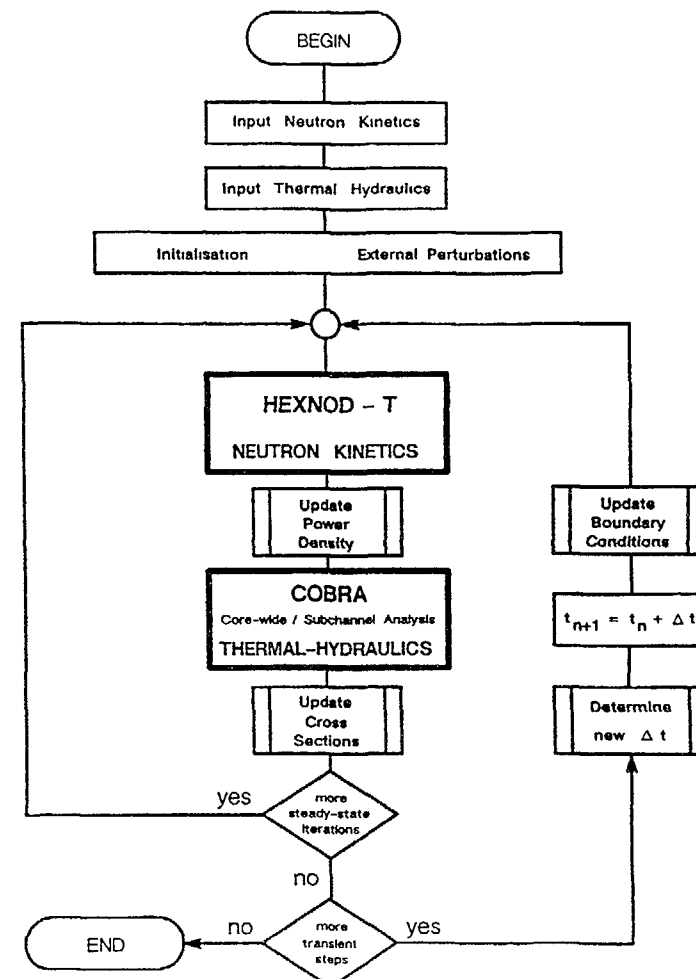


FIG. 1 Calculation scheme hextime.

## 5 Local Safety Margin Evaluation

In both steady-state and transient calculations, HEXTIME yields thermal-hydraulic results for each flow channel node. These results reflect the influences of neutronic feedback coupling and of crossflows between neighbouring channels. For safety-related analyses, they must be checked against the maximum permissible values in order to determine thermal margins. One of the most important safety criteria is the departure from nucleate boiling ratio (DNBR) defined as the ratio between critical heat flux and local heat flux at any particular position on the surface of a fuel rod. Some of the most widely used critical heat flux (CHF) correlations available in HEXTIME are those of W-3-L/R-Grid, B&W, and the KWU CHF Tables.

In standard HEXTIME applications, reactor core subdivision in the horizontal plane is based on the actual hexagonal fuel element arrangement, i.e. both the neutronic and the thermal-hydraulic modules will treat the problem in a comparatively coarse full assembly geometry rather than performing more detailed subchannel analyses. This implies that each of the flow channels is calculated as though containing only one fuel rod representing an average of all the rods actually present. Therefore in such fuel element based calculations only average values of thermal-hydraulic conditions (e.g. quality, enthalpy) of the coolant and of heat flux can be determined.

In DNB evaluations, however, local (pin) values of the thermal-hydraulic quantities would be needed. In order to estimate these values without expensive pin-based subchannel analysis, HEXTIME makes use of the hexagonal local neutron flux reconstruction method described in a previous chapter. The resulting average and maximum nodal neutronic power formfactors serve as multipliers to the average nodal heat flux. The maximum heat flux within a node thus determined is then used in the DNB analysis.

Further HEXTIME development will include a refined methodology for hot channel analysis which has been proved efficient for nodal reactor calculations in Cartesian geometry /12/. In particular, it solves the problems encountered in transient calculations (where neutronic and thermal-hydraulic quantities are not directly coupled any more due to their different time constants) by identification and explicit re-calculation of the relevant hot channels in the core. This re-calculation is based on their respective hot pin axial power distribution and considers the ensuing heat conduction in the fuel and heat transfer to the coolant. Consequently, both maximum rod surface heat flux and hot subchannel thermal-hydraulic conditions are calculated instead of estimated, and hence correctly used in the CHF correlations and in the DNB evaluation.

## 6 Application and Results

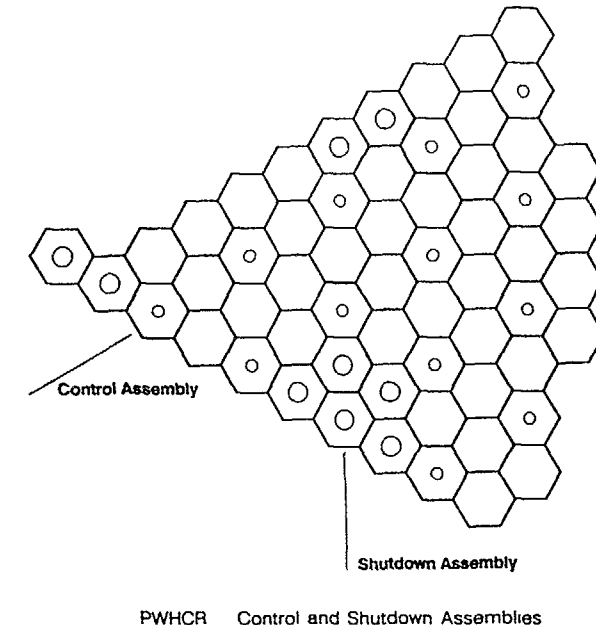
Within the scope of a PWHCR core design and safety study, HEXTIME is currently being applied to the investigation of events involving recriticality of the reactor core. Preliminary results of this study are discussed in this section.

The events quoted above are caused by secondary-side leakages and ruptures during which a substantial subcooling of the reactor core can take place due to the live-steam outflow. Under conservative assumptions and boundary conditions the reactor cannot be prevented from becoming critical again during the cooldown process and, as a result, fission reactions are initiated which oppose a further decrease in coolant temperature.

This return to power involves highly skewed power density distributions combined with far-off-nominal thermal-hydraulic properties of the core (low inlet temperature, pressure and mass flow). Thus core behaviour can be adequately described only by a 3D coupled neutron kinetics / thermal-hydraulics code taking into account local reactivity feedback of fuel temperature and coolant density. On the other hand, the cooldown process is comparatively slow with time constants ranging

from several minutes to about half an hour, depending on the assumed leak size. Thus a quasi-steady-state approximation of the accident sequence is sufficient.

All HEXTIME calculations are performed in a 1/6 core 3D geometry with 1 node per FA radially a radial reflector and 18 axial layers (16 layers within the core plus lower and upper reflector). A radial cross-section of the calculated part of the core including the location of control and shutdown assemblies is given below.



The analyses are carried out using four energy groups. The required cross-sections and cross-section derivatives with respect to thermal-hydraulic variables and boron concentration as well as the cross-section increments for control assemblies are taken from CASMO-3 calculations. All preliminary results quoted in this paper refer to the new core (BOC 1) without soluble boron. A boron concentration of 0 ppm is chosen to maximize the reactivity release during coolant cooldown.

A reactivity balance at cooldown conditions is given in Fig 2. The balance contains the Doppler reactivity, the reactivity release during cooldown and the control assembly worth. The lowest coolant temperature included in the balance (150 °C) is a typical conservative value taken into account in steam line break (SLB) investigations at HZP for PWR's. The whole reactivity balance is normalized to the reference eigenvalue at HFP with no CA's inserted.

The three different control assembly configurations calculated refer to ARO (no control assembly inserted), ARI (all control and shutdown assemblies inserted) and ARI-SR (all control and shutdown assemblies minus one stuck-rod inserted). Due to the limited 1/6 core geometry the stuck-rod is assumed to be the shutdown assembly (7 CA cluster) located in the centre of the core.

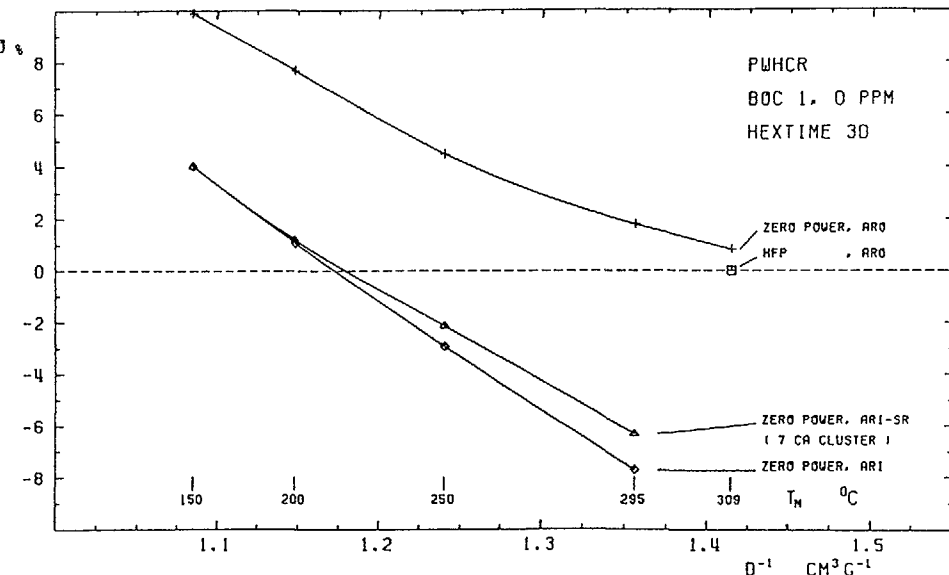


FIG. 2. Reactivity balance at core cooldown conditions (normalized to HFP, ARO).

During cooldown of the plant, even with all or nearly all CA's inserted, the eigenvalue at zero power increases beyond the HFP reference value at coolant temperatures somewhat above 200 °C. Thus return to power cannot be excluded for the present PWHCR concept. The stuck-rod worth of the assumed stuck-rod configuration ( eigenvalue difference between ARI and ARI-SR ) decreases strongly with decreasing temperature – due to strong neutron flux redistribution effects – and almost vanishes at 150 °C. Thus the most efficient stuck-rod at low temperatures is located elsewhere ( probably one of the 6 outer shutdown assemblies ). These stuck-rod positions, however, cannot be described in a 1/6 core geometry. Therefore the investigation of core behaviour following recriticality described below is carried out for the ARI configuration.

Average and local properties of the reactor core after return to power are analyzed assuming thermal-hydraulic boundary conditions typical for SLB investigations in SIEMENS PWR's. Two different flow models are applied, i.e. a closed-channel model ( characterized by a transverse momentum parameter  $s/l = 0$  ) with uniform inlet mass flow distribution and an open-channel model with uniform inlet mass flow distribution and an  $s/l$  value of 0.5. The results are summarized in the following table.

| Case No. | $P/P_N$ % | $s/l$ | $k_{eff}$ | $F_q$ (ring, index, layer) | $q''_{max}$ $W/cm^2$ | $\Delta T_{max}$ °C | $x_{out}^{max}$ | $\theta_{central}^{max}$ °C |
|----------|-----------|-------|-----------|----------------------------|----------------------|---------------------|-----------------|-----------------------------|
| -        | -         | -     | -         | -                          | -                    | -                   | -               | -                           |
| 1        | 10.00     | 0     | 1.0770    | 9.29 (9,2,3)               | 45.3                 | 97.6                | -0.25           | 574                         |
| 2        | 10.00     | 0.5   | 1.0817    | 8.13 (9,2,3)               | 39.7                 | 79.3                | -0.32           | 533                         |
| 3        | 12.93     | 0     | 1.0688    | 9.39 (9,2,3)               | 59.3                 | 114.5               | -0.19           | 705                         |
| 4        | 15.50     | 0.5   | 1.0688    | 8.40 (9,2,3)               | 63.5                 | 101.9               | -0.24           | 743                         |

HEXTIME calculations, 3D, 1/6 core, 18 axial layers, BOC 1, 0 ppm, ARI,  $T_n = 150$  °C,  $p = 100$  bar,  $Gav = 500$  kg/m<sup>2</sup>s closed channel ( $s/l = 0$ ) and open channel ( $s/l = 0.5$ ) model Reference eigenvalue at HFP, ARI.  $k_{ref} = 1.0688$

PWHCR – Core behaviour after return to power

Cases 1 and 2 demonstrate the influence of the open-channel model at a given ( arbitrary ) power level. At SLB conditions, radial and axial power density distributions are highly skewed. Crossflow between adjacent channels ( FA's ) results in a reduction of power peaks and an increase in mass flow at the hot channel exit. At given power level, therefore, maximum local heat flux and fuel centerline temperature as well as maximum temperature rise and steam quality are lower in the open-channel case. However, as the eigenvalues are not identical, cases 1 and 2 are not suitable for comparison of core behaviour at accident conditions.

Cases 3 and 4 are calculated to yield identical eigenvalues, i.e. to compensate a given amount of excess reactivity by power generation. With this requirement, the reduction of local power peaks induced by the open-channel model is over-compensated by an increase in core average power. Thus maximum local heat flux and fuel centerline temperature values even exceed the results of the corresponding closed-channel case, and the closed-channel model cannot be considered to give a conservative description of core behaviour at far-off-nominal conditions.

The present ( preliminary ) results, based on nodal values, do not indicate any danger to the integrity of the PWHCR core during SLB accidents, since maximum heat flux does not exceed the result obtained at nominal HFP conditions (  $q''_{av}$  (HFP) = 48.8 W/cm<sup>2</sup>,  $F_q = 1.78$ , thus  $q''_{max}$  (HFP) = 86.8 W/cm<sup>2</sup> ) and the maximum fuel centerline temperature remains far below the melting temperature.

A more detailed investigation including DNB evaluation requires a refined hot channel analysis methodology. Corresponding HEXTIME development will proceed as outlined in section 5.

## 7 Conclusions

The integrated program system HEXTIME offers important achievements in four areas vital to future high converter reactor design and analysis. Firstly, it couples neutron kinetics and thermal hydraulics, thereby directly taking into account their respective feedback mechanisms. Secondly, it allows 3-dimensional calculation of the reactor core on the basis of fuel assemblies or finer subchannels, also with regard to fluid flow. Thirdly, its equations are formulated and solved including time-dependence, i.e. both steady-state and transient analyses can be performed. Finally, HEXTIME features flexible options for direct evaluation of safety-related parameters such as centerline fuel temperatures and DNB ratios.

HEXTIME is designed for the calculation of reactor core behaviour under conditions ranging from close-to-nominal to far-off-nominal. It may be applied to high converter reactors as well as to any light water reactor with hexagonal fuel rod lattice.

The capability to calculate crossflow effects is essential to achieve the high degree of spatial resolution and accuracy aimed at in the coupled calculation. HEXTIME thus can serve for high accuracy PWHCR core design applications, achieving economically efficient reload strategies. Its capability to evaluate thermal safety margins based on local hot channel fuel pin values is especially valuable in safety analyses for events resulting in highly non-uniform power density distributions and/or low mass flow through the core.

## References

- |  |  |
|--|--|
| <p>/1/ M R Wagner<br/>Three-Dimensional Nodal Diffusion and Transport Theory Methods for Hexagonal-z Geometry<br/>Nuclear Science and Engineering 103 (1989), pp 377-391</p> <p>/2/ M R Wagner<br/>HEXNOD and HEXMED Nodal Reactor Codes for the Design of High Converter Reactors<br/>IAEA Technical Committee Meeting on Technical and Economic Aspects of High Converters, Nuremberg, FRG, 26-29 March 1990</p> <p>/3/ H Finnemann, F Bennewitz, M R Wagner<br/>Interface Current Techniques for Multidimensional Reactor Calculations<br/>Atomkernenergie/Kerntechnik 30 (1977), pp. 123-128</p> <p>/4/ H D. Fischer, H. Finnemann<br/>The Nodal Integration Method – A Diverse Solver for Neutron Diffusion Problems<br/>Atomkernenergie/Kerntechnik 39 (1981), pp. 229-236</p> | <p>/5/ H. Finnemann, H. Raum<br/>Nodal Expansion Method for the Analysis of Space-Time Effects in LWRs.<br/>Proceedings of a Specialists' Meeting on The Calculation of 3-Dimensional Rating Distributions in Operating Reactors, Paris, 26-28 November 1979, NEA/OECD 1980</p> <p>/6/ J. Mackiewicz<br/>Nodal Synthesis – Consistent Nodal Approach for Global Reactor Analysis<br/>Nuclear Science and Engineering 99 (1988), pp. 99-108</p> <p>/7/ M. E. Rose<br/>Weak-element Approximations to Elliptic Differential Equations<br/>Numer. Math. 24 (1975), pp. 185-204</p> <p>/8/ R. Böer, H. Finnemann<br/>MSS-AS: A Pin Power Reconstruction Method Based on Weak Element Approximations to the Neutron Diffusion Equation<br/>to be published</p> <p>/9/ D. S. Rowe<br/>COBRA III C : A Digital Computer Program for Steady State and Transient Thermal Analysis of Rod Bundle Nuclear Fuel Elements BNWL-1695, Battelle-Pacific Northwest Laboratories (1973)</p> <p>/10/ R. E. Masterson, L. Wolf<br/>COBRA III P : An Improved Version of COBRA for Full Core Light Water Reactor Analysis<br/>Nuclear Engineering and Design 48 (1978), p. 293</p> <p>/11/ J.W. Jackson, N.E.Todreas<br/>COBRA IIIC/MIT-2 : A Digital Computer Program for Steady State and Transient Thermal-Hydraulic Analysis of Rod Bundle Nuclear Elements MIT-EL 81-018, Massachusetts Institute of Technology (1981)</p> <p>/12/ R Müller<br/>The Hot Channel Analysis Model for Improved Local Safety Margin Evaluation<br/>Proceedings Jahrestagung Kerntechnik '88, Travemünde, FRG, May 17-19, 1988, pp. 97-100</p> |
|--|--|

**Appendix 1 :**

|                |   |
|----------------|---|
|                | Nomenclature<br>Used in Thermal-Hydraulic Equations   |
| A              | Cross sectional area, (L <sup>2</sup> )   |
| C              | Thermal conduction coefficient, (H/TθL)   |
| C              | Loss function for transverse crossflow, (FT/ML)   |
| D              | Hydraulic diameter, (L)   |
| f              | Friction factor based on all-liquid flow, (dimensionless)   |
| ft             | Turbulent momentum factor, (dimensionless)  |
| g <sub>c</sub> | Gravitational constant, (L/T <sup>2</sup> )   |
| h              | Two-phase enthalpy, Xh <sub>fg</sub> + (1-X)h <sub>f</sub> , (H/M)  |
| h*             | Enthalpy carried by diversion crossflow, (H/M)  |
| m              | Flow rate, (M/T)  |
| p              | Pressure, (F/L <sup>2</sup> )   |
| v              | Liquid specific volume, (L <sup>3</sup> /M)   |
| v'             | Effective specific volume for momentum,<br>(1-X) <sup>2</sup> /ρf(1-α) + X <sup>2</sup> /ρgα, (L <sup>3</sup> /M) |
| w              | Diversion crossflow between adjacent subchannels, (M/TL)  |
| w'             | Turbulent (fluctuating) crossflow between adjacent sub-<br>channels, (M/TL)                                       |
| x              | Distance, (L)   |
| X              | Quality, (dimensionless)  |
| α              | Void fraction, (dimensionless)  |
| Θ              | Orientation of channel with respect to vertical, (radians)  |
| ρ              | Two-phase density, ρgα + ρf(1-α), (M/L <sup>3</sup> )   |
| φ              | Two-phase friction multiplier, (dimensionless)  |
| Subscripts     |   |
| f,g            | Saturated conditions for liquid and vapour, respectively  |
| i,j            | Subchannel identification number  |
| i,j            | Subchannel connection i to j  |

Dimensions are denoted by: L = length, T = time, M = mass, θ = temperature,  
F = ML/T<sup>2</sup> = force and H = ML<sup>2</sup>/T<sup>2</sup> = energy

## IMPROVEMENTS IN THE PREDICTION OF LWHCR LATTICE PARAMETERS

R. BÖHME<sup>1</sup>, J. AXMANN<sup>2</sup>, C.H.M. BROEDERS<sup>1</sup>,  
S. PELLONI, M. SCHATZ<sup>3</sup>

Paul Scherrer Institute,  
Villigen, Switzerland

### Abstract

First analyses of LWHCR lattice experiments carried out at PROTEUS had revealed considerable deficiencies of the calculational methods and available nuclear data. Most codes and their associated data bases used for these studies by different laboratories, were originally tailored for the calculation of fast or thermal reactor lattices and little attention was paid to an elaborate treatment of the resonance region where a large fraction of the reactions takes place in the case of tight LWR lattices. Within the co-operation of PSI, KfK and Siemens-KWU, the availability of more accurate experimental data from the PROTEUS Phase II series of LWHCR lattice experiments has stimulated the development of refined calculational methods and the introduction of new cross section libraries, e.g.:

- The methods for cell calculations in the code systems AARE at PSI and KARBUS at KfK were improved by the introduction of better approximations of the resonance shielding. The cell code KAPER 4 at KfK can now be used for the calculation of water-moderated unit cells and the code SPEKTRA at TUBS is being modified to permit a finer division of the unit cell and the energy scale.
- Considerable progress was made by the creation of suitable multi-group cross-section sets from the nuclear data libraries KEDAK-4, ENDF/B-V and JEF-1.

For most of the LWHCR lattices investigated in PROTEUS it is now possible to predict  $k_{\infty}$  and its changes in the case of voiding within the experimental error limits. However, a comparison of calculated reaction rate ratios with measured indices still reveals compensating discrepancies in the balance equation. This will be demonstrated in the full paper. The spread of results calculated for a benchmark problem proposed by NEACRP has been considerably reduced by the application of the improved methods and data. This holds for properties of burnt-up lattices as well, which cannot be confirmed by PROTEUS experiments. It is expected to obtain more evidence about the remaining discrepancies between calculations and measurements from experiments currently being performed/planned in PROTEUS.

---

<sup>1</sup> Kernforschungszentrum Karlsruhe GmbH, Karlsruhe, Federal Republic of Germany

<sup>2</sup> Technische Universität Braunschweig, Braunschweig, Federal Republic of Germany

<sup>3</sup> Siemens AG, Energieerzeugung KWU, Erlangen, Federal Republic of Germany.

## 1. Introduction

The current series of experiments for the investigation of the physics of a Light Water High Conversion Reactor (LWHCR) at the PROTEUS reactor facility in Switzerland has been progressed since 1985 /1/.

The planning of this so-called PROTEUS Phase II program was made within the framework of a close co-operation between the Paul Scherrer Institute (PSI, formerly EIR) and several German groups interested in the development of an LWHCR. For licensing and for the preparation of the experiments numerous calculations were required. All safety related computations and most reactor calculations were run by the PROTEUS team. However, the co-operating institutions participated in the prediction of the physics characteristics of the unit cells to be investigated in these experiments. Mainly the predicted values of  $k_{\infty}$  (the ratio of neutron production to neutron absorption in a fundamental mode spectrum) and reaction rate ratios were compared among the co-operating teams and with experimental results, as soon as the latter became available. In parallel, the groups involved in the evaluation of PROTEUS experiments participated in the calculation of LWHCR benchmarks proposed by NEACRP /2/. As a result of these comparisons an improvement of the methods and data applied for the calculation of the PROTEUS lattices took place. This has not necessarily meant a continuous reduction of differences between calculated and measured values. The progress made since 1986 in predicting integral parameters measured in PROTEUS will be described in this contribution. The details of the PROTEUS Phase II program itself, the experimental techniques applied as well as the accuracies achieved will be discussed in an accompanying paper to be presented at this Meeting /3/.

## 2. Short Description of the LWHCR Experiments in PROTEUS

Two lattice configurations of the PROTEUS Phase II series with different volumetric moderator-to-fuel ratios ( $V_m/V_f$ ) have been analysed to date. The test lattices of about 0.5 m diameter were built from 7.5 % enriched mixed-oxide fuel rods of 0.84 m length with 0.28 m thick UO<sub>2</sub> blankets on top and bottom. These lattices form the central test zone of the PROTEUS reactor, which is radially surrounded by a uranium metal buffer and thermal driver regions.

The PuO<sub>2</sub>/LO<sub>2</sub> was fabricated from LWR-Pu and clad in stainless steel tubes with an outer diameter (d) of 9.6 mm. The pitch (p) of the hexagonal tight lattice was 10.7 mm. It was increased to 12.0 mm for the study of a wider-spaced lattice. Two different moderators were used in these experiments: water at room temperature and Dowtherm, an organic liquid

containing 42.5 % less hydrogen per unit volume than water. In addition, for the determination of the reactivity change connected with the loss of coolant, completely voided lattices were investigated as well.

In the first set of experiments the ratio of pitch to fuel rod diameter was 1.12. It was increased to 1.26 in the second reference lattice investigated in the PROTEUS Phase II experiments. In the water moderated tight lattice ( $V_m/V_f = 0.48$ ) the ratio of hydrogen to fuel atoms was only slightly less than in the Dowtherm moderated wider lattice ( $V_m/V_f = 0.95$ ). As a measure of effective moderation the relative hydrogen content of the moderator (water = 1.0) multiplied by the ratio  $V_m/V_f$  will be used as a parameter in the comparison of calculated values (C) with experimental data (E).

Of the several types of experimental results obtained in the PROTEUS Phase II experiments /3/ only measured values of  $k_{\infty}$  and the reaction rate ratios for capture in <sup>238</sup>U (C8), capture in <sup>242</sup>Pu (C2) and fission in <sup>238</sup>U (F8) - each expressed relative to fission in <sup>239</sup>Pu (F9) - will be compared with calculated quantities in this paper.

It should be mentioned that a comparison of reaction rate ratios measured in PROTEUS with ratios calculated for a fundamental mode neutron spectrum requires the knowledge of correction factors accounting for differences between the actual spectrum in the central test region of PROTEUS and the fundamental mode spectrum. These correction factors were estimated at PSI and at TUM Braunschweig from one-dimensional calculations of the whole PROTEUS reactor and from both 1D and 2D calculations of IKE Stuttgart /3/. For most reaction rate ratios such independent estimates agree very well. The correction factors deviate < 0.2 % from unity for C8/F9 and C2/F9 and < 1 % for F8/F9 measured in moderated lattices. In dry lattices some measured reaction rate ratios have to be corrected up to 2 %.

## 3. Calculational Methods and Data at the Start of PROTEUS Phase II

Various codes were employed in the analysis of the PROTEUS-LWHCR Phase I experiments /4/. They were either modifications of codes and data libraries used for fast reactor calculations or for thermal reactor design. Some of the codes qualified in these studies were used in 1986 for the prediction of physics parameters of the PROTEUS Phase II lattices /5/. Earlier calculational routes with less suited fast reactor codes (e.g. GRUCAH with the KFKINR cross-section set at KfK) or with older WIMS data libraries were not further pursued at that time. For the cell calculations the most appropriate tools readily available were

1 at PSI, the U.K. lattice code WIMS-D4 /6/ with its so-called 1981 library based on UKAEA data evaluations /7/.

- 2 at KfK, the code system KARBUS with a data set G69COLD derived from KEDAK-4 /8/;
- 3 at TU Braunschweig, the cell code SPEKTRA with a cross-section set DATUBS II derived from the fast reactor cross-section file WIPRO (based on ENDF/B-IV and -V) and complemented with thermal cross-sections from BNL /9/;
- 4 at Siemens-KWU, the Monte Carlo code KMC-MERIT used with nuclear data taken from ENDF/B-IV and -V /10/

The ratios (C/E) of the first predictions of  $k_{\infty}$  of the tight lattices to the corresponding later measured values are shown in the upper part of Figure 1. It can be seen that many predictions deviate by several standard deviations from the measurements. It could be demonstrated that even in cases of reasonable agreement a compensation of considerable discrepancies in calculated and measured reaction rates was taking place /1/.

It is evident that a prediction of the change in  $k_{\infty}$  in the case of voiding was not reliable enough for design purposes at that time. Therefore, efforts were initiated at each of the participating institutes to either improve existing calculational methods and nuclear data libraries or change to alternatives. Some of the developments will be reported here.

It should be mentioned that activities to include JEF-2 data in this development have just been started, but results are not yet available.

#### 4. Improvements of Codes and Data Libraries

##### 4.1 General Improvements in Various Codes

A detailed comparison of the reaction rate balances calculated with data and methods applied within the Swiss/German co-operation revealed some shortcomings of a general nature. Some of them could either be eliminated without great effort or correction factors could be determined by means of supplementary calculations. In several publications /11/, /12/ parameters of considerable influence on the comparison of calculated and measured reaction rate ratios and  $k_{\infty}$  have been identified. Some results of these investigations could be confirmed by additional calculations using the KAPER4 code /13/. A summary of these studies will be given in this section.

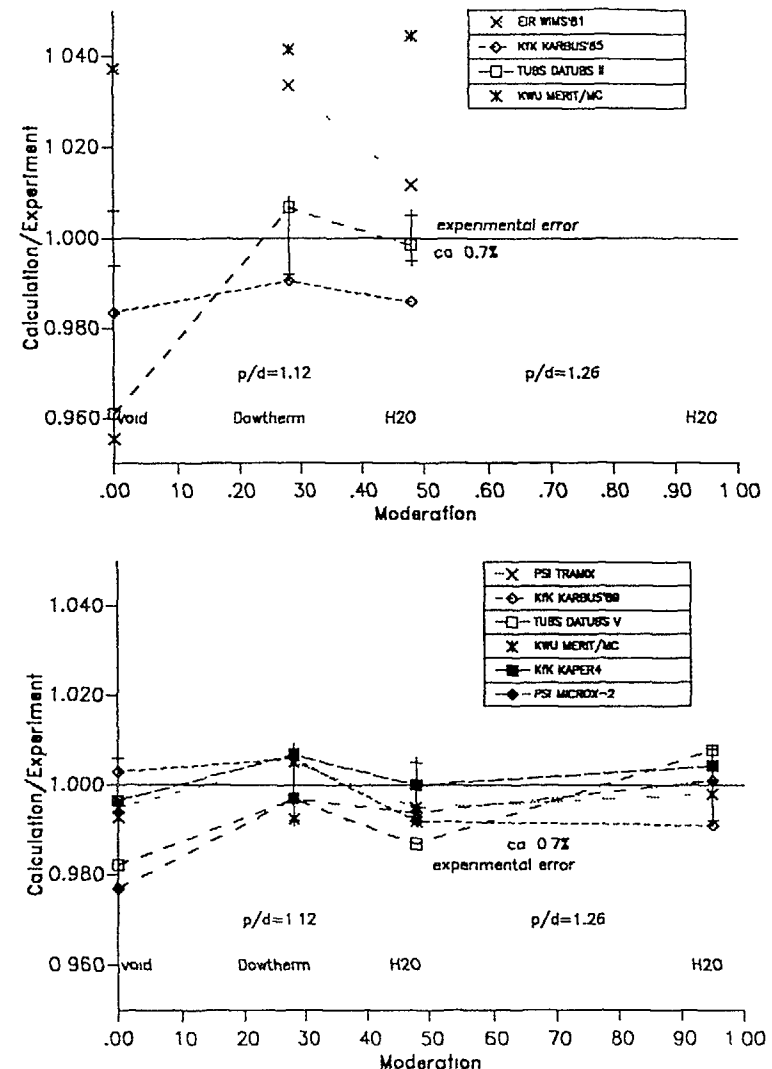


Figure 1 Ratio Calculation/Experiment for  $k_{\infty}$  measured in PROTEUS Predictions 1986 (top) and Status 1989 (bottom)

It should be noted that some of the important improvements introduced at PSI /12/ in the preparation of effective cross-sections, e.g.

- the correction of the elastic removal cross-section accounting for differences between the actual neutron spectrum and the library weighting spectrum in few-group calculations
- application of the IR method instead of the narrow resonance approximation

are not yet common practice in calculational procedures elsewhere

#### 4.1.1 Improvement of the KMC-MERIT Calculations

A particular difficulty was encountered in application of the Monte Carlo code KMC-MERIT 10'. The results of these calculations were found to be very sensitive to the modelling of the unit cells in cases of short linear dimensions (in mean free path) of the lattice calculated. The modelling of a larger portion of the test lattice improved the ratios of calculated to measured reaction rate ratios and  $k_{\infty}$  considerably. This can be seen in the lower diagram of Figure 1

#### 4.1.2 Resonance Shielding of $^{242}\text{Pu}$ and of Structural Materials

In 1986 a method was developed at PSI for the measurement of the ratio of capture in  $^{242}\text{Pu}$  to fission in  $^{239}\text{Pu}$  (C2/F9) with an experimental error of about 4 % /1/. From the comparison with calculated ratios it became evident that some of the data sets used at that time for the analysis (WIMS'81, G69COLD) yielded ratios of calculation to experiment as high as between 1.5 and 1.7 in the wet PROTEUS lattices. This discrepancy was attributed to the inadequate treatment of the 2.7 eV resonance of  $^{242}\text{Pu}$  in the 69-group structure of WIMS. The disagreement of many calculated C2/F9-values was also observed and studied by Ishiguro /14/. The introduction of self shielding factors in the two WIMS energy groups between 2.1 and 3.3 eV was a remedy, although the width of the resonance and its resonance energy near the group boundary makes it not well suited for application of standard self shielding methods. The effect of self shielding this resonance by using such a modified cross-section set is a reduction of the calculated ratio C2/F9 by about 42 % in the tight water-moderated lattice, by about 39 % in the Dowtherm-moderated lattice and < 1 % in the dry lattice. This results in increases of  $k_{\infty}$  by 1.0, 0.8 and 0.0 %, respectively.

Less spectacular effects arose from the neglected self shielding of structural materials in moderated lattices. But a change in  $k_{\infty}$  of 0.6 % was found for the dry lattice /12/. In KARBUS'85 calculations the inaccurate self shielding was due to poor equivalence relations

for the can material. It resulted in an overestimation of  $k_{\infty}$  by about 0.2 % in moderated lattices

#### 4.1.3 Resonance Shielding of Oxygen and Transport Corrections

In some of the 69-group cross-section sets of WIMS structure used in the earlier analyses self shielding of the oxygen resonances above 0.4 MeV was missing for historical reasons. The omission of the self shielding of oxygen has little influence on reaction rate ratios (F8/F9 decreases < 1 %) and  $k_{\infty}$  ( $\approx$  0.1 %) in the wet lattices. But in the dry lattices all reaction rates in the resonance energy region are increased and  $k_{\infty}$  is reduced by 0.8 % (KAPER4 calculation) to 1.1 % (AARE calculation).

A secondary effect of the missing self shielding of oxygen was a reduction of the calculated migration area  $M^2$  of all lattices by about 2 to 3 %. This has an influence on  $k_{\infty}$  determined from measured bucklings  $B^2$ , where leakage is accounted for by a  $M^2 B^2$  term.

$M^2$  is also influenced by the method applied for the calculation of transport corrections to the total cross-section in order to obtain a diffusion coefficient D /11/. Since global currents are a priori not known in many calculational procedures an outflow approximation is made instead of an inflow correction in the calculation of  $\Sigma_v = 1/(3D)$ . An estimate made using KAPER4 has indicated that this approximation reduces the calculated  $M^2$  of the water-moderated lattices by about 2 %. The various errors introduced in the calculation of the migration area were taken into account by corresponding error margins in the experimental evaluation of  $k_{\infty}$ .

#### 4.1.4 Introduction of Problem-Dependent Spectra of Fission Neutrons

Neutron physics calculations are considerably simplified by the assumption of a unique spectrum of fission neutrons. If the fission neutron spectrum provided by the data set agrees well with the effective fission spectrum of the problem only small errors are introduced in reactor calculations. In some of the data sets used for WIMS/D and KARBUS calculations the original fission neutron spectrum was constructed for predominant  $^{235}\text{U}$  fission (Maxwellian temperature of  $\approx$  1.33 MeV), while in the PROTEUS test zone fission of  $^{239}\text{Pu}$  produces a harder spectrum of fission neutrons ( $\approx$  1.37 MeV). These early calculations required, therefore, a correction of the calculated ratio F8/F9 by 2 % and of calculated  $k_{\infty}$  by up to 0.5 % (in the dry lattice) /12/. All calculational procedures currently use either a precalculated effective fission neutron spectrum or a fission neutron spectrum calculated via an iterative procedure.

An early activity at PSI was the creation of a new 69-group set based on the Joint European File JEF to be used in WIMS/D calculations. The WIMS-JEF library was processed using the NJOY module WIMSR in connection with the library management program WILMA<sup>11</sup>. Although the calculated reaction rate ratios were found to be in better agreement with measurements than those obtained using the WIMS 81 library, they showed the well-known weaknesses of former WIMS/D calculations, e.g. no self shielding below a certain energy limit<sup>15</sup>.

A new approach was then the installation of the AARE code system and the generation of suitable data sets from the JEF-1 library. AARE<sup>12</sup> is an update of the DA\DE (applied nuclear DAta, core Neutronics DEpletion) system from Los Alamos<sup>16</sup>. The modular construction of the code package separates the input processing, the solution of the transport equation (by ONEDANT or TWODANT) and the post-processing into distinct, independently executable code modules. The modules are connected to each other solely by means of binary interface files.

For cell calculations two codes are available within the AARE system:

- 1 TRAMIX is a code which reads nuclear data from a library in MATXS format and produces groupwise cross-sections which can be used for succeeding diffusion or transport calculations. TRAMIX is able to shield resonance data in the whole energy range using either the Bondarenko formalism<sup>17</sup> or the intermediate resonance absorption shielding method (IR). Dancoff corrections for different geometries are applied. Fission spectra are calculated from fission matrices.

For LWHCR applications TRAMIX has been run with different energy group numbers, usually 70 to 308. In the few-group calculations elastic scattering matrices are corrected for differences between the actual flux and the library weighting flux.

- 2 MICROX 2<sup>18</sup> is an integral transport theory spectrum code which solves the neutron slowing down and thermalization equations on a detailed energy grid for a two region lattice cell. It produces groupwise cross-sections suitable for use in transport codes, such as ONEDANT and TWODANT. MICROX 2 was developed for the efficient and rigorous preparation of broad group neutron cross sections for poorly moderated systems (such as fast breeder reactors) in addition to the well moderated thermal reactors (such as high temperature reactors and light water reactors). The fluxes in the two regions (fuel and moderator) are coupled by transport corrected collision proba-

bilities. They are computed from escape probabilities and energy dependent Dancoff factors. The flat flux approximation is made in both regions.

In the resonance energy region the balance equations are solved on an ultra fine energy grid. The resonance data include temperature dependent Doppler-broadened resonance cross-sections at about 15000 energy mesh points between 8 keV and 0.414 eV. By this high resolution the code accounts explicitly for overlap and interference effects between different resonance levels in both the resonance and thermal energy range. As pointwise data are also available for the low-energy part of the unresolved range (up to 8 keV) no special provisions for the treatment of resonance shielding in this range are required.

Above a flexible energy limit (< 8 keV), which determines the upper energy boundary for the pointwise resonance calculation, sets of temperature- and dilution-dependent fine-group data are available. Interpolation between temperature- and dilution dependent data enables the calculation of self shielded effective cross-sections in this intermediate and high energy range.

For the calculation of fundamental mode properties in  $B_n$  approximation the program SOLVERB can be run.

For all LWHCR calculations nuclear data have been taken from the JEF-1 library. As an example the influence of different calculational methods on the variation of the ratio of capture in  $^{242}\text{Pu}$  to fission in  $^{239}\text{Pu}$  (C2/F9) with increasing moderation is shown in Figure 2. The curves plotted for the PSI calculations demonstrate that the strong dependence of C/E on the moderation calculated with TRAMIX (70 energy groups) disappears in the case of the pointwise treatment of the 2.7 eV resonance using MICROX 2 (193 energy groups). This figure shows also that the case of the voided lattice (effective moderation = 0) does not fit into the general scheme: the neutron spectrum is much harder in the voided case and contributions of the important 2.7 eV resonance are negligible. The results plotted for this point are a measure of the discrepancies in the fast neutron capture cross-section of  $^{242}\text{Pu}$ . Similar effects, of course less pronounced, are found for other resonance reactions as well.

This can be clearly seen in Figure 3. The ratio of capture in  $^{238}\text{U}$  to fission in  $^{239}\text{Pu}$  (C8/F9) is even in voided lattices strongly influenced by the treatment of resonance shielding. Both calculational methods, TRAMIX and MICROX-2, yield about 3 % different results, although the same data library - JEF-1 - is used. In this case the discrepancy can be explained by the different methods of interpolation applied in the region of unresolved resonances. The discrepancy disappears with increasing effective moderation, which means larger contributions from the resolved resonance region.

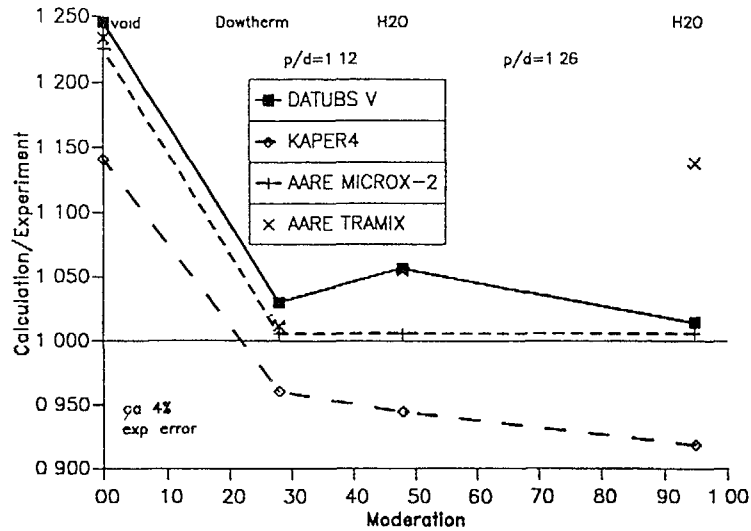


Figure 2 Ratio Calculation/Experiment for C2/F9 measured in PROTEUS

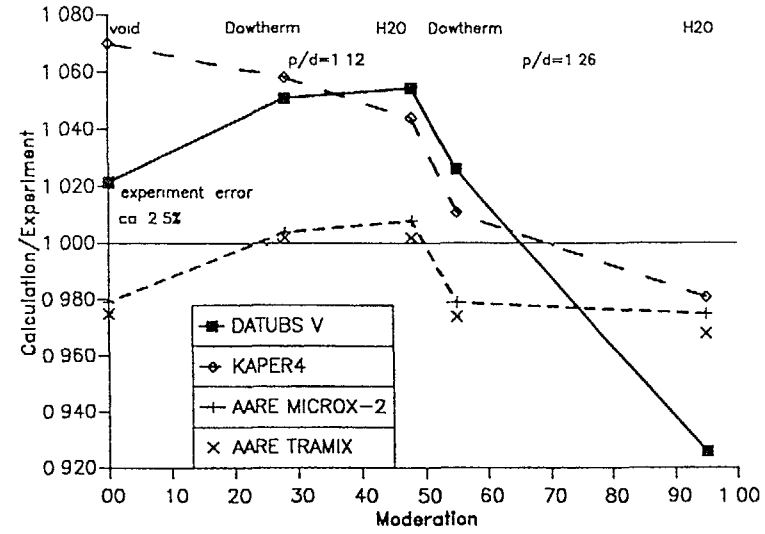


Figure 4 Ratio Calculation/Experiment for F8/F9 measured in PROTEUS

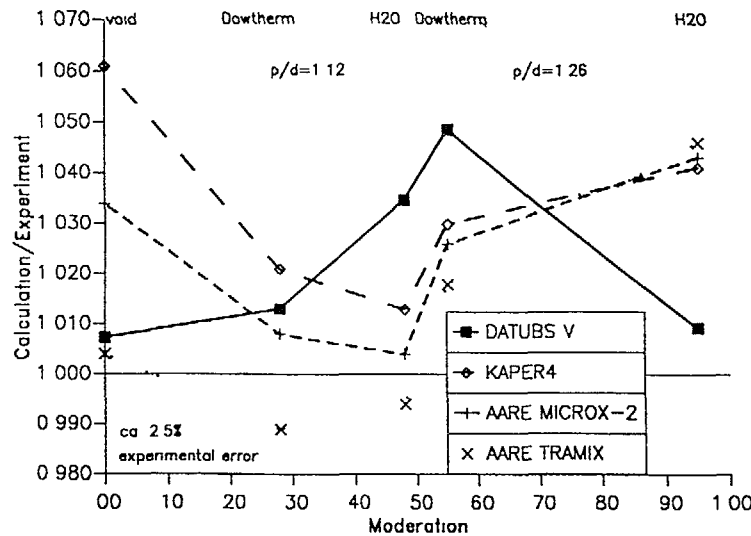


Figure 3 Ratio Calculation/Experiment for C8/F9 measured in PROTEUS

The fast fission index F8/F9, i.e. the ratio of fission in  $^{234}\text{U}$  to fission in  $^{239}\text{Pu}$  shown in Figure 4, is less effected by the calculation of resonance shielding and mainly the basic nuclear data, which are identical for TRAMIX and MICROX-2 calculations, determine the ratio C/E. This results in similar dependence of F8/F9 on the effective moderation for the two cases.

#### 4.3 Development of DITUBS at IfRR

The program system DITUBS /19/ was developed at the Technical University of Braunschweig for the calculation of LWHCRs. Its essential component is the cell code SPEKTRA /9/ mentioned earlier (Section 3). SPEKTRA is a two zone cell program the fuel contained in the central region is surrounded by homogenized structural materials and moderator. It is a collision probability program with Dancoff factor corrections as given by Sauer /20/. The fast and intermediate energy range down to 0.215 eV is divided into 25 energy groups of the Bondarenko structure /17/. In these groups resonance self shielding is taken into account by self shielding factors, as common in fast reactor calculations 10 more energy groups of equal lethargy width cover the range down to  $10^{-4}$  eV.

The cross-section sets DATUBS II and III were derived from fast reactor data (WIPRO data of INTERATOM, based on ENDF/B-IV and -V) and thermal cross-sections from BNL. The predicted  $k_{\infty}$  of tight moderated PROTEUS lattices agreed well with the experiments, as can be seen in Figure 1. But the calculated  $k_{\infty}$  of the voided lattice, and accordingly the change of  $k_{\infty}$  upon voiding, did not agree with the measurements. Thus, a modified cross-section set DATUBS IV was compiled which contained adjusted inelastic scattering data for fuel isotopes taken from the cross-section set KFKINR /21/. Calculated  $k_{\infty}$  for voided lattices were increased by more than 2 %, mainly due to a decrease in the ratio of capture in  $^{234}\text{U}$  to fission in  $^{239}\text{Pu}$  (C8/F9) and an increase of the fast fission index F8/F9.

More recently a new data set for SPEKTRA calculations, DATUBS V, was created at PSI using the NJOY processing code, Version 6/83. All fuel cross-sections were taken from the JEF-1 library, but the thermal scattering cross-sections are still based on BNL data for programming reasons.

$k_{\infty}$  of PROTEUS lattices calculated with SPEKTRA and DATUBS V are shown in the lower part of Figure 1. There is still a slight tendency to underestimate  $k_{\infty}$  of the dry lattices. This must be an effect of not measured reactions, since the measured reaction rate ratios shown in Figures 3 and 4 can be calculated within the experimental error limits.

Somewhat surprising is the dependence of C/E for SPEKTRA/DATUBS V in Figures 3 and 4 on the effective moderation. Especially for the wider water moderated lattice no similarity with TRAMIX and MICROX-2 calculations can be observed, although all the cross-section sets used in these calculations are based on JEF-1 data. In addition, the representation of the unit cell in MICROX-2 calculations is the same as in SPEKTRA calculations. The C/E discrepancies for C8/F9 and C2/F9 are small, but C/E for F8/F9 is very low. Further comparisons are required for an explanation of this effect.

For detailed investigations improvements of the SPEKTRA code are planned. The permitted number of energy groups and the number of regions in the unit cell will be increased.

#### 4.4 Development of KARBUS and KAPER4 at KfK

The code system KARBUS /8/ was introduced in 1985. It is a collection of programs specifically tailored for the calculation of LWHCR lattices. Burn-up calculations and reactor design calculations can be made. A detailed description of these features of KARBUS will be given in another paper at this Meeting /22/.

The cross-section sets used for the evaluation of PROTEUS experiments were usually of the 69-group structure of the WIMS code. They were generated from nuclear data contained in

the KEDAK 4 library. The preparation of effective cross-sections for cell calculations within KARBUS is made with the assumption of equivalence principles. First, effective background cross-sections are determined to take into account the lumping effect and Dancoff factors as proposed by Sauer /20/. For these background cross-sections self shielded cross-sections for the fuel region and the can are then determined according to Bondarenko's method /17/. With these cross-sections a cell calculation is carried out, using either the collision probability routine PERSEUS of WIMS or the transport program ONETRAN. With calculated cell fluxes effective cross-sections for the unit cell can be calculated and forwarded to succeeding routines.

A comparison of cell cross-sections obtained from KARBUS 85 and other codes revealed some deficiencies of the cross-section preparation path especially in cases of voided unit cells. They were removed by the introduction of improved equivalence relations. Other improvements of KARBUS were

- iterative calculation of effective fission neutron spectra,
- iterative calculation of background cross-sections for self shielding (optional),
- elimination of numerical errors in the input cross-section sets

The version KARBUS 89 has two options for the preparation of effective cross-sections for cell calculations in the resonance energy region below a chosen energy limit (recommended < 150 eV)

Application of Bondarenko's self shielding concept, as in former versions of KARBUS,

Use of the fine energy mesh collision probability program RESAB-II of IKE Stuttgart  
23/

The calculation of effective cross-sections using RESAB-II in connection with the well proven cross-section set G69CT005 has not in all cases reduced the differences found between calculated and measured reaction rate ratios. In addition, there seems to be a greater tendency of increasing C/E-values for the ratio C8/F9 with increasing moderation.

The cell program KAPER4 /13/ has been used at KfK for LWHCR studies, too. It was modified for the calculation of water-moderated cells. But there are still approximations in the program which require attention in each case calculated, e.g. the assumption of isotropic scattering. On the other hand, KAPER4 is a useful tool for the study of influences of parameters which cannot easily be varied in other codes. KAPER4 has various options to calculate cell diffusion coefficients, to estimate influences of the flat flux approximation and of transport approximations.

The results of KAPER4 calculations of  $k_{\infty}$  and reaction rate ratios using the 69-group cross section set G69CT005 are shown in Figures 1 to 4. In general, differences between KARBUS 89 and KAPER4 cell calculations are small and accordingly only one set of results is shown in Figures 2 to 4.

Using KAPER4 the influence of various approximations made in collision probability codes on calculated properties of the PROTEUS Phase II lattices has been studied. A summary of the results is

In many LWHCR calculations unit cells are represented by three regions fuel, can and moderator. A further division of the moderator region in three zones increases calculated ratios C8/F9 and C2/F9 of the wider water-moderated lattice of PROTEUS by 0.8 and 0.6 %, respectively.  $k_{\infty}$  decreases by 0.3 %. In the case of moderation by Dowtherm and in the water-moderated tight lattice the ratios are increased by 0.5 and 0.2 %, respectively, and  $k_{\infty}$  is reduced by 0.2 %.

An estimate of the upper limit of a transport correction of collision probabilities was made by replacing the total cross-section and the within-group scattering cross-section by transport corrected cross-sections in the integral transport equation for isotropic scattering. This replacement causes increases of the capture rate ratios and a reduction of  $k_{\infty}$  of the wider water-moderated lattice by 0.1 %.

Anisotropic diffusion has only an indirect influence (via spectral shifts due to leakage) on fundamental mode parameters measured in PROTEUS experiments. The maximum effect was calculated for the wider dry lattice the increase of the migration area by about 6 % causes an increase of  $k_{\infty}$  of the fundamental mode by < 0.1 %.

Thus, most approximations investigated have small effects on the ratios C/E compared with the experimental errors. However, a finer division of the moderator region may be required in calculations based on the collision probability method.

## 5. Present Status of Methods and Data

An overall impression of the progress made in the calculation of reaction rate ratios and  $k_{\infty}$  for the PROTEUS Phase II test lattices can be obtained by comparing the top and bottom of Figure 1. For both diagrams identical scales have been used. It is evident that almost all calculations yield  $k_{\infty}$  within the experimental error band ( $1\sigma$ ). Further improvements of methods or data cannot be achieved by the comparison of measured and calculated  $k_{\infty}$  only. It is mandatory to compare calculated with measured reaction rate ratios as well. For some recent calculations this has been done in Figures 2 to 4. In Figure 3 the ratio of capture

in  $^{238}\text{U}$  to fission in  $^{239}\text{Pu}$  (C8 F9) is shown. This is the most important reaction rate ratio in terms of its influence on  $k_{\infty}$  and the conversion ratio.

It can be seen that some discrepancies, e.g. between the KAPER4 calculation for the dry lattice and the experiment, are much larger than the experimental error. The satisfactory agreement of calculated and measured  $k_{\infty}$  values in such cases is a result of compensating effects in the reaction rate balance, e.g. by fission in  $^{238}\text{U}$  for the KAPER4 dry lattice calculation, as shown in Figure 4.

Most discrepancies between measured and calculated reaction rate ratios can be attributed to the nuclear data used for the calculations. The replacement of WIMS and KFKI/R data by cross-section sets based on the JEF-1 or KEDAK-4 library has reduced many differences considerably. But it could be shown that for some reaction rate ratios, e.g. C2/F9, the treatment of resonance absorption influences the calculated values more than the data itself. Detailed investigation of C/E discrepancies can thus be used to identify shortcomings in methods and data.

## 6. Conclusions

The continuous development of calculational methods and the introduction of new cross-section sets based on modern nuclear data libraries has reduced the differences between calculated and measured  $k_{\infty}$  to values close to the experimental error limit. This is not yet the case for some measurable reaction rate ratios. It must be assumed that a compensation of discrepancies in the various contributions to the reaction rate balance leads to the satisfactory agreement in  $k_{\infty}$ .

It could be shown that deficiencies in nuclear data as well as remaining uncertainties in the treatment of resonance absorption may cause the differences found between calculated and measured reaction rate ratios. More detailed analyses of the PROTEUS LWHCR Phase II experiments - also covering the various other types of integral parameters measured /3/ - should help identify other calculational aspects requiring improvement.

## References

- /1/ R Seiler, R Chawla, K Gmur, H Hager, H-D Berger, R Böhme "Investigation of the Void Coefficient and other Integral Parameters in the PROTEUS LWHCR Phase II Program", Nuclear Technology, 80, 311 (1988)
- /2/ Y Ishiguro, H Akie, H Takano "Summary of NEACRP Burnup Benchmark Calculations for High Conversion Light Water Reactor Lattices", in Proc 1988 International Reactor Physics Conference, III-97, Jackson Hole, Sept 18-22, 1988

- /3/ R. Chawla, H.-D. Berger, H. Hager, R. Seiler: "The PROTEUS Phase II Experiments as Data Base For LWHCR Physics Validation", IAEA Technical Committee Meeting on Technical and Economic Aspects of High Converters, Nuremberg, 26-29 March 1990, 622-I3-TC-700 4.2
- /4/ R. Chawla, R. Bohme: "LWHCR Physics Experiments and their Interpretation", ANS Topical Meeting on Advances in Reactor Physics and Safety, Saratoga Springs, 17-19 September 1986
- /5/ H.-D. Berger, R. Böhme, R. Chawla: "Verification of Calculational Methods for Light Water High Converter Reactors by Critical Experiments", ANS Topical Meeting on Advances in Reactor Physics, Mathematics and Computation, I-107, Paris, April 1987
- /6/ J.R. Askew, F.J. Fayers, P.B. Kemshell: "A General Description of the Lattice Code WIMS", J. Brit. Nucl. Energy Soc., 5, 564 (1966)
- /7/ M.J. Halsall, C.J. Taubman. "The '1981' WIMS Nuclear Data Library", AEEW-R 1442 (1983)
- /8/ C.H.M. Broeders: "Neutron Physics Investigations for Advanced Pressurized Water Reactors", Nuclear Technology, 71, 96 (1985)
- /9/ H.-D. Berger "Neutronenphysikalische Untersuchungen zu einem Fortgeschrittenen Druckwasserreaktor mit hoher Konversion", Thesis, Technische Universität Braunschweig (1984); also GKSS report 85/E/15 (1985)
- /10/ U. Schmidt, G. Ambrosius, C. Shin: "Genauigkeit des Monte Carlo Programms KMC bei Kritikalitätsberechnungen für Kompaktlager", Jahrestagung Kerntechnik '86, p 15, Aachen 1986
- /11/ S. Pelloni, J. Stepanek. "Testing of a JEF-1 Based WIMS-D Cross Section Library for Migration Area and  $k_{\infty}$  Predictions for LWHCR Lattices", EIR-610 (Jan. 1987)
- /12/ S. Pelloni, J. Stepanek, P. Vontobel: "Analysis of PROTEUS Phase II Experiments Performed Using the AARE Modular System and JEF-Based Libraries", Nuclear Science and Engineering, 103, 247 (1989)
- /13/ R. Bohme and E.A. Fischer: "The Fast Reactor Cell Code KAPER4", KfK 4435 (1988)
- /14/ Y. Ishiguro: "Resonance Absorption and Coolant Void Reactivity Coefficient in Tighter Pitch Lattices", IAEA Advisory Group Meeting on Nuclear Data for the Calculation of Thermal Reactor Reactivity Coefficients, Vienna, 7-11 December 1987
- /15/ S. Pelloni, R. Chawla, J. Stepanek: "Application of WIMSD/JEF-1 Data Libraries to the Analysis of LWHCR experiments", ANS Topical Meeting on Advances in Reactor Physics, Mathematics and Computation, Paris, April 1987
- /16/ R. J. LaBauve, T. R. England, D. C. George, R. E. MacFarlane, W. B. Wilson "DANDE - A Linked Code System for Core Neutronics/Depletion Analysis", LA-10412-MS (1985)
- /17/ I.I. Bondarenko: "Group Constants for Nuclear Reactor Calculations", Consultants Bureau, New York (1964)
- /18/ D. Mathews, P. Koch: "MICROX-2 - An Improved Two-Region Flux Spectrum Code for the Efficient Calculation of Group Cross Sections", GA-A-15009 (Vol. 1), UC-77, General Atomics (1979)
- /19/ J.K. Axmann: "Neutronenphysikalische Methoden zur Kernauslegung untermoderierter hoher konvertierender Druckwasserreaktoren", Proc. VGB-Kongress Forschung in der Kraftwerkstechnik (1988)
- /20/ A. Sauer: "Approximate Escape Probabilities", Nucl. Sci. Eng. 16, 329 (1963)
- /21/ E. Kießhaber: "The KFKINR-Set of Group Constants", KfK-1572 (1972)
- /22/ C.H.M. Broeders: "Development of Calculational Procedures for the Neutron Physics Design of Advanced Reactors", IAEA Technical Committee Meeting on Technical and Economic Aspects of High Converters, Nuremberg, 26-29 March 1990, 622-I3-TC-700 3.1
- /23/ B. Rück, R. Ruhle: "RESAB II, Ein Programm zur Berechnung von Gruppenkonstanten im Resonanzbereich nach der Stoßwahrscheinlichkeitsmethode", IKE Stuttgart, internal report (1972)

# EVALUATION OF CRITICAL HEAT FLUX AND FLOODING EXPERIMENTS FOR HIGH CONVERSION PWRs

M. DALLE DONNE

Kernforschungszentrum Karlsruhe GmbH,  
Karlsruhe, Federal Republic of Germany

## Abstract

High converting PWR's (HCPWR or APWR) are based on fuel elements with rod placed in a tight lattice triangular array. The CHF correlation developed at KfK for such geometry has been tested against recently performed experiments. For tests with grid spacers the correlation has been confirmed by various experiments within a scatter band of 10 - 20%. The original KfK correlation prediction for spiral supports is based on tests with single spiral wire and it is not applicable for six integral spiral rib supports. A modification of the correlation, which accounts for this kind of support as well, is proposed in the paper.

The computer code FLUT originally developed at GRS-Garching, for the modelling of the flooding phase during a Loss-of-Coolant Accident in a PWR, has been modified to account for the different APWR core geometry. The new version of the code developed at KfK is able to predict better than FLUT both the tests performed for the APWR as well as for the PWR core geometry. The latest version of FLUT-FDWR, called FLUT-FDWR-MM, allows a finer axial nodalisation of the fuel rod in the region of the quench front. This reduces the oscillations in the rod cladding temperatures and in other physical parameters, and, in some cases improves even the level of the code predictions.

## I INTRODUCTION

The design work for the Kernforschungszentrum Karlsruhe (KfK) concept of an Advanced Pressurized Water Reactor (APWR), also called High Conversion PWR (HCPWR) /1, 2/, has been supported at KfK by theoretical and experimental work in the field of thermohydraulics. In the present paper the latest theoretical work in this field is presented. Two aspects will be dealt with, namely the confirmation and further development of a correlation capable of predicting the

critical heat flux in a tight lattice triangular array of rods, and the improvements of the computer code FLUT-FDWR (FDWR = Fortgeschrittener Druckwasserreaktor, i.e. APWR) developed for the modelling of the reflooding phase of a tight lattice HCPWR after a Loss of Coolant Accident.

## II CRITICAL HEAT FLUX CORRELATION

In 1984 Dalle Donne and Hame developed a new critical heat flux correlation valid for triangular arrays of rod bundles /3/. This correlation should hold for rod bundles with grid spacer supports as well as for spiral wire supports. In the present paper this correlation will be compared with experimental evidence related to rod bundles with tight triangular lattice made available since 1984, both for bundles with grid spacers and with spiral spacers.

The Dalle Donne-Hame correlation is based on the WSC-2 correlation (Table I) /4/, whereby the geometry-dependent parameters  $Q_1$ ,  $Q_2$ ,  $Q_4$  and  $V$  were determined by root mean-square fitting from experimental data of CHF tests performed for rod bundles with tight triangular rod lattices ( $1.02 < p/d < 1.36$ ,  $d$  = rod diameter,  $p$  = lattice pitch).

The new determined values were (for the explanations of the meaning of the symbols see Table I)

$$Q_1 = 1\ 748, Q_2 = 7\ 540, Q_4 = 8\ 783 \quad (1)$$

### For clusters with grid spacers

$$V = -0.252 - 2\ 789 \exp(-3\ 874G) + 1\ 915 \exp(-0\ 234G) \quad (2)$$

and for spiral wire spacers

$$V = 1 - FF(0.336 + 0.09G - 0.697 \exp(-2.68G)) \quad (3)$$

with

$$FF = 2\ 6695(F^{0.915} - 1) \quad (4)$$

Table I WSC-2 correlation

$$\phi \times 10^6 \text{ Btu/hr ft}^2 = \frac{A + B\Delta H_1}{C + ZY'}$$

$$A = \frac{0.25 GD \lambda F_1 Q_1}{Q_3} \quad B = 0.25 GD$$

$$C' = \frac{Q_4 F_3 \sqrt{GDY'}}{D_h}$$

$$C = C' V \left[ 1 + \frac{Y-1}{1+G} \right]$$

where  $D = F_p D_h$ ,  $D_h$  = coolant channel hydraulic diameter (in)

$F_p$  = radial form factor in the considered section of the bundle

$p_r = 10^{-3} p$   $p$  = pressure (p.s.i.a.)

$F_1 = p_r^{0.982} e^{1.17(1-p_r)}$

$F_2 = p_r^{0.841} e^{1.424(1-p_r)}$

$F_3 = p_r^{1.851} e^{1.241(1-p_r)}$

$G$  = mass velocity ( $10^6$  lb/ft<sup>2</sup> hr)

$\lambda$  = latent heat of evaporation (Btu/lb)

$\Delta H_1$  = inlet subcooling (Btu/lb)

$z$  = distance from channel inlet (in)

$Y$  = ratio of average cluster heat flux from entry to  $z$  to local cluster radial-average heat flux at  $z$

$Y'$  = imbalance factor, ratio of the enthalpy increase in the considered subchannel to the heat produced in the subchannel from entry to  $z$

$V$  = grid spacers parameter. For the best fit of experimental data  $V=0.7$ .

| geometry parameter | $Q_1$ | $Q_2$ | $Q_3$ | $Q_4$ |
|--------------------|-------|-------|-------|-------|
| triangular array   | 1.329 | 2.372 | -1    | 12.26 |

$$F = \left( \frac{p}{d} \right)^{0.5} + \left[ 7.6 \frac{(p/d)^3}{H/d} \right]^{2.16} \quad (5)$$

where  $d$  = rod diameter,  $p$  = rod pitch,  $H$  = axial pitch of the spiral spacer

In the correlation of Ref /3/ the parameter  $Y'$  (see Table I) was omitted because the correlation was intended for application to large bundles with a great number of rods, where the effect of the bundle boundary is negligible on the central rods of the bundle and in presence of small power gradients perpendicular to the water flow. In this case  $Y' = 1$

## II 1 Experiments with Bundles with Grid Spacers

### II 1 1 CEA Experiments

In 1987 M Courtaud et al published the results of their CHF experiments /5/. The experiments were performed with Freon-12 and transformed to equivalent water values using the transformation factors suggested by Stevens et al /6/ and by their own experiments. Table II shows the main data of the CEA experiments. For the evaluation of their experiments they used also the KfK correlation /3/. The agreement was rather good, our correlation underpredicting the experimental data of 8.2% with a standard deviation of 9.4%. However, the KfK correlation underpredicted of about 24% the results for a rod cluster with guide tube cells. This is to be expected as our correlation has been developed for uniform rod clusters. On the other hand, the application of the KfK correlation for the prediction of the DNBR (minimum ratio between the CHF and the maximum hot channel heat flux) in the reactor core is still valid, because there will certainly be a region in the large fuel rod bundles of a APWR which is practically unaffected by the presence of guide tubes. Moreover, in the guide tube region the CHF is higher than predicted by the KfK correlation and the DNBR is determined by the bundle region unaffected by the guide tubes.

### II 1 2 JAERI Experiments

In 1989 Sugimoto et al have published the results of their CHF water experiments with a 4 rod bundle /7/. Table III shows the main operating conditions of this

Table II CEA CFH Experiments /5/. Range of Operating Conditions

|  |   |                  |
|--|---|------------------|
| Number of rods = 19                              | } | equivalent water |
| Rod diameter = 8.65 and 9.5 mm                   |   |                  |
| Rod pitch = 9.96 and 12.23 mm                    |   |                  |
| p/d = 1.151 and 1.287                            |   |                  |
| Pressure = 7.6 to 16 MPa                         |   |                  |
| Mass velocity = 2000 to 8000 kg/m <sup>2</sup> s |   |                  |
| Exit steam quality = -0.2 to 0.4                 |   |                  |
| Heat Flux = 500 to 3800 KW/m <sup>2</sup>        |   |                  |

Table III JAERI CHF Experiments /7/ Range of Operating Conditions

|   |
|---|
| Number of rods = 4                              |
| Rod diameter = 9.5 mm                           |
| Rod pitch = 11.4 mm                             |
| p/d = 1.2                                       |
| Pressure = up to 3.9 MPa                        |
| Mass velocity = 560 to 4170 kg/m <sup>2</sup> s |
| Exit steam quality = 0.09 to 0.41               |
| Heat flux = 950 to 2840 KW/m <sup>2</sup>       |

experiment. Due to the relatively low number of rods and the considerable effects of the cluster boundaries, the results of the experiments were also evaluated in terms of local subchannel conditions using the COBRA-IV-I sub-channel analysis. Besides with the KfK /3/, the experiments were compared with the EPRI-B&W /8/, EPRI-Columbia /9/ and Katto /10/ CHF correlations as well. Using the bundle averaged flow conditions, the two latter correlations overpredicted the experimental data by 20 to 100%. Therefore the comparison with the local conditions calculated with COBRA-IV-I was performed only for the first two correlations, which already for the averaged flow conditions gave an agreement better than + 20%. For the case of the KfK correlation, the unbalance factor Y' was used for the comparison with local flow conditions. Fig. 1 shows the results of these comparisons. The CHF ratios obtained from the local flow conditions are

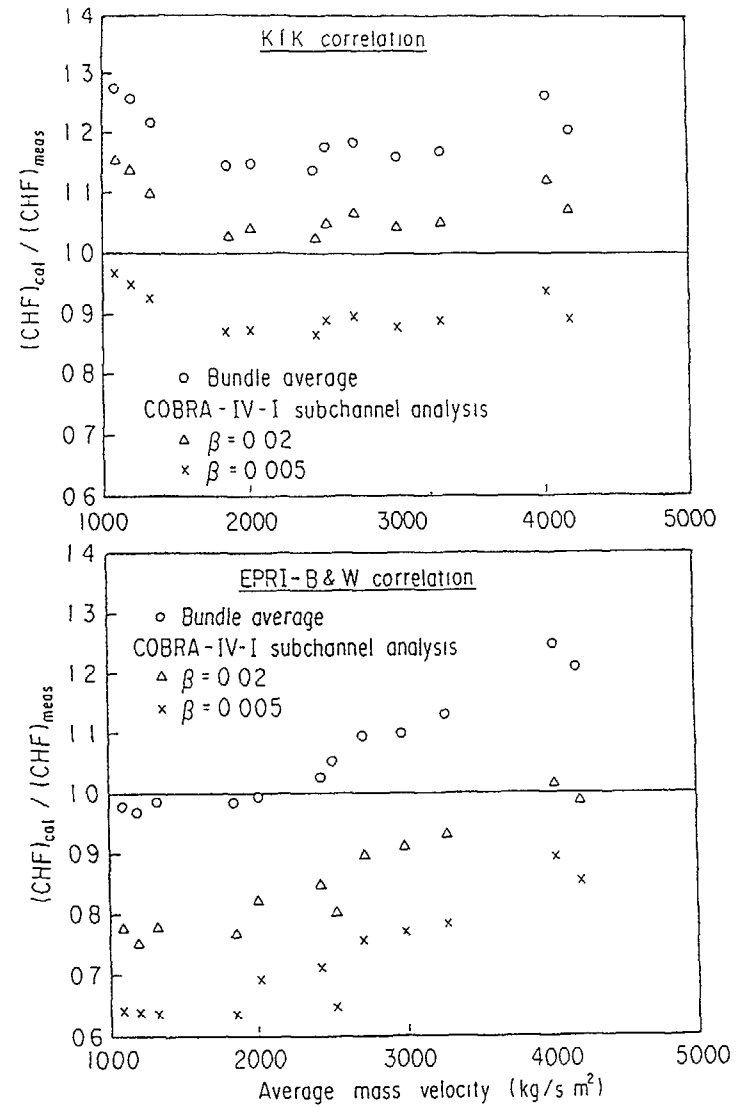


Fig.1. Comparison of the CHF experiments performed at JAERI with water for pressures up to 3.9 MPa and a 4 rod bundle /7/ with the prediction of the KfK /3/ and EPRI-B&W correlations /8/.

smaller than those from the average ones, thus the agreement between experiment and KfK correlation is slightly better of that with the EPRI-B&W correlation

Fig. 2 shows the comparison of experimental data obtained subsequently by JAERI for other test sections with seven rods and  $p/d = 1.2$  as well, and water pressures up to 16 MPa. The agreement with the KfK correlation, on the base of the local flow conditions and using the unbalance factor  $Y'$ , is excellent. JAERI uses now the KfK correlation, with an uncertainty band of  $\pm 15\%$ , for the thermohydraulic core design calculations /11/

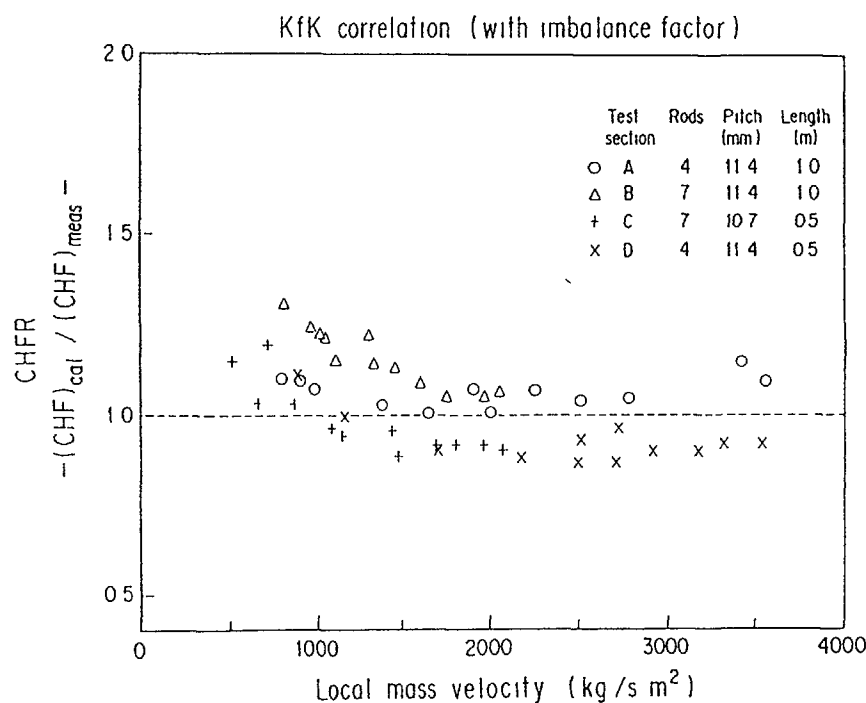


Fig. 2 Comparison of the CHF experiments performed at JAERI with water for pressures up to 16 MPa and bundles with 4 or 7 rods /11/ with the prediction of the KfK correlation /3/.

### II 1.3 Mitsubishi Experiments

Mitsubishi has recently performed CHF experiments with a 7 rod bundle with Freon and water /12/. Table IV shows the main operating conditions of this experiment. Using the local flow conditions and the local subchannel unbalance factor, the experimental results agree quite well with the KfK correlation for heat fluxes up to 2000 KW/m<sup>2</sup>. For higher heat fluxes the KfK correlation overpredicts slightly the experimental data (18% at a flux of 4000 KW/m<sup>2</sup>). Without consideration of the unbalance factor  $Y'$  the overprediction would have been much higher 56% at 4000 KW/m<sup>2</sup> /13/

Table IV. Mitsubishi CHF Experiments /12/. Range of Operating Conditions

|   |               |
|---|---------------|
| Number of rods = 4                              |               |
| Rod diameter = 9.5 mm                           |               |
| Rod pitch = 12 mm                               |               |
| $p/d = 1.263$                                   |               |
| Pressure = 2-2.9 MPa                            | with Freon 12 |
| Mass velocity = 1900-3600 kg/m <sup>2</sup> sec |               |
| Inlet subcooling = 3-36 K                       |               |
| Pressure = 12.3 - 16.7 MPa                      | with water    |
| Mass velocity = 2800-4900 kg/m <sup>2</sup> sec |               |
| Inlet subcooling = 20-170 K                     |               |

### II 1.4 Experiments at KfK - Braunschweig University

Recently KfK and the Braunschweig University have performed a joint experiment with a 7 bundle and Freon-12 /14/. The average flow condition experimental data have been compared with the Dalle Donne-Hame correlation /3/. The agreement is relatively good up to a mass velocity of 3000 Kg/m<sup>2</sup>sec. For higher mass velocities the KfK correlation overpredicts the experimental results quite considerably. The analysis of the JAERI and Mitsubishi experiments (see subchapters II 1.2 and II 1.3) indicate that the agreement would improve very much if the comparison were performed with local flow conditions and under consideration of the local unbalance factor  $Y'$ . The reason for this is of course the relatively low number of rods used in the bundle for this experiment.

## II 2 Experiments with Bundles with Integral Spiral Ribs

The Dalle Donne-Hame CHF correlation /3/ was developed also for rod clusters with spiral wire supports and, to our knowledge, predicts well all the experiments for this kind of bundles available in the literature. However, the proposed APWR's with very tight lattices ( $p/d < 1.2$ ) have the fuel rods supported by six integral spiral ribs /1/. This kind of support offers some advantages in respect of spiral wires, as, for a given axial distance between the supporting sections of the rods, the pressure drops are considerably smaller. This is because, in the case of six spiral starts, the axial pitch of the spiral is only 1/6th of the single start spiral wire for a given axial distance between the supporting sections. At the time of the development of our CHF correlation, no CHF experiment with clusters with six integral spiral ribs was available in the literature. However, recently such an experiment has been performed by KWU /15/. Table VI shows the main operating conditions of this experiment with water.

Table V KfK-Braunschweig Experiments /14/. Range of Operating Conditions

|  |               |
|--|---------------|
| Number of rods = 7                               |               |
| Rod diameter = 9.5 mm                            |               |
| Rod pitch = 10.9 mm                              |               |
| $p/d = 1.147$                                    |               |
| Pressure = 2.3 MPa                               |               |
| Mass velocity = 1000-6000 kg/m <sup>2</sup> /sec | with Freon 12 |
| Exit steam quality = -0.34 - +0.09               |               |
| Heat flux = 100 - 500 kW/m <sup>2</sup>          |               |

Table VI KWU CHF experiment with six spiral ribs cluster /15/. Range of operating correlations

|   |  |
|---|--|
| Number of rods = 37                             |  |
| Rod diameter = 9.5 mm                           |  |
| Rod pitch = 10.6 mm                             |  |
| $p/d = 1.116$                                   |  |
| Axial pitch of the spiral ribs = 600 mm         |  |
| Pressure = 7-16 MPa                             |  |
| Mass velocity = 1000 - 7000 kg/m <sup>2</sup> s |  |

Fig. 3 shows a comparison of the KWU experimental data with the KfK CHF correlation for spiral wire spacers (Eqs. (1), (3), (4) and (5)). The correlation underpredicts the data by up to 40%. As the discrepancy increases with the water mass velocity, it is likely that this may be due to wrong values for the parameter  $V$ , which accounts for the effect of the spacer on the CHF and is mass velocity dependent (Eq. (3)). The reason for this discrepancy may be due to the fact that the correction factor  $FF$  in Eq. (3) has been obtained on the assumption that the increase of CHF caused by the spacer is proportional to the increase of the friction factor caused by the wire spiral spacer. This has been proved to be so for the single wire spiral supports /3/, but it is not true when the results are applied to a different geometry as the six integral spiral ribs kind of support.

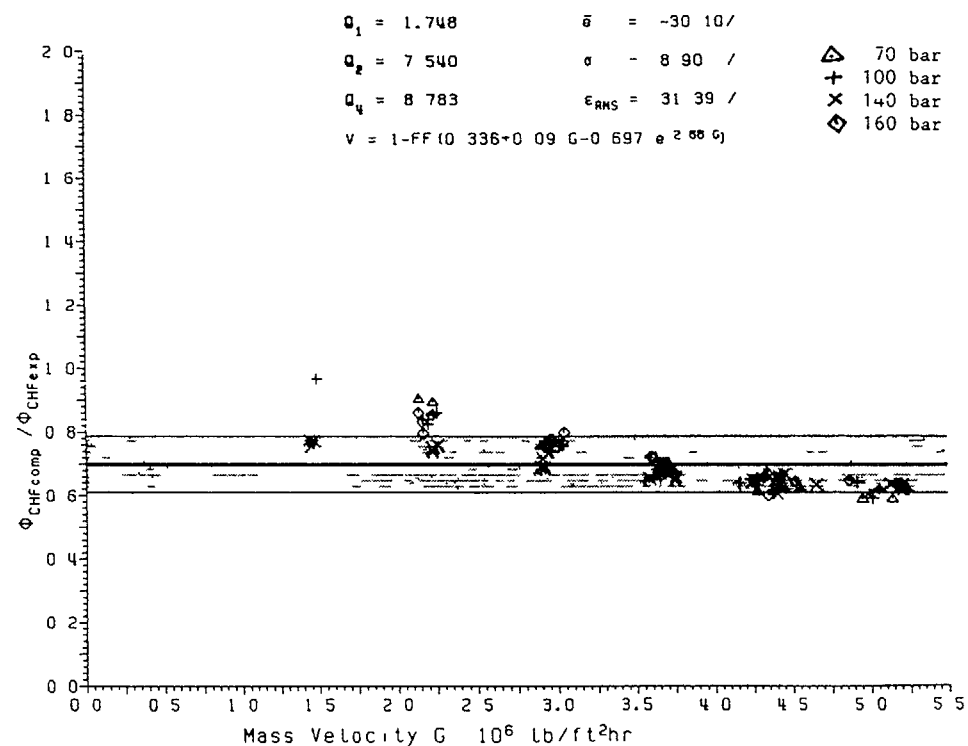


Fig.3 Comparison of the CHF experiments performed at KWU with water for pressures up to 16 MPa and a bundle with 19 rods and six integral spiral ribs support /15/ with the prediction of the KfK correlation with single spiral wire support /3/.

Fig. 4 shows a comparison where the value of  $V$  has been obtained with the factor FF set equal to one. The agreement is excellent, the mean error being 0.9% and the standard deviation 5.6%. I.e. the results with the experiments with six integral spiral ribs ( $H/d = 63.2$ , where  $H$  = axial pitch of spiral rib,  $d$  = rod diameter) agree quite well with those for the bundle with the single spiral wire for which Eq. (3) was obtained. This was a bundle with  $H/d = 13.64/3$ . To account for the different number of starts between a single spiral wire and a six spiral ribs kind of support Eq. (5) should be replaced by

$$F = \left( \frac{p}{d} \right)^{0.5} + n_s^{1.42} \cdot 7.6 \left[ \frac{(p/d)^3}{H/d} \right]^{2.16} \quad (6)$$

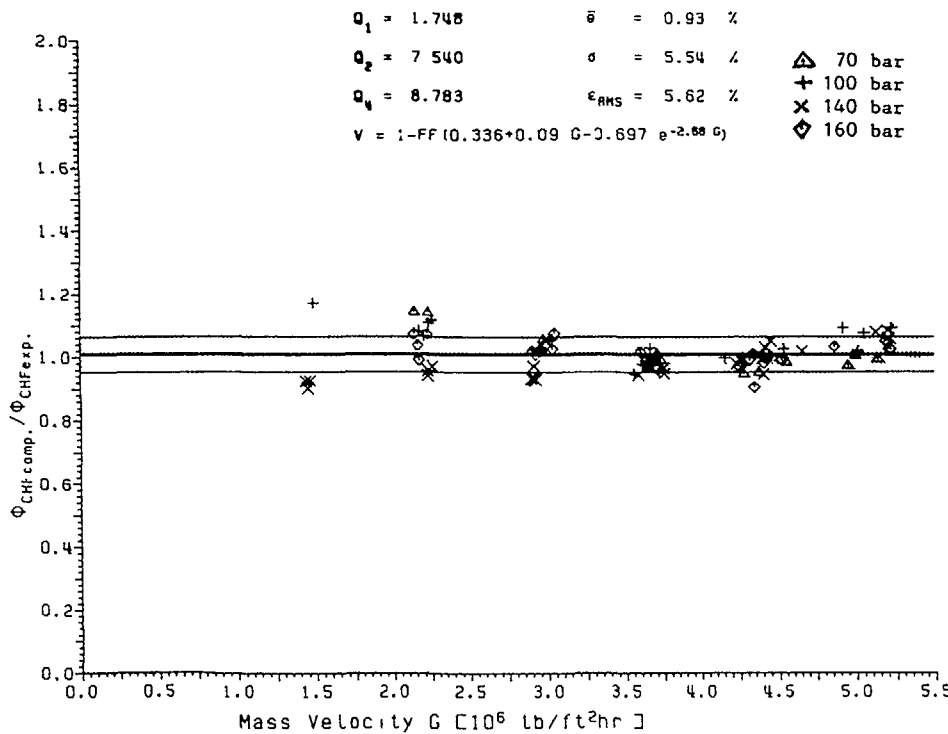


Fig. 4 Comparison of the CHF experiment performed at KWU with water for pressures up to 16 MPa and a bundle with 19 rods and six integral spiral ribs support /15/ with the prediction of the KfK correlation with FF set equal to 1.

Whereby  $n_s$ , number of starts, is equal 1 for the single wire case and equal to 6 for the six integral spiral ribs case respectively. Eq (6) should, however, used with caution, as it is based on only one experiment with a rod cluster with six spiral ribs.

### III DEVELOPMENT OF THE COMPUTER PROGRAMME FLUT-FDWR

For the development of the APWR at KfK, the calculations of the blow-down phase of a Loss-of-Coolant Accident (LOCA) were performed with the computer code RELAP 5 / MOD 1, properly modified to account for the different geometries present in the APWR cores /16/, while the reflood phase was modelled with the code FLUT-FDWR, a further version of the code FLUT, originally developed at GRS-Garching for PWR's /17/, as it was discovered that RELAP 5 / MOD 1, as well as RELAP 5 / MOD 2, was not well suited to model the reflood phase of a core of an APWR.

The hydrodynamic model in FLUT is a two-fluid model with six conservation equations for mass, momentum and energy. The interaction between the phases is modelled by a very simple set of constitutive equations for mass transfer rate, interfacial drag and interfacial heat transfer, which fulfils basic requirements as symmetry of phases, increase of phase interaction with growing deviation from equilibrium and correct behaviour of the disappearing phase (interaction terms gradually decrease as one phase is disappearing), while the dependence on the flow regime appears only indirectly /18/. This proved to be an advantage for the calculations in APWR-geometry. As a matter of fact, most of the presently used flow maps are based on experimental evidence for pipes or for bundles in normal PWR geometry. Their previsions in case of a different geometry may fail completely. The calculations of the first forced reflooding experiment in a very tight APWR geometry with different codes proved this fact /19/. On the other hand the simpler formulation of the FLUT code assures a wider generality and can better cope with this new geometrical configurations /20/.

The one dimensional heat conduction model of the code is able to simulate plates and hollow or full cylinders. Each heat conductor can have up to three material zones separated by gaps. Heat generation can be considered in material zones. Suitable heat transfer correlations depending on the flow regime connect the fluid and the heat conductor model. The positions of the lower and upper

quench-front for each fuel rod is calculated explicitly by means of analytical correlations for the quench-front velocity /21, 22/ This compensates partly the lack of the axial conduction in the one dimensional heat conductor model. For the simulation of a reactor primary system, a network of one dimensional flow elements (pipes) and special plenum cells (lumps) is applied. The reactor core may comprise parallel cells with fuel rods of different power connected to each flow channel. For the primary coolant pumps, a centrifugal pump model is available. The temperatures of the secondary side of the steam generator tubes and the injected mass flow rates of the ECCS must be given as input data.

In the next two subchapters the improvements introduced at KfK to the code FLUT will be reviewed and shortly discussed.

### III 1 FLUT-FDWR Introduction of the Two Diameter Droplets Model for the Flow Regime above the Lower Quench Front and Other Improvements

The modified version FLUT-FDWR contains some new correlations and physical models which improved its preision capability /23, 24/

The criterion of Hsu and Young for the onset of the upper quench-front /25/ was introduced in order to avoid a too early quenching of the rod cladding from above. This criterion allows the beginning of the rewetting process only when the void fraction  $\alpha$  is less than 0.95 and the cladding temperature  $T_{cl}$  is lower than 540°C and gave satisfactory results when applied to the PWR geometry /26/.

A new droplet model for the zone immediately downstream the lower quench-front improved the calculation of the precooling effect in the cases in which the quenching of the cladding takes place at a high void fraction ( $\alpha \leq 0.8$  at the quench-front). Figure 5 shows the flow patterns of the two extreme reflooding situations: flow pattern A occurs usually for high flooding rates (more than 4 cm/s) while flow pattern B is typical of low flooding rates /27/. The establishment of one or the other of these flow patterns is also affected by the inlet subcooling of the flooding water and by the volumetric power density in the bundle. Lower inlet subcooling and high power density favour the pattern B. In an APWR core, where the power density might be higher than in a PWR, pattern B may become of major importance.

The original package of heat transfer correlations of the FLUT code is based on a flow pattern of type A and underestimates the precooling of the cladding before quenching in case of pattern B, where the zone of the dispersed flow film boiling begins directly above the quench-front. A very important parameter in this flow regime is the average droplet diameter used to calculate the heat transfer coefficient and the interfacial area between vapour and water droplets. In the original version of FLUT this parameter was set to a unique constant value. Basing on a study of R. Lee about the generation of droplets at the quench-front and their subsequent evolution /28/, a simplified model was implemented in FLUT-FDWR. Here the region of dispersed flow is divided into two subregions (see Figure 5)

- a) a zone of length  $L$ , immediately downstream the quench-front, in which the calculation uses a value  $d_1 = 0.127$  mm for the droplet average diameter accounting for the presence in this subregion of two kinds of droplets of different diameter generated below (in the zone of transition boiling) by the bursting of bubbles,
- b) the remaining part of the dispersed flow region, in which the value  $d_2 = 2$  mm is used as in the original version of the program (in this zone only the bigger droplets survive, as the smaller ones evaporate completely within the first zone of length  $L$ )

For the length of the zone in which the diameter  $d_1$  is used a reference value  $L_0 = 0.2$  m was determined by means of optimisation calculations of the experiment FLECHT No. 32114 /29/. For the other cases  $L$  was calculated by means of a simplified energy balance. Supposing that the zone of influence of the small droplets depends linearly on the volumetric power density on the fluid  $Q$  and on the initial cladding superheat  $\Delta T$ , referring to the value  $L_0$  we obtain

$$L = L_0(Q_0/Q)(\Delta T_0/\Delta T) \quad (7)$$

where the values with index 0 refer to FLECHT exp. No. 32114 /29/. This method gave good results in the calculation of many experiments in PWR and APWR geometry /23/.

For the calculation of the friction factors, new relations for a proper evaluation in APWR core channels were introduced in FLUT-FDWR /23/.

| Pattern A | Flow regimes  | Pattern B            | Flow regimes  | New droplet model                                   |
|-----------|---|----------------------|---|---|
|           | Annular flow<br>← Upper quench front                |                      | Annular flow<br>← Upper quench front                |   |
|           | Single-phase vapor<br>— $\alpha = 1$                |                      | Single-phase vapor<br>— $\alpha = 1$                |   |
|           | Dispersed flow<br>f m boiling                       |                      | Dispersed flow<br>film boiling                      | Simple droplet population<br>Average diameter $d_2$ |
|           | Inverted annular flow<br>film boiling               | ← Lower quench front | Double droplet population<br>Average diameter $d_1$ |   |
|           | ← Lower quench front                                | Transition boiling   | Bubble burst  |   |
|           | Transition boiling<br>$T_{CHF}$<br>Nucleate boiling | Annular flow         |   |   |
|           | Single-phase liquid                                 | Nucleate boiling     |   |   |
|           |   | Single-phase liquid  |   |   |

Fig.5 Reflood flow regimes and droplet model. L is the length where the double droplet population occurs.

The dependence of the interfacial drag coefficient on the channel geometry can be accounted for in FLUT-FDWR by giving different values of the parameters  $R_v$  and  $R_l$  of the relation of Oseen /30/ in the different components of the system

According to the results of parametric calculations of many reflooding experiments and to the experience of other authors, the following reference values have been established /23/

$$R_v = R_l = 0.70 \text{ m} \text{ for a very tight APWR rod lattice } (p/d = 1.06, d_h = 2.6 \text{ mm})$$

$$R_v = R_l = 0.25 \text{ m} \text{ for a PWR geometry (square rod lattice with } d_h = 12.0 \text{ mm)}$$

$$R_v = R_l = 0.10 \text{ m} \text{ for pipes}$$

(8)

### III 2 FLUT-FDWR-MM Introduction in the Heat Conductor Model of a Mesh Moving with the Quench-Front

The moving mesh has been introduced into the heat conductor model of FLUT FDWR in order to reduce the oscillations caused by the propagation of the quench-front. The conceptual illustration of the moving mesh is given in Fig. 6. The nodalisation shown on the left of this figure is usually used in the FLUT-FDWR calculation. The axial length of each heat conductor is about 4 ~ 6 cm. In the new version of the code, several heat conductor cells around the quench-front are divided into finer ones. Six finer cells for each of the three conductor cells around the quench-front, which are shown in this figure, are used as a standard nodalisation in FLUT-FDWR-MM. The number of divided cells, their location relative to the quench-front and the number of finer cells can be changed by input. The part of the conductor divided into finer cells is moving with the quench-front. When the conductor cell is divided into finer ones, the same temperature distribution as that of the divided cell is assigned to each finer cell. On the other hand, the temperature is assumed to be an arithmetic average of those of the finer cells when the finer cells are combined into one large cell.

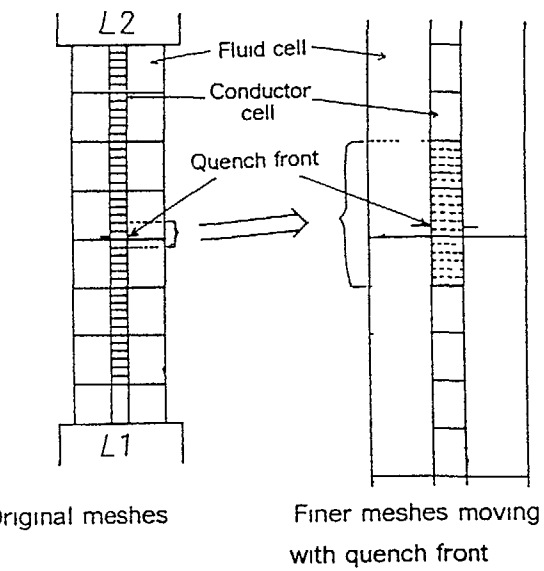


Fig.6 Conceptual illustration of the moving mesh.

The important parameters for the physical model of FLUT-FDWR,  $L$  of the droplet model and  $R_v$  and  $R_l$  of the relation of Oseen for interfacial drag between liquid and vapour phases, were optimised for the coarse mesh used in the FLUT-FDWR calculation /23, 24/. However, the nodalisation effect on the calculation results is very large and very important /23, 31/. This means that the values of these parameters should be reoptimised for the new version with the moving mesh. Through the course of post-test calculations for various reflooding experiments using FLUT-FDWR-MM /32/ the optimum values for  $R_v$  and  $R_l$  were determined as follows:

$R_v = R_l = 0.25 \text{ m}$  for a PWR geometry (square rod lattice with  $d_h = 12.0 \text{ mm}$ )

$R_v = R_l = 0.10 \text{ m}$  for a APWR geometry (triangular rod lattice  $p/d = 1.13$ ,  $d_h = 4.17 \text{ mm}$ )

(9)

Note that smaller values of  $R_v = R_l$  mean stronger interfacial drag.

The optimisation work of Ref /32/ did not allow to better specify the values of  $L$  used in FLUT-FDWR, as the tests used had low sensitivity to this parameter. Thus the values of Eq (7) with  $L_0 = 0.2 \text{ m}$  are still maintained.

### III 3 Comparison of the Calculation Predictions with the Experimental Data

#### III 3.1 Calculations with FLUT-FDWR

Fig. 7 and 8 show the comparisons of the cladding temperatures at certain levels of a heated rod versus time during the core reflooding. In both cases the geometry is typical for a PWR core. Fig. 7 refers to a test performed in USA (experiment FLECHT 32114 /29/) and Fig. 8 to a test performed in Germany (experiment SEFLEX-07 /33,34/). The improvement brought up by FLUT-FDWR in respect of FLUT is evident from the figures. However, especially by the SEFLEX experiment the oscillations in the temperature mentioned in subchapter III 2 are quite considerable.

Fig. 9 shows the cladding temperatures of three heat rods at a certain level versus time for a very tight APWR rod bundle with six integral spiral ribs support ( $p/d = 1.06$ , FLORESTAN 1 experiment /19, 35/). Also here the agreement of the

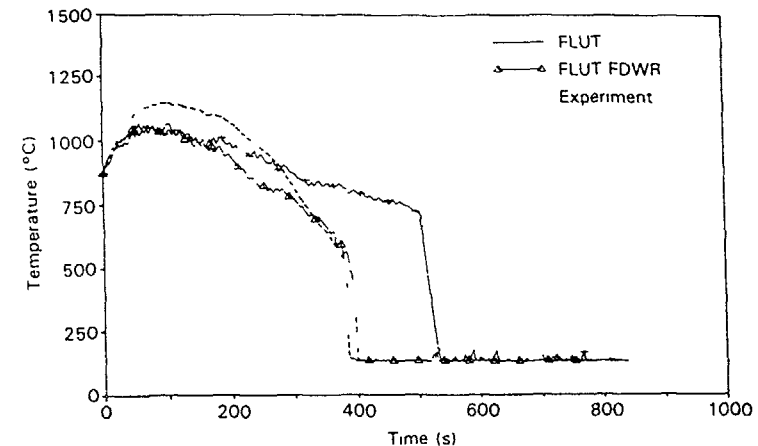


Fig. 7 Rod cladding temperature at 1.83 m high versus time for the FLECHT 32114 experiment /29/ compared with the FLUT and FLUT-FDWR prediction.

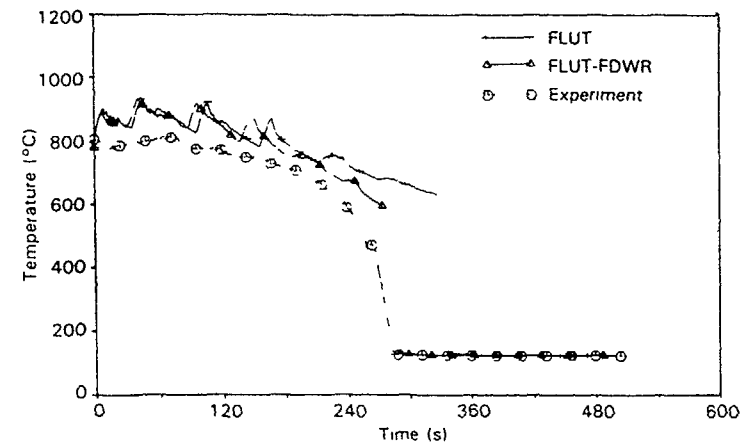


Fig. 8 Rod cladding temperature at 2.30 m high for the SEFLEX-07 experiment /33,34/ compared with the FLUT and FLUT-FDWR prediction.

experimental data is considerably better with FLUT-FDWR than with FLUT. Fig. 10 shows that also the temperature of the steam at the outlet of the test section of the FLORESTAN 1 experiment is better predicted by FLUT-FDWR than by FLUT. Comparison with other experiments gave similar results /23, 24/.

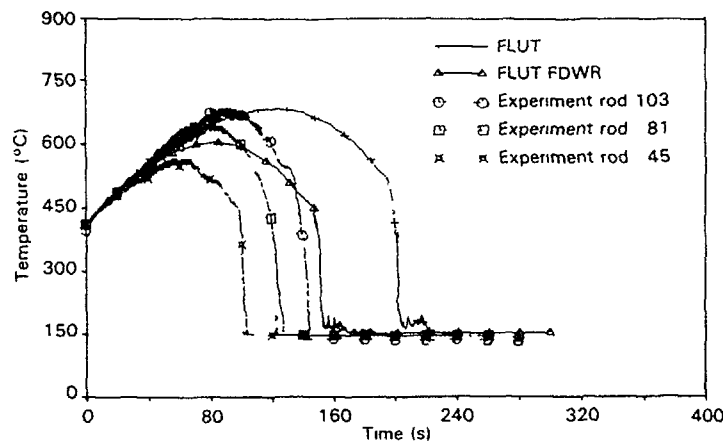


Fig. 9 Cladding temperatures of three rods measured in the FLORESTAN 1 experiment at 1.612 m high /19,35/ and compared with the FLUT and FLUT-FDWR prediction.

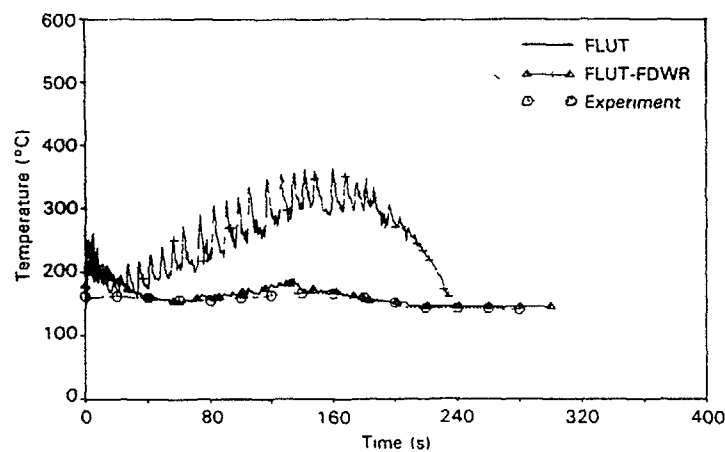


Fig. 10 Steam temperature at test section outlet in the FLORESTAN 1 experiment /19,35/. Comparison with the FLUT and FLUT-FDWR prediction.

### III 3.2 Calculations with FLUT-FDWR-MM

The calculations were performed for PWR as well as APWR geometries, especially in the cases where FLUT-FDWR was producing relatively large oscillations in the cladding temperatures and other physical parameters of the test.

Fig. 11 shows the cladding temperatures calculated with FLUT-FDWR-MM for the same test of Fig. 8 (SEFLEX-07). The temperature oscillations are reduced, if not all, quite considerably in amplitude and the agreement with the experimental values is better. Fig. 12 shows the cladding temperatures calculated with FLUT-FDWR and FLUT-FDWR-MM for another experiment in PWR geometry (NEPTUN 5036/36/). The calculated values are compared with the experimental data of the two measured rods. Also here the improvement caused by FLUT-FDWR-MM in respect of FLUT-FDWR is evident. The same can be said for the calculation of the water carry-over (see Fig. 13).

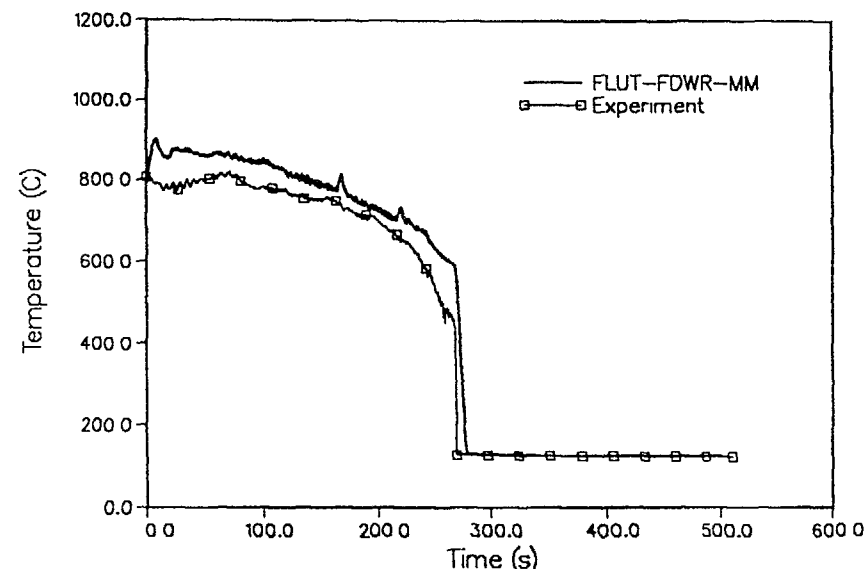


Fig. 11 Rod cladding temperature at 2.30 m high for the SEFLEX-07 experiment /33,34/ compared with the FLUT-FDWR-MM prediction.

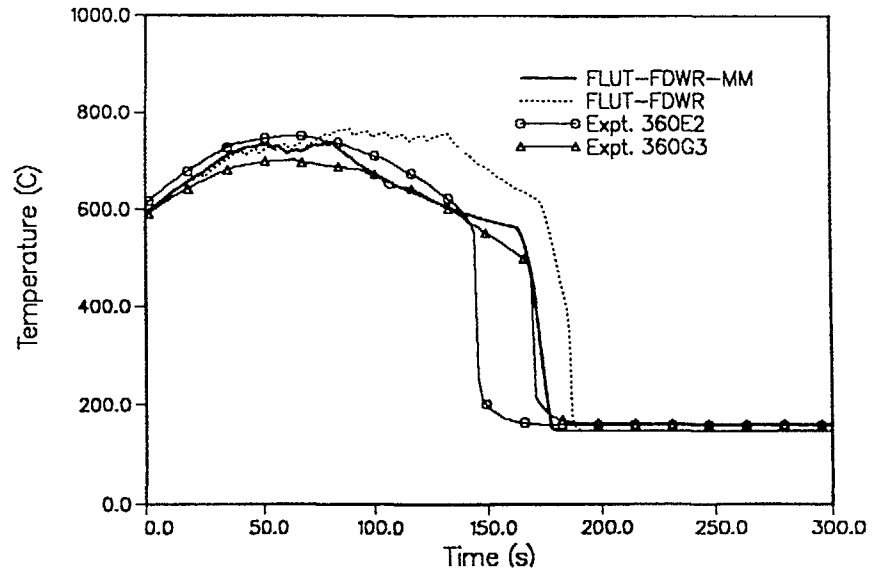


Fig.12 Rod cladding temperatures of two rods measured in the NEPTUN 5036 experiment /36/ at 1.18 m high and compared with the FLUT-FDWR and FLUT-FDWR-MM prediction.

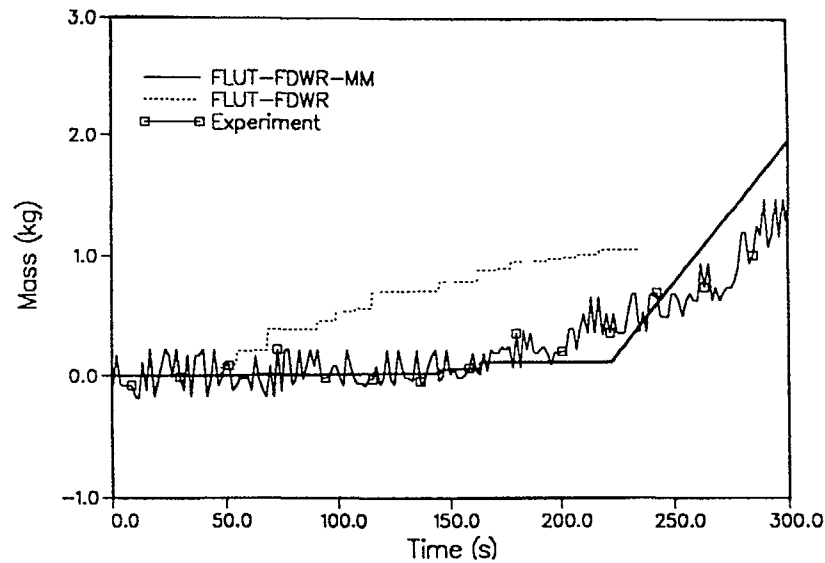


Fig.13 Water carry over at test section outlet in the NEPTUN 5036 experiment /36/. Comparison with the FLUT-FDWR and FLUT-FDWR-MM prediction.

FLUT-FDWR-MM was tested against tests performed in a APWR geometry as well. Fig. 14 shows the cladding temperatures calculated with FLUT-FDWR and FLUT-FDWR-MM for a rod bundle with  $p/d = 1.13$  (NEPTUN III /37, 38/). The calculated temperatures are compared with those of four measured rods. The comparison shows quite clearly the necessity of using with FLUT-FDWR-MM, a considerably lower value of  $R_l = R_v$  than in the case of FLUT-FDWR. The experimental values of the cladding temperatures tend to be slightly underpredicted, however with FLUT-FDWR-MM, the number and amplitude of the temperature oscillations is considerably reduced. Comparisons with other experiments are shown in Ref. /32/

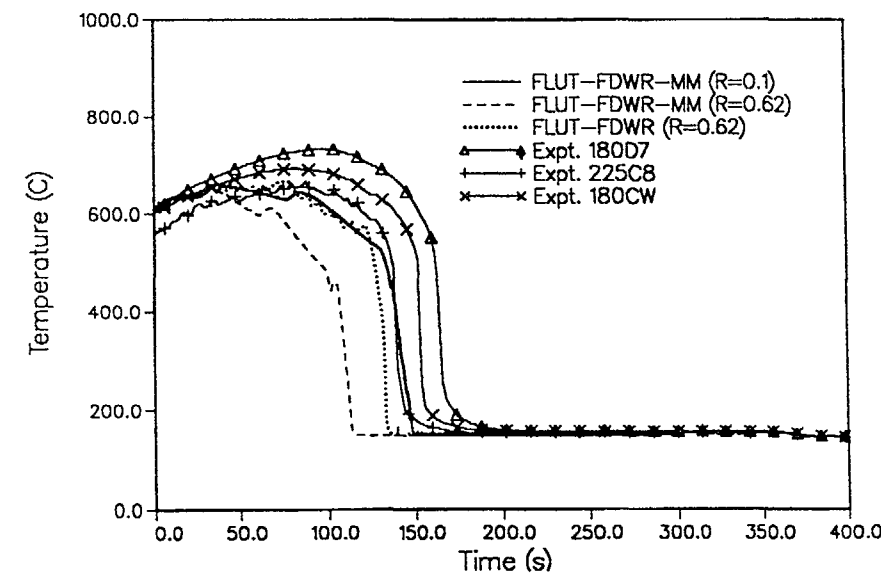


Fig.14 Rod cladding temperatures of four rods at 0.95 m high in the NEPTUN III experiment /37,38/ compared with the FLUT-FDWR ( $R_l=R_v=0.62$ ), with the FLUT-FDWR-MM ( $R_l=R_v=0.62$ ) and with the FLUT-FDWR-MM ( $R_l=R_v=0.1$ ) predictions.

CONCLUSIONS

The latest KfK activities in the field of theoretical thermohydraulics for the APWR have been mainly concentrated

- a) on the development of a reliable correlation for the prediction of a Critical Heat Flux in an APWR core geometry, characterized by fuel rod bundles with relatively tight triangular rod lattices, and
- b) on the development of the computer code FLUT, originally developed by GRS-Garching to model the flooding phase during a Loss-of-Coolant Accident in a PWR, to account for the different core geometry of the APWR

The main results of the KfK work in this field are the following

- 1 ) The KfK CHF correlation for triangular rod clusters with tight lattices and grid supports /3/ has been confirmed within a reasonable scatter band (10 - 20%) by various experiments performed in France, Japan and Germany
- 2 ) The KfK CHF correlation for triangular rod clusters and wire supports /3/ is not directly applicable to the KWU tests with a rod cluster with six integral spiral rib supports. A modification of the CHF correlation is suggested in the present paper, which accounts for both kinds (single wire and six integral spiral ribs) of supports. This new correlation, however, should be used with caution as it based on a relatively low number of experiments
- 3 ) CHF tests with bundles with a larger number of rods (37 or more) and water pressures up to 16 MPa are necessary to reduce the uncertainty band of the correlation
- 4 ) The computer code FLUT has been modified in such a way that it is applicable to core geometries typical of the APWR (tight triangular fuel rod lattice with grid or six integral spiral ribs supports). The new version of the code, FLUT-FDWR, is able to predict better than FLUT tests performed for PWR as well as APWR geometries

5 )

The latest version of FLUT-FDWR, called FLUT-FDWR-MM, allows a finer nodalisation in the rod region, which moves together with the propagation of the quench front. This reduces quite considerably the oscillations in the rod cladding temperatures and other physical parameters. In certain cases also the level of the code predictions is improved in respect of those of FLUT-FDWR

REFERENCES

- /1/ C H M BROEDERS and M DALLE DONNE, "Conceptual Design of a (P,U)O<sub>2</sub> Core with a Tight Fuel Rod Lattice for an Advanced Pressurized Light Water Reactor", Nuclear Technology, 71, 82 (1985)
- /2/ C H M BROEDERS and M DALLE DONNE, "Neutron physics and Thermohydraulics Design of a Reference High Conversion Reactor", IAEA T C Meeting on Technical and Economic Aspects of High Converters, Nuremberg, Germany, 26-29 March 1990
- /3/ M DALLE DONNE and W HAME, "Critical Heat Flux Correlation for Triangular Arrays of Rod Bundles with Tight Lattices, including the Spiral Spacer Effect", Nuclear Technology, 71, 111 (1985)
- /4/ R W BOWRING, "WSC-2 A Subchannel Dryout Correlation for Water-Cooled Clusters over the Pressure Range 3.4-15.9 MPa", AEEW-R983, U K Atomic Energy Authority (1979)
- /5/ M COURTAUD, R DERUAZ and L GROS D'AILLON, "The French Thermal-Hydraulic Program Addressing the Requirements of Future Pressurized Water Reactors", Nuclear Technology, 80, 73 (1987)
- /6/ G F STEVENS et al , "A Comparison between Burnout Data for 19 Rod Cluster Test Sections Cooled by Freon-12 at 155 psia and by Water at 1000 psia in Vertical Upflow", AEEW-R468, U K Atomic Energy Authority (1966)
- /7/ J SUGIMOTO, T IWAMURA, T OKUBO and Y MURAO, "Thermal hydraulic Study on High Conversion Light Water Reactor at JAERI", Proc 4th Int Meet Nuclear Reactor Thermal-Hydraulics, Vol 2, 799, Karlsruhe, Germany, 10-13 Oct 1989
- /8/ V O UOTINEN et al , "Technical Feasibility of a Pressurized Water Reactor Design with a Low-Water Fraction Lattice", EPRI-NP-1833 (1981)

- /9/ D G REDDY and C F FIGHETTI, "Parametric Study of CHF Data, A Generalized Subchannel CHF Correlation for PWR and BWR Fuel Assemblies", EPRI-NP-2609, Vol 2 (1983)
- /10/ Y KATTO, "General Features of CHF of Forced Convection Boiling in Uniformly Heated Rectangular Channels, Int J Heat Mass Transfer, 24, 1413 (1981)
- /11/ Y MURAO, Private communication, JAERI, 1989
- /12/ Y AKIYAMA, K HORI and S TSUDA, "DNB Experiments for High Conversion PWR Core Design", to be published in Nuclear Science and Engineering, see also Proc 4th Int Meet Nuclear Reactor Thermal-Hydraulics, Vol 2, 788, Karlsruhe, Germany, 10-13 Oct 1989
- /13/ Y AKIYAMA, Private communication, Mitsubishi, 1988
- /14/ W ZEGGEL, F J ERBACHER and D C GROENEWALD, "Critical Heat Flux Investigations using a Closely-Spaced Rod Bundle", Proc 4th Int Meet Nuclear Reactor Thermal-Hydraulics, Vol 2, 781, Karlsruhe, Germany, 10-13 Oct 1989
- /15/ U SIMON and G ULRYCH, unpublished, KWU, 1988
- /16/ M DALLE DONNE and C FERRERO, "Loss-of-Coolant Accident and Anticipated Transient Without Scram Calculations for Homogeneous and Heterogeneous Advanced Pressurized Water Reactors", Nuclear Technology, 80, 133 (1988)
- /17/ V TESCHENDORFF, "The Two Fluid Code FLUT for LOCA Reflood Analysis", presented at Workshop International Atomic Energy Agency Program in Uses of Computer Codes for Safety Analysis, Varna, Bulgaria (May 1984)
- /18/ A HORA, CH MICHTSCHLAGER, H G SONNENBURG, V TESCHENDORFF, "Analysis of Reflood Phenomena by the Two Fluid Code FLUT", Proc of NATO Advanced Research Workshop, Spitzingsee/Schliersee, Aug 31-Sept 3, 1982
- /19/ F J ERBACHER and K WIEHR, "Experimental Investigation on Reflooding and Deformation Behaviour of an APWR Tight Lattice Fuel Rod Bundle in a LOCA", Nuclear Technology, 80, 153 (1988)
- /20/ M CIGARINI, "Vorausberechnung des ersten FDWR-Flutexperimentes mit dem FLUT-Rechenprogramm", PNS-Jahresbericht 1986, pp 4100 97, KfK 4100, Karlsruhe (1987)
- /21/ R SEMERIA and B MARTINET, "Calefaction Spots on a Heating Wall Temperature Distribution and Resorption", Proc Inst Mech Engr, 180, 1982
- /22/ A YAMANOUCHI, "Effect of Spray Cooling in Transient State after Loss of Coolant Accident", Journ of Nucl Sci and Techn , 5(11), 547 (1968)
- /23/ M CIGARINI and M DALLE DONNE, "The Reflooding Phase after a Loss-of-Coolant Accident in an Advanced Pressurized Water Reactor", Nuclear Technology, 84, 33 (1988)
- /24/ M CIGARINI, "Thermohydraulische Untersuchungen zu den Vorgangen wahrend der Flutphase nach einem Kuhlmittelverlust bei einem fortgeschrittenen Druckwasserreaktor", KfK-4302, Karlsruhe (1987)
- /25/ Y Y HSU and M W YOUNG, "A Criterion for the Onset of Quench for Low Flow Reflood", NUREG 0915 (1982)
- /26/ M CIGARINI, "Nachrechnung des FEBA-Versuchs Nr 216 mit dem FLUT Programm", PNS-Jahresbericht 1984, pp 4100-61, KfK 3550, Karlsruhe (1985)
- /27/ L E HOCHREITER and K RIEDLE, "Reflood Heat Transfer and Hydraulics in Pressurized Water Reactors", Symposium on the Thermal and Hydraulic Aspects of Nuclear Reactor Safety, Vol 1, ASME, pp 75-107 (1977)
- /28/ R LEE, "Dispersed Flow Heat Transfer above a Quench Front during Reflood in a Pressurized Water Reactor after a Large Break Loss-of-Coolant Accident", University of Maryland, Ph D Thesis (1982)
- /29/ N LEE, S WONG, H C YEH, and L E HOCHREITER, "PWR FLECHT SEASET Unblocked Bundle, Forced and Gravity Reflood Task Data Evaluation Report", NP-2013, Electric Power Research Institute (1982)
- /30/ C W OSEEN, "Neuere Methoden und Ergebnisse in der Hydrodynamik", Akademische Verlagsgesellschaft m b H, Leipzig (1927)

- 226 /31/ M CIGARINI, "Evaluation of Forced Reflooding Experiments in APWR-Geometry (NEPTUN-III Facility) using the Advanced Computer Code FLUT-FDWR", KfK-4585, Karlsruhe (1989)
- /32/ T MORI, M CIGARINI and M DALLE DONNE, "Evaluation of Forced Reflooding Experiments using the FLUT-FDWR-MM (Modified Version of FLUT-FDWR with Moving Mesh in the Heat Conductor Model)", KfK 4658, EUR 11396EN, Karlsruhe (1989)
- /33/ P IHLE and K RUST, "SEFLEX Fuel Rod Simulator Effects in Flooding Experiments - Evaluation Report", KfK-4024, Kernforschungszentrum Karlsruhe (1986)
- /34/ P IHLE and K RUST, "SEFLEX Fuel Rod Simulator Effects in Flooding Experiments - Unblocked Bundle Data", KfK-4025, Kernforschungszentrum Karlsruhe (1986)
- /35/ F J ERBACHER and K WIEHR, "Reflood Heat Transfer in APWR Tight Lattice Fuel Rod Bundles in a LOCA", Trans 4th European Nuclear Conf and 9th Foratom Congress and Int Nuclear Trade Fair, Geneva, Switzerland, June 1-6, 1986
- /36/ F STIERLI and S YANAR, "Flutversuche NEPTUN-2 Übersicht, Unterlagen", EIR Internal Report TM-32-85-30 (1985)
- /37/ J DREIER, G ANALYTIS and R CHAWLA, "NEPTUN-III Reflooding and Boiloff Experiments with an LWHCR Fuel Bundle Simulator Experimental Results and Initial Code Assessment Efforts", Nuclear Technology 80, 93 (1988)
- /38/ J DREIER, unpublished, Paul Scherrer Institut, Wurenlingen (1988)

## **EXPERIMENTS**

(Session 4)

**Chairman**

**R. CHAWLA**

Switzerland

# EXPERIMENTAL SUPPORT TO TIGHT LATTICE AND PLUTONIUM CORE STUDIES

J.L. NIGON, J. MONDOT

CEA, Centre d'études nucléaires de Cadarache,  
Saint-Paul-lez-Durance,  
France

## Abstract

The possible option of a tight lattice core for future PWRs has been considered for the last five years, from 1983 to 1987. EdF, FRAMATOME and CEA conducted a joint R&D programme dealing with undermoderated PWR cores. This R&D programme covered the following domains:

- core physics,
- thermalhydraulics, both under operating and accidental transient conditions,
- fuel behaviour and reactor mechanics.

The conclusions are reported in two feasibility reports prepared by Framatome (1988) and CEA (1987) which are summarized in the present presentation. The core physics experiments covered the following parameters: material buckling, spectrum index, reactivity and power distribution effects and assembly configuration parameters. The thermalhydraulics results deal with DNB (critical heat flux) on one hand, and with reflood after LOCA on the other hand. As for mechanical design, the main feasibility studies concerned the upper plenum, which is much over crowded with guide tubes than in the standard design, and the vibratory behaviour of control/spectral shift rod clusters. At present, an important core physics programme is devoted to the support of plutonium recycling in present PWRs. The EPICURE programme provides useful additional results which could be helpful in further potential HCPWR design activities.

## 1. CONTEXT OF THE FRENCH PROGRAMME

### 1.1 RCVS

Framatome started their first advanced studies in 1980 ; the announcement of a spectral shift reactor has been published in 1982.

From 1983 to 1987, CEA conducted an R&D programme in order to evaluate the concept of undermoderated reactors, and particularly the RCVS concept (that is convertible spectral shift reactor). EdF and FRAMATOME were associated to the progress of this CEA programme. The investigations dealt with core physics, thermohydraulics, fuel behaviour and reactor mechanics. Two feasibility reports have been prepared by FRAMATOME (1988) and CEA (1987).

### 1.2 Pu recycling

The decision of recycling plutonium in EdF PWRs has been taken early in the 1980s ; the feasibility study concluded to the possibility of a 30 % MOX - 70 % UO<sub>2</sub> loading of the french 900 MWe cores.

Core physics and fuel behaviour experimental studies devoted to this recycling programme are of more general interest and may also be useful to the RCVS design study.

### 1.3 Main contributions

The following partial operating chart summarizes the main contributions to the french experimental programme.

|           | <u>J. Mondot</u>                  | <u>Interpretation and Assessment</u>      |   |
|-----------|-----------------------------------|---|---|
|           | <u>DRP/SPRE<br/>M. Salvatores</u> |   | Core  |
| CADARACHE | <u>J.C. Gauthier</u>              | ECOLE reactor<br>MINERVE reactor          | Physics                                       |
|           | <u>DTE/SCOS<br/>J.L. Nigon</u>    | LHC<br><u>A. Mattei</u>                   | Hydraulics & Mechanics                        |
|           |                                   | HERMES facility                           |   |
|           |                                   | Hydraulic tests<br>MAGGY, EIFFEL          |   |
|           | <u>DTE/SETh<br/>M. Courtaud</u>   | LETG<br><u>L. Gros d'Aillon</u>           | GRAZIELLA facility<br>OMEGA facility          |
|           |                                   | LES<br><u>R. Deruaz</u>                   | DNB<br>Thermal-hydraulics<br>LOCA and REFLOOD |
|           |                                   | ECCHO B test section<br>PERICLES facility |   |

## DERPE

SPG  
M. Janvier

## MELUSINE reactor

Core  
physics

## SACLAY

DEMT/SMTS  
P. Jamet

VIB  
M. Axisa

## VIZIR facility

Hydro-  
mechanics

2. CORE PHYSICS (Experimental validations)

From 1984 to 1987 an extensive experimental programme was undertaken to validate the design studies of the Light Water High Conversion Reactors (LWHCR). Three specific experiments were performed :

- \* ERASME/S and ERASME/R : critical experiments in the EOLE facility at the Nuclear Center of Cadarache (Figure II.1).
- \* MORGANE/S and MORGANE/R : critical experiments in the MINERVE pool reactor at the Nuclear Center of Cadarache (Figure II.2).
- \* ICARE/S and ICARE/R : irradiation experiments in the MELUSINE reactor at the Nuclear Center of Grenoble (Figure II.3).

Since 1988 the experimental studies have been particularly devoted to Pu recycling problems. In a first stage, the ERASME/L programme was performed in EOLE using the same pins as those of the previous S and R assemblies (Figure II.5).

A special experiment was also performed in MINERVE in two neighbouring UO<sub>2</sub>-MOX assemblies to validate the pin by pin power distribution derived from in-core fission chamber measurements (Figure II.4).

Finally, in order to reduce the remaining uncertainties, the EPICURE programme, designed to simulate as closely as possible the real conditions encountered in a PWR core with a mixed UO<sub>2</sub>-MOX loading, was decided upon in 1988 (Figure II.6).

This programme started in September 1989 and is planned to last three years.

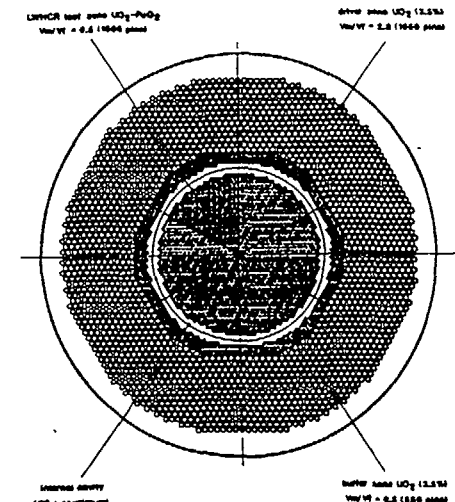


FIG. II.1. ERASME/S: Radial cross-section.

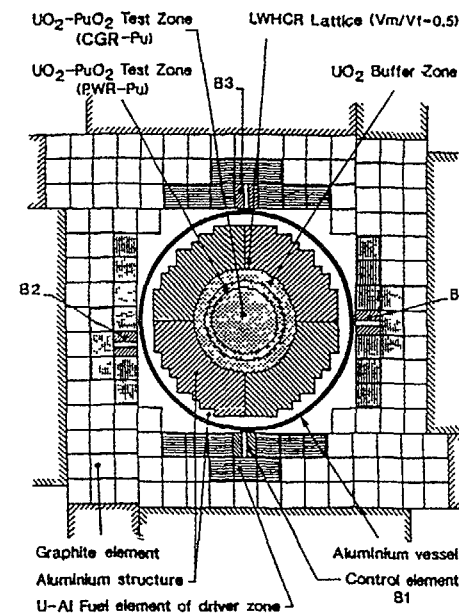


FIG. II.2. MORGANE: Radial cross-section.

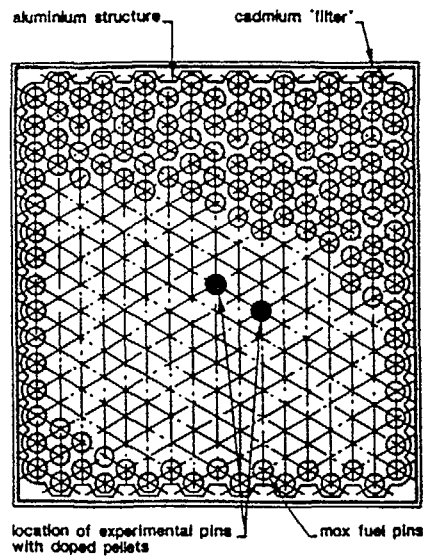


FIG. II.3. ICARE sub-assembly.

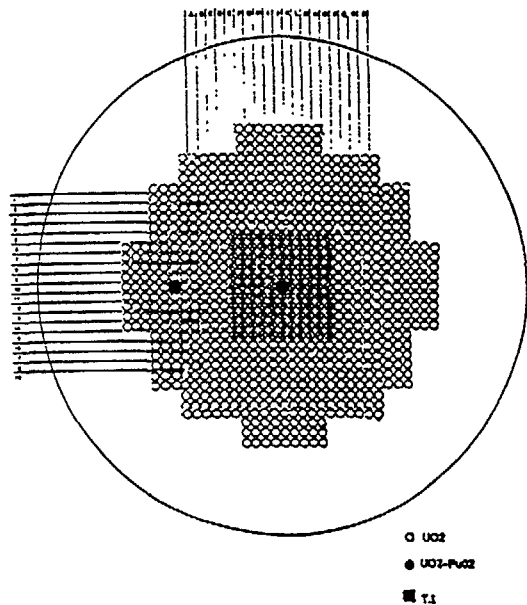


FIG. II.4. MINERVE: MOX-UO<sub>2</sub> configuration.

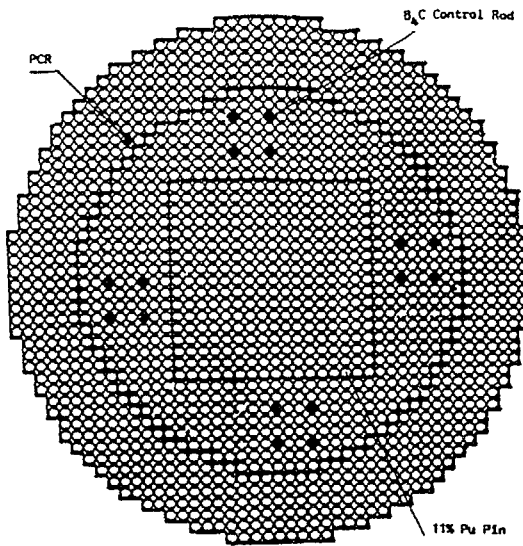


FIG. II.5. ERASME/L: Radial cross-section.

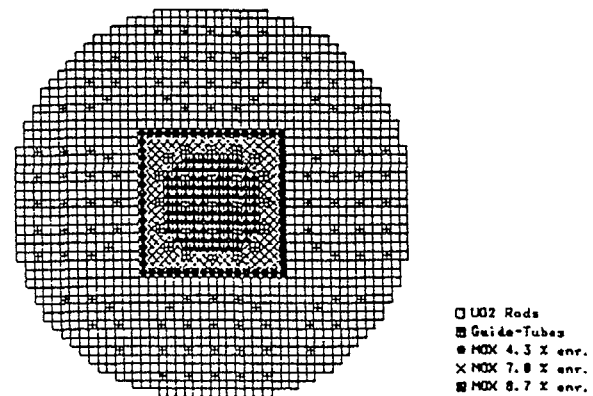


FIG. II.6. EPICURE: Radial cross-section,  
MOX-UO<sub>2</sub> configuration.

## PLANNING OF THE EXPERIMENTS

|         | 1984 | 1985                     | 1986                     | 1987                     | 1988         | 1989 | 1990          | 1991 | 1992 |
|---------|------|--------------------------|--------------------------|--------------------------|--------------|------|---------------|------|------|
| ERASME  |      | $\leftarrow \rightarrow$ | $\leftarrow \rightarrow$ | $\leftarrow \rightarrow$ |              | L    |               |      |      |
| ICARE   |      |                          | $\leftarrow \rightarrow$ | $\leftarrow \rightarrow$ |              | R    |               |      |      |
| MORGANE |      |                          | $\leftarrow \rightarrow$ | $\leftarrow \rightarrow$ |              | R    |               |      |      |
| EPICURE |      |                          |                          |                          | $\leftarrow$ |      | $\rightarrow$ |      |      |

2.1 LWHCR studies

The concept of the Light Water High Conversion Reactor (LWHCR) loaded with mixed oxide fuel allows the improvement of the uranium utilization by increasing the conversion ratio.

This can be obtained by hardening the neutron spectrum (which favours capture in  $^{238}\text{U}$ ) by adapting a tighter lattice pitch.

However, reducing the moderation ratio introduces larger uncertainties in the computed neutronic parameters : the neutron spectrum is intermediate between PWR and FBR lattices and, consequently, most of the fission and capture rates arise in the fast and epithermal energy range where cross-sections are not as well known as in the thermal range.

In order to reduce these uncertainties and to qualify neutronic codes, an extensive programme was launched by CEA.

Concerning neutronic reactor physics research, this programme includes :

- adaptation of codes in particular the cell code APOLLO and its neutronic data library,

- accomplishment of an extensive experimental programme (ERASME, MORGANE and ICARE experiments) in order to reduce the uncertainties in the different neutronic parameters,
- studies of important and specific problems of future PWR designs.

## 2.1.1 The ERASME/S &amp; R Experiments

The ERASME experiments were designed to provide fundamental data relating to the whole moderation ratio range involved in the LWHCR concept. The experiments consist of large-sized cylindrical undermoderated plutonium-fuelled test lattices centered inside a driver-core of the zero power facility EOLE at the Cadarache Nuclear Center.

The driver core is an LWR lattice with 3.5 % enriched  $\text{UO}_2$  fuel rods. In order to improve the spectrum adaptation a buffer zone is located between the test zone and the driver core. It consists of a  $\text{UO}_2$  fuelled (3.5 % enriched uranium) tight lattice.

The test lattice is contained in a watertight stainless steel vessel so as to allow to drain all water from the central zone and to add soluble boron (Fig. II.1).

Core dimensions have been optimized :

- radially in order to obtain a very large area where the fundamental mode is established (test zone radius, properties of the vessel and thickness of the adaptation zone),
- axially in order to avoid 3D effects (uniform fissile height and optimization of axial reflectors).

The ERASME experiments consist of 3 phases :

- The ERASME/S test zone comprises about 1500  $\text{UO}_2\text{-PuO}_2$  fuel rods (11 % Pu enriched) with a moderation ratio  $V_{\text{mod}}/V_{\text{fuel}} = 0.5$ .
- The ERASME/R test zone comprises about 1240  $\text{UO}_2\text{-PuO}_2$  fuel rods with a moderation ratio  $V_{\text{mod}}/V_{\text{fuel}} = 0.9$ .

The measurements carried out in the ERASME experiments concerned :

- Reaction rate distribution for determination of the bucklings.
- Conversion ratio ( $\sigma_c^{238}\text{U}/\sigma_f^{239}\text{Pu}$ ) using metallic foils.
- Fission rates of the major heavy nuclides ( $^{235}\text{U}$ ,  $^{238}\text{U}$ ,  $^{239}\text{Pu}$ ,  $^{240}\text{Pu}$ ,  $^{241}\text{Pu}$  and  $^{242}\text{Pu}$ ) using fission chambers.
- Absorber worth and cluster configurations (stainless steel, natural and 10B enriched  $\text{B}_4\text{C}$ , Hf, Ag-In-Cd, Eu203, Gd203, Zircaloy rods).
- Perturbations produced by heterogeneities in the assembly (guide-tubes and fertile depleted  $\text{UO}_2$  rods).
- Studies of the voided configuration.
- Studies of the configuration with soluble boron.

The main results obtained using the CEA calculational scheme are the followings :

\* The new APOLLO procedure

The French computer code APOLLO was adapted in order to perform hexagonal geometry calculations ; an accurate method to treat resonance overlapping and mutual-shielding of the  $E(^{242}\text{Pu}) = 2.67 \text{ eV}$  and  $E(^{240}\text{Pu}) = 1.057 \text{ eV}$  "thermal" resonances were improved.

New multigroup cross-section sets were generated from the JEF-1 library, or from recent CEA evaluations (for  $^{235}\text{U}$ ,  $^{238}\text{U}$  and  $^{239}\text{Pu}$  primarily).

\* Multiplication factor

Axial measurements with miniature fission chambers demonstrated that axial buckling remained constant in the test zone. The radial buckling was measured using several experimental techniques in order to avoid local moderation ratio fluctuation effects (direct gamma spectrometry on fuel

pins, fission chambers and foils) with epithermal and fast reaction rate distributions. The results,  $(C-E)/E$ , of the analysis of these  $K_{eff}$  measurements are given below :

|                         | ERASME/S<br>$V_m/V_f = 0.5$ | ERASME/R<br>$V_m/V_f = 0.9$ |
|-------------------------|-----------------------------|-----------------------------|
| $(C - E) / E$<br>in pcm | + 860 +/- 560               | + 470 +/- 300               |

\* Conversion ratio and fission rates

The conversion ratio  $\sigma_c^{238}\text{U}/\sigma_f^{235}\text{U}$  was measured using uranium foils placed between nickel clad  $\text{UO}_2$  -  $\text{PuO}_2$  pellets in the central cell of ERASME and in a thermal column for calibration.

The fission rate measurements have been carried out with miniature fission chambers introduced into a voided guide-tube placed in the central cell of ERASME. The experiment-calculation discrepancies for the main parameters are shown below :

| INDICE  | ERASME/S RM = 0.5 | ERASME/R RM = 0.9 |
|---|-------------------|-------------------|
| $\frac{\sigma_c^{238}\text{U}}{\sigma_f^{235}\text{U}}$ | + 1.5 +/- 5.0 %   | - 0.5 +/- 5.0 %   |
| $\frac{\sigma_f^{239}\text{U}}{\sigma_f^{235}\text{U}}$ | + 3.9 +/- 4.0 %   | + 3.8 +/- 4.0 %   |
| $\frac{\sigma_f^{241}\text{U}}{\sigma_f^{235}\text{U}}$ | - 12.0 +/- 8.0 %  | - 3.8 +/- 8.0 %   |

\* Heterogeneity effect study - Reactivity worth of absorbers

Linked to the LWHCR feasibility studies, some realistic heterogeneities involved in the core design were investigated. The reactivity worth and the perturbed power distributions were measured when

introducing an heterogeneity in the central cell. The following table present the main results obtained during these studies (the results are normalized to 100 % for natural  $B_4C$ ).

| ABSORBERS       | ERASME/S<br>$V_m/V_f = 0.5$ |        | ERASME/R<br>$V_m/V_f = 0.9$ |        | ERASME/S<br>Voided Config. |        |
|-----------------|-----------------------------|--------|-----------------------------|--------|----------------------------|--------|
|                 | Exp.                        | Cal.   | Exp.                        | Cal.   | Exp.                       | Cal.   |
| Natural $B_4C$  | -100.0<br>+/- 1.0           | -100.0 | -100.0<br>+/- 1.0           | -100.0 | -100.0<br>+/- 1.0          | -100.0 |
| Enriched $B_4C$ | Not measured                | -199.1 | -179.0<br>+/- 1.0           | -176.0 | -396.0<br>+/- 1.0          | -396.0 |
| Ag - In - Cd    | -62.7<br>+/- 1.5            | -63.3  | -64.7<br>+/- 0.5            | -67.0  | -72.5<br>+/- 0.7           | -75.3  |
| Guide - tube    | + 9.7<br>+/- 0.7            | +11.5  | -11.8<br>+/- 0.2            | +13.3  | /                          | /      |

These measurements allowed us to qualify on the one hand epithermal and thermal cross-sections of the main absorber materials to be used to control LWHCRs, and on the other hand the power peaking calculations using APOLLO multicell routines.

In order to qualify core design methods and to satisfy control safety criteria, we have simulated some realistic clusters allowing us to validate the calculation of the mutual shielding effect and the perturbed power maps between several heterogeneities.

\* Voided configuration

The void coefficient is one of the most important parameters linked to the safety criteria : in a very tight Pu lattice, it could be positive and consequently drastically limit the LWHCR concept.

An extensive experiment has been devoted to the voided configuration in order to reduce the uncertainties in the void coefficient. The "integral" voiding effect was checked by voiding the whole of the water tight vessel containing the LWHCR lattice.

Material buckling, conversion ratio and fission rate ratios were measured in order to validate nuclear data in the fast energy range. The experiment/calculation discrepancy for the void coefficient is :  $-2.5 \pm 6.0$  pcm% of void.

The integral void effect calculation using APOLLO with the new procedure is quite consistent with the measurements.

Control rod and burnable poison efficiencies, fertile rods and cladding materials were also investigated in order to qualify the fast cross-sections of the main absorbers.

\* Borated configuration

The watertight vessel allowed us to add soluble boron in the LWHCR lattice region in order to qualify the boron efficiency in the realistic configuration ERASME/R. The "integral" boron effect was measured by critical size variation and, furthermore, the material buckling was investigated through reaction rate distribution measurements.

The experiment-calculation discrepancy for the boron effect is  $(C-E)/E = +2.0 \pm 3.5\%$  ( $1\sigma$ ) : the new APOLLO procedure gives now the boron effect in a LWHCR lattice, consistent with the experiment.

### 2.1.2 The MORGANE and ICARE Experiments

\* MORGANE S & R

In order to validate depletion calculations, an important research programme was devoted to the study of the fission product effects : they are responsible for an important part of the reactivity losses in Pu fuelled lattices.

To reduce the uncertainties in the reactivity loss, two experimental configurations were built into the zero-power pool reactor MINERVE in order to undertake measurements of the global fission product capture effect performed by the oscillation method.

These experimental configurations consist of two zones (Fig. II.2) :

- A peripheral driver zone in which are located the control rods. The driver fuel elements are 90 % enriched uranium-aluminium plates.
- The central test zone containing the tight lattice. The phase-1 configuration consists of about 720  $\text{UO}_2$ - $\text{PuO}_2$  rods disposed in a triangular pitch ( $V_{\text{mod}}/V_{\text{fuel}} = 0.5$ ) surrounded by an  $\text{UO}_2$  buffer zone (3.5 % enriched). The phase-2 configuration comprises 500  $\text{UO}_2$ - $\text{PuO}_2$  rods ( $V_{\text{mod}}/V_{\text{fuel}} = 0.9$ ) in order to be consistent with the ERASME experiments.

Reactivity effects of samples are measured by the motion of an automatic control device (rotating control rod with cadmium sectors). For small perturbations, it can be demonstrated that the signal delivered by the control device is proportional to the reactivity variation. The global fission product capture is determined by comparing the reactivity worth of a spent fuel sample and that of a sample containing the same concentrations of heavy nuclides but without fission products.

A calibration with well-known worth values ( $^{235}\text{U}$ ,  $^{239}\text{Pu}$ ,  $^{10}\text{B}$ ) is carried out.

Using the new CEA86 procedure, the calculations are in good agreement with the measurements performed in the MORGANE experiments (compared with the old library CEA 79, an amelioration of 10 % to 30 % has been obtained in C/E).

A list of the samples studied is given in the following table :

| P.W.R. spent fuel samples   |               |                                      |
|---|---------------|--------------------------------------|
| B.o.L. enrichment   | Number        | Burn-up                              |
| 3.1 %   | 7             | 20 000 to 60 000 MWd/t               |
| 2.6 %   | 2             | 30 000 to 40 000 MWd/t               |
| $\text{UO}_2$ - $\text{PuO}_2$ Test samples<br>to correct heavy isotopes effect |               |                                      |
| Number  | Pu Enrichment | Isotopic composition (Pu 240/Pu 241) |
| 3   | 0.5 to 1.5 %  | (25 / 5) %                           |
| 1   | 2 %           | (15 / 2) %                           |
| 2   | 6 to 11 %     | (20 / 10) %                          |
| $\text{UO}_2$ Test Samples<br>to normalize experimental effects                 |               |                                      |
| Type  | Number        | Content                              |
| $\text{UO}_2$ with Boron  | 4             | of Boron : 0 to 1200 ppm             |
| Enriched $\text{UO}_2$  | 4             | of $^{235}\text{U}$ : 0.2 to 5 %     |

\* ICARE S & R

In the same way, the ICARE experimental programme was devoted to the measurement of the capture cross-sections of the major heavy isotopes, some important effect fission products and burnable poison nuclides in undermoderated lattices.

The principle of the experiment is as follow :

Depleted UO<sub>2</sub> pellets with small quantities of the nuclides being studied (about 0.1 %) were irradiated at the center of an experimental undermoderated assembly.

The ratio "daughter produced by capture/parent" measured at the beginning and at the end of the irradiation allows us to derive the capture rates of each studied nuclide.

Two phases have been performed :

- The ICARE/S experiment was carried out from April to October 1986. The experimental sub-assembly was located at the center of the MELUSINE core (8.5 MWth) and consisted of about 260 UO<sub>2</sub>-PuO<sub>2</sub> fuel pin (11% Pu) with a 0.5 moderation ratio (Fig. II.3).
- The ICARE/R irradiation started in 1988 in order to study the capture cross-sections in a lattice with a 0.9 moderation ratio.

Due to the cooling and the isotopic analyses time, only a few results are available ; the interpretation is still in progress.

## 2.2 Plutonium recycling studies

### 2.2.1 MINERVE and ERASME/L

EDF and CEA decided in 1987, prior to the first loading of MOX in St LAURENT B.1 to validate experimentally the calculational tools to be used for determining power maps from in-core data in PWR's containing assemblies with recycled plutonium.

For this purpose a special measurement program was carried out in the MINERVE facility. Pin by pin power distributions were determined in a small core with a central zone of 4 % Pu MOX pins (11\*11) surrounded by 3 % enriched UO<sub>2</sub> pins (Fig. II.4).

The power distribution was measured using the classical gamma scanning technique, across the interface between UO<sub>2</sub> and MOX zones. In parallel, measurements were performed with <sup>235</sup>U fission chambers similar to those used for in-core instrumentation in PWRs. These chambers were placed at the center of the MOX zone and in the symmetric position with respect to the interface in the UO<sub>2</sub> zone.

These measurements allowed us to validate our calculational schemes concerning the relative values of the power/activity ratio in MOX and UO<sub>2</sub> assemblies.

At the same time, in the EOLE reactor, the ERASME/L configuration was available. This assembly was both the third stage of the LWHCR studies (with respect to the moderation ratio), and the first step towards the validation of the neutronic "formulaire" for plutonium recycling in PWRs.

The ERASME/L core was composed of about 1600 MOX pins (11 % Pu) with a moderating ratio of 2.1 (Fig. II.5).

Data concerning such parameters as :

- multiplication factors,
- spectral indices,
- worth of several absorbers, etc ...
- reactivity of control rod clusters and associated power distributions, etc ...

were obtained from this experiment.

The experiment/calculation discrepancy in the multiplication factor is  $(C-E)/E = +90 \pm 300$  pcm when using the new APOLLO procedure CEA 86.

At the end of the programme, a power/activity measurement similar to the one performed in MINERVE was repeated in the ERASME/L core to determine the trend of the variation of uncertainties with respect to the plutonium enrichment.

These experimental results provided a first basis to assess the uncertainties in the calculation of MOX subassemblies.

Nevertheless, since 1987 physicists from CEA, EDF, and FRAMATOME have collaborated in a study of the possibility of reducing the remaining uncertainties in the main parameters of a mixed-loaded PWR core. The objective of this exercise was to ensure the same core performance as a classical  $\text{UO}_2$  core, with of course, the same safety criteria.

This group concluded that no experimental programme, available at the moment, was representative enough to lead to a real reduction of the uncertainties, particularly for the calculation of power peaks.

Thus, in 1988 we decided to initiate a new experimental program called EPICURE.

#### 2.2.2 The EPICURE PROGRAMME

The EPICURE programme was started in July 1989. Its main objective is to represent as closely as possible the physical and neutronic conditions encountered in a mixed loaded PWR.

The fuel pins, especially constructed for this experiment, are exactly the same as those at a power reactor, except, of course, for the fissile height (80 cm) and the internal pressure (1 atm).

The composition of the fuel pins is as follow :

1500  $\text{UO}_2$  pins (3.7 %  $^{235}\text{U}$ )

2000 MOX PINS | 200 with 4.3 % Pu contain  
| 1600 with 7.0 % Pu contain  
| 200 with 8.7 % Pu contain

The three Pu contents will allow us to study the real neutronic environment of a three zone MOX assembly, designed to minimise the power peak near the MOX  $\text{UO}_2$  interface.  $\text{UO}_2$  and MOX enrichments were

chosen to be representative also of future core management (i.e. : 1/4 loading and high burn-up).

The fuel pins are over-cladded to match, in the experiment, the moderating ratio of PWR core at operating conditions (water density effect).

A number of configurations like the one presented on the figure II.6 will be devoted to pin by pin power measurements together with fission chamber measurements in the center of assemblies.

"Chequerboard" configurations will also be studied.

In addition, fundamental parameters such as :

- multiplication factors,
- effective fraction of delayed neutrons,
- temperature coefficients (spectrum and water density effects),
- worths of several absorbers (single or in a cluster),
- local void effect, bowing effect on power distributions,

will be investigated successively in clean  $\text{UO}_2$  and MOX cores.

In addition to the EOLE programme, measurements of reactivity effects due to fission product capture, will be performed in MINERVE. These experiments will be similar to MORGANE but with a MOX environment made of EPICURE fuel pins, and successively for the three Pu enrichments.

The EPICURE program, planned to last at least three years, will give us a solid experimental basis to assess present uncertainties and will allow us to reduce these uncertainties through improvements in both :

- basic nuclear data,
- algorithms, models and calculational schemes.

### **2.3 Conclusions**

The experimental information from the tight lattices programmes (ERASME, MORGANE and ICARE) have allowed us to meet the accuracy requirements for LWHCR design.

In particular, the uncertainties in  $K_{eff}$ , conversion ratio and voidage effects have been drastically reduced (by a factor of 2 or 3) and the new CEA 86 procedure for the APOLLO code thus validated has contributed to assess the feasibility of the LWHCR concept.

Concerning Pu recycling in PWRs, the ERASME/L and MINERVE experiments give a first basis for the validation of the calculational scheme and the EPICURE programme will lead to a further reduction of the uncertainties in the main parameters related to safety and operation in a mixed loaded PWR core.

In addition, the large number of measurements obtained in MOX assemblies with different plutonium isotopic compositions and moderation ratios will enable us to improve our knowledge of the uncertainties related to the nuclear data (actinides, fission products, absorbers, ...) and to the computational method included in the APOLLO code.

A synthesis of the whole set of comparisons of experimental results with calculation, together with sensitivity analyses, has been initiated and will form the basis of the validation work for the new APOLLO-II code and its associated library (Recently, the CEA 86 library and, in the future, the library derived from the JEF-2 data file).

## **3. THERMODYNAMICS**

### **3.1 GRAZIELLA and OMEGA DNB tests**

#### **3.1.1 GRAZIELLA and OMEGA facilities description**

GRAZIELLA is a refrigerant-12 facility [Fig. III.1] devoted to DNB tests. The total electric power is around 1 MW ; it is distributed to preheating devices in order to control the fluid inlet temperature and to the test section itself ; a by-pass of the test section allows for mixing of "cold" fluid with the hot fluid leaving the test section, thus avoiding possible saturation outside of the test section, and possible pump cavitation.

The similitude between water and refrigerant-12 is chosen with respect of :

- the vapor to liquid density ratio,
- the vaporization specific heat,
- the local quality of the fluid along the test section.

OMEGA is a water facility devoted to DNB tests [Fig. III.2] ; the maximum pressure is 170 bars, electrical power is 9 MW (for test section only).

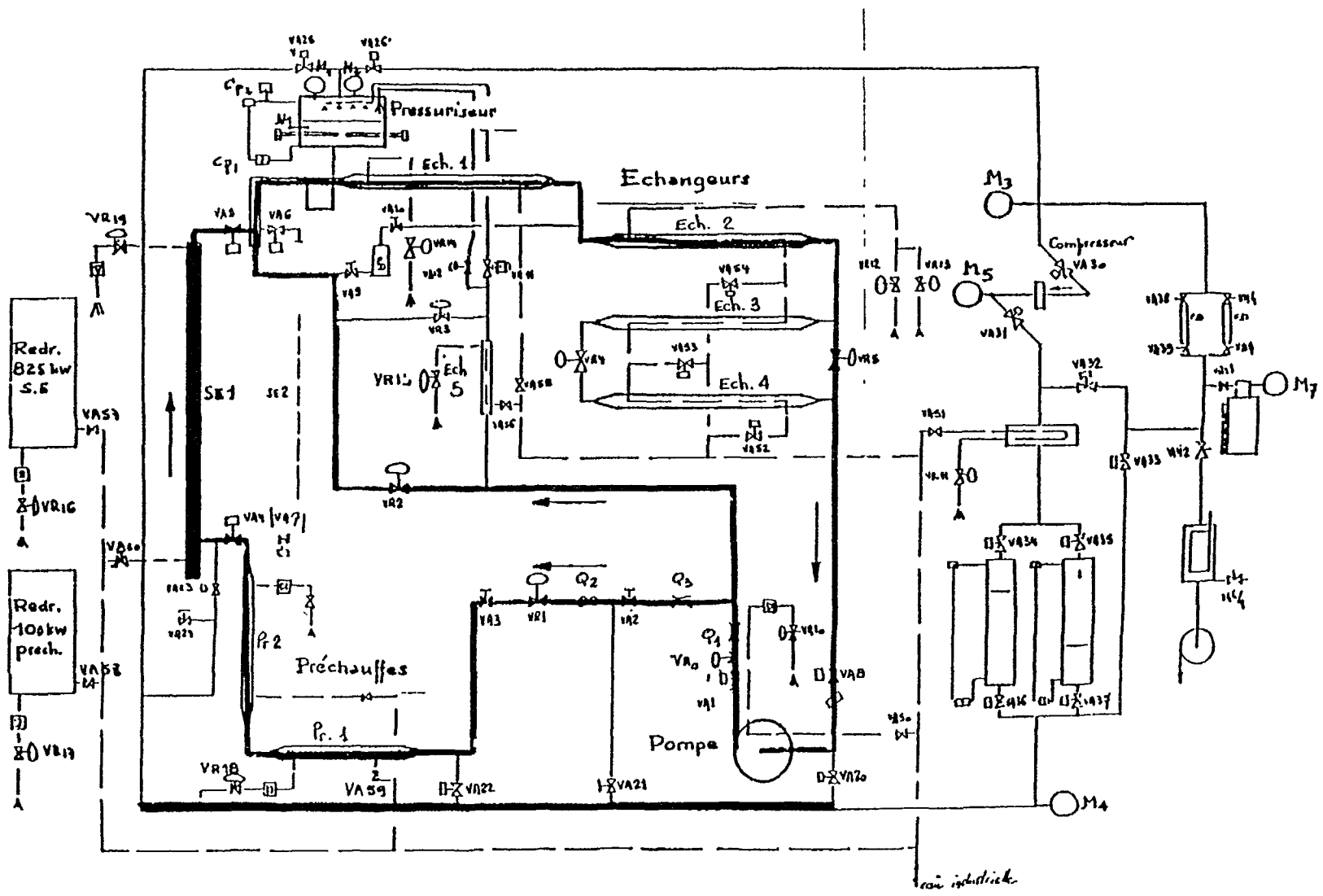


FIG. III.1. Graziella facility.

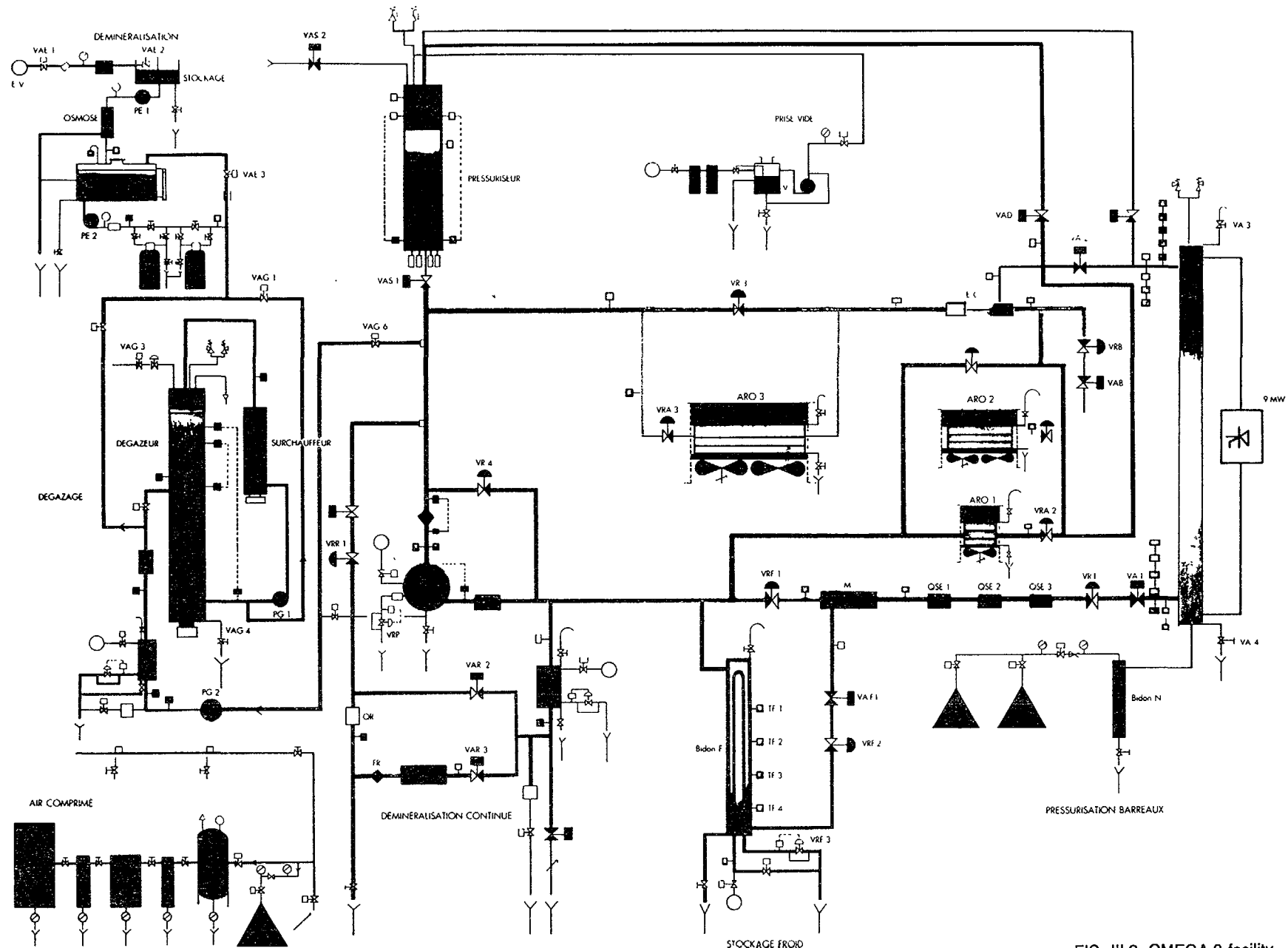


FIG. III.2. OMEGA-2 facility.

3.1.2 DNB hexagonal test sections for tight lattice and semi tight lattices cores

Five test-sections have been tested in the Graziella facility. They are briefly described in the following table :

| Moderator to fuel ratio | Sub-channel type | Clad O-diameter (mm) | Guide tube O-diameter (mm) | Pitch (mm) | Rod number | Heated length (m) |
|-------------------------|------------------|----------------------|----------------------------|------------|------------|-------------------|
| 0.6                     | Standard         | 8.65                 | -                          | 9.96       | 19         | 2.0               |
| 0.6                     | Guide tube       | 8.65                 | 9.8                        | 9.96       | 19         | 2.0               |
| 0.6                     | Inter assembly   | 8.65                 | -                          | 9.96/12.23 | 24         | 2.0               |
|                         |                  |                      |                            |            |            |                   |
| 1.1                     | Standard         | 9.5                  | -                          | 12.23      | 19         | 4.2               |
| 1.1                     | Guide tube       | 9.5                  | 12.5                       | 12.23      | 19         | 4.2               |

The schematic of these test sections is represented on figures III.3 and III.4.

The "standard" channel has also been experimented in water condition on the OMEGA facility both for the tight lattice case and for the semi-tight lattice case.

The equivalent parameter range in water conditions is listed below :

|                      |      |      |    |       |                       |
|----------------------|------|------|----|-------|-----------------------|
| Pressure             | from | 7    | to | 17    | MPa,                  |
| Mass flow            |      | 2400 |    | 11600 | Kg/cm <sup>2</sup> .s |
| Heat flux            |      | 400  |    | 3600  | kW/m <sup>2</sup>     |
| Inlet temperature    |      | 180  |    | 350   | °C                    |
| Outlet vapor quality |      | 0,2  |    | 0,4   |                       |

GRAZIELLA RSM

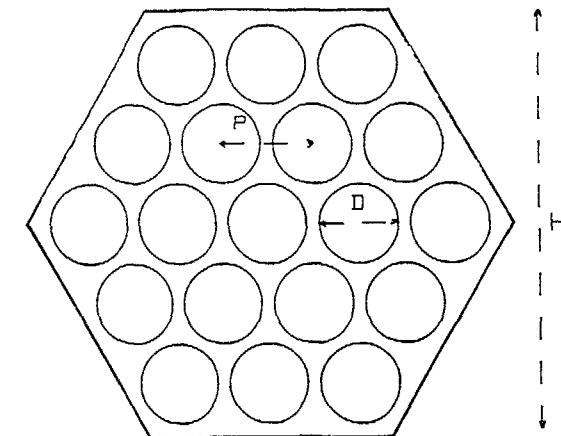


FIG. III.3. 19 rod/standard — DNB test section (GRAZIELLA) (guide tube test section is similar, except the diameter of the non-heated central rod).

GRAZIELLA RSM

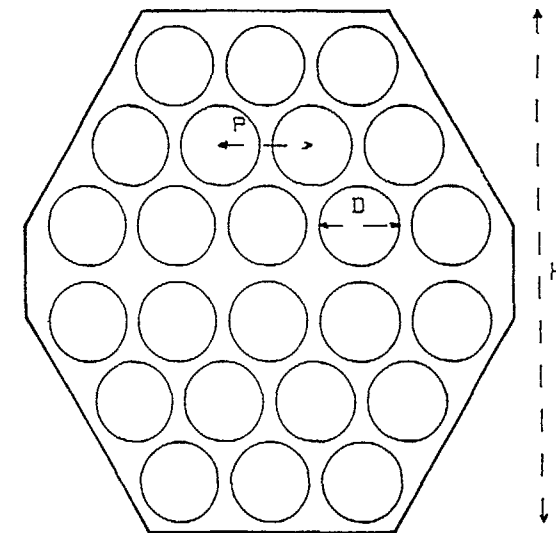


FIG. III.4. 24 rod/inter-assembly — DNB test section (GRAZIELLA).

### 3.2 Main conclusions. DNB correlations and their assessment

For standard subchannels, the results of the three correlations established by Dalle-Done and Hame, by Babcock-Wilcox (Virginia Polytechnic), and by RW.Bowring (AEA Winfrith) are represented on figures III.5, III.6, III.7.

The GRCVSAIL correlation developed in Grenoble fits the experimental results with a 5 % dispersion (quite uniformly over the range of experimental parameters) (fig. III.8).

We assume that the wall effect due to the casing is well represented by the subchannel analysis FLICA code ; we think however that the effect of mixing grids is very important, and is not yet perfectly taken into account.

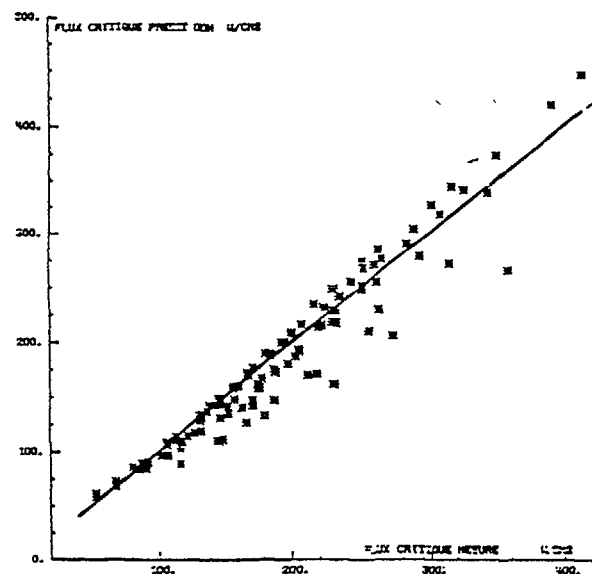


FIG. III.5. Calculated versus measured critical heat flux (using DDH correlation).

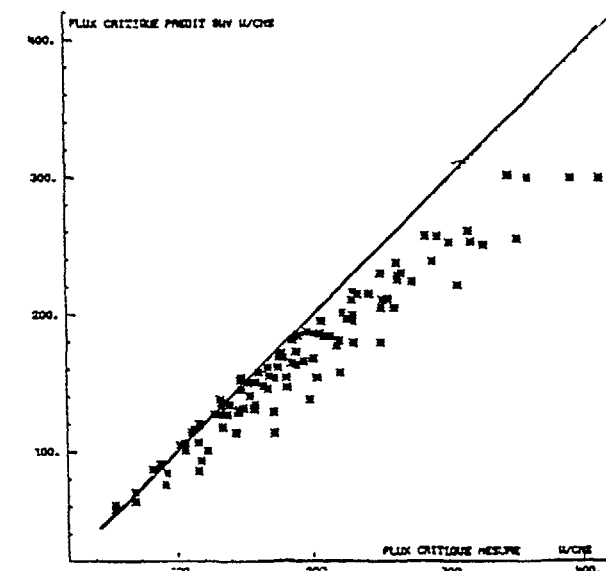


FIG. III.6. Calculated versus measured critical heat flux (using BWV correlation).

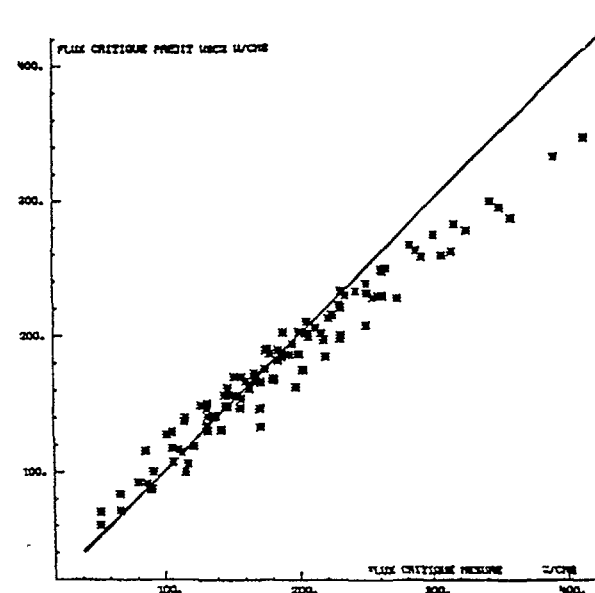


FIG. III.7. Calculated versus measured critical heat flux (using WSC2 correlation).

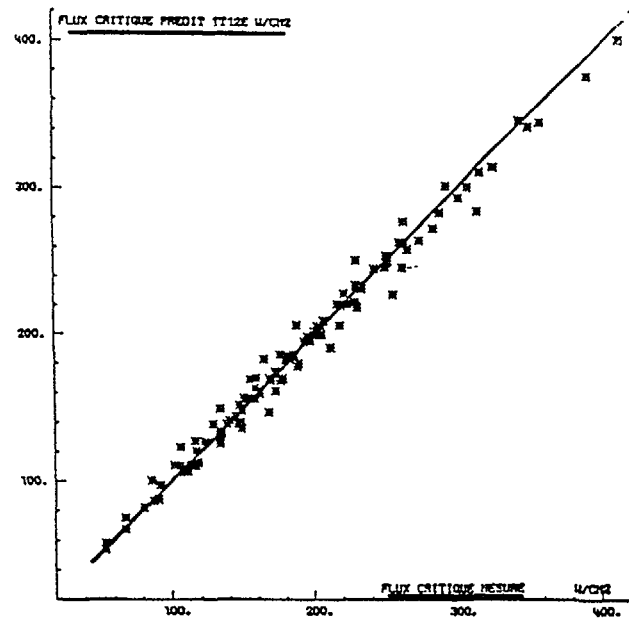


FIG. III.8. Calculated versus measured critical heat flux (using GRVSAIL correlation).

### 3.3 ECCHO-B reflood tests

#### 3.3.1 Facility description - Test sections

The ECCHO-B facility is devoted to reflood tests of rod bundles (37 pins). After an adiabatic heating of the rod bundle up to the "initial" wall temperature, water is injected at the bottom or at both ends of the test section. The mass flow rate is imposed.

The two test sections have following characteristics :

| Moderator to fuel ratio | Heated length (m) | Axial peaking factor | Rod 0-diameter (mm) | Pitch (mm) | Hydraulic diameter (mm) |
|-------------------------|-------------------|----------------------|---------------------|------------|-------------------------|
| 0.6                     | 2.1               | 1.4                  | 8.65                | 9.96       | 4                       |
| 1.1                     | 3.66              | 1.6                  | 9.5                 | 12.23      | 7.9                     |

The test parameter range is given here after :

|                          |      |     |    |     |                          |
|--------------------------|------|-----|----|-----|--------------------------|
| Pressure                 | from | 0.1 | to | 0.2 | MPa                      |
| Heat flux                |      | 1.8 |    | 3.5 | $10^4 \text{ W/m}^2$     |
| Mass flow                |      | 36  |    | 162 | $\text{kg/m}^2.\text{s}$ |
| Inlet subcooling         |      | 30  | or | 60  | $^\circ\text{C}$         |
| Initial wall temperature |      | 300 |    | 800 | $^\circ\text{C}$         |

Bottom injection only has been tested in the tight lattice configuration ; in the semi-tight lattice case, both bottom injection and combined (bottom and top) injection have been investigated.

#### 3.3.2 Main results for tight and semi tight lattice cores

Comparison between tight and semi tight lattice bundles is reported on figures III.9 and III.10. The test parameters are listed here after :

|                          |     |                          |
|--------------------------|-----|--------------------------|
| Pressure                 | 0.2 | MPa                      |
| Mass flow                | 36  | $\text{Kg/m}^2.\text{s}$ |
| Heat flux                | 1.8 | $10^4 \text{ W/m}^2$     |
| Inlet subcooling         | 60  | $^\circ\text{C}$         |
| Initial wall temperature | 600 | $^\circ\text{C}$         |

Similar comparison between the semi tight lattice and the standard PWR cases is reported on figures III.11 and III.12 (heat flux is  $3.35 \cdot 10^4 \text{ W/cm}^2$ ).

Moreover, detailed measurements of steam and liquid flow at the test section outlet (figure III.13) show significant increase of the ratio vapour/liquid in undermoderated bundles. It should thus be expected that reflood and cooling of a ballooned core will be much more questionable in tight lattices than in standard PWR cores.

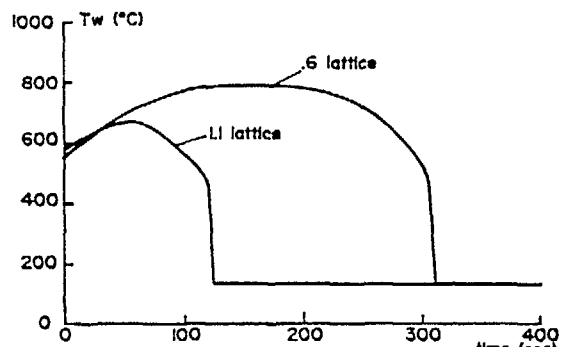


FIG. III.9. Experimental wall temperatures in tight and semi-tight lattice during reflood.

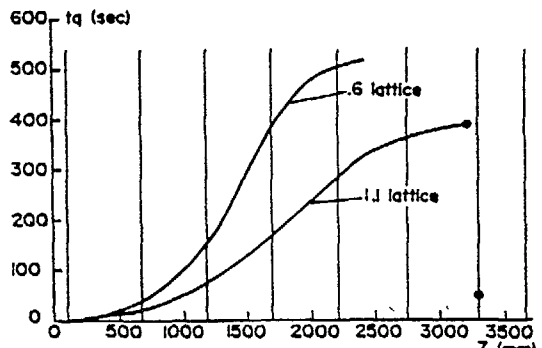


FIG. III.10. Experimental quench time in tight and semi-tight lattice.

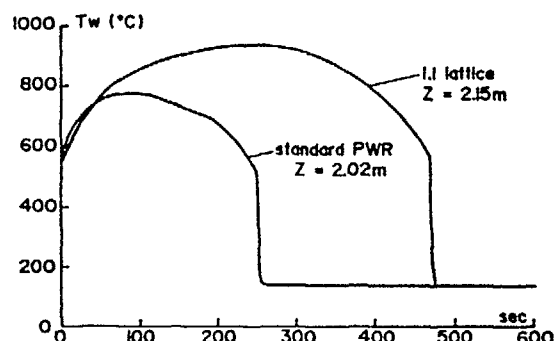


FIG. III.11. Experimental wall temperatures in semi-tight lattice and in standard PWR lattice during reflood.

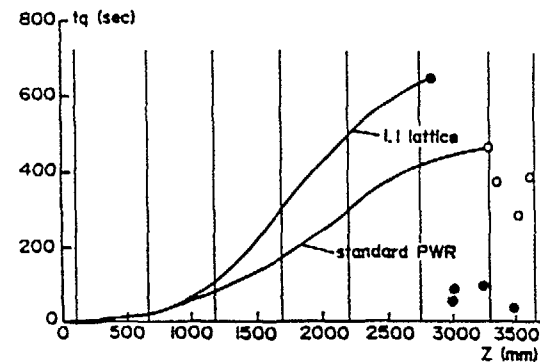


FIG. III.12. Experimental quench time in semi-tight lattice and in standard PWR lattice.

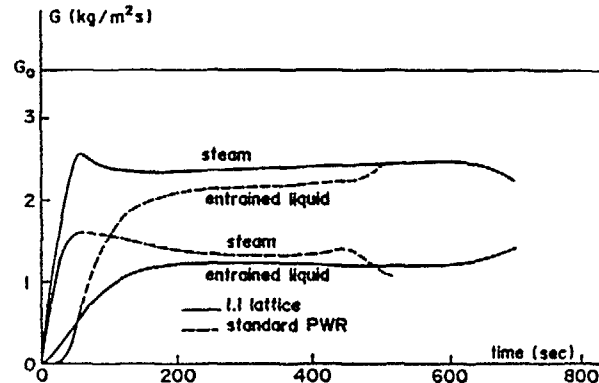


FIG. III.13. Liquid and steam outlet flow rates in semi-tight and standard lattice.

### 3.4 Further tests on PERICLES and present conclusions

The above results are limited to the 37 rod ECCHO-B, without guide-tubes ; they are presently receiving an extension ; additional tests are underway on the PERICLES facility, on a 127 rod test section including guide tubes.

Partial results obtained up to now confirm that the comparisons performed on ECCHO-B should not be altered.

Finally, the figures III.14, III.15, III.16 refer to the comparison of calculated results versus experimental ones ; they reveal a satisfactory validation of CATHARE for 1.1 lattices.

Unless the linear heat rate is decreased, reflood seems to be difficult, even not achieved, in very tight lattice cases.

On the opposite, in the semi tight lattice case, no major problem is expected ; the calculation fits the experimental results well. Further work should be undertaken in order to check that no flow blockage could lead to a lack of core cooling capacity and then to core severe damage.

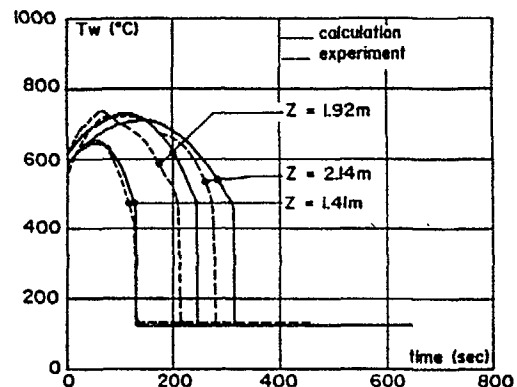


FIG. III.14. Semi-tight lattice reflood comparison between experiment (ECCHO-B) and calculation (CATHARE) ( $\phi = 180 \cdot 10^2 \text{ W/m}^2$ ).

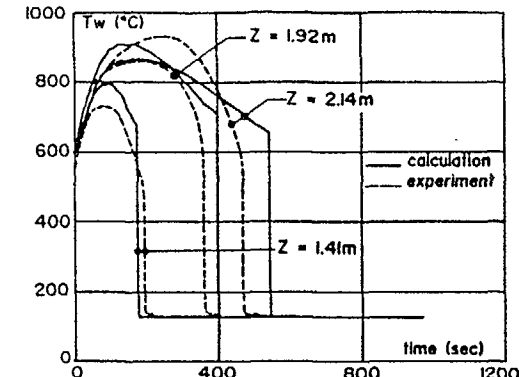


FIG. III.15. Semi-tight lattice reflood comparison between experiment (ECCHO-B) and calculation (CATHARE) ( $\phi = 335 \cdot 10^2 \text{ W/m}^2$ ).

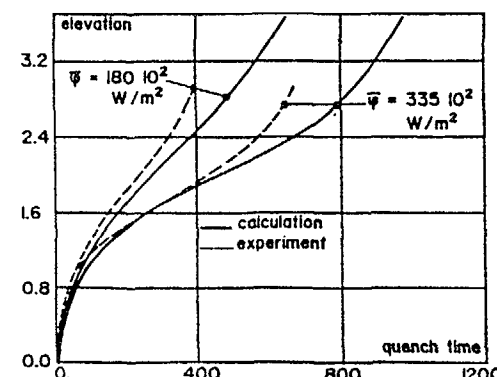


FIG. III.16. Semi-tight lattice calculated and experimental quench times for two values of heat flux.

## IV.1 Fuel assembly characterization in HERMES facility

## IV.1.1 HERMES description (figure IV.1)

The HERMES facility is composed of two loops and a metrology laboratory for surface characterization (wear measurements). The first loop "HERMES T" is operated at intermediate pressure and temperature, thus allowing us to open windows in the casing of the test section, and to use optical methods for velocity and vibration measurements. The second loop "HERMES P" is operated at nominal pressure and temperature, in order to be fully representative of the reactor conditions, and thus to allow us to perform qualification and endurance testing.

The main characteristics are listed below :

|                 | HERMES "T"  | HERMES "P"   |
|-----------------|---|--|
| Fluid           | Water (monitored characteristics)   | Water adjustable characteristics)                            |
| Flow            | 200 to 1.200 m <sup>3</sup> /h<br>(controlled by varying pump speed)        | 200 to 800 m <sup>3</sup> /h                                 |
| Temperature     | 50 to 170°C   | 320°C  |
| Pressure        | 10 to 30 bar  | 150 bar  |
| Electric power  | 500 kW  | 250 kW   |
| Test sections   | Components.<br>Simplex and duplex assemblies of square or hexagonal section | Simplex and duplex assemblies of square or hexagonal section |
| Instrumentation | DP.Liftoff force.<br>Laser anemometry and vibrometry                        | Vibration and impact   |

The typical testing capacities are :

- Control rod assemblies :  
Thermal-hydraulic : pressure loss coefficient, liftoff force ; axial and radial flows.
- Mechanical : Assemblies : compatibility, vibration, endurance.

Control rods : rod drop kinetics, speeds, effects of sudden acceleration, rod cladding wear, absorber material displacement, vibrational behavior of fertile rods.

- Internals : pressure drops, baffle jetting, vibrational behavior of control rod assembly guide tubes close to reactor vessel coolant outlet nozzles, wear phenomena for rod guiding elements, vibrational behavior of fertile rods in the case of downflow.
- Drive mechanisms : performance, wear, endurance of parts subject to fatigue, influence of flow on wear and mechanical behavior.

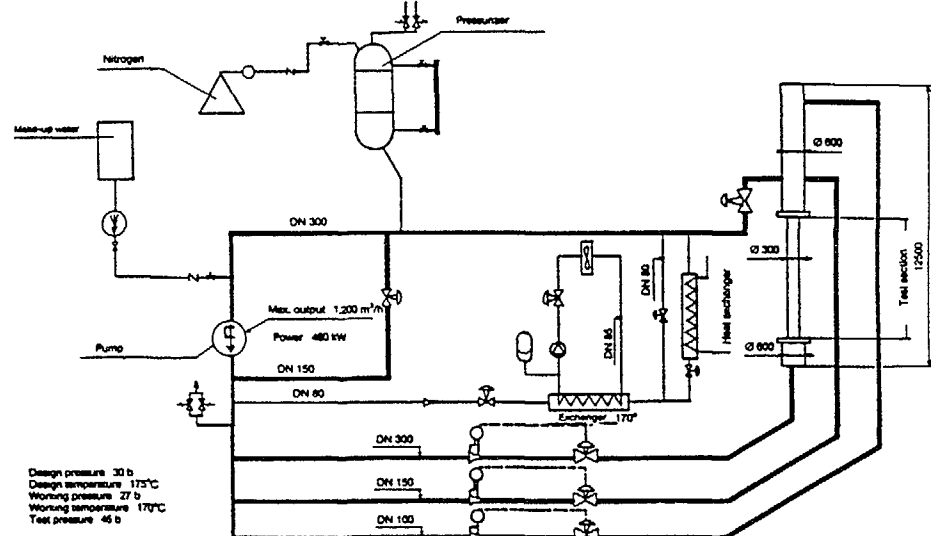


FIG. IV.1. HERMES-T loop schematic.

#### IV.1.2 HERMES test section "SISYPHE" and test results (figure IV.2)

The SISYPHE test section is designed in order to check the feasibility of some technological features required by an hexagonal tight or semi-tight lattice fuel assembly, and required also by the larger number of guide tubes in the upper-plenum (one guide tube per fuel assembly).

The objectives of the tests were :

- the characterization of the fluid flow in the upper region of the assembly, between the upper grid and the assembly head,
- the flow resistance of the different parts of the assembly,
- the induced vibrations of the fuel rods.

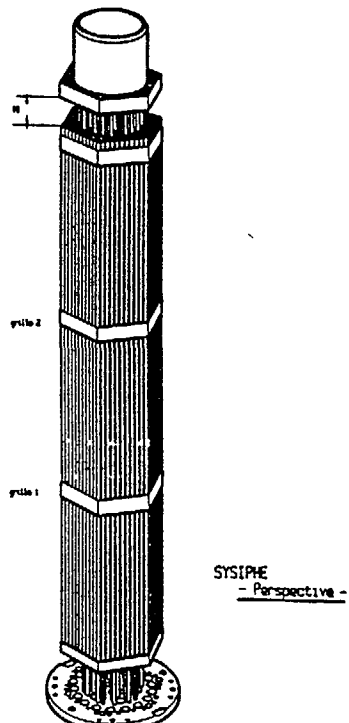


FIG. IV.2. 'SYSIPHE' test section.

The main results lead to the following conclusions :

- the cross-flow in the upper region is acceptable provided that a sufficient distance is kept between the top of the fuel pins and the assembly upper-head,
- in the upper region of the assembly, the central zone is a low velocity region, the cooling of which has to be evaluated carefully,
- no problem appears with regard to the induced vibration of fuel rods.

#### IV.2 Vessel internal testing

##### GRAND-VIZIR, EIFEL and MAGGY experiments

The RCVS concept requires one movable rod cluster per fuel assembly ; around one over three of them are control rods, the other ones are fertile rods devoted to spectral shift. Thus, the upper plenum is rather over-crowded by guide tubes. The feasibility of such a design had to be tested with regard to the vibration of hydrodynamic instabilities, and with regard to the vibration of the fertile or absorbing rods inside the guide tube.

##### IV.2.1 GRAND-VIZIR description and programme

A bundle of 33 guide tubes (so-called GRAND-VIZIR mock-up) is tested on the BEV water loop under transverse water flow conditions (figure IV.3). The geometrical scale is 1/5 ; the Strouhal number and the flow velocity were representative of those of the reactor.

Two situations using cylindrical or hexagonal guide tubes have been investigated (figure IV.4 and figure IV.5).

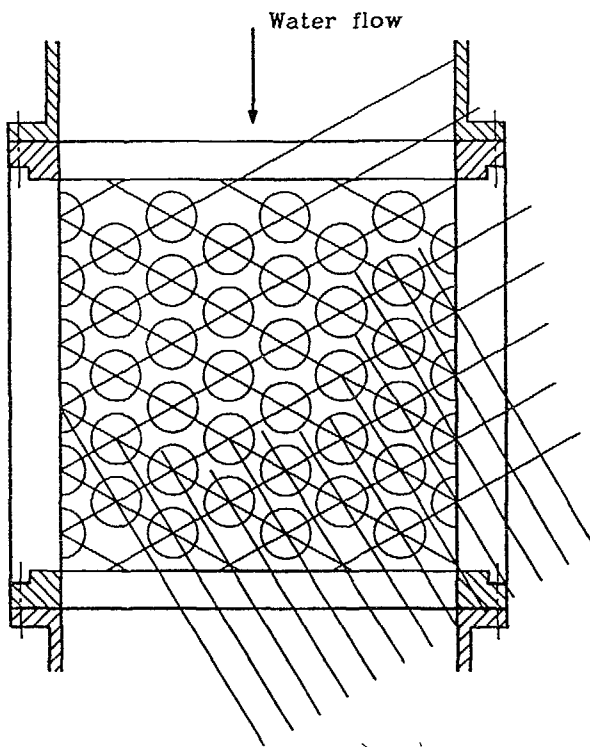


FIG. IV.3. GRAND-VIZIR mock-up.

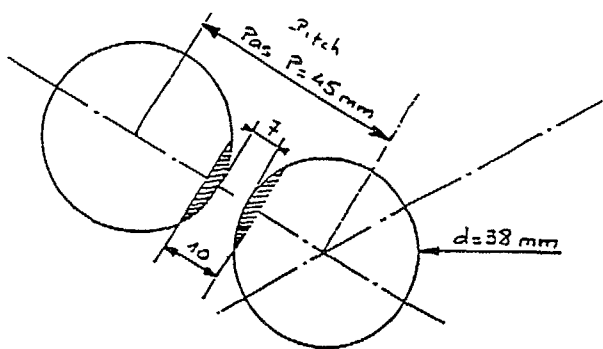
FIG. IV.4. Cylindrical and hexagonal guide-tube:  
external dimensions.

FIG. IV.5. GRAND-VIZIR cylindrical and hexagonal guide tubes.

The tubes themselves were either inserted in the tube-plate or free to rotate at their end.

The velocity between the tubes (hexagonal case) was 25 m/s.

Under such conditions, the reduced dumping coefficients is 0.09, and fluid elastic instability in the case of one "free" tube inside a bundle of "fixed" tubes is reached with a critical velocity of 5.1 m/S, whereas the fluid elastic instability in the case of all tubes free inside the bundle cannot be reached ; thus the critical velocity is larger than 25 m/s.

It has been decided to investigate another domain of experimental parameters -a priori- more representative of what the reactor parameters should be.

#### IV.2.2 EIFEL description and results

The EIFEL test section is designed with the same principle as GRAND-VIZIR, at 1/3 scale, with a nominal velocity of 50 m/s between the tubes, with a reduced dumping coefficient of 0.2 (which is closer to the reactor case, expected to be of the order of 0.6) (figure IV.6).

Under these conditions, the critical velocity in the case of one "free" tube inside a bundle of "fixed" tubes is measured to be around 40 m/s, whereas the critical velocity in the case of a full bundle of "free" tubes is measured at 45.6 m/s.

Although these measured values of critical velocity are higher than the nominal flow velocity between the guide tubes in the reactor, the margin is considered quite small and further investigations should be performed before the final detailed design.

#### IV.2.3 MAGGY experiment and results (figure IV.6)

The objectives of the MAGGY experiments were :

- the evaluation of the vibrations of the absorbing or of the fertile rods induced by the outlet flow of the fuel assembly,
- the evaluation of mechanical forces applied to the rods and to the internals in accident conditions.

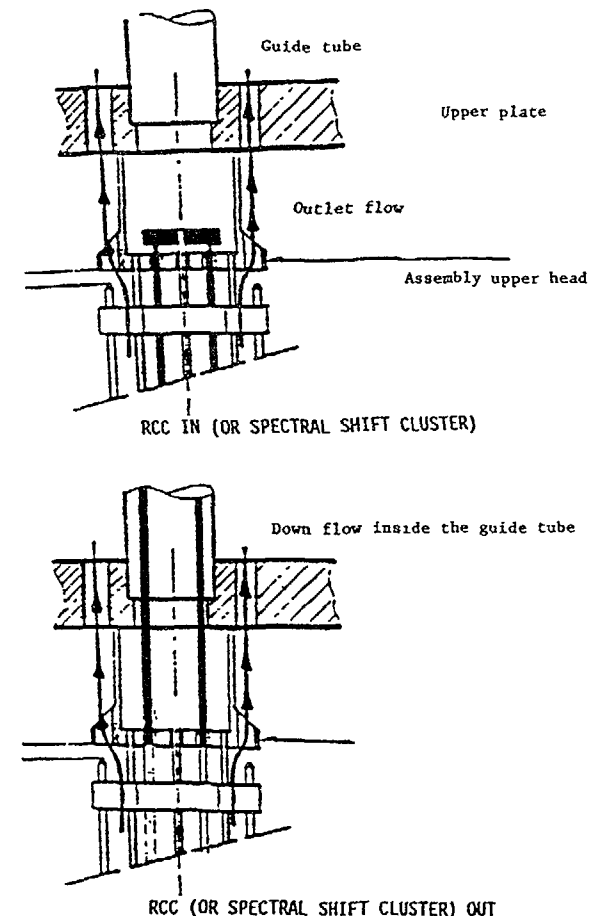


FIG. IV.6. MAGGY experiment.

A first set of tests revealed that whatever the final design should be, it is impossible to avoid excessive vibration of the absorbing rods if the water flows out of the fuel assembly through the guide tubes.

Then, the solution of diverting the outlet flow outside the guide tubes through the periphery of the assembly upper-head has been investigated.

Thanks to these tests, it has been established that such a technological concept was acceptable with regard to any vibration of rods induced by the water flow and with regard to mechanical solicitations both in normal operation and in accident situation.

#### V. GENERAL CONCLUSIONS

V.1. Calculations methods and computer codes have been largely assessed, thanks to the obtained results; the domain of parameters inside which the accuracy is satisfactory has been widely extended.

V.2. Semi-tight lattice cores have been proven to be feasible with regard to core physics, particularly with regard to void effects and with regard to thermalhydraulics both in normal operation and in post-accident situation. On the opposite, very tight lattice cores have to face many difficulties : plutonium content limited by void effect, linear heat rate limited by post LOCA conditions ; then, a very tight lattice core will be very different of a present PWR core, and it looks like a completely new concept.

V.3. In case a detailed design study is decided, further needs will require additional tests :

- core heterogeneities and blankets,
- global core cooling after LOCA, and potential flow blockage,
- DNB assessment through water tests,
- assembly and internals technological testing.

## THE PROTEUS PHASE II EXPERIMENTS AS DATA BASE FOR LWHCR PHYSICS VALIDATION

R. CHAWLA, H.-D. BERGER\*, H. HAGER, R. SEILER

Paul Scherrer Institute,  
Villigen, Switzerland

### Abstract

Twelve different test zones, Cores 7 to 18, have been studied to date in the Phase II program of LWHCR physics experiments at the PROTEUS zero-power facility. This paper reviews the test lattice configurations investigated, the types of integral measurements carried out, experimental techniques and accuracies, the transferability of results to LWHCR design, as also typical comparisons with calculations based on standard LWR methods.

It has been shown that the experimental data base provided is broad – in terms of both high converter design characteristics represented and the types of integral data measured. Thus, the experimental program covers changes in moderation ratio (lattice geometry) and effective fissile-Pu enrichment – with investigations of neutron balance components, moderator voidage effects, influence of lattice poisoning, relative control rod worths and core heterogeneity effects. The importance of having such a broad data base is illustrated by the trends currently reported for the C/E (calculation/experiment) variation for reaction rate ratios with degree of moderation.

## 1 Introduction

The technical – and hence, to some extent, also the economic – feasibility of a given light water high conversion reactor (LWHCR) core design depends on its reactor physics characteristics under normal and accident conditions. It was recognized as early as 1980 at PSI (formerly EIR) that the reliability of calculational results for LWHCRs, e.g. in the prediction of the void coefficient of reactivity, was totally inadequate in the absence of an appropriate experimental data base. A series of relevant integral experiments – the first of its kind worldwide – was accordingly carried out in the PROTEUS zero-power facility during 1981-82 [1]. This so-called PROTEUS-LWHCR Phase I program aroused a great deal of international interest, and a wide range of standard LWR physics methods and data sets have been applied in recent years to its analysis [2,3].

Several features of the earlier, first phase of experiments in PROTEUS prevent its serving as a sufficiently broad base for testing LWHCR physics design calculations.

These include the two-rod nature of the experimental lattices, the non-representative plutonium enrichment and isotopics, as also the fact that certain important reactor design aspects could not be investigated in the relatively short time available. With the above points in mind, a comprehensive five-year program of experiments – PROTEUS-LWHCR Phase II – has been under way at PSI since Summer 1985. Specially fabricated PuO<sub>2</sub>/UO<sub>2</sub> fuel, typical of a homogeneous-design LWHCR, is being used. The principal investigations include those for the void coefficient in terms of detailed neutron balance studies, the effects of changes in moderator-to-fuel ratio (i.e. lattice pitch) and effective Pu enrichment, control rod effectiveness and the influence of core heterogeneities ("hot spot" factors, etc.).

A parallel activity to the PROTEUS-LWHCR Phase II program itself has been the development and testing of calculational codes and data sets on the basis of the experimental results. This is being carried out in a joint, co-operative effort between PSI, Siemens (KWU), the Karlsruhe Nuclear Research Center and the Braunschweig Technical University. Whereas a companion paper written for this Meeting [4] addresses the current status of the code development activity, the present paper deals mainly with details of the experiments themselves, viz. the test lattice configurations investigated to date, the types of integral measurements carried out, experimental uncertainties and the transferability of results to LWHCR design. Comparisons of calculations and measurements are reported on the basis of standard LWR methods and data sets alone.

## 2 The PROTEUS-LWHCR Phase II Cores Investigated to Date

Each reactor configuration for the PROTEUS-LWHCR experiments has basically been a coupled system, with a central test zone driven critical by annular thermal driver zones (Fig. 1). A natural uranium metal buffer, located between the test and driver regions, largely reduces the effects of the mismatch between the thermal driver spectrum and the intermediate or fast spectrum in the test zone. Further details for the reactor, as well as the test zone configurations investigated in the PROTEUS-LWHCR Phase I program, are given in Ref. 1.

The central test zone in the Phase II program has a diameter of 0.50 m, i.e. is somewhat larger than in Phase I with consequently smaller corrections necessary to account for outer reactor-region effects on core-center characteristics (see Section 4). The plutonium-containing part of the test zone extends axially over a length of 0.84 m which, together with the top and bottom blanket regions of depleted UO<sub>2</sub>, results in a total test zone height of 1.40 m.

Up to now, twelve different test zones, Cores 7 to 18, have been studied in the PROTEUS-LWHCR Phase II program (Cores 1 to 6 constituted Phase I). In the first three Cores

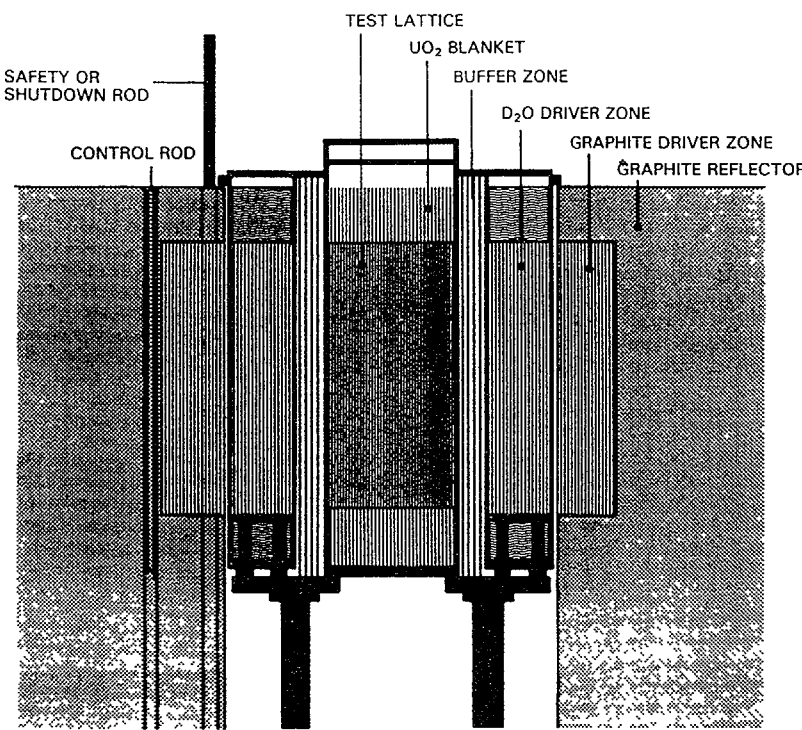


Fig. 1. Basic reactor configuration for the PROTEUS-LWHCR Phase II experiments. The central test zone is 0.50 m in diameter.

(Nos. 7 to 9), measurements were carried out for a reference tight lattice with a volumetric moderator-to-fuel (M/F) ratio of 0.5 – for three simulated voidage states (0, 42.5 and 100% void) using H<sub>2</sub>O, Dowtherm and air (dry lattice), respectively, as moderator [5,6]. Fig. 2(a) indicates the tight lattice geometry employed, about 1900 LWHCR-representative mixed-oxide fuel rods of 7.5% fissile-Pu enrichment (11% total-Pu) making up the 0.5 m-diameter test zone. Apart from detailed neutron balance and  $k_{\infty}$  void coefficient ( $\alpha_v$ ) investigations of the type carried out in the Phase I program [1], relative control rod worths and heterogeneity effects in LWHCR spectra were studied for the first time in Cores 7 to 9 [7,8].

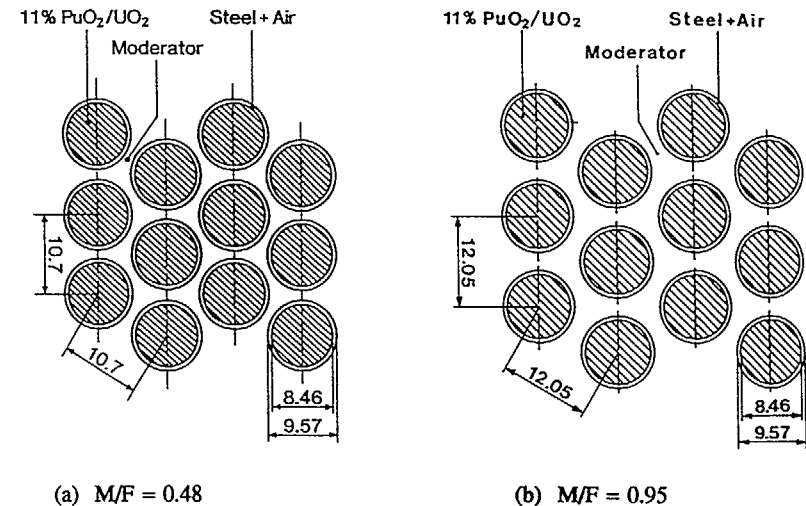


Fig. 2. Reference (a) tight and (b) wider LWHCR test lattices in the Phase II program. The 11% total-Pu corresponds to a fissile-Pu enrichment of ~ 7.5%.

Another new aspect investigated in PROTEUS-LWHCR Phase II has been the influence of a “homogeneous” poisoning of an LWHCR lattice on  $k_{\infty}$  and the void coefficient.

Thus, in Cores 10 to 12, every 37<sup>th</sup> PuO<sub>2</sub>/UO<sub>2</sub> fuel pin in the M/F=0.5 test zone was replaced by a natural-B<sub>4</sub>C rod of identical geometry, measurements of  $k_{\infty}$  for the poisoned “supercell” (see Fig. 3(a)) being carried out again for each simulated voidage state, i.e. with H<sub>2</sub>O, Dowtherm and air [9,10].

The PROTEUS results from the tight lattice (M/F=0.5) experiments have, in effect, been instrumental in shifting the emphasis in the joint Swiss/German LWHCR development effort towards core designs with M/F values somewhat larger than that originally considered desirable [11]. This fact, as well as the need for a broader integral data base per se, have resulted in greater importance being placed more recently on the investigation of wider-spaced LWHCR lattices in PROTEUS. Thus, a second reference test lattice with M/F=1.0 has been studied under clean conditions – for once again, each of the three simulated voidage states – in Cores 13 to 15 [10,12]. Fig. 2(b) indicates the wider LWHCR lattice geometry, about 1500 fuel rods making up the central test zone in this case. Measurements analogous to those for the clean tight lattice (Cores 7 to 9) have been completed for the wider lattice.

The effects of  $B_4C$  poisoning of the M/F=1.0 lattice have been investigated in Cores 16 and 17 – with  $H_2O$  as moderator and dry, respectively [13]. The natural- $B_4C$  loading was increased, relative to that in Cores 10 to 12, such that every 19<sup>th</sup>  $PuO_2/UO_2$  fuel pin was replaced by a  $B_4C$  rod. This increase reflects the greater reactivity of the clean wider LWHCR lattice and the desire to achieve a  $k_\infty$  close to unity (as in an operating power reactor) in the poisoned case. Fig. 3(b) shows the 19-rod supercell investigated in Cores 16 and 17.

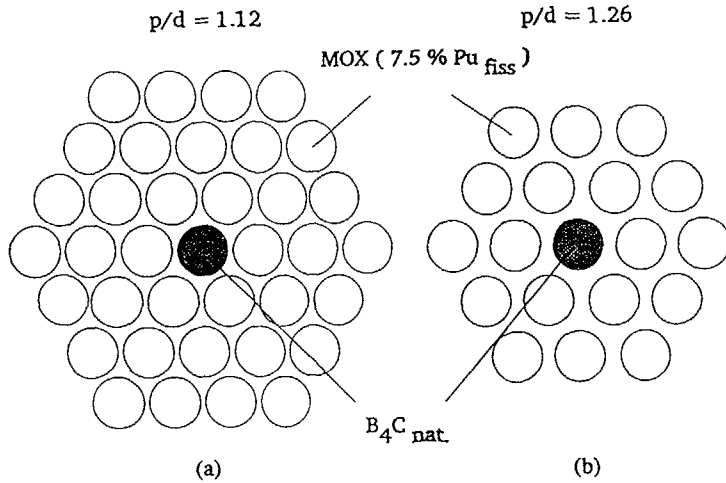


Fig. 3. Poisoned “supercells” investigated in PROTEUS-LWHCR Phase II. The pitch-to-diameter (p/d) values correspond to the respective lattice geometries depicted in Fig. 2.

The analysis of neutron balance components ( $k_\infty$  and central reaction rate ratios) in the tight and wider LWHCR test lattices has revealed significant trends in comparisons of calculational and experimental results (see Section 5.1). The need has thus been indicated of covering an even broader range of moderation ratios in the PROTEUS experiments. It has not been possible, from the viewpoint of operational safety, to install a highly moderated (and hence, highly reactive) test lattice over the full test zone diameter in the current PROTEUS design [10]. Accordingly, Core 18 has been conceived with an  $H_2O$ -moderated test zone, poisoned on the outside and containing a 0.25 m-diameter (effective) central section with an M/F-value of 2.0. The high moderation ratio was achieved by removing every third  $PuO_2/UO_2$  fuel pin from the M/F=1.0 lattice (Fig. 2(b)), so that the “very wide” test lattice essentially consists of Core 13-type unit cells and water holes in the ratio 2:1. Measurements of  $k_\infty$  and central reaction rate ratios are currently in progress in Core 18.

The PROTEUS Phase II program is scheduled for completion this Autumn. Among the experiments still planned to be carried out are ones in which the influence of reducing the effective Pu-enrichment will be investigated (see Section 6).

### 3 Measurement Techniques and Experimental Uncertainties

An important aspect of the Phase II measurements has been the improvement, relative to Phase I, of experimental accuracies in the neutron balance investigations. In this context, new experimental techniques have been developed and applied – mainly for the determination of  $k_\infty$ , but also in extending the earlier range of measured reaction rates. Thus, the cell-worth method, specially developed for  $k_\infty$  measurements in LWHCR lattices [5], has been applied in each Phase II Core. With the buckling method – well established for moderated test zones [1] – continuing to serve as an independent technique, experimental uncertainties ( $1\sigma$ ) on  $k_\infty$  values in the Phase II measurements have been typically about  $\pm 0.7\%$ .

Core-center reaction rate ratios, involving  $^{235}U$  fission ( $F_5$ ),  $^{238}U$  capture and fission ( $C_8$ ,  $F_8$ ) and  $^{239}Pu$  fission ( $F_9$ ), were determined in the clean test lattices using the usual combination of activation-foil and fission-chamber techniques [14]. Due partly to the larger (more LWHCR-representative) fuel-rod diameter in the Phase II experiments, corrections applied for foil effects, etc., have generally been smaller than in Phase I (see also [8]). Moreover, the fact that single-rod lattices have been involved is an additional cause for improved statistical accuracies (relative to those achieved in the earlier two-rod lattices [1]), the typical  $1\sigma$ -error on the “standard” reaction rate ratios ( $C_8/F_9$ ,  $F_8/F_9$  and  $F_5/F_9$ ) being about  $\pm 2\%$  for the Phase II measurements.

Special techniques have been developed for measuring reaction rate ratios involving  $^{241}Pu$  fission ( $F_1$ ) and  $^{242}Pu$  capture ( $C_2$ ) [5]. The errors, due mainly to the poorer statistical accuracies achieved in the counting of the aluminium-backed  $^{241}Pu$  and  $^{242}Pu$  deposits employed, are significantly greater here than for the standard ratios, viz. about  $\pm 4\%$  typically for both  $F_1/F_9$  and  $C_2/F_9$ .

Studies on relative control rod worths and core heterogeneity effects have been new aspects investigated experimentally in the PROTEUS-LWHCR Phase II program. The former type of investigation has involved measurements of rod worths of alternative absorber materials at the center of the test zone in various Cores, the relative values then being LWHCR-specific characteristics [7]. The estimated experimental accuracies for such reactivity worth ratios have been better than  $\pm 1.5\%$ . Questions related to macroscopic heterogeneity effects (“hot spot” factors, etc.) have been addressed by measuring reaction rate distributions in certain benchmark situations, e.g. in the vicinity of a control rod, a water hole and across a core/blacket interface [8]. Standard foil

activation techniques – with errors of less than  $\pm 1\%$  on each experimental point – have generally been employed. Supplementary data have been sought using two other, less painstaking methods, viz.  $\gamma$ -scanning of irradiated fuel rods and radial traverses with miniature fission chambers [15].

#### 4 Transferability of PROTEUS Results to LWHCR Design

The basic approach in the PROTEUS experiments has been one of approximating fundamental-mode conditions in the central region of the test zone for a range of LWHCR designs, moderator voidage states, etc. Measured parameters – such as reaction rate ratios, bucklings,  $k_\infty$  and relative control rod effects – do, however, need to be corrected for the influence of the outer reactor regions. Such corrections have, as mentioned earlier, been smaller in the Phase II program (relative to Phase I) due to the larger quantity of  $\text{PuO}_2/\text{UO}_2$  fuel available for the test zone. In questioning the transferability of the PROTEUS experimental results to LWHCR design, two types of considerations need to be made. These are:

- i. the magnitude of the calculated corrections used in converting measurements to fundamental-mode values, as well as their dependence on the calculational models employed and
- ii. the representativeness of the experimental lattices as such and hence, the value of the measurements in reducing LWHCR design uncertainties [16].

PROTEUS/fundamental-mode differences have been considered most recently for the Phase II experiments in a study employing a range of whole-reactor models for the Core 7 and Core 8 configurations [17]. Table 1 shows, for illustration, some effects of more detailed modeling on the calculated corrections (typically  $<1\%$  in both Cores) for core-center reaction rate ratios. It is seen that these effects are indeed negligible, in comparison to the experimental uncertainties (Section 3).

The second aspect of the transferability of PROTEUS results to LWHCR design, viz. that of representativeness, has been addressed recently using generalized perturbation theory (GPT) methods – “sensitivity profiles” of parameters measured in the test zone being compared with those for a typical power reactor [16]. While establishing the similarity of such profiles is a useful criterion in itself, a quantification of the reduction in calculational uncertainties for the power reactor can be made using correlation coefficients, covariance data and the experimental uncertainties themselves. First results obtained in such an analysis for the Phase II experiments have indeed confirmed that

**Table 1: Whole-Reactor Modeling Effects on Calculated Reaction Rate Ratios at the Center of PROTEUS-LWHCR Cores 7 and 8.**

| Modeling Change<br>Effect (%) on: | 28 $\rightarrow$ 127 gp.calcn.     |         | 1-D $\rightarrow$ 2-D model |         |
|-----------------------------------|------------------------------------|---------|-----------------------------|---------|
|                                   | Core<br>7 ( $\text{H}_2\text{O}$ ) | 8 (air) | 7( $\text{H}_2\text{O}$ )   | 8 (air) |
| $C_8/F_9$                         | 0.0                                | -0.1    | +0.1                        | +0.1    |
| $F_8/F_9$                         | -0.1                               | +0.1    | +0.3                        | -0.1    |
| $F_5/F_9$                         | 0.0                                | 0.0     | 0.0                         | 0.0     |

a considerable reduction in LWHCR design uncertainties can be achieved using the PROTEUS measurements [18].

#### 5 Comparisons of Experiment and Calculation

This section gives – mainly for illustrative purposes – some comparisons of experimental and calculational results obtained using standard LWR physics methods and data sets. As mentioned earlier, the current status of theoretical code development activity in the framework of the Phase II program and the improvements which have resulted in LWHCR lattice predictions are reported separately [4]. Most of the calculational results cited here are based on 1-D whole-reactor calculations in 28 energy groups, the lattice data being generated using the WIMS-D code in conjunction with its 69-group, “1981” cross-section library [5].

##### 5.1 Neutron Balance Components for Different Effective Moderation Ratios

Table 2 gives calculated-to-experimental (C/E) values for neutron balance components, in terms of  $k_\infty$  and explicitly measured reaction rate ratios, in Cores 7 to 9 and Cores 13 to 15, i.e. for a range of effective moderation ratios – from the wider ( $M/F=1.0$ ) LWHCR lattice with  $\text{H}_2\text{O}$ , down to the dry test lattices [5,6,12].

The physics for the dry lattice is clearly quite different from that for the moderated (wet) LWHCR lattices. Even among the latter, however, there are apparently strong trends in the C/E variation with degree of moderation – for both  $k_\infty$  and reaction rate ratios.

**Table 2: C<sup>a)</sup>/E Values for  $k_{\infty}$  and Reaction Rate Ratios for Various Effective Moderation Ratios.**

| Core No.                           | 13               | 15              | 7                | 9     | 8/14      |
|------------------------------------|------------------|-----------------|------------------|-------|-----------|
| M/F                                | 0.95             | 0.95            | 0.48             | 0.48  | 0.48/0.95 |
| Moderator                          | H <sub>2</sub> O | Dowth           | H <sub>2</sub> O | Dowth | air       |
| (M/F) <sub>eff</sub> <sup>b)</sup> | 0.95             | 0.55            | 0.48             | 0.28  | 0.0       |
| C <sub>8</sub> /F <sub>9</sub>     | 1.050            | 1.012           | 0.982            | 0.970 | 1.007     |
| F <sub>8</sub> /F <sub>9</sub>     | 0.986            | 0.986           | 1.030            | 1.019 | 1.026     |
| F <sub>5</sub> /F <sub>9</sub>     | 1.012            | 1.010           | 0.995            | 0.998 | 1.013     |
| F <sub>1</sub> /F <sub>9</sub>     | 1.035            | - <sup>c)</sup> | 1.054            | 1.065 | 1.152     |
| C <sub>2</sub> /F <sub>9</sub>     | 1.745            | - <sup>c)</sup> | 1.729            | 1.650 | 0.962     |
| $k_{\infty}$                       | 1.000            | - <sup>d)</sup> | 1.012            | 1.035 | 1.037     |

<sup>a)</sup> WIMS-D/1981

<sup>b)</sup> defined as M/F [1-(simulated voidage)]

<sup>c)</sup> not measured

<sup>d)</sup> experimental analysis pending

lattice, considered (a) over the partial voidage range 0 to 42.5% void (results deduced from Cores 7 and 9 [6]) and (b) over the total (0 to 100%) voidage range (from Cores 7 and 8 [5]).

**Table 3: The  $k_{\infty}$  Void Coefficient and Its Components for the Tight (M/F=0.5) Test Lattice Between (a) 0 and 42.5% Void and (b) 0 and 100% Void (Units = 10<sup>-4</sup>%).**

|   | (a) 0 to 42.5% void      | (b) 0 to 100% void |                           |              |
|---|--------------------------|--------------------|---------------------------|--------------|
|   | Experiment               | WIMS-D /1981       | Experiment                | WIMS-D /1981 |
| $\alpha_{vi}$ (C <sub>8</sub> /F <sub>9</sub> ) | -14.3 ± 1.2              | -12.9              | -21.5 ± 0.9               | -22.5        |
| $\alpha_{vi}$ (F <sub>8</sub> /F <sub>9</sub> ) | +4.2 ± 0.4               | +4.0               | +5.7 ± 0.3                | +5.5         |
| $\alpha_{vi}$ (F <sub>5</sub> /F <sub>9</sub> ) | +0.9 ± 0.1               | +0.9               | +0.5 ± 0.1                | +0.5         |
| $\alpha_{vi}$ (F <sub>1</sub> /F <sub>9</sub> ) | +1.0 ± 0.6               | +1.3               | -1.3 ± 0.2                | -0.7         |
| $\alpha_{vi}$ (C <sub>2</sub> /F <sub>9</sub> ) | +0.4 ± 0.1               | +0.9               | +1.2 ± 0.1                | +2.3         |
| $\alpha_{vi}$ (others)                          | +5.7 ± 2.2 <sup>a)</sup> | +9.3               | +19.6 ± 1.3 <sup>a)</sup> | +21.6        |
| Net $\alpha_v$                                  | -2.1 ± 1.8               | +3.5               | +4.2 ± 0.8                | +6.7         |

<sup>a)</sup> difference of experimental net  $\alpha_v$  and  $\sum_i (\alpha_{vi})_{meas} R_i$

Other standard calculational routes have been found to yield more consistent results for  $k_{\infty}$ , but this is partly due to compensating errors in the individual neutron balance components [12]. It should be mentioned in passing that the large overprediction of C<sub>2</sub>/F<sub>9</sub> for the wet lattices in Table 2 is mainly due to the inadequate WIMS group structure for treating the dominating <sup>242</sup>Pu resonance at 2.7 eV [5].

In view of the above moderation-dependent C/E trends, results from the experiments currently in progress in Core 18 – involving a central test section with M/F=2.0 (see Section 2) – should be of particular interest.

## 5.2 $k_{\infty}$ Void Coefficients

The results for  $k_{\infty}$  and reaction rate ratios – corresponding to two different H<sub>2</sub>O-voidage states  $v_1$  and  $v_2$ % in an LWHCR test lattice of given geometry – may be combined to yield information on the net  $k_{\infty}$  void coefficient  $\alpha_v$  (between  $v_1$  and  $v_2$ ), as also on its individual components  $\alpha_{vi}$  (due to change in reaction rate ratio  $R_i$ ) [1]. Table 3 gives comparisons of experimental and calculated  $\alpha_v$ ,  $\alpha_{vi}$  values for the tight (M/F=0.5)

It is seen that the experimental  $\alpha_v$ ,  $\alpha_{vi}$  values have larger uncertainties for partial voidage. This is because smaller  $k_{\infty}$ ,  $R_i$  changes are involved, relative to those which occur over the total voidage range. Nevertheless, with  $\alpha_v$  and its components having a marked dependence on the voidage range considered, it is clearly insufficient from the viewpoint of methods validation to refer only to experimental values between 0 and 100% void. Thus, for example, the important negative component due to C<sub>8</sub>/F<sub>9</sub> – while somewhat overestimated by WIMS-D/1981 for the total voidage range – appears to be underpredicted between 0 to 42.5% void. Such effects are, of course, qualitatively consistent with the corresponding C/E variations with voidage (cf. the C/E values for C<sub>8</sub>/F<sub>9</sub> in Cores 7 to 9, Table 2).

Similar arguments to the above may be made against trying to “extrapolate” void coefficient findings from one lattice geometry to another. The importance of an explicit experimental base has been brought out in this context by the  $\alpha_v$ ,  $\alpha_{vi}$  comparisons made for the wider (M/F=1.0) LWHCR lattice in Ref. 12.

### 5.3 Effects of $B_4C$ Poisoning

The availability of integral measurements for clean test lattices, covering a sufficiently broad range of moderation ratios, has been seen to be a fundamental requirement for LWHCR physics validation. In an operating power reactor, however, effects such as leakage, temperature, burnup and the presence of control absorbers are important influences on reactivity and its variation with voidage. Numerical studies, such as the NEACRP LWHCR-burnup benchmark exercise [3], have indicated that the additional calculational uncertainties associated with such effects are relatively small. Nevertheless, related experimental evidence would certainly be desirable.

PROTEUS-LWHCR Cores 10 to 12 and Cores 16 and 17 have addressed a particular such aspect, viz. that of  $B_4C$  poisoning of the tight and wider test lattices,  $k_\infty$  measurements having being carried out for supercells containing a natural  $B_4C$  rod (Section 2). Two types of information could be deduced, viz. (a) the  $\Delta k_\infty$  effect associated with the poisoning and (b) the influence of the  $B_4C$  on the  $k_\infty$  void coefficient [13]. Table 4 compares experiment and calculation for  $\alpha_v$  values in the poisoned tight ( $M/F=0.5$ ) lattice, and it is seen that the presence of  $B_4C$  does not significantly alter – for both partial and total voidage ranges – the corresponding discrepancies observed in the clean lattices (cf. net  $\alpha_v$  values in Table 3).

**Table 4: The  $k_\infty$  Void Coefficient for the Poisoned Tight ( $M/F=0.5$ ) Test Lattice (Units = $10^{-4}/\%$ ).**

|                | (a) 0 to 42.5% void |              | (b) 0 to 100% void |              |
|----------------|---------------------|--------------|--------------------|--------------|
|                | Experiment          | WIMS-D /1981 | Experiment         | WIMS-D /1981 |
| Net $\alpha_v$ | $-3.1 \pm 1.8$      | $+1.6$       | $+4.7 \pm 0.8$     | $+7.6$       |

### 5.4 Relative Control Rod Worths

Integral data related to the relative worths of alternative control rod materials in the center of the test zone were obtained for each of the clean Phase II lattices. These were mainly single-rod studies, although some clusters were also investigated. Information was thereby obtained, not only on the relative effectiveness of different absorber materials in both the tight and wider LWHCR lattices, but also on the variation of such rod-worth ratios with voidage.

Table 5 gives the comparison of calculation and experiment for some of the measurements carried out in Core 7 (tight  $H_2O$ -moderated lattice). As reported earlier [5],  $B_4C$  – even of natural isotopic composition – was the most promising of the various control materials investigated, the reactivity worths of all other rod types in Core 7 being 25 to 45% lower than that of the reference natural- $B_4C$  rod. The significant discrepancy between calculation and experiment which was reported earlier for the relative worth of the 93%  $^{10}B$ -enriched  $B_4C$  rod [5] has since been identified as having resulted from the use of an erroneous WIMS cross-section set for natural boron. The C/E values for the other relative worths shown in Table 5 are, on the other hand, generally poorer than reported earlier – stressing the inadequacy of the WIMS-D/1981 treatment of the alternative control absorbers in the tight-lattice spectrum.

**Table 5: C<sup>a)</sup>/E Values for Control Rod Worth Ratios<sup>b)</sup> in the Tight ( $M/F=0.5$ ) Test Lattice.**

| Control Rod | Material Form | 93% en. $B_4C$ pellet | AgInCd alloy | Hf <sup>c)</sup> metal | Gd <sub>2</sub> O <sub>3</sub> <sup>d)</sup> pellet |
|-------------|---------------|-----------------------|--------------|------------------------|---|
| C/E         |               | 1.020                 | 0.903        | 1.370                  | 0.818   |

<sup>a)</sup> WIMS-D/1981

<sup>b)</sup> relative to natural- $B_4C$  pellet rod

<sup>c)</sup> infinite dilute resonance cross-sections used

<sup>d)</sup> data for the less important isotopes missing

### 5.5 Macroscopic Heterogeneity Effects

Flux depression and peaking effects caused by the insertion and withdrawal, respectively, of control rods in an LWHCR core have been investigated in the clean moderated test lattices in terms of individual reaction rate distributions [8]. Table 6 compares some of the experimental and calculational results obtained in the tight  $H_2O$ -moderated lattice (Core 7), normalisation to unity being carried out via the  $^{239}Pu$  fission rate at a radius of 18.2 cm in the test zone. Significant discrepancies are found to occur in the calculations for both the inserted control rod and the water hole.

**Table 6: Experimental and Calculated<sup>a)</sup> Ratios (With/Without the Central Heterogeneity) for  $^{239}\text{Pu}$  and  $^{238}\text{U}$  Fission Rates in the Vicinity of (a) a Highly Enriched  $\text{B}_4\text{C}$  Rod and (b) a Water Hole in the Tight ( $M/F=0.5$ ) Test Lattice.**

| Radius<br>(cm) | (a) 93% En. $\text{B}_4\text{C}$ Rod |       |       |       | (b) Water Hole |       |       |       |
|----------------|--------------------------------------|-------|-------|-------|----------------|-------|-------|-------|
|                | $F_9$                                |       | $F_8$ |       | $F_9$          |       | $F_8$ |       |
|                | Expt.                                | Calc. | Expt. | Calc. | Expt.          | Calc. | Expt. | Calc. |
| 1.07           | 0.815                                | 0.790 | 0.937 | 0.913 | 1.327          | 1.266 | 1.027 | 1.015 |
| 2.14           | 0.906                                | 0.882 | 0.957 | 0.934 | 1.057          | 1.044 | 1.024 | 1.012 |
| 3.21           | 0.944                                | 0.922 | 0.967 | 0.947 | 1.025          | 1.015 | 1.017 | 1.008 |
| 18.19          | 1.000                                | 1.000 | 1.020 | 0.999 | 1.000          | 1.000 | 1.010 | 1.000 |

<sup>a)</sup> WIMS/1981-based 1-D whole-reactor calculations

## 6 Further Experiments Planned, Conclusions

Some of the experiments carried out for the wider PROTEUS-LWHCR reference lattice ( $M/F=1.0$ ), as also the neutron balance investigations for the highly moderated  $M/F=2.0$  case, are still undergoing final analysis. Further measurements planned in the Phase II program – due for completion this Autumn – include investigations for a reference lattice with an effective fissile-Pu enrichment of 5%. This will be realized for an  $M/F$ -value of 1.0, i.e. in the lattice geometry of Fig. 2(b), by replacing every third  $\text{PuO}_2/\text{UO}_2$  fuel pin by a similarly clad, depleted  $\text{UO}_2$  rod. Fuel enrichment effects were investigated to a limited extent in the Phase I experiments as well [1], but the Phase II experiments planned in this context will be more representative of current LWHCR designs.

It has been seen in the present overview of the PROTEUS-LWHCR Phase II program that the data base provided for physics validation is broad – in terms of both the range of high converter design characteristics represented and the types of integral data measured. Changes in moderation ratio and effective fuel enrichment will have been covered – with investigations of neutron balance components, moderator voidage effects, influence of lattice poisoning, relative control rod effectiveness and power depression/peaking due to core heterogeneities. The trends which have currently been reported for the C/E variation of reaction rate ratios with degree of moderation serve to illustrate the importance of having such a broad data base.

As regards the extent to which calculational uncertainties in LWHCR design will ultimately be reduced by the PROTEUS Phase II measurements, this depends not only on the improved experimental accuracies which have been achieved, but also on the “transferability” of the available integral data. First results from analysis carried out in the latter context have indeed been encouraging.

## References

- [1] R. CHAWLA, K. GMÜR, H. HAGER, R. SEILER, “Measurements and Analyses Pertaining to the PROTEUS Phase I (1981-82) Program”, EIR-Bericht Nr. 608, Swiss Federal Institute for Reactor Research (1986).
- [2] R. CHAWLA, R. BÖHME, “LWHCR Physics Experiments and their Interpretation,” EIR-Bericht Nr. 595, Swiss Federal Institute for Reactor Research (1986).
- [3] W. BERNNAT, Y. ISHIGURO, E. SARTORI, J. STEPANEK, M. TAKANO, “Advances in the Analysis of the NEACRP High Conversion LWR Benchmark Problems”, paper to be presented at the Int. Conf. on the Physics of Reactors: Operation, Design and Computation, Marseille, April 23-27, 1990.
- [4] R. BÖHME, J. AXMANN, C.H.M. BROEDERS, S. PELLONI, M. SCHATZ, “Improvements in the Prediction of LWHCR Lattice Parameters”, Paper 3.5 at this Meeting.
- [5] R. SEILER, R. CHAWLA, K. GMÜR, H. HAGER, H.-D. BERGER, R. BÖHME, “Investigation of the Void Coefficient and Other Integral Parameters in the PROTEUS-LWHCR Phase II Program”, Nucl. Technol., 80, 311 (1988).
- [6] H.-D. BERGER, R. CHAWLA, K. GMÜR, H. HAGER, R. SEILER, R. BÖHME, “Experimentelle Untersuchungen des FDWR-PROTEUS Referenzgitters mit verringelter Moderatordichte und Vergleich mit theoretischen Ergebnissen”, Jahrestagung Kerntechnik ’88, Travemünde, Tagungsbericht (1988).
- [7] H.-D. BERGER, R. CHAWLA, H. HAGER, “Reactivity Control Investigations for LWHCRs”, Trans. ENC’86, Geneva, Vol. 2, 561 (1986).
- [8] R. SEILER, K. GMÜR, H. HAGER, J.M. PARATTE, “Experimental Studies of Macroscopic and Cell Heterogeneities in LWHCRs”, Proc. 1988 Int. Reactor Physics Conference, Jackson Hole, Wyoming, Vol. 2, 353 (1988).
- [9] H.-D. BERGER, R. BÖHME, R. CHAWLA, K. GMÜR, “Investigation of Importance-Weighted Infinite Multiplication Constants in Clean and Poisoned LWHCR Lattices”, Proc. 1988 Int. Reactor Physics Conference, Jackson Hole, Wyoming, Vol. 2, 343 (1988).

- [10] H HAGER, R SEILER, R CHAWLA, H-D BERGER, R BOHME, "Die Realisierung weiterer Untersuchungen zur FDWR-Physik in PROTEUS", Jahrestagung Kerntechnik '89, Dusseldorf, Tagungsbericht (1989)
- [11] R BROGLI, B KUCZERA, H MOLDASCHL, W OLDEKOP, "Lessons Learned from the PWR-HCR Development", Paper 5 1 at this Meeting
- [12] R BOHME, H-D BERGER, R. CHAWLA, H HAGER, S PELLONI, R SEILER, "Comparison of  $k_{\infty}$  Void Coefficient Results from LWHCR Experiments with Different Moderation Ratios", paper to be presented at the Int. Conf on the Physics of Reactors. Operation, Design and Computation, Marseille, April 23-27, 1990
- [13] T WILLIAMS, J ALFONSO, H-D BERGER, R BOHME, R CHAWLA, H HAGER, R SEILER, "Effects of  $B_4C$  Poisoning in Experimental LWHCR Lattices with Different Moderation Ratios", paper to be presented at Jahrestagung Kerntechnik '90, Nurnberg, May 15-17, 1990
- [14] K GMÜR, "Techniques of Reaction Rate Measurements on the PROTEUS Reactor", EIR-Bericht Nr 529, Swiss Federal Institute for Reactor Research (1984)
- [15] H-D BERGER, J ALFONSO, R. CHAWLA, H. HAGER, R. SEILER, "Measurement of Power Distributions in LWHCR Lattices", paper to be presented at ENC '90, Lyon, September 23-28, 1990
- [16] J M KALLFELZ, R CHAWLA, H.-D BERGER, "The Transferability of Integral Physics Data for the Safety Assessment of Tight-Lattice PWRs", Proc. Int. Conf. on Thermal Reactor Safety, Avignon, Vol 5, 2461 (1988)
- [17] W BERNNAT, J KEINERT, M MATTES, "Berechnung integraler Parameter fur hochkonvertierende Leichtwassergitter auf der Basis von JEF-1 und Vergleich mit PROTEUS Phase-II-Experimenten", Jahrestagung Kerntechnik '89, Dusseldorf, Tagungsbericht (1989)
- [18] J R WHITE, T F DeLOREY, "Data Uncertainty Reduction in High Converter Reactor Designs using PROTEUS Phase II Integral Experiments", paper to be presented at the Int. Conf on the Physics of Reactors Operation, Design and Computation, Marseille, April 23-27, 1990

## STATUS OF TIGHT LATTICE THERMAL HYDRAULICS

S BETHKE, W. ZEGGEL,  
X. CHENG, C. MONIR  
Technische Universität Braunschweig,  
Braunschweig, Federal Republic of Germany

### Abstract

This paper contains results and conclusions on Tight Lattice PWR thermal hydraulics which have been mainly obtained in scientific cooperations of Kernforschungszentrum Karlsruhe (KFK) (Inst. für Neutronenphysik und Reaktortechnik (INR) / Inst. für Reaktorbauelemente (IRB)) and Technische Universität Braunschweig (TUBS). This work on High Conversion PWRs (HCPWR) is a part of a cooperative effort between SIEMENS/KWU, KFK, TUBS and the swiss Paul-Scherrer-Institut (PSI).

Since the deterioration of bubbly flow heat transfer (i.e. boiling crisis) depends on local characteristics of fuel assembly (FA) structure, mass flux and fluid quality, there is a need for refined knowledge of these local characteristics while HCPWR-optimization proceeds. In HCPWR bundles flow distribution and mixing become the prevailing modelling factors already under single-phase conditions. Water gaps at the FA boundaries resp. at the thimble cells affect remarkable power peaking. These influences have to be taken into account if the lifetime restrictions by waterside corrosion (wall temperatures) or the minimum Critical Heat Flux (CHF) ratios have to be predicted. Models which are normally used for this kind of analysis are the so called subchannel codes which replace the fine structure of a FA fluid flow by domains of laterally constant properties (subchannels). The constitutive coefficients of these models cannot be deduced from PWR-FA-conditions. Theoretical and experimental investigations are under work at KFK and TUBS to understand the reasons of the high turbulence level in tight lattices and the role of mixing for the CHF event.

The presented investigations are performed with a two-dimensional turbulence model based on the vast amount of Rehme's INR-measurements on turbulence structure. From these flow and temperature field predictions constitutive coefficients for the consecutive subchannel code analysis can be integrated. The application of the latter model depends mainly on additional knowledge about two-phase flow. Actual results of the COBRA-IV-TUBS version will be presented which have been obtained during the analysis of HCPWR-CHF-experiments in water (KWU) and Freon (KFK). Conclusions regarding tight-lattice FA-development and the status of HCPWR thermal hydraulics will be drawn finally.

From a thermal-hydraulic point of view the HCPWR-FA performance can be evaluated as optimistic. More systematical and broader framed prediction models can be very useful especially if the tight lattice bundles are designed for very high burnup. In this context the further experimental and analytical work underway resp. planned within HERA-project/INR-KfK and two-phase mixing KRISTA-measurement/IRB-KfK is very promising.

## 1. Introduction

The tight fuel rod lattice of the PWR with high conversion (PWHCR) makes hitherto unknown demands on the development of interpretation programs. The fundamental difference to conventional PWR lies in the hexagonal lattice of the planned fuel assembly and in the high packing density of the same. It is especially these two aspects of the PWHCR, which rule out the application of the known and wide-spread standard interpretation algorithms of the PWR development.

From the thermal-hydraulic point of view there are two phenomena which are worth being investigated. Firstly, the hydraulic behaviour of the fluid flow in the bundle and the resulting loss of pressure, since they determine the pump capacity to be installed and the constructional layout of the core structure. The second phenomenon is the heat transfer in the single-phase as well as in the two-phase area of flow. Of central importance in connection with this is the critical heat flux phenomenon, which determines the maximum surface heat flux and therewith the maximum power load of the fuel rods.

With reference to both phenomena tests are being conducted within the framework of the scientific co-operation between the Kernforschungszentrum Karlsruhe KfK (Nuclear Research Center Karlsruhe), the SIEMENS AG and the Technical University at Braunschweig. Preliminary results for the CHF-experiments are available. The evaluation of these experiments has already led to interesting conclusions.

## 2. Evaluation method of experimental CHF results

The experimental result of the bundle-CHF-tests is the bundle power upon entry of the critical boiling condition to the rods which are instrument equipped. Entry of the boiling condition is assumed when a specified temperature-excursion in the tube canning has been reached. Therefore, the middle bundle power as a function of differing input data of the fluid in the flow channel is the basis for the numerical evaluation. The thermal condition of the fluid upon exit of the sub-channels is in contrast generally not known. The surface heat flux, which leads to the critical boiling condition is also unknown. In contrast, out of most of the CHF-correlations or CHF-charts follows a local heat flux density, which is valid for the area of the departure from nucleate boiling (DNB). This local heat flux density can be determined from the bundle power using the following formula (slide 1). The average heat flux follows directly out of the measured results and the geometry. Due to manufacturing tolerances etc., the heat production in all rods is not constant. The second factor follows from a measurement of the electrical resistance. Due to differently formed rods (e.g. smooth and finned rods), it can come to a pronounced distribution of the heat flux density along the heated perimeter. The third factor should take these effects into account. It can be derived only with FEM or FDM calculations, and because of the dependence of the heat transfer coefficient on the fluid condition and on the heat flux, is itself not a constant.

The experimental value for the local critical heat flux, which is derived from this calculation, is compared to a mathematically derived value. The concepts, which form the basis of the determination of this value, can be divided into three categories (cf. slide 1, below).

- Input values of the system-parameter-concept are the thermal-hydraulic input data and the geometry of the test channel. Therewith, the geometric parameters of the test in all three dimensions have influence on the CHF-correlation. Verification is very dependent on the utilized test channel.

- The sub-channel-condition-concept calculates, before application of a CHF-correlation, the output conditions of the sub-channels with the help of a sub-channel-analysis (SCA). The results represent the input data of the CHF-correlation, which is therewith not a function of the overall geometry of the bundle. The correlation needs only one geometric parameter, e.g. the hydraulic diameter.
- An additional improvement of the meshed network leads to the local-condition-concept. Calculation of the critical boiling condition follows directly out of the thermal-hydraulic determination of the fluid properties field.

As can be seen in the following diagram (slide 2), the three concepts are linked to an increasing discredit of the calculation area. The calculating segment must be correspondingly limited. The tests, which are necessary for the verification of the complete model, become more costly from top to bottom. Because the excluded single effects must be separately investigated with a decreasing parameter of the CHF-correlation, in order to determine a real as possible local fluid condition, the expenditure for the verification of a procedure increases. On the other hand, the division of the influences of individual effects into separate correlations means, that the total condition process depends less on the geometry and therefore the applications become more universal. The first two concepts are widely applied. For lack of efficient FEM and FDM programs, especially in the two-phase thermal-hydraulic, use of the rigid local concept is far from being realised. For special applications, especially the generating of input data and determination of coefficients for the sub-channel analysis, the FEM programs can gain increasing importance.

## 3. Phases of the design process and related codes

Analogous to the three concepts, according to which the determination of the critical heat flux is conducted, a short survey of the utilized programs and their reticulation in the interpretation shall be presented in the following. The following diagram, Fig. 3, shows the different program systems. The distributed-parameter or hybrid analyses are based on FEM/FDM programs. At the Institut für Raumflug- und Reaktortechnik (IfRR) the FEM program VANTACY (an original development) and a modified braunschweiger version of the famous program VELASCO are available. Small segments from the fuel rod and test bundles can be fluid-mechanically calculated with these programs. By integration over the sub-channels, these programs are suitable for determining input data for the sub-channel-analysis-codes. This can be the mixing parameter, the cross-flow resistance of the gap, the friction coefficient of the sub-channel, heat transfer values and the drag coefficient of the channel structures. Very detailed experiments concerning turbulence were conducted at the Institut für Neutronenphysik und Reaktortechnik (INR) of the KfK. Grid-spacer-less bundles as well as the influence of grating spacers on the turbulence in the fluid channels were investigated. The tests on unheated channel flow were conducted in the past and were also evaluated at the IfRR. They led to statements about the transverse flow behaviour of tight lattices and can lead to valuable input data concerning the sub-channel-analysis.

An experimental circuit for the investigation of heated bundle flows (HERA project) is on the verge of its first test runs. This project will provide detailed information concerning turbulent temperature fields. These tests can be evaluated at the IfRR with an improved version of the VANTACY program, which has been expanded for thermal flows, and which has been coupled with the VELASCO program. Determination of the heat transfer coefficients of the sub-channels is to be expected from the evaluation. A complete coupling of the test evaluation with the calculating programs is ensured for the presented dots. In view of the system programs which are available, application of the distributed-parameter methods has hitherto been restricted to the calculation of single-phase non-boiling flows.

The sub-channel-analysis represents the most widely spread method for the simulation of the flow in individual fuel assemblies. A mean value here characterizes each the thermal and hydraulic relationships for sub-channel. The size and the form of the sub-channels are determined by the geometric structure of the fuel rod cluster. The sub-channel-analysis requires the provision of correlations for the consideration of different individual effects, e.g. the mixing characteristics of the cluster, calculations of the pressure loss etc. The necessary coefficients can either follow out of calculations of the distributed-parameter programs or they are determined directly by tests on cluster segments, whereby the measurement technological expenditure is less here than it must be for the turbulence tests. If larger areas of the cluster are united with the sub-channels — with the appropriate geometric parameters —, this is regarded as a global-analysis.

In the interpretation of the core and for the integration in loop-analysis calculations, the hot-channel model is still used today. Here, there are only two types of channels. The necessary global hot-channel factors, which are not influenced by transverse flow, can be derived using the global-analysis. The local hot-channel factors are the results of a sub-channel-analysis.

Tests concerning the critical heat-flux should be evaluated using a sub-channel-analysis. This can then lead, in special cases, to compilation of system-parameter-correlations, which can be inserted into loop-analysis codes.

### 3.1. Subchannel analysis code

As can be seen in the diagram the sub-channel-analysis describes the central program in the evaluation of the CHF-tests as well as in relation to the interpretation procedure for the cooling loop. It is therefore the link, which connects the single-phase turbulence tests, the single- and two-phase mixing tests and the tests concerning the critical heat-flux with the usual global methods of interpretation.

The principle of the sub-channel-analysis is in the division of the heat exchanger into channels which, hydraulically calculated, are independent of each other. The calculation results from approximation of the generally non-circular channels with circular tubes. The characteristic hydraulic length is the hydraulically equivalent diameter. This concept of the hydraulic diameter holds true for the momentum and heat transfer, as long as the momentum resistance and the heat transfer resistance are independent of the shape of the fluid channel.

The necessary coefficients become clear, when one examines the sub-channel equations. The mass balance of a control volume, Eqn 1, contains a local part, the axial convective part, and the diversion crossflow across the gap. The energy, Eqn 2, also comprises the local part, the axial convective part and the energy part, which is laterally exchanged by the diversion crossflow. Additionally, the heat through the rod and a possible heat given off by the container wall are allowed for. Along with the convective axial and lateral heat flows, in individual cases the axial and the lateral heat conduction must be considered. The turbulent energy exchange appears as final member in the equation. The axial momentum balance, Eqn 3, also shows an analogous setup. The right side of the equation comprises the pressure forces, the wall friction and the drag loss over structure elements and the weight force. Additionally, an axial force is allowed for by the turbulent mixing, as a momentum exchange occurs between the sub-channels. Along with the local and convective axial and lateral components on the right side, the lateral momentum balance, Eqn 4, allows for the pressure force on the gap control volume, the pressure loss over the gap and the lateral weight force, dependent on the slope of the cluster.

### 3.2. Subchannel analysis code input data

The equations show, that application of the sub-channel-analysis calls for the provision of different empirical parameters, the accuracy of which plays a decisive role in the result of the calculation.

- pipe friction coefficient  $f_i$ ,
- drag loss coefficient  $\zeta_i$ ,
- heat transfer coefficient  $h_i$ ,
- turbulent transverse flow per axial length  $w'_i$ , and
- correction factor  $C$  by the formation of the efficient temperature gradient as driving force of the heat conduction

The sub-channel-analysis equations put the turbulent behaviour of heat and momentum transfer into analogous relationships. Constant factors are inserted for correction.

The different components of the transverse flow and the conduction appear in the sub-channel equations separate from each other (Fig 4). The turbulence is specified by the researcher using empirical relationships. The diversion crossflow is calculated using the lateral and the axial momentum balance and is therefore dependent on several incoming factors, e.g. the pipe friction coefficient  $f_i$ , the heat transfer coefficient  $h_i$  and the resistance coefficient of the gap. The result of the lateral mass flow contains the sweeping flow

component. A grouping of the transverse flow components is shown in Fig 4. On the one side are the molecular components of the heat conduction. On the other side are the convective components of the cross-flow, divided into natural and forced effects. A directed and likewise a non-directed flow can be differentiated for both branches. Natural occurrences are the diversion crossflow and the turbulence, forced occurrences are the flow sweeping, caused by fittings and the flow scattering.

The above mentioned coefficients describe the connection of the sub-channel-analysis to the distributed parameter programs. They were inserted in the past mostly on the basis of experimental results and experiences. A theoretically established investigation presents the calculation of these coefficients from FEM/FDM programs. Therewith, suitable coefficients can be computed for special geometries without additional tests on similar channels. But for verification of the FEM and FDM programs, they do require basic research and experiments. The friction coefficient  $f_i$ , Eqn 5, is determined from the experimentally determined wall shear stress distribution, in which the values for a sub-channel are integrated. The heat transfer coefficient  $h_i$ , Eqn 6, follows out of the heat flux and the temperature field of the fluid and in the wall. The mixing-parameter (cf. Eqn 7 and 8) can be determined by an integration of the heat flux over the gap, whereby the exchange in relation to the heat transfer is maintained. Analog equations are used for the momentum exchange. Calculation of the eddy viscosity of heat into that of the momentum occurs using the turbulent PRANDTL-number. The solution to the temperature and the velocity field with the help of the FEM methods offers the possibility to maintain all three values.

#### a Eddy-diffusivity — Crossflow Capabilities

At the INR/KfK, extensive experiments have been carried out in the past few years concerning speed and turbulence distribution. A scheme of the test channel used is shown in Fig 5 [2], [3], [4]. It consists of a rectangular channel with 4 tubes. Air was used as a flow medium. The diameter of the tubes is about 160 mm. The measured section of the cluster is shaded. The diameter and wall distance of the tubes were varied in the course of the test programme.

An extensive evaluation of the speed fields measured, also making use of the results obtained by other experimentors (e.g. TRAPP/AZAD, HOOPER, HEJNA and SEALE) at the IFR was carried out by NEELEN [5] with the VELASCO-BS programme, achieving a new correlation for the wall-parallel eddy viscosity Eqn 10. The natural logarithm of the dimensionless wall-parallel eddy viscosity is accordingly a function of the hydraulic diameter, the profile length, the radius of the rod and the circumference of the null-momentum zone. The measured values and the course of the equation can be seen in Fig 6. The good correspondence over the large area of REYNOLDS-numbers 18,000 to 160,000 can be recognized. As a comparison, the constant value of the eddy viscosity originally implemented in the VELASCO code has been entered.

#### b Wall-shear-stress Distributions — Friction Coefficient

The wall shear stress can, as already stated, be used for the calculation of the sub-channel friction loss coefficient  $f_i$  (cf. Eqn 11), in which the wall shear stress is defined by means of the fluctuating velocities. The following Fig. 7, [6], is to demonstrate the precision of the VELASCO-BS calculations. Experiments by Hooper in two neighbouring rectangular channels were re-calculated. The wall shear stress shows a cosine-shaped course. The maximum values are reached opposite the centres of the channel. A marked minimum is achieved at the narrowest point of the gap. The correspondence between the calculation and the experiment is very good, merely the closed gaps of the flow channel limitation cause problems.

#### c Heat-transfer and Turbulent Temperature Field

In order to solve the transverse flow balance for the heat flow density over the gap between two sub-channels and thus in order to make available the crossflow parameter needed by COBRA, the turbulent PRANDTL-number  $Pr_{turb}$ , Eqn 12, is additionally needed as a conversion factor between the eddy viscosity of momentum  $\epsilon_m$  and that of the heat  $\epsilon_h$ . For this purpose, experiments were prepared at the INR, in which the flow is heated, which means that measurement of the temperature field becomes possible. In this HERA project, we are dealing with a hexagonally arranged 37 rod cluster. Air is again used as a flow medium. The measurements of the wall temperatures, the velocity field and the temperature field, including the turbulent fluctuating quantities, lead to the required thermal-hydraulic crossflow behaviour required, in combination

with a coupled VELASCO-BS/VANTACY calculation. This evaluation will be carried out at the IfRR as soon as the experimental results are available.

The results show that a coupling between an FEM programme such as VANTACY and a sub-channel analysis code is possible. An extensive experimental establishment of the sub-channel coefficients could be unnecessary. Experimental verification of this connection of both packets of programmes is being worked on at present.

#### d Mixing-Experiments

Up to now, the transverse flow coefficients have been established macroscopically from mixing tests. It was possible to distinguish three modes of procedure (cf slide 12). The transverse flow behaviour is determined by feeding hot water or a saline concentration into one of the sub-channels as a tracer. The complete analogy between transportation of material and of heat is presumed in this.

A part of the cluster is heated whereas a different part of the cluster remains unheated. The distribution of the enthalpy-rises gives a measure for the crossflow.

Both methods show the experimentally established enthalpy rises in relation to theoretical enthalpy rises, which would result from simple energy balances over the sub-channels.

SEALE heated the channel on one side, while the other side was cooled in such a way that a stationary temperature field resulted. The heat flux exchanged throughout the installed series of tubes can then be established at the point at which the temperature field also no longer alters in an axial direction. The experimental channel used is shown in the following Fig 8, [7].

The results of an FEM calculation for the SEALE-rectangular channel are shown in Fig 9. Only the speed field in the measured part of the channel is shown.

#### e Two-phase Mixing

In the evaluation of experiments concerning the critical heat flux, the calculation of boiling, two-phase flows is inevitable. From the start of the boiling, the correlations for the single-phase crossflow discussed up to now can merely act as a rough guideline. Both the start of boiling and also the void distribution over the cluster are unknown. ROWE's results [8] are to show the influence of the two-phase flow on the amount of crossflow.

The flow channel used is shown in Fig 10, [8]. This is the simulation of a section from a square lattice. The heating of the cluster is carried out directly by current. These experiments therefore simulate a really boiling flow procedure and the two-phase flow is not realized by feeding air. The results show the concentration of the tracer upon exit from the admitted channel across the exit steam quality. A clear dependence of the course on the mass flux can be seen. The courses show a maximum in positive qualities of exit steam. The course and the height of the maximum are further dependent upon the width of the gap.

To sum up the area of the two-phase mixing, it must be stated that there is a considerable experimental and theoretical gap here. Calculation of the fluid state field in a rod cluster which has a two-phase flow is dependent upon a large number of assumptions and preconditions which are not secured experimentally. Further work is necessary in this field in future, which must lead to an experimentally secured application of the sub-channel analysis codes.

## 4. Evaluation methods for CHF experiments

In the course of the cooperation of KfK/PSI/Siemens-KWU/TU-BS, which is to lead to the development of a high-conversion pressurized water reactor, two projects were planned to establish critical heat flux. Experiments on 37 rod clusters with hexagonal lattice geometry were carried out in the Siemens-KWU laboratories in Karlstein. Water was used as a flow medium. Integral fins and grid spacers were used as spacers. Only 31 of the 37 rods are heated, the six corner rods are unheated.

In the course of the KRISTA experimental stand at the IRB of the KfK, an experiment on a 37 rod cluster is also being prepared. Freon-R12 is acting as a flow medium in this case. The cluster is identical,

from a geometrical point of view, to the Siemens-KWU grid spaced cluster. The experiments will lead to a transmission law between various heat transfer fluids, which means that extensive CHF data banks can be made accessible to application and interpretation, with no restriction with regard to the experimental fluid used. A further component part of the large KRISTA freon circulation is a 7 rod cluster experiment which is used in the investigation of individual effects and has its strength in its flexibility as regards the alteration of peripheral experimental conditions.

An experimental evaluation of the results of these experiments, i.e. of the results of the experiments of the water experiment stand with fin spacers and the experiments with the 7 rod cluster was carried out at the IfRR.

#### a System-Parameter-Evaluation

For the evaluation, the KfK (DALLE-DONNE/HAME) correlation [9], Eqn 13, was used. The relationship is based on the BOWRING-WSC2 correlation. The structure of this equation is discussed briefly below. The critical heat flux is a function of the system pressure, the inlet sub-cooling, the mass velocity, the evaporation heat and the axial distance from the channel inlet. Further, axial and radial heat flux profiles were taken into consideration. The correlation for the factor  $V$  was gained by DALLE-DONNE and HAME by adaptation to the BETTIS-data and is valid for clusters with grid spacers. The influence of the mass flux distribution is taken into consideration by the factor  $F_G$ , which contains the hydraulic diameters and the free flow area of the sub-channels.

Due to the crossflow across the gaps of the cluster, the mass flux distribution does not have such a negative influence as could be deduced from the above equation. This reduction of the enthalpy rise distribution takes an imbalance factor  $Y'$ , Eqn 14, into consideration, which has been integrated into the DALLE-DONNE/HAME relationship in accordance with suggestion by BOWRING [10]. It forms the relationship of the actual enthalpy rise of a channel, calculated from the enthalpy difference, to the power theoretically removed from the heated perimeter, into the calculation of which the heat flux factors of the sub-channel observed enter, as do the circumference heated and the mass flux. However, the problem rises of establishing the actual enthalpy rise. This can be done by measurement. However, in this case there were no sub-channel exit temperatures which would permit the establishment of the enthalpy rise. The actual enthalpy rise was therefore established from a sub-channel analysis calculation. This application of the DALLE-DONNE/HAME correlation thus represents an intermediate step between the system-parameter-correlation of DALLE-DONNE/HAME and the sub-channel condition concept.

#### b Sub channel-Analysis-Evaluation

The sub-channel condition concept is used together with the well-known Russian CHF table. The latter was established on the basis of 8 mm circular tube measurements in water. The critical heat flux is shown as a function of the mass flow, the steam quality at the end of the tube and the pressure. The diameter is considered with an exponent of 1/2. Applied to these cluster flows, this means that the local exit fluid properties of the hottest sub-channels must be used. These can be established by means of a sub-channel analysis. The algorithm of the establishment of the critical heat flux accordingly looks like this (see slide 13). With the critical heat flux which is experimentally established or, in the case of the use of a heat exchanger, with the estimated critical heat flux and the cluster entry data of the experiment, the exit fluid state is established. A value of the critical heat flux in accordance with the CHF look-up table accordingly belongs to this exit fluid state, but it does not have to correspond to the value used. The value for the critical heat flux input into the sub-channel analysis calculation is now varied until the critical heat flux resulting from the CHF look up table and the exit data of the cluster are identical with those on which the establishment of this exit fluid state is based.

The application of the Russian table demands, as already mentioned, statement of a length which characterizes the phenomenon of the critical heat flux. A mere comparison, Fig 11, with the possible layer of bubbles on a heat rod and in a circular tube with the small hydraulic diameter of the experimental cluster used shows that the hydraulic diameter  $d_h$  is unsuited in this comparison of internally flowed circular tubes and externally flowed cylinders. If one presumes that the maximum diameter is independent of the geometrical expansions of the channel, before the latter is released from the wall, but merely depends on the fluid

data, then a comparative diameter  $d_b$  can be defined, which depends on the maximum size of a bubble and is defined as the diameter of a circular tube, on the internal circumference of which the same number of bubbles find space as on a heating rod of the cluster regarded. The maximum diameter of the bubbles was established in the investigation referred to in accordance with a ratio according to KAUFMANN/VAIHINGER [11] as a function of the surface tension  $\sigma$  and the difference in density of steam and liquid, Eqn. 15. Thus, the following relationship results for the diameter. This diameter corresponds in its order of magnitude to the diameter  $d_2$ , which ULRICH had found in a previous investigation.

The differences in the precision of the prediction of the critical heat flux are to be shown through the following two Figs. 12 and 13. The relationship of the heat flux calculated to the heat flux measured is protracted via the mean mass flux of the cluster. The results of the water experiments of the fin-spaced rod cluster of the CHF experiments in Karlstein are protracted. In the use of the stated characteristic diameter  $d_b$ , a considerably better correspondence results with the measurement than use of the hydraulic equivalent diameter  $d_h$ .

With the new characteristic diameter, a first evaluation of the 7 rod cluster experiments is to be presented to finish with. The correlations used as a basis for the sub-channel analysis are collated below. The crossflow is determined in accordance with a correlation Eqn. 16 which was presented by ROGERS/ROSEHART [13]. The transverse mass flux per axial length is calculated as a function of the sub-channel REYNOLDS-number.

The calculation of the pressure losses is carried out on the basis of the well-known NIKURADSE [14] relationship Eqn. 17.

The calculation of the two-phase flow was carried out in accordance with homogeneous models. No void fraction was considered in the sub-cooled area.

As the experiments were carried out with Freon, yet the tables and correlations used were set up for water fluxes, the results between the fluids must be converted. The AHMAD conversion method [12] was used with the dimensionless characteristics for the pressure, the mass flux and the heat flux. The sub-channel analysis was therefore carried out for a Freon flow. The exit results of the calculation were converted to the equivalent water data using the stated equations. These were put into the selected CHF correlations. The heat flux received was then returned to the Freon value.

Fig. 14 shows a cross-section of the 7 rod cluster. The comparatively large edge channels must especially be pointed out. Due to the low total number of channels, a very large cross-section results in the edge area and thus also an extreme mass flux distribution. The cluster is heated over a length of 600 mm. There is a lead-in of equal length under it.

As a comparison, calculations with a ten-fold crossflow were carried out. Via the imbalance factor, the results of these calculations lead to a further result of the DALLE-DONNE/HAME correlation and to a second table result.

The following Fig. 15 show the results of the calculations together with the measured values via the mean exit steam quality  $x_{ex}$  for the various mass fluxes. The DALLE-DONNE/HAME correlation without the imbalance factor produces a clear deviation from the measured values. As a mean, a relationship of the calculated heat flux to the measured heat flux of 0.89 results with a standard deviation of 0.12. In absolute figures, this means that the DALLE-DONNE/HAME correlation underestimates the measured values by an average of 17 kW/m<sup>2</sup>. The height of the deviation is dependent of other fluid parameters, such as the mass flux, the Reynolds number and the steam quality. The introduction of the imbalance factor into the DALLE-DONNE/HAME correlation leads to a reproduction of the measured values which on average is considerably better. The mean value of the deviation in this case is 0.93, with a standard deviation of 0.18 or a mean underestimation of the measured values of 5 kW/m<sup>2</sup>. The increase of the crossflow by a factor of 10 displaces the value towards higher rates.

The use of the sub-channel analysis with the Russian CHF look-up table and the diameter suggested by Ulrich without iteration of the mass flux does not produce any better CHF results. The calculation over measurement ratio is 0.86 on average, with a standard deviation of 0.11. A considerable improvement of the results is achieved by iteration of the heat flux in the course of the sub-channel mass fluxes. Correspondence of calculation and measurement is excellent for all mass fluxes. The mean value of the ratio is 0.96 with a standard deviation of 0.05. As an absolute, this means a mean underestimation of the measurement results of 8 kW/m<sup>2</sup> ± 2.9 kW/m<sup>2</sup> (5 % error probability).

The results of the correlations and tables used for the mean exit steam quality for the mass fluxes observed are shown in the following Fig. 16. The results of the calculations are valid for the DALLE-DONNE/HAME correlation without the imbalance factor, the DALLE-DONNE/HAME correlation with the imbalance factor, the sub-channel analysis calculation with the Russian table, with and without iteration.

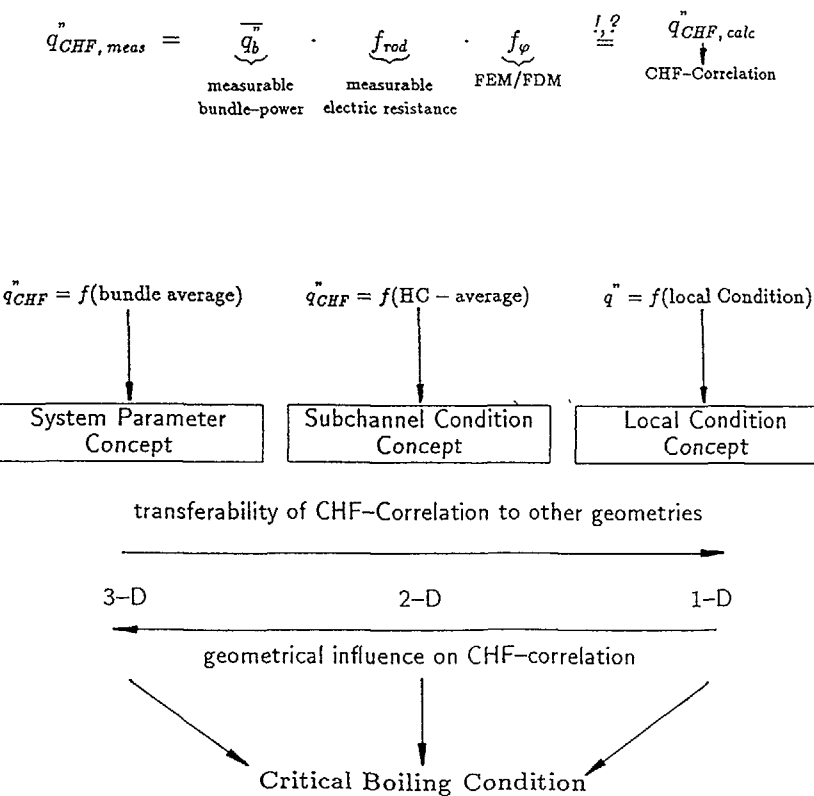
All told, it can be established that the correct application of the sub-channel analysis leads to a very good precision of reproduction of the measurement results. The application of the ROGERS/ROSEHART-mixing-correlation also appears to lead to the best results after evaluation of the results.

## 5. Conclusions

To sum up, the following can be stated:

- The coupling of the FEM calculations with the input data of the sub-channels appears to be very promising. However, extensive individual effect experiments are necessary in order to verify the FEM calculations. The re-calculation of the single-phase turbulence experiments with the VELASCO and VANTACY programmes is very promising.
- In the two-phase thermal hydraulics, there is not yet sufficient experimental data material. Most questions are unanswered yet and there is great uncertainty.
- The system-parameter-correlations lead to useful results as long as one do not move out of the area of the parameters for which the system parameter correlations were set up.
- The sub-channel analysis proves itself to be a useful tool for the evaluation of these CHF experiments. Further calculations will follow here in the near future, also for larger clusters, in order to place this statement on a broader foundation.
- The question of the validity of the conversion law for Freon/water in rod clusters will be investigated as soon as the Freon-CHF experiments of the KfK in the 37 rod clusters are available.

## I. Evaluation-Method of Experimental CHF-Results



## System-Parameter-Concept

$$\overline{q}_c = f(h_{in}, \overline{m}_b, \Delta h_{v,b}, \text{bundlegeometry, incl. heated length})$$

- consideration of the mixing capabilities by optimization of coefficients,
- no local exit-condition and
- the result is one critical heat flux over the bundle exit.

→ Hotchannelmodel

## Subchannel-Condition-Concept

mass velocity    enthalpy    temperature

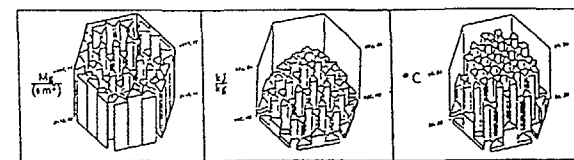


Fig. 1: Mass velocity-, enthalpy- and temperaturedistribution over the bundle exit of a Freon-cooled 37-rodbundle. (COBRA-IV-TUBS—calculation results)

$$\overline{q}_c = f(h_{SC}, \overline{m}_{SC}, \Delta h_{v,SC}, \text{Subchannelgeometry})_{ex}$$

- the influence of transverse flow is considered by calculating the axial progress,
- the heated length is unnecessary in the CHF-Correlation and
- the result is one CHF-data per subchannel.

→ Subchannelanalysis

## Local-Condition-Concept

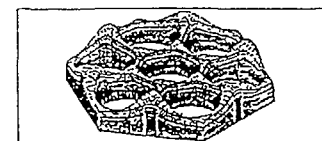
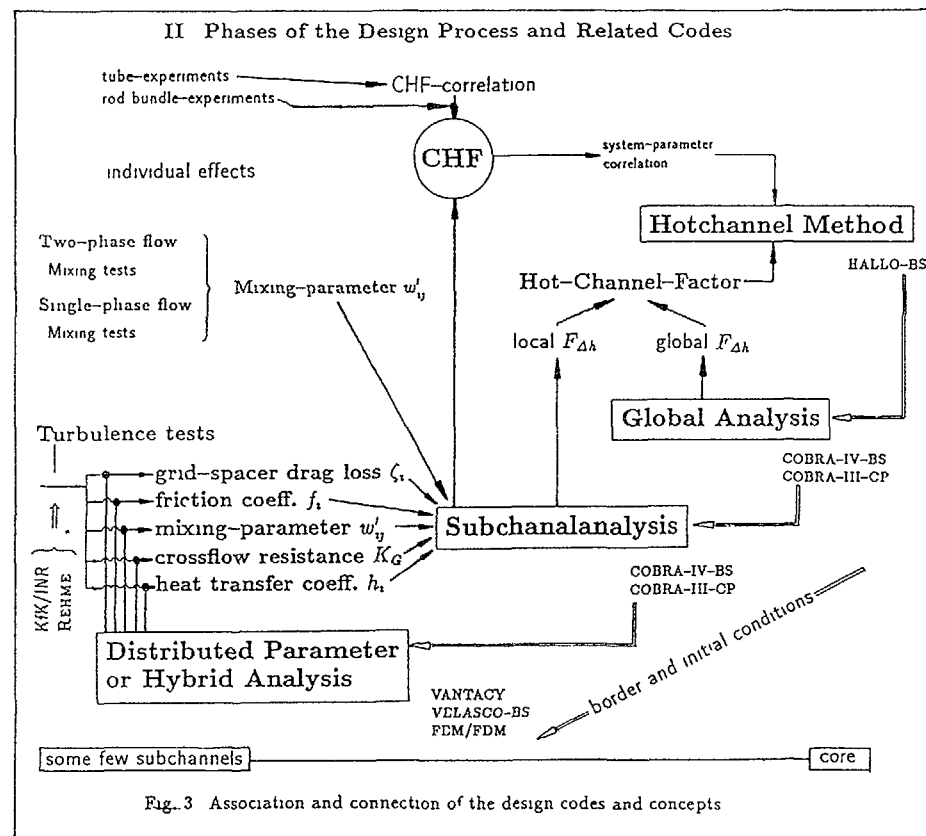


Fig. 2: Velocity-distribution in a 7-rodbundle (single phase flow).

→ FEM/FDM



SLIDE 3

### II.1. Subchannel-Analyses-Code

mass balance

$$A \underbrace{\frac{\partial}{\partial t} \langle \rho \rangle_V}_{\text{local}} + \underbrace{\frac{\partial}{\partial z} \langle \rho u \rangle_A A}_{\text{convection, axial}} + \{D_c^T\} \underbrace{\langle \rho v \rangle_S S}_{\text{Diversion Cross-flow}} = 0 \quad (1)$$

were  
 $S$  gapwidth  
 $A$  flow area  
 $u$  axial velocity  
 $v$  lateral velocity

energy balance

$$\begin{aligned} & A \underbrace{\frac{\partial}{\partial t} \langle \rho h \rangle_V}_{\text{local}} + \underbrace{\frac{\partial}{\partial z} \langle \rho u h \rangle_A A}_{\text{convection, axial}} + \{D_c^T\} \underbrace{\langle \rho v h \rangle_S S}_{\text{Diversion Cross-flow convectiv, laterally}} = \\ & = \underbrace{\{D_r^T\} [P_r \Phi \alpha] [D_r] \{T\}}_{\text{rod heat output}} + \underbrace{\{D_w^T\} [L \alpha] [D_w] \{T\}}_{\text{wall heat transfer}} \\ & + \underbrace{\frac{\partial}{\partial z} A \left\langle \lambda \frac{\partial T}{\partial z} \right\rangle_A}_{\text{axial heat-conduction}} - \underbrace{\{D_c^T\} \left[ \frac{S C(\lambda)}{L_c} \right] [D_c] \{T\}}_{\text{lateral heat-conduction}} - \underbrace{\{D_c^T\} [w'] [D_c] \{h'\}}_{\text{turbulent heat exchange}} \end{aligned} \quad (2)$$

were  
 $h$  spec enthalpy  
 $P_r$  rod-perimeter  
 $\Phi$  portion of perim faced to one SC  
 $\alpha$  heat-transfer coefficient  
 $L$  length of connection SC-wall  
 $L_c$  distance of SC-centres  
 $C$  correction-factor  
 $w'$  turbulence-parameter  
 $h'$  enthalpy of turbulent crossflow

SLIDE 4

axial momentum balance

$$\begin{aligned}
 A \frac{\partial}{\partial t} \langle (\rho u) \rangle_V + \underbrace{\frac{\partial}{\partial z} \langle \rho u^2 \rangle_A}_\text{convection, axial} A + \underbrace{\{D_c^T\} \{(\rho v u)_S S\}}_\text{Diversion Cross-flow convectiv,lateral} = \\
 = \underbrace{A \frac{\partial}{\partial z} \langle P \rangle_A}_\text{pressure force} - \frac{1}{2} \left( \frac{f'}{d_e} + \frac{\zeta}{\Delta z} \right) \langle \rho u^2 \rangle_A A - \underbrace{A \langle (\rho) \rangle_V \cos \Theta g}_\text{force of gravity} \\
 - C_T \{D_c^T\} [w] [D_c] \{u'\} \quad (3)
 \end{aligned}$$

were  
 $P$  pressure  
 $f'$  Darcy-friction coefficient  
 $\zeta$  drag-loss coefficient in  $\Delta z$   
 $\Delta z$  axial length of the volume  
 $\Theta$  slope of the flowchannel  
 $u'$  exchanged axial velocity  
 $C_T$  Correction of the unknown analogy between momentum and heat-transfer

lateral momentum balance

$$\begin{aligned}
 S \frac{\partial}{\partial t} \langle (\rho v) \rangle_{V'} + \underbrace{\frac{\partial}{\partial z} \langle \rho u v \rangle_{A'}}_\text{convection axial} S + C_s \{D_c^T\} [D_c^T] \left\{ (N) \frac{S}{l} \langle \rho v^2 \rangle_S \cos \Delta \beta \right\} = \\
 = \underbrace{\frac{S}{l} \{D_c\} \{(P)_A\}}_\text{total pressure forces} - \frac{1}{2} \frac{S}{l} K_G \langle \rho v^2 \rangle_S - \underbrace{\langle (\rho) \rangle_{V'} S \sin \Theta \cos \beta g}_\text{lateral force of gravity} \quad (4)
 \end{aligned}$$

were  
 $A'$  flow area normal to the flow direction  
 $C_s$  Correction of uncertain coupling of communicating gaps  
 $(N)$  binary operator of flow-direction  
 $\Delta \beta$  difference of gap reference angle  
 $K_G$  pressure loss coefficient of the gap  
 $\beta$  referenzorientatoin of the gap

## II.2. Subchannel-Analyses-Code Input Data

- Darcy-friction coefficient  $f$
- drag-loss coefficient  $\zeta$
- heat-transfer coefficient  $h$
- turbulent lateral flow per unit length  $w'$
- pseudolength  $l$
- correction factor to create the effective gradient of temperature

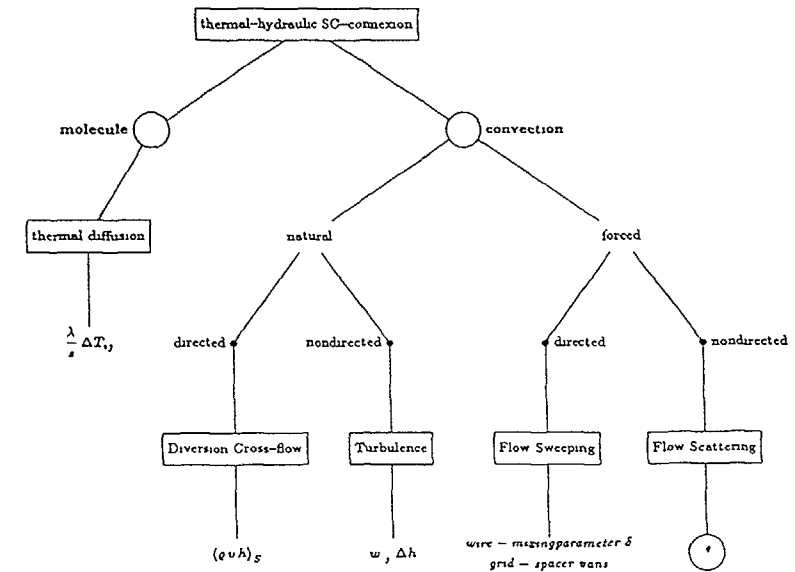


Fig. 4 Mixing-Components according to ROGERS/TODREAS [1]

### Subchannel-Analyses-Code Input Data

#### Connection to Distributed-Parameter-Analysis

- Friction Coefficient  $f_i$ :

$$f_i = 8 \cdot \frac{\overline{u}_i^*}{\overline{u}_i} \quad \text{and} \quad \overline{u}_i^* = \sqrt{\left( \frac{\tau_w}{\rho} \right)_i} \quad (5)$$

were  
 $f_i$ : subchannel friction coefficient  
 $\overline{u}_i^*$ : wall shear stress velocity  
 $\overline{u}_i$ : average SC-velocity  
 $\tau_w$ : wall shear stress

- Heat Transfer Coefficient  $h_i$ :

$$h_i = \frac{\overline{q}_i''}{\overline{T}_{w,i} - \overline{T}_{f,i}} \quad (6)$$

were  
 $h_i$ : SC heat-transfer coefficient  
 $\overline{T}_{w,i}$ : average wall temperature  
 $\overline{T}_{f,i}$ : av. SC fluid temperature  
 $\overline{q}_i''$ : av. rod surface heat flux

- Mixing-Parameter  $w_{ij}'$ :

$$\overline{q}_{ij}'' = \frac{- \left[ \int_{D/2}^{p/2} \rho c_p \left\{ a + (\varepsilon_{h,\varphi})_{\varphi=0} \right\} \left( \frac{1}{r} \frac{\partial T}{\partial \varphi} \right)_{\varphi=0} dr \right]}{\frac{1}{2} (p - D)} \quad (7)$$

were  
 $c_p$ : spec. heat capacity  
 $a$ : thermal diffusivity  
 $p$ : rod pitch  
 $D$ : rod diameter  
 $\varepsilon_{h,\varphi}$ : eddy diffusivity of heat  
 $q_{ij}''$ : heat flux through the rod gap

$$\overline{q}_{ij}'' = \frac{w_{ij}'}{s} \cdot c_p (\overline{T}_i - \overline{T}_j) \quad (8)$$

$$\varepsilon_{h,r} = \frac{-\overline{T}' v_r'}{\partial T} \quad \text{and} \quad \varepsilon_{h,\varphi} = \frac{-\overline{T}' v_\varphi'}{r \partial \varphi} \quad (9)$$

### a. Eddy-diffusivity — crossflow capabilities

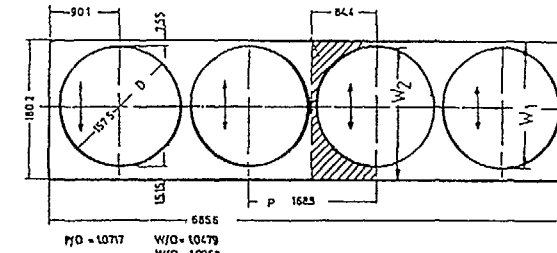
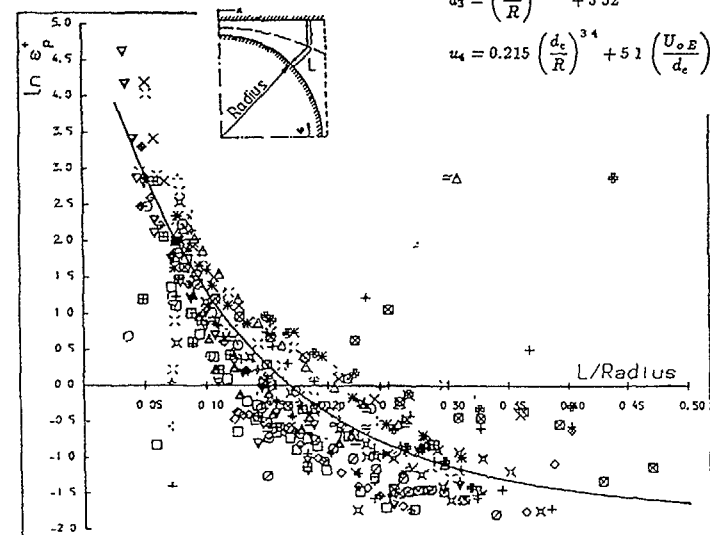


Fig. 5: Cross-cut through the test-channel according to REHME

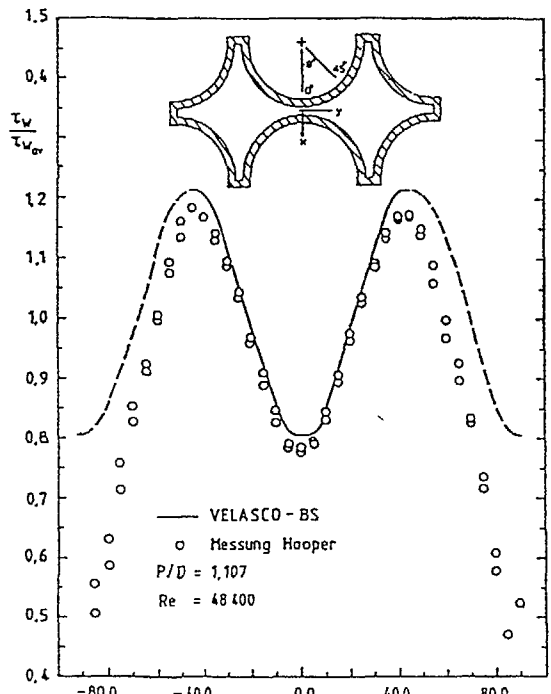
$$\ln \overline{\varepsilon}_{m,\varphi}^+ (\varphi) = u_1 \cdot e^{(u_2 Y_m + u_3)} + u_4 \quad (10)$$

$$\begin{aligned} u_1 &= 0.118 \\ u_2 &= -13.8 \\ u_3 &= \left( \frac{d_c}{R} \right)^{0.236} + 3.52 \\ u_4 &= 0.215 \left( \frac{d_c}{R} \right)^{3.4} + 5.1 \left( \frac{U_{o,E}}{d_c} \right)^{0.149} - 6.94 \end{aligned}$$

Fig. 6: Average normalized wall-parallel eddy-diffusivity vs. the nondimensional length  $Y_m$  [5]

b. Wall-shear-stress Distributions — Friction Coefficient

$$\tau_w = \frac{f_i}{4} \cdot \rho \cdot \frac{\bar{u}_i^2}{2} \quad (11)$$



c. Heat-Transfer and Turbulent Temperature-field

$$\text{turbulent PRANDTL-number: } Pr_{fur} = \frac{\epsilon_m}{\epsilon_h} \quad (12)$$

were  $\epsilon_m$ : eddy diffusivity of momentum  
 $\epsilon_h$ : eddy diffusivity of heat

Project HERA (KfK/INR)

- Wall temperatures
- complete velocity-field
- complete temperature-field } incl. turbulent fluctuations

VELASCO-BS  
VANTACY

$\bar{\alpha}_i, w'_{ij}, \epsilon_{h,\varphi}$  etc.

#### d. Mixing-Experiments

- feeding of hot water
  - feeding of salt-concentration }
  - partial heating of the bundle
  - heating one face and cooling on the other side
- Tracer

#### Analogy of Heat- and Mass-transfer

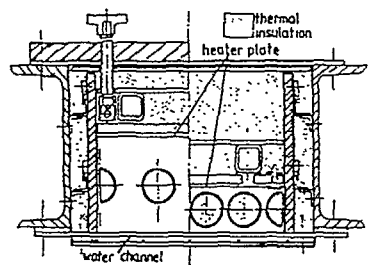


Fig. 8: Cross-section of wind tunnel module and general arrangement of rods according to SEAL [7]

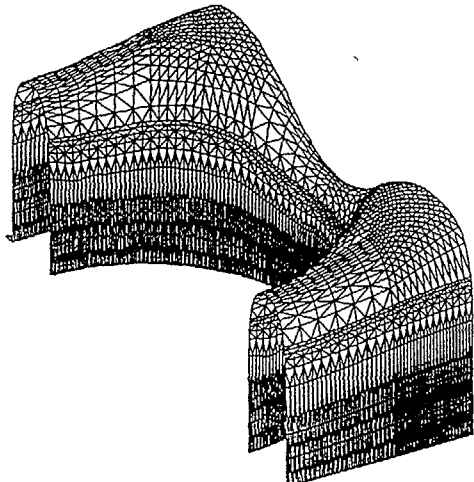


Fig. 9: Turbulent velocity field of the rod arrangement in the wind tunnel from SEAL (FEM-Code VANTACY)

#### e. Two-phase Mixing

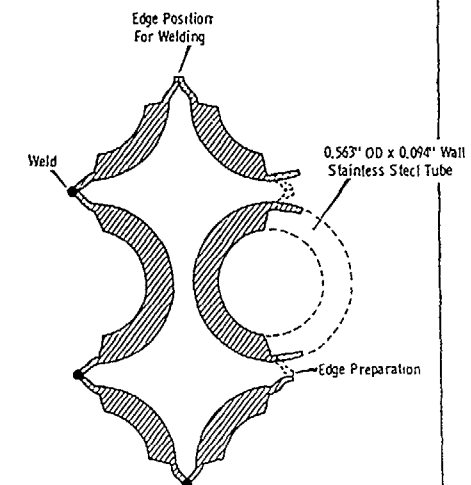
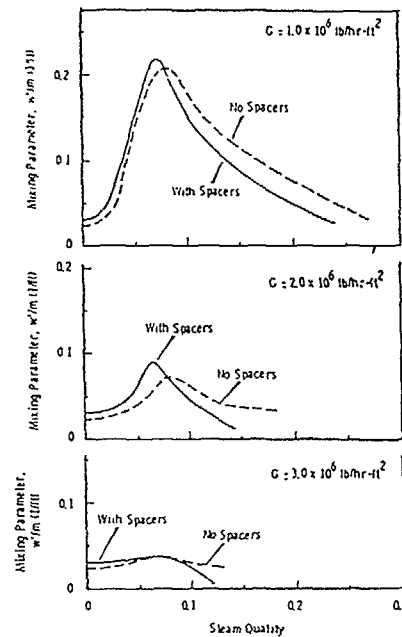


Fig. 10: Estimated variation of mixing with steam quality at 51.7 bar and 2.159 mm gap spacing [8]

### III. Evaluation methods for CHF-Experiments

#### System-parameter-evaluation

Dalle-Donne/Hame [9] (WSC2)  $\dot{q}_{CHF} \left( 10^6 \text{Btu/h} \cdot \text{ft}^2 \right) = \frac{A + B \Delta H_i}{C + Z Y' (Y')} \quad (12)$

$$A = \frac{0.25 G D \lambda F_1 Q_1}{1 + Q_2 F_2 G D}$$

$$B = 0.25 G D$$

$$C' = \frac{Q_1 F_2 \sqrt{G D}}{D_h}$$

$$C = C' V \left[ 1 + \frac{Y - 1}{1 + G} \right]$$

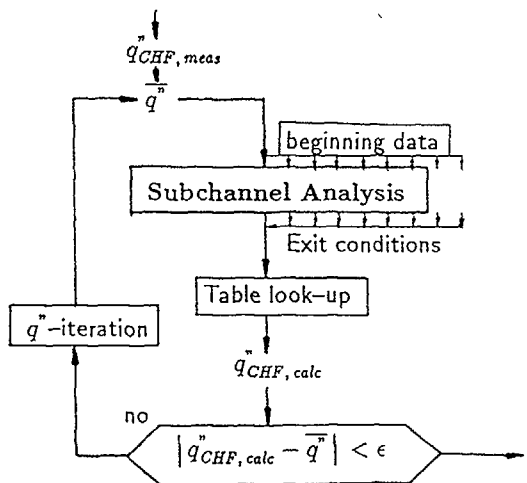
$$V = -0.252 - 2.789 e^{-3.874 G} + 1.915 e^{-0.234 G}$$

Imbalance Factor (BOWRING) [10]  $Y' = \frac{0.25 G D_h (h(z) - h_{in})}{\int_0^z \dot{q} dz} \quad (13)$

#### Subchannel-Analysis

##### Soviet 8 mm tube look-up table

diameter exponent: 1/2



#### CHF-phenomenon Describing Characteristic Length .

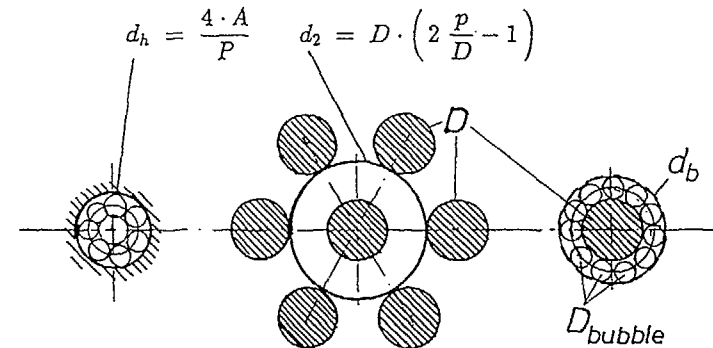


Fig. 11: Several possible characteristic diameters of bundle geometries. On the left hand the equivalent hydraulic diameter, in the centre the second order bundle diameter and on the right hand a bubble size related characteristic diameter.

$$D_{bubble} = 0.837 \Theta \left\{ \frac{2 \sigma}{g (\rho_f - \rho_v)} \right\}^{0.5} \quad d_b = 2 \cdot D_{bubble} + D \quad (14)$$

forced convection, [11]

|      |            |                  |
|------|------------|------------------|
| were | $\Theta$ : | angle of contact |
|      | $\sigma$ : | surface tension  |
|      | $\rho$ :   | density          |
|      | $g$ :      | gravity          |

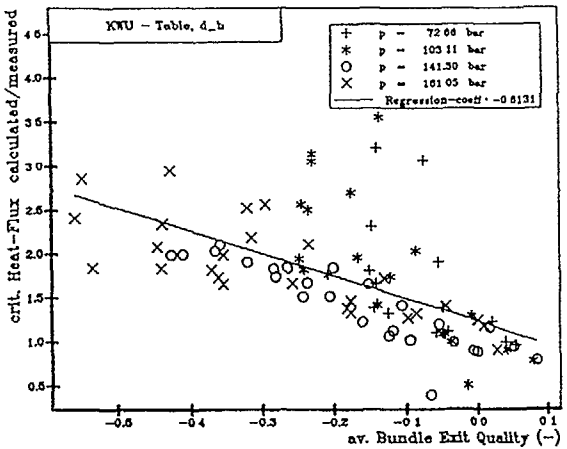


Fig. 12: Rate of the calculated (soviet table) CHF-data to measured data by using the equivalent hydraulic diameter (COBRA-IV-BS results). SIEMENS-KWU Karlstein tests

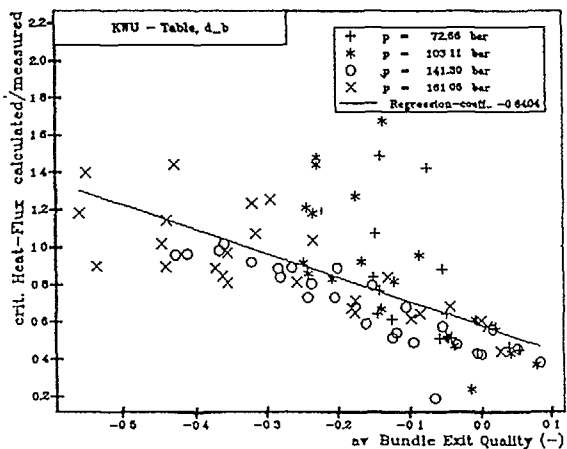


Fig. 13. Rate of the calculated (soviet table) CHF-data to measured data by using the bubble size related diameter  $d_b$  (COBRA-IV-BS results) SIEMENS-KWU Karlstein tests

### 7-Rod-bundle CHF-Evaluation

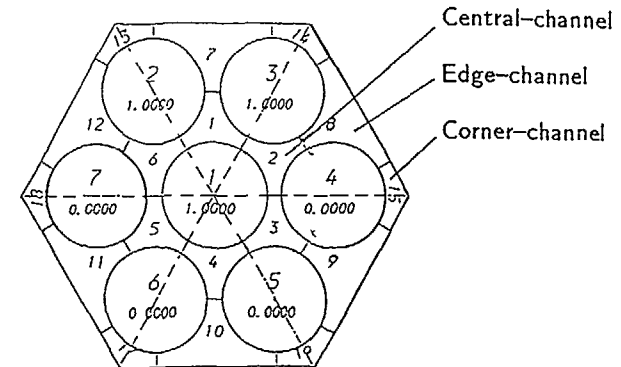


Fig. 14: Cross-cut through the 7-rod-bundle of the KRISTA-FREON-loop at IRB/KfK and axial profil of heat-flux distribution

AHMAD-model [12]

$$\text{mass velocity } \psi = \frac{G \cdot d_e}{\eta'} \left\{ \sqrt{\frac{\gamma}{\rho'}} \frac{\eta'}{d_e} \right\}^{\frac{2}{3}} \cdot \left( \frac{\eta'}{\eta''} \right)^{\frac{1}{8}}$$

$$\text{critical heat flux } \frac{\dot{q}_{\text{CHF}}}{G \Delta H_c} = \text{const.}$$

$$\rho_l / \rho_v = \text{const.}$$

$$x_{\text{inlet}} \text{ and } x_{\text{CHF}} = \text{const.}$$

Mixing-model: ROGERS/ROSEHART [13]

$$w'_y = 0.004 \cdot \overline{G} \overline{d_e} \cdot Re^{-0.1} \quad (16)$$

pressure loss: NIKURADSE [14]

$$f_i = 0.0032 + 0.221 \cdot Re^{-0.237} \quad (17)$$

two-phase flow  
homogeneous models

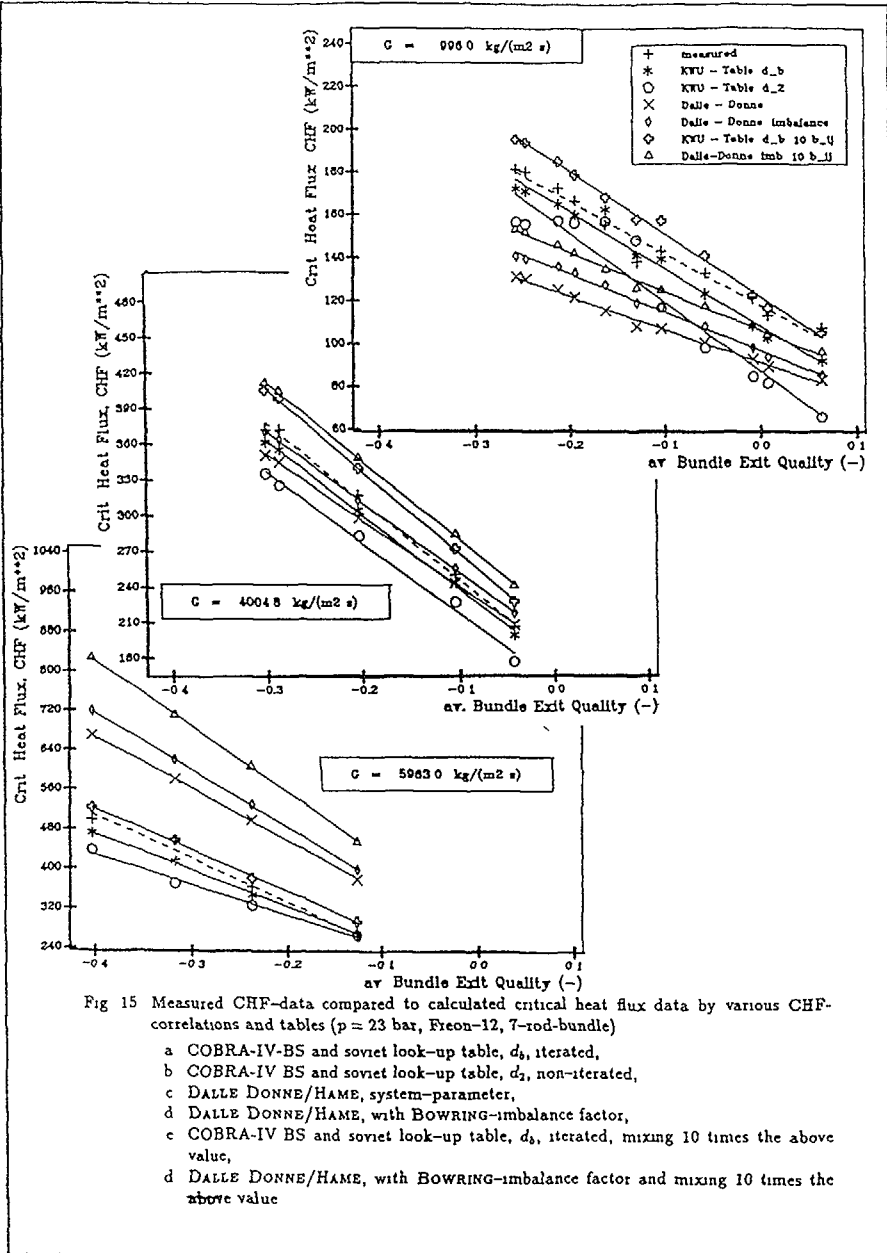


Fig. 15 Measured CHF-data compared to calculated critical heat flux data by various CHF-correlations and tables ( $p = 23$  bar, Freon-12, 7-rod-bundle)

- a COBRA-IV-BS and soviet look-up table,  $d_b$ , iterated,
- b COBRA-IV BS and soviet look-up table,  $d_b$ , non-iterated,
- c DALLE DONNE/HAME, system-parameter,
- d DALLE DONNE/HAME, with BOWRING-imbalance factor,
- e COBRA-IV BS and soviet look-up table,  $d_b$ , iterated, mixing 10 times the above value,
- f DALLE DONNE/HAME, with BOWRING-imbalance factor and mixing 10 times the above value

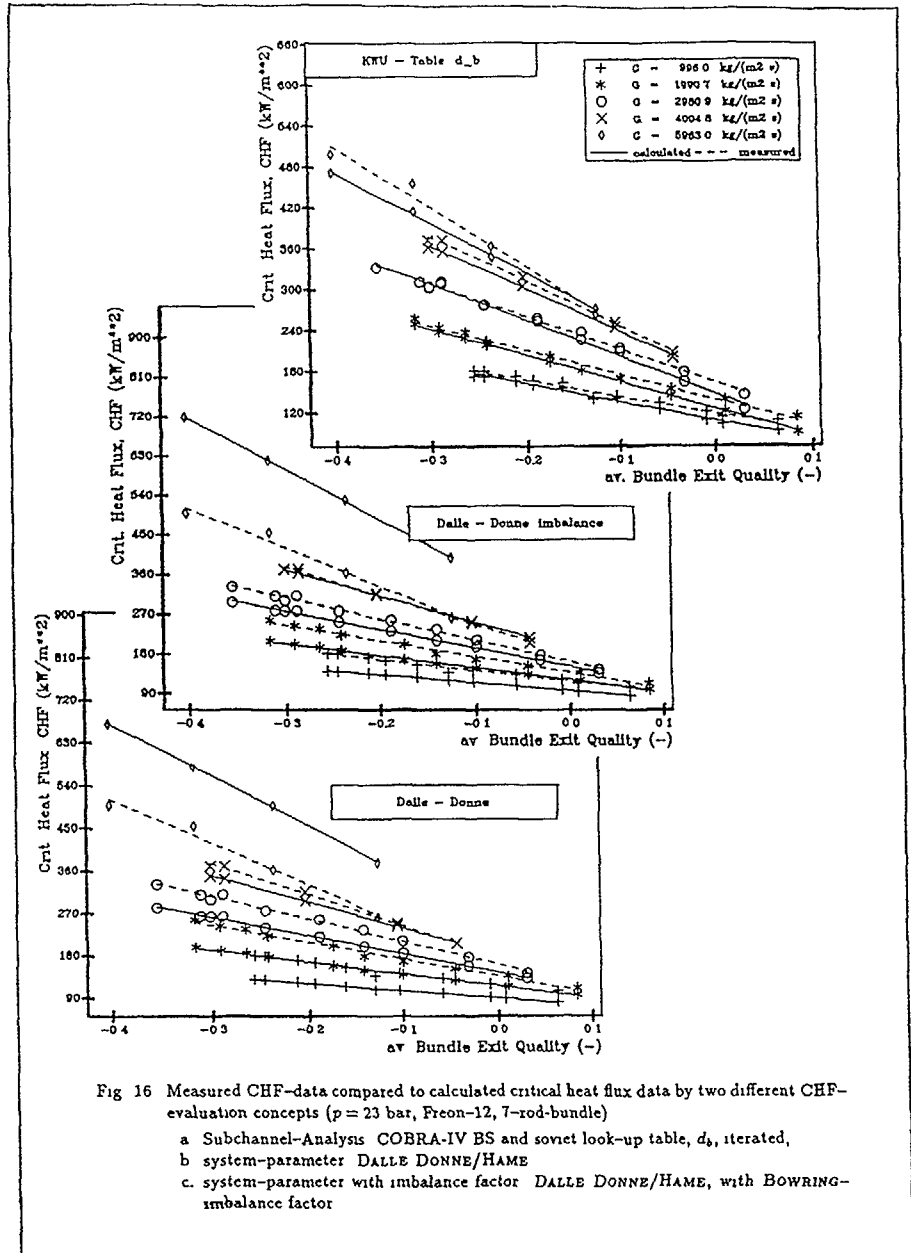


Fig. 16 Measured CHF-data compared to calculated critical heat flux data by two different CHF-evaluation concepts ( $p = 23$  bar, Freon-12, 7-rod-bundle)

- a Subchannel-Analysis COBRA-IV BS and soviet look-up table,  $d_b$ , iterated,
- b system-parameter DALLE DONNE/HAME
- c. system-parameter with imbalance factor DALLE DONNE/HAME, with BOWRING-imbalance factor

## REFERENCES

- [1] Rogers, J T and Todreas, N E Coolant Interchange Mixing in Reactor Fuel Rod Bundles Single-phase Coolants  
*Heat Transfer in Rod Bundles*, The Winter Annual Meeting of The American Society of Mechanical Engineers, New York (1968)
- [2] Rehme, K Turbulente Stromung in einem Wandkanal eines Stabbundels  
KfK 2617, Kernforschungszentrum Karlsruhe (1978)
- [3] Rehme, K Untersuchungen zur Turbulenzstruktur in einem Wandkanal eines Stabbundels ( $p/D = 1.07$ )  
KfK 2983, Kernforschungszentrum Karlsruhe (1980)
- [4] Rehme, K. Turbulenzstruktur in einem Wandkanal eines Stabbundels  
KfK 3177, Kernforschungszentrum Karlsruhe (1981)
- [5] Neelen, N. Modellierung des Impulstransportes achsparalleler turbulenter Strömungen in Stabgittern  
*Dissertation, Techn Univ Braunschweig (1986)*
- [6] Zeggel, W.. Turbulente Strömungen in engen Stabbündeln  
*Kolloquiumsvortrag am INR/KfK (1988)*
- [7] Seal, W. J Experimental and analytical study of mixing by turbulent diffusion and secondary flow between the parallel subchannels or ducts simulating nuclear-fuel rod-bundles.  
*Thesis submitted for the degree of Doctor of Philosophy, School of Mechanical Engineering, University of Bradford (1977)*
- [8] Rowe, D S and Angle, C W Crossflow mixing between parallel channels during boiling, part III Effect of spacers on mixing between two channels  
BNWL-371 PT 3 Pacific Northwest Laboratory, Richland, Washington (1969)
- [9] Dalle Donne, M and Hame, W Critical heat flux correlation for triangular arrays of rod bundles with tight lattices, including the spiral spacer effect  
*Nuclear Technology*, vol 71, no 1, pp 111-124 (1985)
- [10] Bowring, R W WSC-2 A subchannel dryout correlation for water-cooled clusters over the pressure range 3.4 — 15.9 MPa  
AECW-R 983, UK Atomic Energy Authority Atomic Energy Establishment, Dorchester (1979)
- [11] Kaufmann, W D and Vahlungen, D  
*Chem Ing Techn* 921-927 (1972)
- [12] Ahmad, S Y Fluid-to-Fluid Modelling of Critical Heat Flux A Compensated Distortion Model  
AECL-3663 (1971)
- [13] Rogers, J T and Rosehart, R G Mixing by Turbulent Interchange in Fuel Bundles Correlations Inferences  
*ASME-Paper S-72-HT-53 (1973)*
- [14] Nikuradse, J Gesetzmäßigkeiten der turbulenten Stromung in glatten Rohren  
*Forschg-Arb Ing-Wesen H 356 (1932)*

## EXPERIMENTAL INVESTIGATION ON CHF OF TIGHT LATTICE PWRs

W. ZEGGEL

Technische Universität Braunschweig,  
Braunschweig

F.J. ERBACHER

Kernforschungszentrum Karlsruhe GmbH,  
Karlsruhe

Federal Republic of Germany

## Abstract

Improved fuel utilization is possible in tight-lattice PWR cores currently under development within a cooperation of the Karlsruhe Nuclear Research Center (KfK), the Swiss Paul-Scherrer-Institute (PSI), the Siemens/KWU and the Technical University of Braunschweig (TUBS). The hexagonal tightly-packed cores of a Pressurized Water High Converter Reactor (PWHCR) employ higher mass fluxes than conventional PWRs.

PWHCR fuel assemblies (FA) if compared with PWR-FA have distinct fluid flow cross sections and obstructions. Also typical heat flux distributions (local peaks) call for appropriate thermal hydraulic models (average and local heat transfer, mixing, CHF). The scarcity of CHF data available for this kind of problem is obvious.

For this reasons a broad framed investigation program on tight lattice two-phase mixing and boiling heat transfer has been organized at KfK in a scientific cooperation with TUBS. Performance characteristics of the recently erected Freon test facility KRISTA and some principal CHF results will be discussed to describe actual aspects and goals of the thermal hydraulic model fluid based program. The parallel efforts to develop scaling laws for a transformation of Freon flow boiling results into water equivalent data will be outlined. Final concern is related to the long term replacement of CFC-12 by Ozone-harmless fluids.

## 1. INTRODUCTION

A program of experimental and analytical investigations of flow boiling heat transfer and of Critical Heat Fluxes (CHF) in tight hexagonally arranged rod bundles, involving both the Kernforschungszentrum Karlsruhe (KfK), and the Technical University Braunschweig (TUBS), is currently underway at the

Institut für Reaktorbauelemente (IRB) of KfK. The experiments are performed in the recently erected Freon-12 "KRISTA" test facility and are related to the parameter ranges of Pressurized Water High Converter Reactors (PWHCR). This work is a part of a cooperative effort between Siemens AG KWU group (KWU), KfK, TUBS and the Paul-Scherrer-Institut (PSI) in Switzerland.

Table I presents typical data of a pre-convoy and a convoy PWR together with the parameter span of a PWHCR design (confer [1,2]). The lower values of the rod pitch/diameter ratio p/d, the equivalent diameter  $d_e$ , combined with the higher mass flux are typical of the PWHCR which promises a significantly improved fuel utilization.

TABLE I. PWHCR CORE DESIGN PARAMETER RANGE

| Parameter                            | PWR            | PWHCR                                     |
|--------------------------------------|----------------|---|
| rod configuration<br>spacer device   | square<br>grid | hexagonal<br>helical wire /<br>ribs, grid |
| rod diameter, d / mm                 | 10.75/9.5      | 8 - 9.5                                   |
| p/d ratio                            | 1.33           | 1.1 - 1.25                                |
| rod-to-rod gap / mm                  | 3.5/3.1        | 1.0 - 1.24                                |
| equivalent diameter, $d_e$ / mm      | 13             | 3 - 7                                     |
| heated length, l / m                 | 3.9            | 2 - 3.5                                   |
| system pressure, p / MPa             | 15.8           | 15.8                                      |
| mass flux, G / Mg/(m <sup>2</sup> s) | 3.1            | 4 - 7                                     |

PWR design criteria require operation with a certain safety margin to a boiling crisis. Under PWR core design power conditions the occurrence of CHF replaces the efficient nucleate boiling regime by the far less efficient region of departure from nucleate boiling (DNB). This film boiling phenomenon is accompanied with a certain rise of the rod wall temperature. Safe operating conditions of PWR and PWHCR require experimental and theoretical models to describe this problem while the design optimization proceeds.

Though nearly half a thousand CHF-correlations can be found in the open literature it has been assessed that no available prediction methods can be extrapolated to the thermal hydraulic conditions of PWHCR cores. As a consequence experimental and analytical programs on flow boiling resp. CHF behaviour of tight lattice cores have been established in France (e.g. [3]), in Japan (e.g. by JAERI [4] and by Mitsubishi [5]) and also in the Federal Republic of Germany (FRG).

Siemens/KWU performs design-related CHF-tests with light-water as a coolant. An additional systematically organized investigation on flow boiling and CHF in PWHCR lattices is underway at the KRISTA-facility (KRISTA - acronym for Kritische Heizflächenbelastung in Stabbundles; engl.: CHF in rod bundles) of the Institut für Reaktorbauelemente/KfK in cooperation with TUBS in extension of the earlier CHF tests in small tubes (see [6]). Objectives and a description of some results gained at the KRISTA test facility are the content of this paper.

## 2. OBJECTIVES AND EXPERIMENTAL PROGRAM

### 2.1 General

The objective of the thermal hydraulic experimental PWHCR program was to examine various PWHCR parameters in the range indicated in Table I. It consequently was decided to use Freon-12 as a coolant. CFC-12 has been employed successfully in flow boiling tests. Data of measured Freon CHF can be translated into water-equivalent values by fluid-to-fluid modelling laws (see e.g. [7]). This model fluid CFC-12 if compared with light water enables a reduction in power by a factor of 15, and a reduction in pressure by a factor of 6. The CFC-12 fluid and corresponding wall temperatures are near to room temperatures. This results in savings in time and in costs of test section construction and performing flow boiling tests compared to equivalent measurements in pressurized water.

### 2.2 Scope and objectives

The experimental program at the KRISTA facility comprises CHF tests in the following Freon-cooled test-sections: directly heated tubes, indirectly heated 7-rod bundles and 37-rod bundles (see Table II). Additional single and two-phase flow mixing tests will be performed in a 36 rods test section. Efforts are also necessary to replace CFC-12 by fluids which don't deplete Ozone.

The tests in directly heated tubes had the following objectives:

- (i) to commission the KRISTA test facility,
- (ii) to extend the data base [6] for determining the effect of tube diameter on CHF,
- (iii) to compare the CHF data with the CHF tables recently developed in the USSR [8] and by Groeneveld et al. [9],
- (iv) to perform a separate assessment of the modelling laws.

The CHF tests on the 7-rod bundle and 37-rod bundles were primarily designed to investigate the following effects on CHF:

- (i) flow redistribution and mixing in tightly spaced hexagonal rod-bundles,
- (ii) small rod-rod gaps, rod-wall gaps and p/d ratios,

- (iii) axial heat flux distribution, including the effect of heated length,
- (iv) radial heat flux distribution, including the effect of unheated rods,
- (v) rod spacer type and shape.

Parallel to the CHF-tests with gridded 37 rod bundle ( $p/d = 1.18$ ) water-cooled CHF-tests of identical geometry are obtained at the Siemens/KWU Karlstein facility.

TABLE II. SCOPE OF THE FLOW BOILING PROGRAMME UNDER INVESTIGATION AT THE KfK FACILITY KRISTA

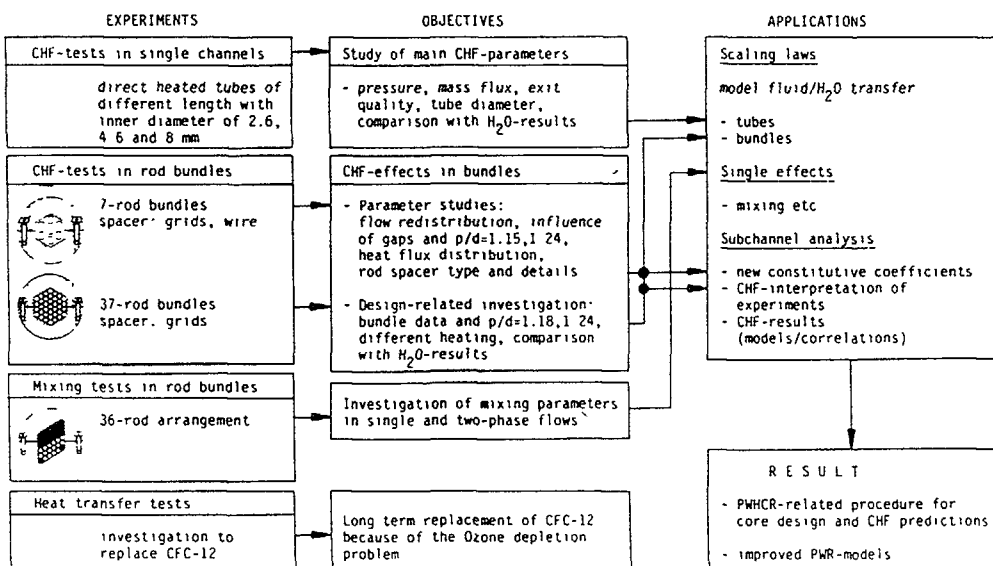


Table II summarizes the application of the observed flow boiling data for the development of scaling laws for bundles, an appropriate description of single effects as two-phase mixing and the formulation of design-relevant CHF-PWHCR-models.

To arrive at these goals the test matrix of the tube and the subsequent 7-rod bundle tests to be discussed in this contribution cover the following conditions:

| Parameter                     | CFC-12       | $H_2O$ -equiv. |
|-------------------------------|--------------|----------------|
| Pressure, MPa                 | 1.05 to 2.72 | 7.0 to 15.8    |
| Mass flux, $Mg/(m^2 \cdot s)$ | 1.0 to 6.0   | 1.4 to 9.0     |
| Critical quality              | -0.2 to +0.2 | -0.2 to +0.2   |

### 3. EXPERIMENTAL EQUIPMENT

#### 3.1 Freon Test Facility

The test facility KRISTA was recently constructed at the Institut für Reaktorbauelemente (IRB) at KfK, Karlsruhe. It has the following performance characteristics (water equivalent values are given in brackets):

Test section power: up to 500 kW (7.5 MW)  
 Flow range: 70 - 112000 kg/h (50 - 80000 kg/h)  
 Pressure range: 1 - 3 MPa (7 - 20 MPa).

Fig. 1 shows a schematic flow diagram of the test facility. The KRISTA facility consists basically of two separate loops, interconnected via the Freon storage tank and the purification system. The left part of the loop will be used for the 37-rod bundle tests while the right part (small KRISTA loop) is used for the single tube and 7-rod bundle tests. The test results reported in this paper were obtained from the small KRISTA loop. Special precautions were taken to minimize Freon leakages to the surroundings.

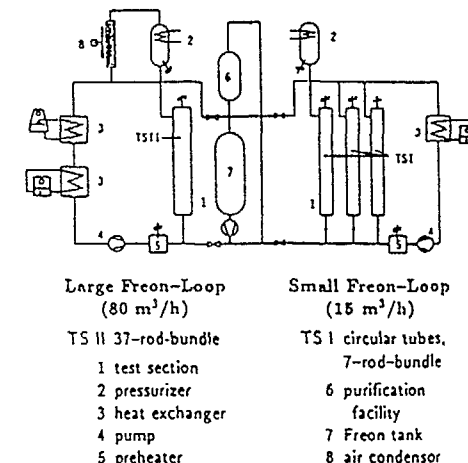


Fig. 1: KRISTA CHF test facility

#### 3.2 7-Rod Test Section

Fig. 2 shows details of the 7-rod bundle channel. The total length is 1.25 m of which 0.6 m is heated. Both the radial and axial flux distribution are uniform. The flow channel is split longitudinally and is bolted together as shown in cross-section A-B of Fig. 2. It is installed inside a pressure tube designed

for pressures up to 4 MPa. Thermocouples are installed inside the flow channel wall and will permit an accurate determination of a heat balance. Local coolant temperatures are measured by fifteen 0.25 mm OD thermocouples positioned in the subchannels at the downstream end of the heated length. Pressure taps are located at various axial positions along the length of the channel as shown in Fig. 2.

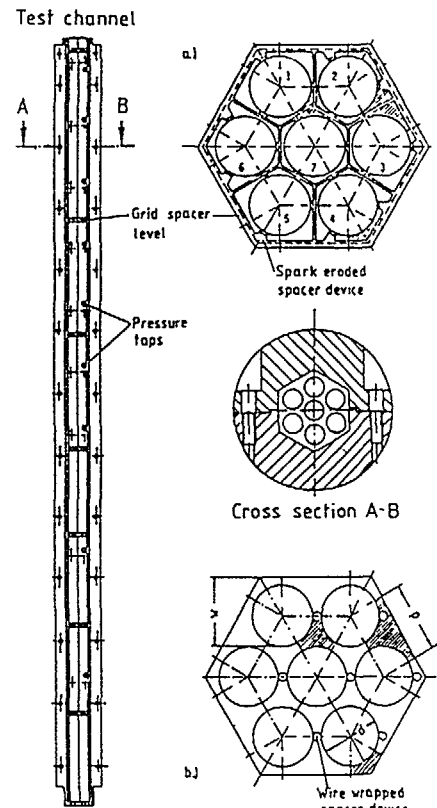


Fig. 2: Schematic of the 7-rod test section

( $p/d = w/d = 1.15$ )

a) Channel with grid spacer test bundle

b) Wire-wrapped test bundle

### 3.3 Fuel Rod Simulator For Freon Tests

Fig. 3 shows design details of the fuel rod simulator. It consists of magnesium oxide ( $MgO$ ) core, a helically-wound heating ribbon, a boron nitride (BN) insulator and a stainless steel cladding. Ni-Cr thermocouples (0.5 mm OD) are embedded in grooves inside the cladding. A plasma spraying process and a subsequent polishing process provided a smooth outer surface in the area where the thermocouples were embedded in the cladding. Eight thermocouples were installed in each of the rods; the junctions were located 15 and 20 mm upstream from the end of the heated length.

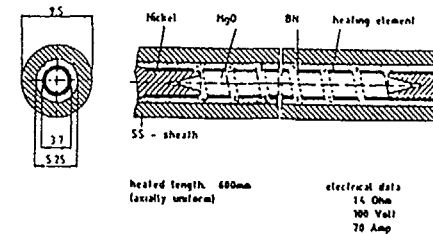


Fig. 3: Details of the fuel-rod simulator construction (all diameters in mm)

## 4. CHF FREON TEST RESULTS

### 4.1 Single Tube CHF Data

Details of the single tube tests performed in the KRISTA facility and the preproject at GKSS can be found elsewhere [6,10,11]. It can be assessed that a comparison of the water converted 8 mm Freon CHF results transferred with Ahmad's scaling law [7] yielded attractive results if compared with 8 mm water tables of Soviet and Canadian authors [8,9]. 344 test data points were compared with Groeneveld's table data and 204 KRISTA data points with the table data of the soviet authors. Table data over the water converted actual CHF results gave the following statistics: average of 0.94 and 1.01 for the Canadian and the Soviet data with standard deviations of 0.087 and 0.116 respectively.

The Soviet and the Canadian CHF look up table recommend a diameter  $d$  exponent

$$q_c \sim d^{-\epsilon} \quad (1)$$

of  $\epsilon = 1/2$  resp.  $\epsilon = 1/3$  as an average. Authors like Kirillov et al. [12] observed pressure dependent values of the exponent. Müller-Menzel and Zeggel [6] reported from Freon CHF tests using Ahmad's scaling law and following equation (1) the functions depicted in Fig. 4. An equivalent characteristic has been derived from  $H_2O$  CHF tube tests by Kirillov and colleagues [13,14]. These first results confirm the well-known scaling law of Ahmad.

A systematical comparison of these water and water converted CHF data is under way. An additional effort is necessary to cope with the conditions of PWHCR test bundles. The recently performed tube measurements also indicated that the diameter exponent of CHF in round tubes depends also from the diameter itself (s. Fig. 5).

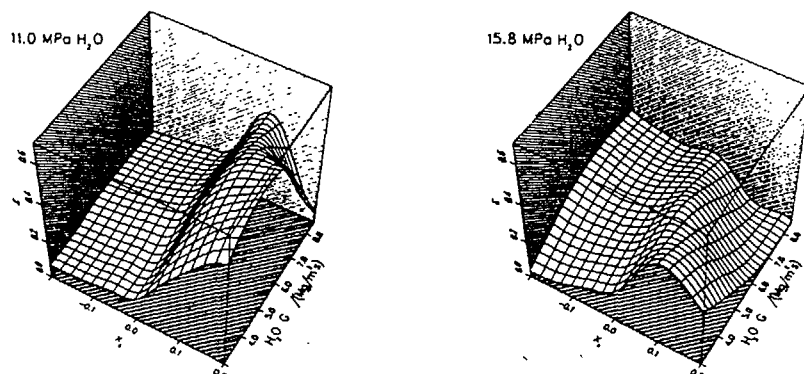


Fig. 4: Diameter exponent  $\epsilon$  as a function of quality and mass flux for two different pressures (water converted CFC-12 data)

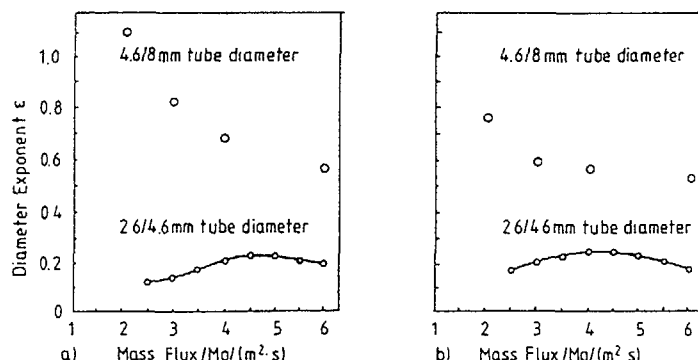


Fig. 5: Diameter exponent as a function of mass flux for  $x_c = 0.0$ :  
a) Freon Pressure 1.78 MPa; b) Freon Pressure 2.72 MPa

#### 4.2 CHF Results in 7-Rod Bundles

The first CHF tests in 7-rod bundles ( $p/d = w/d = 1.15$ ) have been performed in gridded and also in wire-wrapped (axial pitch/diameter  $H/d = 20$ ) rod arrangements. Some data of principal significance will be presented as follows.

The hydraulic behaviour of tightly packed bundles of triangular arranged bare rods are strongly influenced by remarkable differences in fluid flow cross sections of square wall subchannels and triangular center channels. This differences depend on the relative size of the rod-to-rod gaps ( $p/d-1$ ) and rod-to-wall ( $w/d-1$ ) clearings. If the velocities in the different channels are optimistically regarded constant the ratio of the wall to the center channel flow areas defines the mass flow rate ratio. The resulting enthalpy rise ratio is inverse to the mass flow ratio as far as the heating is constant. This geometrically affected flow redistribution is strongly increasing with decreasing  $p/d$  of tight lattices.

Some geometrical and related data of the test bundle between the grid levels are:

| Parameter                  | bundle | center channel | wall channel |
|----------------------------|--------|----------------|--------------|
| Number of subchannels      | 18     | 6              | 6            |
| Flow cross section, $mm^2$ | 348    | 16.0           | 31.8         |
| Hydraulic diameter, $mm$   | 4.4    | 4.3            | 4.9          |

These data could at least in the single phase flow bare rods case result in 100% higher mass flow rates in the wall channels if compared with the center channels. Two thirds of the bundle flow rate pass the wall region of the test section. The enthalpy span in the edge channels will be vice versa 50% of the inner ones. From these rough data it is evident that single and two-phase mixing between these two types of very different channels plays an important role for the retained enthalpy at the exit of the hot channels where CHF will be observed.

From single phase thermal hydraulic investigations performed within the Clinch River Breeder Reactor Project it is also known that wire wraps with decreasing ratio of axial lead  $H$  over diameter affect the described flow redistribution additionally. While discussing some CHF-results obtained with the 7-rod test section ( $p/d = w/d = 1.15$ ) in KRISTA it should be kept in mind, that the following details aggravate the interpretation of CHF-measurements:

- bundle with tight pitch lattice and small rod number,
- small rod-to-rod and rod-to-wall gaps,
- wire wraps with decreasing  $H/d$  and
- short heated length of the test bundles.

the last two problems and the problem of transferring model fluid data into H<sub>2</sub>O flow boiling results will not be stressed in this paper.

#### 4.2.1 CHF in gridded FA with constantly heated seven rods

The following 7-rod bundle results have been obtained in CFC-12 at a system pressure of 1.78, 2.3, and 2.7 MPa. The water equivalent pressure of the second number is 14 MPa resp. 2000 psia. This value is typical of the first generation of PWR cores and consequently well represented in CHF experiments. The Freon bundle average mass fluxes are: 1, 2, 3, 4, 6 Mg/(m<sup>2</sup> s) (water equivalent values are nearly 40% higher).

The CHF data displayed for constant mass fluxes as a function of inlet quality are linear functions. This is a good indicator for judging the consistency of the results. For CHF modeling purposes a plot CHF over critical quality is appropriate. This value  $x_c$  resp. the center channel exit quality has to be calculated. Fig. 6a represents CHF over center subchannel exit qualities. These qualities  $x_c$  are computed by COBRA-TUBS. It has to be noticed that for a given bundle mass flux a span of center channel mass fluxes is realized in the bundle (s. insert in Fig. 6a). The CHF-curves are steeper with increasing bundle mass fluxes. Qualitatively the same picture has been observed with Freon measurements in tubes of the inner diameter of 4.6 mm [6]. The comparison of the Fig. 6a and 6b shows the usefulness of tube table data if certain correction factors for the critical channels of bundles are applied. With water-to-Freon scaling factors (s. [6]) of 15 for CHF and 1.4 for mass fluxes the measured data are positive if PWHCR perspectives are regarded.

Fig. 7 displays calculated over measured data (C/M). The last correlation of Dalle Donne/Hame [15] based on Bowring's WSC-2-correlation [16] is used. This kind of CHF-correlation uses FA inlet conditions (system parameter approach). So local center channel exit conditions where boiling crisis occurs is not directly modeled. For comparison the Dalle Donne-correlated CHF data are converted into CFC-12 equivalent data, by Ahmad's scaling law [7] (note: Ahmad's scaling law has been evaluated for tubes). The values C/M in Fig. 7a (top) are far less one (average: 0.88; s: 0.17).

The prediction improves by application of Bowring's imbalance factor

$$Y' = \frac{\text{heat retained in the hot channel}}{\text{heat generated in the hot channel}}$$

which corrects the actual critical quality at the CHF point. The parameter Y' has been introduced by Bowring [16] and utilized e.g. by Sugimoto et al. [4] for tight lattice

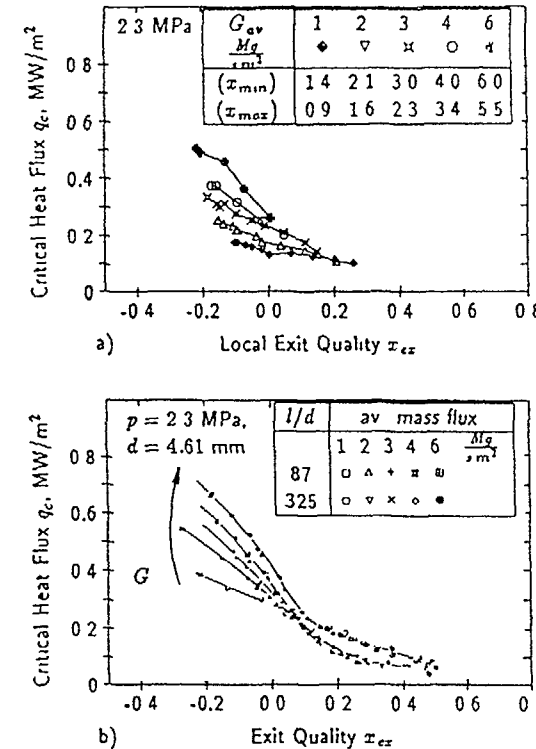


Fig. 6. CHF for the 7-rod bundle conditions  
 a) as a function of predicted central subchannel exit quality using COBRA-IV-TUBS  
 b) round tube (4.61 mm) CHF data as a function of critical quality

applications to account for the enthalpy transfer between subchannels. In our case since the high enthalpy rise in the hot center channels will be reduced by convective heat transfer (mixing) to the wall channels, Y' is less 1.0.

Y' has been computed by COBRA-TUBS. It's application results (s. Fig. 7a, bottom) in C/M closer to one (average: 0.93; s: 0.18). The formerly observed overprediction of high mass flux CHF data (s. [11]) by the CHF-correlation remain constant, if an imbalance factor is applied. The reason is, that the absolute magnitude of the enthalpy spans is reciprocal to the mass flux.

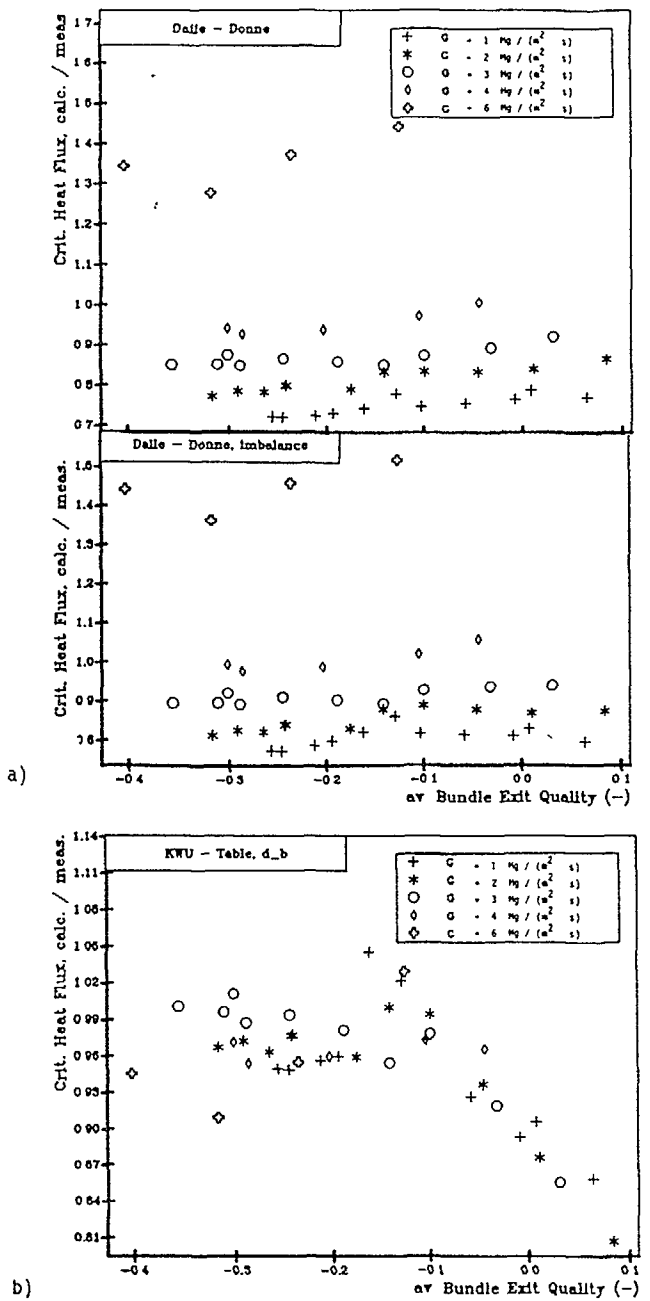


Fig. 7:  
Calculated over measured  
Freon CHF data (2.3 MPa)

a) Dalle Donne / Hame correlation  
b) Soviet round tube table

Fig. 7b gives an impression of table data [8] related predictions (KWU-procedure). It should be emphasized that the COBRA-calculations have been performed iteratively (s. also [17]). The C/M statistics are: average: 0.96, s: 0.05 (!).

An improved representation of all experimental data will be possible with appropriate 2-phase mixing coefficients (s. also [4] and [17]). The respective experiments will be performed at KRISTA.

#### 4.2.2 CHF in gridded FA with unheated rods

The role of subchannel analysis codes (SAC) for evaluation of rod-bundle experiments and the need for refined knowledge of constitutive 2-phase-coefficients becomes evident with Fig. 8.

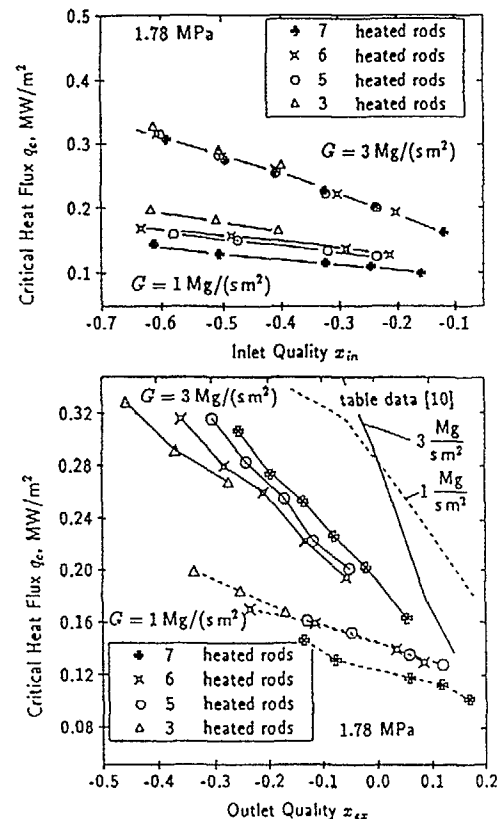


Fig. 8: Effect of unheated rods and comparison with the Canadian table (CHF vs. bundle exit quality)

For a pressure of 1.78 MPa (water equivalent: 11.0 MPa) one, two and four rods have been disconnected from the power supply. This severe non-uniform radial heat source distribution has been investigated with respect to CHF for mass fluxes of 1 and 3  $\text{Mg}/(\text{m}^2 \cdot \text{s})$  (water equivalent: 1.4 and 4.2  $\text{Mg}/(\text{m}^2 \cdot \text{s})$ ). For the higher mass flux the CHF is hardly affected by the amount of power-connected rods. In this case the average bundle power and outlet quality is increasing with the number of heated rods (see bottom plot of Fig. 8). With the lower mass flux the opposite is true. In the latter case the bundle power is roughly constant (s. [11]). The bottom plot of Fig. 8 includes appropriate data of Groeneveld's table. The observed opposing trends of the measured CHF data for two mass fluxes could be influenced by factors as (i) differences in the bypasses along the critical channels, (ii) differences in mixing rates, and (iii) influences of bubble induced wall roughnesses. All these factors can be predicted only by properly formulated two-phase constitutive equations (SAC!).

#### 4.2.3 CHF in 7-rod bundles with different spacers

A final CHF picture Fig. 9 presents CHF data for a grid spaced and a wire-wrapped FA ( $p/d = w/d = 1.15$ ) versus the bundle average exit quality for a system pressure of 2.7 MPa (water equivalent: 15.8 MPa) and a bundle mass flux of  $3 \text{ Mg}/(\text{m}^2 \cdot \text{s})$ . The CHF data of the wire wrapped bundle ( $H/d = 20$ ) are advantageous for high subcooled FA outlet conditions. But the slope of the CHF curve over the exit qualities is twice the value of the gridded bundle. The functions if extrapolated linearly intersect at qualities near zero. This can be understood as a flow regime dependent influence of the wire-wrapping. Low  $H/d$  numbers obviously effect the local two-phase heat transfer deterioration (boiling crisis). The capability of the wire-wraps to flatten the subchannel enthalpy spans is less effective. In both cases of spacer devices the tendency of the CHF data (s. Fig. 9) predicted by the Dalle Donne/Hame correlation follows the observed CHF results. The steeper CHF curve for the wire-wrap case demonstrates the detrimental CHF-characteristics regarding PWHCR purposes of wire-wrapped FA for low  $H/d$  (this case  $H/d = 20$ ) with increasing qualities. An evaluation of these CHF-tests of wire-wrapped bundles is underway. Further tests include wire wraps with larger axial wire pitches.

#### 5. CONCLUSIONS AND FINAL REMARKS

Flow boiling investigations using model fluids is a technology of increasing importance for systematical studies of parameter trends and for a validation of thermal hydraulic simulation codes. Some fundamental work on the validity of Freon two-phase heat transfer results is underway at the KfK with TUBS. Some topics are:

- final comparison of  $\text{H}_2\text{O}$  and Freon CHF data in tubes (in cooperation with D.C. Groeneveld/University of Ottawa).

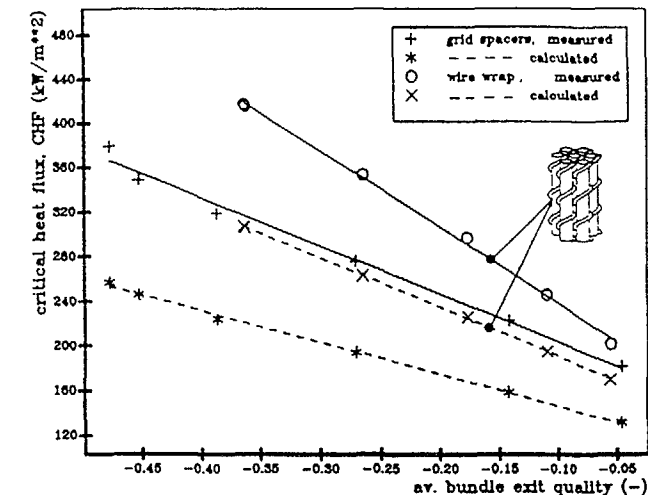


Fig. 9: Measured and predicted Freon CHF data of gridded and wire wrapped 7-rod bundles (System pressure 2.7 MPa, bundle mass flux  $3 \text{ Mg}/(\text{m}^2 \cdot \text{s})$ ;  $H/d = 20$ )

- subchannel code computations of CHF in identical rod arrangements cooled by  $\text{H}_2\text{O}$  and Freon (in cooperation with Siemens/KWU). This study includes square rod lattices as well as triangular rod bundles of 37 rods (s. Fig. 10a).
- further thermal hydraulic experiments with design relevant test sections.
- single and two-phase mixing tests (s. Fig. 10b).
- and last not least research efforts to replace CFC-12 by less Ozone depleting fluids (in cooperation with D.C. Groeneveld/UoO).

It can be concluded that the recently erected KRISTA Freon facility offers the chance to perform systematical thermal hydraulic investigations while the PWHCR-optimization proceeds. Improved knowledge on two-phase flows and limiting phenomena cope with the need to arrive at a safe and economic design. this goal is especially realistic if an international scientific cooperation with respect to the attendants of this TCM might stimulate the national programs, activities and results.

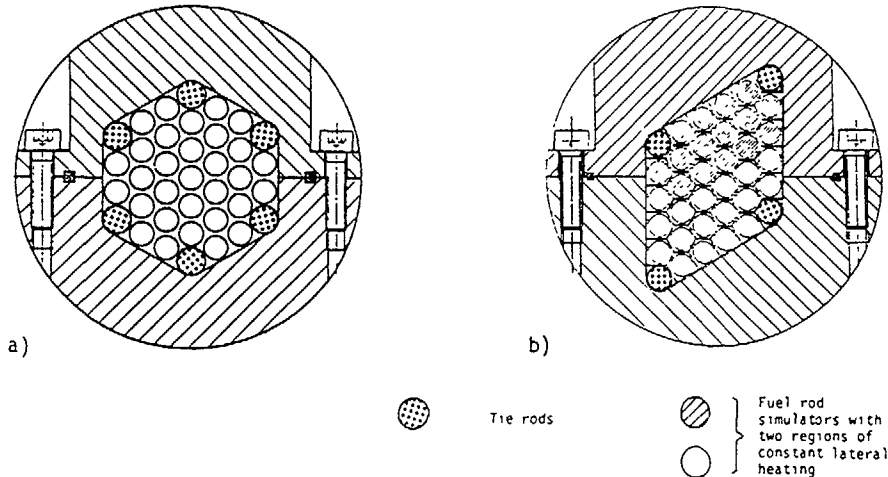


Fig. 10: Test sections for CHF (a.) and mixing (b.) experiments

## 6. SUMMARY

1. CHF experiments in Freon-12 are underway at KfK in cooperation with TUBS as part of the development program for the PWHCR. The objective is to investigate the flow boiling and the CHF behaviour of a tight lattice core. As a part of this program the CHF has been measured in a directly heated tube and 7-rod bundles having a  $p/d = w/d$  of 1.15.
  2. The CHF dependence on tube diameter in Freon was found to be more complicated than recommended by table data. As typical subchannels in PWHCR cores of interest cover smaller sizes than are normally used for the development of CHF prediction methods, more work is required to assess this geometry effect.
  3. The CHF variation with computed center channel exit qualities (gridded 7-rod bundle) has the same tendency as tube CHF data. This confirms the use of well established tubular CHF tables with appropriate correction factors (regarding bundle geometry etc.).
  4. CHF predictions with the Dalle Donne/Hame correlation and the soviet round tube table supported by subchannel computations arrive at satisfying results. The role of subchannel analysis codes for predicting the critical quality where CHF occurs is evident. The constitutive coefficients esp. for two-phase mixing will be improved by measurements at the KRISTA facility.

5. The CHF data on the gridded 7-rod bundle with several unheated rods provide a unique data base to be used for validating and improving subchannel codes. This would be a severe test of the codes as they are usually not designed to predict the CHF for fluids different from water and with such a highly non-uniform radial flux distribution.
  6. The CHF characteristics of wire-wrapped bundles appear disadvantageous for PWHCR purposes at least for low axial lead over diameter wire-wraps ( $H/d = 20$ ).
  7. The scaling laws available to transfer flow boiling results into PWHCR relevant conditions have to be evaluated for bundle flows. This work will be performed with identical 37-rod bundle cross section investigated at the KWW/Karlstein H<sub>2</sub>O and the KfK Freon KRISTA facility.
  8. Studies to replace CFC-12 by non Ozone depleting fluids are underway.
  9. From the actual investigations the potential of tight lattices ( $p/d \geq 1.15$ ) for PWHCR rod bundles is very promising.

## NOMENCLATURE

CHF Critical Heat Flux,  $\text{MW/m}^2$   
 d rod diameter, mm  
 d<sub>e</sub> equivalent/hydraulic diameter, mm  
 G mass flux,  $\text{Mg}/(\text{m}^2\text{s})$   
 H axial wire lead, mm  
 l heated length, m  
 p rod pitch, mm  
 P pressure, MPa  
 q heat flux,  $\text{MW/m}^2$   
 w rod-to-wall gap width + d, mm  
 x fluid quality  
 Y' Bowring's imbalance factor  
 exponent of diameter effect on CHF

### Subscripts:

|    |                      |
|----|----------------------|
| av | bundle average value |
| c  | critical             |
| ex | outlet, exit         |
| in | inlet                |

## ACKNOWLEDGEMENTS

The authors gratefully acknowledge the contributions of the IRB team of the KRISTA facility. They also acknowledge the contributions of their TUBS colleagues, especially X. Cheng who was responsible for the experiments and analysis and S. Bethke who performed the calculations.

## REFERENCES

- [ 1] Oldekop, W., Berger, H.D., Zeggel, W.: General Features of Advanced Pressurized Water Reactors with Improved Fuel Utilization. Nuclear Technology 59 (1982) 212-227
- [ 2] Moldaschl, H., Brogli, R., Kuczera, B.: Status and Prospects of the Cooperative KWU High Converter Development 1989. Proc. of the ICENES '89 Conference, Karlsruhe, FRG (1989)
- [ 3] Courtaud, M., Deruaz, R., Gros-Delion, L.: The French Thermal Hydraulic Program Adressing the Requirements of Future Pressurized Water Reactors. Nuclear Technology 80 (1988) 73-82
- [ 4] Sugimoto, J., Iwamura, T., Okubo, T., Murao, Y.: Thermal-Hydraulic Study on High Conversion Light Water Reactor at JAERI. Proc. of the NURETH-4 Topical Meeting, Karlsruhe, FRG (1989) 799-804
- [ 5] Akiyama, Y., Hori, K., Tsuda, S.: DNB Experiments for High Conversion PWR Core Design. Proc. of the NURETH-4 Topical Meeting, Karlsruhe, FRG (1989) 788-793
- [ 6] Müller-Menzel, T., Zeggel, W.: CHF in the Parameter Range of Advanced Pressurized Water Reactor Cores. Nuclear Engineering and Design 90 (1987) 265-273
- [ 7] Ahmad, S.Y.: Fluid-to-Fluid Modelling of Critical Heat Flux: A Compensated Distortion Model. Int. J. Heat Mass Transfer 16 (1973) 641-662
- [ 8] Working Party of the Heat and Mass Transfer Section of the Scientific Council of the Academy of Science USSR, Table Data for Calculating Burnout when Boiling Water in Uniformly Heated Tubes. Thermal Engineering 23 (1977) 77-79
- [ 9] Groeneveld, D.C., Cheng, S.C., Doan, T.: 1986 AECL-UO CHF Look-up Table. Heat Transfer Engineering 7 (1986) 46-62
- [10] Cheng, X., Zeggel, W.: Parameters of CHF in Small Diameter ( $\leq 8$  mm) Round Tubes. Proc. of the NURETH-4 Topical Meeting, Karlsruhe, FRG (1989) 121-126
- [11] Zeggel, W., Erbacher, F.J., Groeneveld, D.C.: Critical Heat Flux Investigations Using a Closely-Spaced Rod Bundle. Proc. of the NURETH-4 Topical Meeting, Karlsruhe, FRG (1989) 781-787
- [12] Kirillov, P.L., Bobkov, V.P., Vinogradov, V.N., Ivashkevich, A.A., Smogalev, I.P.: Recommendations on calculating the heat-transfer crisis in pipes on the Basis of a bank of experimental Data. Soviet Atomic Energy 59 (1986) 531-539
- [13] Kirillov, P.L., Bobkov, V.P., Vinogradov, V.N., Denisov, V.S., Ivashkevich, A.A., Katan, I.B., Paniutchev, E.I., Smogalev, I.P., Salnikova, O.B.: On Standard Critical Heat Flux Data for Round Tubes. Proc. of the NURETH-4 Topical Meeting, Karlsruhe, FRG (1989) 103-107
- [14] Kirillov, P.L.: Personal communication at the NURETH-4 Conference (1989)
- [16] Bowring, R.W.: WSC-2: A Subcooled Dryout Correlation for Water-Cooled Clusters Over the Pressure Range 3.4-15.9 MPa (500-2300 PSIA). Report AEEW - R 983 (1979)
- [15] Dalle Donne, M., Hame, W.: A Critical Heat Flux Correlation for Triangular Arrays of Rod Bundles with Tight Lattices, Including the Spiral Spacer Effect. Nuclear Technology 71 (1985) 111-124
- [17] Bethke, S., Zeggel, W., Cheng, X., Monir, C.: Status of Tight-Lattice Thermal-Hydraulics. IAEA-Meeting on Technical and Economic Aspects of High Converters, Nürnberg, IAEA-TECDOC 622-I3-TC-700 4.3 (1990)

## EXPERIMENTAL INVESTIGATIONS ON EMERGENCY CORE COOLING OF TIGHT LATTICE PWRs IN A LOCA

F.J. ERBACHER, K. WIEHR

Kernforschungszentrum Karlsruhe GmbH,  
Karlsruhe, Federal Republic of Germany

### Abstract

The work performed in the FLORESTAN program at the Karlsruhe Nuclear Research Center on the reflooding and deformation behavior of a tight-lattice fuel rod bundle in a loss-of-coolant accident (LOCA) of an advanced pressurized water reactor (APWR) is described. The present reflooding tests in an undeformed extremely tight bundle with a pitch-over-diameter ratio  $p/d = 1.06$  show a different thermal-hydraulic behavior compared to a standard pressurized water reactor. Gravity-feed tests exhibited long quench times and high peak cladding temperatures. A deformation test on internally pressurized Zircaloy cladding tubes has shown that a hexagonal tight-lattice bundle has the potential of large circumferential burst strains and a high coolant channel blockage.

### INTRODUCTION

The incentive to further develop the proven pressurized water reactor (PWR) is its potential to improve fuel utilization in a closed uranium/plutonium fuel cycle. This can be achieved by neutron spectrum hardening via significant reduction of the moderator-to-fuel ratio in the core. For this reason the wide square fuel rod lattice typical of a PWR is modified into a tight triangular lattice with a rod pitch-over-diameter ratio ( $p/d$ ) ranging from 1.06 to 1.30 depending on the design. By such modifications a conversion ratio of approx. 0.8 to 0.9 can be achieved.

A major problem of such tight lattice fuel elements is the emergency core cooling in a loss-of-coolant accident (LOCA). Since no experimental data exist, the FLORESTAN program is under way at KfK. This program is part of a trilateral cooperation with Siemens/KWU, the Swiss Paul Scherrer Institute and the Technical University of Braunschweig.

In this paper reflooding tests in a very tight 61-rod bundle ( $p/d = 1.06$ ) and a deformation test in a 61-rod bundle ( $p/d = 1.20$ ) with internally pressurized Zircaloy claddings are described. The bundle with  $p/d = 1.06$  represents the blanket region of a heterogeneous reactor design, whereas the  $p/d$ -ratio of 1.20 is typical of a homogeneous design.

### EXPERIMENTAL

The test bundle for the reflooding tests shown in Figure 1 consists of 61 electrical heated fuel rod simulators with a cosine shaped axial power profile, a heated length of 2024 mm and a total length of 5600 mm. The stainless steel (SS) cladding

tubes have six integral helical fins. The dimensions of the cladding tubes were chosen to fit with the existing REBEKA electrical fuel rod simulator, i.e., the cladding inner diameter is 9.3 mm, the outer diameter of the SS-cladding tubes is 10.1 mm. The main characteristics of this fuel rod simulator are largely identical with the REBEKA fuel rod simulator. Its excellent thermal simulation compared to nuclear fuel rods has been proven in extensive experimental work [1, 2].

Figure 2 shows schematically the FLORESTAN test loop. An essential feature of this loop is that by providing representative emergency cooling conditions during reflooding and by using electrically heated fuel rod simulators of high simulation quality, the temperature and pressure transients of the cladding tubes are established automatically in a representative way without controlling the temperature by the power supply.

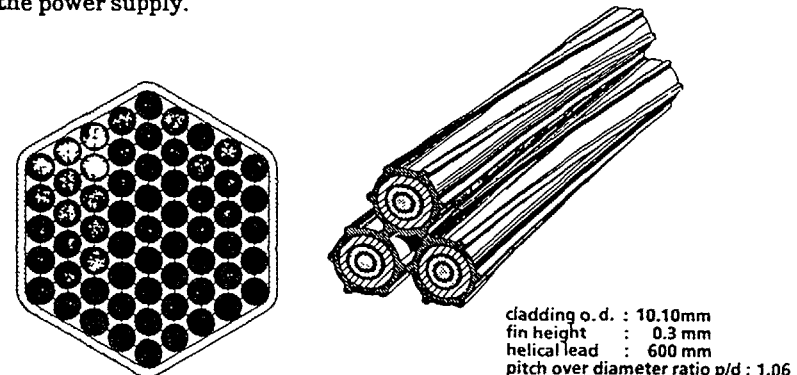


Fig. 1 FLORESTAN test bundle

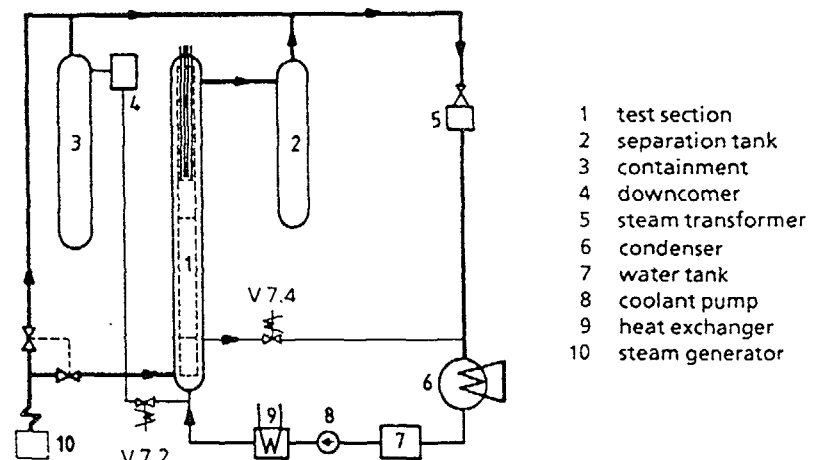


Fig. 2 FLORESTAN test loop

- 1 test section
- 2 separation tank
- 3 containment
- 4 downcomer
- 5 steam transformer
- 6 condenser
- 7 water tank
- 8 coolant pump
- 9 heat exchanger
- 10 steam generator

## RESULTS

### Forced feed reflooding

Forced feed reflooding tests in a tight rod bundle are important as baseline tests in order to study the basic phenomena. The boundary conditions of forced feed reflooding tests are well defined, the reflood water mass flow through the bundle can easily be measured and the results can be compared with the existing data base of forced feed reflooding tests in PWR geometries. Furthermore, mainly such well defined tests are suited to assess and improve computer codes.

In the following, a forced feed FLORESTAN test in a tight test bundle is compared with a forced feed REBEKA test in a more open PWR geometry. At the start of flooding (SOF), a relatively low temperature of 600°C was chosen for the FLORESTAN test on the basis of blowdown calculations. The corresponding temperature of the REBEKA test was 765°C. The average linear rod power during reflooding was 20.7 W/cm (axial peaking factor 1.2) for the REBEKA test and 14.7 W/cm (axial peaking factor 1.3) for the FLORESTAN test. The flooding water mass flow for the FLORESTAN test bundle was selected by using the same superficial water velocity as in the REBEKA test section. This resulted in a corresponding cold flooding rate of 8.1 cm/s compared to 3.2 cm/s in the REBEKA test. The temperature of the reflood water was 130°C for both tests.

Figure 3 shows the measured cladding temperature transients within the upper half of the heated length of the REBEKA and the FLORESTAN test bundle. In the REBEKA test, the peak cladding temperature develops at the axial midplane. Also, after the start of flooding the cladding temperatures decrease very soon. In contrast to this the tight lattice exhibits the peak cladding temperature relatively late and at a higher position. Also, the temperature increase after SOF is substantially higher. This different temperature characteristic of the tight lattice is evidently the result of the small water volume in the bundle and the helical fins. They produce an enhanced turbulence and subchannel cross-mixing. Both effects result in a relatively fast evaporation of the water so that in the upper part of the bundle the cooling takes place extensively by superheated steam. With rising water level and enhanced water entrainment the precursory cooling increases also for the upper elevations of the bundle. This causes a relatively fast temperature drop from the peak temperature to quenching temperature.

Figure 4 shows the total pressure drop of the tight lattice compared to a PWR geometry. It is evident that the pressure drop development is very different and that the two-phase flow pressure drop in the tight lattice bundle is considerable. After SOF the pressure drop increases almost instantaneously due to the high two-phase flow pressure drop over the full bundle length. With rising water level the effective length, which produces two-phase pressure drop, becomes smaller, resulting in a decreasing pressure drop with time. When the upper end of the bundle is rewetted the pressure drop reaches a constant level which corresponds to the pressure drop of the convective water cooling with nucleate boiling.

### Gravity feed reflooding

In a LOCA the mass flow of the emergency core cooling water through the core is mainly determined by the available downcomer head, the two-phase pressure drop in the core and system effects in the core and the primary loops. Consequently,

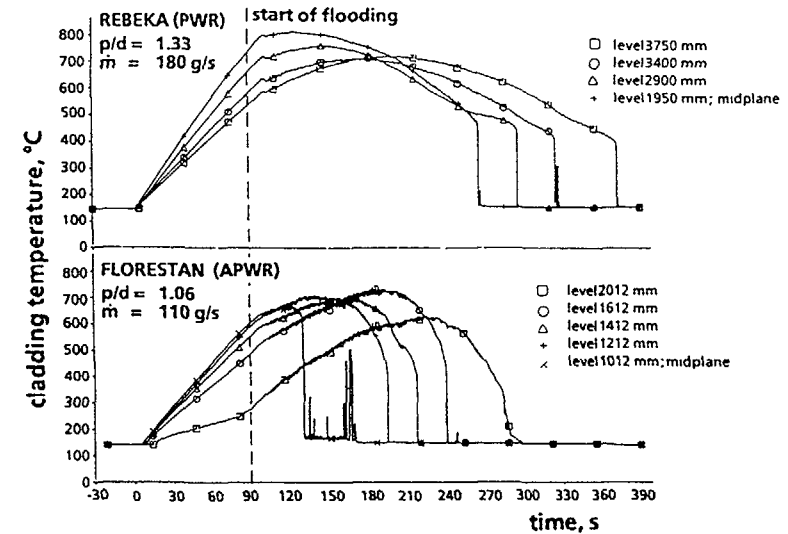


Fig. 3 Cladding temperatures in the upper half of heated bundle length

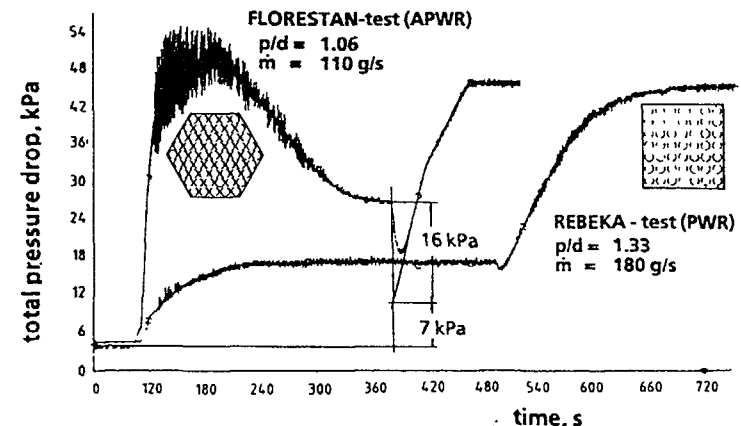


Fig. 4 Pressure drop

only large scale integral tests with a proper loop simulation are able to deliver representative data which can be applied directly to the reactor.

In the FLORESTAN gravity feed separate effect tests the downcomer was simulated by a tube with a pressure head which is identical to the downcomer in the reactor of nearly 6 meters height. The height of the water level in the downcomer represents the driving force for the mass flow of the water into the test bundle. Oscillations of the liquid can develop between the bundle test section and the downcomer simulator. Depending on the two-phase flow pressure drop in the bundle and the dynamics of the oscillation, water can be carried over through the downcomer into the containment simulator as well as through the test bundle into the separation tank. In this way, an artificial overfeeding of the test bundle possible in forced feed is prevented.

The test procedure for gravity feed was selected such that, at initiation of flooding, the downcomer was filled up to a level of about 4500 mm with hot water. At SOF, the filled downcomer tube was connected to the test section by opening the valve V 7.2. After initiation of reflooding, the water column in the downcomer started to oscillate with a frequency of about 1.5 Hz. It was found that the total pressure drop in the test section also oscillated with the same frequency and a high initial amplitude.

In Figure 5 two experiments with nearly the same temperature at SOF of 500°C and also nearly the same flooding water injection rate of 110 g/s are compared, one with forced feed and the other with gravity feed reflooding. - The upper part of Fig. 5 shows temperature transients and the water level in the separation tank of the forced feed test. The 1612 mm elevation shows the maximum cladding temperature of about 690°C and a quench time of 213 s. At 270 s the upper end of the heated length of the bundle is rewetted. The water level in the separation tank remains constant until 290 s, i.e. no water was carried over during the whole reflooding period. - The lower part of Fig. 5 shows temperatures and water levels of the gravity feed test. It is evident that the maximum cladding temperatures develop also in the upper part of the bundle and relatively late after SOF. However, at the axial level of 1612 mm, the peak cladding temperature of the gravity feed test is about 880°C, i.e. approx. 200 K higher compared to the forced feed test. The time at maximum temperature is also much longer. The upper end of the heated length of the bundle is rewetted only at approx. 750 s compared to 270 s in the forced feed test, i.e. the quench time in the gravity feed test is more than three times longer compared to the forced feed test. These relatively high temperatures and long quench times in the gravity feed test are the result of the high pressure pulses in the test section which cause a substantial water entrainment from the test section into the separation tank, right from SOF. The corresponding increase of the water level in the separation tank is indicated in the lower part of Fig. 5.

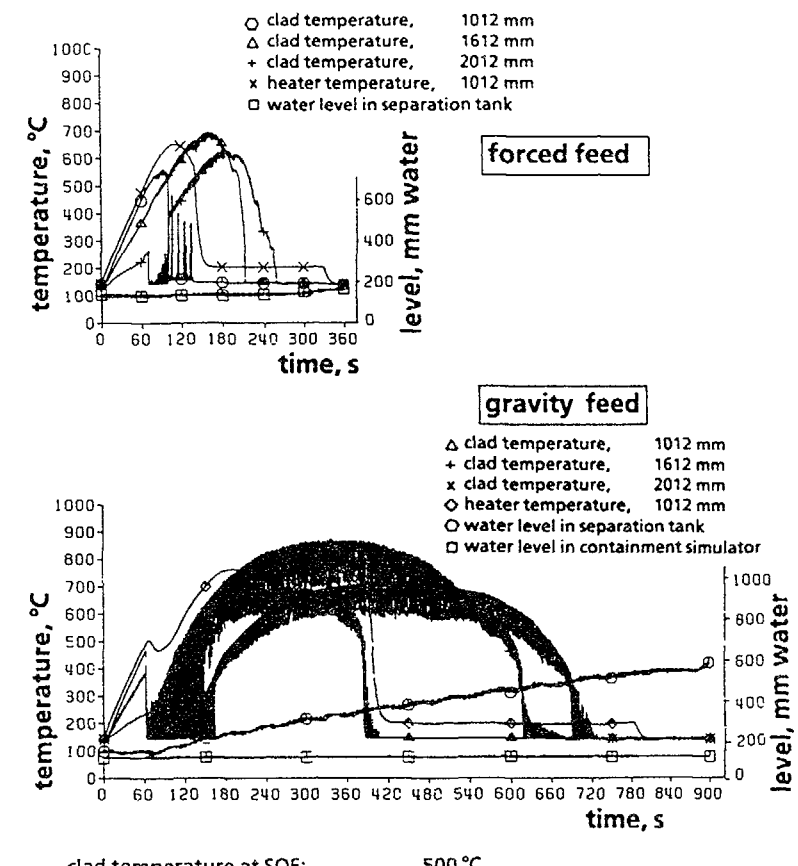


Fig. 5 Temperatures and water levels in FLORESTAN forced- and gravity feed tests

This gravity feed reflooding behavior of the very tight test bundle is in contrast to a PWR geometry which under gravity feed shows an improved reflooding heat transfer.

### Cladding deformation and coolant channel blockage

In the LOCA analysis the number of ruptured fuel rod claddings, the extent and distribution of cladding deformations and their influence on coolability must be predicted.

In order to determine the deformation potential and maximum possible coolant channel blockage of a hexagonal tight-lattice bundle with Zircaloy cladding tubes, a special FLORESTAN material test was performed on a 61-rod bundle with a pitch-over-diameter ratio of 1.20. The dimensions of the Zircaloy claddings were  $10.75 \times 0.725$  mm. The test conditions were untypical of a LOCA and chosen to obtain the theoretically maximum cladding deformation (Figure 6). At a nearly constant cladding temperature of  $800^{\circ}\text{C}$  the Zircaloy cladding tubes were internally pressurized with Helium of 8.4 MPa. The outer fluid atmosphere was nearly stagnant steam at 0.4 MPa system pressure. The rod power was untypically low compared to the decay heat and chosen to compensate only for the heat losses. Therefore, the deformation of the Zircaloy claddings developed under nearly isothermal and adiabatic conditions. The internal rod pressures developed according to the individual cladding deformations. The time of deformation from pressurization to burst was less than one minute.

Figure 7 is a plan view and cross-section of the deformed 61-rod bundle. A pronounced coplanarity of the burst locations and large cladding deformations are evident from the left side photograph. This resulted even in a deformation of the 1 mm thick bundle housing. - The coplanarity of the maximum cladding deformations is the result of the axial power profile and mainly the almost adiabatic test procedure, i.e. nearly no cooling. Under cooling and power conditions typical of a LOCA the interaction between the ballooning cladding tubes with their increasing cladding surface and the outer cooling efficiency would result in less deformation and coplanarity.

The right side photograph of Fig. 7 is a cross-section of the deformed bundle in the axial level of maximum flow blockage. The photograph illustrates the serious cladding deformations of the inner 37 claddings. The deformation of the Zircaloy claddings in the outer ring is influenced by cold wall effects of the bundle housing. Their non-symmetric wall weakening with the thicker wall facing the cold housing is typical of the strain behavior of Zircaloy claddings deformed under azimuthal cladding temperature differences.

Figure 8 shows the circumferential strains and the calculated coolant channel blockage of the inner 37 rods. The strains plotted in the diagram illustrate the coplanarity and the location of the maximum strains slightly above the midplane. The maximum circumferential burst strains reached values up to about 90 %. From the individual strains a theoretical coolant channel blockage ratio of 100 % extending over a length of 7 cm was calculated. However, this calculation does not take into account the wrinkles of the outer cladding contours which still leave open many small passages for the coolant even in the area of the maximum flow blockage.

The relatively high cladding deformation and coolant channel blockage found in the FLORESTAN material test is in contrast to a REBEKA material test performed under similar "worst case" conditions. This test typical of a wide PWR lattice resulted in a maximum flow blockage of 85 % only.

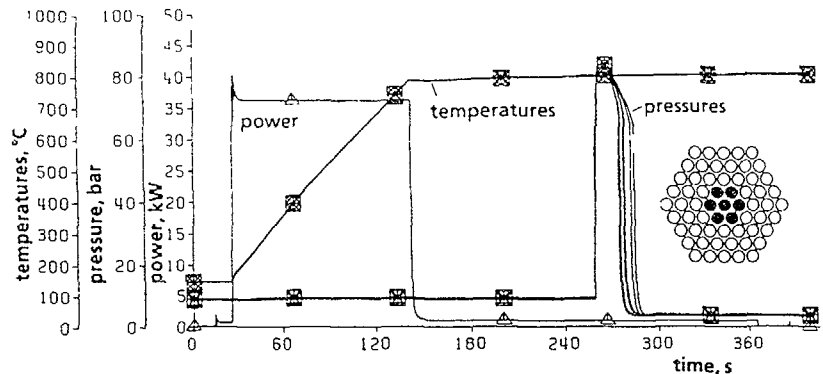


Fig. 6 Test procedure of FLORESTAN - material test (inner 7 rods)

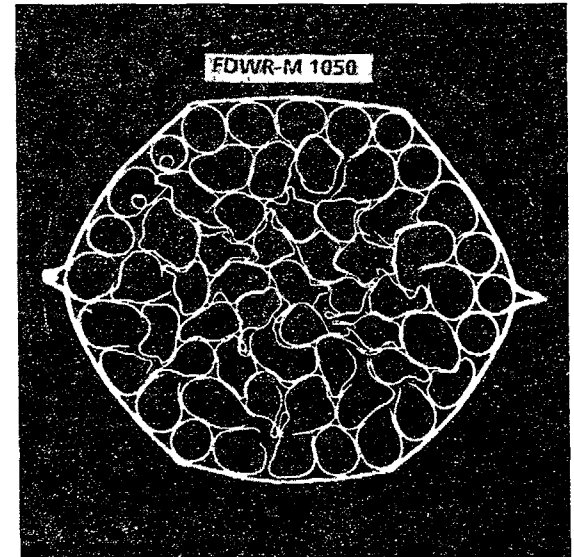
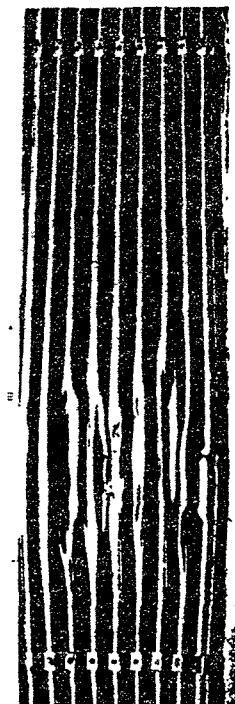


Fig. 7 Plan view and cross-section of the deformed bundle

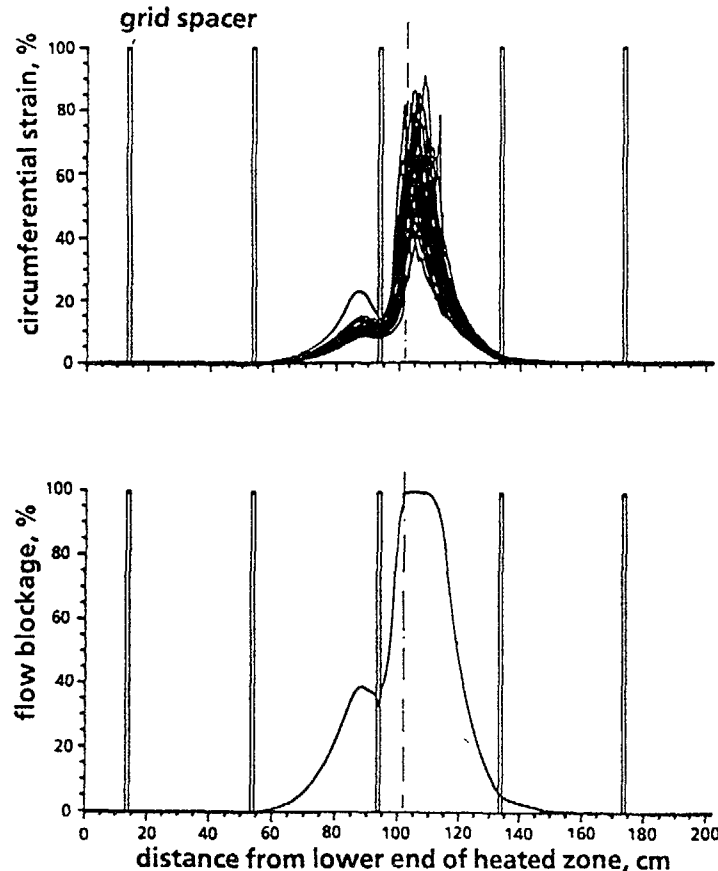


Fig. 8 Strain profile and flow blockage of 37 inner rods

In order to prove reliably a sufficient coolability of a hexagonal tight lattice bundle experiments are needed which simulate in a representative way the interaction between deforming fuel rod claddings and the emergency core cooling.

## SUMMARY AND CONCLUSION

The essential results of the FLORESTAN reflooding tests in a very tight rod bundle ( $p/d = 1.06$ ) and of the FLORESTAN deformation test ( $p/d = 1.20$ ) can be summarized as follows:

- The reflood heat transfer in a tight-lattice fuel rod bundle is quite different compared to the wide lattice of a standard PWR.
- The peak cladding temperature develops relatively late in the upper part of the bundle.
- The highest pressure drop develops shortly after start of flooding.
- Gravity-feed flooding tests in tight lattice bundles with flooding rates comparable to forced feed tests result in more entrainment. This leads to higher peak cladding temperatures and longer quench times.
- A hexagonal tight-lattice bundle has the potential of large circumferential burst strains and a high coolant channel blockage.

These findings underline that substantial research work needs to be done in order to study the phenomena associated with the reflooding and deformation behavior of tight-lattice fuel rod bundles.

Future experiments within the FLORESTAN program will concentrate on reflooding tests on 61-rod bundles with Zircaloy claddings of 9.5 mm outer diameter and a pitch-over-diameter ratio of 1.24.

## REFERENCES

- [1] F.J. Erbacher, P. Ihle, K. Rust, K. Wiehr: Temperature and Quenching Behavior of Undeformed, Ballooned and Burst Fuel Rods in a LOCA. Fifth International Meeting on Thermal Nuclear Reactor Safety, September 9-13, 1984, Karlsruhe, FRG.
- [2] K. Wiehr: REBEKA-Bündelversuche, Untersuchungen zur Wechselwirkung zwischen aufblähenden Zircaloyhüllen und einsetzender Kernnotkühlung. Abschlußbericht, KFK 4407, April 1988, Kernforschungszentrum Karlsruhe GmbH, Karlsruhe, FRG.

# THE NEPTUN EXPERIMENTS ON LOCA THERMAL HYDRAULICS FOR TIGHT LATTICE PWRs

J. DREIER, R. CHAWLA, N. ROUGE, S. YANAR  
Paul Scherrer Institute,  
Villigen, Switzerland

## Abstract

The NEPTUN test facility at the Paul Scherrer Institute is currently being used to provide a broad data base for the validation of thermal-hydraulics codes used in predicting the reflooding behaviour of a tight-lattice PWR (light water high conversion reactor, LWHCR). The present paper gives a description of the facility and the test matrix to be covered in the experimental program. Results are presented from a number of forced-feed, bottom-reflooding experiments, comparisons being made with (a) measurements carried out earlier for standard-PWR geometry and (b) the results of a calculational benchmark exercise conducted in the framework of a Swiss/German LWHCR-development agreement.

Rewetting for the tight, hexagonal-geometry ( $p/d = 1.13$ ) NEPTUN-III test bundle has been found to occur in all tests carried out to date, in which reasonably LWHCR-representative values for the various thermal-hydraulics parameters are used. Results of the calculational benchmark exercise have confirmed the need for further code development efforts for achieving reliable predictions of LWHCR reflooding behaviour.

## 1 Introduction

The concept of the Light Water High Conversion Reactor (LWHCR) – being developed in the framework of a trilateral co-operation between Siemens (KWU), Kernforschungszentrum Karlsruhe and the Paul Scherrer Institute – is mainly based on standard, commercially well established, pressurized water reactor (PWR) technology. As a consequence, many of the components of a future LWHCR power plant, and even certain aspects of system behaviour, may be considered to have already been adequately studied. However, characteristics directly effected by the tight, hexagonal-lattice core design (which leads to a harder neutron spectrum and hence, the higher fuel conversion ratio) clearly do need detailed investigation.

One of the key questions in the above context is that related to the coolability of an LWHCR core after a loss-of-coolant-accident (LOCA) event. In considering the thermal-hydraulics behaviour during the different phases of a LOCA event for an LWHCR, various

initial conditions – such as rod temperature and flooding rate – would be expected to be quite different to those for a standard PWR. Integral system calculations, which take the modified core design explicitly into account, are necessary to determine these conditions. Current-day thermal-hydraulics codes and data bases, on the other hand, have not been adequately assessed for the tight, hexagonal-lattice geometry of LWHCR cores. In effect, therefore, experimental investigations are needed for each of several different phases of an LWHCR LOCA event, viz. depressurization, core dryout and reflooding.

The NEPTUN test facility at the Paul Scherrer Institute was designed and constructed for studying reflooding and low-pressure boil-off characteristics in electrically heated, fuel bundle simulators. In 1985, the facility was modified to enable a program of LWHCR-relevant experiments to be conducted using a 37-rod, tight-pitch bundle [1]. The present paper gives an overview of the NEPTUN-LWHCR program and includes comparisons of experimental results with (a) measurements carried out earlier for standard-PWR geometry and (b) the results of a calculational benchmark exercise conducted under the Swiss/German co-operation agreement.

## 2 NEPTUN Description

### 2.1 General

Figure 1 gives a simplified flow diagram of the NEPTUN test facility and shows also the principal instrumentation of the test loop. In preparation for a given experiment, the reflooding water is first circulated in the water loop in order to adjust the desired conditions. The water mass flow rate is determined via volume flow rate (turbine flowmeter), temperature and pressure measurements. Over the test section itself, a series of pressure difference measurements is carried out. At the top of the test section, the expelled fluid is divided into its two phases in the steam/water separator. The water is collected in the carryover tank, and the accumulated mass is measured via a pressure difference measurement. The separated steam is discharged over the exhaust steam line and a pressure regulating valve, and the steam mass flow rate is again measured over a turbine/pressure/temperature measurement system. A special steam boiler is used for adjusting conditions in the test loop before the start of a reflooding experiment, as well as for maintaining a desired test section pressure.

For all experiments conducted to date at the NEPTUN test facility, the same type of fuel rod simulators has been used. The rods have a 10.72 mm o.d. and a total length of 1940 mm, of which 1680 mm is electrically heated with a cosine-shaped power distribution (see Figure 2). Some constructional details are given in the sectional view also shown in Figure 2. Each heater rod is instrumented with eight, inconel-sheathed, chromel-alumel thermocouples, located at a depth of 0.47 mm from the heater rod surface.

Due to the different thermal behaviour of the electrical rod simulators and actual fuel rods (e.g. gas gap), the NEPTUN results cannot be directly applied to a power reactor core.

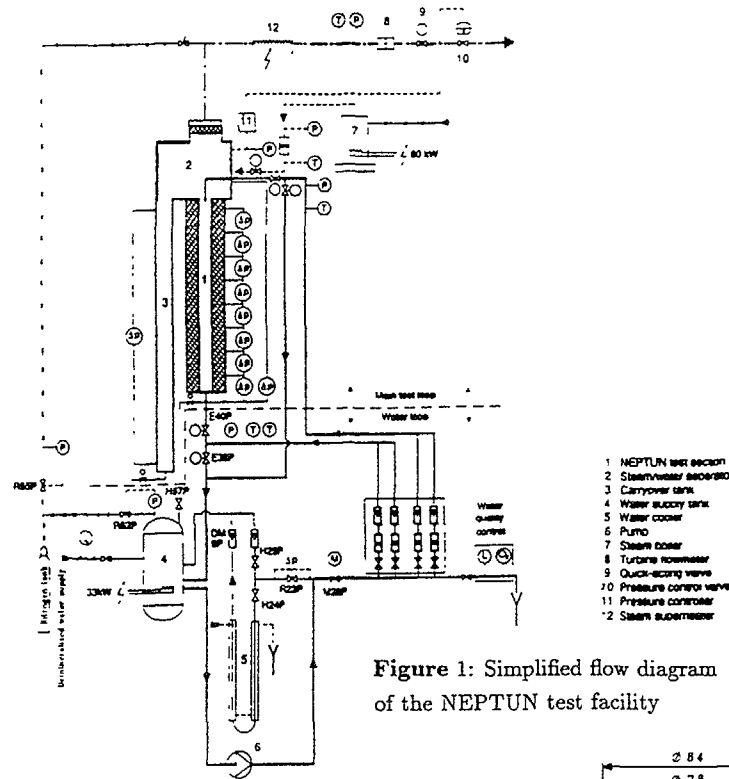


Figure 1: Simplified flow diagram of the NEPTUN test facility

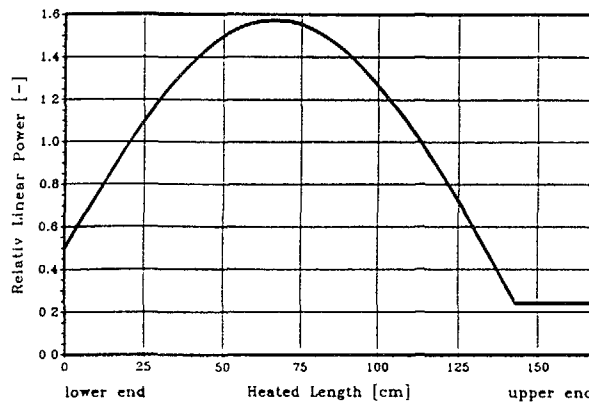


Figure 2: NEPTUN heater rod: power distribution and constructional details

However, a validation of reflooding models on the basis of a range of NEPTUN-type experiments is clearly necessary for thermal-hydraulics codes meant to yield reliable predictions of LWHCR core behaviour.

## 2.2 NEPTUN-III Bundle

There have been several alternative designs proposed for a "homogenous" LWHCR core with pitch-to-diameter ratios for the fuel assemblies ranging from 1.12 up to about 1.30. Largely as a result of the experimental physics investigations, the emphasis has shifted in recent years towards the somewhat wider lattices [2]. The first LWHCR-relevant NEPTUN test bundle (NEPTUN-III), for which the first measurements were made in 1986, has had a relatively low pitch-to-diameter ratio, viz. 1.13.

A horizontal cross-section of the NEPTUN-III test bundle, along with the low heat capacity housing, is shown in Figure 3. The azimuthal positions of the recording thermocouples for the instrumented heater rods are indicated by letters and numbers which, together with the details indicated in the vertical sectional view of Figure 4, give the actual temperature measurement positions. The measurement levels 1 to 8 are exactly the same as used for the pressure difference and fluid temperature measurements (Figure 4). Due to geometrical reasons, the fluid temperature can only be measured between the two outer rings of heater rods. The radial positioning of the rods is fixed by five grid spacers, the vertical positions for which are also indicated in Figure 4.

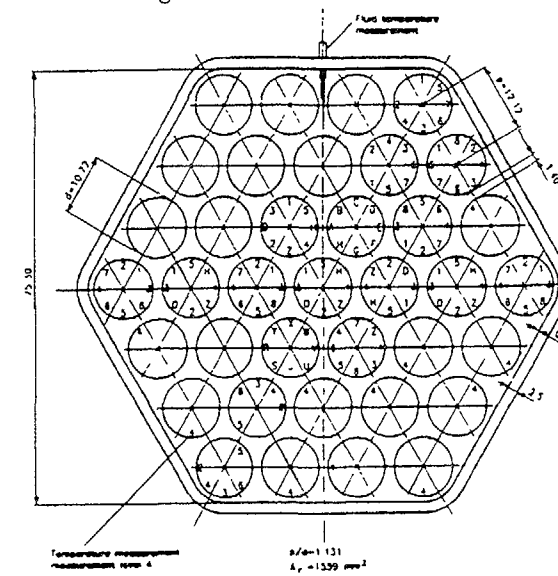


Figure 3: Horizontal cross-section of the NEPTUN-III test section, showing the thermocouple positions

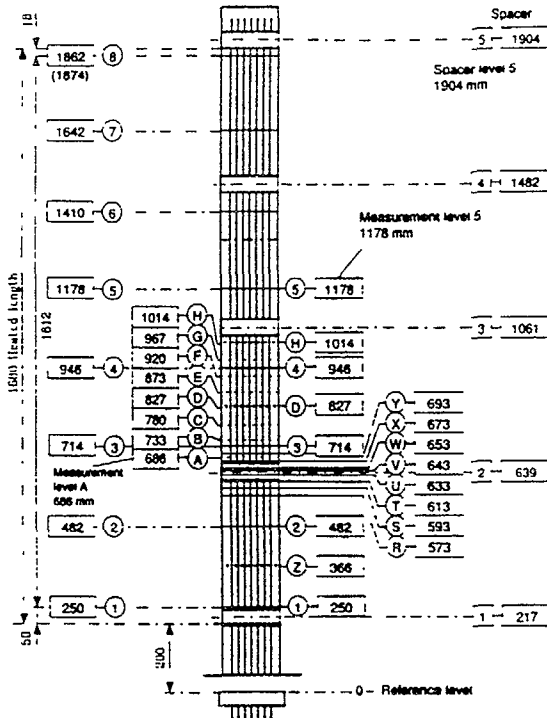


Figure 4: Vertical sectional view of the NEPTUN-III test bundle, showing the spacers and the various measurement levels

### 3 Test Matrix for LWHCR Reflooding Experiments

Considering the planning for the NEPTUN-LWHCR program as a whole, the effects to be studied include those of varying the bundle geometry, the reflooding mode and various thermal-hydraulics parameters. Thus, following the shift in emphasis towards wider lattices, a second LWHCR-representative bundle (NEPTUN-IV), with a pitch-to-diameter ratio of 1.27, is to be investigated later. In order to be able to simulate hot-leg and combined injection – in addition to the cold-leg injection (bottom reflooding) simulated till now – the test section has been modified recently. Investigation of the two other reflooding modes is considered important since these could in practice also occur in an actual reactor core. Together with the variation of thermal-hydraulics parameters, the above aspects result in the test matrix given in Table 1.

Table 1: Test Matrix for the NEPTUN-LWHCR Reflooding Experiments

|                               |   |                             |
|-------------------------------|---|-----------------------------|
| Geometry                      | hexagonal, $p/d = 1.13$ , grid spacers        |                             |
|                               | hexagonal, $p/d = 1.27$ , grid spacers        |                             |
| Reflooding Mode               | forced-feed, bottom reflooding                |                             |
|                               | forced-feed, top reflooding                   |                             |
|                               | combined injection (i.e. from bottom and top) |                             |
| Thermal-hydraulics Parameters | test section pressure                         | 1.0, 4.1, 5.0 bar           |
|                               | rod power                                     | 1.19, 2.45 kW               |
|                               | initial rod temperature                       | 477, 597, 757 °C            |
|                               | flooding rate                                 | 1.5, 2.5., 4.5, 10, 15 cm/s |
|                               | flooding water subcooling                     | 10, 80 °C                   |

Due to the fact that the NEPTUN results cannot be directly applied to a power reactor, all reflooding experiments are carried out as forced-feed experiments and the thermal-hydraulics parameters are, as indicated, chosen over a wide range. This, on the one hand, ensures that the local conditions during reflooding in an actual LWHCR are covered and, on the other hand, provides an adequate data base for reflooding model development in a general sense.

The part of the above NEPTUN-LWHCR test matrix which has been completed is that for the tight ( $p/d = 1.13$ ) bundle with forced-feed, bottom-reflooding conditions. This has involved over 60 individual experiments. The combined-injection and top-reflooding modes are currently being investigated, and the facility will be modified in the second half of 1990 for experiments with the wider ( $p/d = 1.27$ ) bundle.

### 4 Comparisons with Standard PWR Results

To date, a variety of parametric studies has been carried out in forced-feed, bottom-reflooding tests with the NEPTUN-III ( $p/d = 1.13$ ) bundle. Early findings from some of these studies were presented in [1].

The choice of thermal-hydraulics parameters for the NEPTUN-LWHCR program has partly been determined by the need to provide certain direct comparisons of experimental results with those from earlier NEPTUN measurements in standard PWR geometry (square,  $p/d = 1.33$ , grid spacers). Thus, the single such comparison reported in [1] led to

the conclusion that similar flooding water mass flow rates for the two geometries (i.e. about a three times larger flooding velocity in the NEPTUN III case) yield similar bundle quench times. This indicates the important influence of the flooding rate – a result confirmed by the more detailed parametric studies.

The flooding rate which is established in an actual power reactor, however, depends strongly on other factors such as the pressure difference occurring across the core. Accordingly, results from a parameter study are presented here to provide a somewhat more complete comparison for the standard PWR and tight LWHCR geometries. This involves the consideration of quench times, midplane temperatures and pressure differences for the two different sets of NEPTUN experiments. Table 2 gives the thermal-hydraulics parameters and other identification data for the individual experiments for which results are currently compared.

**Table 2 Thermal-Hydraulics Parameters and Other Experiment Identification Data for the Results Compared in Figures 5 to 7**

| Line/<br>Symbol | Geometry | Experiment<br>No | Thermal-hydraulics Parameters |   |                                      |                      |   |
|-----------------|----------|------------------|-------------------------------|---|--------------------------------------|----------------------|---|
|                 |          |                  | Flooding<br>Rate<br>[cm/s]    | Flooding<br>Water<br>Subcooling<br>[°C] | Test<br>Section<br>Pressure<br>[bar] | Rod<br>Power<br>[kW] | Initial<br>Rod Surface<br>Temperature<br>[°C] |
| —●—             | LWHCR    | 6017             | 4.5                           | 80                                      | 4.1                                  | 2.45                 | 597   |
| —+—             | LWHCR    | 6005             | 10                            | 80                                      | 4.1                                  | 2.45                 | 597   |
| —*—             | LWHCR    | 6030             | 15                            | 80                                      | 4.1                                  | 2.45                 | 597   |
| -●-             | PWR      | 5055             | 1.5                           | 80                                      | 4.1                                  | 2.45                 | 597   |
| -+-             | PWR      | 5032             | 2.5                           | 80                                      | 4.1                                  | 2.45                 | 597   |
| -*-             | PWR      | 5054             | 4.5                           | 80                                      | 4.1                                  | 2.45                 | 597   |

Thus, Figure 5 gives the quench front propagation curves for the six experiments – three from NEPTUN-III and three from the standard PWR series. Considering the two cases with the same flooding velocity (viz. Experiment Nos 6017 and 5054, each with 4.5 cm/s), the ratio of the quench times for the two bundles is about 4, i.e. significantly higher than the factor of 3 for the earlier reported comparison [1]. This is a consequence of the different set of thermal-hydraulics parameters currently considered. Figure 5 also shows that the quench time for the LWHCR bundle for the highest flooding rate (15 cm/s) is greater than for the standard PWR case with a flooding velocity of as low as 2.5 cm/s.

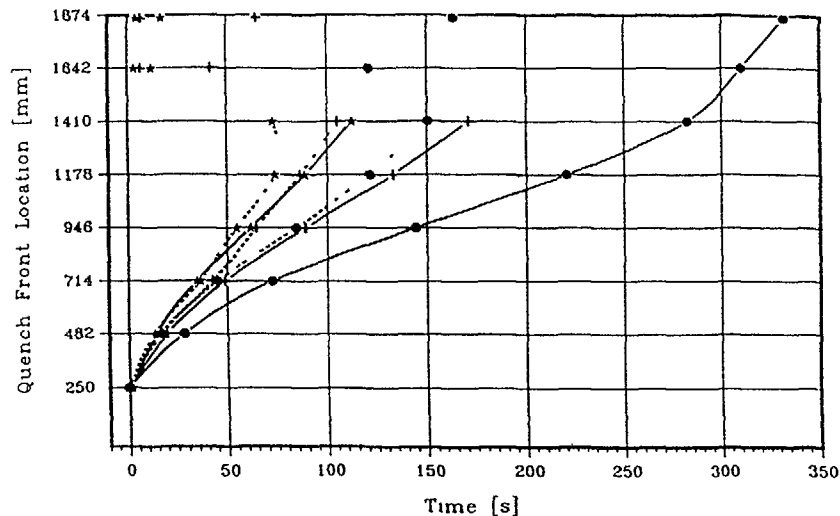


**Figure 5** Quench-front propagation curves for the NEPTUN experiments specified in Table 2

Figure 6 compares the rod-surface temperature profiles at Level 4 (bundle midplane) for the six experiments. Considering again the two experiments with the same flooding rate, there is seen to be a difference of 250 °C in the maximum temperatures reached. For higher flooding rates, the maximum temperature for the LWHCR bundle is strongly reduced. This indicates that Experiment 6017 (see Table 2) was close to the rewetting limit. In fact, with a lower flooding rate of 2.5 cm/s and the same value for the other parameters, quenching of the NEPTUN-III bundle was no longer possible. It should, of course, be noted that the constant rod-power basis for such direct PWR/LWHCR-geometry comparisons is over pessimistic from the LWHCR viewpoint.

For a given set of thermal hydraulics parameters, curves of the type shown in Figure 5 allow an estimate to be made of the flooding rate necessary to achieve rewetting within a certain time. The question as to whether such a flooding rate could be made available in an actual LWHCR core may be addressed qualitatively by comparing measured pressure differences across the NEPTUN-III bundle with corresponding results from the standard PWR geometry experiments. Figure 7 gives such a comparison for the six, currently considered NEPTUN experiments, the measured total pressure differences having been plotted as a function of quench-front location in each case. At the beginning of the reflooding phase, the pressure differences for the NEPTUN-III case are significantly higher than those for the standard-PWR geometry experiments (by up to a factor of about 4). As a general trend, this difference becomes smaller as the quench-front propagates higher. For the two experiments with the same flooding velocity (4.5 cm/s), the pressure difference

for the tight LWHCR geometry is about twice that for the LWR case at the beginning of the experiment. Beyond a quench-front location of about 630 mm, however, the pressure difference in the LWR case actually becomes the greater.

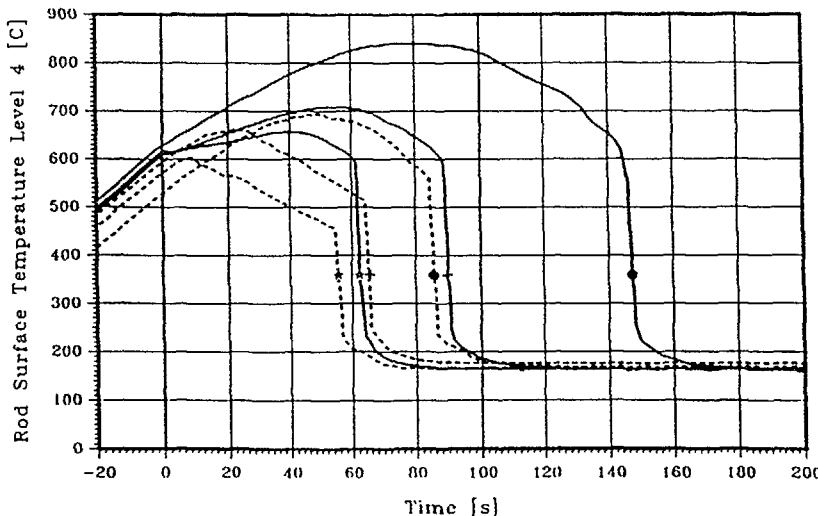
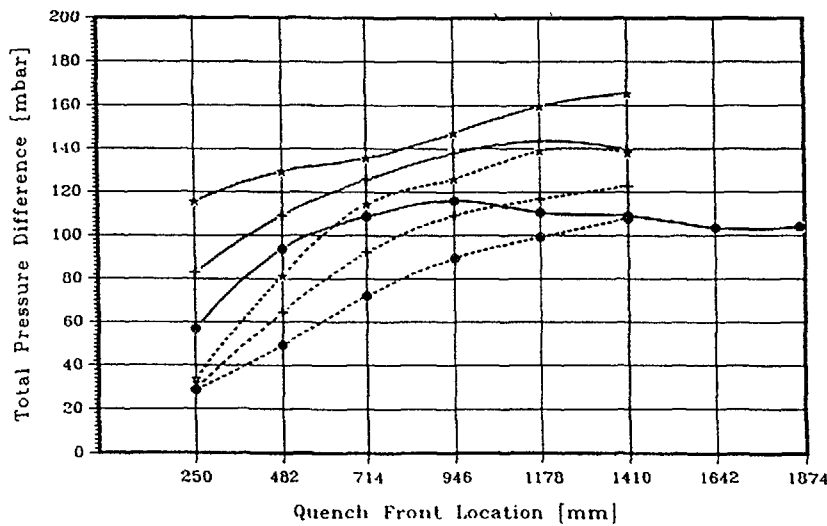


Figure 6: Rod-surface temperature profiles for the NEPTUN experiments specified in Table 2



291 Figure 7: Total pressure differences for the NEPTUN experiments specified in Table 2

## 5 NEPTUN-III Benchmark

As mentioned in the introduction, thermal-hydraulics codes and their data bases have to be validated against the results of reflooding experiments in tight hexagonal bundles before they can be used for reliable predictions for an LWHCR. A first “blind” benchmark exercise was conducted for a reflooding experiment carried out with a very tight ( $p/d = 1.06$ ) bundle in the FLORESTAN test facility at Karlsruhe [3]. The considerable systematic differences between this experiment and the NEPTUN-III series (e.g. type of spacers,  $p/d$ -value, rod-simulator construction and design of the test section’s upper end) have provided ample justification for a similar benchmark exercise to be carried out for one of the NEPTUN-III reflooding tests.

From the wide range of forced-feed, bottom-reflooding experiments available for the  $p/d = 1.13$  bundle, the benchmark was chosen as one with a relatively low flooding rate, high initial rod temperature and large flooding water subcooling. This choice has been intentional since these characteristics are known, from experience, to render code predictions more difficult. The various thermal-hydraulics parameters for the NEPTUN-III benchmark experiment – which may otherwise be considered “reasonably representative” for a tight LWHCR design – are given in Table 3.

Table 3: Effective Values of Thermal-Hydraulics Parameters for the NEPTUN-III Benchmark (Experiment No. 6035)

|                                 |           |
|---------------------------------|-----------|
| Mean test section pressure      | 4.18 bar  |
| Mean rod power                  | 1.20 kW   |
| Initial rod surface temperature | 624 °C    |
| Mean flooding rate              | 2.42 cm/s |
| Mean flooding water subcooling  | 79.8 °C   |

RELAP5/MOD2 and FLUT-FDWR were the two basic codes applied in producing the four different, blind benchmark solutions which are currently compared with experimental results. Two of the code versions used had been modified earlier on the basis of the FLORESTAN test.

Figure 8 compares the rod-surface temperature profiles for Level 5 (just above the mid-plane; see Figure 4). The general trends for all four calculations are an overestimation of the precooling downstream of the quench-front and an underprediction of the quench temperature, leading to too low maximum temperatures and large errors in the rewetting time. These trends were found to be more pronounced in the upper part of the test bundle.

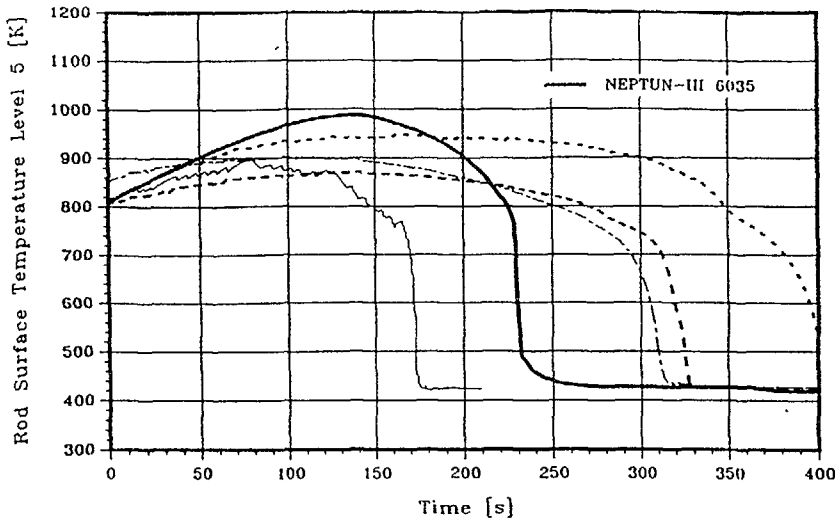


Figure 8: Comparison of experimental and calculated rod surface temperatures (Level 5) for the NEPTUN-III benchmark

The total pressure difference measured across the NEPTUN-III test section is compared with the calculational results in Figure 9. If the large oscillations are ignored, there is seen to be significant underprediction of the pressure difference in each case.

The comparison of expelled water masses is shown in Figure 10, the calculated values being seen to be considerably erroneous. It should be mentioned that the overpredictions in this case were obtained with the standard-version codes, the two partly LWHCR-adapted codes yielding too low values. Finally, Figure 11 compares results for the exhaust steam mass flow rate at the test section's upper end, large oscillations in the calculated values being seen here as well.

The results of the NEPTUN-III benchmark exercise may be summarized as follows. Errors in the blind calculations are generally of similar magnitude as for the FLORESTAN benchmark, although the geometry of the test bundle lies in between those for the very tight FLORESTAN case and a standard PWR. The principal shortcomings of the currently used thermal-hydraulics codes – e.g. in the treatment of droplet generation, interphase drag, heat transfer downstream of the quench-front and spacer effects – seem to be in evidence equally for both benchmark problems. This underlines the need for further code development efforts on the basis of a broader range of experiments.

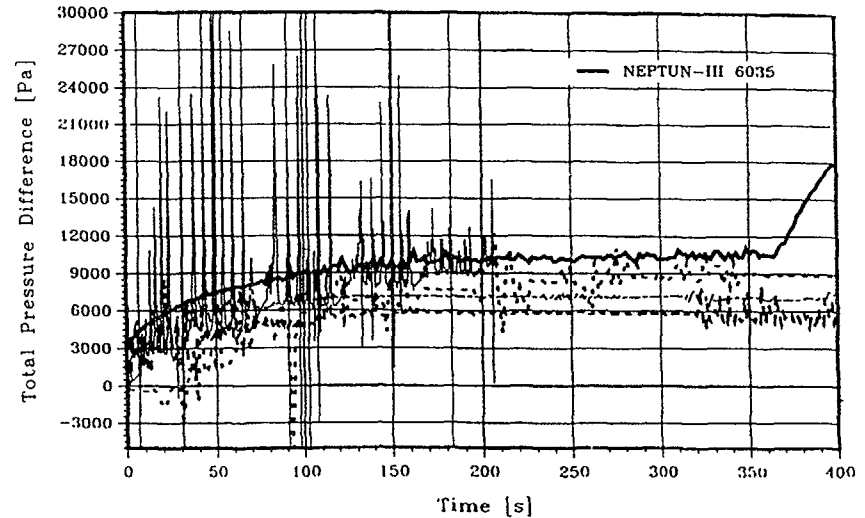


Figure 9: Comparison of experimental and calculated total pressure differences across the test bundle for the NEPTUN-III benchmark

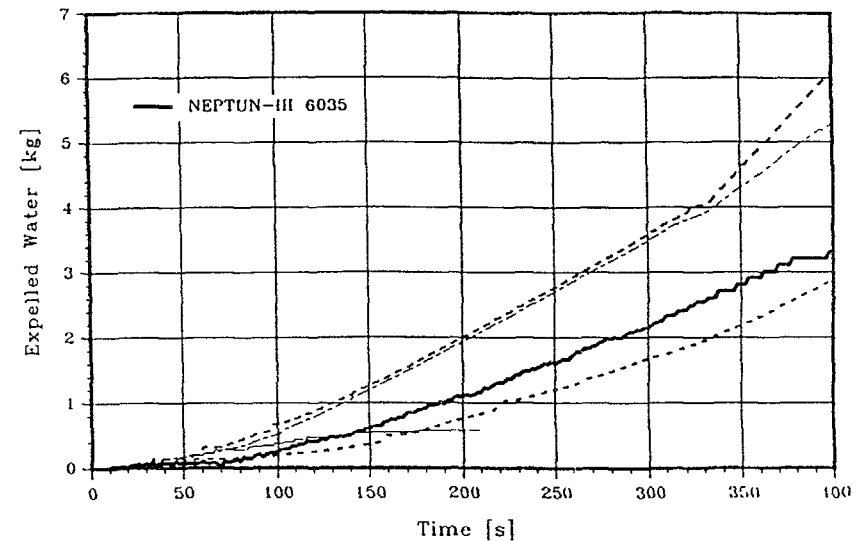


Figure 10: Comparison of experimental and calculated expelled water masses for the NEPTUN-III benchmark

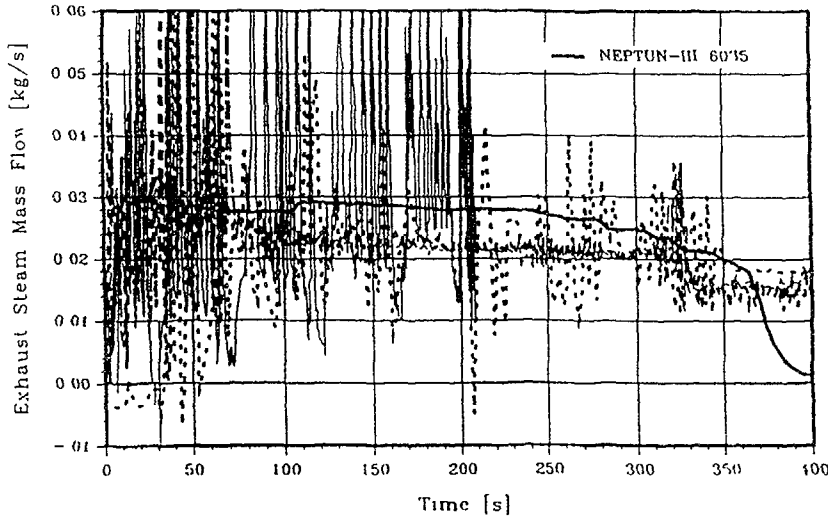


Figure 11: Comparison of experimental and calculated exhaust steam mass flow rates for the NEPTUN-III benchmark

## References

- [1] J. Dreier, G. Analytis, R. Chawla  
"NEPTUN-III Reflooding and Boiloff Experiments with an LWHCR Fuel Bundle Simulator: Experimental Results and Initial Code Assessment Efforts"  
Nucl. Technol. 80(1988)93
- [2] R. Chawla, H.-D. Berger, H. Hager, R. Seiler  
"The PROTEUS Phase II Experiments as Data Base for LWHCR Physics Validation"  
Paper 4.2 at this Meeting
- [3] F.J. Erbacher and K. Wiehr  
"Experimental Investigations on the Reflooding Behaviour of an Advanced Pressurized Water Reactor Tight-Lattice Fuel Rod Bundle in a Loss of Coolant Accident"  
Nucl. Technol. 80(1988)153

## 6 Conclusions

An overview has been given of the NEPTUN-LWHCR program of reflooding experiments – covering two LWHCR geometries, three different reflooding modes and a wide range of thermal-hydraulics parameters. Results from forced-feed, bottom-reflooding experiments in NEPTUN-III have indicated that, in comparison to standard-PWR geometry cases, the maximum rod-surface temperatures for a  $p/d = 1.13$  test bundle are generally higher and the quench times significantly longer. Rewetting for the tight-geometry bundle, however, does occur in all experiments with reasonably LWHCR-representative values for the various thermal-hydraulics parameters.

The results of a calculational benchmark exercise, based on one of the NEPTUN-III experiments, have confirmed that further code development efforts are needed in order to reduce the considerable, current-day uncertainties in LWHCR reflooding predictions.

R&D PROGRAMMES  
(Session 5)

Chairman

**R.H. BROGLI**  
Switzerland

## LESSONS LEARNED FROM THE PWHCR DEVELOPMENT

R. BROGLI

Paul Scherrer Institute,  
Villigen, Switzerland

B. KUCZERA

Kernforschungszentrum Karlsruhe GmbH,  
Karlsruhe, Federal Republic of Germany

H. MOLDASCHL

Siemens AG,  
Unternehmensbereich KWU,  
Erlangen, Federal Republic of Germany

W. OLDEKOP

Technische Universität Braunschweig,  
Braunschweig, Federal Republic of Germany

### Abstract

The MOX-fuelled, tight lattice LWR-concepts like the German/Swiss FDWR (Fortgeschritten Druckwasserreaktor) as well as the French RSM (Reacteur Sous-Moderé) are supposed to make good use of plutonium and to save uranium resources while utilizing the standard LWR technology. Despite the fact that implementation of PWR-HCR is some years away early resolution of the specific R&D is of highest importance in order to be able to maintain an acceptable implementation schedule in todays environment of very strict licensing. Recognizing this and directing the development towards a flexible fuel utilization is a prudent way allowing to adapt the fuel operations to the desired conditions.

Thus Siemens/KWU, Karlsruhe Nuclear Research Center (KfK), Paul Scherrer Institute (PSI) and Technical University of Braunschweig as an associated member joined efforts to solve the pertinent open technical questions. Each organization was leading the task-forces where it has its strength. This mode of cooperation for the development of the PWR-HCR proved to be very successful so far. During the conceptual design work and the related research to acquire the necessary data base for our PWR-HCR concept development we got a lot of valuable experience.

The most enjoyable aspect of the PWR-HCR development was the successful scientific work and lessons learned through the experiments and their analytical evaluations:

- in the reactor-physics area the importance of the epithermal spectra was recognized. With the validation of the PROTEUS experiments the calculational methods were considerably improved through an adapted group structure and a better resonance shielding
- core physics problems such as reactivity compensation and power density optimization can be solved almost classically for intermediate pin lattices
- the reflood experiment and the CHF experiments showed that reflooding as well as stationary cooling are quite feasible despite of the rather narrow dimensions
- the design codes were adapted and checked against critical experiments and theoretical benchmark tests to provide a calculational basis for neutronic and thermalhydraulic design of the core
- the first results for mechanical design were very encouraging since among patents directly related to the HCR design a lot of spin-offs were detected which might be also of some advantage for classical reactors

By this the essential features of the first design stage of the PWR-HCR, the socalled PWR-C1 were defined to be the basis for all further investigations which will be performed e.g. by harmonizing known concepts for an advanced and fuel saving core design. Such harmonisation would also have to address the new safety features that are being discussed for thermal LWR.

The key lesson learned from the cooperation is that interdisciplinary R+D work of high sophistication can still contribute substantially to concepts like the HCR that build largely on proven technology.

---

### 1. Introduction

The last years were and the next few years may be in terms of orders for new nuclear power plants rather dismal. The reasons for this are the actual overcapacity of electricity generation and the lacking public acceptance in many countries. But with the worldwide growing electricity demand new electrical capacity will have to be established. Whether this additional amount will be nuclear or not, of course will depend on public's acceptance and on the utilities with respect to economics:

- the public will accept the nuclear option only if people are aware, that accident probabilities are very low and severe consequences to the environment can be excluded

- the utilities will ask for safe, reliable and economic plants with a reasonable long lifetime.

The first point would imply that the new plants should demonstrate a higher degree of safety. Since essential features of those concepts might hold till the middle of the next century, all further improvements of safety features for standard LWRs will also be relevant for next generation reactors.

Although any shortages of fuel cannot be foreseen today, in only a few decades cheap uranium might well be exhausted and some utility decision makers may select a power plant which has reasonable fuel cycle cost for various conceivable fuel availabilities.

Both boundary conditions ask for plants reliable but safer as before, able to operate with various types of fuel like UO<sub>2</sub> or PuO<sub>2</sub>, in a high or low conversion mode: energy autarky aspects and energy cost ask for a high conversion rate, for high reload a burnup, a large burnup cycle potential and last not least a high degree of standardization.

A few years ago some of the reactor designers looked for possibilities to activate standard LWR's potentials. This resulted in an advanced but semi-classical design, Light Water High Converter Reactor (LWHCR) / 1, 2 /. It seemed to be clear that the future role of nuclear power and the need to balance energy resources will enhance those trends of LWR improvements. Thus several MOX-fuelled, tight lattice LWR-concepts were designed like the German/Swiss FDWR (Fortgeschrittener Druckwasserreaktor / 3-10 /) as well as the French RSM (Reacteur Sous-Moderé / 11 /), using well proven and highly standardized LWR technology and supposed to use plutonium in order to save uranium resources.

Despite the fact that implementation of PWR-HCR is some years away, early resolution of the specific R&D is of high importance in order to maintain an acceptable implementation schedule in todays environment of very strict licensing. Recognizing this and directing the development toward a flexible fuel utilization is an attractive way allowing to adapt the fuel operations to the desired conditions.

## 2. The Cooperation Goals and the Cooperation Program

To meet the goal of designing a reliable High Converter concept in a fairly good time, Siemens KWU, the Karlsruhe Nuclear Research Center (KfK), the Paul Scherrer Institute (PSI) and the Technical University of Braunschweig (TUBS) as an associated member joined efforts to solve the pertinent open technical and safety related questions. Each organization was leading task-forces of high expertise.

After an initial period of investigations which were directed to a very tight lattice to sharpen the design tools mainly of physics and thermal-hydraulics, the near term objective was defined to be a medium size lattice. A short development period and a low cost-benefit ratio can be gained if one relies to the greatest possible extent on well-known technology. The PWHCR is a concept derived directly from the German Convoy PWR. It can be adapted to utilities' needs by different stages of development, the starting point being defined Convoy's moderation ratio VMF = 2.

The generic goal of our joint development was to show the licensability of a HCR core with a much tighter lattice than is realized in the standard light water reactor. Since the technical feasibility of a given HCR core design rests on several key questions related to reactor physics and thermal-hydraulics behaviour under normal and accident conditions, a number of experiments and the theoretical analyses of the results were necessary. Within the joint cooperation the partners have been conducting, on a complementary basis an R&D program, the main items of which are summarized in table 1.

## 3. Theoretical and Experimental Cooperation Findings

### 3.1 Neutron Physics

Defining the main parameters like moderation ratio and enrichment one has to obey the requirements of inherent safety which is mainly based on nuclear design. Following the generic parametric design stages, detailed investigations were performed with the design codes SPECTRA, established by Technical University of Braunschweig, AARE from the Paul Scherrer Institute, Wurenlingen, CASMO at Siemens KWU and KAPER4 at the Nuclear Research Center Karlsruhe. Considerable progress was made by the creation of suitable multigroup cross section sets from the nuclear data libraries KEDAK-4, ENDF/B-V and JEF-1. Additional investigations were made by the University of Stuttgart and the University of Lowell (Mass.). Extensive core design and burnup calculations were performed with the KfK KARBUS code and the standard design and burnup code MEDIUM of KWU. A hexagonal standard design code HEXMED compatible to MEDIUM, based on the same solution technique is under test.

Due to the fact that for an advanced tight lattice design with fairly high fissile enrichment the effective void coefficient is expected to be markedly less negative than in current-day LWRs, the application of a 3D-dynamics code is a matter of urgent necessity. Therefore KWU developed the coupled neutron kinetics (thermal-hydraulics) program system HEXTIME, based on the well proven code system PANBOX, which allows 3D steady state and transient full core as well as subchannel analyses to be performed.

**Table 1: Development Items and Results**

| Technical Key Area     | Main Activity  | Institution         | Preliminary Results   |
|------------------------|--|---------------------|---|
| Neutron physics        | measurements of reaction rates                                 | PSI, TUBS, KfK, KWU | <ul style="list-style-type: none"> <li>- void coefficient negative for PWHCR lattice</li> </ul>                   |
|                        | code verification  | KfK, TUBS KWU, PSI  | <ul style="list-style-type: none"> <li>- substantial uncertainty reduction</li> </ul>                             |
| Thermal-hydraulics     | high pressure experiments                                      | KfK, KWU, TUBS      | <ul style="list-style-type: none"> <li>- coolability guaranteed</li> <li>- detailed analysis necessary</li> </ul> |
| Emergency core cooling | reflooding experiments   | KfK, PSI            | <ul style="list-style-type: none"> <li>- emergency core coolability for VMF &gt; 1.5 verified</li> </ul>          |
| Mechanical design      | fuel assembly core internals core assemblies shut down systems | KWU                 | <ul style="list-style-type: none"> <li>- generic problems solved</li> </ul>                                       |
| Material behaviour     | irradiation experiments  | KWU                 | <ul style="list-style-type: none"> <li>- under irradiation</li> </ul>   |

A benchmark of tight lattice cell burnup calculation was approved at the 29th meeting of the NEACRP September 1986, to identify the problems of data and calculational methods. Fifteen organisations from eight countries submitted twenty sets of benchmark results / 12 /, which were helpful to clarify some of HCR's specific neutron physics problems.

The technical feasibility of a given PWHCR design rests on several key questions mainly related to reactor physics under normal and accident conditions. The void reactivity behaviour between nominal and highly voided conditions after a LOCA accident influences crucially the inherent safety behaviour of a reactor core. To provide experimental data for testing neutron physics codes and cross-section libraries employed for HCR studies, many integral neutron physics measurements representative for tight  $\text{PuO}_2/\text{UO}_2$  lattices were carried out at the PROTEUS zero power facility.

### 3.2 Thermal-hydraulics

An important thermohydraulic tool has been provided by the KfK code HADA, which has been applied extensively for core design parameter investigations. With Braunschweig's hydraulic flow distribution code HALLO the hydraulic properties of the PWHCR circuit components can be formulated jointly with the detailed PWHCR core structure, whereas subchannel effects can be treated with the well-known COBRA-IV code. The published sets of coefficients were checked and supplemented by results of KWU's critical heat flux experiments at the  $\text{H}_2\text{O}$  high pressure facility in Karlstein and at KfK's FREON facility in Karlsruhe. The result, the code system, COBRA-TUBS, thoroughly verified by application of FREON-R12 CHF results to CHF results of a water-cooled high pressure experiment has a lot of important properties. Additional codes to be mentioned here are the VELASCO-TUBS code for the hot-spot analysis, based on a turbulence model and supported by the comprehensive empirical material of KfK, and the VANTACY code, devised for design purposes which ask for a rapid solution of the momentum equations.

### 3.3 Emergency Core Cooling

KfK's FLORESTAN test loop is used for reflooding bundle tests at forced feed and gravity feed conditions. PSI's NEPTUN test facility, used for investigation of tight and medium-tight rod bundles was originally designed and previously used to study reflooding heat transfer and two-phase flow phenomena in standard PWR lattices. The facility can also be used for carrying out low-pressure boiloff experiments. In complementary theoretical activities a special tight lattice version of the FLUT code has been provided and applied for corresponding LOCA analyses.

Boiloff experiments, performed for the standard LWR geometry at NEPTUN were analyzed in the past by TRAC-BD 1/MOD 1 and RELAP 5/MOD 2/CY 36.02. It was felt that the analysis of high pressure and boiloff experiments with HCR geometry would provide a valuable check of applicability of the new interfacial shear correlation to bundles with much smaller hydraulic diameter. For a definite answer concerning e.g. the discrepancies between the predicted and the measured liquid carryover, a careful analysis of a number of boiloff experiments is required, which could be the basis for an international cooperation.

### 4. The Results

Our mode of cooperation for the joint development of the PWHCR proved to be very successful: during the conceptual design work and the related research to acquire the necessary

data base for the concept development we got a lot of valuable experience, which would be a good basis for any continuation. We would like to sum up as follows.

- in the reactor-physics area the importance of a refined modeling of the epithermal spectra was recognized. With the validation of the PROTEUS experiments the calculational methods were considerably improved through an adapted group structure and a better treatment of resonance shielding; theoretical uncertainty was substantially reduced
- the reflood experiments and the CHF experiments have demonstrated that reflooding as well as stationary cooling are quite feasible in spite of the rather narrow fuel pin lattice
- the core design codes were adapted and checked against critical experiments and theoretical benchmark test to provide a calculational basis for neutronic and thermal-hydraulic design of the core
- the first results for mechanical design were very encouraging since among patents directly related to the PWHCR design a lot of spin-offs were detected which might be also of a certain advantage for classical reactors
- core design problems such as reactivity compensation and power density optimization can be solved in an almost classical way for medium-tight pin lattices
- certain advantages of the hexagonal subassembly geometry were quantified and checked.

By the initial comprehensive analyses of neutron-physics and thermal-hydraulic properties of various PWHCR geometries we could jointly confirm that there is no conflict between the different objectives "high conversion", "high reload burnup", "large cycle length potential" and the overall requirements for negative reactivity feedback and stationary and transient coolability of the core.

The results of the experimental and theoretical investigations and the evaluation activities preceding the KWU High Converter Reactor development performed in our cooperation pointed out that a core concept with a topologically uniform core, the socalled "PWHCR" (former PWR-C1) as the first HCR-design stage has the potential for the desired flexibility with regard to fuel utilization. Based on this concept one has the choice of putting the main emphasis either on progressive fuel saving or low fuel cycle cost. This goal is attainable by choosing a hexagonal fuel rod lattice enabling a fairly small moderation ratio. The main technical parameters of the PWHCR design are:

#### Fuel Assembly Design Parameters

|  |   |
|--|---|
| - Fuel rod lattice pitch                   | 11.8 mm                                 |
| - Cladding outside diameter                | 9.5 mm                                  |
| - Pitch-to-diameter ratio                  | 1.24                                    |
| - Cladding material                        | Zry                                     |
| - Cladding wall thickness                  | 0.6 mm                                  |
| - Volumetric moderation (VMF)              | approx. 1.2                             |
| - Fuel assembly (FA) distance across flats | 200 mm                                  |
| - Spacer type                              | grid                                    |
| - Number of fuel rods per assembly         | 247                                     |
| - Active core height                       | 300 cm                                  |
| - Fuel                                     | UO <sub>2</sub> /PuO <sub>2</sub> (MOX) |
| - Maximum fissile Pu enrichment            | 7-8 w/o                                 |
| - Maximum average discharge burnup         | 55-60 MWd/kg                            |

#### Core Design Parameters

|  |          |
|--|----------|
| - Thermal output                                 | 3765 MW  |
| - Average linear heat generation rate            | 146 W/cm |
| - Average volumetric power density               | 105 kW/l |
| - Total number of fuel assemblies                | 349      |
| - Number of control assembly drives              | 85       |
| - Number of FAs that can hold a control assembly | 127      |

The PWHCR is an excellent link between the LWR and the fast breeder generation. With the accumulation of Pu, better use of it in HCRs will provide sufficient fuel for the next century. The extensive theoretical and experimental investigation of the different HCR problems and tasks has been performed with a very good efficiency in the cooperation with the partners / 5-9 /.

#### 5. Outlook on Further Activities

##### Physics

The investigations actually performed indicated that a moderator-to-fuel ratio somewhat larger than that of the tight lattice which was originally considered, would be advantageous with respect to increased safety margins. However, since conversion ratio increases exponentially with reduction of moderation ratio, it will be an economic challenge to know the real physical margins available.

##### Thermal-hydraulic

Thermal-hydraulic and neutron-physical core design are closely coupled together via power distribution, pressure drop and heat

transfer at a defined total H<sub>2</sub>O flow rate. They all strongly depend on the configuration of the core and the fuel assembly type. Principally the thermal-hydraulic analysis of an HCR core has to solve the problems on three consecutive levels. Due to the advantages of hexagonal geometry there will be a large economic and safety incentive for further development.

#### Emergency core cooling

Blind code predictions of gravity feed test with a very tight lattice showed that most thermal-hydraulic computer codes do not adequately predict the reflooding behaviour of this type of bundle. Although a HCR core will be shorter than a normal PWR core and therefore it will generally be easier to reflood the reactor after LOCA, the hydraulic resistance of the HCR core will be always higher than that of a conventional PWR, and this will, to a certain amount outweigh the advantage.

Thus for a definite answer concerning e.g. the discrepancies between the predicted and the measure liquid carryover, a careful analysis of a number of boiloff experiments and representative transient blowdown tests to determine the cladding temperatures at end of blowdown and start of reflooding, also the investigation of the effects of the hot leg injection are required, which would justify a more intensive cooperation on a broader international basis.

#### 6. Conclusion

The analytical and experimental work to evaluate the conceptual idea of a higher converting MOX PWR core showed that

- within certain limits such a design is feasible from a safety design and operational standpoint.
- the phenomena within a tight lattice MOX core are understood and can accurately be calculated.
- the potential for the LWR-evolution can be expanded into an area of flexible and better fuel utilization.

The scientific achievements to enlarge the knowledge basis for LWR-systems was very successful and this applies the possibility to realize a reactor with improved safety and fuel flexibility.

#### REFERENCES

- / 1 / M. C. Edlund  
Physics of the Uranium-Plutonium Fuel Cycle in Pressurized Water Reactors  
Trans. Am. Nucl. Soc., 24, 508 (1976)
- / 2 / H. H. Hennies, H. Markl  
Überlegungen zur Modifizierbarkeit eines LWR im Hinblick auf eine bessere Uranausnutzung  
Proc. Jahrestagung Kerntechnik 1980, p. 853 (1980)  
(in German)
- / 3 / W. Oldekop, H.-D. Berger, W. Zeggel  
General Features of Advanced Pressurized Water Reactors with Improved Fuel Utilization  
Nucl. Technol. 59 (1982) 212
- / 4 / R. Brogli, B. Kuczera, H. Moldaschl  
Technical Feasibility Investigations Related to Advanced Tight-Lattice Cores in Standard PWRs  
Conference Internationale Sur le Developments en Physique de Reacteurs et Methodes de Calcul, 27-30 Avril 1987, Paris, Proc. Vol. 1, 231
- / 5 / H. Moldaschl, R. Brogli, B. Kuczera  
Light Water High Converter Reactor - the LWR Technology of the late 90s  
Int. Conf. on Nuclear Power Performance and Safety, Vienna, Austria, September 28 - October 2, 1987
- / 6 / H. Moldaschl, W. Zeggel  
Gradual Commercialization of Advanced PWR Tight Lattice Cores  
ANS Winter Meeting, Los Angeles, November 15 - 19, 1987  
TANSAO 55 1-760 (1987) 126-127
- / 7 / R. Brogli, C. Goetzmann, B. Kuczera  
Research and Development Efforts for the Light Water High Conversion Reactor  
Nucl. Technol. 80 (1988) 61
- / 8 / H. Markl, C. Goetzmann, H. Moldaschl  
KWU's High Conversion Reactor Concept - An Economical Evolution of Modern Pressurized Water Reactor Technology Toward Improved Uranium Ore Utilization  
Nucl. Technol. 80 (1988) 65
- / 9 / H. Moldaschl, R. Chawla  
Could Even High Conversion PWRs be "Inherently Safe"?  
Proc. Int. Top. Meeting on Safety of Next Generation Power Reactors. Seattle, Washington, May 1-5, 1988

302 / 10 / H. Moldaschl, R. Brogli, B. Kuczera  
Status and Prospects of the Cooperative KWU High  
Converter Development 1989  
ICENES'89, Karlsruhe, July 1989

/ 11 / J. P. Millot  
Considérations sur les réacteurs PWR sous-modére  
RGN-Actualités, 4, 405 (1982)

/ 12 / H. Akie, Y. Ishiguro, H. Takano  
Summary Report on the International Comparison of  
NEACRP Burnup Benchmark Calculations for High  
Conversion Light Water Reactor Lattices  
Oct. 1988, JAERI-M 88-200, NEACRP-L-309

## OVERVIEW OF BELGIAN ACTIVITIES IN THE FRAME OF IMPROVED FUEL UTILIZATION AND HIGH CONVERSION REACTORS

G. MINSART  
SCK/CEN,  
Mol, Belgium

### Abstract

Since many years, Belgium has been actively involved in R & D related to improved fuel utilization in nuclear reactors.

In the frame of water reactors, a Belgian spectral shift project proposed in the early sixties has been supported by UKAEA and its development, jointly performed by SCK/CEN, BN and UKAEA Winfrith and Risley, has led to a critical experiment realized at Mol in the VENUS facility, followed by the successfull power operation of the VULCAIN reactor in the BR3 installation, also at Mol.

Another way to improve the fuel utilization is to recycle the plutonium in PWR's. A large series of benchmark experiments involving mixed-oxide fuels have been conducted in the VENUS facility, enabling the core designers to improve and calibrate their calculational procedures.

Numerous types of fuels (MOX fuels, burnable poisoned fuels, advanced concepts) have been irradiated in the BR3 (PWR) reactor by Belgian and foreign manufacturers, and extensive testing has been made on these fuels, including power cycling in the materials testing reactor BR2.

The possibility of using the VENUS facility for experiments related to "advanced PWR" (tight lattices) has been also envisaged. Up to now, preliminary orientation studies have been performed; lattices with rather low water-to-fuel ratios could be realized, but at the expense of new supporting grids and fuel pins having higher enrichments similar to those considered for the power reactors.

The materials testing reactor BR2 provides unique facilities for irradiating LWR, ALWR and FBR fuel bundles in representative conditions (neutron spectrum, pressure, temperature, power density, coolant thermohydraulics, ...) in steady-state as well as in transient regimes, loops of several types and sizes are available or can be tailored to the experimenter's needs.

Finally, activities related to the fast breeders, and more particularly to FBR fuels, should also be mentioned : development of MOX fuel and of improved canning materials (ferritic steels, ...), extensive fuel and cladding qualification and testing (irradiations in BR2), physics-dosimetry and safety studies, ...

---

Since many years, Belgium has been actively involved in R & D related to improved fuel utilization in nuclear reactors; this work was related to both fast breeders and thermal reactors, fuel composition and fabrication, cladding materials, testing of reactor components, ...

#### The VULCAIN concept

In the early sixties, the Belgian spectral shift project VULCAIN has been proposed. The main objective was to realize core loadings having a large excess reactivity controlled by spectral variation; in this way, the reactor can be operated for long periods of time without reshuffling or reloading, and the way of controlling the excess of reactivity reduces parasitic neutron absorptions and enhances captures in fertile  $^{238}\text{U}$ , leading to improved conversion factor. The development of the VULCAIN project has been jointly performed by SCK/CEN, Belgonucleaire and UKAEA Winfrith and Risley. The VULCAIN core was made of hexagonal assemblies containing each 37 fuel pins (triangular pitch), of inner moderator zones and tubular safety and control rods acting as neutron flux traps when they were inserted. The spectral shift is realized by a mixture of light and heavy water : at the start of life, nearly pure heavy water is used; it is progressively diluted by light water when the burnup proceeds and the core life ends with pure light water.

This concept has been extensively analysed both theoretically and experimentally : near to the BR1 reactor at Mol a critical facility has been built; the VENUS zero power installation, where a full-size VULCAIN core has been realized. Hot conditions were partially simulated by water density reduction (in several proportions). Numerous core parameters were measured for several  $\text{H}_2\text{O}/\text{D}_2\text{O}$  proportions; the same core conditions were computed and the agreement between calculations and experiments was good; on that basis, studies needed for power operation were actively pursued, with an important contribution by UKAEA : thermohydraulics problems, burnout limit, Doppler effect, ... were analysed; at the end of the zero power measurement campaign in VENUS, the fuel has been transferred to BR3 for the power demonstration. In the meantime, the BR3 internal pieces had been adapted to the VULCAIN design.

The VULCAIN core has been successfully operated in power : during two years (nov.66 - nov.68), it produced  $160 \cdot 10^6$  KWh electricity and its availability factor reached 90 %.

One should notice that the VULCAIN core operated in BR3 contained already one experimental MOX fuel assembly.

#### MOX fuel fabrication

The MOX fuel irradiated in VULCAIN had been produced by a joint team Belgonucleaire - SCK/CEN installed in MOL, who developed fabrication techniques for mixed oxide fuels. Several fabrication processes were investigated and that activity resulted in a small pilot installation in the Pu-lab of the SCK/CEN. Mox fuels produced in this way were tested in many different conditions (power density, temperature and pressure, burnup limit, ...) both in power reactors and in BR2 experimental loops. The next step has been the installation by Belgonucleaire of a Mox fuel fabrication plant in DESSEL, near to MOL. The development of improved fabrication techniques has been pursued and the DESSEL plant has already produced a large amount of Mox fuels for several reactors, including fast breeders.

#### Pu recycling studies

Recycling the plutonium in PWR's is a way to improve the fuel utilization. Be able to produce high quality Mox fuel rods and assemblies is not sufficient : one should also demonstrate his ability to correctly compute the nuclear characteristics of that fuel and the evolution during irradiation. A large series of benchmark experiments involving mixed-oxide fuels have thus been conducted in the VENUS facility, enabling the core designers to improve and calibrate their calculational procedures. An interesting particularity of the VENUS facility is its fast dump used as safety shut down; in this way, it is possible to realize very clean core loadings, without any local perturbation required for safety reasons. A variety of local discontinuities or boundaries were investigated, and the attention was mainly focused on the detailed fission density distribution and some reactivity effects.

The first large Pu-recycling programme in VENUS started in 1967; it was a direct collaboration between SCK/CEN, who performed the measurements, and Belgonucleaire, who made the calculations. The checked (and/or improved) computational procedures were then applied to the analysis of the Mox fuel evolution in power reactors. A new Pu-recycling experimental programme in VENUS has just been started : the VIP programme will be presented at the PHYSOR-90 meeting, end of April 1990 in Marseille, France [1].

#### Fuel testing

The Mox fuels, produced first by the joint team BN-SCK/CEN and later by the BN plant at Dessel, have been extensively tested and their good performance has been well established both for boiling and for pressurized water reactors on one hand, and for fast breeders on the other hand. R&D work on Mox fuels for LWR's is being pursued [2].

The BR3 (PWR) reactor has been a particularly useful and efficient tool for testing new fuel concepts under realistic conditions. Numerous types of fuels (Mox fuels, burnable poisoned fuels, advanced concepts) produced by Belgian and foreign manufacturers have been irradiated in the BR3 during the many years of operation after the VULCAIN core (see table 1). An typical BR3 core loading is illustrated on Fig. 1. Advantage has been taken of the vicinity of the materials testing reactor BR2 : combined irradiations alternating normal operation in BR3 and power cycling in the loops of the BR2 allowed to check the ability of fuel rods to withstand power transients after significant irradiation levels. Indeed, the materials testing reactor BR2 provides unique facilities for irradiating LWR, ALWR and FBR fuel bundles in representative conditions (neutron spectrum, pressure, temperature, power density, coolant thermohydraulics, ...) in steady-state as well as in transient regimes. Loops of several types and sizes are available or can be tailored to the experimenter's needs. Fig. 2 shows a cross section of the BR2 matrix : capsules and loops can be located in standard channels and/or in one of the five large channels; examples of such loops are shown on fig. 3 to 6.

In addition to these irradiation capabilities, a series of post-irradiation examinations can be performed at Mol, thus enabling the experimenters to obtain an additional set of information useful for their analysis.

#### APWR orientation studies

The possibility of using the VENUS facility for performing critical experiments related to "advanced PWR" (tight lattices) has been investigated. At the end of 1985, at least two concepts were examined in several countries, and mainly in France :

- spectral variation by exchange or progressive extraction of pins (fuel and/or poison rods),

- highly undermoderated lattices enhancing the conversion factor.

In fact, the VULCAIN project was already focused on the same idea : the spectral variation was obtained by changing the ratio  $H_2O/D_2O$  of the moderator. The orientation studies performed at the SCK/CEN in 1985 addressed the other concept : a strong reduction of the moderating ratio  $V_{H2O}/V_{fuel}$  in the lattice. Several ways allow to attain in VENUS the desired low water to fuel ratios :

- designing new supporting grids, with a small pitch in triangular geometry; simultaneously, other fuel pin diameters could be considered

- using the presently available grids and using aluminium microtubes and/or microrods to remove part of the water in the lattice (square pitch); according to the number and size of these Al pieces, the ratio water to fuel can be varied, enabling thus to investigate several values for that parameter

- combining new triangular pitch grids and Al microtubes can extend the range of possible water to fuel ratios

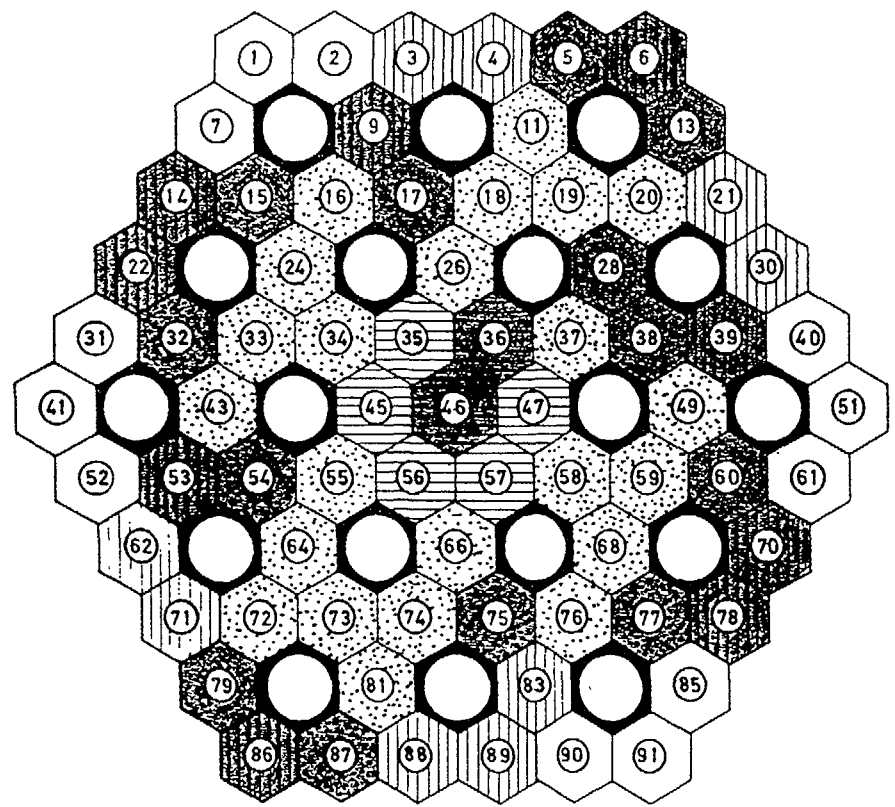
In all cases, it is useful to have long fuel pins ( $H_{act} = 1 \text{ m}$ ) in order to reduce the axial leakage and to attain criticality with a core loading compatible with the limited size of the VENUS vessel, possibly, an outer feeding zone would be used, and/or higher fuel enrichments could be required. For such applications, Mox fuel is very convenient and Pu contents up to 10 to 12 % have been envisaged.

TABLE 1 : THE ELEVEN BR3 OPERATION CAMPAIGNS (1962 - 1987)

| Operation period        | Electrical energy in millions of kWh |                            | EFPH<br>(1) | Availability factor of the plant % (2) | Main characteristics   | Denomination of the successive cores |
|-------------------------|--------------------------------------|----------------------------|-------------|--|--|--------------------------------------|
|                         | Gross (produced)                     | Net (provided to the grid) |             |  |  |                                      |
| 10.10.62 up to 21.08.63 | 45.8                                 | 40.8                       | 4008        | 62                                     | Oxide core, stainless steel cladded, cooled and moderated by light water, control by rods (one plutonium enriched fuel assembly in core 1B).   | Core BR3/1A                          |
| 02.12.63 up to 31.07.64 | 55.5                                 | 51.1                       | 4848        | 90                                     |  | Core BR3/1B                          |
| 29.11.66 up to 18.11.68 | 159.9                                | 142.9                      | 13944       | 90                                     | Oxide core, stainless steel cladded, cooled and moderated by H <sub>2</sub> O/D <sub>2</sub> O mixture-spectral shift reactor (Vulcain project); one plutonium enriched fuel assembly. | Core BR3/2                           |
| 31.07.69 up to 20.12.70 | 79.2                                 | 67.1                       | 7339        | 91                                     | Oxide core, stainless steel and Zircaloy cladded, cooled and moderated by borated light water; three plutonium enriched fuel assemblies.   | Core BR3/2B                          |
| 25.09.72 up to 11.01.74 | 89.4                                 | 78.7                       | 7944        | 80                                     | Oxide core, Zircaloy cladded, cooled and moderated by borated light water; 24 (3A) and 22 (3B) plutonium enriched assemblies from a total of 73 assemblies.                            | Core BR3/3A                          |
| 02.07.74 up to 27.06.75 | 47.9                                 | 40.2                       | 4416        | 76                                     |  | Core BR3/3B                          |
| 15.07.76 up to 15.04.78 | 132.0                                | 117.1                      | 11916       | 96                                     | Oxide core, Zircaloy cladded, cooled and moderated by borated light water.   | Core BR3/4A                          |
| 22.06.79 up to 26.09.80 | 97.5                                 | 87.2                       | 8663        | 86                                     |  | Core BR3/4B                          |
| 21.09.81 up to 01.04.83 | 98.0                                 | 86.3                       | 8641        | 90                                     | Dismountable fuel assemblies; UO <sub>2</sub> ,  | Core BR3/4C                          |
| 13.07.84 up to 11.11.85 | 89.5                                 | 79.2                       | 8008        | 85                                     | UO <sub>2</sub> -PuO <sub>2</sub> and UO <sub>2</sub> -Gd <sub>2</sub> O <sub>3</sub> (burnable poison) fuels.   | Core BR3/4D <sub>1</sub>             |
| 03.07.86 up to 30.06.87 | 69.6                                 | 61.2                       | 6232        | 92                                     |  | Core BR3/4D <sub>2</sub>             |

(1) Equivalent Full Power Hours (Full power : 40.9 MWth).

(2) The availability factor of the plant, in %, is defined as the ratio of the number of hours on line, to the total number of hours of the operation period, this ratio being multiplied by a factor of 100.



1F<sub>7</sub> (12)

ZO (7)

G (36)

UO<sub>2</sub>-PuO<sub>2</sub> fuel pins (24)

FIG. 1. BR3 core 3A.

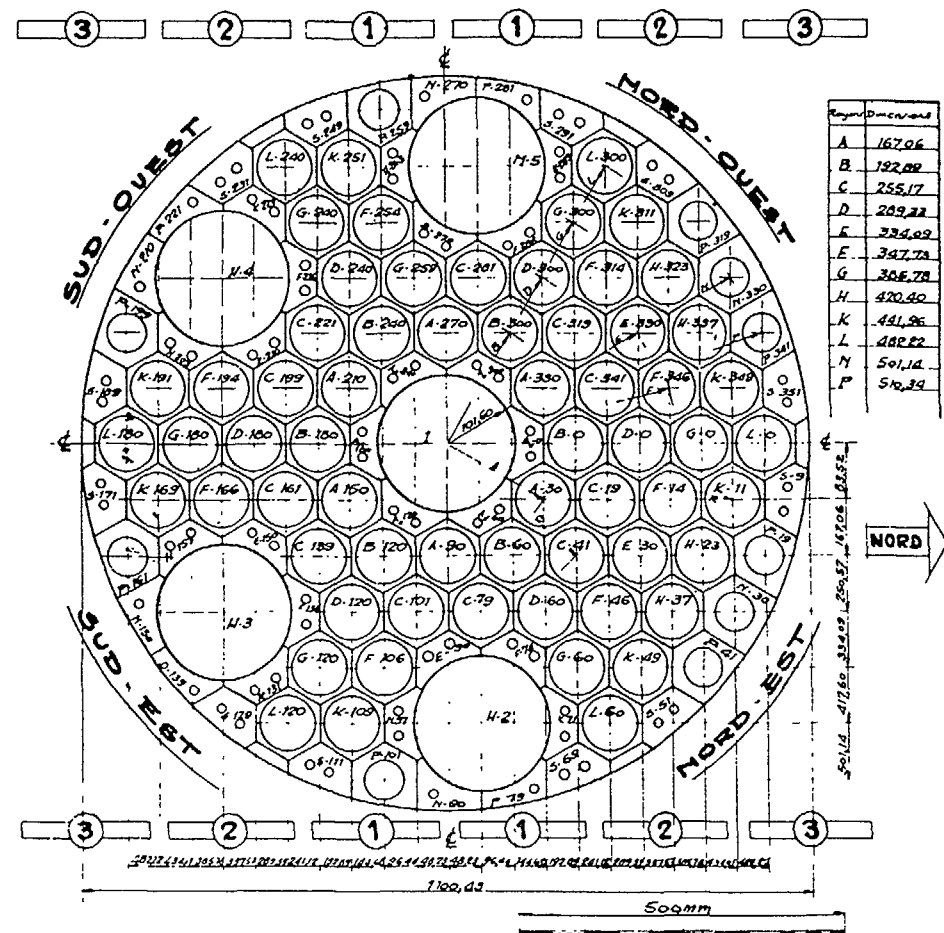
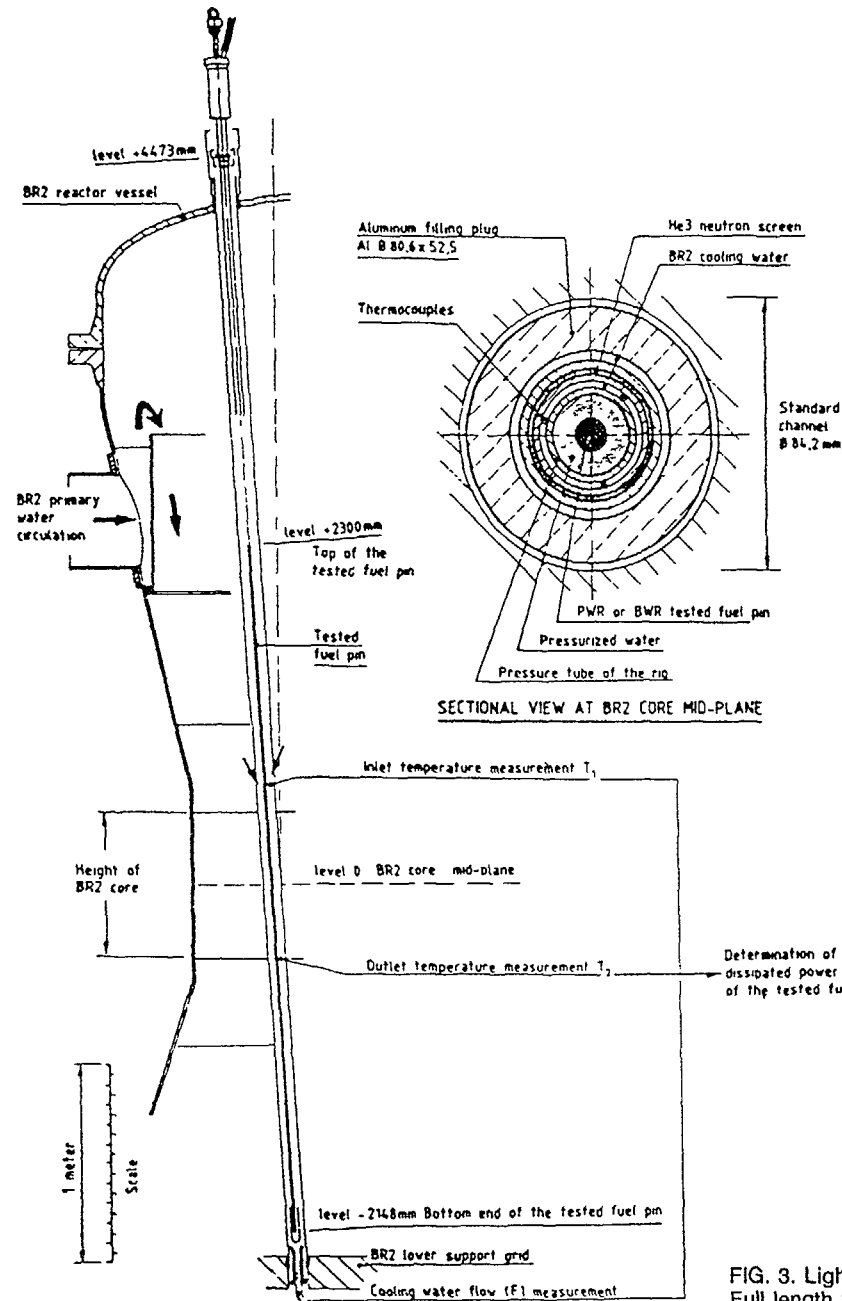


FIG. 2. Cross-section of the BR2 matrix.



307

FIG. 3. Light water reactor fuel irradiation in the BR2 reactor.  
Full length fuel pin irradiation testing.

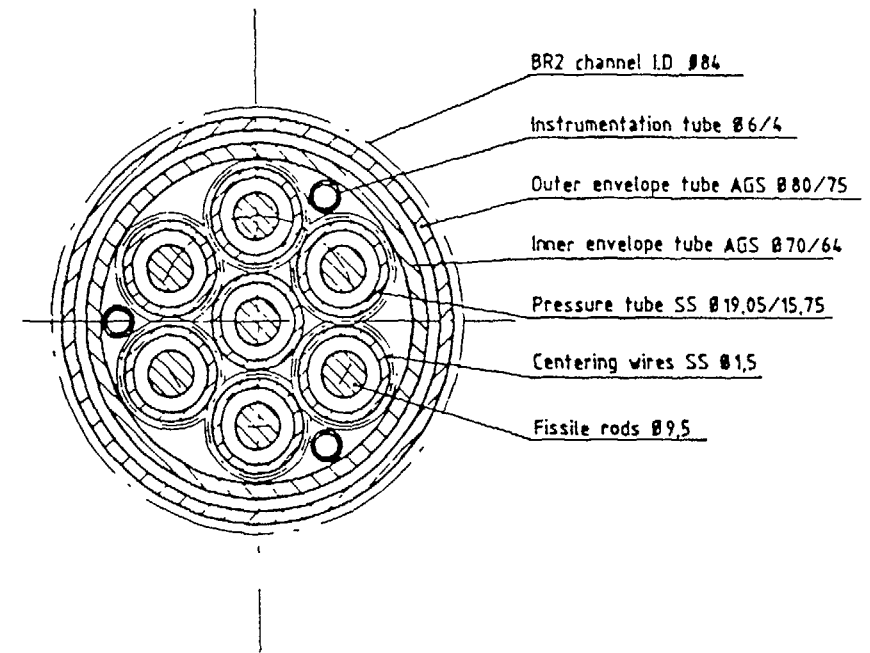


FIG. 4. Multi-rods in a pressurized water capsule.

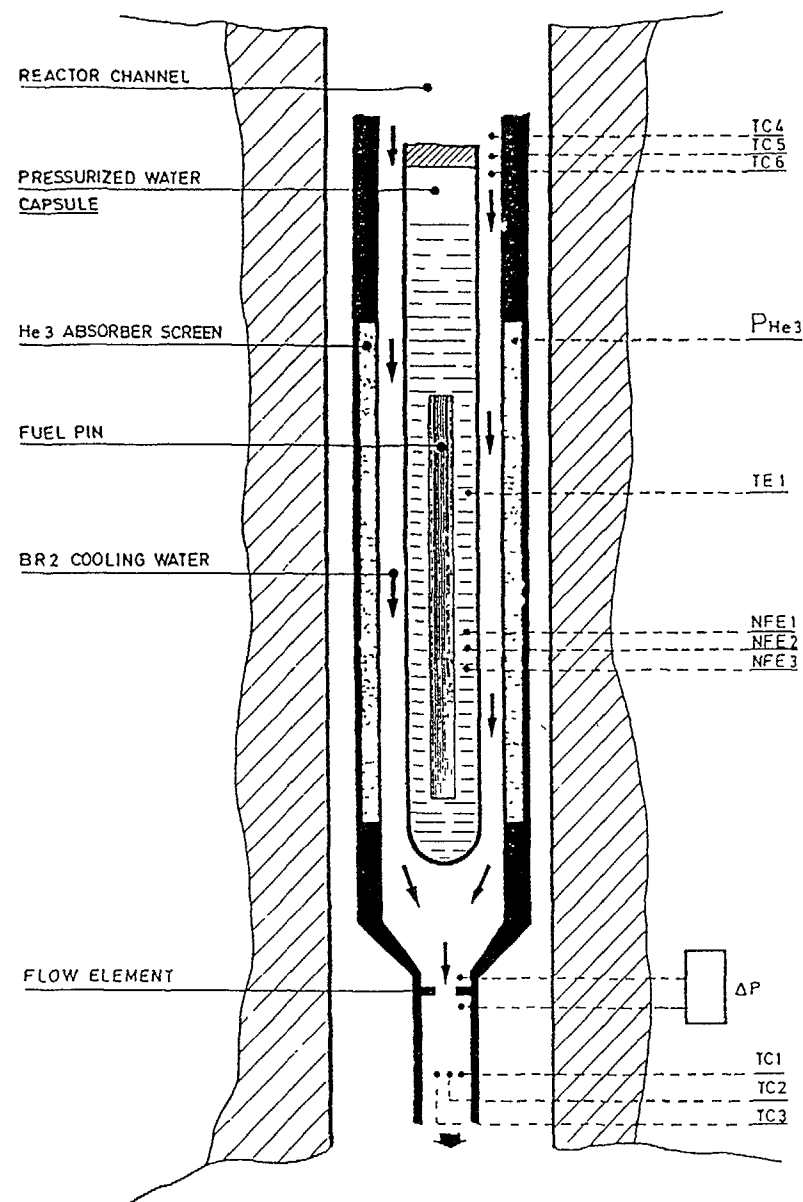


FIG. 5. Example of test rig in BR2.

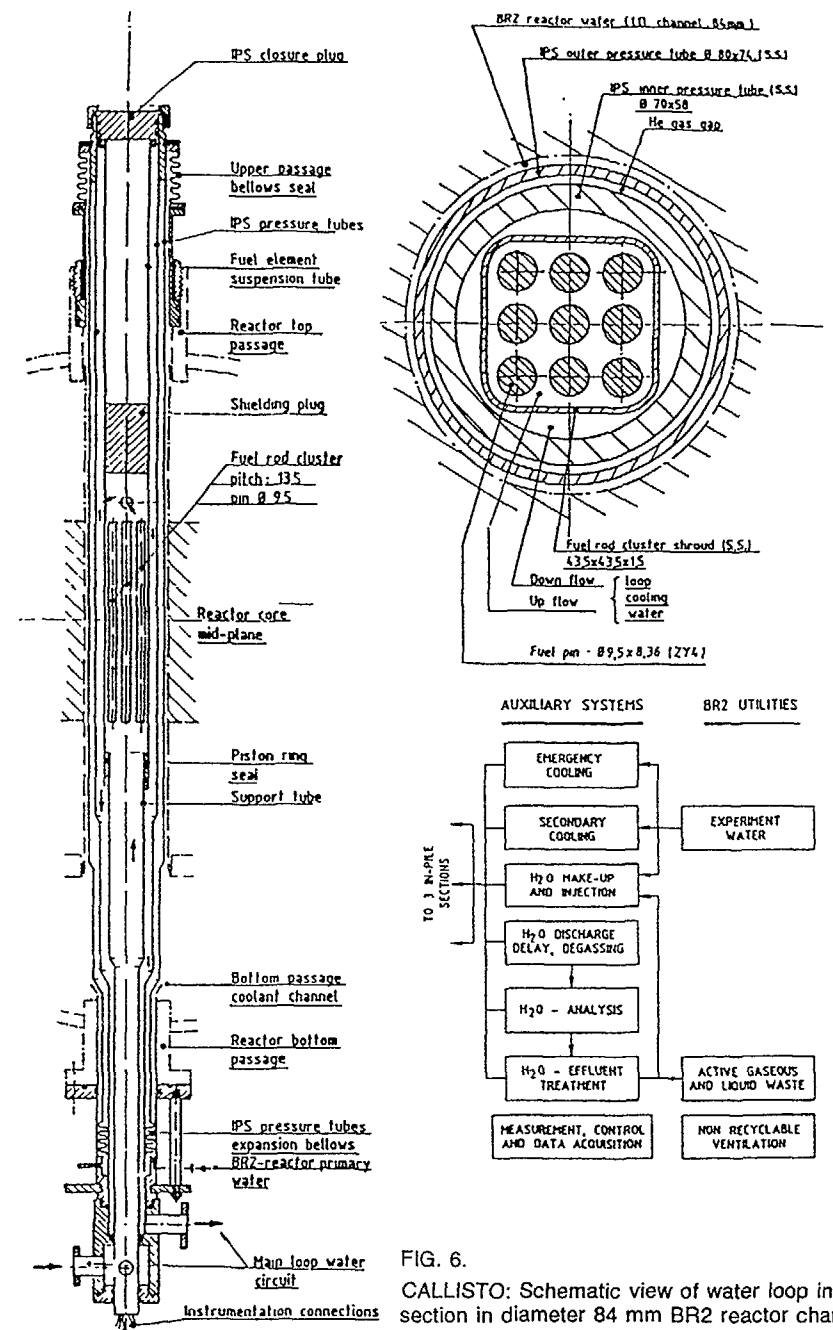


FIG. 6.

CALLISTO: Schematic view of water loop in-pile section in diameter 84 mm BR2 reactor channel.

The selection of the optimum values for the various parameters ( $V_{H2O}/V_{fuel}$ , enrichment or Pu content, core size, ...) has to be done by the core designers, according to thermal-hydraulics constraints, to safety criteria such as the sign of the void coefficient in the central part of the core, and to possible requirements imposed by the reprocessing technology. In VENUS, several sets of optimum parameters could be investigated experimentally : the main restriction is to realize a critical core within the limited space available in the vessel; this could require to use either a higher enrichment (or fissile Pu content) or a larger  $V_{H2O}/V_{fuel}$  than the optimized values, if a feeding zone is not retained as an acceptable environment. In any case, the needed critical mass is large when very tight lattices are to be realized, and such an experimental programme can be best envisaged in the frame of an international cooperation.

#### References

- [1] VENUS International Programme (VIP), a Nuclear Data Package for LWR Pu recycle.  
A. Charlier (BN), J. Basselier (BN), L. Leenders (SCK/CEN)  
to be presented at the PHYSOR-90 Conference (Marseille, April 23-26, 1990).
- [2] Belgian R&D programme in the field of MOX fuel for LWRs.  
D. Haas (BN) - J.-M. Baugnet (SCK/CEN)  
IAEA Technical Committee Meeting on Recycling of Plutonium and Uranium in Water Reactor fuels. Cadarache 13-16, Nov. 1989.

## INVESTIGATION OF INTERMEDIATE CONVERSION PRESSURIZED WATER REACTORS FOR SMALL OR MEDIUM NUCLEAR SYSTEMS

V. KNAPP, D. PEVEC  
Faculty of Electrical Engineering,  
University of Zagreb

D. GRGIĆ  
Rade Končar Institute  
Zagreb, Yugoslavia

#### Abstract

High conversion in water cooled and moderated reactors combines familiar technology backed by extensive experience with desirable feature of efficient fuel utilization. However, economy considerations result in reprocessing installation capacity placing a lower limit on the size of nuclear programme within which fuel cycles requiring reprocessing can be considered. Direct fuel cycles will therefore remain preference for small and medium nuclear systems, as well as for a number of developing countries that will be entering nuclear energy field in 15-20 years time

Feasibility and gains of combining intermediate conversion core of pressurized water reactor, i.e. semitight lattice, and correspondingly increased fuel utilization with the convenience of open fuel cycle are investigated.

At this stage conceptual calculations are in progress with the aim of determining the range of variation of  $V_m/V_f$  ratios at the BOL and EOL of fuel compatible with reactivity requirements and with efficient plutonium burning.

---

#### Background and Project Motivation

The long term nuclear strategies as formulated in early seventies assumed rapid expansion of nuclear power, corresponding increase of uranium cost and consequently early introduction of fast breeder reactors. However, already at that time several general industrial and politico-economical trends operated against this expectations becoming reality, although their effects depended essentially on the country in question. Of primary importance in industrialized countries was continuous reduction of energy use per unit production. US survey shows since 1970 an accelerated decrease of energy consumption per unit production<sup>(1)</sup>. If energy consumption per unit production was 100 in 1970, it came close to 60 in 1985. Even though the fraction of electricity in total energy use was increasing, consumption of electric energy per unit production was decreasing as well. With excess of production capacities sharp competition was developing between oil producers and nuclear equipment manufacturers.

This tendency of reduction of energy consumption per unit national product had a clear effect on nuclear power plant construction programme in USA already in early seventies. Its effects were delayed in countries such as France, Japan, or FR Germany which wanted to reduce their dependence on imported oil after the oil crisis of 1973. This stimulus to construction of nuclear power plants was short lived and limited, and again country dependent Anti nuclear movements increased their activity. Accident at the Three Mile Island power station in 1979 resulted in cancellation of many orders in US and increase of costs of nuclear power stations by addition of more safety and control systems. Reduced demand of uranium kept prices low, even with tendency to decrease. Fuel reprocessing cost on the other hand had a steady upward trend, partly due to stricter safety requirements. Both of these tendencies operated against early introduction of fast breeders, which could be economic at higher uranium cost and at lower fuel cycle costs. Thus the general tendency of nuclear industry in 80-ties was to pass through difficult period with proven thermal technology. The time when fast breeders could be economic moved further into future, not only because of uranium cost decrease and fuel cycle costs increase, but also because of higher than hoped for investment costs of fast breeders. Previously assumed short period for economic use of thermal reactors is extended for at least several decades. Rather than being a transitory reactor type, thermal reactors are now viewed upon as the main suppliers of nuclear electricity for many decades, which gave new motivations and reasons for their development and improvement. Most major nuclear industries responded with priorities specific to the state of nuclear programmes in their respective countries. In addition to the safety and environmental consideration better uranium utilization is the obvious aim of these developments.<sup>(2,3)</sup> Traditional approach via fuel reprocessing and recycle offers considerable opportunities. However it requires reprocessing facilities in the country, or alternatively international fuel cycle services with international fuel and waste transport with handling and transport of plutonium or of plutonium containing fuel. With a list of problems and difficulties this possibility does not appear a realistic one. First one, on the other hand, is open to countries with nuclear programmes sufficiently large to sustain reprocessing facility of economic capacity.

We can therefore conclude that there is a category of countries with small and medium nuclear systems interested in better utilization in open once through fuel cycle. A number of countries which will be entering nuclear energy early in next century will also fall into this category. There are, of course, several known lines of development to improve fuel utilization with once through fuel cycle such as extended burnup, spatial variation of enrichment, frequent refueling, low power density, low leakage core, higher thermodynamic efficiency and others.<sup>(4)</sup>

On the assumption that once through fuel cycle will remain best choice for a number of countries for several decades, it would seem appropriate to investigate whether fuel utilization in once through fuel cycle has reached its optimum. Of course, the best choice, as with any fuel cycle is not the one which gives lowest fuel cost, but one which gives lowest energy costs. We believe that it should be IAEA task to stimulate and coordinate this research of interest for many of its member states. Countries with small or medium nuclear programmes, interested in efficient once through fuel cycle are unlikely to possess resources for such research and development. Several lines of development are possible, as mentioned before, all with minor effects in comparison with what can be attained in high conversion reactors with reprocessing and recycle. We believe that an effort can be justified to establish to what extent the benefits of tight lattice, or semitight lattice could be utilized in the once through fuel cycle. The aim is to combine high plutonium production with the ability to burn in situ as much as possible of it. Two requirements are contradictory to considerable extent, as under-

moderation which gives high plutonium production, leads to too low reactivity at assumed low Pu content at EOC. Some use of spectral shift would remedy the situation. We intend to evaluate the feasibility and gains of combining intermediate conversion core with the convenience of once through fuel cycle.

### Conceptual Investigation

The work we wish to report here has been initiated with the aim to evaluate what effect on fuel utilization can be attained in pressurized water reactor, in once through fuel cycle, using spectral shift to vary the water to fuel ratio during the life of the fuel.

We are beginning with determination of main physics parameters, at this stage we are not considering fuel design beyond putting an upper limit on the range of maximum and minimum values of moderator to fuel ratios during the life of the fuel.

Calculations are at present in the phase of conceptual investigation in order to determine the ratio of final and initial  $V_m/V_f$  ratio compatible with reactivity requirement of core. In order to limit the number of variable parameters we select the values of  $V_m/V_f$  ratios at the EOL of fuel in the range 1.8-2.2, such as to secure efficient fissioning of plutonium. Lower value 1.8 corresponds to the core of NPP Krško. From this research we also hope to be able to judge and evaluate the effects of introducing spectral shift into existing core without any changes in the core other than displacer rods. We start with a core radially divided in zones with maximum, minimum and intermediate values of  $V_m/V_f$  ratio. In order to reduce neutron leakage lowest  $V_m/V_f$  ratio with fresh fuel is in central region, while the highest value of ratio is at the core periphery with the fuel in the last stage of its burnup. Change of  $V_m/V_f$  ratio is assumed to be effected through use of water displacer rods, absent in peripheral region, and in maximal number in central region of the core. Enrichment values for the fresh fuel are assumed to be in standard range of pressurized water reactors. The values in the range 3.0-3.8 w/o in U-235 were selected.

### Calculational Model

In order to perform preliminary cell and fuel assembly calculations the PSU-LEOPARD code<sup>(5)</sup> will be used. The PSL-LEOPARD code is spectrum dependent non-spatial fuel depletion code which fits fast and thermal group constants to a fourth degree polynomial. We expect that PSU LEOPARD will give reasonable results for semitight lattices we intend to use in this study. As the range of validity of PSU LEOPARD results is not known, we will check PSU-LEOPARD results by comparison with results of more accurate set of codes, NITAWL<sup>(6)</sup> (performs resonance shielding calculations by Nordheim integral treatment and produces working library) and XSD-RNPM<sup>(7)</sup> (one dimensional discrete ordinates transport code) for cell calculations, and DOT IV, version 4.2,<sup>(8)</sup> (two dimensional discrete ordinates transport code) for fuel assembly calculations.

Global core modeling will be performed using the MCRAC code<sup>(9)</sup> in order to obtain preliminary results. The MCRAC code is two-dimensional, two-group diffusion code suitable for scoping and preliminary in-core fuel management studies. Therefore, the MCRAC results will be checked by more accurate codes, CITATION<sup>(10)</sup> (multigroup multidimensional finite-difference diffusion code) and/or ILLICO<sup>(11)</sup> (multigroup multidimensional nodal diffusion code).

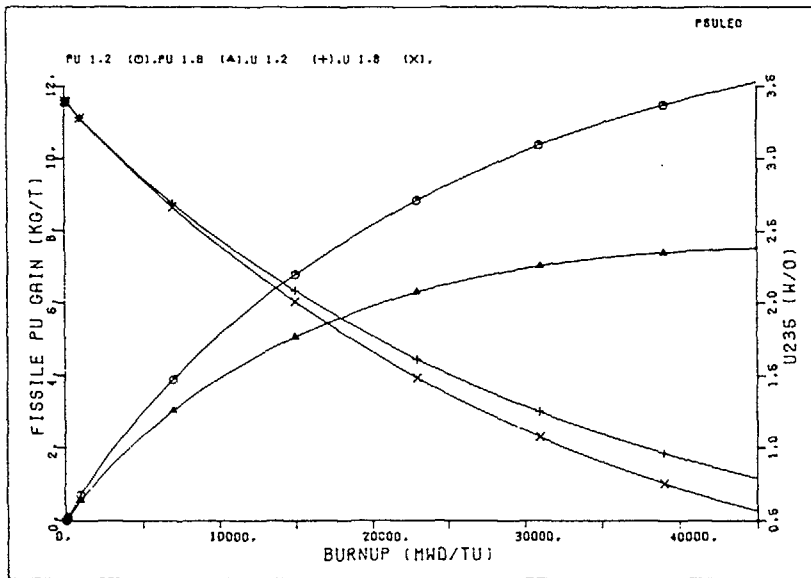


Figure 1. Fissile plutonium gain and U-235 enrichment as a function of burnup for semitight lattice ( $V_m/V_f = 1.2$ ) and standard lattice ( $V_m/V_f = 1.8$ )

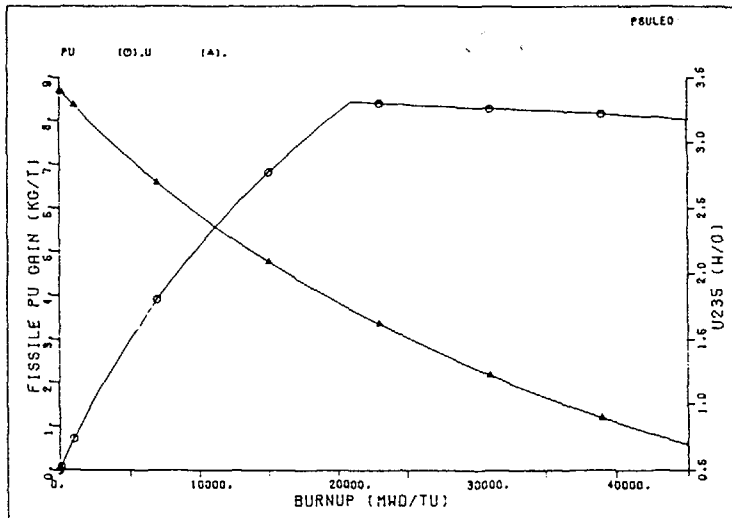


Figure 2. Fissile plutonium gain and U-235 enrichment as a function of burnup for lattice with spectral shift (moderator to fuel volume ratio increased from 1.2 to 1.8 at burnup of 21000 MWd/tU)

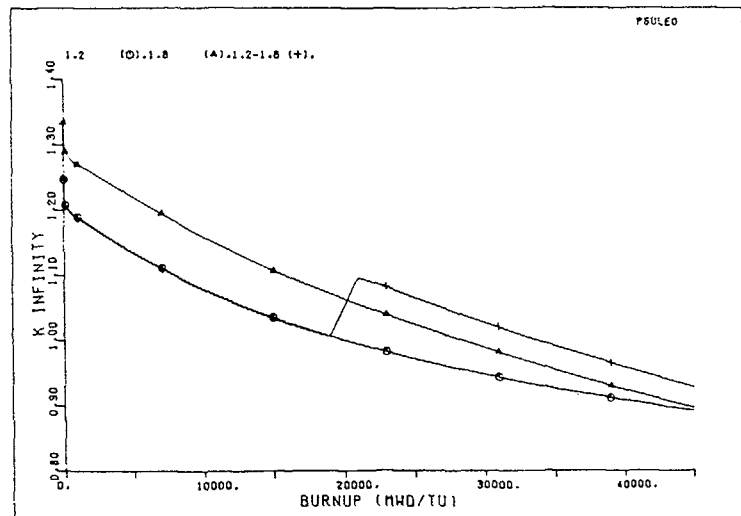


Figure 3. K-infinity as a function of burnup for semitight lattice, standard lattice, and lattice with spectral shift.

### Initial Results

We present a selection of cell calculations performed for various  $V_m/V_f$  ratios and initial fuel enrichment of 3.4 w/o using PSU-LEOPARD code. Physics cell parameters were calculated as function of fuel depletion in steps up to 45 000 MWD/tU. Figure 1. depicts fissile plutonium and U-235 contents as a function of burnup for semitight lattice ( $V_m/V_f = 1.2$ ) and standard lattice ( $V_m/V_f = 1.8$ ). Figure 2. shows fissile plutonium and U-235 as a function of burnup for lattice with spectral shift,  $V_m/V_f$  from 1.2 to 1.8. A comparison of Figures 1. and 2. indicates the more efficient burning of plutonium and U-235 after change of lattice  $V_m/V_f$  ratio to 1.8 at burnup value of 21 000 MWD/tU.

Figure 3. presents  $k$ -infinity as a function of burnup for under-moderated semitight lattice ( $V_m/V_f = 1.2$ ), standard lattice ( $V_m/V_f = 1.8$ ), and lattice with spectral shift, by change of moderator to fuel volume ratio from 1.2 to 1.8 at burnup value of 21 000 MWD/tU.

To evaluate the effects of enrichment change analogous calculations were performed also with lower and higher enrichments (3.0 w/o and 3.8 w/o). More complete presentation will be given after global core calculations are performed.

## References

- 1 M Ross, 'Improving the Efficiency of Electricity Use in Manufacturing', Science (1989)
- 2 "Status of Advanced Technology and Design for Water Cooled Reactors Light Water Reactors", IAEA TECDOC 479, IAEA (1988)
- 3 M C Edlund, "On High Conversion Ratio Light Water Reactors", Nucl Tech 80, 9 (1988)
- 4 P M Lang, "Review of Concepts to Improve Uranium Utilization in Light Water Reactors, with Emphasis on Nonbackfitable Options", IAEA TC Meeting on Advanced Light and Heavy Water Technology, Vienna (1984)
- 5 R F Barry, "LEOPARD A Spectrum Dependent Non Spatial Depletion Code for the IBM-7094", WCAP-3269 25 (1963)
- 6 R M Westfall et al, 'NITAWL-S, Scale System Module for Performing Resonance Shielding and Working Library Production', NUREG/CR 0200 (1981)
- 7 N M Greene, L M Petre, 'XSDRNPMS A One Dimensional Discrete Ordinates Code for Transport Analysis', NUREG/CR 0100 (1983)
- 8 W A Rhoades et al, "DOT IV Version 4.2 Two Dimensional Discrete Ordinates Radiation Transport Code System", CCC-320, Oak Ridge National Laboratory (1982)
- 9 H Y Huang et al, "MCRAAC Multiple Cycle Reactor Analysis Code, User's Guide", Penn State University (1981)
- 10 T B Fowler, D R Vondy, and G W Cunningham, "Nuclear Reactor Core Analysis Code CITATION", ORNL-TM 2496, Rev 2 (1971)
- 11 H L Rajic, A M Ougouag, "ILLICO A Vectorized Multigroup Multidimensional Nodal Neutron Diffusion Code", Trans Am Nucl Soc 54, 192 (1987)

## PROGRESS REPORT ON THE RESEARCH ACTIVITIES ON HIGH CONVERSION REACTORS AT THE CENTRO ATOMICO BARILOCHE, ARGENTINA

M.J. ABBATE, M.M. SBAFFONI, N.E.PATIÑO  
Centro Atómico Bariloche,  
Comisión Nacional de Energía Atómica,  
San Carlos de Bariloche,  
Argentina

### Abstract

The present progress report covers the activities performed by the High Conversion Reactors Group of the Neutrons and Reactors Division of the Centro Atómico Bariloche (CAB). This group previously devoted mainly to neutron physics problems, started some years ago its activities in the field of this reactor concept, which were initially focused on the neutronic problems related with the design of these facilities.

The main results obtained up to the moment and the experience acquired are reported, and they cover

- description of preliminary work
- implementation and validation of the calculational system
- study of the sensitivity of cell calculations to geometrical treatment
- evaluation of resonance self-shielding correction and heterogeneities effects
- local values for the NEACRP international benchmark at zero burn up

Moreover, the activities under way are also presented

- provisions for burn-up calculations
- PROTEUS Phase I and II and JAERI's FCA-HCLWR cell calculations
- fuel element and whole core calculations.

### 1 INTRODUCTION

New conceptions in nuclear power reactors are presently being studied, i.e. high conversion reactors (HCR). Their inclusion in a strategy of nuclear energy generation would bring significant advantages over the one presently applied, mainly because of their high fuel utilization, /1/ to /5/

Their technology implies, among other ideas, the use of a compact lattice in the core, which hardens the neutron spectra and poses new and very interesting and important problems to solve in the neutron and reactor physics area.

The present progress report covers the activities performed by the High Conversion Reactors Group of the Neutrons and Reactors Division of the Centro Atómico Bariloche (CAB), which were initially focused on the neutronic problems related with the design of these facilities.

## 1.1. WORKS PERFORMED

- The works performed up to the moment were as follows:
- establishment of a preliminary work plan.
  - determination of the state-of-the-art in HCRs.
  - determination of the principal present-day problems in neutronic calculation and design of this kind of reactors.
  - improvement and updating of the available experimental facilities including the data handling and processing system.
  - completion and discussion of the present calculational system.
  - implementation of the complete capability to process nuclear data and to obtain problem-dependent group constants, and its validation with benchmarks.
  - study of the sensitivity of the cell calculation to geometrical treatment.
  - calculation of local values for the NEACRP HCLWR international benchmark /6/, without burn-up.
  - analysis of sensitivity of the problem to the use of different theories to calculate the resonance self-shielding effect.
  - study of the influence of the treatment of heterogeneities.

## 1.2. ACTIVITIES UNDER WAY

Moreover, a brief summary on the activities under way is done, which covers:

- development and implementation of a burn-up code, and burn-up calculations.
- fuel elements modelling, calculation and design.
- calculations related with theoretical benchmarks and with experiments, as: PROTEUS Phase I and II /7/, /8/ and FCA-HCLWR/9/.
- preliminary calculations of the core, oriented to perform parametric studies.
- definition of the future work plan.

## 2. PRELIMINARY WORK

As a previous work, the state-of-the-art in High Conversion Reactors (HCR) was established, from a wide bibliographical study, identifying the open problems in research and development in this field /10/.

The first conclusion seemed to be that the status of reactor physics needed to design HCR, in which the power is generated with a mixed spectra, with neutron energies from thermal to fast with great importance of the epithermal energy range, is somehow similar to the status of reactor physics thirty years ago.

Of course, during the years one has learned a great deal about thermal and fast reactors, but very little about "resonance" reactors and a combination of all of them.

The "somehow similar" referred to above, concerned mainly with the lacking of experimental differential and integral measurements which were not being carried out at that moment for this type of reactors, the need of rigorous tests on nuclear data processing and preparation, especially in the resonance region, and on the most suitable calculation methods to be used with tight lattices.

Great differences were seen at that time in the main representative parameters among different laboratories, and many were the open problems then identified to work on.

Neutronic calculation and nuclear data problems were specifically observed /11/.

The void reactivity coefficient is one of the most sensitive and important parameters; it must be noted that an intermediate energy neutron spectrum will be present in normal operating conditions, while a fast one in case of a loss-of-coolant accident, so the neutron physics of the reactor will be very different in operating or accidental conditions, and so should be the neutron data treatment and calculational methods used.

The most important parameters which influence the reactor behaviour are enrichment, structural and control materials and tightness of the lattice, and a great variety of proposed designs were found at the time: homogeneous or heterogeneous, enriched mainly with plutonium, or with mixed oxides (MOX) with greater proportions of uranium, with cladding of stainless steel or zircalloy, with different configurations and materials for control systems.

Because of the very special type of problems one is dealing with, working libraries should be carefully and specially evaluated and obtained from recommended master data libraries.

On the nuclear data processing, self-shielding and shadowing effects should be carefully considered, so methods widely used up to now must be fully tested.

Heterogeneity effects and homogenization models require also special treatment to assure the conservation of the reaction rates.

As one of the main goals of these facilities is to obtain high conversion ratio and fuel utilization (burn-up), at least on the first steps suitable nuclear data should be selected and tested considering a big number of isotopes, to permit a detailed study of the problem and to prevent undesirable effects from approximations.

For the first studies, a design mainly based in the SIEMENS (KWU) - TUBS design was selected /5/ ( TUBS: Technische Universitaet zu Braunschweig).

From the experimental point of view, an effort has been dedicated to improve and update the present experimental facilities /12/, in order to try to set up a simple system where to observe the changes produced in the neutron spectra by changes in fuel composition, moderator or grid pitch.

The existent facilities comprise a complete time-of-flight spectrometer, with a pulsed neutron source and capabilities for neutron activation. The idea was to extend the energy range of the measurements in order to cover the resonance region.

The on-line data acquisition system was totally changed, incorporating new elements that rendered possible to receive information simultaneously by two lines, with different channel width, one for the measurements on the thermal and epithermal range and the other one for part of the epithermal and the fast ranges.

The electronic chain was improved adding new fast NIM modules and reducing considerably all the dead times.

The Lithium-6 glass detector was revised in order to diminish the gamma-flash dead time and to conform the response pulses. Its efficiency was also revised, new and better values were calculated by Sn adjoint method, and several tests were done measuring neutron spectra in a dummy moderated fuel element for two different p/d relations /12/ and in bulk media /13/.

The system was fully improved and the energy range extended, but there are still some problems to solve, especially how to treat the long mean emission times involved in this kind of multiplicative systems, compared with the flight times.

Besides that, at present no new experiments are planned, because of the very hard difficulties found to get an adequate assembly containing enriched fuel.

### 3 CALCULATIONAL SYSTEM

The first problem found was the necessity to have enough capability to process and generate suitable working libraries, then, a nuclear data group was also created.

AMPX-II processing system and ENDF-B/IV library were used, as they were the ones we had available, and a detailed check with benchmarks was done.

The best calculation method is an open problem, but it can be asserted that any of the well known methods, previously evaluated, could be used, if correct nuclear data treatment and geometrical models are applied.

#### 3.1 DESCRIPTION

Figure 3.1 shows the computer code system employed

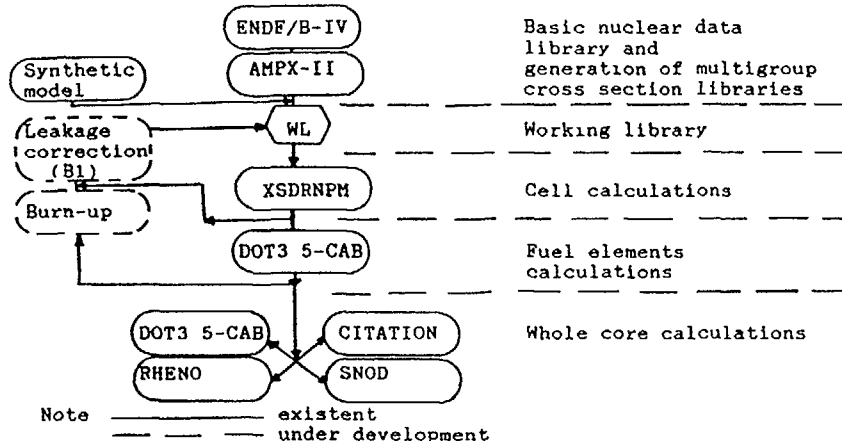


FIGURE 3.1 Computer code system

#### a Basic Nuclear Data Library and Generation of Multigroup Cross Section Libraries

The ENDF/B-IV library is available in our country as the source of basic nuclear data.

The AMPX-II system /14/ was employed for generating the working libraries using mainly the modules NPTXS, reconstruction of point cross sections; XLACS-IIA, generation of multipurpose multigroup master libraries, and, NITAWL, resonance self-shielding calculation, according to Nordheim's integral treatment.

At this level, multigroup cross sections may also be obtained from a synthetic model /15/, which allows the obtention of these of moderating atoms and molecules from analytic kernels.

#### b Cell Calculations

The XSDRNPMP code of the AMPX-II system is utilized. It is a one-dimensional code, providing the capacity for discrete ordinates (Sn - Pl) and diffusion calculations, plus a subsequent homogenization and/or condensation of cross sections.

#### c Fuel Element Calculation

The DOT3 5-CAB /16/ code is employed in this stage, which allows two-dimensional Sn and diffusion calculations.

#### d. Whole Core Calculations

The codes available are:

- DOT3 5 CAB for 2-D calculations
- CITATION used for 2-D and 3-D diffusion calculations
- RHENO this code has been developed at CAB, and allows 2-D and 3-D calculations. It is based on a nodal method in which the local problem is solved by diffusion theory
- SNOD also developed at CAB, allowing a 3-D nodal calculation in which the local problem is solved by the Sn method

#### e Leakage correction and Burn-up calculations

The corresponding computer codes are presently being locally developed. They are intended to perform a leakage correction on the neutron flux following the B1 method, plus a subsequent flux expansion and scaling of power (already programmed) ending with a burn-up calculation. The required interfaces will be provided to allow burn-up calculations at pin-cell level as well as at fuel element level.

#### f. Energy mesh

As a recommended energy mesh is not defined yet, the tendency is to use the most refined one, compatible with the computer memory and with reasonable calculation times. This has the additional advantage of making possible a detailed consideration of the physical behaviour of this type of reactors. In the present work, a 108/110 groups energy grid was used for cell calculations, including most of the WIMS limits in order to facilitate comparisons with other authors results, while 20, 8 and 3 groups were used for assembly, core and burn-up calculations.

Two cross section libraries have been generated in this group structure: a HOT library, at reactor operating temperature and a COLD library, at room temperature, for the analysis of the experiments.

#### 3.2 VALIDATION

The whole system has been successfully validated in the generation of multigroup cross sections for thermal and fast critical facilities. The benchmark systems considered were:

#### a Thermal Benchmarks

Enriched uranium and plutonium fueled critical spheres were employed as benchmark cases. Table 3 I shows the results obtained in the validation.

It can be seen that a good agreement is found in the uranium-fueled spheres, with a maximum difference of 0.6%  $\Delta/k/k$ .

In the plutonium-fueled systems, the results obtained with AMPX-II present a much better agreement with the experiments than other results, which were also calculated by means of transport theory. As the discrepancies found in the AMPX-II results are not negligible, they were further investigated, a curve-fitting analysis of the results presented in table 3 I shows that the reactivity excess of the AMPX-II results can be attributed to an excess in the Pu239 fission cross section in the region of its 0.3 eV resonance, of the order of 2%.

TABLE 3.I

Thermal benchmarks results

| Benchmark                | Fuel | Experiment          | AMPX-II | Other results | Difference<br>(*1.E+05) |
|--------------------------|------|---------------------|---------|---------------|-------------------------|
| Eigenvalue: k-effective. |      |                     |         |               |                         |
| ORNL-1                   | U    | 1.00026             | 0.99687 | 0.98812       | -339                    |
| ORNL-2                   | U    | 0.99975             | 0.99687 | 1.00346       | -288                    |
| ORNL-3                   | U    | 0.99994             | 0.99399 | 1.00059       | -595                    |
| PNL-1                    | Pu   | 1.00000             | 1.01580 | -----         | 1580                    |
| PNL-2                    | Pu   | 1.00000             | 1.00586 | -----         | 586                     |
| PNL-3                    | Pu   | 1.00000             | 0.99647 | 1.00815       | -353                    |
| PNL-4                    | Pu   | 1.00000             | 1.00424 | 1.01714       | 424                     |
| PNL-5                    | Pu   | 1.00000             | 1.00890 | 1.02661       | 890                     |
| Eigenvalue: Buckling.    |      |                     |         |               |                         |
| PNL-1                    | Pu   | 0.02182 +/- 0.00015 | 0.02134 |               |                         |

**b. Fast benchmarks**

The well-known GODIVA and JEZEBEL critical assemblies were employed as benchmark cases. The validation involved the calculation of k-effective, spectral indeces, reactivity contributions, and leakage spectrum. Tables 3.II and 3.III show the main results of the validation.

A very good agreement is found between the calculated results and the experimental measurements, in both critical assemblies.

TABLE 3.II

Fast benchmarks results: GODIVA

| Parameter                            | Isotope | C/E ratio<br>This work | Other<br>results (C/E)     |
|--------------------------------------|---------|------------------------|----------------------------|
| k-effective                          |         | 1.00519                | 1.0048<br>0.99254<br>0.992 |
| Spectral indeces<br>(Fission ratios) | U238    | 1.020                  | 1.020                      |
|                                      | Np237   | 1.053                  | 1.006                      |
|                                      | U233    | 0.947                  | 0.944                      |
|                                      | Pu239   | 0.986                  | 0.994                      |

TABLE 3.III

Fast benchmarks results: JEZEBEL

| Parameter                            | Isotope | C/E ratio<br>This work |
|--------------------------------------|---------|------------------------|
| k-effective                          |         | 1.00325                |
| Spectral indeces<br>(Fission ratios) | U238    | 1.020                  |
|                                      | Np237   | 1.055                  |
|                                      | U233    | 0.945                  |
|                                      | Pu239   | 0.989                  |

**4. SENSITIVITY TO GEOMETRICAL TREATMENT OF HCLWR's MICROCELL CALCULATIONS**

The aim of this work was to evaluate the error introduced in some of the main design parameters of HCR, as the k infinite, neutron spectra and reaction rates, by the use in cell calculations of geometrical models that do not consider explicitly all the real zones.

To study the mentioned differences three typical microcells were considered:

- TUBCAB1 was taken as reference because it is an accurate picture of the real cell, and it was described by three homogeneous zones in cylindrical geometry: fuel (plus gap), clad (and structural material), and moderator.

- TUBCAB2 where only two zones were considered, mixing in the first one the fuel and the clad and considering in the second one the moderator.

- TUBCAB3 where again two zones were used, with the fuel considered alone as first zone, and the clad mixed with the moderator as the second one. This case is equivalent to the one defined by TUBS for its design calculations, and all the cell data for this analysis were taken from their data /5/.

All the cases were calculated for a moderator to fuel ratio of 0.6865, which implies a relation between pitch and diameter of 1.1845.

The working libraries were obtained in a 110 groups energy mesh, with temperatures of 900 K for the fuel and 585 K for the moderator and clad.

The calculations were made using the DOT3.5-CAB code in its transport option with P0 and S6 approximations, and suitable tests were done to assure an adequate convergence of the results.

The k-infinite obtained for the three cases, averaging a number of converged runs, are shown in Table 4.I. Also, a k-infinite mean value from the NEACRP benchmark results /6/ was included, even if the cell there defined is somehow different from the one reported here, just to show orders of magnitude.

TABLE 4.I

K-Infinite values for the three calculated cases

| Case            | K infinite | Standard Deviation |
|-----------------|------------|--------------------|
| TUBCAB1 (f/c/m) | 1.09538    | 0.00356            |
| TUBCAB2 (f+c/m) | 1.08576    | 0.00285            |
| TUBCAB3 (f/c+m) | 1.08172    | 0.00172            |
| NEACRP          | 1.09250    | 0.00240            |

As it can be seen there, mixing the clad with the fuel underestimates the k-infinite in 0.98% (1000 pcm), while diluting the clad into the moderator produces an underestimation of 1.35% (1350 pcm), so from the point of view of the calculation of multiplication factors, the second is the case which is closest to the reference.

From the point of view of the calculation of fluxes the effect is opposite, and the most convenient model is to mix the clad with the moderator, because otherwise it dilutes the fuel and increases the importance of the resonances; no noticeable differences can be seen between TUBCAB1 and TUBCAB3 cases.

Typical zonewise neutron spectra are shown in Figure 4.1.

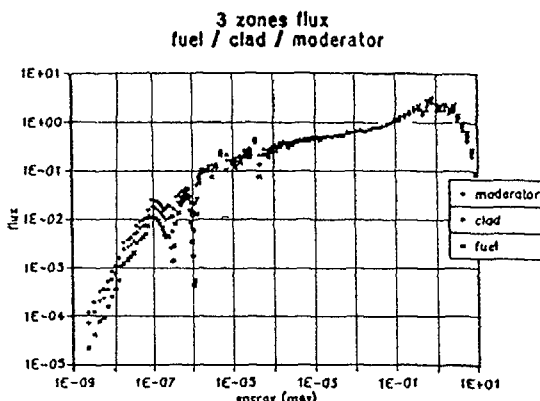


FIGURE 4.1 Typical zonewise neutron spectra. TUBCAB1 (3 zones)

Referring to the reaction rates, total cell absorption and production were calculated for the three cases, as well as total production and absorption rates for some isotopes, and the same but groupwise for Pu239, Pu241 and Pu242. Defining three energy groups, thermal from 10<sup>-5</sup> eV to 4 eV, epithermal from 4 eV to 9 118 KeV, and fast from 9 118 KeV to 10 MeV, it could be seen that in this kind of cells 57 % of the total absorptions is produced in the epithermal range, while 25 % occur in the thermal range and 18 % in the fast one.

The values can be seen in table 4.III, NEACRP benchmark mean values were also included

TABLE 4.III  
Comparison of reaction rates

| Reaction          | Case | TUBCAB1 | TUBCAB2 | TUBCAB3 | NEACRP |
|-------------------|------|---------|---------|---------|--------|
| <b>Production</b> |      |         |         |         |        |
| Pu239             |      | 0 679   | 0 675   | 0 669   | 0 685  |
| Pu240             |      | 0 0296  | 0 0291  | 0 0294  | 0 030  |
| Pu241             |      | 0 227   | 0 226   | 0 225   | 0 220  |
| Pu242             |      | 0 0058  | 0 0057  | 0 0058  | < 0 01 |
| U235              |      | 0 0126  | 0 0126  | 0 0126  | 0 020  |
| U238              |      | 0 125   | 0 121   | 0 125   | 0 125  |
| <b>Absorption</b> |      |         |         |         |        |
| Pu239             |      | 0 366   | 0 365   | 0 362   | 0 370  |
| Pu240             |      | 0 131   | 0 132   | 0 132   | 0 125  |
| Pu241             |      | 0 0955  | 0 0952  | 0 0948  | 0 090  |
| Pu242             |      | 0 0310  | 0 0317  | 0 0314  | 0 035  |
| U235              |      | 0 0073  | 0 0073  | 0 0073  | 0 012  |
| U238              |      | 0 336   | 0 340   | 0 341   | 0 335  |

Looking at the importance of each isotope, 62% of the productions come from Pu239, 21% from Pu241 and 11% from U238. Regarding to the absorptions, 37% occur in the Pu239, 34% in U238, 13% in Pu240 and 9 7% in Pu241.

While the total absorption is practically equal for all the cells, concerning the neutron production, mixing the clad with the fuel underestimates its 0 8 %, while mixing it with the moderator produces an underestimation of approximately 1 %. From other side, the absorption of the clad changes in more than 10%, but it has a weight of less than 2% on the total values. The absorption of the moderator diminishes in both cases, especially in the thermal range.

Comparing the values obtained for the three cases, the tendency is the same that the one observed in k-infinite calculation, so, considering the great importance of these reaction rates on conversion ratios and fuel utilization, it is recommended, for present case, to mix the clad with the fuel (TUBCAB2), to obtain better values of k and CR, even if for spectra calculations the classical model of diluting the clad into the moderator produces the closest spectra.

This work was also used as a first check-point of the quality of the results of the local system. This was the reason for the inclusion of the NEACRP benchmark preliminary results. Comparing all the values, including total and group-by-group reaction rates, all are in good agreement and within the dispersion of the rest of the participants.

#### 5 EVALUATION OF NORDHEIM'S METHOD FOR RESONANCES SELF-SHIELDING

As it was said, the neutron spectra of the HCRs have a high epithermal component, and its fuel is enriched in fissile plutonium therefore, the treatment of the resonances self-shielding becomes very important.

Reported results have shown that the use of different methods and data for this correction can produce large discrepancies among calculated values of k-infinite, conversion ratio and void coefficient.

At present the most widely utilized method is Bondarenko's technique (BT), and a hyperfine energy mesh method (HEM) is also sometimes used and recommended. The latter is the most refined and accurate one, but is enormously time consuming, and therefore not adequate for design work, while Bondarenko is more practical and fast, but less exact.

In this work the evaluation of the Nordheim integral treatment (NIT) was done, to test its accuracy and speed /17/. It was performed calculating two typical HCR's microcells which corresponds to the proposed NEACRP HCLWR benchmark /18/.

Cell number one has a moderator to fuel ratio of 0 6, while number two has a Vm/Vf equal to 1 1.

Three groups of calculations were carried out, using group constants where the resonance self-shielding effect was treated by the mentioned method.

Hyperfine with ROLAIDS code, which performs a detailed (45000 energy groups) calculation with collision probabilities method.

Bondarenko with FOBOS code, especially developed for this work, and which includes the usual approximations to consider the heterogeneities, i.e narrow resonances and Bell-Wigner's rational expression.

- Nordheim with NITAWL code, included in the mentioned AMPX-II

The hyperfine calculation was taken as reference, and its results were also compared with the mean value of the results of the benchmark, but it should be noted that this value is highly influenced by Bondarenko treatment because this is the method most widely used

Calculations were performed with XSDRNPM code. The k-infinite values obtained, as a function of the void fraction, for the two  $V_m / V_f$  relations are shown in Figures 5.1 and 5.2

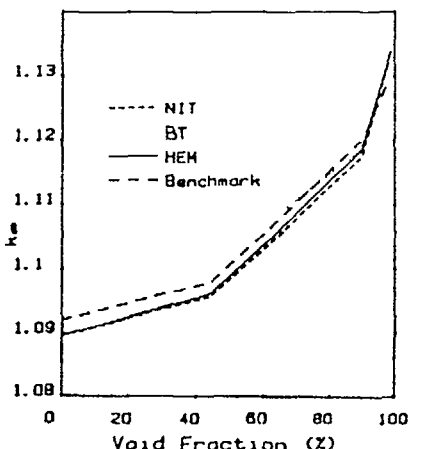


FIGURE 5.1  $V_m/V_f = 0.6$

Effect on k-infinite of self-shielding treatment

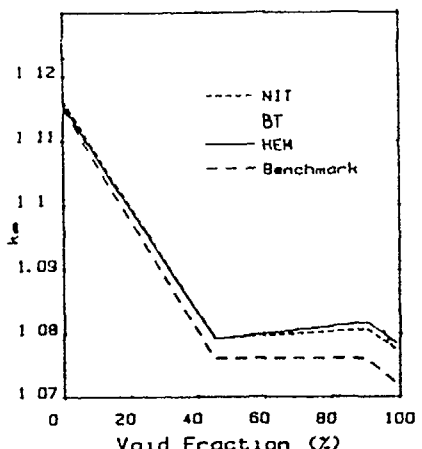


FIGURE 5.2  $V_m/V_f = 1.1$

Effect on k-infinite of self-shielding treatment

As it can be seen, Nordheim's method shows a very good agreement with the HEM, better than BT.

Moreover, the correspondent CPU times are 5 hours and 30 minutes for HEM, 2 minutes for BT and 8 minutes for NIT, all of them ran in a VAX-11/780 computer.

Calculated conversion ratios can be seen in Table 5.1, the agreement is also very good and HEM as well as NIT predict values bigger than BT and the benchmark which, as it was said, are correlated. The differences diminish with the increasing of the void fraction, because the importance of the resonance region is lower when the spectrum is hardened.

TABLE 5.1  
Calculated Conversion Ratios

| Cell Number | Void Fraction | Nordheim | Method Bondarenko | Hyperfine | NEACRP mean value |
|-------------|---------------|----------|-------------------|-----------|-------------------|
| 1           | 0 %           | 0.879    | 0.861             | 0.876     | 0.837             |
|             | 45 %          | 0.974    | 0.927             | 0.940     |                   |
|             | 90 %          | 1.149    | 1.145             | 1.147     |                   |
|             | 99 %          | 1.310    | 1.310             | 1.310     |                   |
| 2           | 0 %           | 0.782    | 0.768             | 0.785     | 0.754             |
|             | 45 %          | 0.919    | 0.900             | 0.932     |                   |
|             | 90 %          | 1.155    | 1.147             | 1.167     |                   |
|             | 99 %          | 1.468    | 1.472             | 1.469     |                   |

Finally, reaction rates for fuel isotopes were calculated for the two cells.

From these results one can conclude that the high multiplication factor and low conversion ratio obtained with Bondarenko's method come from the low absorption in U238, and from the high calculated production rates.

Looking at all these results, and considering also the involved processing times, it can be inferred that in this kind of cells Nordheim method can be used with results very similar to the hyperfine method, without extraordinary consumptions of time.

For the future, it is convenient to implement some improvements on the code which calculates with Nordheim's methods, as to include corrections for the interaction of resonance isotopes and to develop the possibility of interpolating in working libraries.

#### 6 EFFECT OF RESONANCE SELF-SHIELDING AND OF HETEROGENEITIES TREATMENT

As it has said, results reported up to now have shown that well known procedures used for thermal and fast reactors calculations can not be directly applied for HCRs.

In this part of the work, the effect of considering or not the self-shielding correction in some isotopes, and of different approximations to take into account the heterogeneities are studied [17].

The calculations were carried out in the two cells mentioned in 5, as a function of the void fraction.

Calculation of multiplication factors was done using group constants where self-shielding was treated by Nordheim method, and also with some isotopes treated as infinitely diluted. The studied isotopes were Pu240, Pu241, Pu242, and some structural materials. The differences in k-infinite between both cases are shown in table 6.1.

As it can be seen, the lack of treatment of self-shielding on Pu240 and Pu241 produces an underestimation of approximately 2%, while on Pu242 and structural material produces overestimations up to 0.5%.

TABLE 6.1

Effect of the lack of treatment of self-shielding on some isotopes Differences on k-infinite in p.c.m.

| Cell number | Void fraction | Material infinitely diluted |       |       |          |     |
|-------------|---------------|-----------------------------|-------|-------|----------|-----|
|             |               | Pu240                       | Pu241 | Pu242 | Fe+Cr+Ni | Mn  |
| 1           | 0 %           | -2035                       | -1306 | 287   | -108     | -32 |
|             | 45 %          | -1755                       | -849  | 261   | -58      | -42 |
|             | 90 %          | -644                        | -124  | 40    | 73       | -41 |
|             | 99 %          | -300                        | -8    | 7     | 138      | -30 |
| 2           | 0 %           | -2085                       | -1717 | 214   | 196      |     |
|             | 45 %          | -1991                       | -1475 | 392   | 228      |     |
|             | 90 %          | -834                        | -399  | 141   | 214      |     |
|             | 99 %          | -379                        | -19   | 4     | 37       |     |

Note 1 p.c.m. = delta k \* 1.0E+05

Moreover, when the void fraction increases the spectrum is harder and the effect of the resonances decreases producing an important overestimation of the void coefficient. This effect, in Pu240 generates an error in the conversion ratio of 5 %.

Normally, the self-shielding treatment methods include the heterogeneities effect by equivalence relations based on fuel escape probabilities and Dancoff factors. The sensitivity of the neutronic calculations to the different approximations applied was also studied.

Fuel escape probabilities were calculated with the expressions of Sauer, Carlvik, Wigner, and Bell-Wigner, using as reference value the exact one of the probabilities obtained from the expression of Case, included in the NITAWL code. In Table 6.II the maximum error in k-infinite is shown (in p.c.m.) for the four void fractions.

TABLE 6.II

Differences (in p.c.m.) in k-infinite, using different approximations for fuel escape probabilities calculation

| Void Fraction | Approximation: |         |             |        |
|---------------|----------------|---------|-------------|--------|
|               | Sauer          | Carlvik | Bell-Wigner | Wigner |
| 0 %           | 9              | - 28    | - 36        | 462    |
| 45 %          | 5              | - 10    | 70          | 377    |
| 90 %          | 4              | - 6     | 105         | 160    |
| 99 %          | 3              | - 1     | 40          | 120    |

At it can be seen, most of the expresions are accurate enough, with the exception of Wigner's.

It was also proved that this kind of compact cells is much more sensible to the Dancoff factor used than the PWR's ones. A change of 5% in the Dancoff factor produces a change of 0.5% in k-infinite, which is more than 3 times higher than the change produced in PWR cells. Moreover, as the difference changes with the void coefficient, it modifies the void reactivity coefficient.

In view of this high sensitivity, the models normally used to calculate this factor were also evaluated. They are: Sauer, Fukai and Two rods. The comparisons were done on the cell 1, because it is more compact and so the effects are bigger, and for cross sections of clad which correspond to stainless-steel ( $0.30 \text{ cm}^{-1}$ ) and zircalloy-2 ( $0.70 \text{ cm}^{-1}$ ), and cross sections of moderator which covers the range from cold to a practically voided core.

The results can be seen in Table 6.III, expressed as differences in k-infinite referred to the exact value of the Dancoff factor calculated with the collision probabilities code COLPROB /19/.

Sauer, Fukai, and Two rods, consider the clad mixed with the moderator, while in the fourth case the clad cross section is neglected and in the fifth is treated explicitely in a separate zone. Sauer method shows very good results, even without treating the three zones separately, and showed that the clad can not be neglected; the other two imply discrepancies from 0.5% to 1.5%.

As summary, it can be said that the self-shielding effect should be considered in all the resonant isotopes, including the structural material, because the individual effects could be accumulative. There is also a high sensitivity to the Dancoff factor, but it can be calculated properly with some of the models already known, for homogeneous lattices; nevertheless, special care will be needed in the case of heterogeneous lattices.

TABLE 6.III

Differences (in p.c.m.) produced in k-infinite using Dancoff factors calculated by different methods

| Clad's<br>XS(cm <sup>-1</sup> ) | Model                      | Moderator XS (cm <sup>-1</sup> ) |        |        |       |       |
|---------------------------------|----------------------------|----------------------------------|--------|--------|-------|-------|
|                                 |                            | 0.01                             | 0.1    | 0.6    | 1.0   | 1.5   |
| 0.30                            | Sauer                      | - 10                             | 10     | - 20   | - 30  | - 50  |
|                                 | Fukai                      | - 630                            | - 590  | - 510  | - 320 | - 260 |
|                                 | Two rods                   | - 1530                           | - 1450 | - 1320 | - 820 | - 640 |
|                                 | Sauer (clad's<br>XS = 0.0) | 610                              | 600    | 670    | 510   | 550   |
|                                 | Sauer (3 zones)            | 30                               | 20     | - 20   | - 20  | 10    |
| 0.70                            | Sauer                      | 10                               | 10     | 40     | 40    | 40    |
|                                 | Fukai                      | - 540                            | - 490  | - 380  | - 220 | - 150 |
|                                 | Two rods                   | - 1340                           | - 1270 | - 1110 | - 670 | - 500 |
|                                 | Sauer (clad's<br>XS = 0.0) | 1450                             | 1430   | 1600   | 1200  | 1210  |
|                                 | Sauer (3 zones)            | 30                               | 10     | 60     | - 70  | - 60  |

## 7. NEACRP HCLWR CELL BURNUP BENCHMARK CALCULATION

This benchmark was proposed at the 29th meeting of the Nuclear Energy Agency Committee on Reactor Physics (NEACRP). It aims to extract some problems included in the data and methods employed in the neutronic calculations and design of high conversion reactors, and to accelerate the developing works in the field of nuclear data and methods.

Participants were requested to calculate the nuclear characteristics of a tight lattice hexagonal cell with moderator-to-fuel volume ratio ( $V_m/V_f$ ) of 0.6, with 8% fissile enrichment, though results for the cell of volume ratio of 1.1 (7% enrichment) were also received.

The following results were required: k-infinite and conversion ratio; one-group and 3-groups effective cross sections; fractional reaction rates for fuel and fission products at 0, 30 and 50 GWD/T burn-up, number densities at 30 and 50 GWD/T burn-up, and, void behaviour: k-infinite and reaction rates when the moderator void fraction changes from 0% to 45%, 90% and 99%, at burn-ups of 0, 30 and 50 GWD/T.

The calculations carried out up to now at the Centro Atómico Bariloche comprise the obtention of all the requested results at 0 GWD/T (without burn-up) for both volume ratios. The obtention of the results at burn-ups different from zero is now in progress (See point 8.1).

The results obtained in the calculations of this benchmark have been partially presented in point 5.

Figures 7.1 to 7.4 show (in a solid straight line) the locally calculated values of k-infinite, conversion ratio, and reaction rates for both cells.

A very good agreement was found at any void fraction between the mean value of the integral and differential parameters reported by the participants in the benchmark and the local results.

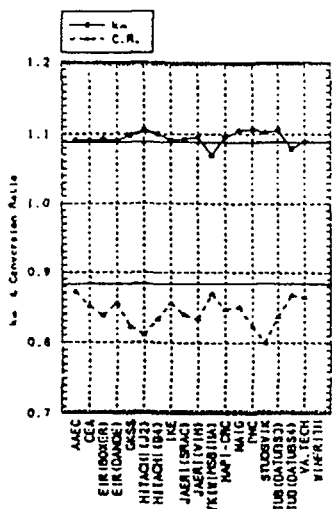


FIGURE 7.1: K-infinity and conversion ratio.  
( $V_m/V_f \approx 0.6$ )

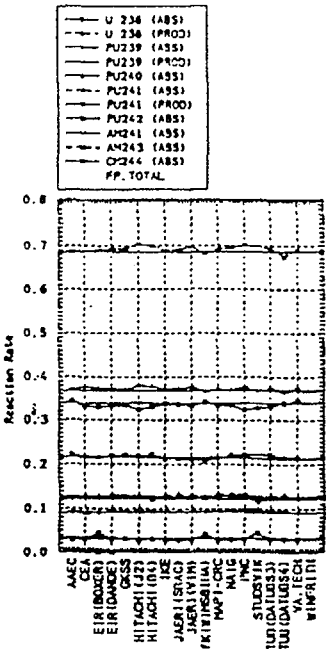


FIGURE 7.2: Reaction rates.  
(void 0% 0 GWD/T)

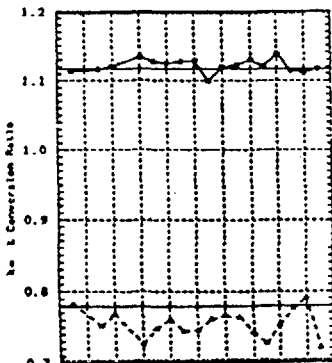


FIGURE 7.3: K-infinity and conversion ratio.  
( $V_m/V_f \approx 1.1$ )

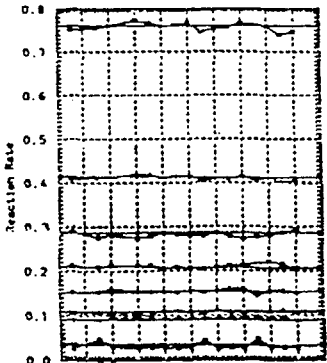


FIGURE 7.4: Reaction rates.  
(void 0% 0 GWD/T)

The rest of the results (not shown here for the sake of brevity) also present a very good agreement with the mean value of the benchmark, and we consider these favorable results as a first validation of our computational system for the calculation of HCLWRs.

## 8. ACTIVITIES UNDER WAY

Under this point, the work which is currently being performed is summarized.

Considering that the next objective of this research program is to acquire enough local design capacity, it is very important to have a complete and efficient calculating system and independent possibilities for nuclear data processing.

Therefore, the present calculational system is being completed with burn-up, fuel assemblies and whole core calculation capabilities. The corresponding steps should be fully validated against experimental and calculated results to arrive, finally, to the design work itself.

For this part, it was considered convenient to use only one reference or starting design that is the based in a proposal of SIEMENS(KWH) - TUBS /5/.

### 8.1 BURN-UP CALCULATIONS

A complete analysis of HCRs requires a good calculation of burn-up to determine conversion ratio and fuel utilization. As the calculational system available up to now does not have a burn-up module, it was a primary need to implement one, as it was said in point 3.

In a first step the burn-up at microcell level will be considered and studied but, the final goal is to include burn-up calculations at all levels, including fuel assemblies and fuel management.

The definition of a burn-up chain is not obvious, and different criteria can be found in the bibliography, so one recommended for other types of reactors (thermal) will be used as starting point /19/, and adjustments and improvements will be made later, after the evaluation of the present chain.

As it was said in 3.1., at present, power scaling and leakage correction have been programmed, as well as the interfacing between some of the stages defined in Figure 3.1.

Next step of this work will cover NEACRP calculations with burn-up, as it was said in point 7..

### 8.2 BENCHMARK CALCULATIONS

The validation of nuclear data and calculation methods for HCR is difficult because of the lack of experimental data. On this respect, experiments have been and are being carried out in Switzerland, France and Japan. To test the calculational system, the following experiments were chosen to compare with:

- the experiments which are being carried out in the Paul Scherrer Institute (formerly EIR), Wuerenlingen, at the PROTEUS reactor
- the experiments of the Fast Critical Assembly performed in JAERI

#### a. PROTEUS

This experiment has been divided in two phases:  
- Phase I, /7/, heterogeneous, where some rods contained a mixed oxide (MOX) enriched up to 15% and some depleted UO<sub>2</sub>; they were arranged in different relations: 1 to 1, simulating an enrichment

of 8% in fissile materials, and 1 to 2 simulating an enrichment of 6 %. In both cases experiments were done for 0%, 42.5% and 100% void fraction.

- Phase II, /8/, homogeneous, where the test region contains only MOX fuel with an enrichment equivalent to 7%. Only results for 0% and 100% of void fraction are known.

The first calculated case was the Phase II because, being homogeneous, it was easier to interpret, but there are very few published results. Therefore, only multiplication factors were obtained, and they are presented in table 8.2.I, for 0 % of void fraction.

TABLE 8.2.I

## Multiplication factor for PROTEUS Phase II. Void Fraction 0%

| Code               | Library    | C/E   | k-infinite | Difference<br>(p.c.m.) |
|--------------------|------------|-------|------------|------------------------|
| Experimental value |            | 1.000 | 1.1217     |                        |
| WIMS               | WIMS81     | 1.012 | 1.1352     | 1350                   |
| KARBUS             | KEDAK      | 0.986 | 1.1060     | -1570                  |
| WIMS               | WIMS/Stan. | 0.976 | 1.0953     | -2640                  |
| WIMS               | JEF I      | 0.983 | 1.1030     | -1870                  |
| This work:         |            |       |            |                        |
| AMPX-II            | ENDF/B-IV  | 0.981 | 1.1009     | -2080                  |

Note: C/E calculated to experimental ratio

For 0% void fraction, the results of this work underestimate k-infinite, as the most of the reported values, in the order of 2000 p.c.m..

Similar situation was found in the case with 100% void fraction. The conclusion is that the results presented here are as good as the already known ( showing discrepancies of the same order ), in particular, better than the obtained with the WIMS standard library.

For a deeper analysis more results are needed, for instance reaction rates, therefore calculations of Phase I were started. Only preliminary results are available because the analysis is not complete up to now. A first set of results is given at Tables 8.2.II and 8.2.III with 0 and 100 % void fraction respectively, also 42.5 % case was calculated.

The first calculated case was the '1 to 1', simulating 8% of enrichment; as this enrichment is reached with depleted and 15% enriched rods, the equivalent cell should include one of each, so an homogenization model must be used.

In the results named AMPX-II(1) the calculations were carried out with a working library where the self-shielding correction was applied to the equivalent cell, that means, after mixing; while in the AMPX-II(2), the correction was applied to the individual rods and then, these cross sections were mixed.

A number of values is presented for each case; they correspond to different homogenization factors applied.

The results show bigger discrepancies than the ones of Phase II, especially for low void fractions (from 1 to 4 %), and are very sensitive to the order in which mixing procedures and resonance self-shielding treatment are done.

TABLE 8.2.II

## K infinite for PROTEUS Phase I. Void Fraction 0%

| Code               | Library   | C/E    | k-infinite | Difference<br>(p.c.m.) |
|--------------------|-----------|--------|------------|------------------------|
| Experimental value |           | 1.000  | 1.045      |                        |
| WIMS               | WIMS81    | 0.990  | 1.035      | -1045                  |
| EPRI               | CPM       | 1.012  | 1.058      | 1254                   |
| SRAC               | JENDL-2   | 1.002  | 1.047      | 209                    |
| SRAC               | ENDF/B-IV | 0.985  | 1.029      | -1560                  |
| This work:         |           |        |            |                        |
| AMPX-II(1)         | ENDF/B-IV | 0.9618 | 1.003      | -3595                  |
|                    |           | to     | to         | to                     |
|                    |           | 0.9959 | 1.009      | -4195                  |
| AMPX-II(2)         | ENDF/B-IV | 1.019  | 1.067      | -1973                  |
|                    |           | to     | to         | to                     |
|                    |           | 1.025  | 1.071      | -2612                  |

TABLE 8.2.III

## K infinite for PROTEUS Phase I. Void Fraction 100%

| Code               | Library   | C/E   | k-infinite | Difference<br>(p.c.m.) |
|--------------------|-----------|-------|------------|------------------------|
| Experimental value |           | 1.000 | 0.905      |                        |
| WIMS               | WIMS81    | 1.023 | 0.926      | 2100                   |
| EPRI               | CPM       | 1.070 | 0.968      | 6300                   |
| SRAC               | JENDL-2   | 0.990 | 0.895      | -1000                  |
| SRAC               | ENDF/B-IV | 0.957 | 0.866      | -3900                  |
| This work:         |           |       |            |                        |
| AMPX-II(1)         | ENDF/B-IV | 1.012 | 0.916      | 1122                   |
|                    |           | to    | to         | to                     |
|                    |           | 1.025 | 0.927      | 2227                   |
| AMPX-II(2)         | ENDF/B-IV | 1.013 | 0.917      | 1152                   |
|                    |           | to    | to         | to                     |
|                    |           | 1.025 | 0.928      | 2257                   |

A great deal of work should still be done, reviewing the Pu239 resonance self-shielding, the mixing/homogenization method, a more adequate Dancoff correction taking into account the cell heterogeneities.

Moreover, the configuration '1 to 2' must also be calculated, and a complete analysis should be done considering that, from the calculation point of view, the cell is infinite and the fundamental mode effect ( $k_{eff} = 1$ ) should be taken into account.

## b. FAST CRITICAL ASSEMBLY - HIGH CONVERSION LIGHT WATER REACTOR (FCA-HCLWR)

A series of experiments have been initiated in 1986 at the FCA at the Japan Atomic Research Institute (JAERI), to investigate the nuclear characteristics of the HCLWR core: the infinite multiplication factor, the moderator voidage effect, the conversion ratio, the control rod worth, etc. /9/

The FCA-HCLWR core is a coupled system, consisting of a controlled test zone (which simulates the neutron spectrum of the HCLWR core), surrounded by a stainless steel buffer zone, a driver zone and a blanket zone of depleted uranium metal.

The experimental program consists of two phases. Phase 1 for enriched uranium fueled cores, and Phase 2 for plutonium fueled cores. The results of Phase 1 experiments have already been published, and they are being used for the validation of our code system for HCLWR calculations.

In these experiments, two moderator-to-fuel volume ratios are used: 0.6 and 1.0, and two different voidage states: 0% and 45%.

Since Phase 1 experiments do not contain plutonium, its results are easier to interpret, and several steps of the calculational sequence may anyway be checked in its application for HCLWR calculations, leaving the validation of the code system for the calculation of void coefficient, and of the plutonium cross sections for the next phase.

The calculation of Phase 1 experiments is now in progress in Bariloche. The obtention of the correspondent effective cross sections is presently under way.

### 8.3 FUEL ELEMENT CALCULATIONS

This work was started validating the system and methods already described, with the Montecarlo HCBWR benchmark reported in /20/. It comprises one fuel element of 199 fuel cells and 18 control rods.

The controlled assembly was calculated to -10% and 40% void fraction, and uncontrolled ones for the cold reactor (-10%) and for 0, 40 and 85 % of void fraction.

Comparisons were performed of integral parameters like multiplication factor and conversion ratio, and differential ones, like power maps and peak factors, against Montecarlo (MC), and HELIOS.HX code /20/ results.

Unidimensional and bidimensional Sn and diffusion calculations were done and the first conclusions are:

- k-infinite: discrepancies for the uncontrolled element are of approximately 1000 pcm with the MC and much lower with the HELIOS, in both the unidimensional and bidimensional cases, which is a very good agreement with the reference.

- for the controlled case there is a very good agreement with the bidimensional calculation.

- the power map has an excellent agreement with the reference calculations.

- power peaks are within the statistical deviations of MC and HELIOS in controlled and uncontrolled cases.

- the conversion ratio shows a systematic upward shift of 0.1 for all the void fractions, which was not explained up to now.

- comparisons between transport and diffusion calculations showed that diffusion is accurate enough for this calculations and, of course, considerably faster.

This work should be continued, and completed with HCR calculations.

### 8.4 ANALYSIS AND OPTIMIZATION OF MAIN PARAMETERS OF A HCR DESIGN

The objective of this part of the work is twofold:

- a. To complete the calculational system to include whole core calculations, including suitable modules and developing the

interfaces required, and to analize the advantages and drawbacks of each of the available codes for this stage

- b. Based on the starting design described above, to evaluate design changes at core level, mainly concerning the reflector and the size of the core, in order to improve the void behaviour of the reactor

The present status of this work is that group constants of the homogenized fuel elements have already been obtained and the first whole core calculations have been done.

Once this first stage of the work is completed, design studies at cell, fuel element and core level will be initiated, specially focused on the void coefficient of the reactor

## 9 CONCLUSIONS AND OUTLOOK

In the frame of High Conversion Reactors neutronic calculations and design, the main goal of the research and development activities carried out up to the moment at the Neutrons and Reactors Division of the Centro Atómico Bariloche has been the development of the design capacities, as well as the achievement of a comprehensive knowledge of the neutronic behaviour of these reactors. As one of the results, a neutronic calculational sequence is now available, which can be confidently applied for HCR design.

A future work plan will be defined during 1990 with the cooperation of experts in the field. Anyway, the activities which are presently in progress will be completed, and improvements in the calculation system will be introduced (cross section treatment, burn-up chains, new codes, etc).

It should also be mentioned that a thermohydraulics group of this center is now starting first studies in HCRs.

## 10. ACKNOWLEDGEMENTS

A significant part of the presented results was contributed by: P.C. Florido, S.E. Gomez, R. Cervieri, V. Ishida and M. Salvatore, members of our group.

We are also indebted to the help we received from other colleagues from abroad, specially to the stimulating suggestions and discussions with Prof. Dr. Oldekop and his group at TUB.

Special mention want to be done of Prof. Edlund and Tom Parkinson, who attracted our attention on this matter.

This work is partially supported by the UNDP and the IAEA through the project ARG/78/020, ARG/89/012 "Nuclear Engineering" from 1985.

## REFERENCES

- /1/ "Advanced light and heavy water reactors for improved fuel utilization", Proc. of a technical committee and workshop on advanced light and heavy water reactor technology, IAEA-TECDOC -344 (1985).
- /2/ C.H.M. Broeders, Nucl. Technol., 71, 96 (1985).
- /3/ V.O. Uotinen et al., "Technical feasibility of a pressurized water reactor design with a low water volume fraction lattice", EPRI, NP-1833 (1981).

- /4/ M.C.Edlund, "An evolutionary approach to improved fuel cycles in PWR", research proposal to USDOE (1981).
- /5/ - W.Oldekop, H.D.Berger and W.Zeggel, Nucl. Technol., 59, 212 (1982).  
- H.Maerkli, G.Goltzmann and H.Moldaschl, Nucl. Technol., 80, 65 (1988).
- W.Zeggel et al., Nuc. Technol., 80, 292 (1988).
- /6/ H. Akie et al., "Preliminary report of HCLWR cell burnup benchmark calculation", Tokai,JAERI (1986).
- /7/ - R.Chawla et al., "Comparisons of calculated and measured parameters for a Pu-fueled LWHCR lattice", EIR Rep.N. 463 (1982)  
- R.Chawla et al., Nucl. Technol., 67, 360 (1984).
- R.Chawla et al., Nucl. Technol., 73, 296 (1986).
- R.Chawla, H.M.Hsieh and M.J.Halsall, Ann. Nuc. Energy, 13, 9, 523 (1986).
- /8/ - S. Pelloni and J.Stepanek, "Testing of a JEF-1 based WIMSD cross section library for migration area and k-infinite predictions for LWHCR lattices", EIR Report 610 SFI for RR (1987).  
- R.Seiler et al., Nuc. Technol., 80, 311 (1988).
- /9/ T. Osugi et al., J. Nucl. Sci. Technol. 26, 5, 477 (May 1989).
- /10/ M.M. Sbaaffoni and M.J.Abbate, "Estado del arte en las investigaciones en reactores avanzados", commun. to XIV scientific meeting of the AATN, Córdoba (Argentina), (1986).
- /11/ M.J. Abbate and M.M. Sbaaffoni, "Problemas de cálculo neutrónico de reactores de alta conversión", commun. to XIV scientific meeting of the AATN, Córdoba (Argentina), (1986).
- /12/ P.C. Florido, M.J. Abbate, M.M.Sbaaffoni and N.Patiño, "Desarrollo de una cadena de medición por tiempo de vuelo, para energías térmicas y epitérmicas", commun. to XVI scientific meeting of the AATN, Mendoza (Argentina), (1988).
- /13/ - S.E. Gómez, P.C. Florido, M.M.Sbaaffoni and M.J.Abbate, "Cálculo de la eficiencia de vidrios de litio utilizando el método de ordenadas discretas", commun. to XVII scientific meeting of the AATN, Buenos Aires (Argentina), (1989).  
- S.E.Gómez, P.C.Florido, M.M.Sbaaffoni and M.J.Abbate, "Medición y cálculo de espectros neutrónicos en sistemas de sodio, homogéneos", commun. to XVII scientific meeting of the AATN, Buenos Aires (Argentina), (1989).
- /14/ N.M. Greene et al., "AMPX-II Modular code system for generating coupled multigroup neutron-gamma-ray cross-section libraries from data in ENDF format", PSR-63, RSIC, (1978).
- /15/ V.H. Gillette, N.E.Patiño, R.Granada and R.Mayer, Nucl. Inst. and Methods in Physics Research A280, 273, (1989).
- /16/ M.M. Sbaaffoni and M.J.Abbate, "DOT 3.5 CAB - A new version of DOT 3.5 code", CNEA NT 18/85, sent to RSIC and NEA data bank (1985).
- /17/ N.E. Patiño, M.J.Abbate and M.M.Sbaaffoni, "Influence of the resonance treatment in HCPWR's cell calculations", accepted to be presented in PHYSOR conference, Marsella (1990).
- /18/ H. Akie, Y. Ishiguro and H.Takano, JAERI-M 88-200, NEACRP-L-309, JAERI (1988).
- /19/ R.J.J. Stamm'ler and M.J. Abbate, "Methods of steady-state reactor physics in nuclear design", Academic Press, London (1983).
- /20/ M. Yamamoto et al., Nucl. Technol., 80, 240 (1988).

## REACTOR PHYSICS RESEARCH CONNECTED WITH THE LR-O REACTOR

J. BÁRDOŠ

Nuclear Research Institute,  
Řež, Czechoslovakia

### Abstract

In the first part of the paper a review of the Czechoslovak R + D programme for industrial applications of nuclear energy is presented. In the period of searching for the most advantageous type of a nuclear power reactor suited to industrial application, CSSR concentrated almost exclusively on the HWGCR type. As a results of work a prototype of the 150 MW reactor was implemented. In the middle of the 1970's, a fundamental change in the orientation of the Czechoslovak nuclear power branch took place, namely to PWR of the VVER type. Reactor physics research work connected with these philosophies were started on the heavy water zero power reactor TR-O in Nuclear Research Institute, Rez. This reactor was according to the change in the mentioned orientation reconstructed to the zero power light water reactor LR-O. Description of the LR-O is presented in the paper. Aditioanly are briefly described so caled inserting light water cores LVZ-1 and LVZ-2 prepared for the TR-O reactor to speed up the initiation of research work for the implementation of light water reactors in CSSR. Reactor LR-O is described as very flexible research tool for reactor physics experiments connected with light water cores.

In the paper the present work performed on the LR-O reactor are described. The works are mainly oriented to develop a fuel eycles for VVERs with BAF e.g. a fuel containing  $Gd_2O_3$  as burnable absorber. Part of the work is performed under the IAEA research contract N° 5328/RB "Safety Aspects of Using Gd Poisoned Fuel in the VVER Reactors". In adition to the BAF containing a homogeneous  $Gd_2O_3$ -admixture in fuel

pellets, specimens of duplex type fuel pellets containing a homogeneous  $Gd_2O_3$ -admixture in a part of pellets only (DUBAF pellets) were prepared. In the paper the DUBAF pellets for burn-up modelation and for  $k_{inf}$  management are described.

In the final part of the paper future plans and possibilities are described. Mainly experiments with different nominal value of the burnable absorber particle radius in BAF and experiments with  $(Th,U)O_2$  fuel are discussed.

---

#### INTRODUCTION

In the period of searching for the most advantageous type of a nuclear power reactor suited to industrial applications, Czechoslovakia concentrated, owing to the international division of work principles valid at that time, almost exclusively on the HWGCR reactor. As a result of work a prototype of the reactor in question with a capacity of 150 MW was implemented. The centre ensuring the necessary physical research and irradiation experiments became then the Nuclear Research Institute (NRI) Rež near Prague, where for the physical research purposes, the TR-0 heavy water zero-power reactor [1] was build. Nuclear Fuel Institute (NFI) Prague manufactured and delivered for this reactor i.a. about 40 t of fuel in the form of natural metallic uranium pins, 6.3 mm in diameter, with a 1 mm thick magnesium sheath.

In the middle of the 1970's, a fundamental change in the orientation of the Czechoslovak nuclear power branch took place, namely to PWR type reactors, by initiating the construction of Soviet type VVER reactors.

In order to speed up the initiation of research works necessary for the implementation of the VVER reactors in Czechoslovakia insertion cores LVZ-1 and LVZ-2 for the

experimental TR-0 reactor were prepared [2]. Idea of using the TR-0 reactor as a driver zone to operate a small light water core situated in its centre appeared to be very progressive. The light water internal lattice operation was enabled without any changes in the control and protection system of the TR-0 reactor, respecting all safety aspects and operating instructions.

To fabricate LVZ-1, an Al tube of the TR-0 fuel assembly was used. The inner tube diameter was 186 mm, the wall thickness 3 mm. The fuel charge for LVZ-1 consisted of metal uranium pins enriched with 2.94% U235; the pin diameter and the Al cladding thickness were 6.3 mm and 0.9 mm respectively. Regular hexagonal lattice pitches 13.6 mm, 12.7 mm and 11 mm were ready for LVZ-1.

Based on experience with LVZ-1, an advanced version LVZ-2 was prepared. For LVZ-2 a double-tube variant with inner diameter 310 mm and outer diameter 338 mm was chosen. In the hermetic interspace was a sensor indicating the ingress of water into this space. The LVZ-2 version was prepared mainly to use VVER-type fuel pins in the VVER-type fuel lattices.

At the same time, the reconstruction of the TR-0 heavy water reactor to the LR-0 light water reactor was intensively prepared. The LR-0 reactor was put into operation in 1983. Description of the LR-0 reactor is in the following section of this paper.

Main areas of research performed on the LR-0 reactor were [3]:

- experiments for VVER pressure vessel neutron exposure evaluation,
- space kinetics,
- nuclear fuel storage subcriticality investigation,
- experiments with Gd poisoned fuel for VVER reactors.

Some ideas from the last mentioned area of research could be interesting for this meeting. These are included into the last section of this paper.

## LR-0 EXPERIMENTAL REACTOR

The LR-0 experimental reactor [4] serves for modelling core configurations of VVER-1000 or VVER-440 type assemblies in symmetric or asymmetric arrangements with the standard or variable triangular lattice pitch. The fission chain reaction in the core is controlled mainly by changing moderator level in the reactor vessel. The  $H_3BO_3$  concentration in the moderator may be of 0 to 12 g  $H_3BO_3$  per liter  $H_2O$ , the moderator may be externally heated up to 70°C. The heat from uranium fission in fuel elements is dissipated into the moderator. The thermal power of the reactor is limited to 5 kW for 1 hour and the thermal neutron flux density in the centre of the core to  $10^{13} m^{-2}s^{-1}$ .

The aluminium reactor vessel (Fig. 1) is situated in a concrete shield and covered with mobile shielding platforms. The bottom cylindrical part of the vessel has a diameter of 3.5 m a height of 6.5 m, the upper part of the square cross section 6x6 m and height of 1.5 m is covered with square cover. On it, there is a rotational circular cover with a system of openings which provide accessibility of any site in the cylindrical part of the vessel. In the bottom of the vessel, there are three openings of I.D. 200 mm. Two of them are assigned for the release of the moderator, the central neck serves for the moderator inlet. Simultaneously, a dry channel passes through the inlet neck serving for inserting a neutron source closely to the heel of the central assembly. The mantle of the vessel is covered with 1 mm Cd sheet and removable thermal shielding.

The main part of the technology equipment is the reactor core located on a supporting system in the reactor vessel. The design of the standard supporting system makes it possible to modify easily configurations of the reactor core. A supporting plate (Fig. 2) with

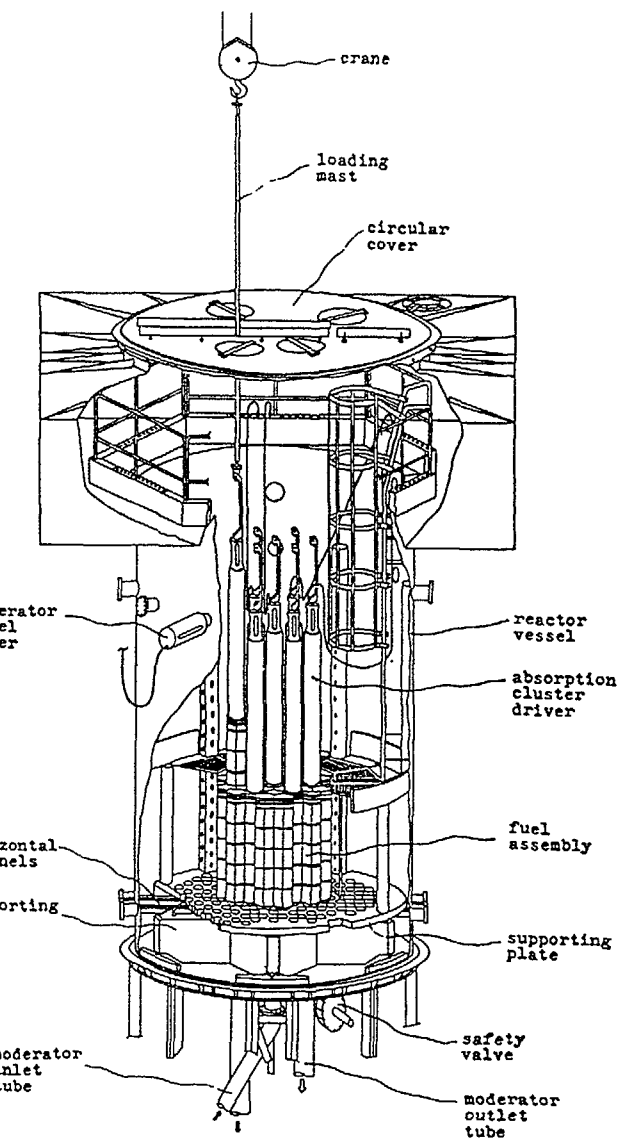


FIG. 1. Reactor vessel and its equipment.

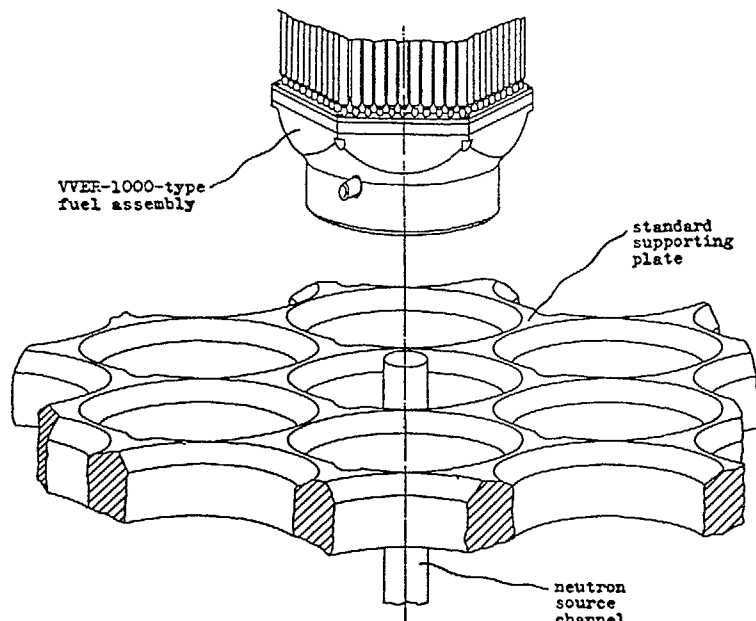


FIG. 2. Standard supporting plate.

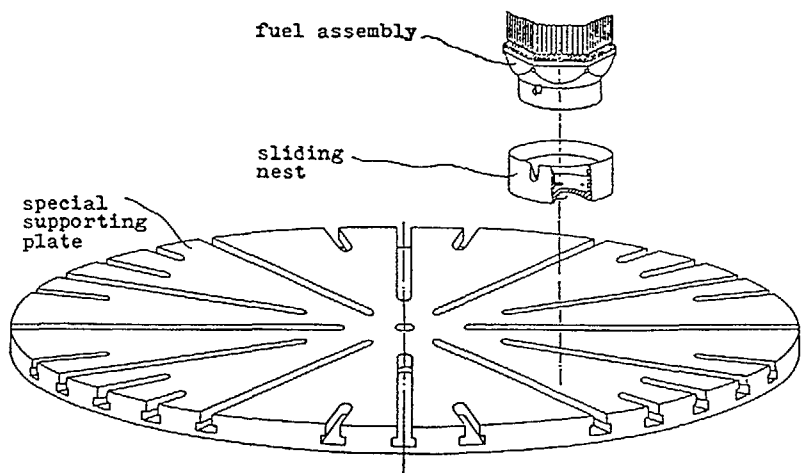


FIG. 3. Special supporting plate with grooves.

openings for situating fuel assemblies of the VVER-1000 type forms a triangular lattice with a pitch of 236 mm. Experiments of VVER-440 type fuel assemblies are being performed using a special supporting plate enabling arrangement of assemblies one from another in different distances keeping the triangular lattice. Instead of holes, this plate has radial grooves (Fig. 3) which actually create a radial fitting of sliding nests for placing assembly heels. The angles between the grooves are chosen in such a manner that, at a fixed pitch, the assembly lattice is triangular and symmetric with respect to the central point of the plate. The nests are variable according to the type of the assembly. Consequently, it is possible to compile a core containing the VVER-440 or VVER-1000 type assemblies, a core with various pitches of assemblies in the inner and outer part (a driven and a driving core), etc.

The basic types of fuel assemblies used are the shortened dismountable models of the VVER-1000 and VVER-440 assemblies (Fig. 4). Fuel elements are filled with sintered UO<sub>2</sub> pellets with an outer diameter of 7.53 mm and internal central hole of 1.4 mm in diameter. The height of the fuel filling in the element is 1357 mm. The fuel enrichment varies from 1.6% to 4.4% of U235. In addition to the fuel element type mentioned, further fuel elements containing Gd to be used in the LR-0 reactor were prepared in NFI. Up to now, 3605-, 3610-, 3615-, 3620-, and 4460-type fuel elements containing a homogeneous Gd<sub>2</sub>O<sub>3</sub> - admixture in the fuel pellets were prepared. The first group of two digits gives the uranium enrichment with U235 isotope (e.g. 36 designates 3.6% U235), the second one the weight content of Gd<sub>2</sub>O<sub>3</sub> in a fuel pellet (e.g. 15 designates 1.5 w% of Gd<sub>2</sub>O<sub>3</sub>). In addition to the fuel elements containing a homogeneous Gd<sub>2</sub>O<sub>3</sub>-admixture in fuel pellets (BAF) specimens of duplex type fuel pellets containing a homogeneous Gd<sub>2</sub>O<sub>3</sub>-admixture in a part of the

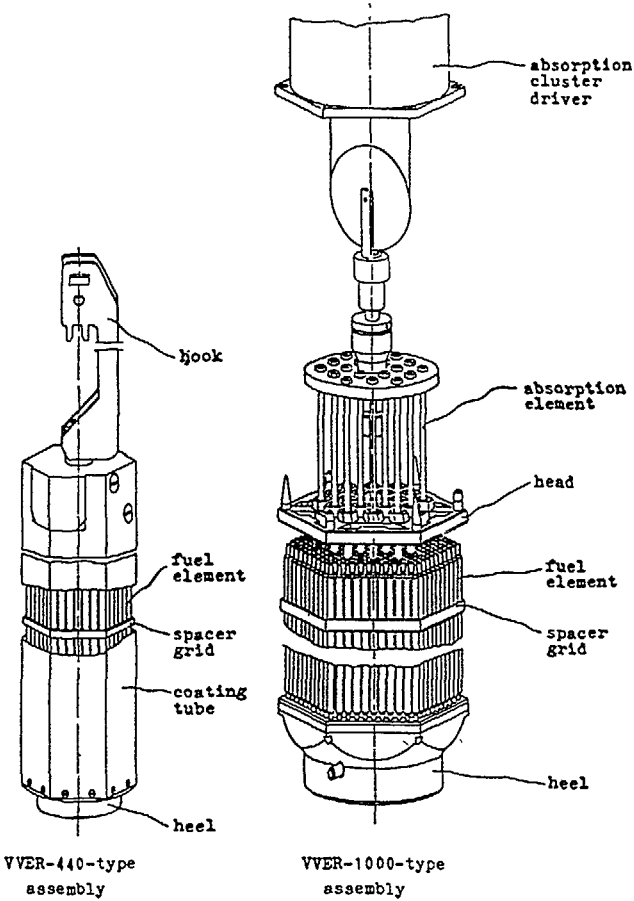


FIG. 4. Fuel assemblies.

pellet only (DUBAF) were prepared for experiments planned in future. The cladding tube all of the elements is Zr+1%Nb of O.D. 9.15 x 0.72 mm. Several fuel elements may be opened at both ends and fuel pellets may be removed.

The hexagonal coatless fuel assembly VVER-1000 for LR-0 may be equipped with an absorption cluster which is a model of an analogous element in a power reactor. A Zr+1%Nb tube of O.D. 10.3 x 0.65 mm passes through the

centre of each assembly for in-pile instrumentation. In the assembly, there are 312 fuel elements in a triangular lattice with a pitch of 12.75 mm. The distribution of fuel elements, guide tubes for cluster absorption elements and the central tube is provided by means of five stainless steel spot-welded honeycomb spacer grids. Their number and height in the assembly may be modified according to experimental requirements.

The VVER-440 assembly for LR-0 has 126 elements in a triangular lattice with a pitch of 12.2 mm. The stainless steel spacer grids used are either spot-welded honeycomb ones or drilled plates. The hexagonal Al coating tube of the assembly is 2 mm thick and its outer size is 144 mm. A Zr+1%Nb tube of O.D. 10.3 x 0.65 mm goes through the centre of the assembly. Under experimental conditions, it is also possible to model the disturbances in the VVER-440 power reactor core caused by the insertion of a control element assembly. The control element assembly is represented here by a storeyed assembly whose absorption section has exchangeable segments. The insertion of the control element assembly is simulated by changing the number of the absorbing segments.

#### SPECIAL FUEL

#### Physical models

The burning up process in BAF pellets differs substantially from that encountered in a current ceramic fuel which does not contain burnable absorber. This dissimilarity is due to the presence of Gd in itself which, considering the high absorption cross section for thermal neutron capture, causes the thermal neutrons incident on the surface of an unburned BAF pellet to be probably captured in the vicinity of this surface already. The probability of the thermal neutron penetration into the subsurface and inner BAF layers increases step by step

in the course of a fuel campaign as Gd burning up in the surface layer.

Supposing that an ideal BAF pellet consists of a homogeneous mixture of  $\text{UO}_2$  and  $\text{Gd}_2\text{O}_3$  molecules, a partially burnt up pellet may be considered as a cylinder showing two concentric layers. The outer layer contains partially burnt up  $\text{UO}_2$  without Gd absorber and the inner layer shows the original  $\text{UO}_2$  and  $\text{Gd}_2\text{O}_3$  composition. When designing this model a relation given in [5] may be used

$$R(t) = R(0) - \phi t / (4C) \quad (1)$$

where

$R(t)$  is the radius of the absorbing portion of pellet in time  $t$ ,

$t$  is the burning up time (i.e. time from the beginning of the campaign),

$\phi$  is the neutron flux density,

$C$  is the initial burnable absorber concentration in the pellet.

In reality, a partially burnt up pellet exhibits a more complicated inner structure as the outer layer burn-up is not homogeneous, the layer boundary is not sharp, etc.

Despite this, we consider this model applicable to testing computer programs since it models with sufficient accuracy the most substantial factor, namely the change in the effective radius of the BAF pellet absorbing portion.

The knowledge of  $\text{UO}_2$  enrichment in the outer and inner layers,  $\text{Gd}_2\text{O}_3$  concentration in the inner layer, as well as the knowledge of the layer size provide a very solid basis enabling accuracy testing of this burn-up model when performing direct measurements with such pellets in the LR-0 reactor.

However, a BAF pellet prepared in reality consists of free  $\text{UO}_2$  and  $\text{Gd}_2\text{O}_3$  particles in a  $\text{UO}_2\text{-Gd}_2\text{O}_3$  solid solution matrix. Even in an ideal plane of the first approximation no homogeneity at the level of single molecules may be envisaged. Considering an absorber particle (or particle agglomerate) in a homogeneous matrix as the space unit, we can transpose the aforementioned considerations for a BAF pellet in their entirety to any particle. Accepting further idealisation, namely spherical shape particles, their radius in a surface layer will then decrease during burning up process also according to the relation (1). Using our model it is possible to expect the layer boundary to be out of focus and the relation (1) not to hold for a real  $\text{Gd}_2\text{O}_3$  concentration in  $\text{UO}_2$  but for a certain effective concentration, function of the initial particle diameter. This effect can be also used for  $k_{\text{inf}}$  management.

Subsurface layer shielding by BAF surface layer absorber shows further accompanying effects. Neutron spectrum in these subsurface layers is shifted to higher energies with consequences of higher Pu production. For illustration of mentioned effect some results of calculations [6] performed in order to carry out the benchmark problems given under International Atomic Energy Agency CRP "Safe Core Management with Burnable Absorbers in VVERs" are presented on Fig. 5. Clean fuel lattice in this benchmark consists of VVER fuel pins ( $\text{UO}_2$  pellets diameter 7.72 mm, outer diameter of Zr+1%Nb cladding 9.1 mm, triagonal lattice pitch 12.75 mm, fuel enrichment 4.2% U235), poisoned lattice consist of the same geometry BAF pins (BAF enrichment 1.6% U235, Gd content 4 w%).

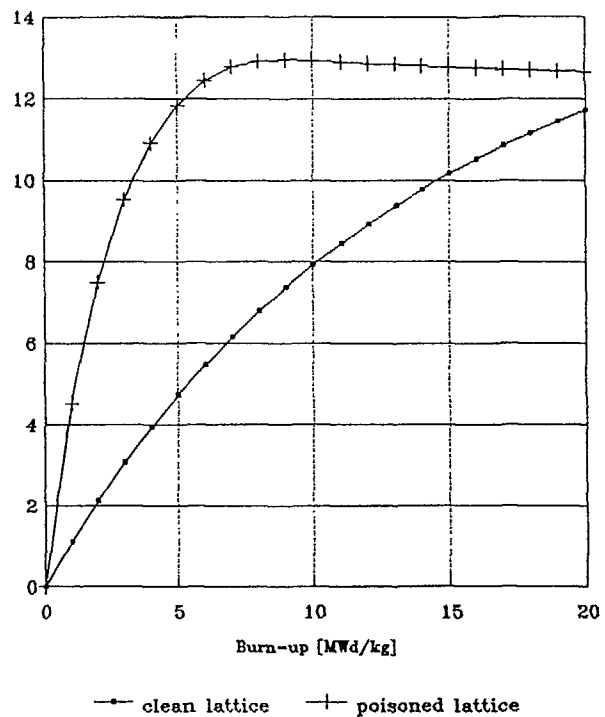


FIG.5. Pu-239 number densities.

### Experiments

The first part of experiments with BAF in frame of mentioned CRP on reactor LR-0 was performed in 1989. Experiments were performed with a simple BAF pin in the infinite lattice of the VVER type fuel pins [7]. Results for BAF containing 0.5, 1, 1.5 and 2%  $Gd_2O_3$  in  $UO_2$  with enrichment 3.6% U235, gives good set of values for corresponding benchmark calculations. In the 1990 experiments will be performed using BAF 6%  $Gd_2O_3$  in  $UO_2$  of 4.4% U235 enrichment, as well as experiments using DUBAF pellets e.g. duplex type BAF pellets modelling partially

burned-up BAF. For 1991 we prepare experiments connected with already mentioned idea of higher conversion core created by BAF.

Other interesting part of new experiments now under preparation is experiment with simple pin of  $ThO_2$  in infinite VVER type lattice of  $UO_2$  fuel pins. This experiment is foreseen for preparation of modified first core loading to start  $ThO_2$  -  $U^{235}O_2$  cycle in unmodified VVERs and to escape of using Pu for this purpose.

### ACKNOWLEDGMENT

Part of the results included in this paper was obtained under International Atomic Energy Agency Research Contract № 5328/RB. Author wish to acknowledge for this financial support.

### REFERENCES

- [1] M. Čapek: Experiences from Operation of the TR-0 Reactor,  
CMEA Symposium on Experiences from Using of Research Reactors, Predeal, Romania, 1974  
(in Russian)
- [2] M. Hron, J. Bárdóš: Physical Research of the VVER-type Lattices on Inserted Cores of the TR-0 Reactor,  
*Jaderná energie* 25 (1979) 297  
(in Czech)
- [3] B. Ošmera et al.: Studies of VVER Physics on LR-0 Experimental Reactor,  
Report to be presented on PHYSOR-90, Marseille,  
April 23-26, 1990
- [4] Q. Sochor, R. Starý: The Experimental Reactor LR-0 after Five Years Operation,  
*Nukleon*, A Special Issue (1988) 5

- [5] L. Mortensen: Absorber Management Using Burnable Poisons,  
Risø Report № 341 (1977)
- [6] J. Vacek, P. Mikolas: Experience with the WIMS Computer Code at Skoda Plzen,  
A Technical Committee/Workshop on In-Core Fuel Management, IAEA, Vienna, December 4-7, 1989
- [7] J. Bárdóš et al.: Burnable absorbers in VVER-type Fuel Lattices,  
Meeting of participants in the co-ordination Research Programme on "Safe Core Management with Burnable Absorbers in VVERs", IAEA, Vienna, December 11-14, 1989

## LIST OF PARTICIPANTS

|                  |   |  |   |
|------------------|---|--|---|
| Abbate, M.J.     | Centro Atómico Bariloche<br>8400 Bariloche (Río Negro)<br>Argentina   | Broeders, C.H.M.                       | Kernforschungszentrum Karlsruhe GmbH<br>Postfach 3640<br>7500 Karlsruhe, Germany  |
| Arai, K.         | Nuclear Engineering Laboratory<br>TOSHIBA Corporation<br>4-1 Ushimado-cho, Kawasaki-ku<br>Kawasaki 210, Japan | Brogli, R.H.                           | Paul Scherrer Institute<br>5232 Villigen<br>Switzerland   |
| Axmann, J.       | Institut für Raumflug und Reaktortechnik<br>Hans-Sommer-Str. 5<br>3300 Braunschweig<br>Germany                | Bryumin, S.V.                          | Scientific Research and Design<br>Institute for Power Engineering<br>2/8, M. Krasnosel'skaja Street<br>Moscow 107113, USSR    |
| Baker, J.N.      | United Kingdom Atomic Energy Authority<br>CH 475, Risley, Warrington<br>United Kingdom                        | Chawla, R.                             | Paul Scherrer Institute<br>5232 Villigen PSI<br>Switzerland   |
| Balakrishnan, K. | BARC, Reactor Engineering Division<br>Bhabha Atomic Research Centre<br>Bombay 85, India                       | Crijns, M.J.<br>(Scientific Secretary) | IAEA, Division of Nuclear Power<br>Wagramerstrasse 5<br>P.O. Box 100, A-1400 Vienna<br>Austria                                |
| Bardos, J.       | Reactor Physics Division<br>Nuclear Research Institute<br>25068 Rez<br>The Czech and Slovak Federal Republic  | Dalle Donne, M.                        | Kernforschungszentrum Karlsruhe GmbH<br>Postfach 3640<br>7500 Karlsruhe, Germany  |
| Berbey, P.       | EDF/SEPTEN<br>12/14 Avenue Dutrievoz<br>69628 Villeurbanne Cedex<br>France                                    | Dreier, J.                             | Paul Scherrer Institute<br>Laboratory for Thermohydraulics<br>Würenlingen und Villigen<br>CH-5232 Villigen PSI<br>Switzerland |
| Berger, H.D.     | Siemens AG/KWU, B314<br>Power Generation Group KWU<br>Hammerbacher Str. 12+14<br>8520 Erlangen, Germany       | Dumitache, I.                          | Institute for Nuclear Power Reactors<br>Ministry of Electrical Power<br>P.O. Box 78, 0300 Pitesti<br>Romania                  |
| Bethke, S.       | Institut für Raumflug und Reaktortechnik<br>Hans-Sommer-Str. 5<br>3300 Braunschweig<br>Germany                | Edlund, M.C.                           | Virginia Polytechnic Institute<br>and State University<br>Blacksburg, VA 24061<br>United States of America                    |
| Boehm, R.        | Siemens AG/KWU<br>Hammerbacher Str. 12+14<br>8520 Erlangen, Germany   | Erbacher, F.J.                         | Kernforschungszentrum Karlsruhe GmbH<br>Institut f. Reaktorbauelemente<br>Postfach 3640<br>7500 Karlsruhe, Germany            |
| Boehme, E.R.     | Kernforschungszentrum Karlsruhe GmbH<br>Postfach 3640<br>7500 Karlsruhe, Germany                              | Finnemann, H.                          | Siemens AG/KWU<br>Hammerbacher Str. 12+14<br>8520 Erlangen<br>Germany   |

|               |   |               |  |
|---------------|---|---------------|--|
| Goetzmann, C. | Siemens AG/KWU, R 1/R 115<br>Hammerbacher Str. 12+14<br>Postfach 3220<br>8520 Erlangen, Germany   | Kuesters, H.  | Kernforschungszentrum Karlsruhe GmbH<br>Institut für Neutronenphysik und<br>Reaktortechnik<br>Postfach 3640, 7500 Karlsruhe 1<br>Germany |
| Guengoer, S.  | Physics Department<br>Gukurova University<br>Bakali-Adana<br>Turkey   | Lee, J.C.     | Department of Nuclear Engineering<br>University of Michigan<br>Ann Arbor, MI 48109-2104<br>United States of America                      |
| Hishida, H.   | Mitsubishi Atomic Power Ind., Ltd.<br>2-14-1 Shibakouen, Minato-ku<br>105 Tokyo, Japan  | Longhi, B.    | Framatome, Tour Fiat<br>92080 Paris la Défense Cedex 16<br>France  |
| Huesken, J.   | Siemens AG/KWU<br>Hammerbacher Str. 12+14<br>8520 Erlangen, Germany   | Maerkli, H.   | Siemens/KWU, R<br>Hammerbacher Str. 12+14<br>8520 Erlangen<br>Germany  |
| Ishiguro, Y.  | Reactor System Laboratory<br>Department of Reactor Engineering<br>Japan Atomic Energy Research Institute<br>319-11 Tokai-mura, Naka-gun<br>Ibaraki-ken, Japan | Meier, W.     | Siemens AG/KWU, B421<br>Hammerbacher Str. 12+14<br>8520 Erlangen<br>Germany  |
| Janssen, A.J. | Netherlands Energy Research Foundation<br>Business Unit Nuclear Energy<br>Postbus 1, Westerduinweg 3<br>1755 ZG Petten<br>Netherlands                         | Meyer, P.J.   | Siemens AG/KWU, N253<br>Hammerbacher Str. 12+14<br>8520 Erlangen<br>Germany  |
| Khalid, M.    | IAEA, Division of Nuclear Power<br>Wagramerstrasse 5<br>P.O. Box 100, A-1400 Vienna<br>Austria  | Minsart, G.   | S.C.K./C.E.N.<br>Boeretang 200,<br>B-2400 MOL, Belgium   |
| Kluever, B.   | Institut für Raumflug und Reaktortechnik<br>Hans-Sommer-Str. 5<br>3300 Braunschweig<br>Germany  | Millot, J.P.  | Framatome - Tour Fiat<br>92080 Paris la Défense Cedex 16<br>France   |
| Knapp, V.     | Faculty of Electrical Engineering<br>University of Zagreb<br>Unska 3, P.O. Box 170,<br>41000 Zagreb<br>Yugoslavia   | Moldaschl, H. | Siemens AG/KWU, U 7,331<br>Hammerbacher Str. 12+14<br>Postfach 3220<br>8520 Erlangen, Germany  |
| Koban, J.     | Siemens AG/KWU, R 281<br>Hammerbacher Str. 12+14<br>8520 Erlangen, Germany  | Murao, Y.     | Department of Reactor Engineering<br>Tokai Establishment, JAERI<br>Tokai-mura 319-11<br>Ibaraki-ken, Japan                               |
| Kuczera, B.   | Kernforschungszentrum Karlsruhe GmbH<br>Postfach 3640<br>7500 Karlsruhe 1<br>Germany  | Nigon, J.L.   | CEN Cadarache DTE/SCOS<br>BP No.1<br>13108 Saint-Paul-lez-Durance-Ceaca<br>France  |

|     |                 |  |                  |  |
|-----|-----------------|--|------------------|--|
| 332 | Oh, Se Kee      | Korea Advanced Energy Research Institute<br>P.O. Box 7<br>Daeduck-danji, Daejun<br>Korea, Federal Republic of                      | Sekiya, T.       | Osaka University, Dept. of<br>Nuclear Engineering<br>2-1 Yamada-oka, Suita-shi<br>565 Osaka Pref., Japan     |
|     | Oldekop, W.     | Institut für Raumflug und Reaktortechnik<br>Hans-Sommer-Str. 5<br>3300 Braunschweig<br>Germany                                     | Serghiuta, D.    | Institute for Nuclear Power Reactors<br>Ministry of Electrical Power<br>P.O. Box 78<br>0300 Pitesti, Romania |
|     | Pelloni, S.     | Paul Scherrer Institute<br>CH-5232 Villigen PSI<br>Switzerland   | Seiler, R.       | Paul Scherrer Institute<br>CH-5232 Villigen PSI<br>Switzerland   |
|     | Pshenin, V.V.   | I.V. Kurchatov Institute of Atomic Energy<br>I.V. Kurchatov Sq. 1<br>Moscow 123182<br>USSR   | Takeda , R.      | Energy Research Laboratory<br>HITACHI Ltd.<br>1168 Moriyama-cho, Hitachi-shi<br>Ibaraki-ken, 316<br>Japan    |
|     | Rajamaeki, K.   | Technical Research Center of<br>Finland Nuclear Engineering Lab.<br>P.O. Box 169<br>SF-00181 Helsinki<br>Finland                   | Vandenberg, C.N. | Rue du Champ de Mars, 25<br>Belgonucleaire S.A.<br>1050 Bruxelles<br>Belgium                                 |
|     | Rau, P.J.       | Siemens AG/KWU, B42<br>Bunsenstr. 42<br>8520 Erlangen, Germany   | Vivante, C.      | DG of Science Research and<br>Development<br>Rue de la Loi 200<br>B-1049 Brussels<br>Belgium                 |
|     | Rummel, I.      | Siemens AG/KWU, R115<br>Hammerbacher Str. 12+14<br>Postfach 3220<br>8520 Erlangen, Germany   | Wagner, M.R.     | Siemens AG/KWU, Dept. B3<br>Postfach 3220<br>8520 Erlangen, Germany  |
|     | Santos, A.D.    | IPEN/CNEN/SP<br>Travessa R, 400-Cidade Universitária<br>Armando de Salles Oliveira<br>Pinheiros, Sao Paulo, SP CEP 05508<br>Brazil | Xu, C.           | Institut für Raumflug und Reaktortechnik<br>Hans-Sommer-Str. 5<br>3300 Braunschweig<br>Germany               |
|     | Sbaffoni, M.M.  | Centro Atomico Bariloche<br>Av. da Bastillo Km.9.5<br>Rio Negro<br>San Carlos de Bariloche 8400<br>Argentina                       | Zeggel, W.       | Institut für Raumflug und Reaktortechnik<br>Hans-Sommer-Str. 5<br>3300 Braunschweig<br>Germany               |
|     | Schatz, M.      | Siemens AG/KWU Group<br>Hammerbacher Str. 12+14<br>8520 Erlangen<br>Germany  | Zverkov, Yu.A.   | I.V. Kurchatov Institute of Atomic Energy<br>I.V. Kurchatov Sq. 1<br>Moscow 123182<br>USSR                   |
|     | Schlosser, G.J. | Siemens AG/KWU Group<br>Hammerbacher Str. 12+14<br>8520 Erlangen<br>Germany  |                  |  |